

Institute of Nutritional Science
Chair of Food Science
Justus Liebig University Giessen

**Non-target screening of emerging bioactive and
hazardous compounds in complex matrices via
multi-hyphenated techniques**

Cumulative dissertation

for the degree of

Doctor rerum naturalium (Dr. rer. nat.)

Submitted to the

**Faculty of Agricultural Science, Nutritional Science, and Environmental
Management**

Justus Liebig University Giessen

by

Tamara Schreiner (M. Sc.)

Fulda, Germany

Giessen, 2022

With permission of the faculty Agricultural Science,
Nutritional Science, and Environmental Management
Justus Liebig University Giessen

Examining committee:

1st Reviewer: Prof. Dr. Gertrud Morlock
2nd Reviewer: Prof. Dr. Bernd Lindemann
3rd Examiner: Prof. em. Dr. Wolfgang Schwack
3rd Examiner: Prof. em. Dr. Bernd Honermeier

Table of Contents

Declaration	V
Acknowledgments	VII
Scientific contributions.....	IX
List of figures	XIII
List of abbreviations	XV
1. Introduction	1
1.1. <i>Non-target screening for bioactivity in food</i>	1
1.2. <i>Status-quo high-performance thin-layer chromatography hyphenations</i>	3
1.2.1. <i>High-performance thin-layer chromatography–effect-directed analysis</i>	4
1.2.2. <i>Microplate assays versus planar assays</i>	7
1.2.3. <i>High-performance thin-layer chromatography–effect-directed analysis– high-resolution mass spectrometry</i>	7
1.2.4. <i>On-surface metabolisation</i>	8
1.3. <i>Online desalting and orthogonal separation</i>	9
1.4. <i>Mass analysers: single quadrupole versus orbitrap</i>	10
1.5. <i>Diffusion susceptibility of silica gel layers</i>	11
1.6. <i>Scope</i>	12
1.7. <i>Progress achieved through multi-hyphenated techniques</i>	12
1.7.1. <i>Establishment of an eight-dimensional hyphenation (Publication 1)</i>	13
1.7.2. <i>Application field study using the eight-dimensional hyphenation (Publication 2)</i>	15
1.7.3. <i>Ten-dimensional hyphenation for non-target screening (Publication 3)</i>	17
1.7.4. <i>Application field study using the ten-dimensional hyphenation (Publication 4)</i> ...	19
1.7.5. <i>Diffusion reduction permitting multiplexed assay formats (Publication 5)</i>	19
1.7.6. <i>Application field study for multiplexed estrogen screen (Publication 6)</i>	20
1.8. <i>References</i>	23
2. Publication 1	33
3. Publication 2	57
4. Publication 3	109
5. Publication 4	155
6. Publication 5	173
7. Publication 6	227
8. Summary.....	253
9. Zusammenfassung	255

Declaration

I declare: this dissertation submitted is a work of my own, written without any illegitimate help by any third party and only with materials indicated in the dissertation. I have indicated in the text where I have used texts from already published sources, either word for word or in substance, and where I have made statements based on oral information given to me. At any time during the investigations carried out by me and described in the dissertation, I followed the principles of good scientific practice as defined in the “Justus Liebig University Giessen Statute for Ensuring Good Scientific Practice”.

Giessen, August 2022

Tamara Schreiner

Acknowledgments

My special thanks go to my first supervisor Prof. Dr. Gertrud Morlock, who gave me the opportunity to do my doctorate in her research group. Thank you very much for this instructive time and your dedicated support in all matters.

I would also like to thank Prof. Dr. Bernd Lindemann for proving the second review for my doctorate.

Further, a big thank you to my wonderful colleagues Stefanie Kruse, Annabel Mehl, Alisa Ronzheimer und Isabel Müller, who have always been there to help and advise me, and who have also sometimes cushioned my bad mood. I could not think of any better collegial support.

I am also grateful for the good souls of the working group Julia Heil and Simone Cutts. Without you, the team would not be the same.

I would also like to extend my sincere thanks to the thesis students Dorena Sauter, Maren Friz, and Naila Eggerstorfer for assistance in laboratory work.

Last but not least, I want to thank my beloved family, my parents and my sister, for their support during my studies and my PhD. Without you I would never have made it. I love you.

Scientific contributions

Peer-reviewed original research papers

- 1) Schreiner, T., Morlock, G.E.: Non-target bioanalytical eight-dimensional hyphenation including bioassay, heart-cut trapping, online desalting, orthogonal separations and mass spectrometry, *J. Chromatogr. A* 1647, **2021**, 462154

Author contributions: **Tamara Schreiner:** Conceptualization, Methodology, Experimental Analysis, Data Analysis, Writing – Original Draft. **Gertrud E. Morlock:** Conceptualization, Methodology, Supervision, Writing – Review and Editing.

- 2) Schreiner, T., Sauter, D., Friz, M., Heil J., Morlock, G.E.: Is our Natural Food our Homeostasis? Array of A Thousand Effect-Directed Profiles of 68 Herbs and Spices, *Front. Pharmacol.* 12, **2021**, 755941

Author contributions: **TS** carried out all bioassays and mass spectrometry experiments, analyzed the data, and wrote the manuscript draft. **DS** and **MF** prepared the *B. subtilis*, α -/ β -glucosidase, β -glucuronidase, pYAS, pYES, pYAAS, pYAES (bio)autograms. **JH** prepared the samples and *A. fischeri*, tyrosinase, and α -amylase (bio)autograms. **GM** initiated the project, concept and methodology, obtained research funding, supervised the study, and revised the manuscript.

- 3) Schreiner, T., Eggerstorfer, N., Morlock, G.E.: Effects of gastrointestinal digestion on the bioactivity of convenience tomato products examined by ten-dimensional hyphenation – submitted to *J. Agric. Food Chem.*, **2022**

Author contributions: **Tamara Schreiner:** Conceptualization, Methodology, Investigation, Data Analysis, Writing – Original Draft. **Naila M. Eggerstorfer:** Investigation. **Gertrud E. Morlock:** Conceptualization, Methodology, Supervision, Writing – Review and Editing.

- 4) Schreiner, T., Eggerstorfer, N., Morlock, G.E.: Effects of gastrointestinal digestion on bioactivity of meal replacement products studied by ten-dimensional hyphenation – submitted to *Food Funct.*, **2022**

Author contributions: **Tamara Schreiner:** Conceptualization, Methodology, Investigation, Data curation, Writing – Original Draft. **Naila M. Eggerstorfer:** Investigation. **Gertrud E. Morlock:** Conceptualization, Methodology, Supervision, Funding Acquisition, Writing – Review and Editing.

- 5) Schreiner, T., Ronzheimer, A., Friz, M., Morlock, G.E.: Multiplex planar bioassay with reduced diffusion on normal phase, identifying androgens, verified antiandrogens and synergists in botanicals via 12D hyphenation, *Food Chem.* 395, **2022**, 133610

Author contributions: **T. Schreiner:** Methodology, Investigation, Formal analysis, Writing – original draft. **A. Ronzheimer:** Methodology, Investigation, Formal analysis, Writing – original draft. **M. Friz:** Investigation. **G.E. Morlock:** Conceptualization, Methodology, Supervision, Funding acquisition, Project administration, Writing – review & editing.

- 6) Ronzheimer, A., Schreiner, T., Morlock G.E.: Multiplex planar bioassay detecting estrogens, antiestrogens, false-positives and synergists as sharp zones on normal phase, *Phytomedicine* 103, **2022**, 154230

Author contributions: **A. Ronzheimer:** Conceptualization, Methodology, Investigation, Data curation, Writing – original draft. **T. Schreiner:** Conceptualization, Methodology, Investigation, Data curation, Writing – original draft. **G.E. Morlock:** Conceptualization, Methodology, Supervision, Writing – review & editing.

Peer-reviewed original research paper (co-authorships)

- 1) Morlock, G.E., Ziltener, A., Geyer, S., Mehl, A., Schreiner, T., Kamel, T., Tersteegen, J., Brümmer, F.: Indo-Pacific bottlenose dolphins self-medicate with invertebrates in coral reefs, *iScience*, **2022**, 104271

Author contributions: Conceptualization: A.Z., F.B., T.K. (sampling), G.E.M. (analysis); Methodology: A.Z., J.T., F.B. (sampling), G.E.M. (analysis); Sampling: A.Z., J.T.; Investigation: S.G. (all HPTLC-assay experiments), A.M. (HRMS), T.S. (hormonal-effective bioassays and respective MS), J.T. (HPTLC-*A. fischeri* assay); Funding acquisition: A.Z., G.E.M., F.B.; Project administration: A.Z., G.E.M.; Supervision: F.B. (dive protocol), A.Z. (sampling), G.E.M. (analysis); Writing – original draft: G.E.M., A.Z.; Writing – review & editing: G.E.M., A.Z., F.B., J.T.

- 2) Schreiner, T., Morlock, G.E.: Investigation of the phytoestrogenic potential of rose, red and white wines via effect-directed 9D hyphenation – submitted to *J. Chromatogr. A*, **2022**

Author contributions: **Tamara Schreiner:** Conceptualization, Methodology, Investigation, Data Analysis, Writing – Original Draft. **Gertrud E. Morlock:** Conceptualization, Funding acquisition, Methodology, Supervision, Writing – Review and Editing.

Poster presentations

Presenter in italics

- 1) Curious2022 Future Insight™ conference, Darmstadt, 12-14.07.2022: *Morlock, G.E.*, Ziltener, A., Geyer, S., Mehl, A., Schreiner, T., Kamel, T., Tersteegen, J., Brümmer, F.: Dolphins' beauty secrets, poster presentation, awarded with the poster prize

List of figures

Figure 1. Common hyphenation possibilities for non-target screening	2
Figure 2. Schematic representation of the eight-dimensional hyphenation	13
Figure 3. Calculated salt and nutrient load on a HPTLC silica gel 60 F ₂₅₄ MS-grade plate for respective (bio)assays.	15
Figure 4. Irreversible mitochondrial conversion of the blue dye resazurin	21

List of abbreviations

10D	ten-dimensional
12D	twelve-dimensional
8D	eight-dimensional
AChE	acetylcholinesterase
BChE	butyrylcholinesterase
DAD	diode array detector
ddMS2	data-dependent MS2
EDA	effect-directed analysis
F ₂₅₄	fluorescence indicator, green fluorescent at 254 nm
fix	fixated zones through Degalan coating
FLD	fluorescence light detection
hAR	human androgen receptor
hER	human estrogen receptor
HPLC	high-performance liquid chromatography
HPTLC	high-performance thin-layer chromatography
R _F	retention factor
HRMS(/MS)	high-resolution (tandem) mass spectrometry
LC	liquid chromatography
MS	mass spectrometry
MU	4-methylumbelliferone
MUG	4-methylumbelliferyl β-D-galactopyranoside
<i>m/z</i>	mass-to-charge ratio
NP	normal phase
NTS	non-target screening
pYAS	planar yeast androgen screen
pYAAS	planar yeast antagonist androgen screen
pYAVAS	planar yeast antagonist verified androgen screen
pYES	planar yeast estrogen screen
RP	reversed phase
RP-18 W	wettable reversed phase
TAGs	triacylglycerols
TIC	total ion current
TLC	thin-layer chromatography

TOF	time-of-flight
UV	ultra violet
V	verification
Vis	visible light, white light illumination

1. Introduction

Current non-target screening (NTS) strategies for food focus mainly on illicit adulterations [1, 2], emerging contaminants [1–3], or pesticides [4, 5]. For the screening of new drugs, nature offers an invaluable rich source of plant-based bioactive secondary metabolites [6–9]. Imposing pharmacological effects in humans, nature-derived bioactive constituents could help in preventing diseases or maintaining the health status [7]. Considering thousands of unknown compounds in natural products, the need for comprehensive technologies to determine unknown natural features is increasing [10]. To cover and record this diversity of substances, high-performance liquid chromatography (HPLC) coupled with high-resolution mass spectrometry (HRMS) is usually used [11, 12]. The enormous datasets resulting from HPLC–HRMS analyses need substantial reduction and prioritisation for further evaluation [10, 12]. Data processing can bias the results of NTS strategies by focusing on the most abundant compounds, neglecting those of minor abundance [12]. Since the experimentally generated datasets cannot be handled properly without processing, the amount of data to be evaluated must be reduced otherwise, *e.g.*, by prioritising bioactive compounds [10]. To implement the bioactivity aspect in current NTS strategies, HPLC–HRMS methods have to be expanded by biological and biochemical detection methods. The direct combination of analytical methods and biological activity testing still remains challenging [13]. Enzymatic and microbiological assays require neutral, aqueous, or buffered conditions, while identification methods, such as HPLC–HRMS, need salt-free, pure organic solvents. In recent years, different groups worked on natural product research and the identification of unknown bioactive compounds by *in silico* combination of data from analytical and biological screenings [6, 14–17].

1.1. Non-target screening for bioactivity in food

Screening approaches for biologically active compounds from natural products are expensive, time-consuming, elaborate, and require a lot of equipment [8, 13]. The two major challenges for the NTS for bioactivity are genericity and multidisciplinary. Sample preparation is a critical step concerning selectivity and sensitivity. To avoid any loss of substances or discrimination of some analytes, sample preparation requires non-selective and wide-scope methods. However, an utmost generic sample preparation goes along with matrix interferences, especially for complex samples [18]. The second challenge is

the interdisciplinary hyphenation of chemical analysis and biological detection [10] which makes it difficult to assign the bioactivity to individual compounds from complex matrices [11, 15, 19]. Effect-directed analysis (EDA) commonly comprises several analytical methods, such as fractionation, chromatography, bioassay, and mass spectrometry [11] embedded in off-line [17, 20, 21], at-line [9, 16], or on-line [6] workflows (Figure 1). The most commonly employed chromatographic technique for EDA is HPLC [6, 9, 11, 15–17, 21]. The advantage of HPLC is its high separation capacity. Nevertheless, HPLC coupled with (bio)assays could be problematic due to solvent incompatibility and limited combination possibilities with assay variants.

Off-line screenings usually consist of iterative microfractionation into microplate format, followed by respective (bio)assays, and subsequent HPLC–HRMS analysis of bioactive fractions [16, 17, 21]. This technique harbours the risk of overlooking bioactivity as only the whole fraction is determined as sum parameter and opposing effects can cancel each other out [22]. A clear assignment of a substance to an effect is biased since there are usually several chemically related analytes in one fraction. Off-line formats on the other hand are compatible with almost any (bio)assay regardless of incubation time or assay material [16]. For at-line and on-line methodologies, a flow-split is embedded after chromatographic separation. In at-line approaches, one part is fractionated in

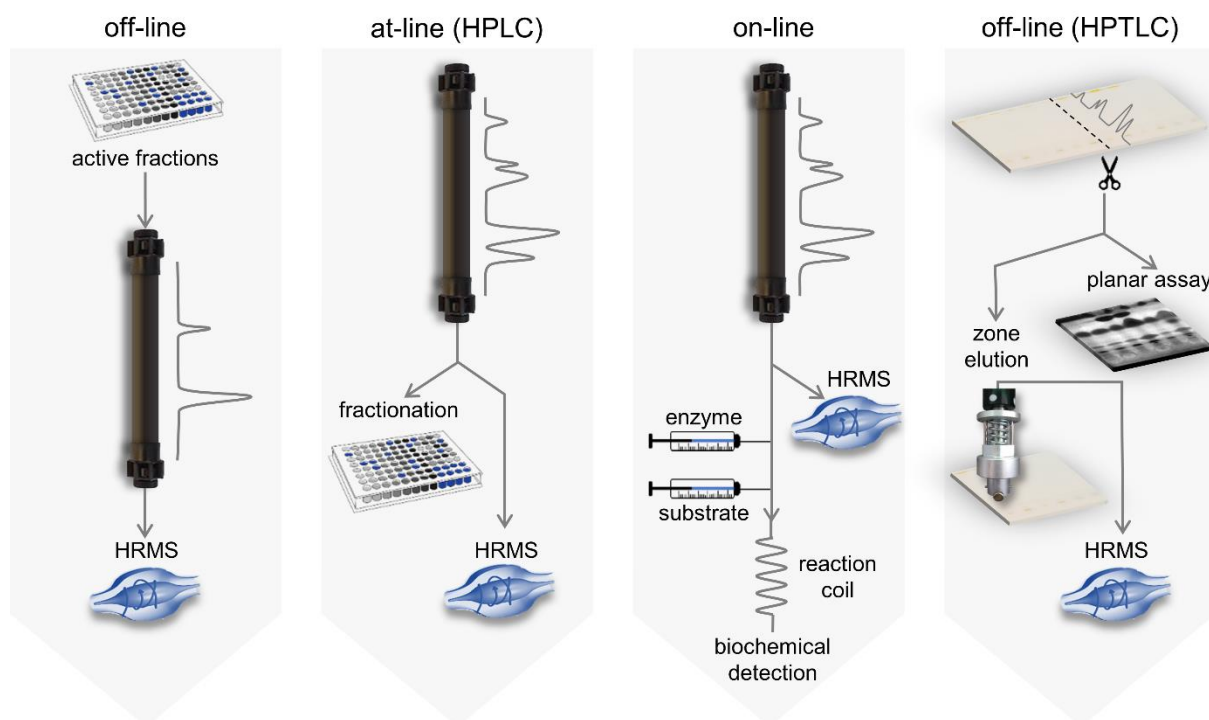


Figure 1. Common hyphenation possibilities for non-target screening by combining separation techniques, such as high-performance liquid chromatography (HPLC) or high-performance thin-layer chromatography (HPTLC), with high-resolution mass spectrometry (HRMS), and (bio)assays. Comparison of off-line, at-line, and on-line hyphenation options proposed in the literature [6, 11, 16, 17, 23].

microplates, while the other part is analysed via HRMS [16]. In on-line variants, chromatographed effluent is divided proportionally into HRMS and to a completely automated (bio)assay procedure realised through continuous injection of necessary reagents into a reaction coil [6]. Computational correlation in at-line and on-line approaches enables precise assignment of the detected effect to an individual molecule while being limited in (bio)assay variants [16]. On-line variants are additionally restricted to fast-reacting biological systems and influenced by the organic solvent inevitably present after HPLC separation, interfering with biological or biochemical assays [11]. Besides HPLC, other separation methods, such as gas chromatography [20] and high-performance thin-layer chromatography (HPTLC) [10, 11, 23–25] are also used in EDA but are less reported. In Figure 1, the currently performed off-line NTS for bioactivity with HPTLC is displayed for the sake of completeness but firstly introduced in section 1.2.3.

1.2. Status-quo high-performance thin-layer chromatography hyphenations

HPTLC is an optimised version of thin-layer chromatography (TLC), employing advanced instrumentation and improved layer properties (smaller particle size, more homogenous particle distribution), which allow reliable results through standardisation. The capability in selectivity options, application volumes, and derivatisation possibilities, renders HPTLC an emerging technology for various applications [26]. In particular, the matrix robustness of HPTLC is attractive to handle complex samples without time-consuming sample preparation [10]. Although HPTLC has less separation power compared to HPLC, it is superior in some regards. The whole sample is stored on the plate and can be detected by different exposures (white light illumination, ultra-violet light, or fluorescence light). In HPLC, compounds that do not interact with the stationary phase are rushing through the column, eluting within the dead volume, and thus are not captured by any detector. While in HPTLC multiple samples are chromatographed side-by-side under the same conditions, HPLC has a lower throughput and a greater variation in analysis conditions due to sequential execution. After chromatography, HPTLC plates could be chemically, biochemically, and biologically derivatised [10, 11, 26]. For HPLC, common detectors are limited in versatility or even destructive, and implementations of derivatisations within the analysis are still technically complex [19].

1.2.1. High-performance thin-layer chromatography–effect-directed analysis

EDA as a form of post-chromatographic derivatisation is therefore easier to combine with HPTLC. A great advantage of HPTLC–EDA is the complete evaporation of the organic solvent from the silica gel layer [11]. Although, a disadvantage, especially for normal phase (NP)-HPTLC, is the diffusion susceptibility of zones in aqueous bioassays during long incubation times [11, 27]. HPTLC–EDA techniques can be divided into bioautography and biochemical assays. Both are performed post-chromatographically. Besides the differentiation in bioautography and biochemical detection, two application variants of planar assays can be distinguished. First, the whole-plate assay, where the biological material is distributed all over the plate after chromatography [28]. Second, the start zone assay, where *e.g.* an enzymatic metabolisation process takes place exclusively on the application zone, and chromatography is performed after the assay [29–31].

To ensure the viability of the organisms and the proper quaternary structure of enzymes on the (HP)TLC plate, appropriate conditions on the silica gel layer must be given, *i.e.*, almost neutral pH, moist environment, and optimal working temperature for the respective organism or enzyme [11]. In case of acidic or alkaline mobile phases, a neutralisation step has to be involved before the assay procedure. To prevent the (HP)TLC plate from drying, moist and humid conditions during incubation can be achieved by placing the plate in a closed, humidity-controlled environment, *e.g.* a tight and moistened box.

Both, biochemical assays and bioautography, are commonly used for bioprofiling for new effective substances from natural complex matrices [10, 28, 32]. The focus of the subsequent assay description is on the EDA applied in the present work, which targets physiological effects which play a role in the development of human diseases.

In general, biochemical assays are based on the principle of enzyme-substrate interaction. Commonly employed biochemical assays, used in both microplate and HPTLC, include cholinesterases, glucuronidase, tyrosinase, glucosidases, and amylase. Executing planar biochemical assays, enzyme solutions are applied onto the plate and after an incubation period, inhibiting effects are visualised using substrates that are usually enzymatically converted to colourful products. Zones in which the enzymatic function is inhibited, remain colourless [11], except for the α -amylase assay, where enzyme-inhibiting zones are dyed blue-violet [33]. The enzymes acetylcholinesterase (AChE) and butyrylcholinesterase (BChE) are involved in neurotransmission processes. The disease pattern of Alzheimer's is characterised by a deficiency of the neurotransmitter acetylcholine in the synapses of the cerebral cortex. AChE and BChE catalyse the

degradation of this neurotransmitter, which leads to a further deterioration of neuronal transmission. Inhibition of these enzymes is the main target in the deceleration of Alzheimer's disease [34, 35].

For detoxification, substance elimination from the human body is often regulated via glucuronidation pathways. Compounds are marked by adding a glucuronide moiety to the molecule. In the intestine, these processes can be reverted by bacterial β -glucuronidase, resulting in gastrointestinal malfunction and disease. Enzyme inhibitors address explicitly the extra loop of the bacterial enzyme, which is missing in the human ortholog, to prevent bacterial deglucuronidation of the molecule to be eliminated [36].

Tyrosinase is a key regulator of melanogenesis. Also, it is responsible for the browning of foods. By using molecular oxygen, tyrosinase converts monophenols via the intermediate diphenols to the final quinones [37]. Polymerisation of built quinones results in the respective pigments, such as melanin. Excessive production of melanin results in hyperpigmentation, acne, and freckles [38]. The inhibition of tyrosinase activity is of high interest to the cosmetics industry, as it can prevent skin abnormalities and be used as skin whitening agent [37, 38].

The three enzymes α -glucosidase, β -glucosidase, and α -amylase are involved in the breakdown of oligosaccharides into monomers. The small Greek letter indicates which kind of bond, they are able to cleave, either α - or β -linked oligosaccharides. The released glucose molecules are absorbed from the intestine and lead to an elevation of the blood glucose level. Since diabetes patients are poor in lowering hyperglycaemia levels, the inhibition of these enzymes is desirable for the treatment of diabetes. By the prevention of oligosaccharide hydrolysis, less free glucose is available for absorption and thus a balanced blood glucose level could be maintained [33, 39].

In bioautography, living organisms are applied onto the (HP)TLC surfaces to detect biological effects [11]. As a result, a bioautogram is obtained. Recently, several microorganisms were employed for HPTLC-EDA, e.g., *Aliivibrio fischeri* (*A. fischeri*) [40], *Bacillus subtilis* (*B. subtilis*) [41], *Salmonella typhimurium* (*S. typhimurium*) [42], or *Saccharomyces cerevisiae* (*S. cerevisiae*) [27, 43, 44]. In direct bioautographic assays, the bioactivity can be instantly measured, for example as enhanced or attenuated bioluminescence of the Gram-negative *A. fischeri* bacteria. The natively bioluminescent *A. fischeri* immediately shows a change in photon emission when exposed to harmful or toxic substances for the marine bacteria. Reduced photon emission is an indicator for antimicrobial and toxic substances [11, 40, 45], whereas an increased photon emission

indicates a stimulated energetic cell metabolism. Weins and Jork (1996) introduced this *in situ* bioassay to TLC plates [45]. Indirect approaches firstly expose reporter organisms equipped with specific operons to their trigger molecules. This exposure induces the production of enzymes decoded in the operon. Bioactivity is then measured indirectly through enzymatic substrate conversion. As examples of indirect bioautography, the yeast estrogen and androgen screens (YES and YAS), the SOS-Umu-C assay, and the *B. subtilis* bioassay are described more precisely.

The endocrine system regulates the hormonal homeostasis of almost all vertebrates. An imbalance has severe impacts on juvenile development, menstrual cycle, fertility, and other hormonal regulated processes [44]. Endocrine-disrupting chemicals are detected in the YAS and YES as well as in their antagonistic versions. Employed yeast strains are genetically modified to contain the human androgen/estrogen receptor (hAR/hER) [46, 47]. In presence of hormone-like substances, the ligand-receptor interaction induces the expression of β -galactosidase through the cleavage of the repressor protein, which formerly prevented gene transcription of the enzyme [43]. Hormonal effects are indirectly measured as enzymatic activity mediated through hydrolysis of chromogenic or fluorescing substrates. For antagonistic assays, an agonist is artificially introduced to the bioassay system. Agonists and antagonists compete for free binding sites at the receptors. Antagonists block the receptor so that less enzyme expression is induced. Antagonistic effects are determined as reduction of β -galactosidase activity [48]. For planar antagonist screening, the right side of each track is oversprayed with an agonist-stripe along with the chromatographed track (see Publication 5, Figure 1). β -Galactosidase activity is then detectable over the whole track, except for those zones containing antagonistic substances [44].

To screen for genotoxic substances, the SOS-Umu-C assay can be used. The principle is based on the SOS DNA repair mechanism which is regulated via several genes [49]. In response to DNA damage induced by mutagens and genotoxins, the genetically modified *S. typhimurium* TA1535/pSK1002 activates the SOS signal cascade, resulting in the expression of the enzyme β -galactosidase. Comparable to hormonal effects, genotoxicity can be determined indirectly as β -galactosidase activity [42, 49, 50].

Antibiotics are commonly used to treat bacterial infections. EDA for potential drug candidates can be realised with the Gram-positive *B. subtilis* bioassay. Present substances with antibiotic-like properties lead to cell death or bacteriostatic conditions. The cell

viability is detected indirectly via a tetrazolium salt that is converted into a violet formazan by the dehydrogenases of intact *Bacilli* [41, 51].

1.2.2. *Microplate assays versus planar assays*

Microfractionation for microplate assays require an upstream separation technique, such as chromatography or electrophoresis (Figure 1). Fractions are usually collected time-controlled or peak-wise [19]. In case of chromatography-based fractionation, vessel capacity and flow should match, otherwise a split must be installed, resulting in a considerable loss of sample. Time-controlled fractionation often collects several analytes with similar chemical properties in one vessel which leads to the determination of the sum of all biological responses comprised in this well. Evaporating organic solvent from the microwells is mandatory for (bio)assay procedures, but some compounds only show slight solubility in aqueous media and therefore are not re-dissolved after drying [19].

Planar (bio)assays are a good alternative to microplate assays where HPTLC serves as an upstream separation technique. After chromatography, the complete solvent can be evaporated and aqueous assay media, buffers, and substrates can be applied on the same surface without analyte loss. Biological effects can be directly assigned to specific zones on the plate, which can be further evaluated to individual substances causing the bioactivity. Planar (bio)assays showed to be more sensitive compared to microplate assays, probably due to lower matrix interferences [30, 42, 51].

1.2.3. *High-performance thin-layer chromatography–effect-directed analysis– high-resolution mass spectrometry*

State-of-the-art HPTLC–EDA–HRMS hyphenations are comparable to off-line NTS methods (Figure 1), whereby HPTLC–EDA and HPTLC–HRMS are performed in a time-shifted manner, which only allows indirect coupling. On one plate (20 cm × 10 cm) samples were chromatographed in duplicate as two sets, and cut into two identical halves (10 cm × 10 cm), of which only one was subjected to the (bio)assay [23]. According to the effect profile of the (bio)autogram, zones of interest were selected on the remaining clean chromatogram, either manually [23] or automated [52]. Plates were imprinted by an elution head, eluting the selected zones to an HRMS instrument. After the MS recording, accurate positioning of the elution head was verified by performing the same (bio)assay on the imprinted chromatogram [23, 52].

This procedure has disadvantages in several respects. Duplicate application on one HPTLC plate reduces the number of samples being analysed in a single chromatographic run. Zone marking on the identical half without (bio)assay must be as precise as possible. Incorrectly placed imprints cannot be re-analysed so easily. Correction attempts, which are often only a few millimetres away, would result in a leakage of the elution head, since the silica gel layer is already damaged near this zone. Moreover, the (bio)assay procedure has to be performed twice, requiring twice the time, effort, and material [53]. Currently, the high matrix and salt load of the (bio)assay hampers direct hyphenation of HPTLC–EDA–HRMS. The aim to directly elute the bioactive zone from the (bio)autogram into HRMS can only be realised by including a desalting step, reducing the interfering matrix and salts.

1.2.4. *On-surface metabolism*

NTS for bioactive compounds in food is reasonable as it is more straightforward compared to random, non-prioritised NTS strategies. Considering effects on living organisms, compound distribution, half-life, resorption, and metabolism *in vivo* have to be taken into account. Effective constituents from the diet may not reach the organism in the same form as they were applied [13]. Digestion plays a major role in the breakdown of macronutrients such as saccharides, lipids, and proteins [31, 54]. The three main digestive enzyme classes are proteases, lipases, and amylases, which are distributed differently throughout the gastrointestinal tract (GIT) [55]. Enzymes involved in digestion processes are delivered by the salivary gland, liver, and pancreas [54]. Most accurate results in the prediction of food breakdown, nutrient release, and absorption into the bloodstream are provided by *in vivo* experiments [54, 55]. To avoid ethical issues, static digestion models were standardised *in vitro* to mimic oral, gastric, and intestinal metabolism [31, 56]. Current *in vitro* models are a good alternative to animal or human studies providing comparable results for the digestion of macronutrients. Prediction models for the *in vitro* digestion of micronutrients, such as bioactive compounds, carotenoids, or polyphenols are deviating from *in vivo* results [57]. The realistic simulation of the digestion requires the right pH and composition of enzymes, electrolytes, and co-factors [56]. Morlock *et al.* (2021) recently introduced the harmonised digestion procedure [56] from solution-based assays to planar surfaces. In brief, samples are applied to the silica gel layer. Digestive enzymes and respective co-factors are oversprayed. To set humid conditions, the plate is wetted and incubated.

After simulated digestion, samples are chromatographed and derivatised either chemically, biochemically, or biologically. On-surface digestion with subsequent HPTLC showed comparable results to *in vitro* digestion followed by planar chromatography. The on-surface nanoGIT^{+active} system is advantageous because enzyme and sample consumption is kept minimal (nano). Metabolisation and separation are performed on the same layer and could further be combined with multiple detection options [31].

Especially drugs or toxins are metabolised in the liver. Liver metabolism plays a major role in activation or inactivation of compounds introduced to the human body. To transfer the complex liver biotransformation processes to *in vitro* models, a homogenised liver extract from rats, the so-called S9 mixture, is commonly used. S9 metabolisation affects bioactivity, *e.g.*, metabolic activation of estrogenic properties of bisphenol A [58], stimulation of mutagenic potential of aflatoxin B1 [59], or conferment of neurotoxic attributes to chlorpyrifos [30]. Planar on-surface assays exploiting the S9 activation system could either be performed as start-zone assay [30], or whole-plate assay [60] by adding the liver homogenate directly to the (bio)assay material applied.

1.3. Online desalting and orthogonal separation

By eluting active zones directly from the (bio)autogram, assay salts and media components are co-transferred automatically. In case of alkaline or acidic mobile phases, additional salt load from neutralisation buffers is co-eluted to HRMS. Therefore, employing a desalting step is crucial to prevent ion suppression, clogging of the ion source through crystallisation, and signal suppression [61]. In the fields of proteomics [62], genomics [63], and metabolomics [61, 64], on-line desalting is already embedded in HPLC–HRMS analyses due to very saline sample preparation. Technically they all follow more or less the same principle. A second stationary phase is introduced in form of a guard column [63, 64], second separation column [62], or a solid-phase-extraction column [61] before [61, 63, 64] or after [62] the analytical column. Analytes are retained on the stationary phase, while salts and buffer materials are discarded [63]. After the desalting step, samples are transferred to HPLC–MS.

With embedding a desalting step into the HPTLC–EDA–HRMS workflow, it might be unnecessary to perform HPLC, since the chromatographic separation has already occurred on the HPTLC plate. Nevertheless, an orthogonal chromatography is reasonable for several aspects. As already mentioned, HPTLC has a lower separation capacity compared to HPLC [11]. Chemically similar compounds could retard at the same

migration distance on the plate, which makes an orthogonal separation mandatory to assign the bioactivity to an individual substance. As it is technically less complex to combine EDA with HPTLC, rather than HPLC, the latter can be used to separate potentially co-eluting analytes from the planar (bio)autogram. Moreover, additional information about the unknowns is gained as two retention factors (R_F) are determined within a single workflow: First, the migration distance on NP-HPTLC plates and second, the retention time on the reversed phase (RP) HPLC column.

1.4. Mass analysers: single quadrupole versus orbitrap

Usually, mass analysers are selected according to the research purpose. For targeted approaches, MS instruments with low resolution power are adequate, *e.g.*, for the quantification of known analytes. For example, single quadrupole mass spectrometers are applied in routine analysis. The operating principle of single quadrupole instruments is based on four metal rods arranged in parallel. A radio frequency voltage is applied to the rods. Opposite rods have opposite potential. The resulting voltage field forces the ions on amplitudes through the quadrupole. The mass-to-charge ratio (m/z) can be calculated from the ion trajectories [65]. Single quadrupole instruments do not provide enough resolution to calculate a molecular formula from the obtained m/z ratio. Only with a list of suspected compounds, this MS is sufficient as identifying detector, since the assumed candidates can be confirmed against available standards.

For NTS purposes, higher resolution instruments are required, *e.g.*, time-of-flight (TOF) or orbitrap mass analysers. Since its launch in 2005, orbitrap technology has replaced several TOF instruments that were most commonly used until then [66, 67]. The basic operating principle is relying on outer electrodes and a central electrode on which voltages are applied. Ions are introduced in the gas phase between the outer and inner electrodes. The electric field resulting from the outer electrodes forces the ions to oscillate along the axis, while the inner electrode induces rotation. The trajectory of the ions can be described as circular spirals which can be mathematically converted into a mass spectrum via Fourier transformation [67]. Several technological advances made the orbitrap even more attractive for NTS. The possibility of pulsed injection via an external storage device, the so-called curved linear trap, decoupled the mass analyser from the ion source and was a prerequisite to introduce a fragmentation option. A higher-energy collision induced dissociation cell in form of a multipole was added to obtain structural information by fragmentation [67, 68]. To implement this advantageous mass analyser in

routine analysis and for research purposes, the orbitrap technology was produced in benchtop format as hybrid quadrupole-orbitrap instrument [68].

Since the orbitrap is superior compared to the single quadrupole concerning resolution, exact mass analysis, and fragmentation option, it is preferred in suspect screening and NTS.

1.5. Diffusion susceptibility of silica gel layers

NP-silica gel layers are most commonly used in HPTLC. Unfortunately, they are susceptible to diffusion due to long incubation times with aqueous bioassay media [27, 69, 70]. State-of-the-art HPTLC–bioautography methods are based on immersion of the HPTLC plate into the cell suspension for a few seconds. Incubation of an immersed NP plate at nearly 100% humidity causes band broadening, zone distribution over the plate, and blurred signals [27, 70, 71]. Salts from bioassay and neutralisation buffers additionally promote these effects.

Klingelhöfer and Morlock (2014) tried to counteract the problem by introducing a hybrid layer, the so-called wettable reversed phase (RP-18 W) HPTLC plate. As a result, they obtained sharp-bounded bands at the expense of sensitivity [71, 72]. To reduce the diffusion on NP layers, the immersion step was replaced by a spray-on technology, considerably improving the assay quality [69, 72]. By spraying, the cell suspension is applied in a more controlled fashion and a defined cell layer thickness on the planar chromatogram [72]. Nevertheless, signals are still blurred after the bioassay.

For planar immunoassays, several washing and incubation steps are required in which the silica gel layer could flake from the support [73]. By fixation of the layer with a plastic, usually polyisobutyl methacrylate [74], the silica is kept stable throughout the procedure [73, 75]. Besides the layer stability through long incubation times, the impregnation with the plastic showed another advantage, in particular sharp-bounded zones on NP. Other options to modify the silica gel layer are polyethylene glycol or poly-D-lysine. Through chemical reactions of the silanol groups with the coating agent, a change in interaction, surface topology, and chemistry of the silica conferred biocompatible properties to the layer [76, 77]. Realising low-diffusion bioassays on NP plates is the prerequisite for multiplex assays.

1.6. Scope

The lack of easy, information-rich, and highly-streamlined NTS strategies for bioactive ingredients in food initiated the development of new, innovative, fast, and multi-hyphenated techniques. To obtain the most comprehensive information possible, chromatographic, biological, biochemical, spectroscopic, and spectrometric methods were drawn from the analytical toolbox. A few of the main advantages of HPTLC were decisive for the use of this methodology as a basis for further hyphenations. First, HPTLC offers the possibility for high-throughput screening, second, the matrix robustness, and third, the variety in biological and (bio)chemical hyphenation options. As most NTS strategies exploit HRMS as an identification method, a direct hyphenation of HPTLC, (bio)assay, and HRMS was sought to be investigated. State-of-the-art HPTLC–EDA–HRMS experiments require doubled time, material, and effort. The aim is to simplify the commonly executed workflow. Bioactive zones should be directly eluted out of the planar (bio)autogram to an MS instrument. Saline (bio)assay media are co-transferred with the analytes from the plate causing interferences with ionisation and noisy backgrounds in MS recording. This fact makes the reduction in salt load an inevitable step to realise a direct coupling. The variety in possible HPTLC–EDA hyphenations demands a generic desalting before further analyses. To overcome the problematical occurrence of co-elutions, a second chromatographic step is desired. Up to now, HPTLC–EDA cannot be completely automated, which is why the subsequent identification analysis steps should be as automated and standardised as possible. New NTS multi-hyphenated workflows based on HPTLC–EDA–HRMS require therefore the simplification of the current workflow, online-desalting, automation, and a second separation technique to reach the ultimate goal of structure elucidation of unknown bioactive compounds.

1.7. Progress achieved through multi-hyphenated techniques

For elucidation of unknown bioactive compounds in food, it is essential to obtain as much information as possible. As already stated by Wilson and Brinkman (2007), “it is often necessary to have data from more than one spectroscopic technique” to identify a compound from complex mixtures [78]. Each information gained in the established multi-hyphenated workflows was denoted as a dimension. In this study, a comprehensive highly streamlined NTS strategy with up to twelve dimensions was developed which is presented in the following sections. The method is versatile and can be used both in routine and research, *e.g.*, for monitoring of food quality and authenticity, discovery of

new drugs, or generally for the identification of unknown bioactive substances from any matrix.

1.7.1. Establishment of an eight-dimensional hyphenation (Publication 1)

The first multi-hyphenation resulted in an eight-dimensional (8D) workflow (Figure 2) arranged in the following order, *i.e.*, separation on NP-HPTLC plate (1D), detection under white light illumination (Vis, 2D), UV light (UV at 254 nm, 3D), and fluorescence light (FLD at 366 nm, 4D), bioprofiling (5D), and subsequent heart cut elution, on-line desalting, and RP-HPLC separation (6D) with diode array detection (DAD, 7D) and single quadrupole mass spectrometry (MS, 8D) [53]. The dimensions 1D–4D are routinely performed in HPTLC analysis. By focusing on bioactivity (5D), antibacterial effects, or those stimulating the energetic cell metabolism of the marine *A. fischeri* bacteria, were screened in *Cinnamomum verum* and *C. cassia*. Once a biological effect is detected, it is of highest interest to identify the compound(s) responsible. As identification strategy, the dimensions 6D–8D were provided. The direct hyphenation of the first five dimensions with the following three turned out problematic. The transfer of the bioactive zone from the planar medium to RP-HPLC–DAD–MS was performed using an elution-based TLC–MS interface. Thereby, not only the analyte(s), but the saline and nutrient-rich bioassay media were eluted from the plate. Those media or buffers from biochemical and microbiological

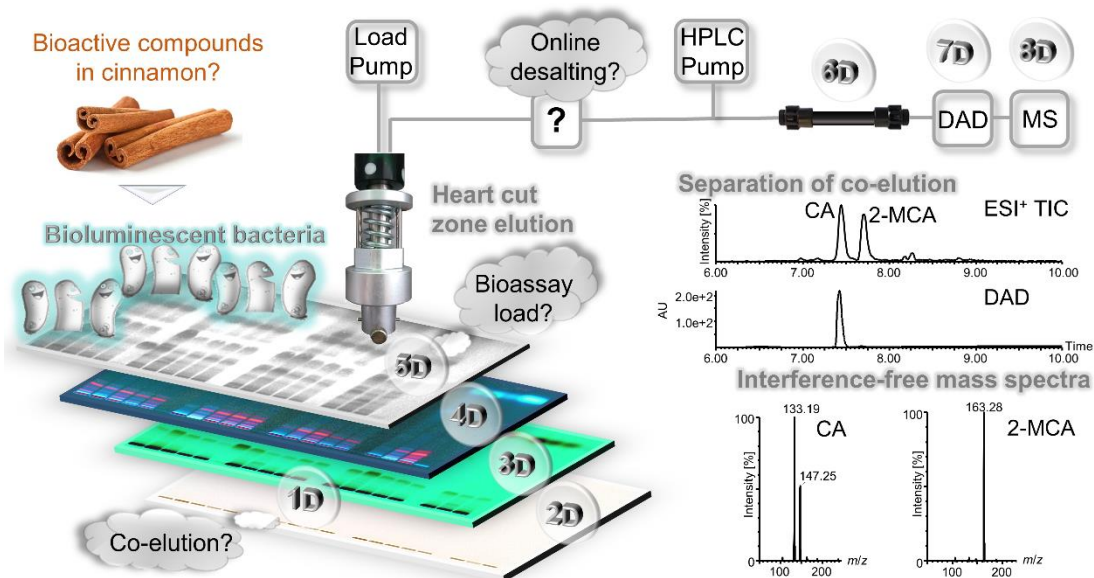


Figure 2. Schematic representation of the eight-dimensional hyphenation exploiting NP-HPTLC separation (1D), multi-imaging detection (UV/Vis/FLD, 2D–4D), bioassay (5D), heart cut elution, analyte trapping/online desalting, RP-HPLC separation (6D) with diode array detection (DAD, 7D) and mass spectrometric detection (MS, 8D), resulting in separation of the co-eluting cinnamaldehyde (CA) and 2-methoxy cinnamaldehyde (2-MCA), and interference-free mass spectra [53].

assays (5D) would interfere with ionisation and mass spectrometric detection (8D). Thus, salts and media components had to be eliminated before MS measurement. The very saline (approx. 45 g/L [79]) *A. fischeri* bioassay was selected to establish a desalting step between HPTLC and MS.

For the reduction of MS interferences, four different approaches were tested: no desalting, desalting with an RP/ion exchange hybrid column, and with two different short guard columns (stationary material either capped with phenyl moieties or RP alkyl chains). All were mounted on a 2-position, 6-port switching valve as suggested by Fountain *et al.* (2004) [63]. Salt reduction capacities of the devices were determined by the elution of *A. fischeri* medium from a sample-free plate and comparison of MS total ion current (TIC) intensities in both polarity modes [53]. The RP guard column showed the best TIC reductions with -44.2% in ESI-positive ion mode, and -32.2% in negative ion mode, compared to non-desalted TICs. After the implementation of the RP guard column as a desalting device, the optimal elution solvent and time were evaluated. The selected guard column fulfilled two tasks simultaneously: trapping the analyte(s) on RP material while discarding the salts solved in the aqueous elution solvent. Since water has the greatest elution strength on silica gel plates, and a higher organic portion would cause analyte breakthrough, the best choice was 10% aqueous methanol as elution solvent. The duration of elution was set to 45 s, as enough analytes were transferred to give a strong signal response and breakthrough from desalting cartridge was kept minimal.

As the example of cinnamon extracts showed, the orthogonal RP-HPLC separation proved to be reasonable. In the *A. fischeri* bioassay of the NP-HPTLC-separated samples, a dominant antibacterial zone near the solvent front was detected. To prove the functionality of the just established 8D hyphenation, it was aimed to identify this zone via RP-HPLC-DAD-MS. Results revealed two distinct signals of 2-methoxy cinnamaldehyde and cinnamaldehyde hidden behind this antibacterial zone. Both substances were retained at the same migration distance on the plate so it was impossible to assign the effect to one or the other. Standards confirmed that both contributed to the antibacterial effect detected in bioautography [53].

In conclusion, all information gained with the 8D workflow was essential to identify unknown substances exhibiting bioactivity. In this first multi-hyphenated pilot study the compounds identified were not unknown for cinnamon or their biological activity. Nevertheless, even more dimensions and better MS instrumentation would facilitate compound elucidation and identification.

1.7.2. Application field study using the eight-dimensional hyphenation (Publication 2)

The functionality of the 8D hyphenation was shown for the *A. fischeri* assay and cinnamon as a sample. To prove the versatility and robustness, the workflow was transferred to 13 other biochemical and microbiological assays and 68 botanical samples [28]. As the previously investigated mobile phase for the botanical screening contained 12% acid [80], a neutralisation step was integrated into the workflow directly before (bio)assay. Interpretation of the effect-directed analyses (EDAs) is summarised in Table 1. The variety of (bio)assays required different neutralisation agents, buffers, and substrates. Salt and nutrient load of the individual assays are plotted in Figure 3. A detailed description of (bio)assay materials, preparation, and volume applied onto 20 cm × 10 cm HPTLC silica gel 60 F₂₅₄ MS-grade plates is given in Publication 2 [28]. Calculations were based on the total (bio)assay load applied onto the 20,000 mm² area, and downsized to the given format of the elution head (2 mm × 4 mm), resulting in an overall area of 8 mm² of co-transferred analyte(s), neutralisation and (bio)assay salts, and nutrients.

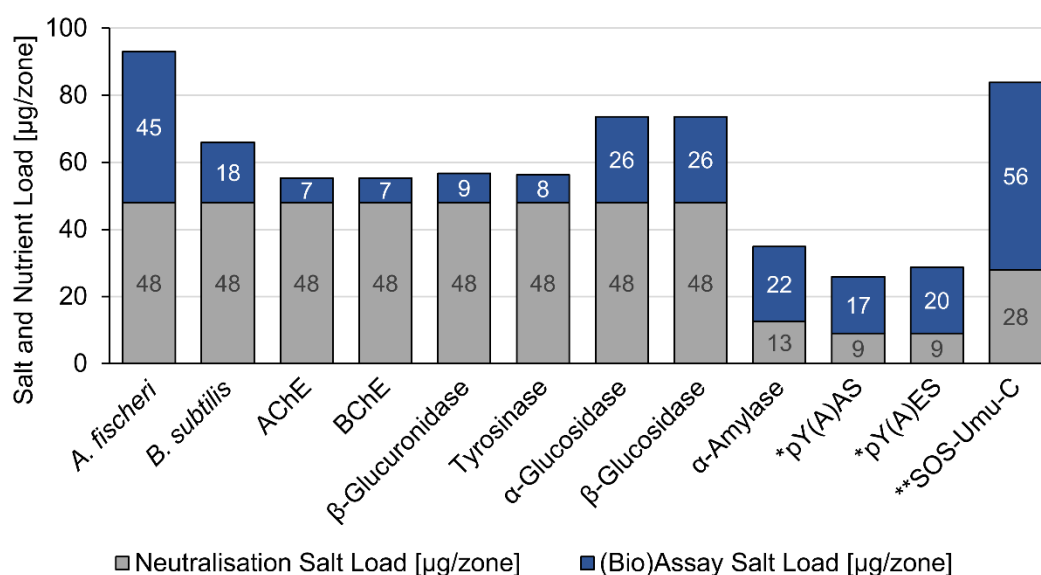


Figure 3. Calculated salt and nutrient load on a HPTLC silica gel 60 F₂₅₄ MS-grade plate for respective (bio)assays. Salt load is given in µg per 8-mm² zones, for neutralisation buffers and assay material (buffers, enzymes, substrates, dyes) respectively. Calculations were based on the experimental design described in the material and method section of Publication 2 [28]. For hormonal assays the amount of agonist stripe is negligible and calculations were made for 4-methyl umbelliferyl β-D-galactopyranoside as a substrate (*). SOS-Umu-C assay load was calculated with resorufin-β-D-galactopyranoside substrate and as it was performed on the thicker HPTLC silica gel 60 plates, requiring twice the volume, the amounts were halved for comparability (**).

Table 1. Interpretation of applied planar biochemical and biological assays (modified [25]). Chromogenic or fluorescent response depended on the used substrates (see Publication 2).

biochemical assay	response	evaluation
acetylcholinesterase [34]	colourless on rose background	improvement of cholinergic neurotransmission, prevention of acetylcholine hydrolysis
butyrylcholinesterase [34]	colourless on rose background	improvement of cholinergic neurotransmission, prevention of acetylcholine hydrolysis
β -glucuronidase [36]	colourless on blue background	normalised detoxification via glucuronidation pathways, otherwise hampered by bacterial enzyme orthologs
tyrosinase [37, 38]	colourless on greyish-brown background	balanced melanogenesis, prevention of hyperpigmentation and skin abnormalities
α -glucosidase [39]	colourless on rose background	balanced blood glucose levels by inhibiting the lysis of oligosaccharides into its glucose monomers
β -glucosidase [39]	colourless on rose background	balanced blood glucose levels by inhibiting the lysis of oligosaccharides into its glucose monomers
α -amylase [33]	violet on colourless background	balanced blood glucose levels by inhibiting the lysis of oligosaccharides into its glucose monomers
bioautography		
Gram-negative bacteria	<i>Atiivibrio fischeri</i> [40, 45, 79]	probiotic-like effect, increased bioluminescence is related to enhanced energetic cell metabolism (photon emission)
	<i>Salmonella typhimurium</i> TA1535/pSK1002 [42]	antibacterials, decreased bioluminescence is related to reduced cell viability and decreased energetic cell metabolism
Gram-positive bacteria	<i>Bacillus subtilis</i> [41]	genotoxins, mutagens
	<i>Saccharomyces cerevisiae</i> B 1991 [44]	antibacterials
yeast cells	<i>Saccharomyces cerevisiae</i> B 1991 [44]	endocrine disrupting chemicals, agonists of the human androgen receptor (hAR)
	<i>Saccharomyces cerevisiae</i> B 3505 [43]	endocrine disrupting chemicals, antagonists of the hAR

The 8D hyphenation showed robust and reliable results through all assays and media. Since the used MS instrument had only a single quadrupole mass analyser, the resolution was too low to calculate the molecular formula. Evaluation of obtained data was based on literature and database research. One of the following criteria had to be true for a tentative assignment of the signal to a respective compound: Either the spectral data (at least absorbance maximum and mass) matched any database, the compound was already described for the botanical, or the substance already proved to have the respective biological properties. Some of the tentative assignments were verified or rebutted against available standards. For further optimisation of a non-target screening strategy for bioactive unknowns in complex mixtures, the 8D workflow was improved by the application of an MS instrument with higher resolving power and fragmentation option. Moreover, the question arose, if bioactive compounds can unfold their effective potential after passage through the digestive tract, or if they were metabolised to a related, but inactive molecule.

1.7.3. Ten-dimensional hyphenation for non-target screening (Publication 3)

A combination of NTS, bioactivity studies, and identification of effect-compounds is highly desirable but still neglects human metabolisation pathways after oral administration [7, 13]. Harsh conditions in gastrointestinal food processing, residence time, absorption capability, and solubility of bioactive compounds influence their effectiveness [7].

The incorporation of the recently established nanoGIT system [31] and the upgrade to HRMS/MS, expanded the workflow to ten dimensions (NP-HPTLC-nanoGIT^{+active}-UV/Vis/FLD-EDA-heart cut-RP-HPLC-DAD-HRMS/MS, see Publication 3, Figure 1) [81]. The change to another mass spectrometer required the development of a new HRMS/MS method. The first HRMS dimension was a full scan in polarity switching mode as usual for NTS strategies [82–84]. For fragmentation scans, four options were evaluated: all ion fragmentation, data-dependent MS2 (ddMS2) in Top5 mode, and variable or multiplexed data-independent acquisition. The advantages and drawbacks of each MS2 acquisition method were considered, and finally, the best agreement was rated with the ddMS2 mode. The newly developed ten-dimensional (10D) hyphenation provided the following information:

- 1) Gastrointestinal on-surface metabolisation gave evidence about lipids, sugars, and proteins and whether these macronutrients were hydrolysed by the respective enzymes (lipases, amylases, and proteases).

- 2) Metabolic changes were tracked by NP-HPTLC separation. The observed R_F values also provided relative details about substances' polarity.
- 3–5) The visualisation of the planar chromatogram revealed information about compounds with UV activity (UV 254 nm), native fluorescence (FLD 366 nm), or chromophores (white light illumination, Vis).
- 6) Screening for bioactivity was realised with one of the proposed (bio)assays as in Table 1. In the presented cases concerning the 10D hyphenation, EDA particularly targeted AChE, BChE, α -, and β -glucosidase inhibitors, as well as substances affecting the energetic cell metabolism of the *A. fischeri* bacteria.
- 7) After heart cut elution and online-desalting, an orthogonal information on substances' polarity was obtained by means of the retention time on RP-HPLC column.
- 8) The wavelength scan of the DAD gave evidence about absorbance maxima, and absorbance spectra in the wavelength range of 200–400 nm.
- 9–10) Exact mass and fragmentation data were recorded by HRMS/MS from which a molecular formula was calculated and structural properties were derived.

This workflow was applied to ten convenience tomato products in the matter of sauces or soups. The HPTLC layout allowed a side-by-side comparison of the bioactivity profile of metabolised and non-metabolised samples. Changes in bioactivity caused by intestinal metabolism were determined with the five (bio)assays AChE, BChE, *A. fischeri*, α -glucosidase and β -glucosidase. The most emerging metabolic bioactivity change identified through all (bio)assays was caused by fatty acids as products of the digestion of triacylglycerols (TAGs). Lipases from the used pancreatic enzyme mixture hydrolysed the TAGs into glycerol and their respective fatty acids. Plant-based products revealed saturated and unsaturated long-chained fatty acids ($\geq C14$), while products blended with cream or skim milk powder of animal origin, also showed short-chained fatty acids. The latter were only active in the *A. fischeri* bioassay. Other bioactive ingredients were found not to be affected by digestion, *e.g.* piperine, the main alkaloid from black pepper, which is active against the *A. fischeri* bacteria [81]. Beside the possibility to track metabolic changes, the most outstanding improvement of the 10D hyphenation, compared to the previous 8D version, is the opportunity to get structural information of the unknowns through tandem HRMS and thus enable an unambiguous substance assignment.

1.7.4. Application field study using the ten-dimensional hyphenation (Publication 4)

The recently developed streamlined and information-rich 10D workflow was applied to six highly-processed differently-flavoured meal replacement products. The totality of the data obtained led to the identification of 13 substances and proved the functionality and robustness of the new NTS strategy for bioactive compounds in foods [85].

Despite the miniaturised simulation of the intestinal digestion processes, resorption is still neglected. As an example, physostigmine, a known alkaloid from plants, is cited. The compound has pronounced AChE inhibitory potential but is only poorly absorbed by humans, while its synthetic analogue rivastigmine possesses better transepithelial permeability and is commonly used as a therapeutic agent against Alzheimer's disease [34]. Various protocols describe analytic approaches to determine pharmacokinetics and resorption [86]. Embedding an additional dimension concerning the substance uptake through membranes would complete the comprehensive workflow. Other options to gain more dimensions and associated information are multiplexed assay formats, which allow the detection of several biological effects in a single run.

1.7.5. Diffusion reduction permitting multiplexed assay formats (Publication 5)

As stated already for the 8D hyphenation, the problem of analyte diffusion on NP plates still remained. Currently, planar yeast androgen/estrogen screens (pYAS/pYES), as well as their antagonistic (A) versions are performed on both plate types silica gel 60 and RP-18 W [27, 44, 69–72]. The latter is not prone to diffusion but is less sensitive compared to NP plates [22]. To overcome the diffusion susceptibility of NP plates and to further improve the workflow, several optimisations were investigated. For fixation of zones after chromatography, different coatings, *i.e.*, poly-D-lysine, PEG 2000, PEG 8000, and a polyisobutyl methacrylate resin (Degalan), were investigated. Out of the tested agents, only Degalan showed a reduction in the observed zone diffusion. As vertical immersion of the plate in Degalan solution caused streaks when taken out and the solution was too low in viscosity to be piezoelectrically sprayable, the final coating procedure took place horizontally in a glass dish. The fixation of zones on NP plates was a precondition and crucial for the further development of the HPTLC-pYAAS bioassay procedure to a multiplex version.

The bioassay pYAAS was already performed in a multiplex format to detect androgens and antiandrogens in parallel on one RP-18 W plate. Androgenic properties were determined as β -galactosidase activity, cleaving the non-fluorescent substrate

4-methylumbelliferyl β -D-galactopyranoside (MUG) in its fluorescent product 4-methylumbelliferone (MU) and galactose [44]. In zones containing hAR antagonists, enzyme production was not triggered and a substrate conversion was missing. Antagonistic effects are therefore detectable as fluorescence-diminishing zones in an oversprayed agonist track. The reduction in fluorescence originated either from an antagonistic effect or from absorption properties of a substance. Since those two observations cannot be distinguished, a verification (V) for true antiandrogenicity was required. Verification was achieved by applying a second stripe of the fluorescing product MU parallel to the agonist (see Publication 5, Figure 1). If the fluorescence was reduced in both stripes, an absorbing substance was assumed (false-positive). A true antagonistic effect was stated if fluorescence reduction in the agonist stripe appeared, while MU stripe was non-fluorescent at this position. This design offered two more information that were about false-positives and synergists, which locally enhanced the fluorescence of the testosterone stripe but not of the MU-stripe.

As proof-of-principle, 68 botanicals were screened for androgens and antiandrogens on RP-18 W, NP, and Degalan coated NP plates (^{fix}). The twelve samples suspected to comprise antagonists were subjected to the verification procedure. Ten zones were verified to exhibit true antiandrogenic properties, while seven synergistic zones were determined. Those zones were further evaluated with heart cut-RP-HPLC-DAD-HRMS, resulting in 29 potential candidates responsible for the observed effects. The overall NP-HPTLC^{fix}-UV/Vis/FLD-pYAVAS-FLD-heart cut-RP-HPLC-DAD-HRMS/MS hyphenation resulted in twelve dimensions (12D), of which four are comprised in the multiplexed pYAVAS bioassay, namely androgens, antagonists, false-positives, and synergists [22].

1.7.6. Application field study for multiplexed estrogen screen (Publication 6)

The previously established 12D hyphenation was transferred to the closely related pYES assay for the detection of estrogens, antiestrogens, false-positives, and synergists [87]. With this multiplex assay, even additive effects were distinguishable from synergistic effects, which is hardly achievable in common approaches [88]. With a modified mathematical analogy [89, 90], those two effects are described as follows. Additive effects are observed as two effective compounds (1) summing up their signal when applied in combination ($1 + 1 = 2$), while synergy yielded intensified signals by the combination of a non-effective compound (0) with an effective substance (1) to the equation $0 + 1 > 1$ [87]. Further optimisations were realised with the alternative green fluorescent substrate

fluorescein-di-(β -D-galactopyranoside). It was preferred over the blue fluorescent MUG, because botanical samples showed less green native fluorescence than blue. For the first time, it was also considered that antagonistic responses could also be caused by cytotoxic properties which could not be proven or excluded by the verification stripe. Apoptosis of the yeast cells as a result of contact with cytotoxic substances automatically prevents β -galactosidase expression and ultimately leads to a lack of substrate conversion. Cytotoxicity was determined using resazurin as a dye. Viable cells irreversibly convert the blue dye via mitochondrial processes into the pink fluorescing product resorufin (Figure 4, detectable at FLD 366 nm) [91]. Since the botanical samples contain fluorescence-diminishing pigments, cytotoxicity was evaluated in white light illumination (Vis) mode, where the positive response appeared as colourless on purple background (as depicted for the positive control menadion, Figure 4) [87].

With the 12D NP-HPTLC^{fix}-UV/Vis/FLD-pYAVAS-FLD-heart cut-RP-HPLC-DAD-HRMS/MS hyphenation, 17 hormonal active substances could be assigned to specific molecules of which only seven were known for their biological properties towards the estrogen receptor. Of the remaining ten, four were structurally related to known phytoestrogens and the other six had not previously appeared in an endocrine context. In conclusion, the 12D hyphenation showed the potential to assign hormonal effects to individual compounds, to distinguish between different hormonal effects, and to identify unknown hormonally active substances from complex mixtures.

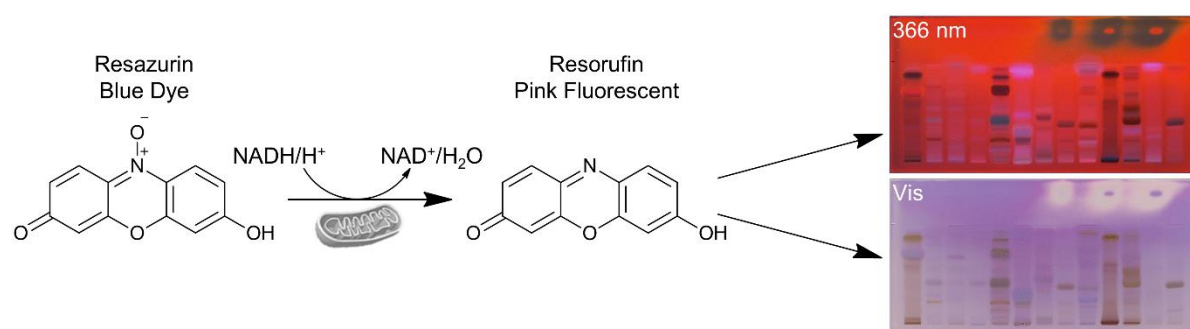


Figure 4. Irreversible mitochondrial conversion of the blue dye resazurin into its pink fluorescent product resorufin (modified [87, 91]), and corresponding NP-HPTLC^{fix}-planar cytotoxicity (yeast)-FLD/Vis bioautograms.

1.8. References

- [1] Y. Fu, C. Zhao, X. Lu, G. Xu. Nontargeted screening of chemical contaminants and illegal additives in food based on liquid chromatography–high resolution mass spectrometry, *TrAC, Trends Anal. Chem.* 96 (2017) 89–98. doi:10.1016/j.trac.2017.07.014.
- [2] R. Díaz, M. Ibáñez, J.V. Sancho, F. Hernández. Target and non-target screening strategies for organic contaminants, residues and illicit substances in food, environmental and human biological samples by UHPLC-QTOF-MS, *Anal. Methods* 4 (2012) 196–209. doi:10.1039/C1AY05385J.
- [3] A.M. Knolhoff, T.R. Croley. Non-targeted screening approaches for contaminants and adulterants in food using liquid chromatography hyphenated to high resolution mass spectrometry, *J. Chromatogr. A* 1428 (2016) 86–96. doi:10.1016/j.chroma.2015.08.059.
- [4] J.W. Wong, J. Wang, W. Chow, R. Carlson, Z. Jia, K. Zhang, D.G. Hayward, J.S. Chang. Perspectives on Liquid Chromatography-High-Resolution Mass Spectrometry for Pesticide Screening in Foods, *J. Agric. Food Chem.* 66 (2018) 9573–9581. doi:10.1021/acs.jafc.8b03468.
- [5] J.F. García-Reyes, M.D. Hernando, A. Molina-Díaz, A.R. Fernández-Alba. Comprehensive screening of target, non-target and unknown pesticides in food by LC-TOF-MS, *TrAC, Trends Anal. Chem.* 26 (2007) 828–841. doi:10.1016/j.trac.2007.06.006.
- [6] D.Q. Li, J. Zhao, J. Xie, S.P. Li. A novel sample preparation and on-line HPLC-DAD-MS/MS-BCD analysis for rapid screening and characterization of specific enzyme inhibitors in herbal extracts: case study of α -glucosidase, *J. Pharm. Biomed. Anal.* 88 (2014) 130–135. doi:10.1016/j.jpba.2013.08.029.
- [7] B. Da Vieira Silva, J.C. Barreira, M.B.P. Oliveira. Natural phytochemicals and probiotics as bioactive ingredients for functional foods: Extraction, biochemistry and protected-delivery technologies, *Trends Food Sci. Technol.* 50 (2016) 144–158. doi:10.1016/j.tifs.2015.12.007.
- [8] Ł. Cieśla, R. Moaddel. Comparison of analytical techniques for the identification of bioactive compounds from natural products, *Nat. Prod. Rep.* 33 (2016) 1131–1145. doi:10.1039/C6NP00016A.

- [9] M. Mladic, D.J. Scholten, W.M.A. Niessen, G.W. Somsen, M.J. Smit, J. Kool. At-line coupling of LC-MS to bioaffinity and selectivity assessment for metabolic profiling of ligands towards chemokine receptors CXCR1 and CXCR2, *J. Chromatogr. B* 1002 (2015) 42–53. doi:10.1016/j.jchromb.2015.08.004.
- [10] G.E. Morlock. High-performance thin-layer chromatography combined with effect-directed assays and high-resolution mass spectrometry as an emerging hyphenated technology: A tutorial review, *Anal. Chim. Acta* 1180 (2021) 338644. doi:10.1016/j.aca.2021.338644.
- [11] S.C. Weiss, N. Egetenmeyer, W. Schulz. Coupling of In Vitro Bioassays with Planar Chromatography in Effect-Directed Analysis, *Adv. Biochem. Eng./Biotechnol.* 157 (2017) 187–224. doi:10.1007/10_2016_16.
- [12] B. González-Gaya, N. Lopez-Herguedas, D. Bilbao, L. Mijangos, A.M. Iker, N. Etxebarria, M. Irazola, A. Prieto, M. Olivares, O. Zuloaga. Suspect and non-target screening: the last frontier in environmental analysis, *Anal. Methods* 13 (2021) 1876–1904. doi:10.1039/d1ay00111f.
- [13] J. Schwager, M.H. Mohajeri, A. Fowler, P. Weber. Challenges in discovering bioactives for the food industry, *Curr. Opin. Biotechnol.* 19 (2008) 66–72. doi:10.1016/j.copbio.2008.02.016.
- [14] J.J. Kellogg, D.A. Todd, J.M. Egan, H.A. Raja, N.H. Oberlies, O.M. Kvalheim, N.B. Cech. Biochemometrics for Natural Products Research: Comparison of Data Analysis Approaches and Application to Identification of Bioactive Compounds, *J. Nat. Prod.* 79 (2016) 376–386. doi:10.1021/acs.jnatprod.5b01014.
- [15] L.K. Caesar, J.J. Kellogg, O.M. Kvalheim, N.B. Cech. Opportunities and Limitations for Untargeted Mass Spectrometry Metabolomics to Identify Biologically Active Constituents in Complex Natural Product Mixtures, *J. Nat. Prod.* 82 (2019) 469–484. doi:10.1021/acs.jnatprod.9b00176.
- [16] R.A. Otvos, M. Mladic, G. Arias-Alpizar, W.M.A. Niessen, G.W. Somsen, A.B. Smit, J. Kool. At-Line Cellular Screening Methodology for Bioactives in Mixtures Targeting the α 7-Nicotinic Acetylcholine Receptor, *J. Biomol. Screening* 21 (2016) 459–467. doi:10.1177/1087057115625307.
- [17] K.T. Kongstad, C. Özdemir, A. Barzak, S.G. Wubshet, D. Staerk. Combined use of high-resolution α -glucosidase inhibition profiling and high-performance liquid chromatography-high-resolution mass spectrometry-solid-phase extraction-nuclear

- magnetic resonance spectroscopy for investigation of antidiabetic principles in crude plant extracts, *J. Agric. Food Chem.* 63 (2015) 2257–2263. doi:10.1021/jf506297k.
- [18] P. Hajeb, L. Zhu, R. Bossi, K. Vorkamp. Sample preparation techniques for suspect and non-target screening of emerging contaminants, *Chemosphere* 287 (2022) 132306. doi:10.1016/j.chemosphere.2021.132306.
- [19] M.G. Weller. A unifying review of bioassay-guided fractionation, effect-directed analysis and related techniques, *Sensors (Basel)* 12 (2012) 9181–9209. doi:10.3390/s120709181.
- [20] L. Torras-Claveria, S. Berkov, O. Jáuregui, J. Caujapé, F. Viladomat, C. Codina, J. Bastida. Metabolic profiling of bioactive *Pancreaticum canariense* extracts by GC-MS, *Phytochem. Anal.* 21 (2010) 80–88. doi:10.1002/pca.1158.
- [21] S.G. Wubshet, J.S. Schmidt, S. Wiese, D. Staerk. High-resolution screening combined with HPLC-HRMS-SPE-NMR for identification of potential health-promoting constituents in sea aster and searocket--new Nordic food ingredients, *J. Agric. Food Chem.* 61 (2013) 8616–8623. doi:10.1021/jf402949y.
- [22] T. Schreiner, A. Ronzheimer, M. Friz, G.E. Morlock. Multiplex planar bioassay with reduced diffusion on normal phase, identifying androgens, verified antiandrogens and synergists in botanicals via 12D hyphenation, *Food Chem.* 395 (2022) 133610. doi:10.1016/j.foodchem.2022.133610.
- [23] N.G.A.S.S. Chandana, G.E. Morlock. Eight different bioactivity profiles of 40 cinnamons by multi-imaging planar chromatography hyphenated with effect-directed assays and high-resolution mass spectrometry, *Food Chem.* 357 (2021) 129135. doi:10.1016/j.foodchem.2021.129135.
- [24] Á.M. Móricz, P.G. Ott, I. Yüce, A. Darcsi, S. Béni, G.E. Morlock. Effect-directed analysis via hyphenated high-performance thin-layer chromatography for bioanalytical profiling of sunflower leaves, *J. Chromatogr. A* 1533 (2018) 213–220. doi:10.1016/j.chroma.2017.12.034.
- [25] G.E. Morlock, A. Ziltener, S. Geyer, J. Tersteegen, A. Mehl, T. Schreiner, T. Kamel, F. Brümmer. Evidence that Indo-Pacific bottlenose dolphins self-medicate with invertebrates in coral reefs, *iScience* 25 (2022) 104271. doi:10.1016/j.isci.2022.104271.
- [26] G. Morlock, W. Schwack. Hyphenations in planar chromatography, *J. Chromatogr. A* 1217 (2010) 6600–6609. doi:10.1016/j.chroma.2010.04.058.

- [27] S. Buchinger, D. Spira, K. Bröder, M. Schlüsener, T. Ternes, G. Reifferscheid. Direct coupling of thin-layer chromatography with a bioassay for the detection of estrogenic compounds: applications for effect-directed analysis, *Anal. Chem.* 85 (2013) 7248–7256. doi:10.1021/ac4010925.
- [28] T. Schreiner, D. Sauter, M. Friz, J. Heil, G.E. Morlock. Is Our Natural Food Our Homeostasis? Array of A Thousand Effect-Directed Profiles of 68 Herbs and Spices, *Front. Pharmacol.* 12 (2021). doi:10.3389/fphar.2021.755941.
- [29] I. Müller, G.E. Morlock. Validation and quantification of the saccharide release of hydrothermally treated flours after salivary and pancreatic amylolysis by the HPTLC nanoGIT^{active} method, *in submission*.
- [30] E. Azadniya, J. Mollergues, T. Stroheker, K. Billerbeck, G.E. Morlock. New incorporation of the S9 metabolizing system into methods for detecting acetylcholinesterase inhibition, *Anal. Chim. Acta* 1129 (2020) 76–84. doi:10.1016/j.aca.2020.06.033.
- [31] G.E. Morlock, L. Drotleff, S. Brinkmann. Miniaturized all-in-one nanoGIT^{active} system for on-surface metabolization, separation and effect imaging, *Anal. Chim. Acta* 1154 (2021) 338307. doi:10.1016/j.aca.2021.338307.
- [32] G.E. Morlock, J. Heil. HI-HPTLC-UV/Vis/FLD-HESI-HRMS and bioprofiling of steviol glycosides, steviol, and isosteviol in Stevia leaves and foods, *Anal. Bioanal. Chem.* (2020) 1–18. doi:10.1007/s00216-020-02618-4.
- [33] S. Agatonovic-Kustrin, D.W. Morton. High-performance thin-layer chromatography HPTLC-direct bioautography as a method of choice for alpha-amylase and antioxidant activity evaluation in marine algae, *J Chromatogr A* 1530 (2017) 197–203. doi:10.1016/j.chroma.2017.11.024.
- [34] A. Marston, J. Kissling, K. Hostettmann. A rapid TLC bioautographic method for the detection of acetylcholinesterase and butyrylcholinesterase inhibitors in plants, *Phytochem. Anal* 13 (2002) 51–54. doi:10.1002/pca.623.
- [35] H.-R. Adhami, U. Scherer, H. Kaehlig, T. Hettich, G. Schlotterbeck, E. Reich, L. Krenn. Combination of bioautography with HPTLC-MS/NMR: a fast identification of acetylcholinesterase inhibitors from galbanum, *Phytochem. Anal.* 24 (2013) 395–400. doi:10.1002/pca.2422.
- [36] E. Mahran, M. Keusgen, G.E. Morlock. New planar assay for streamlined detection and quantification of β -glucuronidase inhibitors applied to botanical extracts, *Anal. Chim. Acta: X* 4 (2020) 100039. doi:10.1016/j.acax.2020.100039.

- [37] S. Wangthong, I. Tonsiripakdee, T. Monhaphol, R. Nonthabenjawan, S.P. Wanichwecharungruang. Post TLC developing technique for tyrosinase inhibitor detection, *Biomed. Chromatogr.* 21 (2007) 94–100. doi:10.1002/bmc.727.
- [38] J. Taibon, A. Ankli, S. Schwaiger, C. Magnenat, V.-I. Boka, C. Simões-Pires, N. Aligiannis, M. Cuendet, A.-L. Skaltsounis, E. Reich, H. Stuppner. Prevention of False-Positive Results: Development of an HPTLC Autographic Assay for the Detection of Natural Tyrosinase Inhibitors, *Planta Med.* 81 (2015) 1198–1204. doi:10.1055/s-0035-1546250.
- [39] C.A. Simões-Pires, B. Hmicha, A. Marston, K. Hostettmann. A TLC bioautographic method for the detection of alpha- and beta-glucosidase inhibitors in plant extracts, *Phytochem. Anal.* 20 (2009) 511–515. doi:10.1002/pca.1154.
- [40] G. Eberz, H.-G. Rast, K. Burger, W. Kreiss, C. Weisemann. Bioactivity screening by chromatography-bioluminescence coupling, *Chromatographia* 43 (1996) 5–9. doi:10.1007/BF02272814.
- [41] M. Jamshidi-Aidji, G.E. Morlock. Bioprofiling of unknown antibiotics in herbal extracts: Development of a streamlined direct bioautography using *Bacillus subtilis* linked to mass spectrometry, *J. Chromatogr. A* 1420 (2015) 110–118.
- [42] D. Meyer, M. Marin-Kuan, E. Debon, P. Serrant, C. Cottet-Fontannaz, B. Schilter, G.E. Morlock. Detection of low levels of genotoxic compounds in food contact materials using an alternative HPTLC-SOS-Umu-C assay, *Altex* (2020). doi:10.14573/altex.2006201.
- [43] M.B. Müller, C. Dausend, C. Weins, F.H. Frimmel. A New Bioautographic Screening Method for the Detection of Estrogenic Compounds, *Chromatographia* 60 (2004) 207–211. doi:10.1365/s10337-004-0315-8.
- [44] I. Klingelhöfer, N. Hockamp, G.E. Morlock. Non-targeted detection and differentiation of agonists versus antagonists, directly in bioprofiles of everyday products, *Anal. Chim. Acta* 1125 (2020) 288–298. doi:10.1016/j.aca.2020.05.057.
- [45] C. Weins, H. Jork. Toxicological evaluation of harmful substances by in situ enzymatic and biological detection in high-performance thin-layer chromatography, *J. Chromatogr. A* 750 (1996) 403–407. doi:10.1016/0021-9673(96)00601-2.
- [46] I.J. Purvis, D. Chotai, C.W. Dykes, D.B. Lubahn, F.S. French, E.M. Wilson, A.N. Hobden. An androgen-inducible expression system for *Saccharomyces cerevisiae*, *Gene* 106 (1991) 35–42. doi:10.1016/0378-1119(91)90563-Q.

- [47] D.P. McDonnell, Z. Nawaz, C. Densmore, N.L. Weigel, T.A. Pham, J.H. Clark, B.W. O'Malley. High level expression of biologically active estrogen receptor in *Saccharomyces cerevisiae*, *J. Steroid Biochem. Mol. Biol.* 39 (1991) 291–297. doi:10.1016/0960-0760(91)90038-7.
- [48] J.A. Buckley. Quantifying the antiestrogen activity of wastewater treatment plant effluent using the yeast estrogen screen, *Environ. Toxicol. Chem.* 29 (2010) 73–78. doi:10.1002/etc.11.
- [49] Y. Oda. Development and progress for three decades in umu test systems, *Genes Environ.* 38 (2016) 24. doi:10.1186/s41021-016-0054-8.
- [50] G. Reifferscheid, J. Heil, Y. Oda, R.K. Zahn. A microplate version of the SOS/umu-test for rapid detection of genotoxins and genotoxic potentials of environmental samples, *Mutat. Res. Environ. Mutagen. Relat. Subj.* 253 (1991) 215–222. doi:10.1016/0165-1161(91)90134-T.
- [51] A. Marston. Thin-layer chromatography with biological detection in phytochemistry, *J. Chromatogr. A* 1218 (2011) 2676–2683. doi:10.1016/j.chroma.2010.12.068.
- [52] A. Mehl, W. Schwack, G.E. Morlock. On-surface autosampling for liquid chromatography-mass spectrometry, *J. Chromatogr. A* 1651 (2021) 462334. doi:10.1016/j.chroma.2021.462334.
- [53] T. Schreiner, G.E. Morlock. Non-target bioanalytical eight-dimensional hyphenation including bioassay, heart-cut trapping, online desalting, orthogonal separations and mass spectrometry, *J. Chromatogr. A* 1647 (2021) 462154. doi:10.1016/j.chroma.2021.462154.
- [54] R. Lucas-González, M. Viuda-Martos, J.A. Pérez-Alvarez, J. Fernández-López. In vitro digestion models suitable for foods: Opportunities for new fields of application and challenges, *Food Res. Int.* 107 (2018) 423–436. doi:10.1016/j.foodres.2018.02.055.
- [55] S.J. Hur, B.O. Lim, E.A. Decker, D.J. McClements. In vitro human digestion models for food applications, *Food Chem.* 125 (2011) 1–12. doi:10.1016/j.foodchem.2010.08.036.
- [56] M. Minekus, M. Alminger, P. Alvito, S. Ballance, T. Bohn, C. Bourlieu, F. Carrière, R. Boutrou, M. Corredig, D. Dupont, C. Dufour, L. Egger, M. Golding, S. Karakaya, B. Kirkhus, S. Le Feunteun, U. Lesmes, A. Macierzanka, A. Mackie, S. Marze, D.J. McClements, O. Ménard, I. Recio, C.N. Santos, R.P. Singh, G.E. Vegarud, M.S.J. Wickham, W. Weitschies, A. Brodkorb. A standardised static in vitro digestion method suitable

- for food - an international consensus, *Food Funct.* 5 (2014) 1113–1124. doi:10.1039/c3fo60702j.
- [57] T. Bohn, F. Carriere, L. Day, A. Deglaire, L. Egger, D. Freitas, M. Golding, S. Le Feunteun, A. Macierzanka, O. Menard, B. Miralles, A. Moscovici, R. Portmann, I. Recio, D. Rémond, V. Santé-Lhoutelier, T.J. Wooster, U. Lesmes, A.R. Mackie, D. Dupont. Correlation between in vitro and in vivo data on food digestion. What can we predict with static in vitro digestion models?, *Crit. Rev. Food Sci. Nutr.* 58 (2018) 2239–2261. doi:10.1080/10408398.2017.1315362.
- [58] S. Yoshihara, M. Makishima, N. Suzuki, S. Ohta. Metabolic activation of bisphenol A by rat liver S9 fraction, *Toxicol. Sci.* 62 (2001) 221–227. doi:10.1093/toxsci/62.2.221.
- [59] J.L. Suit, A.E. Rodgers, M. Jetten, S.E. Luria. Effects of diet on conversion of aflatoxin B1 to bacterial mutagen(s) by rats in vivo and by rat hepatic microsomes in vitro, *Mutat. Res. Environ. Mutagen. Relat. Subj.* 46 (1977) 313–323. doi:10.1016/0165-1161(77)90009-7.
- [60] E. Debon, P. Rogeboz, H. Latado, G.E. Morlock, D. Meyer, C. Cottet-Fontannaz, G. Scholz, B. Schilter, M. Marin-Kuan. Incorporation of metabolic activation in the HPTLC-SOS-Umu-C assay to detect low amounts of genotoxic chemicals, *in submission* (2022).
- [61] C.-H. Tung, C.-C. Lin, C.-C. Tung, S.-F. Chen, F. Sheu, T.-J. Lu. Combination of on-line desalting and HPLC-UV-ESI-MS for simultaneous detection and identification of FIP-5 and flammutoxin in *Flammulina velutipes*, *J. Food Drug Anal.* 26 (2018) 1045–1053. doi:10.1016/j.jfda.2017.12.004.
- [62] H. Luo, W. Zhong, J. Yang, P. Zhuang, F. Meng, J. Caldwell, B. Mao, C.J. Welch. 2D-LC as an on-line desalting tool allowing peptide identification directly from MS unfriendly HPLC methods, *J. Pharm. Biomed. Anal.* 137 (2017) 139–145. doi:10.1016/j.jpba.2016.11.012.
- [63] K.J. Fountain, M. Gilar, J.C. Gebler. Electrospray ionization mass spectrometric analysis of nucleic acids using high-throughput on-line desalting, *Rapid Commun. Mass Spectrom.* 18 (2004) 1295–1302.
- [64] J. Bengtsson, B. Jansson, M. Hammarlund-Udenaes. On-line desalting and determination of morphine, morphine-3-glucuronide and morphine-6-glucuronide in microdialysis and plasma samples using column switching and liquid chromatography/tandem mass spectrometry, *Rapid Commun. Mass Spectrom.* 19 (2005) 2116–2122.

- [65] P.E. Miller, M.B. Denton. The quadrupole mass filter: Basic operating concepts, *J. Chem. Educ.* 63 (1986) 617. doi:10.1021/ed063p617.
- [66] P. Eichhorn, S. Pérez, D. Barceló. Time-of-Flight Mass Spectrometry Versus Orbitrap-Based Mass Spectrometry for the Screening and Identification of Drugs and Metabolites, in: A.R. Fernández-Alba (Ed.), TOF-MS within food and environmental analysis: Comprehensive analytical chemistry, Elsevier, Amsterdam, 2012, pp. 217–272.
- [67] R.A. Zubarev, A. Makarov. Orbitrap mass spectrometry, *Anal. Chem.* 85 (2013) 5288–5296. doi:10.1021/ac4001223.
- [68] S. Eliuk, A. Makarov. Evolution of Orbitrap Mass Spectrometry Instrumentation, *Annu. Rev. Anal. Chem.* 8 (2015) 61–80. doi:10.1146/annurev-anchem-071114-040325.
- [69] C. Riegraf, G. Reifferscheid, S. Belkin, L. Moscovici, D. Shakibai, H. Hollert, S. Buchinger. Combination of yeast-based in vitro screens with high-performance thin-layer chromatography as a novel tool for the detection of hormonal and dioxin-like compounds, *Anal. Chim. Acta* 1081 (2019) 218–230. doi:10.1016/j.aca.2019.07.018.
- [70] A. Schönborn, A. Grimmer. Coupling sample preparation with effect-directed analysis of estrogenic activity - Proposal for a new rapid screening concept for water samples, *JPC - J. Planar Chromat.* 26 (2013) 402–408. doi:10.1556/JPC.26.2013.5.3.
- [71] I. Klingelhöfer, G.E. Morlock. Sharp-bounded zones link to the effect in planar chromatography-bioassay-mass spectrometry, *J. Chromatogr. A* 1360 (2014) 288–295. doi:10.1016/j.chroma.2014.07.083.
- [72] A. Schönborn, P. Schmid, S. Bräm, G. Reifferscheid, M. Ohlig, S. Buchinger. Unprecedented sensitivity of the planar yeast estrogen screen by using a spray-on technology, *J. Chromatogr. A* 1530 (2017) 185–191. doi:10.1016/j.chroma.2017.11.009.
- [73] J. Müthing, U. Distler. Advances on the compositional analysis of glycosphingolipids combining thin-layer chromatography with mass spectrometry, *Mass Spectrom. Rev.* 29 (2010) 425–479. doi:10.1002/mas.20253.
- [74] M. Brockhaus, J.L. Magnani, M. Blaszczyk, Z. Steplewski, H. Koprowski, K.A. Karlsson, G. Larson, V. Ginsburg. Monoclonal antibodies directed against the human Leb blood group antigen, *J. Biol. Chem.* 256 (1981) 13223–13225. doi:10.1016/S0021-9258(18)43031-1.
- [75] D. Steil, C.-L. Schepers, G. Pohlentz, N. Legros, J. Runde, H.-U. Humpf, H. Karch, J. Müthing. Shiga toxin glycosphingolipid receptors of Vero-B4 kidney epithelial cells

- and their membrane microdomain lipid environment, *J. Lipid Res.* 56 (2015) 2322–2336. doi:10.1194/jlr.M063040.
- [76] N.A. Alcantar, E.S. Aydil, J.N. Israelachvili. Polyethylene glycol-coated biocompatible surfaces, *J. Biomed. Mater. Res.* 51 (2000) 343–351. doi:10.1002/1097-4636(20000905)51:3<343:AID-JBM7>3.0.CO;2-D.
- [77] Y.H. Kim, N.S. Baek, Y.H. Han, M.-A. Chung, S.-D. Jung. Enhancement of neuronal cell adhesion by covalent binding of poly-D-lysine, *J. Neurosci. Methods* 202 (2011) 38–44. doi:10.1016/j.jneumeth.2011.08.036.
- [78] I.D. Wilson, U.A. Brinkman. Hype and hypernation: multiple hyphenation of column liquid chromatography and spectroscopy, *TrAC, Trends Anal. Chem.* 26 (2007) 847–854. doi:10.1016/j.trac.2007.07.007.
- [79] European Committee for Standardization. Water quality - Determination of the inhibitory effect of water samples on the light emission of *Vibrio fischeri* (Luminescent bacteria test): Part 1: Method using freshly prepared bacteria (2009).
- [80] S. Krüger, L. Hüsken, R. Fornasari, I. Scainelli, G.E. Morlock. Effect-directed fingerprints of 77 botanical extracts via a generic high-performance thin-layer chromatography method combined with assays and mass spectrometry, *J. Chromatogr. A* 1529 (2017) 93–106. doi:10.1016/j.chroma.2017.10.068.
- [81] T. Schreiner, N.M. Eggerstorfer, G.E. Morlock. Effects of gastrointestinal digestion on bioactivity of convenience tomato products studied by ten dimensional hyphenation, *in submission* (2022).
- [82] I.-L. Wu, S.B. Turnipseed, J.M. Storey, W.C. Andersen, M.R. Madson. Comparison of data acquisition modes with Orbitrap high-resolution mass spectrometry for targeted and non-targeted residue screening in aquacultured eel, *Rapid Commun. Mass Spectrom.* 34 (2020) e8642. doi:10.1002/rcm.8642.
- [83] W. Jia, L. Shi, X. Chu, J. Chang, Y. Chen, F. Zhang. A strategy for untargeted screening of macrolides and metabolites in bass by liquid chromatography coupled to quadrupole orbitrap mass spectrometry, *Food Chem.* 262 (2018) 110–117. doi:10.1016/j.foodchem.2018.04.090.
- [84] J. Wang, W. Chow, J.W. Wong, D. Leung, J. Chang, M. Li. Non-target data acquisition for target analysis (nDATA) of 845 pesticide residues in fruits and vegetables using UHPLC/ESI Q-Orbitrap, *Anal. Bioanal. Chem.* 411 (2019) 1421–1431. doi:10.1007/s00216-019-01581-z.

- [85] T. Schreiner, N.M. Eggerstorfer, G.E. Morlock. Effects of gastrointestinal digestion on bioactivity of meal replacement products studied by ten dimensional hyphenation, *in submission* (2022).
- [86] E.J. Carrasco-Correa, J. Ruiz-Allica, J.F. Rodríguez-Fernández, M. Miró. Human artificial membranes in (bio)analytical science: Potential for in vitro prediction of intestinal absorption-A review, *TrAC, Trends Anal. Chem.* 145 (2021) 116446. doi:10.1016/j.trac.2021.116446.
- [87] A. Ronzheimer, T. Schreiner, G.E. Morlock. Multiplex planar bioassay detecting estrogens, antiestrogens, false-positives and synergists as sharp zones on normal phase, *Phytomedicine* 103 (2022) 154230. doi:10.1016/j.phymed.2022.154230.
- [88] X. Zhou, S.W. Seto, D. Chang, H. Kiat, V. Razmovski-Naumovski, K. Chan, A. Bensoussan. Synergistic Effects of Chinese Herbal Medicine: A Comprehensive Review of Methodology and Current Research, *Front. Pharmacol.* 7 (2016) 201. doi:10.3389/fphar.2016.00201.
- [89] N. Rajapakse, E. Silva, Kortenkamp Andreas. Combining Xenoestrogens at Levels below Individual No-Observed-Effect Concentrations Dramatically Enhances Steroid Hormone Action, *Environ. Health Perspect.* 110 (2002) 917–921.
- [90] K.R. Roell, D.M. Reif, A.A. Motsinger-Reif. An Introduction to Terminology and Methodology of Chemical Synergy-Perspectives from Across Disciplines, *Front. Pharmacol.* 8 (2017) 158. doi:10.3389/fphar.2017.00158.
- [91] J.L. Chen, T.W.J. Steele, D.C. Stuckey. Metabolic reduction of resazurin; location within the cell for cytotoxicity assays, *Biotechnol. Bioeng.* 115 (2018) 351–358. doi:10.1002/bit.26475.

2. Publication 1

Non-target bioanalytical eight-dimensional hyphenation including bioassay, heart-cut trapping, online desalting, orthogonal separations and mass spectrometry

Tamara Schreiner, Gertrud E. Morlock*

Chair of Food Science, Institute of Nutritional Science, and Interdisciplinary Research
Center (iFZ), Justus Liebig University Giessen, Heinrich-Buff-Ring 26-32, 35392 Giessen,
Germany

Published in

Journal of Chromatography A, 1647 (2021) 462154

Received 5 November 2020; Revised 22 March 2021; Accepted 8 April 2021; Available online 20 April 2021



Non-target bioanalytical eight-dimensional hyphenation including bioassay, heart-cut trapping, online desalting, orthogonal separations and mass spectrometry

Tamara Schreiner, Gertrud E. Morlock*

Chair of Food Science, Institute of Nutritional Science, and Interdisciplinary Research Center (iFZ), Justus Liebig University Giessen, Heinrich-Buff-Ring 26-32, 35392 Giessen, Germany

ARTICLE INFO

Article history:

Received 5 November 2020
Revised 22 March 2021
Accepted 8 April 2021
Available online 20 April 2021

Keywords:

Eight-dimensional hyphenation
Non-target screening
High-performance thin-layer chromatography
Online desalting
Effect-directed analysis of cinnamon
Allivibrio fischeri bioassay

ABSTRACT

It is still a challenge to discover and identify individual bioactive compounds directly in multicomponent mixtures. Current workflows are too tedious for routine use. Hence, the hyphenation of separation and detection techniques is a powerful tool to maximize the information obtained by a single sample run. A robust eight-dimensional (8D) hyphenation was developed. Orthogonal separations, biological assay detection, analyte trapping, desalting, and physico-chemical detections were arranged in the following order, i.e. 1) normal phase high-performance thin-layer chromatography (NP-HPTLC) separation, 2) Vis detection, 3) UV detection, 4) fluorescence detection (FLD), 5) bioassay for effect-directed analysis (EDA), 6) heart-cut trapping/desalting/elution to reversed phase high-performance liquid chromatography (RP-HPLC) separation, 7) photodiode array (PDA) and 8) mass spectrometry (MS) detection. For the first time, the hyphenation exploited online analyte trapping to desalt the eluted bioactive zone from the plate containing highly salted bioassay media. Subsequent valve switching guided the trapped analyte(s) to the main column, followed by multiple detection. As proof-of-principle, cinnamon samples were analyzed by NP-HPTLC–UV/Vis/FLD–EDA–RP-HPLC–PDA–MS, whereby a bioactive zone was separated into two distinct peaks detected by PDA and MS to be 2-methoxy cinnamaldehyde and cinnamaldehyde. The developed 8D hyphenation is applicable for routine, allowing the non-target high-throughput screening of complex samples for individual bioactive compounds.

© 2021 Elsevier B.V. All rights reserved.

1. Introduction

State-of-the-art non-target screening exploits liquid chromatography (LC) coupled to high-resolution mass spectrometry (HRMS) or time-of-flight mass spectrometry (TOF-MS) [1–4]. On the one hand most detected features in a complex sample can not be assigned to a molecule. On the other hand not all detected features can be elucidated in its structure. Hence, a decision has to be made which ones are most important to be subjected to further characterization. Integrating the biological detection helps to find out the compounds of highest priority. Thus, non-target bioanalytical screening strategies are the ultimate tool [5]. Comprehensive information on bioactive compounds in complex samples is obtained by hyphenated methods exploiting orthogonal separation and multiple inclusive effect-directed detection principles to maximize the information obtained by a single sample run [6,7].

The detection of individual bioactive substances in complex samples is possible using high-performance thin-layer chromatography (HPTLC–UV/Vis/FLD) hyphenated to effect-directed assays (EDA) and HRMS [2,5,6,8,9]. Unknown bioactive compounds are heart-cut eluted and online transferred to the electrospray ionization (ESI) interface [2,6,8,10,11]. However, two HPTLC plates have to be prepared, one for the bioassay and one for structure elucidation by HRMS or nuclear magnetic resonance spectroscopy. This requires twice the time and doubles material consumption. To ensure that the bioactive zone has properly been eluted and transferred, the bioassay must be applied on the post-HRMS plate once again. A non-target bioanalytical screening strategy should guarantee the proper assignment of a single compound inducing the bioactivity. However in HPTLC, a bioactive zone could contain several components, whereby each can be responsible for the bioactivity. As for 2D HPLC [12,13], potentially coeluting bioactive substances on the bioautogram obtained by normal phase (NP)-HPTLC-EDA can be separated by subsequent reversed phase (RP)-HPLC-PDA-MS. In other words, only the selected bioactive zone (not matrix, not background) is orthogonally separated and detected for a

* Corresponding author: Phone +49-641-99-39141; Fax +49-641-99-39149.
E-mail address: gertrud.morlock@uni-giessen.de (G.E. Morlock).

second time. Thus, such an arrangement is utmost efficient. Consequently, there is huge potential and high interest in the development of a multidimensional hyphenation like HPTLC–EDA–heart-cut–HPLC–PDA–MS [14–17]. Such a hyphenation is challenging because the heart-cut zone elution via an elution head-based interface transfers the desired analyte(s) together with the bioassay medium (salts, amino acids, proteins etc.) to the MS. This causes high background signal (baseline) intensities, ion suppression and more cleaning cycles [5,15]. Thus, there is need for online desalting to reduce or even get rid of the intense bioassay background signals. Desalting concepts used in HPLC–MS may also be applied to HPTLC–EDA–MS. For example, either a solid phase extraction (SPE) cartridge [18], second chromatographic column [19] or short guard column [20,21] was exploited in two dimensional LC systems for nucleic acid or plasma online desalting [20,21] or peptide purification [19]. However, these concepts can not simply be transferred for on-surface elutions, for which also solubility and elution strength have to be taken into account.

In this study, an orthogonal eight-dimensional (8D) hyphenation was developed which explored online analyte trapping for a robust desalting for the first time. Different desalting devices [20] were investigated by installing them on a switching valve to allow a two-position load-elution variant. The optimal elution parameters were studied, such as elution time, elution volume and solvent composition. As proof-of-principle, 18 different cinnamon samples along with well-known bioactive marker compounds were investigated with the developed NP-HPTLC-UV/Vis/FLD-EDA-heart-cut/trapping/elution-RP-HPLC-PDA-ESI-MS hyphenation.

2. Materials and methods

2.1. Chemicals and materials

Magnesium sulfate heptahydrate ($\text{MgSO}_4 \cdot 7 \text{H}_2\text{O}$, 99.5%) and HPTLC plates silica gel 60 F_{254} MS-grade were purchased from Merck, Darmstadt, Germany. Toluene ($\geq 99\%$), acetic acid (99.8%), sodium dihydrogen phosphate monohydrate ($\text{NaH}_2\text{PO}_4 \cdot \text{H}_2\text{O}$, 98%), dipotassium hydrogen phosphate trihydrate ($\text{K}_2\text{HPO}_4 \cdot 3 \text{H}_2\text{O}$, 99%) and glycerol (86%) were obtained from Roth, Karlsruhe, Germany. Diammonium hydrogen phosphate ($[\text{NH}_4]_2\text{HPO}_4$, $\geq 99\%$) was delivered by Acros Organics, NJ, USA. Sodium chloride (NaCl , $\geq 99.5\%$), tryptone, ammonium acetate ($\geq 99\%$) and coumarin (Co, $\geq 99\%$) were purchased from Fluka Sigma Aldrich, Steinheim, Germany. Yeast extract and ethyl acetate (99.8%) were delivered by Th. Geyer, Renningen, Germany. 2-Methoxycinnamaldehyde (2-MCA) was obtained from PhytoLab, Vestenbergsgreuth, Germany and cinnamaldehyde (CA, $\geq 98\%$) from Fluka. Methanol (HPLC grade) and cinnamic acid (Ci, 98%) were purchased from vwr, Darmstadt, Germany, whereby LC-MS grade methanol was from Honeywell, Muskegon, MI, USA. Bidistilled water was prepared using a Destamat Bi 18E (Heraeus, Hanau, Germany). The marine microorganism *Aliivibrio fischeri* (strain 7151) was provided by Leibniz Institute, DSMZ, German Collection of Microorganisms and Cell Cultures, Berlin, Germany.

2.2. Sample preparation and standard solutions

Cinnamomum verum and *Cinnamomum cassia* samples were bought on the market (Table S1). Each cinnamon sample (200 mg) was dissolved in 2 mL methanol – water (4:1, V/V), ultrasonicated (15 min, Sonorex Digiplus, Bandelin, Berlin, Germany), centrifuged ($3000 \times g$, 5 min, Labofuge 400, Heraeus, Hanau, Germany) and the supernatant was used. Co, Ci, CA and 2-MCA were dissolved each as 1-mg/mL methanolic stock solution and diluted 1:10 with methanol (0.1 mg/mL).

2.3. NP-HPTLC/UV/Vis/FLD method

A set of HPTLC plates silica gel 60 F_{254} MS-grade were pre-washed two times with methanol – water (4:1, V/V) and dried in an oven (Mettler, Schwabach, Germany) at 110°C for 20 min. The sample (2.5 μL) and diluted standard solutions (5 μL) were applied as 7-mm bands with a track distance of 7.5 mm (Automated TLC Sampler ATS 4, CAMAG, Muttenz, Switzerland). The development of the plate was performed in a Twin-Trough Chamber with toluene – ethyl acetate – methanol (6:3:1, V/V/V) up to a developing distance of 65 mm (further mobile phases in Table S2 and Fig. S1). The chromatogram was dried in a stream of cold air for 5 min and documented at 254 nm, 366 nm and white light illumination (TLC Visualizer 3, CAMAG). For removal of residual organic solvent traces, the HPTLC plate was dried again for 15 min (Automated Development Chamber ADC2, CAMAG). The instrument control and data evaluation was performed with VisionCATS v2.5 software (CAMAG).

2.4. *Aliivibrio fischeri* bioassay

The cell culture medium was prepared according to DIN EN ISO 11348-1, section 5 [22] as reported [23]. The *A. fischeri* suspension (2 mL) was piezoelectrically sprayed on the MS-grade plate using the blue nozzle at level 6 (Derivatizer, CAMAG). The bioluminescence was recorded instantly and in trigger interval of 3 min until 30 min. Thus, 10 images at a 120-s exposure time were taken (Bioluminizer, CAMAG).

2.5. Instrumental setup of the 8D hyphenation

The UPLC system (Acquity H Class, Waters, Eschborn, Germany) was equipped with the quaternary solvent manager, solvent degasser, sample manager, column oven, photodiode array detector (PDA) and ESI-MS (single quadrupole QDa, Waters). The elution solvent was pumped by a standalone pump (515 HPLC pump, Waters) to the TLC-MS Interface (CAMAG) or Plate Express (Advion, Idaho, ID, USA). The bioactive target zone was isolated by the oval elution head (4 \times 2 mm) and heart-cut eluted for 45 s at a flow rate of 0.1 mL/min through a biocompatible filter to different online desalting devices: RP/IEC (short Oasis MCX column, 20 mm \times 3 mm, 30 μm , Waters), RP and Phenyl-X (pre-column/defender guard in a cartridge: Accucore RP-MS, 10 mm \times 2.1 mm, 2.6 μm , or Accucore Phenyl-X, 10 mm \times 2.1 mm, 2.6 μm , both Thermo Scientific, Bellefonte, PA, USA). The biocompatible inline filter (IDEX Health & Science, Oak Harbor, WA, USA) containing a PEEK frit (0.5 μm , Techlab, Braunschweig, Germany) was installed in between the elution head-based interface and two-position switching valve (MXT-Series PD715-000, Rheodyne IDEX Health & Science). In the latter, the desalting device was installed, which trapped the analyte(s) on the respective material and discarded the bioassay salts into the waste. By switching, regulated via remote control and Rheodyne TitanMX software (Rheodyne IDEX Health & Science), the HPLC gradient flushed the desalting device and guided the analyte(s) to the main column (Accucore RP-MS 100 mm \times 2.1 mm, 2.6 μm , Thermo Scientific) thermostated at 40°C in a column oven (instrumental set up in Fig. S2). The HPLC gradient consisted of 2.5 mM ammonium acetate, adjusted to pH 4.5 with acetic acid (A) and methanol (B). The final gradient with a flow rate of 0.6 mL/min started with 98% A for the first 2 min. The organic portion (B) increased linearly to 20% until 4.5 min and to 90% within the following 3.5 min. The ratio 10/90 A/B was held for the next 2 min, then immediately felt down to 98% A within 0.1 min. The gradient time included 3 min re-equilibration time. The generated system pressure reached max. 600 bar. After HPLC separation the analytes were detected by PDA and then ESI-MS. The latter was operated

in polarity switching mode with ESI probe set to 600°C and ESI source to 120°C as well as optimized scan frequency of 5 Hz and cone voltage of 10 V in both ionization modes (Fig. S3). The MassLynx V4.2 software (Waters) was used.

2.6. Investigation of elution solvent and elution time

The four standards (5 µL) were applied as 4 mm bands (sized to the elution head geometry) on pre-washed plates (ATS4 with FreeMode option of winCATS software V.1.4.7, CAMAG). Various solvent mixtures were prepared in 50 mL flasks in a linearly descending series from 90% methanol in bidistilled water to completely aqueous. With the respective solvent mixture installed, the system (load pump) was purged at a flow rate of 1 mL/min for 5 min.

3. Results and discussion

As not every detected unknown compound in complex mixtures can be elucidated in its structure, a decision on priority has to be made. The effect-directed detection supports decision makers and points to bioactive compounds considered as first priority compounds. Hence, a NP-HPTLC–UV/Vis/FLD–EDA–RP-HPLC–PDA–ESI-MS hyphenation was developed (Figs. 1 and S2). A total of eight dimensions of different separation and detection principles were combined to obtain as much information as possible in a single sample run. It exploited heart-cut trapping, online desalting of the bioactive zone, and an orthogonal alignment of the two chromatographic dimensions in a minimalistic way, as only the selected bioactive zone (not matrix, not background) is separated and detected for a second time. The *A. fischeri* bioassay was selected to evaluate the effect of highly salted cultivation media [22]. Additionally, this bioassay detects bioactive compounds more generally via its impact on the energetic cell metabolism [16]. Cinnamon samples were selected because they are rich in bioactive marker compounds and complex matrix [24,25].

3.1. Calculated bioassay salt load

The *A. fischeri* bioassay medium [22] contains an overall calculated amount of ca. 45 g/L of nutrients and salts. On a 20 cm × 10 cm plate, 2 mL of the bacterial suspension are adsorbed. The elution head elutes a zone of 2 mm × 4 mm, and thus an area of 8 mm². Thereby, 36 µg of salt load is transferred to the MS. Less salt amounts are already sufficient to cause ion suppression, interfering signals and adduct ion formation (e.g., Na⁺, K⁺, NH₄⁺), instead of the protonated [M+H]⁺ and deprotonated molecule [M-H]⁻ [15]. Consequently, the bioassay medium is an unacceptable source of contamination for the MS system. The transfer of the coeluting assay medium has to be reduced for a direct hyphenation, in particular for use in routine and in combination with an HRMS system.

3.2. Reduction of MS interferences by online desalting

MS-grade plates show enhanced sensitivity and low background signals according to the manufacturer's specification. About half of the interferences were avoided using MS-grade plates with a reduced plate thickness. Further, only half of the material needs to be applied on the plate, which is advantageous for expensive samples and cell cultures, to obtain comparable results to regular plates (e.g., HPTLC plates silica gel 60 F₂₅₄). Therefore, MS-grade plates were studied with regard to the total ion count (TIC) intensities after application of the *A. fischeri* bioassay.

The concepts of online desalting systems reported so far [18,20,21] cannot be simply transferred to on-surface elutions. Solubility in relation to desorption from the planar adsorbent and

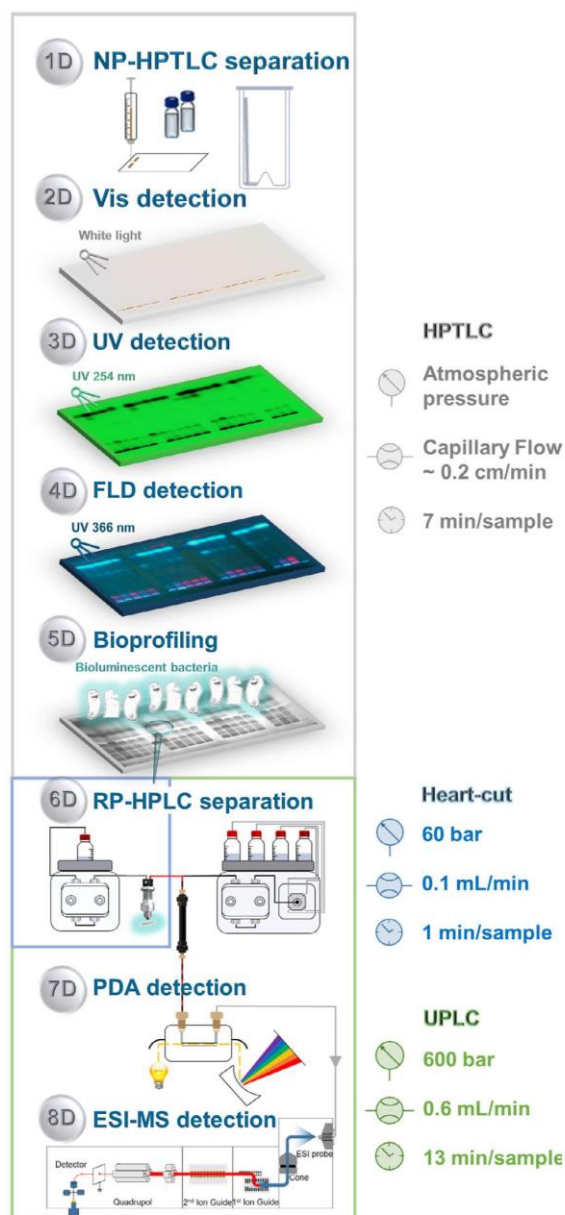


Fig. 1. Scheme of the developed 8D hyphenation exploiting heart-cut trapping and online desalting, arranged in the following sequence: NP-HPTLC–UV/Vis/FLD–EDA–RP-HPLC–PDA–MS (for 18 samples on a plate, analysis time was calculated per sample).

HPLC start gradient as well as elution strength in relation to planar adsorbent and column are also crucial aspects for successful desalting of the sample eluted from the bioassay plate. Three different desalting devices were one after the other installed on the switching valve and tested for their salt load reduction capacity (Fig. 2). The load pump command led the eluent through the elution head and thus bioactive zone. In the load position, the analytes were eluted from the plate and guided to a desalting trap installed on the switching valve. Analytes were trapped on the re-

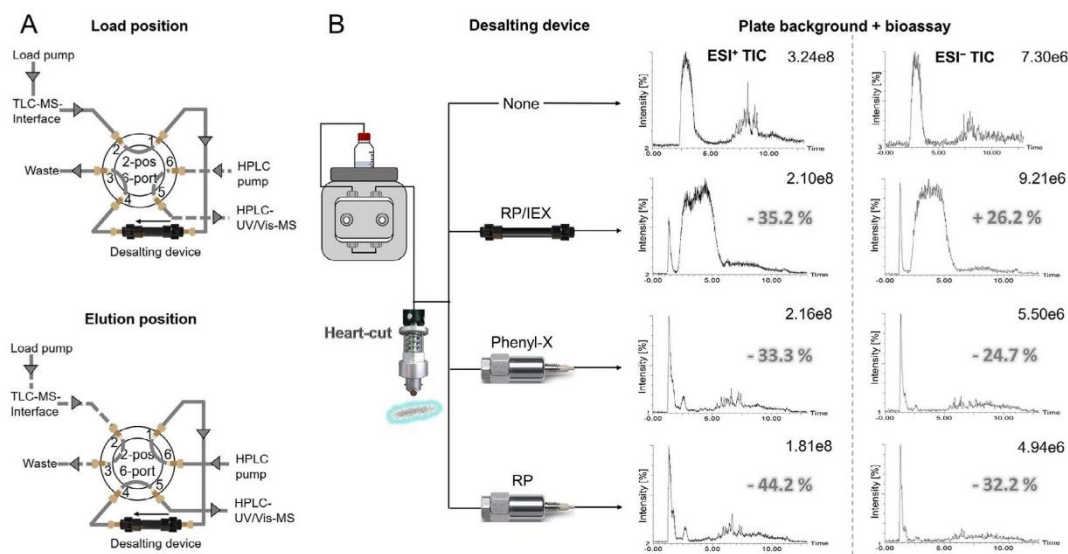


Fig. 2. Reduction of the *A. fischeri* bioassay medium load by heart-cut trapping and online desalting: Scheme of the two-position six-port switching valve (A) and mean TIC reduction of the bioassay load/plate background ($n = 2$) via the three tested desalting devices (B); eluted with 90% bidistilled water for 45 s at a flow rate of 0.1 mL/min from pre-washed MS-grade plates with 2 mL *A. fischeri* medium adsorbed; respective full scan MS spectra in Fig. S4.

spective RP/IEX, Phenyl-X or RP material of the different desalting devices, while salts and polar nutrients of the bioassay medium were flushed into the waste. In the elution position, the gradient of the quaternary HPLC pump was guided through the desalting device and carried the analyte(s) to the main column, followed by subsequent PDA and MS detection. In the positive and negative ionization mode, TIC-MS intensities of the plate background with and without bioassay were compared (Fig. 2B) as well as the obtained full scan mass spectra (Fig. S4).

Comparing the three desalting devices, the short RP/IEX hybrid column reduced the bioassay plate background only in the positive ionization mode, and contrarily, increased it in the ESI⁻ TIC. This mixed mode column, consisting of cation exchange and RP material, bound the positively charged salt ions via ionic forces and trapped apolar substances via hydrophobic interactions, whereas the anions accumulated in the aqueous solvents. By the valve switch, the anion load, plate background molecules and further retarded molecules were transferred to the MS. Usually in ion exchange chromatography, the still bound counter ions were washed from the column during a regeneration process by rinsing with a high ionic strength buffer. In this process, the bound ions were replaced by counter ions of the buffer [26]. However, no regeneration process was integrated in this 8D hyphenation, which would cause the column to lose its ESI⁺ TIC reduction potential over time. Due to the weak salt reduction capacity and slowly progressing cation saturation, the RP/IEX hybrid column was excluded as possible desalting device.

The RP pre-column showed the lowest TIC intensities regarding the bioassay load for both ionization modes. The mean high TIC intensities of the bioassay plate background, caused by the high salt amounts transferred to MS, were reduced by 44% in the ESI⁺ TIC and 32% in the ESI⁻ TIC. The Phenyl-X desalting pre-column showed almost comparable TIC reduction properties like the RP material.

All in all, the RP pre-column showed the highest desalting capacity, and thus was employed for further analysis. The automated valve switching, analyte trapping and online desalting are the key

elements making the new workflow generic and robust compared to the initial setup [15]. Due to the poor pressure stability of the elution head-based interface (max. 60 bar for the TLC-MS Interface), its isolation via the switching valve from the high-pressure UPLC gradient (up to 600 bar) is mandatory. First this allows the integration of sophisticated UPLC columns with a better separation power, if required. An additional feature of the valve switching/analyte trapping/online desalting strategy was the simplicity to guide the solvent flow to waste in the elution position, and thus clean the elution head (Fig. 2A). This elution head rinsing was performed during the UPLC gradient at no extra time.

3.3. Optimization of zone transfer and ionization

To ensure that the analytes are eluted from the adsorbent layer and retarded on the second separation column, the elution time and elution solvent were studied. The higher the elution time was, the higher was the sample volume transferred to RP-HPLC. A commonly used elution solvent is methanol to transfer substances from the HPTLC plate into the (HR)MS system [2,10,27]. Water (or aqueous buffer) and methanol (or acetonitrile) were the only eligible elution solvents for adapting the used HPLC gradient. Methanol has a high elution strength on the RP adsorbent. Thus, for elution solvents with a high methanol portion, no hydrophobic analyte interactions are expected towards the RP column. In contrast, water has the highest solvent strength on the NP adsorbent. This was proven by the retention behavior of typical marker compounds of cinnamon, i.e., Ci, Co, CA and 2-MCA, eluted with different ratios of methanol and bidistilled water (Fig. 3A-D). Elution solvents containing less than 20% water were not able to extract the analytes out of the adsorbent layer. The mass traces revealed that Ci and Co were partially front-eluted with the elution solvent (injection mark). Moreover, the peak shapes were bimodal and broad for all tested substances. Elution in the range of 30-60% aqueous solvent caused bimodal peaks especially for Ci. The analytes were split up between the methanolic fraction of the elution solvent and methanolic fraction of the HPLC gradient. Co, CA and 2-MCA eluted

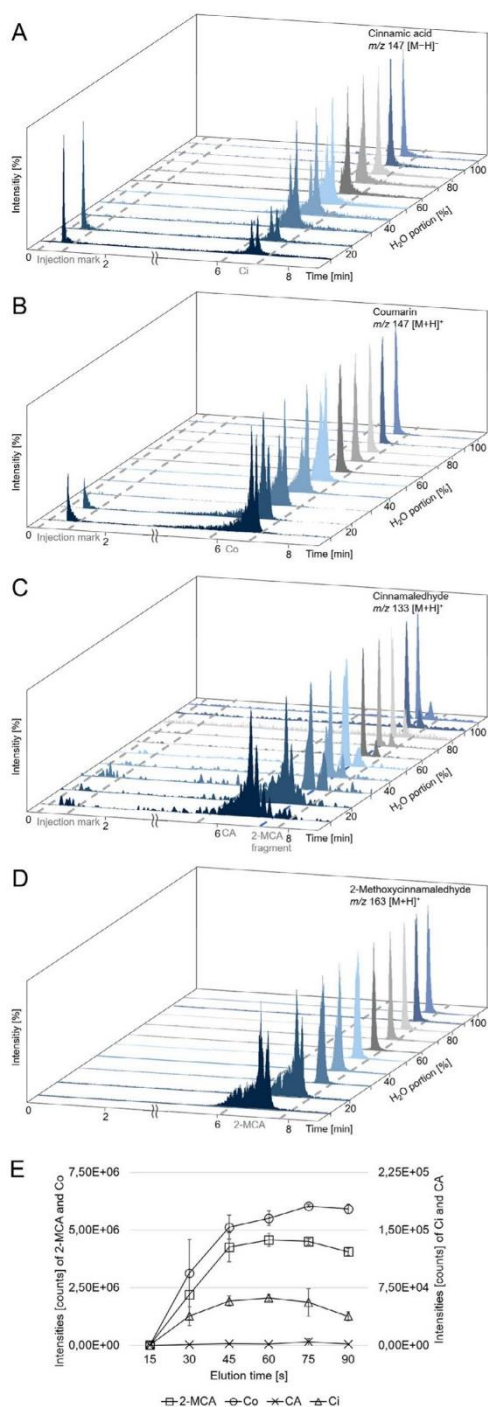


Fig. 3. Different ratios of methanol and bidistilled water were studied to elute the bioactive compounds Ci (A), Co (B), CA (C) and 2-MCA (D; each 500 ng/band, only applied) off the adsorbent for transfer to RP-HPLC-PDA-MS at a 0.1-mL/min flow rate for 45 s. The latter optimal elution time was found plotting signal intensities against duration of elution (E; $n = 3$).

later than Ci, and thus for the latter, the bimodal peak shape was more obvious. Using only 30% to 0% methanol, the retention behavior and peak shapes were satisfying. Since the standards are more middle polar to apolar, the elution with 90% bidistilled water was preferred.

In order to avoid a loss of analytes by a too short or too long elution time, it was studied and optimized for the given transfer lines over a wider polarity range of analytes. The elution time depended on solvent strength, selectivity and solubility. Eluting with 90% bidistilled water, the optimal elution time was figured out by plotting signal intensities against the duration of the elution (Fig. 3E). Within 15 s to 30 s the transferred analyte amount was too low to achieve repeatable results. Heart-cut analyte aliquots partially remained in the transfer tube from the elution head to the RP desalting device installed on the switching valve. The used 70-cm capillary tubing had an inner diameter of 0.13 mm, and thus a calculated volume of 9.3 μ L. Further, the unknown dead volume of the biocompatible inline filter had to be taken into account, just as the 50- μ L steel capillary, connecting the first position of the switching valve and the desalting device. At a flow rate of 0.1 mL/min an elution volume of 25 μ L (50 μ L) fills the capillaries on the way to the RP desalting device within 15 s (30 s), which explains the partial analyte loss for short elution times. A longer elution time of 45 s to 75 s led to repeatable results and did not differ considerably between analyses. Even longer elution times resulted in analyte losses due to breakthrough. Hence, a 45-s elution was found to be optimal, as it was considered as best compromise for a generic operation in a wide polarity range. Not only middle to apolar compounds (Fig. 3), but also highly polar compounds such as phenolic acids (Fig. 4) were successfully transferred to the second separation dimension.

3.4. 5D screening of 18 cinnamon samples

An overall screening of 18 different cinnamon extracts (Table S1) for their bioactive potential was performed. Along with these samples, important marker compounds of cinnamon, i.e. CA, 2-MCA, Co and Ci, were applied. The simultaneous separation of 18 samples under the same chromatographic conditions allows a reliable comparison [6]. The developed mobile phase toluene – ethyl acetate – methanol (6:3:1, V/V/V; MP6) was a good choice among the mobile phases investigated (Table S2 and Fig. S1) [28]. Although one mobile phase (MP5, containing *o*-phosphoric acid) showed a better zone resolution in FLD 366 nm, the acidic plate background could not be satisfyingly neutralized for the *A. fischeri* bioassay application.

For the same plate, versatile information was obtained due to the multi-imaging detection. The detection at white light illumination (Fig. 5A) showed that the co-extracted visual matrix remained on each application zone. This highlights a crucial advantage of HPTLC separations which is matrix robustness. The detection at UV 254 nm (Fig. 5B) showed the signals for Ci and the coeluting CA or 2-MCA in all samples. The amount of these analytes evident as dark zones of different intensity varied from sample to sample. The Co was only detected in samples 2, 6, 11 and 12. The detection at FLD 366 nm (Fig. 5C) showed only the blue fluorescent 2-MCA in all samples. Note that other not naively fluorescent components like CA can be hidden in the same zone. By comparing all the individual profiles only little differences were visible between the 18 screened cinnamon samples. In samples 2, 4, 6, 7, 11 and 14-16 comparatively fewer red fluorescent bands (chlorophylls) were visible in the lower part of the planar chromatogram.

In contrast, the *A. fischeri* bioautogram showed especially in the lower plate part much more differences in the bioactive compound profiles of the 18 cinnamons (Fig. 5D). Even after 30 min, the same active metabolites were detected in the bioactive compound pat-

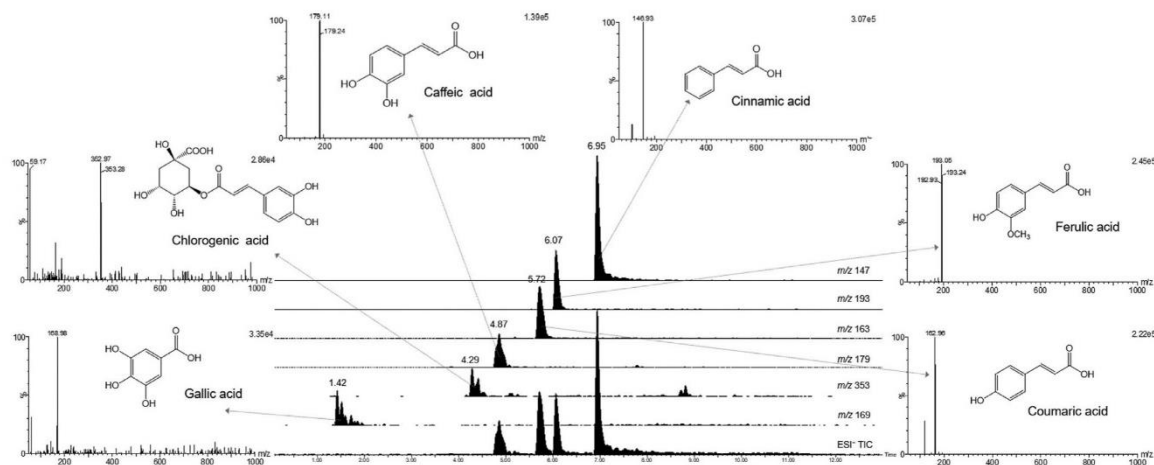


Fig. 4. Proof-of-concept for more polar phenolic acids (gallic, chlorogenic, caffeic, cinnamic, ferulic and coumaric acids, only applied) in ESI-TIC and respective XICs, eluted with 90% bidistilled water for 45 s at a flow rate of 0.1 mL/min from pre-washed MS-grade plates with 2 mL *A. fischeri* medium adsorbed.

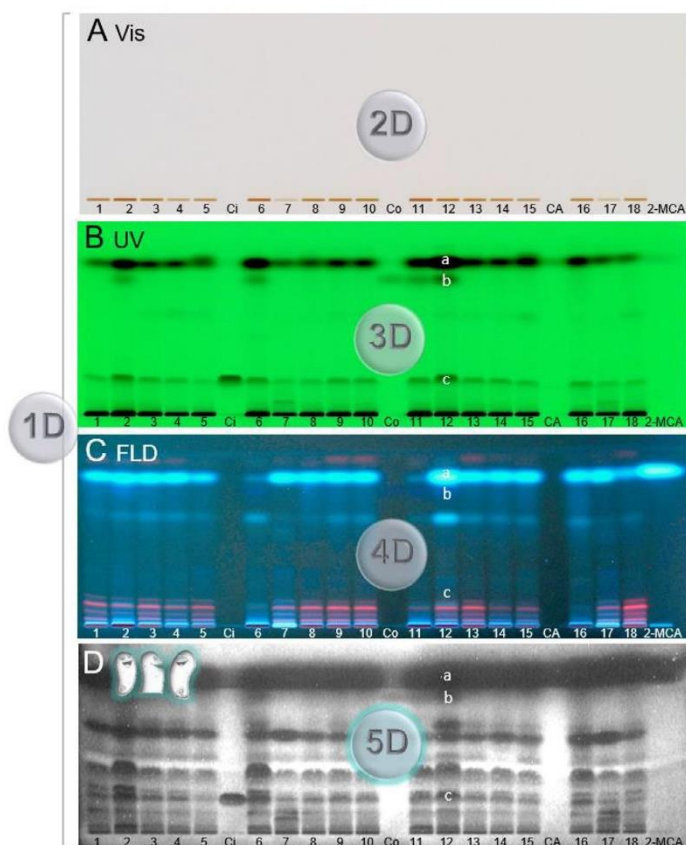


Fig. 5. Simultaneous screening of 18 cinnamon samples (Table S1) and important marker compounds Ci, Co, CA and 2-MCA (zones a-c in sample 12) developed with toluene – ethyl acetate – methanol (6:3:1, V/V/V) and detected at white light illumination (A), UV 254 nm (B), FLD 366 nm (C) and biologically via Gram-negative *A. fischeri* bacteria (the impairment of their bioluminescence and thus energetic metabolism was depicted as greyscale image, D).

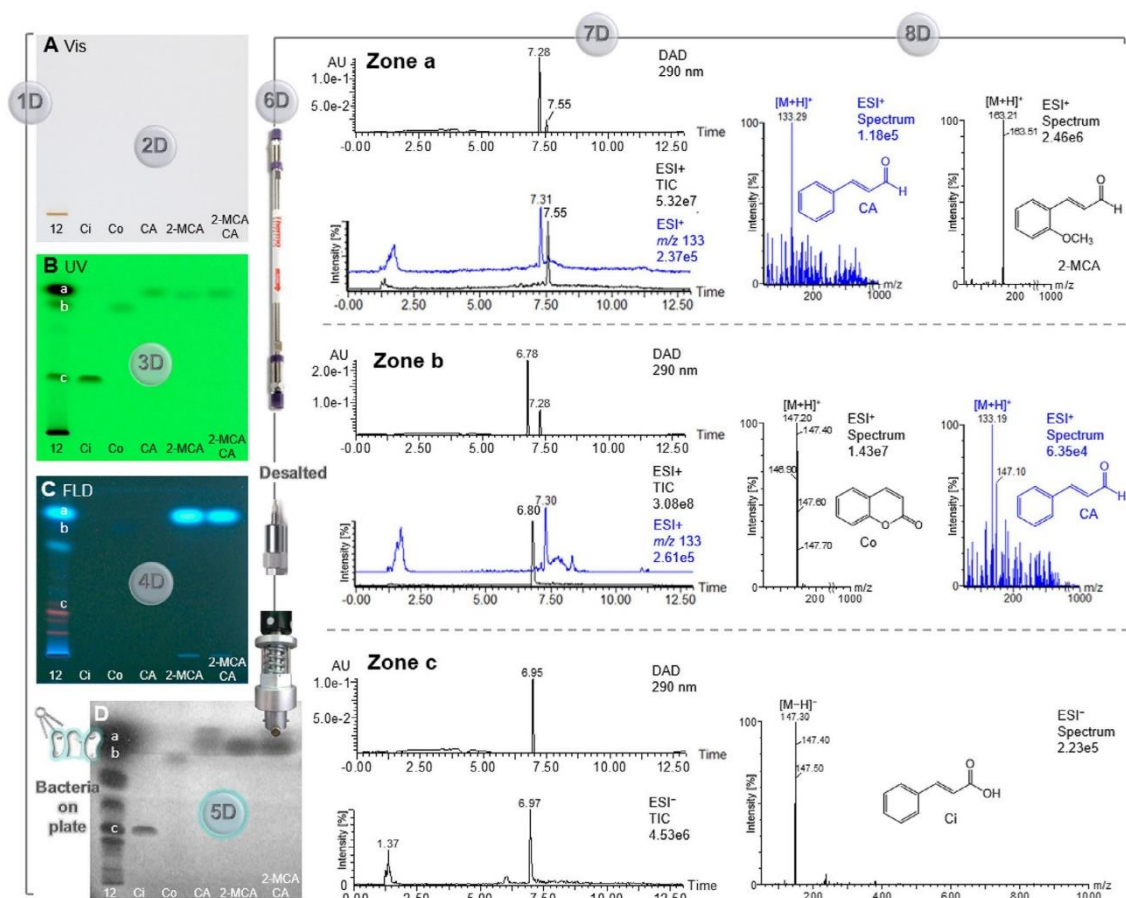


Fig. 6. HPTLC chromatograms of cinnamon extract 12 and four bioactive marker compounds Ci, Co, CA and 2-MCA developed with toluene – ethyl acetate – methanol (6:3:1, V/V/V) and documented at white light illumination (A), UV 254 nm (B), FLD 366 nm (C) and biologically via Gram-negative *A. fischeri* bacteria (D), followed by heart-cut elution of the active zones a–c, online desalting of bioassay medium salts and respective RP-HPLC–PDA–MS chromatograms and ESI-MS spectra (further spectral data in Fig. S7).

tern (Fig. S5). The aqueous/buffered bioassay environment caused that the *a priori* sharp zones of CA and 2-MCA diffused, resulting in a broadened dark inhibition zone (further information on diffusion effects in Fig. S6). Beside CA and 2-MCA, which are known for their antibacterial effects [29–32], Ci, Co and lots of further unidentified components induce a pathogenic impact on Gram-negative *A. fischeri* bacteria.

3.5. 8D hyphenation shown for cinnamon sample 12

Since there were only little differences in the compound profiles of the 18 different samples, sample 12 provided a comparatively high amount of 2-MCA and was chosen. It was subjected to the whole 8D hyphenation as proof-of-principle (Fig. 6). From the *A. fischeri* bioautogram (Fig. 6D), the bioactive zones of interest were immediately heart-cut eluted to the RP desalting device, and by valve switch, subjected to RP-HPLC–PDA–MS. Only the analytes together with residual bioassay ingredients were transferred to the orthogonal separation and detection. The filter frit at the output of the elution head and the biocompatible inline filter frit have pore sizes of 2 μm and 0.5 μm , respectively. Bacteria of the genus *Aliivibrio* have a width of 0.5 μm to 0.8 μm and a length of 1.4 μm to 2.6 μm [33] and cannot pass the filter frits. The bioassay

salt load was decreased by online desalting. Thus, interference-free chromatograms of the second orthogonal separation were obtained by PDA and MS (Fig. 6, 7D/8D).

Zone a showed two different signals at retention times of 7.28 min and 7.55 min at UV 290 nm, whereas only one dominant signal at 7.55 min (m/z 163 [M+H]⁺) was detected in the ESI⁺ TIC. Another very weak signal (m/z 133 [M+H]⁺) was revealed and the mass trace was extracted for a better visualization. The two coeluting substances in the planar chromatogram were now well separated due to the orthogonal column chromatographic separation and assigned to be CA and 2-MCA. The spectrum of CA was not interference-free and contained more noise compared to that of 2-MCA. This is explained by diffusion effects, as the *A. fischeri* medium consists mainly of water and salts [22]. CA has a water solubility of 1.72 g/L [34,35]. By spraying 2 mL culture suspension over a 20000-mm² area, 0.7 μL medium is sprayed over the 7-mm² CA zone of 500 ng. The quotient out of 500 ng CA and 700 μL medium load is 0.7 ng/nL, and thus the complete amount of CA is soluble in the over-sprayed medium. Comparing images at UV 254 nm before and after the *A. fischeri* bioassay, it is evident that the CA bands diffused (Fig. S6). A similar diffusion effect is evident for zone b (Co). In the initial image at UV 254 nm, the zones are well separated (Fig. 6B). Contrarily, the MS and PDA data showed

a diffusion of CA into zone b (Co) due to its diffusion caused by the very polar bioassay medium. The weak CA signal proved that it (zone a) was spread over a wider area, and thus on the adjacent zone b. However, the Co signal at m/z 147 $[M+H]^+$ was undoubtedly identified in the ESI⁺ TIC and PDA chromatograms. Zone c (Ci) showed only a single well-shaped peak both via the ESI⁻ TIC and PDA at 290 nm and was verified by its mass signal at 6.97 min (m/z 147 $[M-H]^-$). This is a good example for the outstanding, but underestimated separation quality of HPTLC. All spectral data were compared to standards (Fig. S7), undoubtedly identifying the analyzed bioactive compounds in the cinnamon samples with the new 8D hyphenation. All four identified compounds in the cinnamon samples were proven to be active against Gram-negative *A. fischeri* bacteria.

3.6. Benchmarking with status quo

The minimalistic sample preparation and matrix robustness of HPTLC is a key feature with regard to complex samples. The sample remains as native as possible, which is important for the non-target screening for bioactive unknown unknowns. In contrast, status-quo microtiter plate assays can only provide a sum parameter as result and are prone to matrix effects (as there is no separation). The ultimate objective is to find the most important bioactive substances in complex mixtures. Selecting a comprehensive technique of highest separation efficiency and sensitivity would increase the complexity, would make data acquisition/processing tedious and would distract from the essential. In the end, not all detected compounds can be clarified in the structure anyway. Why create a complexity that is then simplified to make it manageable? We judge the separation efficiency of HPTLC to be ideal for the transfer to the orthogonal dimension. A second separation of quite different selectivity is most efficient and structure elucidation is only made for the most bioactive zones [36,37]. The whole 8D procedure took 4 h for screening of 18 samples and characterization of 4 marker compounds (including recording of 2 background zones). In contrast, status-quo HPLC–HESI–HRMS non-target screening, regardless of bioactivity, takes about 30 min per sample, summing up to 9 h for 18 complex samples [36]. And yet the bioactivity is still not assigned, which needs additional labor time. In comparison, the 4-h all-inclusive bioanalytical 8D hyphenation is more efficient and straightforward. One could predict bioactivity of unknowns via Big Data tools, but it still poses a challenge in assigning individual components in complex mixtures, due to the diversity of identity and abundance of compounds [37]. In any case, the real biological evidence is required in the end. If compared to status-quo microtiter plate assays, planar assay workflows by HPTLC–EDA were faster and less expensive [38]. The serious question therefore arises as to whether the currently used mainstream techniques are still the best choice. With the routine use of this 8D hyphenation, savings in costs and analysis time are estimated to be higher than 60%.

4. Conclusions

The proof-of-principle of the developed robust 8D hyphenation was successfully demonstrated. The valve switching permitted analyte trapping, online desalting and the employment of high-pressure gradients. The second orthogonal separation column and gradient can easily be adjusted depending on the purpose, making it highly flexible. The salt load transfer to the MS system was reduced by up to 44% in ESI⁺-TIC-MS and >32% in ESI⁻-TIC-MS by a simple RP pre-column (compliant to the second separation column). The cinnamon samples showed that there are still some challenges. Due to the aqueous bioassay medium load on the plate,

diffusion of analytes may occur as observed for CA, but not for 2-MCA, Co and Ci. Such a phenomenon can be discovered and explained by comparison of the images before and after the bioassay. Low analyte concentrations are hardly recognizable in PDA chromatograms and in full scan MS spectra used for the presented non-target screening strategy. Apart from this, the focus on the most important bioactive compounds might already be sufficient work for the analyst. Hence, this 8D workflow is an outstanding approach to get a wealth of information on most potent bioactive unknown compounds in complex samples and any coeluting compounds in planar chromatography. The 8D workflow was developed and optimized based on mass spectral data directly recorded from the *A. fischeri* bioautogram. It showed that even highly salted medium did not influence the detection of coeluting substances. Hence, it is also a very good solution for the analysis of salt-rich industrial samples. This hyphenation can also be exploited for the integration of other bioassays and their respective media. The transfer to more sensitive HRMSⁿ systems can now be dared based on the progress. Depending on the available instrumentation, even 12D hyphenations are possible and focus of future studies.

Appendix A. Supplementary data

Supplementary data to this article (Tables S1 and S2; Figs. S1–S7) can be found online at...

CrediT authorship contribution statement

Tamara Schreiner: Conceptualization, Methodology, Experimental Analysis, Data Analysis, Writing – Original Draft. **Gertrud E. Morlock:** Conceptualization, Methodology, Supervision, Writing – Review and Editing.

Declaration of Competing Interest

The authors declare that they have no known competing financial interests or personal relationships that could have appeared to influence the work reported in this paper.

Acknowledgements

Thank is owed to Merck, Darmstadt, Germany for providing the plates as well as to Waters, Eschborn, Germany for technical support. Instrumentation was partially funded by the Deutsche Forschungsgemeinschaft (DFG, German Research Foundation) – INST 162/471-1 FUGG; INST 162/536-1 FUGG.

Supplementary materials

Supplementary material associated with this article can be found, in the online version, at doi:10.1016/j.chroma.2021.462154.

References

- [1] J.F. García-Reyes, M.D. Hernando, A. Molina-Díaz, A.R. Fernández-Alba, Comprehensive screening of target, non-target and unknown pesticides in food by LC-TOF-MS, *TrAC, Trends Anal. Chem.* 26 (2007) 828–841, doi:10.1016/j.trac.2007.06.006.
- [2] M. Jamshidi-Aidji, G.E. Morlock, Fast Equivalency Estimation of Unknown Enzyme Inhibitors *in Situ* the Effect-Directed Fingerprint, Shown for *Bacillus* Lipopeptide Extracts, *Anal. Chem.* 90 (2018) 14260–14268.
- [3] R. Díaz, M. Ibáñez, J.V. Sancho, F. Hernández, Target and non-target screening strategies for organic contaminants, residues and illicit substances in food, environmental and human biological samples by UHPLC-QTOF-MS, *Anal. Methods* 4 (2012) 196–209, doi:10.1039/C1AY05385J.
- [4] Y. Fu, C. Zhao, X. Lu, G. Xu, Nontargeted screening of chemical contaminants and illegal additives in food based on liquid chromatography–high resolution mass spectrometry, *TrAC, Trends Anal. Chem.* 96 (2017) 89–98, doi:10.1016/j.trac.2017.07.014.

- [5] G.E. Morlock, Chromatography Combined with Bioassays and Other Hyphenations – The Direct Link to the Compound Indicating the Effect, in: K. Jayaprakasha, B.S. Patil, Pillati F. (Eds.), *Instrumental Methods for the Analysis and Identification of Bioactive Molecules*, Washington D.C., 2014, pp. 101–121.
- [6] I.D. Wilson, U.A.T. Brinkman, Hype and hypernation: multiple hyphenation of column liquid chromatography and spectroscopy, *TrAC, Trends Anal. Chem.* 26 (2007) 847–854, doi:10.1016/j.trac.2007.07.007.
- [7] G. Morlock, W. Schwack, Hyphenations in planar chromatography, *J. Chromatogr. A* 1217 (2010) 6600–6609, doi:10.1016/j.chroma.2010.04.058.
- [8] M. Jamshidi-Aidji, G.E. Morlock, Bioprofiling of unknown antibiotics in herbal extracts: Development of a streamlined direct bioautography using *Bacillus subtilis* linked to mass spectrometry, *J. Chromatogr. A* 1420 (2015) 110–118.
- [9] Á.M. Mórícz, P.G. Ott, I. Yüce, A. Darcsi, S. Béni, G.E. Morlock, Effect-directed analysis via hyphenated high-performance thin-layer chromatography for bio-analytical profiling of sunflower leaves, *J. Chromatogr. A* 1533 (2018) 213–220, doi:10.1016/j.chroma.2017.12.034.
- [10] G.E. Morlock, I. Klingelhöfer, Liquid chromatography-bioassay-mass spectrometry for profiling of physiologically active food, *Anal. Chem.* 86 (2014) 8289–8295, doi:10.1021/ac501723j.
- [11] S. Krüger, L. Winheim, G.E. Morlock, Planar chromatographic screening and quantification of coumarin in food, confirmed by mass spectrometry, *Food Chem* 239 (2018) 1182–1191, doi:10.1016/j.foodchem.2017.07.058.
- [12] C.J. Pickens, I.A. Haidar Ahmad, A.A. Makarov, R. Bennett, B.F. Mann, E.L. Regalado, Comprehensive online multicolumn two-dimensional liquid chromatography-diode array detection-mass spectrometry workflow as a framework for chromatographic screening and analysis of new drug substances, *Anal. Bioanal. Chem.* 412 (2020) 2655–2663, doi:10.1007/s00216-020-02498-8.
- [13] C. Lotter, E. Poehler, J.J. Heiland, L. Mauritz, D. Belder, Enantioselective reaction monitoring utilizing two-dimensional heart-cut liquid chromatography on an integrated microfluidic chip, *Lab Chip* 16 (2016) 4648–4652, doi:10.1039/c6lc01138a.
- [14] C. Oellig, W. Schwack, Strategies of Coupling Planar Chromatography to HPLC-MS, in: T. Kowalska, M. Sajewicz, J. Sherma (Eds.), *Planar chromatography - mass spectrometry*, CRC Press, Boca Raton, London, New York, 2016, pp. 173–198.
- [15] S. Kirchert, G.E. Morlock, Orthogonal Hyphenation of Planar and Liquid Chromatography for Mass Spectrometry of Biomarkers out of the Bioassay Matrix (NP-HPTLC-UV/vis/FLD-Bioassay-RP/IEH-HPLC-UV/vis-ESI-MS), *Anal. Chem.* 92 (2020) 9057–9064, doi:10.1021/acs.analchem.0c01251.
- [16] W. Kukula-Koch, T. Mroczek, Application of hydrostatic CCC–TLC–HPLC–ESI–TOF–MS for the bioguided fractionation of anticholinesterase alkaloids from *Argemone mexicana* L. roots, *Anal. Bioanal. Chem.* 407 (2015) 2581–2589, doi:10.1007/s00216-015-8468-x.
- [17] W. Schwack, E. Pellissier, G. Morlock, Analysis of unauthorized Sudan dyes in food by high-performance thin-layer chromatography, *Anal. Bioanal. Chem.* 410 (2018) 5641–5651, doi:10.1007/s00216-018-0945-6.
- [18] H.-K. Min, S.-W. Hyung, J.-W. Shin, H.-S. Nam, S.-H. Ahn, H.J. Jung, S.-W. Lee, Ultrahigh-pressure dual online solid phase extraction/capillary reverse-phase liquid chromatography/tandem mass spectrometry (DO-SPE/cRPLC/MS/MS): a versatile separation platform for high-throughput and highly sensitive proteomic analyses, *Electrophoresis* 28 (2007) 1012–1021, doi:10.1002/elps.200600501.
- [19] H. Luo, W. Zhong, J. Yang, P. Zhuang, F. Meng, J. Caldwell, B. Mao, C.J. Welch, 2D-LC as an on-line desalting tool allowing peptide identification directly from MS unfriendly HPLC methods, *J. Pharm. Biomed. Anal.* 137 (2017) 139–145, doi:10.1016/j.jpba.2016.11.012.
- [20] Kenneth J. Fountain, Martin Gilar, John C. Gebler, Electrospray ionization mass spectrometric analysis of nucleic acids using high-throughput on-line desalting, *Rapid Commun. Mass Spectrom.* 18 (2004) 1295–1302.
- [21] Jörgen Bengtsson, Britt Jansson, Margareta Hammarlund-Udenaes, On-line desalting and determination of morphine, morphine-3-glucuronide and morphine-6-glucuronide in microdialysis and plasma samples using column switching and liquid chromatography/tandem mass spectrometry, *Rapid Commun. Mass Spectrom.* 19 (2005) 2116–2122.
- [22] *European Committee for Standardization, Water quality - Determination of the inhibitory effect of water samples on the light emission of Vibrio fischeri (Luminescent bacteria test): Part 1: Method using freshly prepared bacteria*, 2009.
- [23] S. Krüger, L. Hüsken, R. Fornasari, I. Scainelli, G.E. Morlock, Effect-directed fingerprints of 77 botanical extracts via a generic high-performance thin-layer chromatography method combined with assays and mass spectrometry, *J. Chromatogr. A* 1529 (2017) 93–106, doi:10.1016/j.chroma.2017.10.068.
- [24] G.K. Jayaprakasha, P.S. Negi, B.S. Jena, L. Jagan Mohan Rao, Antioxidant and antimutagenic activities of *Cinnamomum zeylanicum* fruit extracts, *J. Food Compos. Anal.* 20 (2007) 330–336.
- [25] P. Kawatra, R. Rajagopalan, Cinnamon: Mystic powers of a minute ingredient, *Pharmacogn. Res.* 7 (2015) 1–6.
- [26] C. Selkirk, Ion-exchange chromatography, in: P. Cutler (Ed.), *Protein purification protocols*, second ed., Humana, Totowa N.J., 2004, pp. 125–131.
- [27] H.-R. Adhami, U. Scherer, H. Kaehlig, T. Hettich, G. Schlotterbeck, E. Reich, L. Krenn, Combination of bioautography with HPTLC-MS/NMR: a fast identification of acetylcholinesterase inhibitors from galbanum(?), *Phytochem. Anal.* 24 (2013) 395–400, doi:10.1002/pca.2422.
- [28] N.G.A.S. Sumudu Chandana, G.E. Morlock, Eight different bioactivity profiles of 40 cinnamons by multi-imaging planar chromatography hyphenated with effect-directed assays and high-resolution mass spectrometry, *Food Chem* (2021) 129135, doi:10.1016/j.foodchem.2021.129135.
- [29] R. Di Pasqua, G. Betts, N. Hoskins, M. Edwards, D. Ercolini, G. Mauriello, Membrane toxicity of antimicrobial compounds from essential oils, *J. Agric. Food Chem.* 55 (2007) 4863–4870, doi:10.1021/jf0636465.
- [30] P. Domadia, S. Swarup, A. Bhunia, J. Sivaraman, D. Dasgupta, Inhibition of bacterial cell division protein FtsZ by cinnamaldehyde, *Biochem. Pharmacol.* 74 (2007) 831–840, doi:10.1016/j.bcp.2007.06.029.
- [31] M. Friedman, Chemistry, Antimicrobial Mechanisms, and Antibiotic Activities of Cinnamaldehyde against Pathogenic Bacteria in Animal Feeds and Human Foods, *J. Agric. Food Chem.* 65 (2017) 10406–10423, doi:10.1021/acs.jafc.7b04344.
- [32] F. Huang, J. Kong, J. Ju, Y. Zhang, Y. Guo, Y. Cheng, H. Qian, Y. Xie, W. Yao, Membrane damage mechanism contributes to inhibition of *trans*-cinnamaldehyde on *Penicillium italicum* using Surface-Enhanced Raman Spectroscopy (SERS), *Sci. Rep.* 9 (2019) 490.
- [33] S.L. Drake, A. DePaola, L.-A. Jaykus, An Overview of *Vibrio vulnificus* and *Vibrio parahaemolyticus*, *Compr. Rev. Food Sci. Food Saf.* 6 (2007) 120–144, doi:10.1111/j.1541-4337.2007.00022.x.
- [34] I.M. Helander, H.-L. Alakomi, K. Latva-Kala, T. Mattila-Sandholm, I. Pol, E.J. Smid, L.G.M. Gorris, A. von Wright, Characterization of the Action of Selected Essential Oil Components on Gram-Negative Bacteria, *J. Agric. Food Chem.* 46 (1998) 3590–3595.
- [35] H. Chen, P.M. Davidson, Q. Zhong, Impacts of sample preparation methods on solubility and antimicrobial characteristics of essential oil components in milk, *Appl. Environ. Microbiol.* 80 (2014) 907–916, doi:10.1128/AEM.03010-13.
- [36] E. Azadnia, L. Goldoni, T. Bandiera, G.E. Morlock, Same analytical method for both (bio)assay and zone isolation to identify/quantify bioactive compounds by quantitative nuclear magnetic resonance spectroscopy, *J. Chromatogr. A* 1628 (2020) 461434, doi:10.1016/j.chroma.2020.461434.
- [37] L.K. Caesar, J.J. Kellogg, O.M. Kvalheim, N.B. Cech, Opportunities and Limitations for Untargeted Mass Spectrometry Metabolomics to Identify Biologically Active Constituents in Complex Natural Product Mixtures, *J. Nat. Prod.* 82 (2019) 469–484, doi:10.1021/acs.jnatprod.9b00176.
- [38] E. Azadnia, J. Mollergues, T. Stroheker, K. Billerbeck, G.E. Morlock, New incorporation of the S9 metabolizing system into methods for detecting acetylcholinesterase inhibition, *Anal. Chim. Acta* 1129 (2020) 76–84, doi:10.1016/j.aca.2020.06.033.

Supplementary information

Non-target bioanalytical eight-dimensional hyphenation including bioassay, heart-cut trapping, online desalting, orthogonal separations and mass spectrometry

Tamara Schreiner, Gertrud E. Morlock*

Chair of Food Science, Institute of Nutritional Science, and Interdisciplinary Research Center
(iFZ), Justus Liebig University Giessen, Heinrich-Buff-Ring 26-32, 35392 Giessen, Germany

*Corresponding Author: phone +49-641-99-39141; fax +49-641-99-39149

gertrud.morlock@uni-giessen.de

Table of Contents

Page S-3	Table S1. Compilation of the investigated 18 cinnamon samples, including weight (W) extracted in 2 mL methanol – water (4:1, V/V).
Page S-4	Table S2. Investigation of mobile phase (MP) systems for cinnamon extract separation on HPTLC plates silica gel 60 F ₂₅₄ MS-grade.
Page S-5	Fig. S1. HPTLC chromatograms at UV 366 nm of cinnamon extracts 3 and 7 (Table S1) on HPTLC plates silica gel 60 F ₂₅₄ MS-grade with mobile phase (MP) systems 1–16 (Table S2).
Page S-6	Fig. S2. Instrumental set up for zone elution with online desalting and subsequent RP-HPLC-DAD-MS analysis.
Page S-7	Fig. S3. Development of the full scan MS method with regard to cone voltage (CV) and scan frequency (SF) on the examples of 2-methoxycinnamaldehyde (2-MCA), coumarin (Co), cinnamaldehyde (CA) and cinnamic acid (Ci).
Page S-8	Fig. S4. Reduction of <i>A. fischeri</i> bioassay medium load by online desalting: mean full scan MS spectra of the bioassay load/plate background ($n = 2$) via the tested desalting devices; eluted with 90% bidistilled water for 45 s at a flow rate of 0.1 mL/min from pre-washed MS-grade plates with 2 mL <i>A. fischeri</i> medium adsorbed; respective mean TIC reduction in Fig. 2.
Page S-9	Fig. S5. Documentation of the bioautographic profile over 30 min (10 images were taken): Simultaneous screening of 18 cinnamon samples and the important marker compounds 2-methoxycinnamaldehyde (2-MCA), coumarin (Co), cinnamaldehyde (CA) and cinnamic acid (Ci) developed with toluene – ethyl acetate – methanol (6:3:1, V/V/V) and detected biologically (bioluminescence of Gram-negative <i>A. fischeri</i> bacteria depicted as greyscale image). Even 30 min after the bioassay application, the bioactive compound pattern of the 18 cinnamons was comparable and still the same active metabolites were detected.
Page S-10	Fig. S6. Major diffusion effects (framed red) caused by the <i>A. fischeri</i> bioassay medium after separation of cinnamon sample 12 as well as 2-methoxycinnamaldehyde (2-MCA), coumarin (Co), cinnamaldehyde (CA) and cinnamic acid (Ci) with toluene – ethyl acetate – methanol (6:3:1, V/V/V); documented before versus after the <i>A. fischeri</i> bioassay at UV 254 nm (A) and 366 nm (B).
Page S-11	Fig. S7. Further spectral data of zones a–c in cinnamon sample 12, analyzed as in Fig. 5.

Table S1. Compilation of the investigated 18 cinnamon samples, including weight (W) extracted in 2 mL methanol – water (4:1, V/V).

No.	Label	Manufacturer	Origin	Plant	W [mg]
1	Ceylon cinnamon, ground	Gewürzkarawane, Freiburg, Germany	Ceylon	<i>C. verum</i>	200.8
2	Cinnamon, ground	Ezogelin Gewürze, Heilbronn, Germany	not specified	<i>C. cassia</i>	200.5
3	Ceylon cinnamon, ground	Alnatura, Bickenbach, Germany	Madagaskar	<i>C. verum</i>	201.9
4	Ceylon cinnamon	Gewürze-Kräuter-Tee Jorge Gonzalez, Sasbach Germany	Ceylon	<i>C. verum</i>	201.4
5	Cinnamon sticks, ground	NGR Products, Bremen, Germany	Sri Lanka	<i>C. verum</i>	200.7
6	Cinnamon, ground and germ-reduced	Fa. Koninklijke Euroma B.V., Wapenveld, Netherlands	not specified	not specified	200.0
7	Organic ceylon cinnamon, ground, fine and sweet	H F Hanseatic Fine Food, Bad Oldesloe, Germany	Sri Lanka	<i>C. verum</i>	199.9
8	Ceylon cinnamon, ground	Siegfried-Klein, Bönningheim, Germany	Ceylon	<i>C. verum</i>	205.4
9	Ceylon cinnamon, ground	Alnatura, Bickenbach, Germany	Madagaskar	<i>C. verum</i>	197.7
10	Ceylon cinnamon, ground	Alnatura, Bickenbach, Germany	Madagaskar	<i>C. verum</i>	201.4
11	Cinnamon, ground	Omega Großhandel, Essingen, Germany	not specified	<i>C. cassia</i>	200.3
12	Cinnamon, ground	Hela, Ahrensburg, Germany	not specified	not specified	202.0
13	Ceylon cinnamon, ground	Lebensbaum Diepholz, Germany	Madagaskar	<i>C. verum</i>	202.4
14	Cinnamon, ground premium quality	1001 Frucht, Regensburg, Germany	Ceylon	<i>C. verum</i>	201.4
15	Organic ceylon cinnamon, ground	Cosmoveda, Berlin, Germany	Ceylon	<i>C. verum</i>	200.2
16	Tansania ceylon cinnamon	Pfefferkontor, Berlin, Germany	Tansania	<i>C. verum</i>	200.3
17	Organic ceylon cinnamon	Simone Wertz, Gersten, Germany	Ceylon	<i>C. verum</i>	201.4
18	Cinnamon, ground, type: Ceylon-mild	Sonnentor Kräuterhandel, Sprögnitz, Austria	Madagaskar	<i>C. verum</i>	202.9

Table S2. Investigation of mobile phase (MP) systems for cinnamon extract separation on HPTLC plates silica gel 60 F₂₅₄ MS-grade.

No.	MP system ¹	Ratio (all V/V)	Distance	Literature
1	Petroleum ether:CH ₂ Cl ₂ :FA	20:40:1		[1]
2	Toluene:EtOAc	93:7		[2]
3	<i>n</i> -Hexane:EtOAc	18:7		[3]
4	Toluene:EtOAc:MeOH:H ₂ O:FA	60:85:45:10:5		-
5	Toluene:EtOAc:MeOH:H ₂ O: <i>o</i> -phosphoric acid	60:85:45:10:1		-
6	Toluene:EtOAc:MeOH	6:3:1		-
7	<i>n</i> -Hexane:toluene:EtOAc:MeOH	2:4:3:1		-
8	Toluene:EtOAc:MeOH	3:1:1		-
9	1) Toluene:EtOAc:MeOH 2) ACN:H ₂ O:FA	5:3:2 41:8:1	70 mm 30 mm	-
10	EtOAc:pyridine:MeOH:H ₂ O	80:20:10:5		[4]
11	Toluene:diethyl ether:FA	10:10:1		-
12	Toluene:EtOAc:MeOH:FA	12:10:1:1		-
13	1) Toluene:diethyl ether:FA 2) ACN:H ₂ O:FA	10:10:1 41:8:1	70 mm 30 mm	-
14	CHCl ₃ :EtOAc:MeOH:FA	4:3:2:1		[5]
15	MeOH:H ₂ O:EtOAc: <i>n</i> -hexane	gradient		[6]

¹Dichloromethane CH₂Cl₂, formic acid FA, ethyl acetate EtOAc, methanol MeOH, bidistilled water H₂O, chloroform CHCl₃, acetonitrile ACN

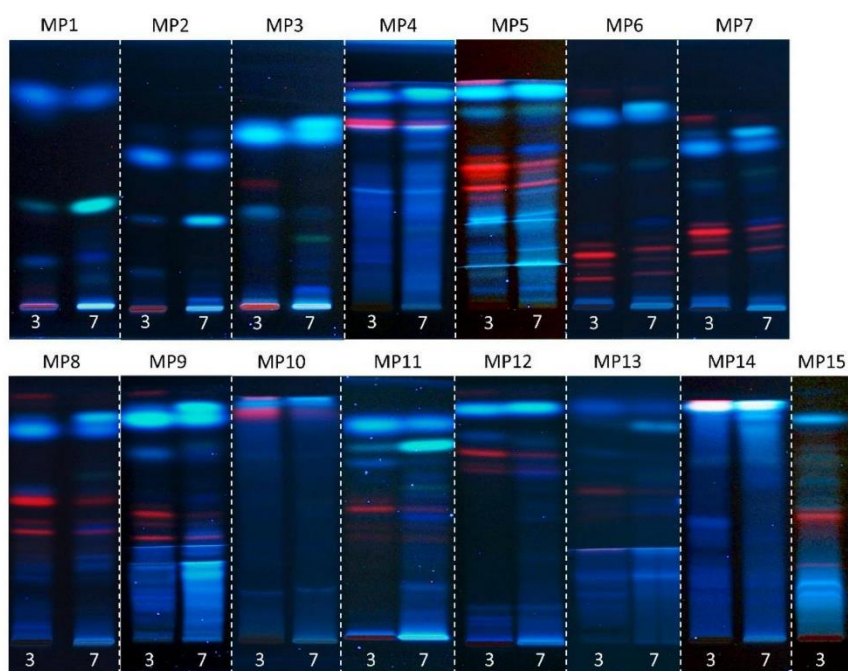


Fig. S1. HPTLC chromatograms at UV 366 nm of cinnamon extracts 3 and 7 (Table S1) on HPTLC plates silica gel 60 F₂₅₄ MS-grade with mobile phase (MP) systems 1–16 (Table S2).

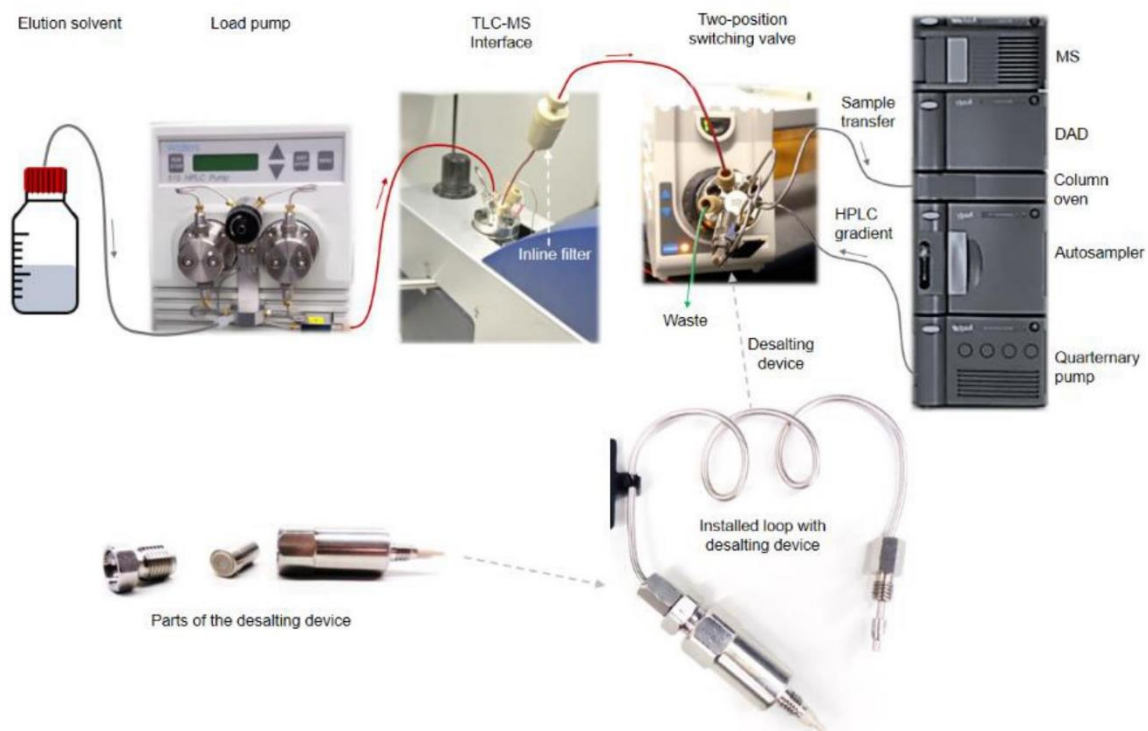


Fig. S2. Instrumental set-up for zone elution with installed online desalting device and subsequent RP-HPLC-DAD-MS analysis.

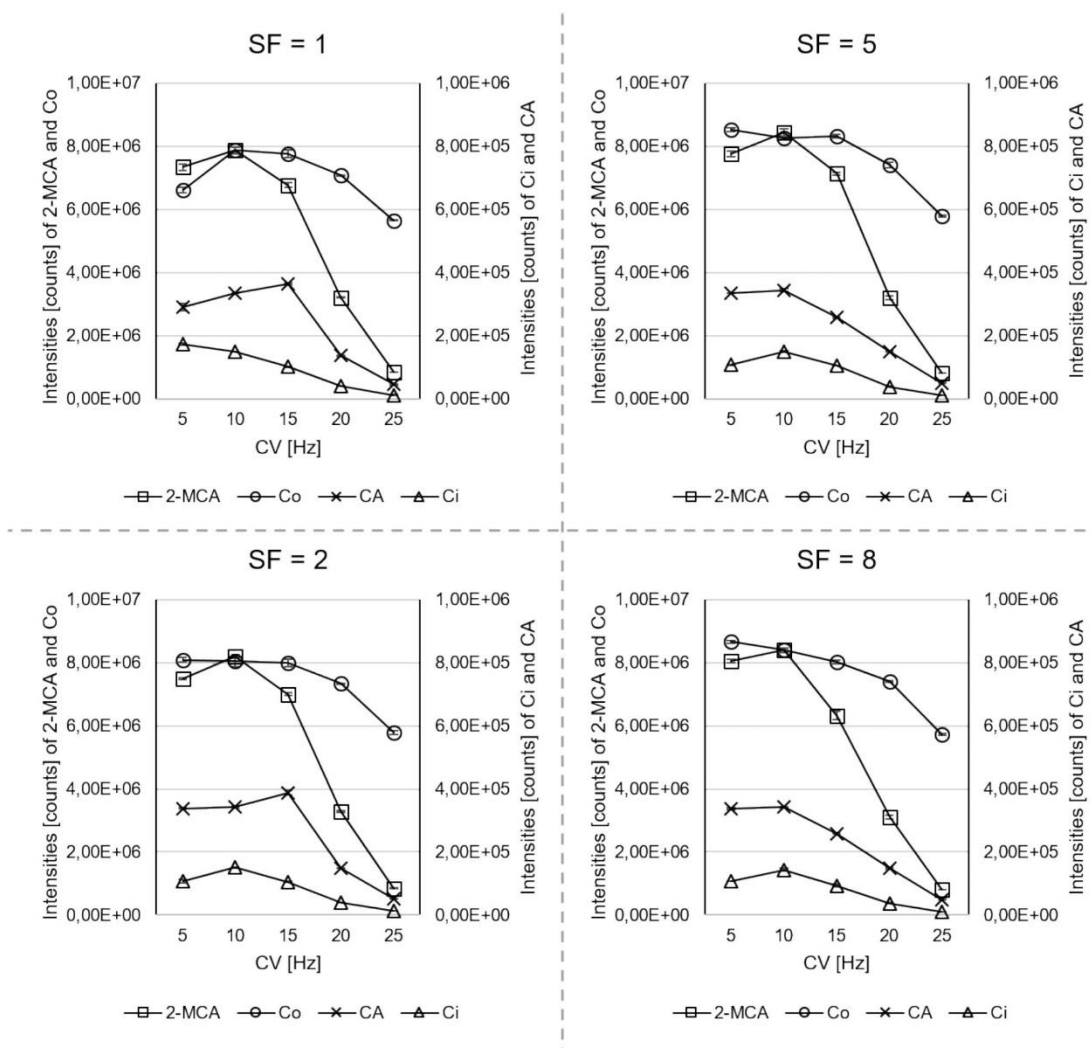


Fig. S3. Development of the full scan MS method with regard to cone voltage (CV) and scan frequency (SF) on the examples of 2-methoxycinnamaldehyde (2-MCA), coumarin (Co), cinnamaldehyde (CA) and cinnamic acid (Ci).

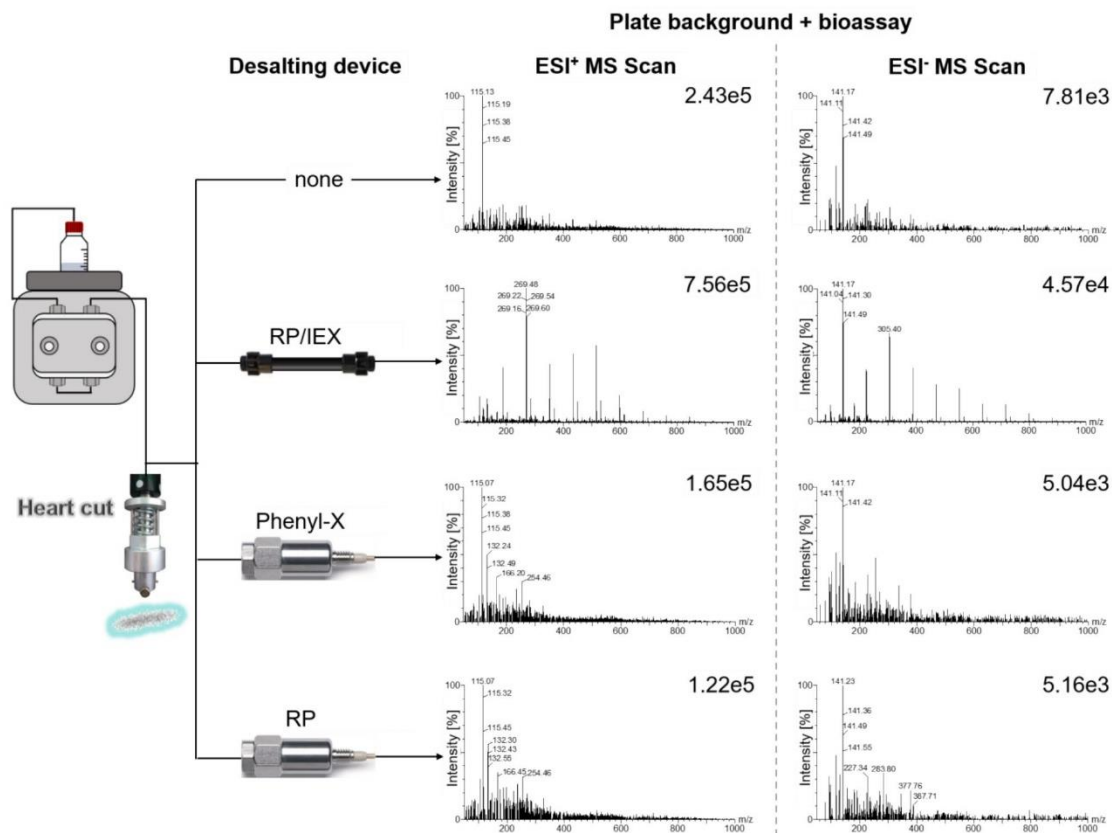


Fig. S4. Reduction of *A. fischeri* bioassay medium load by online desalting: mean full scan MS spectra of the bioassay load/plate background ($n = 2$) via the tested desalting devices; eluted with 90% bidistilled water for 45 s at a flow rate of 0.1 mL/min from pre-washed MS-grade plates with 2 mL *A. fischeri* medium adsorbed; respective mean TIC reduction in Fig. 2.

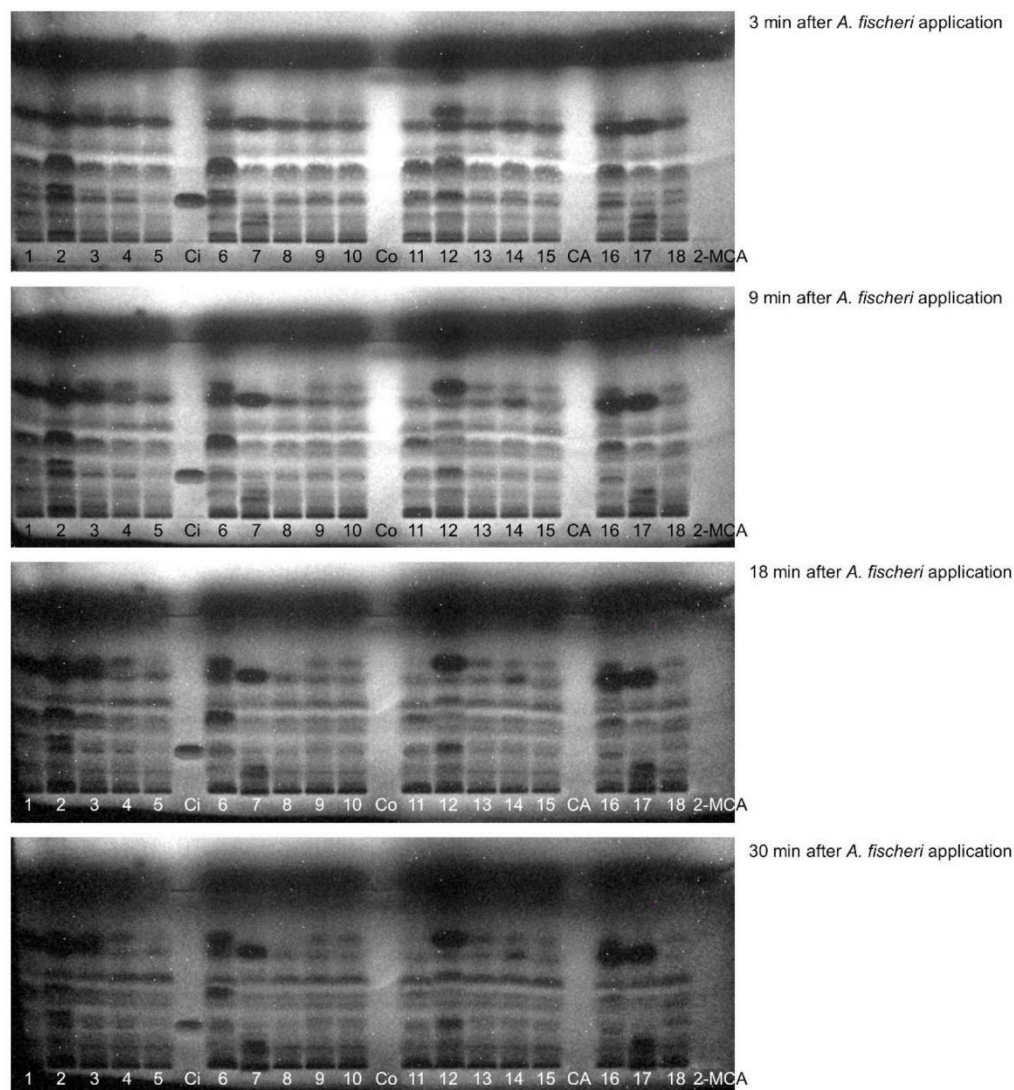


Fig. S5. Documentation of the bioautographic profile over 30 min (10 images were taken): Simultaneous screening of 18 cinnamon samples and the important marker compounds 2-methoxycinnamaldehyde (2-MCA), coumarin (Co), cinnamaldehyde (CA) and cinnamic acid (Ci) developed with toluene – ethyl acetate – methanol (6:3:1, V/V/V) and detected biologically (bioluminescence of Gram-negative *A. fischeri* bacteria depicted as greyscale image). Even 30 min after the bioassay application, the bioactive compound pattern of the 18 cinnamons was comparable and still the same active metabolites were detected.

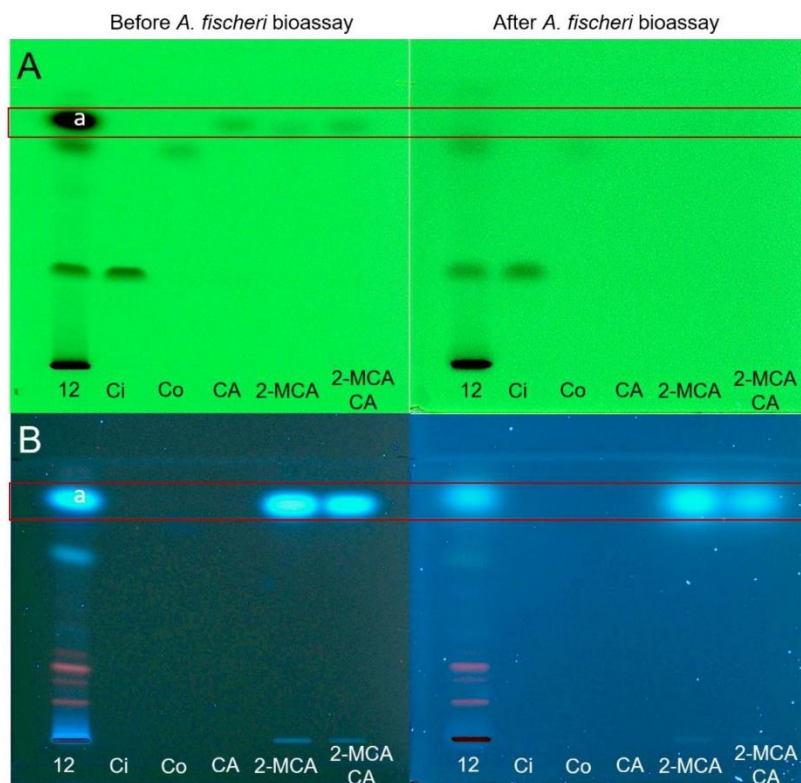
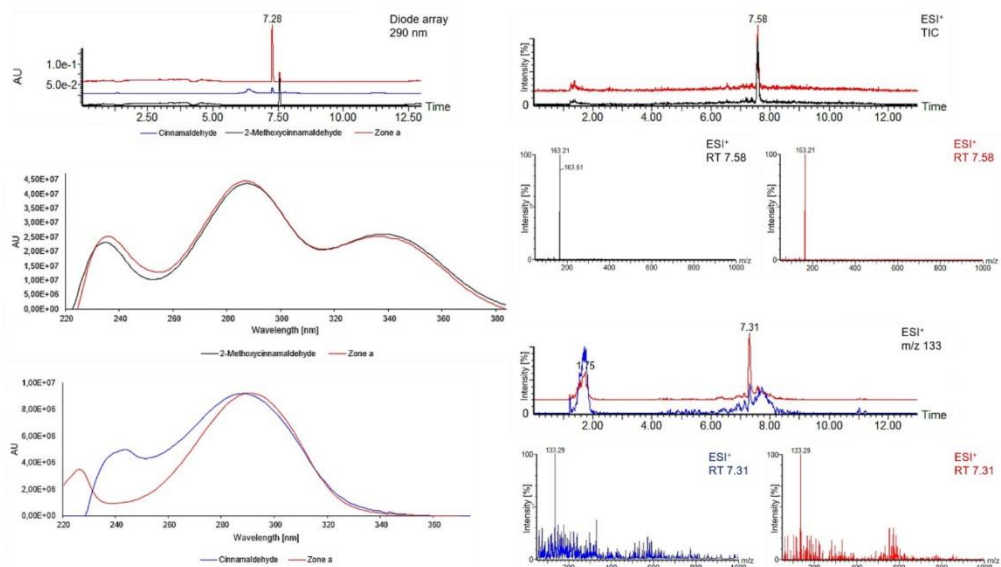
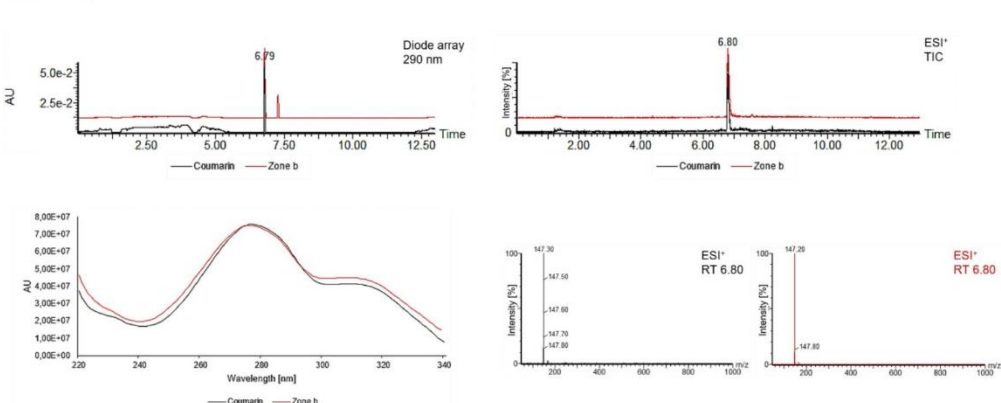


Fig. S6. Major diffusion effects (framed red) caused by the *A. fischeri* bioassay medium after separation of cinnamon sample 12 as well as 2-methoxycinnamaldehyde (2-MCA), coumarin (Co), cinnamaldehyde (CA) and cinnamic acid (Ci) with toluene – ethyl acetate – methanol (6:3:1, V/V/V); documented before *versus* after the *A. fischeri* bioassay at UV 254 nm (A) and 366 nm (B).

Zone a



Zone b



Zone c

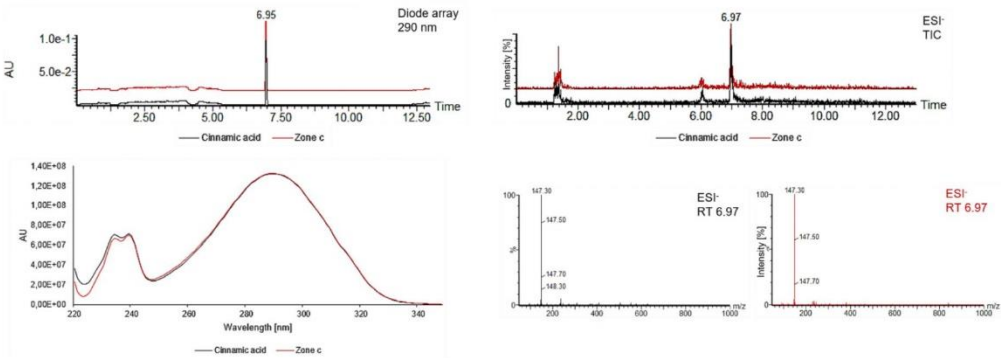


Fig. S7. Further spectral data of zones a-c in cinnamon sample 12, analyzed as in Fig. 5.

References

- [1] C.L. Gopu, S. Aher, H. Mehta, A.R. Paradkar, K.R. Mahadik, Simultaneous determination of cinnamaldehyde, eugenol and piperine by HPTLC densitometric method, *Phytochem Anal* 19 (2008) 116–121.
- [2] G. Horváth, N. Jámor, A. Végh, A. Böszörményi, É. Lemberkovics, É. Héthelyi, K. Kovács, B. Kocsis, Antimicrobial activity of essential oils: the possibilities of TLC-bioautography, *Flavour Fragr. J.* 25 (2010) 178–182.
- [3] M. Yamunadevi, E.G. Wesely, M. Johnson, Phytochemical studies on the terpenoids of medicinally important plant *Aerva lanata* L. using HPTLC, *Asian Pacific Journal of Tropical Biomedicine* 1 (2011) 220-225.
- [4] M. Medić-Šarić, I. Jasprica, A. Mornar, Ž. Maleš, Application of TLC in the Isolation and Analysis of Flavonoids, in: M. Waksmundzka-Hajnos, J. Sherma, T. Kowalska (Eds.), *Thin Layer Chromatography in Phytochemistry: 16 Application of TLC in the Isolation and Analysis of Flavonoids*, CRC Press, 2008, pp. 405–424.
- [5] W. Jesionek, B. Majer-Dziedzic, I.M. Choma, Separation, Identification, and Investigation of Antioxidant Ability of Plant Extract Components Using TLC, LC–MS, and TLC–DPPH •, *J. Liq. Chromatogr. Related Technol.* 38 (2015) 1147–1153.
- [6] K. Misra, R. Tulsawani, R. Shyam, D.K. Meena, G. Morlock, Hyphenated High-Performance Thin-Layer Chromatography for Profiling of some Indian Natural Efficiency Enhancers, *J. Liq. Chromatogr. Related Technol.* 35 (2012) 1364–1387.

3. Publication 2

Is Our Natural Food Our Homeostasis? Array of a Thousand Effect-Directed Profiles of 68 Herbs and Spices

Tamara Schreiner, Dorena Sauter, Maren Friz, Julia Heil, Gertrud E. Morlock*

Institute of Nutritional Science, Chair of Food Science, and TransMIT Center for
Effect-Directed Analysis, Justus Liebig University Giessen, Giessen, Germany

Dedicated to the 75th birthday of Prof. Dr. Teresa Kowalska, University of Silesia, Poland

Published in

Frontiers in Pharmacology, 12 (2021) 755941

Received 9 August 2021; Accepted 3 November 2021; Published 9 December 2021



Is Our Natural Food Our Homeostasis? Array of a Thousand Effect-Directed Profiles of 68 Herbs and Spices

Tamara Schreiner, Dorena Sauter, Maren Friz, Julia Heil and Gertrud Elisabeth Morlock*

Institute of Nutritional Science, Chair of Food Science, and TransMIT Center for Effect-Directed Analysis, Justus Liebig University Giessen, Giessen, Germany

OPEN ACCESS

Edited by:

Michael Heinrich,
UCL School of Pharmacy,
United Kingdom

Reviewed by:

Yusuf Kamisah,
Universiti Kebangsaan Malaysia,
Malaysia
David Morton,
La Trobe University, Australia

*Correspondence:

Gertrud Elisabeth Morlock
gertrud.morlock@uni-giessen.de

Dedicated to the 75th birthday of Prof.
Dr. Teresa Kowalska,
University of Silesia, Poland

Specialty section:

This article was submitted to
Ethnopharmacology,
a section of the journal
Frontiers in Pharmacology

Received: 09 August 2021

Accepted: 03 November 2021

Published: 09 December 2021

Citation:

Schreiner T, Sauter D, Friz M, Heil J
and Morlock GE (2021) Is Our Natural
Food Our Homeostasis? Array of a
Thousand Effect-Directed Profiles of
68 Herbs and Spices.
Front. Pharmacol. 12:755941.
doi: 10.3389/fphar.2021.755941

The beneficial effects of plant-rich diets and traditional medicines are increasingly recognized in the treatment of civilization diseases due to the abundance and diversity of bioactive substances therein. However, the important active portion of natural food or plant-based medicine is presently not under control. Hence, a paradigm shift from quality control based on marker compounds to effect-directed profiling is postulated. We investigated 68 powdered plant extracts (botanicals) which are added to food products in food industry. Among them are many plants that are used as traditional medicines, herbs and spices. A generic strategy was developed to evaluate the bioactivity profile of each botanical as completely as possible and to straightforwardly assign the most potent bioactive compounds. It is an 8-dimensional hyphenation of normal-phase high-performance thin-layer chromatography with multi-imaging by ultraviolet, visible and fluorescence light detection as well as effect-directed assay and heart-cut of the bioactive zone to orthogonal reversed-phase high-performance liquid chromatography–photodiode array detection–heated electrospray ionization mass spectrometry. In the non-target, effect-directed screening via 16 different on-surface assays, we tentatively assigned more than 60 important bioactive compounds in the studied botanicals. These were antibacterials, estrogens, antiestrogens, androgens, and antiandrogens, as well as acetylcholinesterase, butyrylcholinesterase, α -amylase, α -glucosidase, β -glucosidase, β -glucuronidase, and tyrosinase inhibitors, which were on-surface heart-cut eluted from the bioautogram or enzyme inhibition autogram to the next dimension for further targeted characterization. This biological-physicochemical hyphenation is able to detect and control active mechanisms of traditional medicines or botanicals as well as the essentials of plant-based food. The array of 1,292 profiles (68 samples \times 19 detections) showed the versatile bioactivity potential of natural food. It reveals how efficiently and powerful our natural food contributes to our homeostasis.

Keywords: botanical, effect-directed analysis, 8D hyphenation, high-performance thin-layer chromatography, high-performance liquid chromatography, mass spectrometry

1 INTRODUCTION

Herbs and spices are widely used for nutrition, flavoring, cosmetics, dyeing, or fragrances (Guldiken et al., 2018). They are also applied in medicine due to their known beneficial effects on human health (Yuan et al., 2016; Caesar et al., 2019), inspired by traditional healers who have used botanical extracts since ancient times (Belwal et al., 2018b). The knowledge of biologically active plants, their harvesting, production, preparation, and administration has been passed down through thousands of years of traditional medicine (Yuan et al., 2016). Particularly phenols were reported to have antibacterial, antiviral, and antioxidant effects, as well as the ability to modulate enzyme activity and transduction pathways (Krüger et al., 2017; Tresserra-Rimbau et al., 2018). Some studies have quantified the total amount of healthful constituents in herbal extracts and calculated the recommended intake of antioxidants from culinary herbs (Halvorsen et al., 2002; Wojdylo et al., 2007). However, their multifactorial relevance in homeostasis is underexplored. It is evident that the use of the whole natural plant extract is more powerful for homeostasis due to the versatility of the gentle mechanisms of active compounds than the use of isolated compounds (Morlock and Heil, 2020).

In a typical screening for potential drug candidates, plant extracts are currently freed from assay-interfering tannins by solid-phase extraction, separated with an HPLC gradient (42 min/sample including equilibration), and collected in fractions, which are screened for bioactivity in a microtiter plate assay (Kongstad et al., 2015). Therefore, bioactivity can only be assigned to a fraction containing several analytes via a costly and time-consuming workflow, which subsequently requires analytical separation and testing of each peak to assign the individual bioactive compounds (Caesar et al., 2019). In routine, there has only been a little progress in non-target screening of food for bioactive compounds at an affordable price. Most methods deal with illicit additions, organic contaminants (Fu et al., 2017), adulterated foods (Díaz et al., 2012), and migrants from packaging (Rusko et al., 2020; Su et al., 2020). Also, generic chromatography-based high-resolution mass spectrometric methods were examined to cover as many substances as possible within a single analysis (Díaz et al., 2012). However, one drawback is the high load of interfering matrix caused by the diversity and abundance of substances in such natural products as spices and herbs (Caesar et al., 2019; Morlock and Heil, 2020). Elaborate sample preparation (which is selective and error-prone) would otherwise limit the validity and significance of the results. The state of the art is setting an intensity threshold and focusing on highly abundant signals (Wu et al., 2016). But even the smallest signal can have an important biological effect. Ignoring minor signals from the set instrumental threshold will produce grossly negligent results. Moreover, compounds may not ionize well or at all with standard settings of mass spectrometric recording. That is why routine analysis of natural extracts is still tailored and limited to marker compounds. However, the important active portion of natural food needs to be under (analytical) control, which is presently not the case.

To overcome these limitations and expand the analytical toolbox, a high-throughput eight-dimensional (8D) hyphenation was recently developed, and its proof of principle was shown for cinnamon samples detected with an antibacterial bioassay (Schreiner and Morlock, 2021). It demonstrated the information gained by combining effect-directed assays (EDA) with normal-phase high-performance thin-layer chromatography including multi-imaging by ultraviolet, visible, and fluorescence light detection (NP-HPTLC–UV/Vis/FLD) (Morlock, 2021). Heart-cut elution and transfer of the bioactive compound zone to an orthogonal reversed-phase high-performance liquid chromatography (RP-HPLC) system was exploited to separate potentially coeluting bioactive substances. The subsequent photodiode array detection (DAD) and heated electrospray ionization mass spectrometry (HESI-MS) were used for additional straightforward characterization of the bioactive substances. The advantage of NP-HPTLC–UV/Vis/FLD–EDA–heart-cut RP-HPLC–DAD–HESI-MS is that it prioritizes and reduces the thousands of compounds in such natural samples to the most important bioactive compounds. As the previously developed hyphenation was only shown for cinnamon and one antibacterial bioassay, this study intended to examine the influence of 68 different plant matrices and 16 different assays on the robustness of the new 8D hyphenation. It was of interest to prove its universal validity and significance, to figure out potential limitations, and to verify its suitability as generic activity screening. Such straightforward effect-directed profiling could be applied to reveal, understand, and control the mode of action of traditional medicines, botanicals, and plant-based food.

2 MATERIALS AND METHODS

2.1 Chemicals and Materials

Purity grades were listed when available. All salts were of p. a. quality and water free unless stated otherwise. Ethanol, toluene (all solvents of chromatography grade), bovine serum albumin (BSA, fraction V, $\geq 98\%$), dipotassium hydrogen phosphate (K_2HPO_4 , $\geq 99\%$), sodium dihydrogen phosphate monohydrate ($NaH_2PO_4 \cdot H_2O$, $\geq 98\%$), glycerol (Rotipuran, 86%), potassium dihydrogen phosphate (KH_2PO_4 , $\geq 99\%$), dipotassium hydrogen phosphate trihydrate ($K_2HPO_4 \cdot 3 H_2O$, $\geq 99\%$), sodium hydroxide (NaOH, $\geq 98\%$), disodium hydrogen phosphate (Na_2HPO_4 , $\geq 99\%$), potassium chloride (KCl, 98.5%), polyethylene glycol (PEG) 8000 (Ph. Eur.), kojic acid ($>98\%$), acetic acid (100%), sulfuric acid (96%), hydrochloric acid (37%, HCl, purest), citric acid (p. a.), 3-[4,5-dimethylthiazol-2-yl]-2,5-diphenyltetrazolium bromide (MTT, $\geq 98\%$), 3-[(3cholamidopropyl)dimethylammonio]-1-propanesulfonate (CHAPS, $\geq 98\%$), dimethyl sulfoxide (DMSO), and tris(hydroxymethyl)aminomethane (TRIS, $\geq 99.9\%$) were obtained from Carl Roth, Karlsruhe, Germany. Diammonium hydrogen phosphate ($[(NH_4)_2HPO_4]$, $\geq 99\%$) was purchased from Acros Organics, Morris Plains, NJ, United States. Butyrylcholinesterase (BChE) from equine serum (≥ 140 U/mg) was provided by SERVA, Heidelberg, Germany. Acarbose ($\geq 95\%$), α -glucosidase from *Saccharomyces cerevisiae*

TABLE 1 | Compilation of 68 botanicals, including botanical name, plant part, and sample weights (W) extracted with 5 ml methanol (*filtered through 0.45 µm PTFE filter).

No	Common name	Botanical name	Plant part	W [mg]
1	Acerola	<i>Malpighia glabra</i> L. [Malpighiaceae]	fruits	501.5
2	Horehound, white	<i>Marrubium vulgare</i> L. [Lamiaceae]	herb	500.1
3	Apple*	<i>Malus sylvestris</i> (L.) Mill. [Rosaceae]	peel	500.7
4	Artichoke, globe	<i>Cynara cardunculus</i> subsp. <i>scolymus</i> (L.) [Asteraceae]	leaves	501.3
5	Basil	<i>Ocimum basilicum</i> L. [Lamiaceae]	herb	500.6
6	Fenugreek	<i>Trigonella foenum-graecum</i> L. [Fabaceae]	seeds	499.9
7	Stinging nettle*	<i>Urtica dioica</i> L. [Urticaceae]	leaves	501.5
8	Blackberry	<i>Rubus fruticosus</i> L. [Rosaceae]	leaves	500.6
9	<i>Eucalyptus</i>	<i>Eucalyptus globulus</i> Labill. [Myrtaceae]	leaves	499.7
10	Fennel	<i>Foeniculum vulgare</i> Mill. [Apiaceae]	fruits	499.9
11	Fruit tea, yellow	not available	unknown	501.3
12	Fruit tea, red	not available	unknown	502.6
13	Galangal	<i>Alpinia officinarum</i> Hance. [Zingiberaceae]	roots	501.8
14	Ginkgo	<i>Ginkgo biloba</i> L. [Ginkgoaceae]	leaves	502.7
15	Ginseng	<i>Panax ginseng</i> C.A.Mey. [Araliaceae]	roots	502.3
16	Guarana	<i>Paullinia cupana</i> Kunth [Sapindaceae]	seeds	498.8
17	Dog rose	<i>Rosa canina</i> L. [Rosaceae]	fruits	501.0
18	Blueberry, European	<i>Vaccinium myrtillus</i> L. [Ericaceae]	fruits	501.2
19	<i>Hibiscus</i>	<i>Hibiscus rosa-sinensis</i> L. [Malvaceae]	blossoms	499.6
20	Raspberry	<i>Rubus idaeus</i> L. [Rosaceae]	juice concentrate from fruits	503.0
21	Elderberry	<i>Sambucus nigra</i> L. [Adoxaceae]	fruits	501.4
22	Elder flower	<i>Sambucus nigra</i> L. [Adoxaceae]	blossoms	502.5
23	Honeybush*	<i>Cyclopia genistoides</i> (L.) R.Br. [Fabaceae]	leaves, branches, blossoms	499.3
24	Hop	<i>Humulus lupulus</i> L. [Cannabaceae]	blossoms	502.1
25	Ginger	<i>Zingiber officinale</i> Roscoe [Zingiberaceae]	roots	499.0
26	Jasmine*	<i>Jasminum officinale</i> L. [Oleaceae]	blossoms	499.2
27	Cassis	<i>Ribes nigrum</i> L. [Grossulariaceae]	juice concentrate from fruits	500.7
28	Chamomile	<i>Matricaria chamomilla</i> L. [Asteraceae]	blossoms	499.3
29	Cardamom*	<i>Elettaria cardamomum</i> (L.) Maton [Zingiberaceae]	fruits	499.6
30	Garlic	<i>Allium sativum</i> L. [Amaryllidaceae]	bulbs	499.9
31	Kola*	<i>Cola nitida</i> (Vent.) Schott and Endl. [Malvaceae]	seeds	500.8
32	Coriander	<i>Coriandrum sativum</i> L. [Apiaceae]	fruits	501.3
33	Caraway	<i>Carum carvi</i> L. [Apiaceae]	fruits	500.0
34	Lovage	<i>Levisticum officinale</i> W.D.J.Koch [Apiaceae]	roots	499.6
35	Marjoram	<i>Origanum majorana</i> L. [Lamiaceae]	herb	502.4
36	Yerba mate*	<i>Ilex paraguariensis</i> A.St.-Hil. [Aquifoliaceae]	leaves, roasted	499.6
37	Yerba mate	<i>Ilex paraguariensis</i> A.St.-Hil. [Aquifoliaceae]	leaves	500.2
38	Lemon balm	<i>Melissa officinalis</i> L. [Lamiaceae]	leaves	500.6
39	Clove*	<i>Syzygium aromaticum</i> (L.) Merr. and L.M.Perry [Myrtaceae]	flower buds	501.9
40	Orange	<i>Citrus × aurantium</i> L. [Rutaceae]	blossoms	499.7
41	Orange	<i>Citrus × aurantium</i> L. [Rutaceae]	peel	501.1
42	Oregano	<i>Origanum vulgare</i> L. [Lamiaceae]	herb	501.5
43	Passionflower	<i>Passiflora incarnata</i> L. [Passifloraceae]	blossoms	501.1
44	Peppermint	<i>Mentha × piperita</i> L. [Lamiaceae]	leaves	500.3
45	Rooibos*	<i>Aspalathus linearis</i> (Burm.f.) R.Dahlgren [Fabaceae]	leaves	500.7
46	Rosemary*	<i>Salvia Rosmarinus</i> Spenn. [Lamiaceae]	leaves	500.9
47	Sage	<i>Salvia officinalis</i> L. [Lamiaceae]	leaves	499.9
48	Sea buckthorn	<i>Hippophae rhamnoides</i> L. [Elaeagnaceae]	fruits	501.9
49	Horsetail	<i>Equisetum arvense</i> L. [Equisetaceae]	herb	499.3
50	Yarrow*	<i>Achillea millefolium</i> L. [Asteraceae]	herb	501.6
51	Celeriac	<i>Apium graveolens</i> L. [Apiaceae]	bulb	501.3
52	Coneflower	<i>Echinacea angustifolia</i> DC. [Asteraceae]	herb and roots	499.1
53	Plantain	<i>Plantago lanceolata</i> L. [Plantaginaceae]	leaves	500.5
54	Star anise	<i>Illicium verum</i> Hook.f. [Schisandraceae]	fruits	500.3
55	Licorice	<i>Glycyrrhiza glabra</i> L. [Fabaceae]	roots	500.3
56	Siberian ginseng	<i>Eleutherococcus senticosus</i> (Rupr. and Maxim.) Maxim. [Araliaceae]	roots	503.4
57	Thyme	<i>Thymus vulgaris</i> L. [Lamiaceae]	herb	499.6
58	Grape*	<i>Vitis vinifera</i> L. [Vitaceae]	seed	499.9
59	Grape	<i>Vitis vinifera</i> L. [Vitaceae]	peel	499.7
60	Juniper	<i>Juniperus communis</i> L. [Cupressaceae]	fruits	501.5
61	Grape	<i>Vitis vinifera</i> L. [Vitaceae]	leaves	501.2
62	Hawthorn	<i>Crataegus</i> sp. [Rosaceae]	leaves and blossoms	499.7
63	Hawthorn leaves (Batch 1)	<i>Crataegus</i> sp. [Rosaceae]	leaves	501.8
64	Hawthorn leaves (Batch 2)	<i>Crataegus</i> sp. [Rosaceae]	leaves	499.9
65	Chicory	<i>Cichorium intybus</i> L. [Asteraceae]	roots	501.1
66	Cinnamon	<i>Cinnamomum verum</i> J.Presl [Lauraceae]	bark	501.5
67	Lemon peel	<i>Citrus × limon</i> (L.) Osbeck [Rutaceae]	peel	500.7
68	Lemon verbena	<i>Aloysia citridora</i> Paláu [Verbenaceae]	leaves	500.4

(1,000 U/vial), tyrosinase from mushroom ($\geq 1,000$ U/mg, 25 kU/vial), β -glucuronidase from *Escherichia coli* (5,000 U/vial), acetylcholinesterase (AChE) from *Electrophorus electricus* (≥ 245 U/mg, 10 kU/vial), peptone from casein (for microbiology), sodium acetate, sodium chloride (NaCl), Müller-Hinton broth (for microbiology), D-(+)-glucose (99.5%), rivastigmine ($\geq 98\%$), imidazole ($\geq 99.5\%$), copper sulfate, 7-hydroxy-4-methylcoumarin (4-methylumbelliferone, $>98\%$), yeast nitrogen base without amino acids (for molecular biology), quercetin-3-O-glucoside ($\geq 90\%$), liquiritigenin ($\geq 97\%$), naringenin ($\geq 95\%$), syringic acid ($\geq 95\%$), pinobanksin ($\geq 95\%$), sodium hydrogen carbonate (99.7%), lysogeny broth (containing 5 mg/ml sodium chloride) powder, ampicillin sodium salt, α -amylase from hog pancreas (50 U/mg), Gram's iodine solution (for microscopy) and testosterone ($\geq 99\%$) were delivered by Sigma-Aldrich, Steinheim, Germany. 2-Naphthyl- β -D-glucopyranoside (95%) and β -glucosidase from almonds (3,040 U/mg) were provided by ABCR, Karlsruhe, Germany. 1-Naphthyl acetate ($\geq 98\%$) and 2-naphthyl- α -D-glucopyranoside were obtained from AppliChem, Darmstadt, Germany. Fast Blue B salt (95%) was purchased from MP Biomedicals, Eschwege, Germany. 5-Bromo-4-chloro-3-indolyl- β -D-glucopyranosid-uronic sodium salt was obtained from Carbosynth, Compton-Berkshire, United Kingdom. Methanol (MS quality) and formic acid (99%) were delivered from VWR, Darmstadt, Germany. D-Saccharolactone and (2S)-2-amino-3-(3,4-dihydroxyphenyl) propionic acid (levodopa) was obtained from Santa Cruz Biotechnology, Dallas, TX, United States. 17- β -Estradiol (98.5%) was obtained from Dr. Ehrenstorfer, Augsburg, Germany. Ethyl acetate ($\geq 99.8\%$) and yeast extract powder (for microbiology) were purchased from Th. Geyer, Renningen, Germany. The medium for the Gram-negative, naturally luminescent marine *Aliivibrio fischeri* bacteria (DSM-7151, German Collection of Microorganisms and Cell Cultures, Berlin, Germany) is listed elsewhere (European Committee for Standardization, 2009). Gram-positive soil bacteria *Bacillus subtilis* subsp. *spizizenii* (DSM-618), magnesium sulfate heptahydrate ($\text{MgSO}_4 \cdot 7 \text{H}_2\text{O}$, 99.5%), citric acid monohydrate ($\geq 99.5\%$), 4-methyl-umbelliferyl- β -D-galactopyranoside, phosphate-buffered saline (without Ca^{2+}), soluble starch, as well as HPTLC plates silica gel 60 F₂₅₄ MS-grade and HPTLC plates silica gel 60 (both 20 cm \times 10 cm) were provided by Merck, Darmstadt, Germany. Bidistilled water was prepared by a Heraeus Destamat Bi-18 E (Thermo Fisher Scientific, Dreieich, Germany). *Saccharomyces cerevisiae* BJ 1991, equipped with the human androgen receptor, S9 enzyme mixture (from rat liver), nicotinamide adenine dinucleotide phosphate (NADP), and glucose 6-phosphate were delivered by Xenometrix, Allschwil, Switzerland. Additional chemicals and reagents used for planar yeast ant-/agonistic androgen/estrogen screens were reported elsewhere (Klingelhöfer and Morlock, 2015; Klingelhöfer et al., 2020). The *Saccharomyces cerevisiae* cells equipped with the hER β were obtained from the Erwin Herberle-Bors, University of Vienna, Austria (Kirchmayer, 2009). Reference substances acacetin (99%), eriocitrin (96%), naringin (92%), ginkgolide A (99%) and B (99%), isorhamnetin (99%), liquiritin apioside ($\geq 95\%$), hesperidin ($>96\%$), (-)-epicatechin (100%), (+)-catechin (98%), rutin (90%), and meranzin (98%) were

obtained from PhytoLab, Vestenbergsgreuth, Germany. Rosmaric acid ($\geq 98\%$), galangin ($\geq 98\%$), chlorogenic acid, kaempferol, and daidzein were delivered by Cayman Chemical, Ann Arbor, MI, United States. Glycyrrhizic acid and 4-nitroquinoline-1-oxide (98%) were purchased from TCI, Eschborn, Germany. The strain TA1535 of *Salmonella typhimurium* (genetically modified to contain the plasmid pSK1002) was purchased as cryostock from Trinova Biochem, Giessen, Germany. Resorufin- β -D-galactopyranoside was obtained from Toronto Research Chemicals, Toronto, Canada.

2.2 Standard Solutions and Sample Preparation

Standards solutions were prepared in methanol (1 mg/ml). Samples were obtained as dried, homogenized (mostly aqueous) extracts from Martin Bauer Group, Vestenbergsgreuth, Germany. For a 10% extract solution, an aliquot (0.5 g, Table 1) of each botanical powder was suspended in 5 ml methanol, ultra-sonicated for 30 min (Sonorex Digiplus, Bandelin, Berlin, Germany), and centrifuged at $3,000 \times g$ for 15 min (Labofuge 400, Heraeus, Hanau, Germany). Each supernatant was transferred in an autosampler vial. Some extracts were additionally filtered (Table 1, marked*) through a $0.45 \mu\text{m}$ polytetrafluoroethylene filter (VWR, Darmstadt, Germany).

2.3 HPTLC–UV/Vis/FLD

Plates were pre-washed with methanol–water (4:1 V/V), dried in an oven (Memmert, Schwabach, Germany) for 20 min at 110°C (Morlock, 2014), and stored wrapped in aluminum foil. All botanical extracts (4 μL /band) were applied as 6 mm bands on a pre-washed plate (Automatic TLC Sampler 4, CAMAG, Muttenz, Switzerland). The plate was developed up to a migration distance of 70 mm with 7 ml ethyl acetate–toluene–formic acid–water (16:4:3:2 V/V/V/V) (Krüger et al., 2017). Separation was performed in a twin trough chamber (20 cm \times 10 cm, CAMAG) followed by drying for 4 min with a stream of cold air (hair dryer) and for 20 min in a laminar flow of air (Automated Development Chamber 2, CAMAG). The developed plates were documented at Vis, UV 254 nm, and FLD 366 nm (TLC Visualizer 2, CAMAG). The software winCATS (version 1.4.7.2018) or visionCATS (version 2.5.18262.1, both CAMAG) controlled the instruments.

2.4 HPTLC–EDA

For bioprofiling, 16 silica gel 60 F₂₅₄ MS-grade chromatograms were prepared. The buffer and assay solutions were piezoelectrically sprayed (Derivatizer, CAMAG) if not stated otherwise. To remove acidic traces left on the planar chromatogram (which can interfere with pH-sensitive bioassays), the chromatogram was neutralized with 1.5 ml phosphate buffer (80 mg/ml Na_2HPO_4 , pH 7.5 adjusted with NaOH; yellow/green nozzle, level 6) for enzymatic and bacterial assays, 1.4 ml citrate buffer (6 mg/ml citric acid monohydrate, 10 mg/ml Na_2HPO_4 , adjusted to pH 12 with NaOH, yellow ultra-nozzle, level 2) (Klingelhöfer et al., 2020) for the hormonal-effective bioassays, 1.25 ml sodium bicarbonate buffer (2.5%, yellow nozzle, level 3) for

α -amylase bioassay or twice with 2.8 ml sodium bicarbonate buffer for SOS-Umu-C bioassay (neutralization procedure for SOS-Umu-C bioassay was investigated during this study, **Supplementary Figure S1**). The moist chromatogram was dried as mentioned in 2.3. A positive control was applied at three different concentrations at the top plate edge to verify the proper bioassay performance. The assay solutions/suspensions were applied as follows. For incubation, the plates were horizontally placed in a moistened polypropylene KIS box (26.5 cm \times 16 cm \times 10 cm, ABM, Wolframs-Eschenbach, Germany) pre-saturated with 30 ml water at 37°C (30°C for hormonal-effective bioassays) for 30 min. The procedure was documented at FLD 366 nm and white light illumination in transmission, reflection, and reflection/transmission mode.

2.4.1 *Bacillus subtilis* Bioassay

For the Gram-positive *B. subtilis* inhibition bioassay, 80 μ l of stock solution was suspended in 20 ml Müller-Hinton Broth and incubated overnight at 37°C. Before usage, the cell number was determined using a spectrophotometer (M501, Camspec, Garforth, United Kingdom) at 600 nm. At an optical density (OD₆₀₀) between 0.8 and 1.1, the culture was ready to use for EDA. An aliquot of the bacteria suspension (2 ml) was sprayed on the planar chromatogram (red nozzle, level 6) (Morlock et al., 2021b). The plate was incubated at 37°C for 2 h. As substrate solution (2 mg/ml), MTT was freshly prepared in phosphate-buffered saline. After the application of 250 μ l substrate solution (blue nozzle, level 6), the plate was incubated again for 30 min at 37°C. Inhibitory zones appeared colorless (white) on a formazan-purple background. The positive control was tetracycline (10 μ g/ml in ethanol, 0.4, 0.8, and 1.2 μ l/band).

2.4.2 *Aliivibrio fischeri* Bioassay

The bioluminescent marine Gram-negative bacteria *A. fischeri* were cultured according to DIN EN ISO 11348-1, Section 5 (European Committee for Standardization, 2009). Therefore, 200 μ l of cryostock were suspended in 20 ml medium. The cultivation was performed overnight (18–24 h) in a 100 ml Erlenmeyer flask at room temperature by shaking at 75 rpm. Once the culture showed brilliant blue fluorescence by shaking in the dark, it was ready for use. An aliquot of the bacteria suspension (3 ml) was sprayed on the plate (blue nozzle, level 6) and directly recorded (BioLuminizer 2, CAMAG) (Morlock et al., 2021a; Morlock et al., 2021b). The native bioluminescence (depicted as a greyscale image) was documented in ten images at time intervals of 3 min. Exposure time was set to 120 s. Antibacterial components were detected as dark zones, whereas metabolism-enhancing substances appeared as bright zones on the bioluminescent background. The positive control was caffeine (1 mg/ml in methanol, 0.5, 1.5, and 3 μ l/band).

2.4.3 Cholinesterase Inhibition Assays

The initial AChE and BChE inhibition assays (Marston et al., 2002) were modified (Hage and Morlock, 2017; Morlock et al., 2021b). The plates were pre-wetted with 0.5 ml TRIS-HCl buffer (7.55 mg/ml TRIS, pH 7.8 adjusted with HCl, green nozzle, level 6). Then, 1.5 ml of enzyme solution (AChE 6.66 U/ml, BChE 3.34 U/ml, and each 1 mg/ml BSA in TRIS-HCl buffer) were

applied (green nozzle, level 6) and the chromatogram was subsequently incubated at 37°C for 30 min. For detection, 0.5 ml substrate mixture (1 mg/ml 1-naphthyl acetate, 2 mg/ml Fast Blue B salt) was sprayed (red nozzle, level 6) onto the plate to obtain colorless (white) inhibition zones on a purple background. The positive control was rivastigmine (0.1 mg/ml in methanol, 2, 4, and 8 μ l/band).

2.4.4 Glucosidase Inhibition Assays

An improved version of Simões-Pires *et al.* (Simões-Pires et al., 2009) was used to detect α - and β -glucosidase inhibitors. The substrate solution (12 mg 2-naphthyl- α -D-glucopyranoside or 2-naphthyl- β -D-glucopyranoside in 9 ml ethanol and adding 1 ml of 10 mM NaCl solution) was sprayed (1 ml, red nozzle, level 6) onto the plate, followed by drying in a stream of cold air. Pre-wetting was carried out by spraying 0.5 ml sodium acetate buffer (41 mg/ml, pH 7.5 adjusted with 0.1 mM acetic acid, green nozzle, level 6). An aliquot of the respective enzyme solution (α -glucosidase 10 U/ml, β -glucosidase 1,000 U/ml in sodium acetate buffer) was applied (1 ml; green nozzle, level 6) and the plate was subsequently incubated at 37°C for 30 min. The antidiabetic effect was visualized by Fast Blue B salt staining (2 mg/ml in water, 0.5 ml, red nozzle, level 6), resulting in colorless (white) inhibitory zones on a purple background. The positive controls were acarbose (3 mg/ml in ethanol, 1, 3, and 6 μ l/band) for the α -glucosidase assay and imidazole (1 mg/ml in ethanol, 3, 5, and 7 μ l/band) for the β -glucosidase assay.

2.4.5 β -Glucuronidase Inhibition Assay

The β -glucuronidase inhibition assay was run as described recently (Mahran et al., 2020) The chromatogram was pre-wetted with potassium phosphate buffer (0.5 ml; 9.34 mg/ml K₂HPO₄ and 6.31 mg/ml KH₂PO₄; green nozzle, level 6). Then, 750 μ l enzyme solution (25 U/ml in potassium phosphate buffer with 1 mg/ml BSA) were sprayed onto the chromatogram (green nozzle, level 6). Incubation followed for 15 min at 37°C. As substrate, 750 μ l of a 2 mg/ml 5-bromo-4-chloro-3-indolyl- β -D-glucuronide sodium salt solution was sprayed. The plate was incubated again for 60 min for producing colorless (white) inhibitory zones on a blue background. The positive control was D-saccharolactone (0.1 mg/ml in water, 1, 1.5, and 2 μ l/band).

2.4.6 Tyrosinase Inhibition Assay

The tyrosinase inhibitor potential was investigated according to an improved (Morlock et al., 2021b) workflow (Taibon et al., 2015). To prepare the substrate solution, 45 mg levodopa, 25 mg CHAPS, and 75 mg PEG 8000 were dissolved in 10 ml of phosphate buffer (1.4 mg/ml K₂HPO₄, 1.68 mg/ml Na₂HPO₄, pH 6.8) and stored at 4°C until use. The levodopa substrate solution was sprayed onto the chromatogram (1 ml, blue nozzle, level 6) and subsequently dried for 2 min in a stream of cold air. Then, 1 ml of enzyme solution (400 U/ml in phosphate buffer) was sprayed onto the plate (blue nozzle, level 6), followed by incubation at room temperature for 20 min. After incubation, the plate was immediately dried and documented. Tyrosinase

inhibition activity was apparent as colorless (white) zones on a greyish-brown background. The positive control was kojic acid (0.1 mg/ml in ethanol, 1, 3, and 6 μ l/band).

2.4.7 Planar Yeast Androgen/Estrogen Screen (pYAS/pYES) Bioassay

The hormonal-effective bioassays were run as recently described (Klingelhöfer et al., 2020). Cryogenic YAS or YES cell culture (1 ml each) was suspended in 39 ml or 29 ml medium, respectively. The suspensions were cultivated by shaking at 70–75 rpm and 30°C overnight (20–22 h). The cell number was determined with a hemocytometer after diluting 50 μ l culture in 950 μ l 0.9% NaCl solution. The required cell count of 0.8×10^8 cells/ml was adjusted via centrifugation ($2,500 \times g$, 5 min) of 5 ml yeast cell culture and resuspension in the required amount of medium plus 50 μ l copper sulfate. This suspension was sprayed on the plate (1.4 ml, red nozzle, level 6), followed by incubation for 4 h (pYAS) or 3 h (pYES) at 30°C. Substrate solution (2 mg 4-methylumbelliferyl- β -D-galactopyranoside, 100 μ l DMSO, 3 ml citrate buffer) was sprayed onto the chromatogram (1.5 ml, yellow ultra-nozzle, level 2). Subsequently, the plates were incubated for 1 h at 37°C. Bioautograms were recorded at FLD 366 nm. Endocrine agonists appeared as 4-methylumbelliferone-blue fluorescent zones on a dark blue background. As a positive control, testosterone (for pYAS: 0.5 μ L, 1.5 μ g/ml in methanol) or 17- β -estradiol (for pYES: 5 μ l, 100 ng/ml in ethanol) were applied.

2.4.8 Metabolization via S9-pYES Bioassay

Potential estrogens resulting from liver metabolism were investigated by adding the S9 enzyme mixture (500 μ l) and respective cofactors (166 μ l NADP, 42 μ l glucose 6-phosphate, 958 μ l phosphate buffer) to 3,334 μ l *Saccharomyces cerevisiae* cell culture (0.8×10^8 cells/ml). The assay was performed as described above.

2.4.9 Planar Yeast Antagonistic Androgen/Estrogen Screen (pYAS/pYES) Bioassay

To screen the antagonistic activity, the pYAS or pYES bioassays were extended by overspraying along the middle of each track a 1 mm \times 70 mm area of testosterone (4 μ l, 1.5 μ g/ml in methanol) or 17- β -estradiol (5 μ l, 2 ng/ml in ethanol), respectively, with the Freemode option of winCATS (Klingelhöfer et al., 2020). Endocrine antagonists appeared as fluorescence-reducing bands in the 4-methylumbelliferone-blue fluorescent testosterone or 17- β -estradiol track part.

2.4.10 SOS-Umu-C Bioassay

The planar SOS-Umu-C bioassay was run on HPTLC silica gel plates without a fluorescence indicator. After development, the plates were additionally scanned at 546/>580 nm using the TLC Scanner 3 (CAMAG). *Salmonella typhimurium* cells (50 μ l cryostock) were suspended in 35 ml Lysogeny broth (20 mg/ml with 1 mg/ml D-(+)-glucose and 106 mg/L ampicillin sodium salt) and incubated overnight at 75 rpm and 37°C for 16 h. Before use, the cells were centrifuged ($3,000 \times g$, 10 min). The pelleted cells were re-suspended in fresh medium to obtain the

required OD₆₆₀ of 0.2 (Meyer et al., 2020). The chromatogram was sprayed with *Salmonella* suspension (2.8 ml, yellow nozzle, level 3) and incubated at 37°C for 3 h. Substrate solution [15 μ l resorufin- β -D-galactopyranoside solution (20 mg/ml in DMSO) in 2.1 ml phosphate buffer and 0.9 ml glycerol] was sprayed onto the plate (2.5 ml, red nozzle, level 6). Incubation followed at 37°C for 1 h. The plates were documented at white light illumination and 366 nm. The generated resorufin fluorescence was measured at 546/>580 nm. Genotoxic substances were detectable either as pink zones on the colorless background at white light illumination or as pink fluorescent zones on a brown-reddish background at 254 nm or 366 nm. The positive control was 4-nitroquinoline-1-oxide (1 μ g/ml in methanol, 1 μ l/spot).

2.4.11 α -Amylase Inhibition Assay

The latest α -amylase inhibition method, which used immersion of the plate into enzyme and substrate solutions (Agatonovic-Kustrin and Morton, 2017; Agatonovic-Kustrin et al., 2019), was adjusted and transferred to a piezoelectric spraying procedure, in which the enzyme solution (62.5 U/mL in sodium acetate buffer) was sprayed onto the chromatogram (1 ml, red nozzle, level 5), followed by 30 min incubation at 37°C. As substrate 2%-soluble starch solution was sprayed onto the wet plate (0.5 ml, red nozzle, level 5). After 20 min incubation at 37°C, Gram's iodine solution was sprayed (250 μ l, yellow nozzle, level 5) for visualization. The α -amylase inhibition activity was observed as violet zones on a colorless background. The positive control was acarbose (0.1 mg/ml in methanol, 0.3, 0.6, and 0.9 μ l/band).

2.5 Instrumental Setup of the 8D-Hyphenation

The multipotent bioactive zones were further characterized with RP-HPLC-DAD-HESI-MS directly after EDA. The UPLC system (Acquity H Class, Waters, Eschborn, Germany) was equipped with the quaternary solvent manager, solvent degasser, sample manager, column oven, photodiode array detector (DAD), and HESI-MS (single quadrupole QDa, Waters). The bioactive target zone was heart-cut eluted with an oval elution head (4 mm \times 2 mm) of the TLC-MS Interface 2 (CAMAG) with 90% aqueous methanol. A standalone pump supplied the solvent (515 HPLC pump, Waters). Analytes were transferred through a biocompatible inline filter (IDEX Health and Science, Oak Harbor, WA, United States) containing a PEEK frit (0.5 μ m, Techlab, Brunswick, Germany) to an online desalting RP pre-column/defender guard (Accucore RP-MS, 10 mm \times 2.1 mm, 2.6 μ m, Thermo Scientific, Bellefonte, PA, United States). The online desalting device was installed onto a two-position switching valve (MXT-Series PD715-000, Rheodyne IDEX Health and Science) and served as an analyte trap while discarding the bioassay salts as waste. By switching, controlled via remote control and Rheodyne TitanMX software, the analytes were transferred to the main RP column (Accucore RP-MS 100 mm \times 2.1 mm, 2.6 μ m, Thermo Scientific) and separated orthogonally. The column was thermostated at 40°C. The 13 min HPLC gradient consisted of (A) 2.5 mM ammonium acetate (pH 4.5 adjusted with acetic acid) and (B) methanol. Starting

conditions were 98% A at a flow rate of 0.6 ml/min for the first 2 min. The methanolic portion increased linearly to 20% within the following 2.5 min. At 8 min, a ratio of 10/90% A/B was reached and held for the next 2 min; then it fell to 98% A within 0.1 min, followed by 3 min equilibration time. Detection parameters were set to a wavelength scan from 190 to 400 nm for DAD. The MS was operated in polarity-switching mode, while the ESI probe was heated to 600°C and ESI source to 120°C. The sampling frequency was set to 5 Hz and cone voltage to ± 10 V in both ionization modes (Schreiner and Morlock, 2021). The MassLynx V4.2 software (Waters) was used to evaluate and process the data.

3 RESULTS AND DISCUSSION

3.1 Outline of the Study

A total of 68 very different powdered plant extracts (botanicals added to food products in food industry) and 16 different effect-directed assays were selected to investigate and prove the suitability of the biological–physicochemical 8D hyphenation for generic screening (Figure 1). Among the plants (Table 1) were such ones that are commonly used as culinary spices and herbs or in traditional medicine. Their diverse and varying compositions represent different matrix loads for the analytical system. Moreover, the nine biological and seven biochemical assay media differed over a wide range in salt and nutrient composition. This represents the diversity of possible compositions of a bioactive zone (to be heart-cut and transferred to the next dimension) and was therefore considered a good worst-case scenario to test whether the developed generic hyphenation method is suitable for routine analyses. First, the bioactivity screening was evaluated per assay (Figures 2–6), whereby some botanicals were mentioned repeatedly, *i.e.* galangal (no. 13) yerba mate (no. 37), orange peel (no. 41), licorice (no. 55), and Siberian ginseng (no. 56). Then, these botanicals were subjected to heart-cut RP-HPLC–DAD–HESI-MS analysis (Figures 7–11). All botanicals were extracted and applied analogously. Thus, the effect profiles of each assay could directly be compared by their response pattern. The most effective and important botanicals were highlighted at a glance in side-by-side comparison. The band broadening (diffusion) depended on the assay incubation time. The most important bioactive compounds discovered were tentatively assigned based on information obtained about spectral (UV/Vis/FLD), polarity (hR_F values with a deviation of ± 1), and molecular (mass signal) properties. Since there was no access to a high-resolution mass spectrometry system, the assignments were verified by comparing with reference standards.

Using the Gram-negative *Aliivibrio fischeri* and Gram-positive *Bacillus subtilis* bioassays, natural antibacterial compounds were detected that can subtly fight infections and contribute to longer shelf life and better preservation of products. Natural AChE and BChE inhibitors, which can provide symptomatic benefits for the cognitive decline of Alzheimer's patients (Tundis et al., 2016), were revealed by the respective planar enzyme inhibition assays. The tyrosinase inhibition assay was used to screen for plant-based

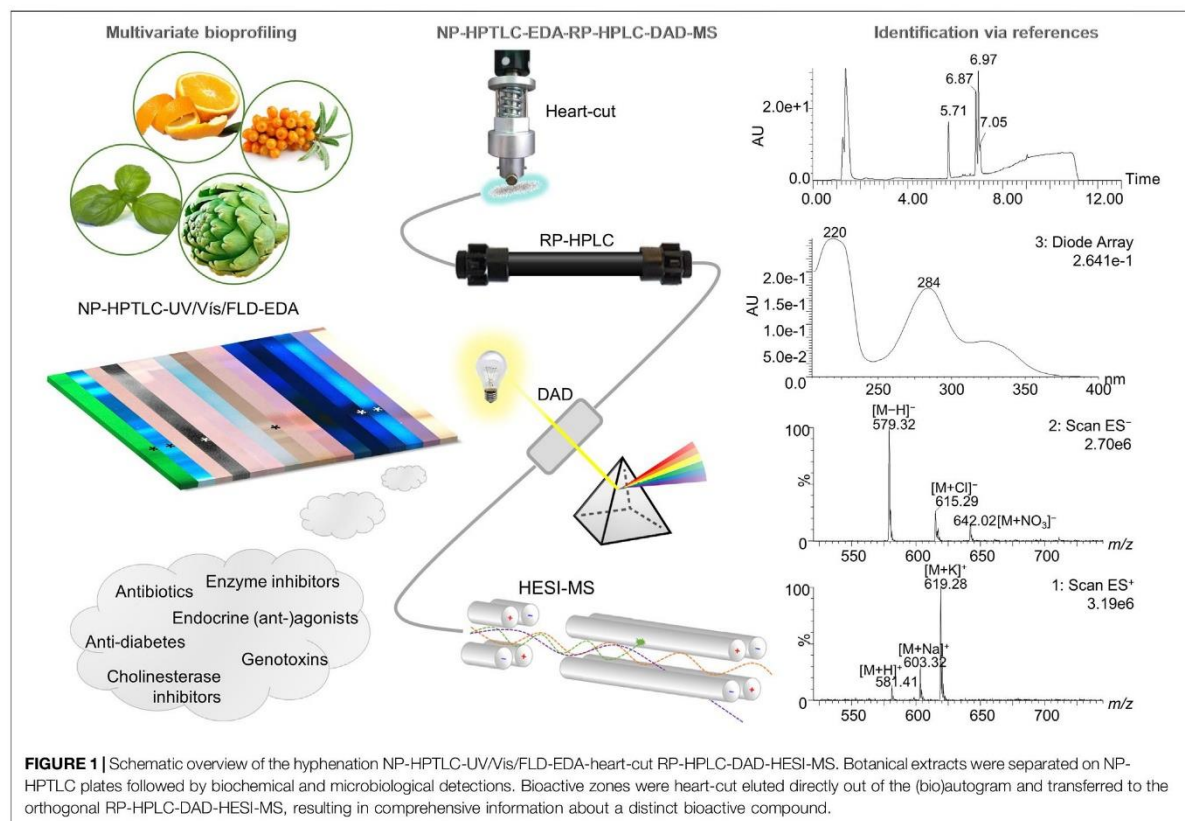
skin whiteners or inhibitors of the enzymatic food browning. The β -glucuronidase inhibition assay was used to detect compounds that prevent the gut-bacterial reversion of detoxification via glucuronidation. Additional α -amylase, α - and β -glucosidase inhibition assays were employed to determine natural compounds with benefits for diabetes patients. Phytoandrogens and phytoestrogens were detected via the human estrogen receptor α (hER α) or hER β or in combination with the S9 enzyme mixture simulating liver metabolism, and respective antagonists were investigated using recombinant yeast cells equipped with the human estrogen/androgen receptor. Genotoxins were detected with a recombinant *Salmonella typhimurium* strain equipped with the SOS-Umu-C repair mechanism. Hence, the spectrum of effects in the investigated botanicals may be linked to the mitigation of bacterial infections, the improvement of cholinergic transmission for Alzheimer's patients, the decrease of blood glucose levels in diabetics, the reduction of skin abnormalities, and to the balance of the steroid hormonal system, among other disorders.

3.2 Screening Results

3.2.1 Compounds Inhibiting Bacteria

In traditional medicines, plant-based extracts are used to assist in the treatment of bacterial infections (Brantner and Grein, 1994; Palombo and Semple, 2001). Antibacterial activities can be so effective that plant extracts are also used as preservatives in food products. For example, the ingredients carnosol and carnosic acid of rosemary extract are marketed as preservative E 392. Rosemary (no. 46) is also screened here, using non-pathogenic bacterial representatives which are easier to handle in the laboratory. The Gram-positive *B. subtilis* bioassay is based on an oxidoreductase enzyme reaction. Intact enzymes of viable *B. subtilis* cells reduce the tetrazolium salt MTT to the insoluble purple formazan (Marston, 2011). Cell death is visualized as colorless zones indicating antibacterial compounds. Most antibacterials detected were located at hR_F values ≥ 90 (Figures 2–4C). In eucalyptus (no. 9), marjoram (no. 35), yerba mate green (no. 37), Siberian ginseng (no. 56), thyme (no. 57), hawthorn leaves (nos. 63 and 64), and cinnamon bark (no. 66) additional antibacterials were detected in the lower hR_F range. Essential oils from herbs such as oregano and thyme are known for their antimicrobial activity, especially against Gram-positive bacteria (Soković et al., 2010).

The Gram-negative *A. fischeri* bacteria are able to convert metabolic energy into turquoise bioluminescence via luciferase. A change in bioluminescence intensity is correlated with substances enhancing or reducing the cell metabolism. Such effects are visualized as lightened or dark zones on the bioluminescent background of the bioautogram (depicted as greyscale image). Almost all botanical extracts showed antimicrobial activity against *A. fischeri* (Figures 2–4D). Intense antimicrobial zones were detected in yerba mate green (no. 37), passionflower (no. 43), peppermint (no. 44), rooibos (no. 45), licorice (no. 55), Siberian ginseng (no. 56), and cinnamon bark (no. 66). Most samples showed at least one dark antimicrobial zone, while more than half of all samples had two or more. The more universally and sensitively detecting *A. fischeri* bioassay proved to be a good starting assay to investigate complex mixtures.



3.2.2 Compounds Inhibiting AChE and BChE

In traditional or ayurvedic medicine, plants and their phytoconstituents are used to assist in the treatment of Alzheimer’s disease (Azadniya et al., 2021). The pathophysiology of Alzheimer’s disease is often associated with cholinergic system dysfunction. Therefore, many synthetic drugs target the inhibition of cholinesterases. Both AChE and BChE catalyze the hydrolysis of the neurotransmitter acetylcholine into acetic acid and choline. While AChE is highly selective for acetylcholine, BChE can also convert other substrates, e.g., butyrylcholine, succinylcholine, or organophosphates. Besides synthetic drugs, also natural compounds are able to inhibit this enzyme mechanism. Particularly polyphenols interact with amino acid residues of the active side of the enzymes terminating the splitting from acetylcholine into acetic acid and choline and thus maintaining colinergic neurotransmission and improve cognition of Alzheimer’s patients (Jabir et al., 2018). The enzyme-inhibiting potential is revealed as colorless zones on a purple background. Acerola fruit (no. 1) showed a remarkably strong inhibition zone at hR_F 41 (Figures 2E,F). While roots and branches from the acerola tree are known to have anti-cholinesterase activity through the norfriedelins A-C (Liu et al., 2013), only cytotoxic, anti-HIV, antioxidant, antihyperglycemic, skin whitening, and antimicrobial activities are described for extracts

from the fruits (Motohashi et al., 2004; Belwal et al., 2018a). This zone showed not only a strong response in the AChE and BChE assays, but also in most other assays (Figure 2). Other inhibitory zones were detected in ginger (no. 25, hR_F 99), kola (no. 31, hR_F 68), marjoram (no. 35, hR_F 99), yerba mate green (no. 37, hR_F 88), lemon balm (no. 38, hR_F 32), peppermint and rooibos (nos. 44 and 45, both hR_F 34), Siberian ginseng (no. 56, hR_F 93), and hawthorn (nos. 62–64, hR_F 60 and 85) (Figures 2–4E,F). Some typical traditional medicines used in the treatment of Alzheimer’s disease, such as *Panax notoginseng*, *Ginkgo biloba* (no. 14), *Melissa officinalis* (no. 38), and *Salvia officinalis* (no. 47), are also screened here. Among these, *Melissa officinalis* (no. 38) possess cholinesterase-inhibiting potential, the others operate according to a different mechanism to treat the neurodegenerative disease (Sharma et al., 2019).

3.2.3 Compounds Inhibiting β -Glucuronidase

The detoxification mechanism via glucuronidation can be reversed with β -glucuronidase from opportunistic *Enterobacteriaceae* such as *Escherichia coli*, resulting in gastrointestinal malfunction. This can be prevented by inhibiting the microbial β -glucuronidase, where such inhibitors address the extra loop in the bacterial enzyme (in contrast to the mammalian one) (Mahran et al., 2020). The enzyme inhibitors do not cleave the chromogenic substrate and are therefore detected

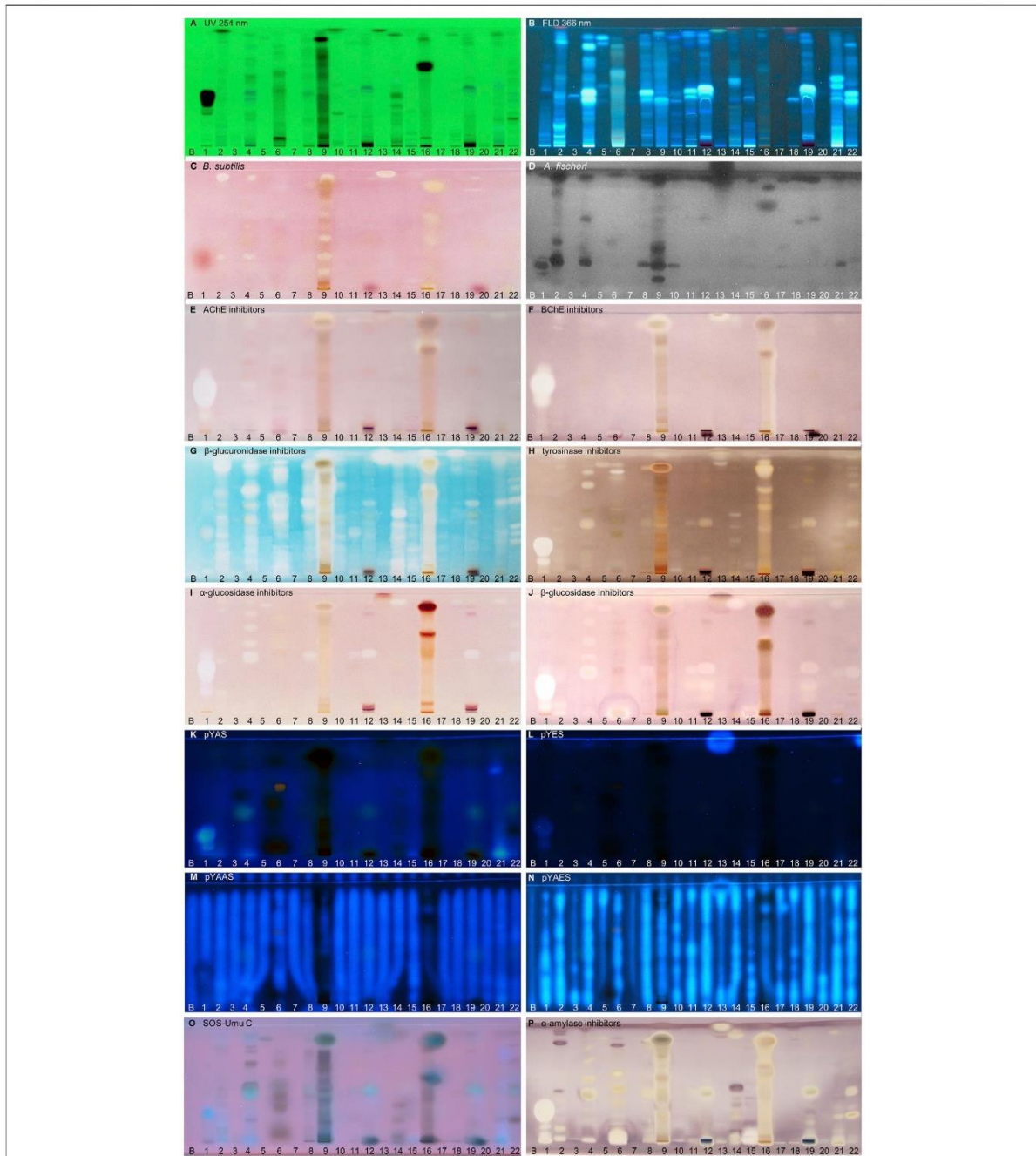


FIGURE 2 | NP-HPTLC–UV/Vis/FLD–EDA profiles of the plant extracts no. 1–22. Separation of the applied botanicals (4 μL/band, assignments in **Table 1**; solvent blank B for comparison) on HPTLC plate silica gel 60 F₂₅₄ MS-grade with ethyl acetate–toluene–formic acid–water (16:4:3:2, V/V/V/V) up to 70 mm, detected at UV 254 nm (**A**), FLD 366 nm (**B, K–O**) and white light illumination (**C, E–J, P**) after the *B. subtilis* bioassay (**C**), *A. fischeri* bioassay with bioluminescence depicted as a greyscale image, (**D**) and AChE (**E**), BChE (**F**), β-glucuronidase (**G**), tyrosinase (**H**), α-glucosidase (**I**), β-glucosidase (**J**) and α-amylase (**P**) inhibition assays, as well as pYAS (**K**), pYES (**L**), pYAAS (**M**), pYAES (**N**), SOS-Umu-C (**O**) bioassays.

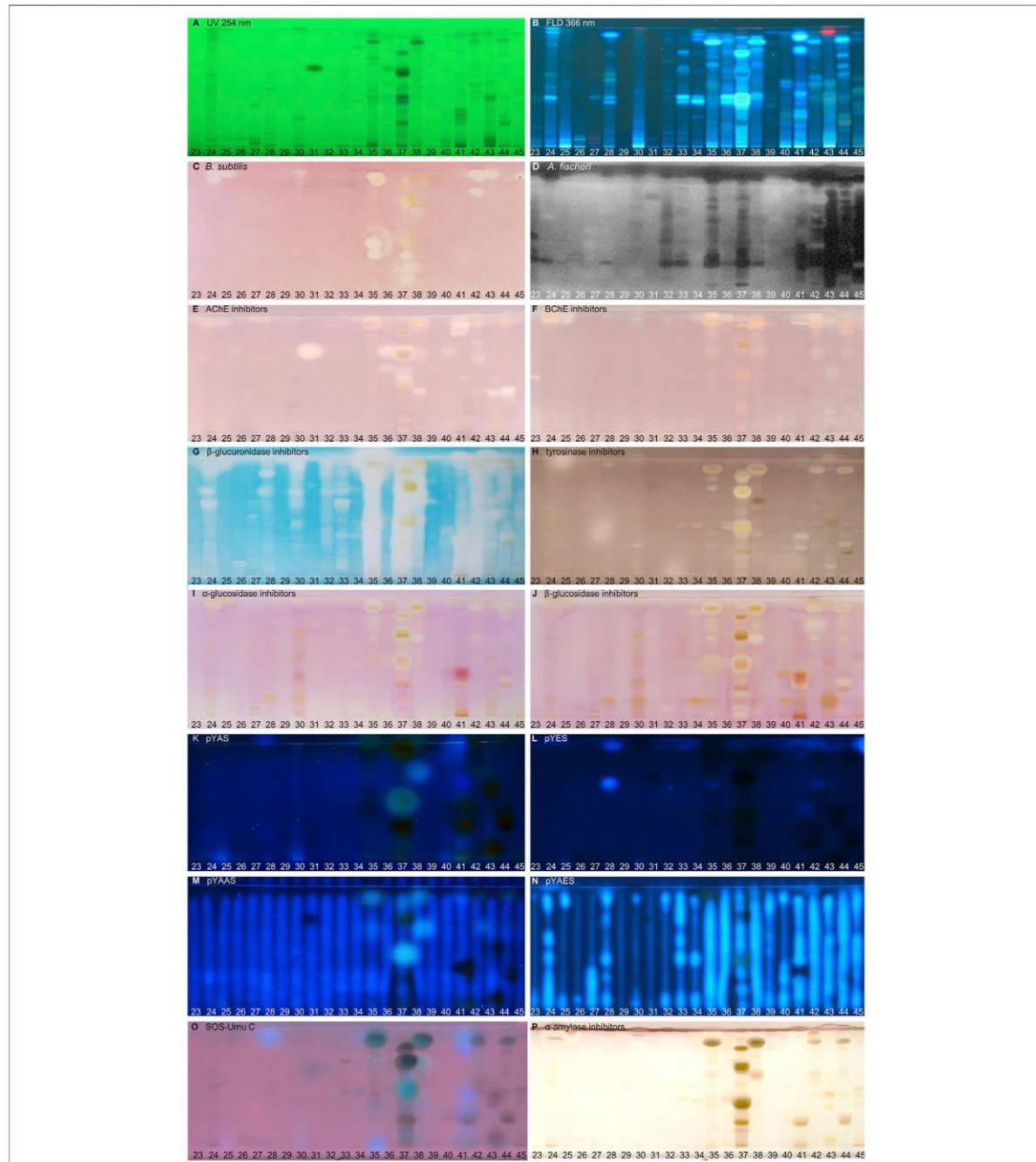


FIGURE 3 | NP-HPTLC–UV/Vis/FLD–EDA profiles of the plant extracts no. 23–45. Separation of the applied botanicals (4 μ L/band, assignments in **Table 1**) on HPTLC plate silica gel 60 F_{254} MS-grade with ethyl acetate–toluene–formic acid–water (16:4:3:2, V/V/V/V) up to 70 mm, detected at UV 254 nm (**A**), FLD 366 nm (**B**, **K–O**) and white light illumination (**C**, **E–J**, **P**) after the *B. subtilis* bioassay (**C**), *A. fischeri* bioassay with bioluminescence depicted as a greyscale image, (**D**) and AChE (**E**), BChE (**F**), β -glucuronidase (**G**), tyrosinase (**H**), α -glucosidase (**I**), β -glucosidase (**J**), and α -amylase (**P**) inhibition assays, as well as pYAS (**K**), pYES (**L**), pYAAS (**M**), pYAES (**N**), SOS-Umu-C (**O**) bioassays.

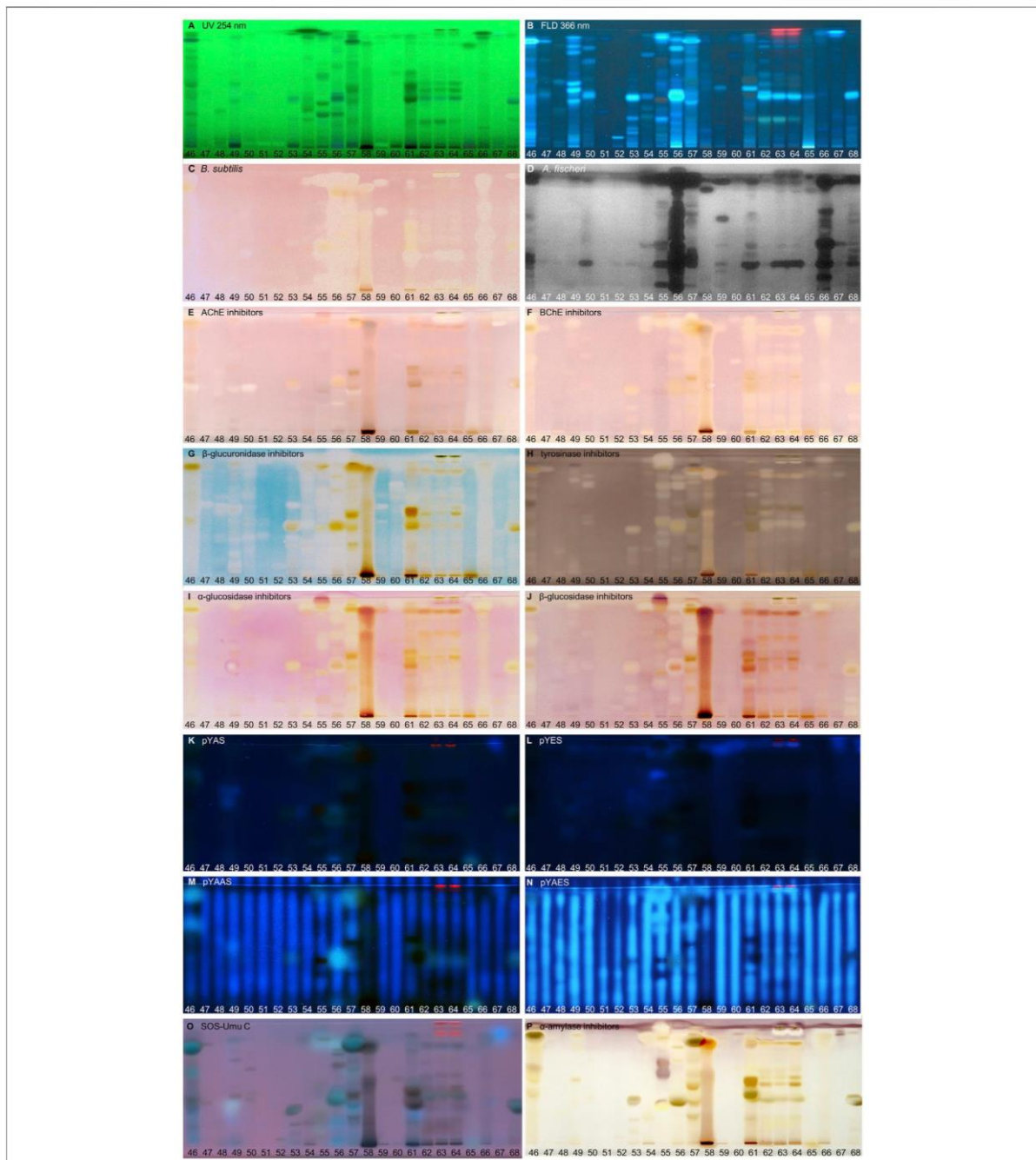
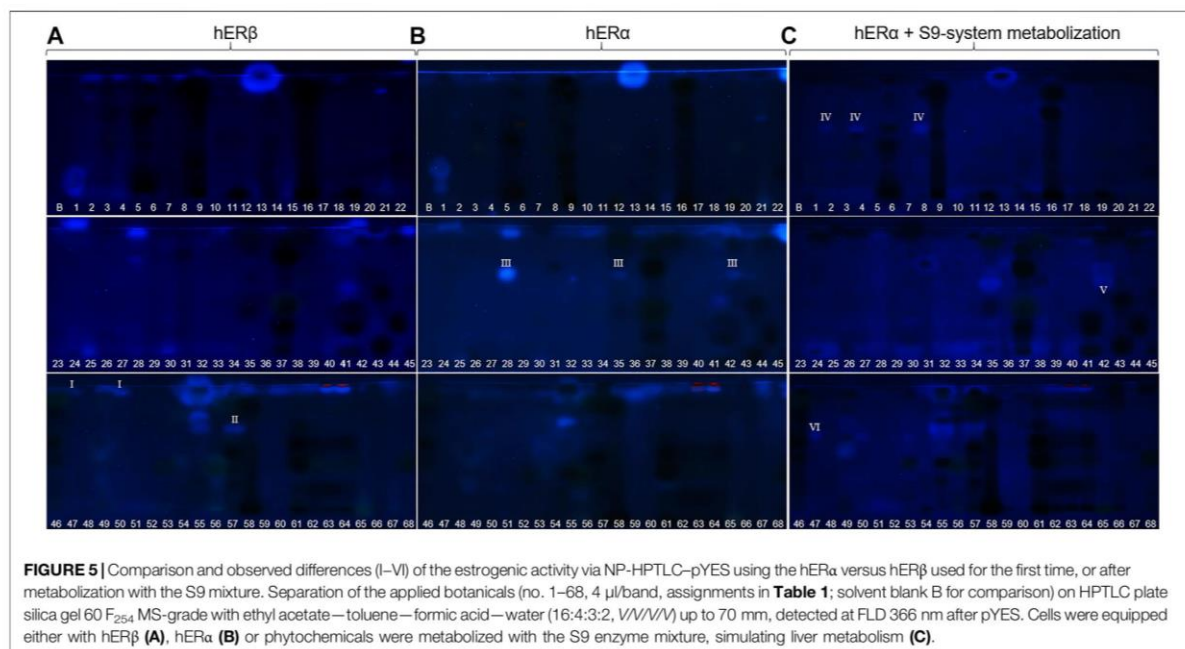


FIGURE 4 | NP-HPTLC–UV/Vis/FLD–EDA profiles of the plant extracts no. 46–68. Separation of the applied botanicals (4 μ L/band, assignments in **Table 1**; solvent blank B for comparison) on HPTLC plate silica gel 60 F₂₅₄ MS-grade with ethyl acetate–toluene–formic acid–water (16:4:3:2, V/V/V/V) up to 70 mm, detected at UV 254 nm (**A**), FLD 366 nm (**B, K–O**), and white light illumination (**C, E–J, P**) after the *B. subtilis* bioassay (**C**), *A. fischeri* bioassay with bioluminescence depicted as a greyscale image, (**D**) and AChE (**E**), BChE (**F**), β -glucuronidase (**G**), tyrosinase (**H**), α -glucosidase (**I**), β -glucosidase (**J**), and α -amylase (**P**) inhibition assays, as well as pYAS (**K**), pYES (**L**), pYAAS (**M**), pYAES (**N**), SOS-Umu-C (**O**) bioassays.



as colorless zones on an indigo-blue background. In each eucalyptus (no. 9), guarana (no. 16), marjoram (no. 35), yerba mate green (no. 37), oregano (no. 42), Siberian ginseng (no. 56), and cinnamon bark (no. 66), the whole sample track appeared white on the indigo-blue background due to the comparatively high abundance of β -glucuronidase inhibitors (**Figures 2–4G**). If the application volume is reduced by a factor of 4 for these botanicals, the individual inhibitors become evident (**Supplementary Figure S2**). All botanical extracts showed β -glucuronidase inhibitory potential at least in the solvent front (hR_F 99). For such screening results, repetition using a mobile phase of reduced solvent strength is recommended in order to better differentiate the individual inhibitors (**Supplementary Figure S3C,D**). Some isolated flavonoid standards, *i.e.*, isorhamnetin, kaempferol, liquiritigenin, daidzein, *etc.*, already proved to be active against β -glucuronidase (Sun et al., 2020). Their activity and also that of additional flavonoids have been confirmed by our study directly in herbs and spices.

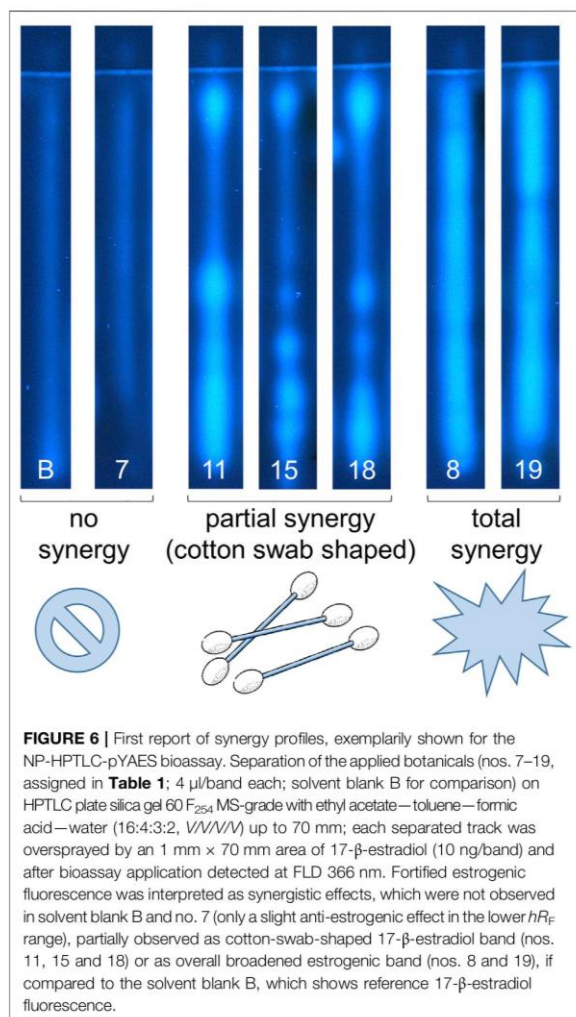
3.2.4 Compounds Inhibiting Tyrosinase

Polyphenoloxidases are responsible for the browning of cut or injured fruits or plant tissues. In mammalian cells, the corresponding tyrosinase controls melanogenesis by catalyzing the hydroxylation of phenols with subsequent oxidation to quinones. An overproduction of melanin induces pigmentary abnormality, freckles, or age spots. Preferably, the cosmetics industry is interested in naturally derived tyrosinase inhibitors (Taibon et al., 2015). In this context, ethnobotanicals are brought into focus. In South Africa, herbal extracts are traditionally used as skin care products to treat burns, abscesses, wounds and acne

(Lall and Kishore, 2014). Chinese herbal medicines with anti-tyrosinase activity are traditionally used as folk skin whiteners. Among the studied botanicals, *Ginkgo biloba* (no. 14), *Panax ginseng* (no. 15), and *Zingiber officinale* (no. 25) were reported to inhibit mushroom tyrosinase (Ye et al., 2010; Hu et al., 2020). Our screening results showed that ginseng (no. 15) and ginger (no. 25) played a minor role in tyrosinase inhibition compared to other botanicals. However, differences in effects can be caused for example by plant subspecies, climate, soil, environmental and agricultural conditions as well as extraction mode. In the planar assay, tyrosinase inhibitors are shown as colorless zones on a greyish-brown background. Many botanical extracts showed multiple tyrosinase inhibitors (**Figures 2–4H**). While acerola (no. 1) (Belwal et al., 2018a), ginkgo (no. 14) (Shu et al., 2020), licorice (no. 55) (Li et al., 2017), and hawthorn (nos. 62–64) (Rocchetti et al., 2020) are known for their anti-tyrosinase activity, the screening results proved similarly potent tyrosinase inhibitors in artichoke (no. 4), plantain (no. 35), yerba mate green (no. 37), rosemary (no. 46), and yarrow (no. 50).

3.2.5 Compounds Inhibiting α - and β -Glucosidase

The enzymes α - and β -glucosidase hydrolyze the saccharide dimers and oligomers, as well as glucosides dependent on the anomeric glycosidic bond, into resorbable monomers such as glucose and into aglycones. In the treatment of hyperglycemic blood levels of type 2 diabetes patients, enzyme inhibitors are of therapeutic interest by reducing postprandial glucose uptake (Simões-Pires et al., 2009; Turkiewicz et al., 2019). Screening results showed several α - and β -glucosidase inhibitors as a specific pattern (at hR_F 42, 48, 62, and 80) for artichoke (no. 4) in both assays (**Figures 2I,J**). Although the α - (Turkiewicz et al., 2019)



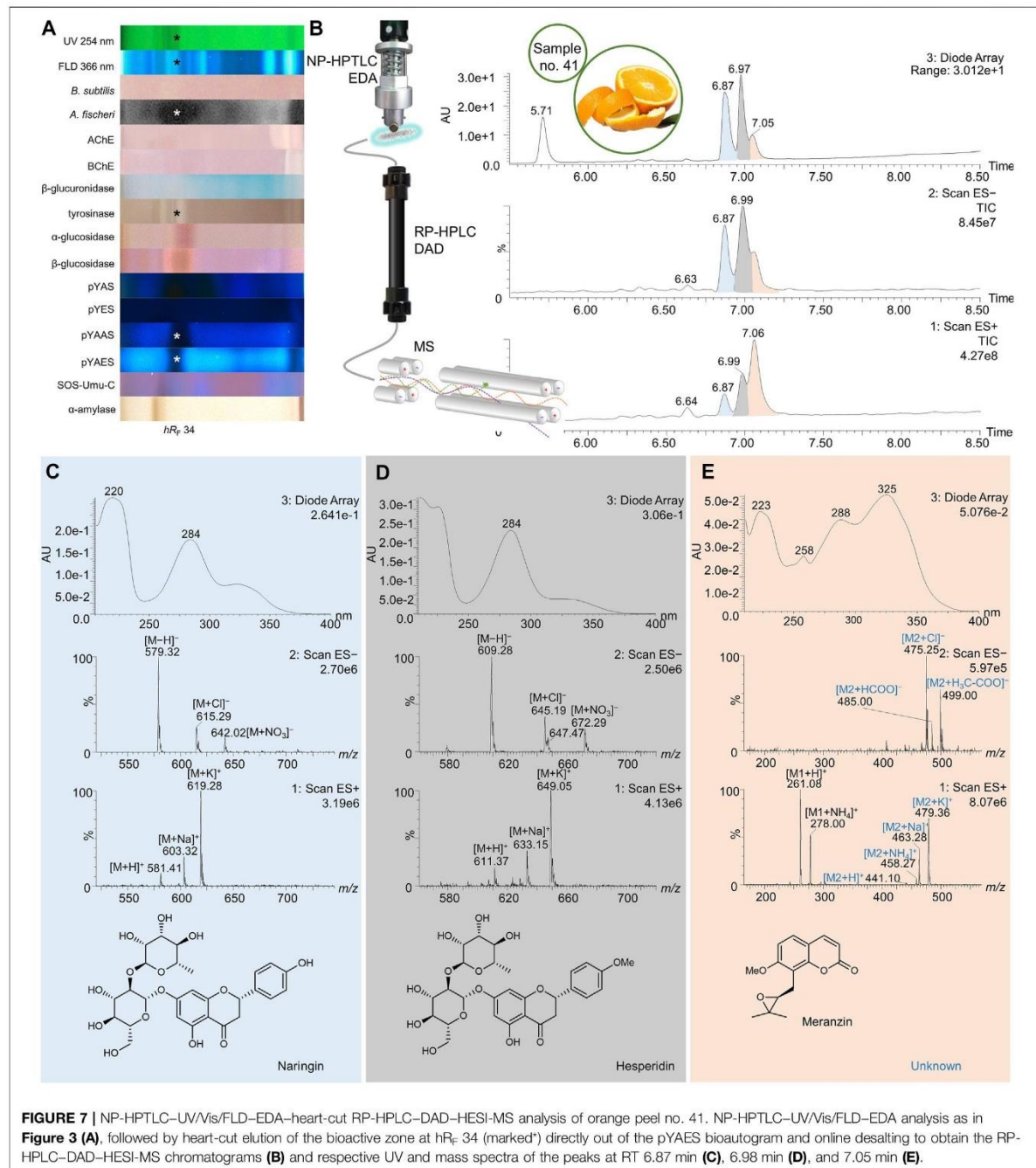
and β -glucosidase (Morlock et al., 2021a) inhibitory potential and chemical composition of extracts of different artichoke cultivars have already been described, the distinct bioactive components have been scarcely assigned in literature. In both glucosidase inhibition assays, samples of blackberry leaves (no. 8), yellow fruit tea (no. 11), red fruit tea (no. 12), elderflower (no. 22), yerba mate green (no. 37), horsetail (no. 49), plantain (no. 53), Siberian ginseng (no. 56), and lemon verbena (no. 68) showed a positive response at hR_F 42 (**Figures 2–4I,J**). In all of them, the same bioactive compound was assumed. Another remarkably similar active compound was observed at hR_F 94 for basil (no. 5), ginkgo (no. 14), European blueberry (no. 18), elderberry (no. 21), hop (no. 24), yerba mate green (no. 37), lemon balm (no. 38), oregano (no. 42), peppermint (no. 44), rosemary (no. 46), star anise (no. 54), Siberian ginseng (no. 56), thyme (no. 57), and cinnamon bark (no. 66). All of them showed both α - and β -glucosidase inhibitory activities. Worldwide more than 1,000 herbal remedies were

traditionally deployed for the maintenance and treatment of high blood glucose levels and thus diabetes. Both, the ethnobotanicals used and their mode of application (as tincture or extract, orally or as infusion) differ between local communities (Cock et al., 2021). Since western medical treatment methods for type 2 diabetes focus on hypoglycemic drugs, such as insulin, ethnopharmacological remedies are considered to be safe and to have less toxic side effects. According to the theory of traditional Chinese medicine, flavonoids (Bai et al., 2019) and polyphenols (Umeno et al., 2016) are attributed to have antidiabetic effects via several mechanisms. Glycyrrhizic acid from *Glycyrrhiza glabra* (no. 55), apigenin and its derivatives as well as quercetin, found in many botanicals (**Table 2**), are known to target α -glucosidase (Bai et al., 2019).

3.2.6 Compounds With Agonistic/Antagonistic Hormonal Effects

Disrupting endocrine signaling pathways can have a severe impact on hormonal balance and cause feminization/masculinization, infertility, acne, and menstrual cycle disorders. Also phytochemicals present in food (Morlock and Klingelhöfer, 2014) or commodities in daily use (Klingelhöfer et al., 2020) can affect the human hormone system. HPTLC hyphenated to the planar yeast androgen/estrogen screens (pYAS/pYES) and their antagonistic versions (pYAAS/pYAES) showed positive reactions to a limited extent (**Figures 2–4K–N**). In the pYAS bioassay, a few 4-methylumbelliferone-blue and thus androgenic responses were detected in acerola (no. 1, hR_F 16), elderberry (no. 21, hR_F 72), chamomile (no. 28, hR_F 99), orange peel (no. 41, hR_F 67 and 98), horsetail (no. 49, hR_F 49 and 61), lemon peel (no. 67, hR_F 99), and for several samples at the application zone (nos. 4, 15, 25, 30, and 56). In the pYES bioassay, 15 botanicals showed estrogen-like activity. In some samples, phytoestrogens were known and expected, e.g., 8-prenylnaringenin in hop (no. 24) (Prencipe et al., 2014; Mbachu et al., 2020), (iso-)liquiritigenin in licorice (no. 55) (Boonmuen et al., 2016), or pesticide residues from fruit surfaces (Schulte-Oehlmann et al., 2011) such as orange peel (no. 41), grape peel (no. 59), or lemon peel (no. 67). However, in acerola (no. 1, hR_F 15 and 27), galangal (no. 13, hR_F 99), chamomile (no. 28, hR_F 63 and 95), lovage (no. 34, hR_F 97), marjoram (no. 35, hR_F 62), oregano (no. 42, hR_F 45), juniper (no. 60, hR_F 89), grape leaves (no. 61, hR_F 92), and hawthorn (nos. 62–64, hR_F 94), estrogen-like responses were also detected. Since steroid hormone-like compounds are known to have a greater affinity to hER α , but several phytoestrogens (e.g., daidzein or genistein) to hER β (Mbachu et al., 2020), the pYES bioassay was also performed via the hER β for the first time. The assay was analogously run for both receptors, but no remarkable difference was observed in the results obtained by both (**Figure 5A** versus **Figure 5B**). The hER α seemed to be less selective. However, a significant difference in the estrogenic pattern was observed after metabolization with the S9 mixture (**Figure 5C**). The use of genetically modified yeast cells containing the hER β for the pYES bioassay and the simulated metabolization via the S9 liver enzyme system were reported here for the first time.

In the respective antagonistic assays, only a few zones were detected. For acerola (no. 1, hR_F 99), fenugreek (no. 6, hR_F 99),



eucalyptus (no. 9, hR_F 5 or 89), ginseng (no. 15, hR_F 96), guarana (no. 16, hR_F 60), kola (no. 31, hR_F 73), orange peel (no. 41, hR_F 25 or 32), licorice (no. 55, hR_F 27), thyme (no. 57, hR_F 24 or 50), and lemon verbena (no. 68, hR_F 99), the possibly antiandrogenic zones were also investigated using an overlaid area of the fluorescent 4-

methylumbelliferone (**Supplementary Figure S4**) to exclude any false-positive response as observed for the physicochemical fluorescence reduction by pigments or dyes (Klingelhöfer et al., 2020). Seven botanical samples (nos. 6, 15, 16, 31, 41, 55, and 68) showed truly antiandrogenic activities. The same verification test was

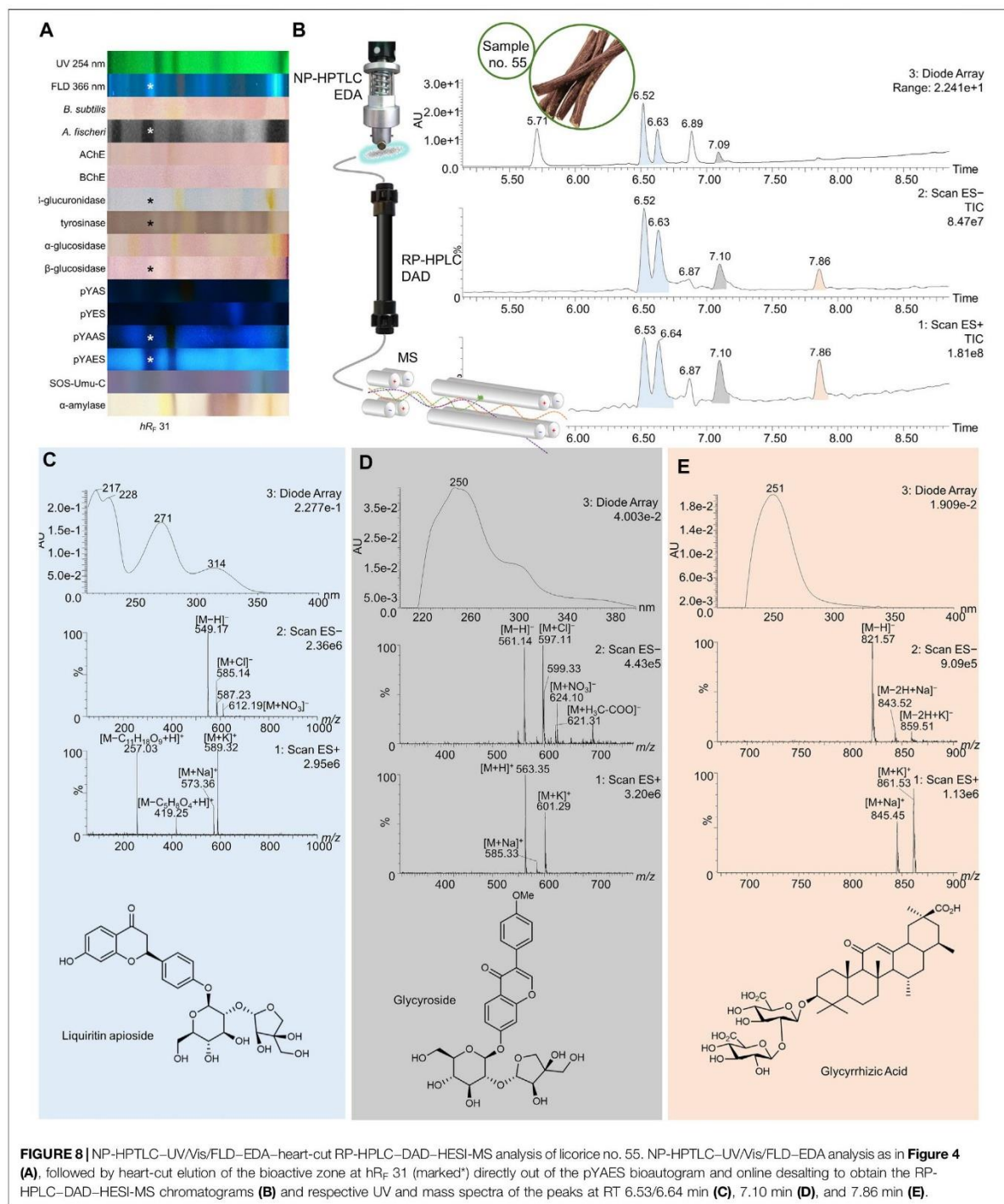


FIGURE 8 | NP-HPTLC–UV/Vis/FLD–EDA–heart-cut RP-HPLC–DAD–HESI-MS analysis of licorice no. 55. NP-HPTLC–UV/Vis/FLD–EDA analysis as in **Figure 4 (A)**, followed by heart-cut elution of the bioactive zone at *hR_F 31* (marked*) directly out of the pYAES bioautogram and online desalting to obtain the RP-HPLC–DAD–HESI-MS chromatograms **(B)** and respective UV and mass spectra of the peaks at RT 6.53/6.64 min **(C)**, 7.10 min **(D)**, and 7.86 min **(E)**.

run for possible antiestrogens in galangal (no. 13, *hR_F 99*), guarana (no. 16, *hR_F 72* or 91), garlic (no. 30, *hR_F 99*), kola (no. 31, *hR_F 99*), orange peel (no. 41, *hR_F 34*), licorice (no. 55, *hR_F 31* or 43), thyme

(no. 57, *hR_F 31*), grape seeds/leaves (nos. 58/61, *hR_F 48*, 61 or 92), and lemon verbena (no. 68, *hR_F 99*). Seven botanicals (nos. 16, 30, 41, 55, 57, 58, and 68) revealed true antiestrogenic properties

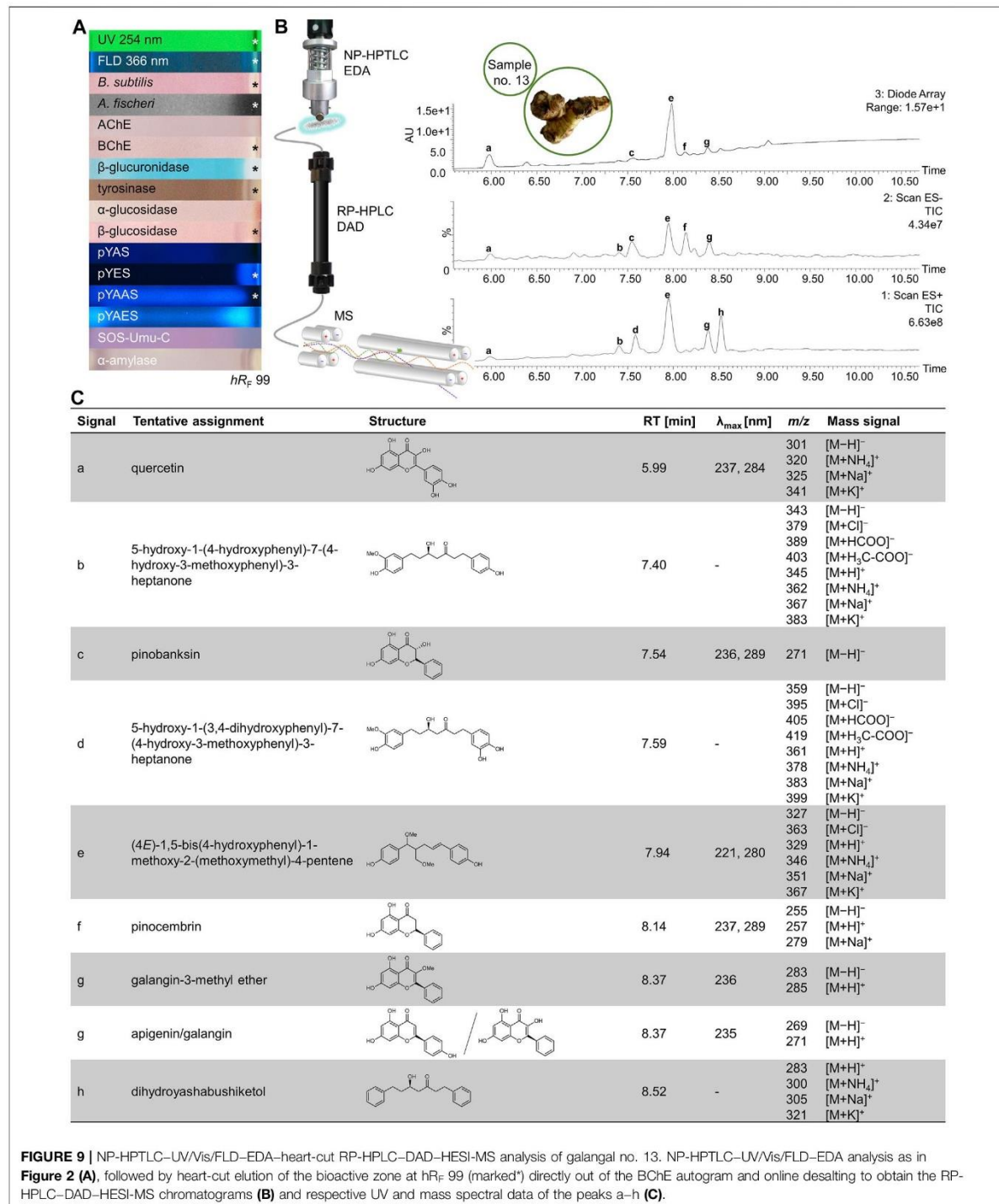
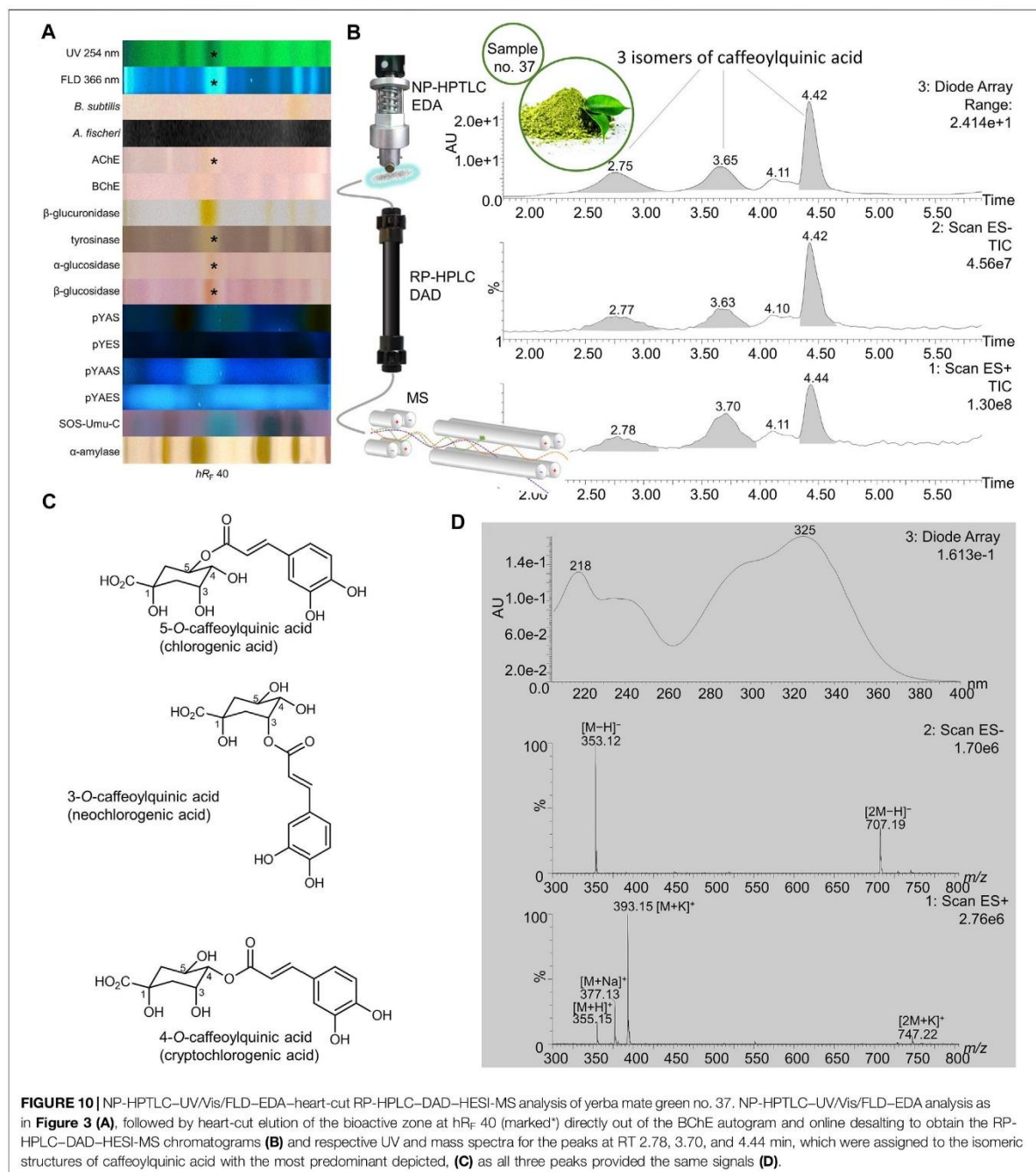


FIGURE 9 | NP-HPTLC–UV/Vis/FLD–EDA–heart-cut RP-HPLC–DAD–HESI-MS analysis of galangal no. 13. NP-HPTLC–UV/Vis/FLD–EDA analysis as in Figure 2 (A), followed by heart-cut elution of the bioactive zone at *hR_f* 99 (marked*) directly out of the BChE autogram and online desalting to obtain the RP-HPLC–DAD–HESI-MS chromatograms (B) and respective UV and mass spectral data of the peaks a–h (C).



(Supplementary Figure S5). In the antiestrogenic assay, synergistic effects were evident. The overlapping 17- β -estradiol area (10 pg/70 mm area) is partially enhanced on sample tracks, apparent as a cotton swab shape if compared to the solvent blank (Figures 2–4N). This

observation revealed synergistic effects between distinct botanical ingredients in most samples (except for nos. 7, 29, and 31) and 17- β -estradiol, resulting in fortified estrogenic activities (Figure 6). This overlapped experimental setup can be transferred to all other assays to identify synergy. Such a

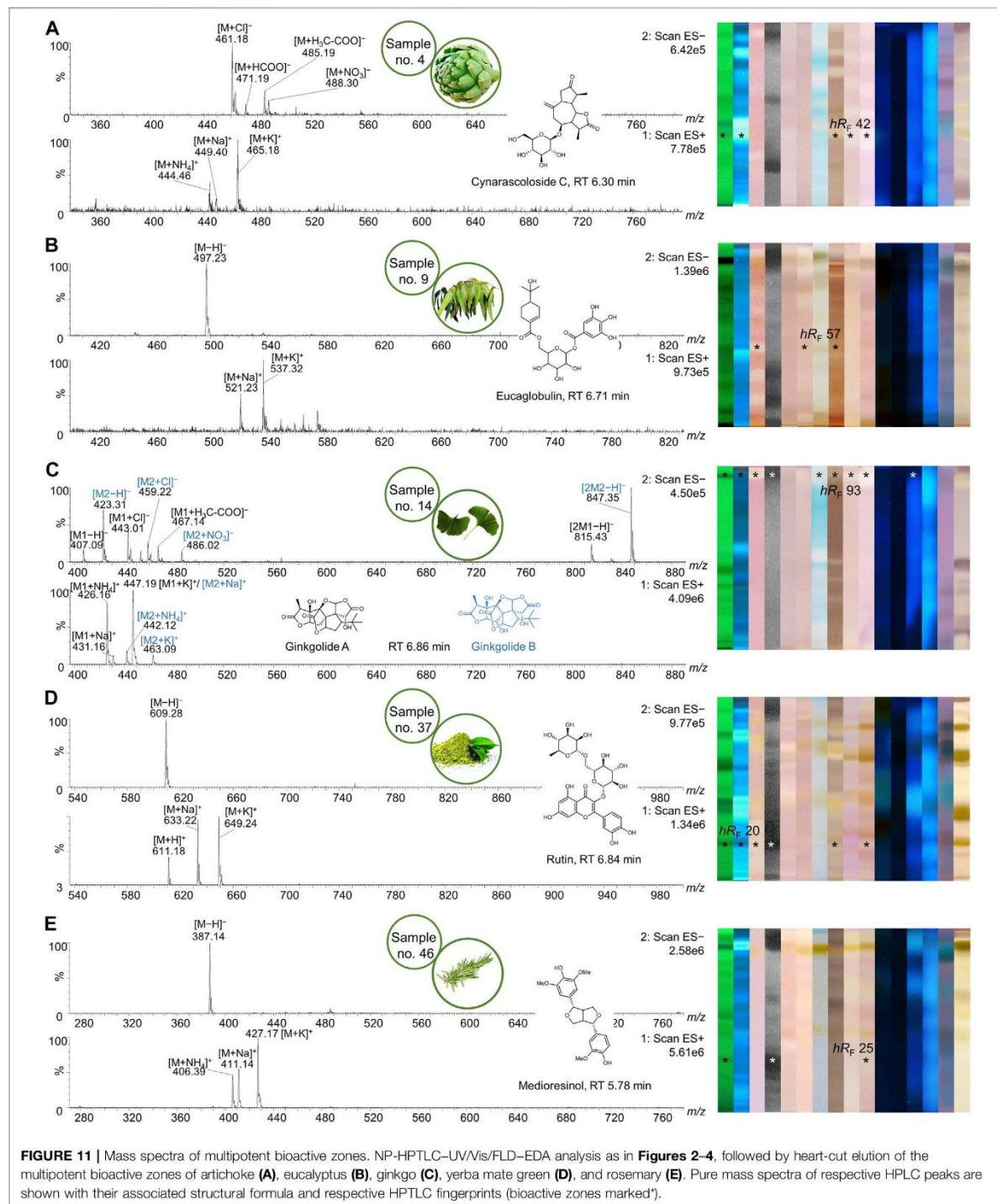


FIGURE 11 | Mass spectra of multipotent bioactive zones. NP-HPTLC-UV/Vis/FLD-EDA analysis as in **Figures 2–4**, followed by heart-cut elution of the multipotent bioactive zones of artichoke (**A**), eucalyptus (**B**), ginkgo (**C**), yerba mate green (**D**), and rosemary (**E**). Pure mass spectra of respective HPLC peaks are shown with their associated structural formula and respective HPTLC fingerprints (bioactive zones marked*).

TABLE 2 | NP-HP TLC-EDA-RP-HPLC-DAD-HESI-MS signals of bioactive zones and respective activity (X) in *B. subtilis* (A), *A. fischeri* (B), AChE/BChE (C), α - β -glucosidase (D), β -glucuronidase (E), tyrosinase (F), pYAS (G), pYES (H), pYAAS (I), pYAES (J) and α -amylase (K). In blue: analyses and respective bioactivity, which were confirmed by a standard; in rose: rebutted ones.

No	Botanical	hRF (\pm 1)	RT [min]	UV λ_{max} [nm]	m/z	Mass signal	Tentative assignment	Literature	A	B	C	D	E	F	G	H	I	J	K				
2	Horehound, white	90	7.38	—	431	[M-H] ⁻	apigenin-O-glucoside	Amessis-Ouchermoukh et al. (2014)	X	X	X	X	X	X	X					X			
					467	[M + Cl] ⁻																	
4	Artichoke	42	3.27/ 3.91/ 4.43	234, 322	455	[M + Na] ⁺																	
					471	[M + K] ⁺																	
					353	[M-H] ⁻										X	X						
					355	[M + H] ⁺																	
					372	[M + NH ₄] ⁺																	
					377	[M + Na] ⁺																	
					393	[M + K] ⁺																	
					461	[M + Cl] ⁻																	
					471	[M + HCOO] ⁻																	
					485	[M + H ₃ C-COO] ⁻																	
9	<i>Eucalyptus</i>	57	6.71	232, 276	444	[M + NH ₄] ⁺																	
					449	[M + Na] ⁺																	
					465	[M + K] ⁺																	
					519	[M-H] ⁻																	
					555	[M + Cl] ⁻																	
					538	[M + NH ₄] ⁺																	
					543	[M + Na] ⁺																	
					559	[M + K] ⁺																	
					447	[M-H] ⁻																	
					483	[M + Cl] ⁻																	
12	Fruit tea, red	41	3.74	—	433	[M-H] ⁻																	
					469	[M + Cl] ⁻																	
					496	[M + NO ₃] ⁻																	
					497	[M-H] ⁻																	
					521	[M + Na] ⁺																	
					537	[M + K] ⁺																	
					449	[M-H] ⁻																	
					449	[M + H] ⁺																	
					466	[M + NH ₄] ⁺																	
					471	[M + Na] ⁺																	
13	Galangal	99	5.99	237, 284	487	[M + K] ⁺																	
					519	[M-H] ⁻																	
					185	[M + H] ⁺																	
					202	[M + NH ₄] ⁺																	
					207	[M + Na] ⁺																	
					223	[M + K] ⁺																	
					353	[M-H] ⁻																	
					353	[M-H] ⁻																	
					355	[M + H] ⁺																	
					372	[M + NH ₄] ⁺																	
2	Horehound, white	90	5.23/ 6.18	233, 326	377	[M + Na] ⁺																	
					377	[M + Na] ⁺																	
					393	[M + K] ⁺																	
					301	[M-H] ⁻																	
					320	[M + NH ₄] ⁺																	
					325	[M + Na] ⁺																	
					341	[M + K] ⁺																	
					449	[M-H] ⁻																	
					449	[M + H] ⁺																	

(Continued on following page)

TABLE 2 | (Continued) NP-HPTLC-EDA-RP-HPLC-DAD-HESI-MS signals of bioactive zones and respective activity (X) in *B. subtilis* (A), *A. fischeri* (B), AChE/BChE (C), α -/ β -glucosidase (D), β -glucuronidase (E), tyrosinase (F), pYAS (G), pYES (H), pYAES (I), pYAES (J) and α -amylase (K). In blue: analytes and respective bioactivity, which were confirmed by a standard; in rose: rebutted ones.

No	Botanical	hR_f (± 1)	RT [min]	UV λ_{max} [nm]	m/z	Mass signal	Tentative assignment	Literature	A	B	C	D	E	F	G	H	I	J	K										
14	Ginkgo	46	7.40	—	343	[M-H] ⁻	5-hydroxy-1-(4-hydroxyphenyl)-7-(4-hydroxy-3-methoxyphenyl)-3-heptanone	Zhou et al. (2018)	X	X	X	X	X	X	X	X	X	X	X	X									
					379	[M + Cl] ⁻																							
					389	[M + HCOO] ⁻																							
					403	[M + H ₃ C-COO] ⁻																							
					345	[M + H] ⁺																							
					362	[M + NH ₄] ⁺																							
					367	[M + Na] ⁺																							
					383	[M + K] ⁺																							
					271	[M-H] ⁻			236, 289	pinobanksin	Zhou et al. (2018)	X	X	X	X	X	X	X	X	X	X	X	X	X					
					359	[M-H] ⁻																							
					395	[M + Cl] ⁻																							
					405	[M + HCOO] ⁻																							
					419	[M + H ₃ C-COO] ⁻																							
					361	[M + H] ⁺																							
378	[M + NH ₄] ⁺																												
383	[M + Na] ⁺																												
399	[M + K] ⁺																												
327	[M-H] ⁻	221, 280	(4E)-1,5-bis(4-hydroxyphenyl)-1-methoxy-2-(methoxymethyl)-4-pentene	Zhou et al. (2018)	X	X	X	X	X			X	X	X	X	X	X	X	X	X									
363	[M + Cl] ⁻																												
329	[M + H] ⁺																												
346	[M + NH ₄] ⁺																												
351	[M + Na] ⁺																												
367	[M + K] ⁺																												
255	[M-H] ⁻	pinoembrin			Zhou et al. (2018)	X	X	X	X	X	X	X	X	X	X	X	X	X	X	X									
257	[M + H] ⁺																												
279	[M + Na] ⁺																												
283	[M-H] ⁻																												
285	[M + H] ⁺																												
269	[M-H] ⁻																												
271	[M + H] ⁺																												
283	[M + H] ⁺																												
300	[M + NH ₄] ⁺																												
305	[M + Na] ⁺																												
321	[M + K] ⁺																												
344	[M + NH ₄] ⁺																												
349	[M + Na] ⁺																												
365	[M + K] ⁺																												
439	[M-H] ⁻	galangin-3-methyl ether	Zhou et al. (2018)	X	X	X	X	X	X	X	X	X	X	X	X	X	X	X											
475	[M + Cl] ⁻																												
458	[M + NH ₄] ⁺																												
463	[M + Na] ⁺																												
479	[M + K] ⁺																												
407	[M-H] ⁻			galangin	Krüger et al. (2017); Zhou et al. (2018)	X	X	X	X	X	X	X	X	X	X	X	X	X	X	X									
443	[M + Cl] ⁻																												
453	[M + HCOO] ⁻																												
467	[M + H ₃ C-COO] ⁻																												
815	[2M-H] ⁻																												
426	[M + NH ₄] ⁺																												
14	Ginkgo					93	6.86	—	407	[M-H] ⁻	dihydroyashabushiketol	Zhou et al. (2018)	X	X	X	X	X	X	X	X	X	X	X	X					
									443	[M + Cl] ⁻																			
									453	[M + HCOO] ⁻																			
		467	[M + H ₃ C-COO] ⁻																										
		815	[2M-H] ⁻																										
		426	[M + NH ₄] ⁺																										
		14	Ginkgo						46	4.03			230, 267	321	[M + K] ⁺	biobalide	Mauri et al. (1999), Niu et al. (2017)	X	X	X	X	X	X	X	X	X	X	X	X
														344	[M + NH ₄] ⁺														
				349	[M + Na] ⁺																								
				365	[M + K] ⁺																								
				439	[M-H] ⁻																								
				475	[M + Cl] ⁻																								
				458	[M + NH ₄] ⁺																								
				463	[M + Na] ⁺																								
479	[M + K] ⁺																												
407	[M-H] ⁻																												
443	[M + Cl] ⁻																												
453	[M + HCOO] ⁻																												
467	[M + H ₃ C-COO] ⁻																												
815	[2M-H] ⁻																												
426	[M + NH ₄] ⁺																												
14	Ginkgo	93	6.42	—	439	[M-H] ⁻	ginkgolide C	Chen et al. (2005); Ding et al. (2006); Niu et al. (2017)	X	X	X	X	X	X	X	X	X	X	X	X									
					475	[M + Cl] ⁻																							
					458	[M + NH ₄] ⁺																							
					463	[M + Na] ⁺																							
					479	[M + K] ⁺																							
					407	[M-H] ⁻																							
					443	[M + Cl] ⁻																							
					453	[M + HCOO] ⁻																							
					467	[M + H ₃ C-COO] ⁻																							
					815	[2M-H] ⁻																							
					426	[M + NH ₄] ⁺																							
					14	Ginkgo			93	6.86	—	407	[M-H] ⁻	ginkgolide A	Wang et al. (2016), Niu et al. (2017)	X	X	X	X	X	X	X	X	X	X	X	X		
												443	[M + Cl] ⁻																
												453	[M + HCOO] ⁻																
467	[M + H ₃ C-COO] ⁻																												
815	[2M-H] ⁻																												
426	[M + NH ₄] ⁺																												

(Continued on following page)

TABLE 2 | (Continued) NP-HPTLC-EDA-RP-HPLC-DAD-HESI-MS signals of bioactive zones and respective activity (X) in *B. subtilis* (A), *A. fischeri* (B), AChE/BChE (C), α - β -glucosidase (D), β -glucuronidase (E), tyrosinase (F), pYAS (G), pYES (H), pYAS (I), pYAS (J) and α -amylase (K). In blue: analytes and respective bioactivity, which were confirmed by a standard; in rose: rebutted ones.

No	Botanical	<i>h</i> R _F (\pm 1)	RT [min]	UV λ_{max} [nm]	<i>m/z</i>	Mass signal	Tentative assignment	Literature	A	B	C	D	E	F	G	H	I	J	K																		
15	Ginseng	16	7.60	243	431	[M + Na] ⁺	ginsenoside Rg1/Rf	Du et al. (2018); Wilson and Sander (2018)	X	X	X	X	X	X	X	X	X	X	X																		
					447	[M + K] ⁺																															
					423	[M - H] ⁻																															
					459	[M + Cl] ⁻																															
					847	[2M - H] ⁻																															
					442	[M + NH ₄] ⁺																															
					463	[M + K] ⁺																															
					836	[M + Cl] ⁻																															
					846	[M + HCOO] ⁻																															
					860	[M + H ₃ C-COO] ⁻																															
					824	[M + Na] ⁺																															
					840	[M + K] ⁺																															
					800	[M - H] ⁻																															
					836	[M + Cl] ⁻																															
					846	[M + HCOO] ⁻																															
16	Guarana	91	5.12/ 5.98	203, 279	289	[M - H] ⁻	(epi)catechin	da Silva et al. (2017), Morlock et al. (2021b)	X	X	X	X	X	X	X	X	X	X	X																		
					325	[M + Cl] ⁻																															
					291	[M + H] ⁺																															
					329	[M + K] ⁺																															
					577	[M - H] ⁻																															
					579	[M + H] ⁺																															
					601	[M + Na] ⁺																															
					617	[M + K] ⁺																															
					353	[M - H] ⁻																															
					353	[M - H] ⁻																															
					355	[M + H] ⁺																															
					372	[M + NH ₄] ⁺																															
					377	[M + Na] ⁺																															
					393	[M + K] ⁺																															
					447	[M - H] ⁻																															
19	Hibiscus Elder flower	45 40	4.57 3.80/ 4.67	234, 322 233, 326	353	[M - H] ⁻	chlorogenic acid ^b chlorogenic acid ^b	da Silva et al. (2017), Morlock et al. (2021b)	X	X	X	X	X	X	X	X	X	X	X																		
					353	[M - H] ⁻																															
					355	[M + H] ⁺																															
					372	[M + NH ₄] ⁺																															
					377	[M + Na] ⁺																															
					393	[M + K] ⁺																															
					447	[M - H] ⁻																															
					449	[M + H] ⁺																															
					471	[M + Na] ⁺																															
					487	[M + K] ⁺																															
					317	[M - H] ⁻																															
					319	[M + H] ⁺																															
					336	[M + NH ₄] ⁺																															
					341	[M + Na] ⁺																															
					357	[M + K] ⁺																															
24	Hop	92	7.05	264, 347	393	[M + K] ⁺	kaempferol-3-O-glucoside (astragalin)	Önder et al. (2013)	X	X	X	X	X	X	X	X	X	X	X																		
					447	[M - H] ⁻																															
					449	[M + H] ⁺																															
					471	[M + Na] ⁺																															
					487	[M + K] ⁺																															
					317	[M - H] ⁻																															
					319	[M + H] ⁺																															
					336	[M + NH ₄] ⁺																															
					341	[M + Na] ⁺																															
					357	[M + K] ⁺																															
					293	[M - H] ⁻																															
					295	[M + H] ⁺																															
					312	[M + NH ₄] ⁺																															
					317	[M + Na] ⁺																															
					333	[M + K] ⁺																															
25	Ginger	94	8.06	297	293	[M - H] ⁻	6-gingerol	Krüger et al. (2018)	X	X	X	X	X	X	X	X	X	X	X																		
					295	[M + H] ⁺																															
					312	[M + NH ₄] ⁺																															
					317	[M + Na] ⁺																															
					333	[M + K] ⁺																															
					431	[M - H] ⁻																															
					433	[M + H] ⁺																															
					28	Chamomile														50	6.95	237, 266, 335	237	[M - H] ⁻	apigenin-7-O-glucoside	Lin and Harnly, (2012)	X	X	X	X	X	X	X	X	X	X	X
																							266	[M + H] ⁺													
																							335	[M + K] ⁺													
																							431	[M - H] ⁻													
																							433	[M + H] ⁺													

(Continued on following page)

TABLE 2 | (Continued) NP-HPTLC-EDA-RP-HPLC-DAD-HESI-MS signals of bioactive zones and respective activity (X) in *B. subtilis* (A), *A. fischeri* (B), AChE/BChE (C), α -/ β -glucosidase (D), β -glucuronidase (E), tyrosinase (F), pYAS (G), pYES (H), pYAES (I), pYAES (J), pYAES (K), in blue: analytes and respective bioactivity, which were confirmed by a standard; in rose: rebutted ones.

No	Botanical	hR_f (± 1)	RT [min]	UV λ_{max} [nm]	m/z	Mass signal	Tentative assignment	Literature	A	B	C	D	E	F	G	H	I	J	K	
		63	7.51	241, 257, 331	455 471 473 475 497 513 447 471	[M + Na] ⁺ [M + K] ⁺ [M-H] ⁻ [M + H] ⁺ [M + Na] ⁺ [M + K] ⁺ [M-H] ⁻ [M + Na] ⁺	apigenin-7-O-(2''-O-acetylglucoside)	Lin and Harnly, (2012)				X							X	
33	Caraway	43	7.04	—	487 433 469 452 457 473	[M + K] ⁺ [M-H] ⁻ [M + Cl] ⁻ [M + NH ₄] ⁺ [M + Na] ⁺ [M + K] ⁺	luteolin-7-O glucoside	Hossain et al. (2014)		X		X	X						X	
35	Majoram	78	6.52	236, 278	359 395 719 378 383 399 301 337 303 343 365 381 452 457 473	[M-H] ⁻ [M + Cl] ⁻ [2M-H] ⁻ [M + NH ₄] ⁺ [M + Na] ⁺ [M + K] ⁺ [M-H] ⁻ [M + Cl] ⁻ [M + H] ⁺ [M + H] ⁺ [M + Na] ⁺ [M + K] ⁺ [M + NH ₄] ⁺ [M + Na] ⁺ [M + K] ⁺	quercetin arabinoside	Hossain et al. (2014), Çelik et al. (2017)	X	X	X	X	X						X	
		93	6.20	219, 326	482 487 473	[M + K] ⁺ [M + Na] ⁺ [M + K] ⁺	rosmarinic acid	Hossain et al. (2014), Çelik et al. (2017)	X	X	X	X	X							X
		97	7.85	235, 287	381 381 381	[M + K] ⁺ [M-H] ⁻ [M + K] ⁺	hesperetin/quercetin	Hossain et al. (2014); Erenler et al. (2016)	X	X	X	X	X	X						X
37	Yerba mate green	6	3.90	—	452 457 473	[M + NH ₄] ⁺ [M + Na] ⁺ [M + K] ⁺	dicafeic acid	Souza et al. (2011)	X	X	X	X	X	X						X
		14	7.07	—	482 487 503	[M + NH ₄] ⁺ [M + Na] ⁺ [M + K] ⁺	quercetin arabinoside	Souza et al. (2011)	X	X	X	X	X	X						X
		14	7.07	—	482 487 503	[M + NH ₄] ⁺ [M + Na] ⁺ [M + K] ⁺	quercetin glucoside	Bravo et al. (2007); Souza et al. (2011), Mateos et al. (2018)	X	X	X	X	X	X						X
		20	6.84	256, 356	364 381 609 611 633 649 353 355 372 377 393 367 369 391 407	[M + Na] ⁺ [M + K] ⁺ [M-H] ⁻ [M + H] ⁺ [M + Na] ⁺ [M + K] ⁺ [M + H] ⁺ [M + NH ₄] ⁺ [M + Na] ⁺ [M + K] ⁺ [M-H] ⁻ [M + H] ⁺ [M + H] ⁺ [M + Na] ⁺ [M + K] ⁺	dicafeic acid	Bravo et al. (2007); Souza et al. (2011)	X	X	X	X	X	X						X
		20	6.84	256, 356	364 381 609 611 633 649 353 355 372 377 393 367 369 391 407	[M + Na] ⁺ [M + K] ⁺ [M-H] ⁻ [M + H] ⁺ [M + Na] ⁺ [M + K] ⁺ [M + H] ⁺ [M + NH ₄] ⁺ [M + Na] ⁺ [M + K] ⁺	rutin	Krüger et al. (2017), Mateos et al. (2018)	X	X	X	X	X	X						X
		40	2.75/ 3.65/ 4.42	217, 324	353 355 372 377 393 367 369 391 407	[M-H] ⁻ [M + H] ⁺ [M + NH ₄] ⁺ [M + Na] ⁺ [M + K] ⁺ [M-H] ⁻ [M + H] ⁺ [M + Na] ⁺ [M + K] ⁺	chlorogenic acid ^b	Mateos et al. (2018), Morlock et al. (2021a)	X	X	X	X	X	X						X
		47	5.11	236, 322	367 369 391 407	[M-H] ⁻ [M + H] ⁺ [M + Na] ⁺ [M + K] ⁺	feruloylquinic acid	Bravo et al., 2007; Souza et al. (2011), Mateos et al. (2018)	X	X	X	X	X	X						X

(Continued on following page)

TABLE 2 | (Continued) NP-HPTLC-EDA-RP-HPLC-DAD-HESI-MS signals of bioactive zones and respective activity (X) in *B. subtilis* (A), *A. fischeri* (B), AChE/BChE (C), α - β -glucosidase (D), β -glucuronidase (E), tyrosinase (F), pYAS (G), pYES (H), pYAES (I), pYAES (J) and α -amylase (K), in blue: analytes and respective bioactivity, which were confirmed by a standard; in rose: rebutted ones.

No	Botanical	<i>h</i> R _F (\pm 1)	RT [min]	UV λ _{max} [nm]	<i>m/z</i>	Mass signal	Tentative assignment	Literature	A	B	C	D	E	F	G	H	I	J	K			
38	Lemon balm	92	6.21	219, 326	515	[M-H] ⁻	dicaffeoylquinic acid	Krüger et al. (2017), Mateos et al. (2018)	X	X	X	X	X	X	X	X	X	X	X	X		
					517	[M + H] ⁺																
					539	[M + Na] ⁺																
					555	[M + K] ⁺																
					359	[M-H] ⁻																
					395	[M + Cl] ⁻																
41	Orange peel	21	5.74	229, 278	719	[2M-H] ⁻	rosmarinic acid	Krüger et al. (2017), Yilmaz (2020)	X	X	X	X	X	X	X	X	X	X	X	X		
					361	[M + H] ⁺																
					378	[M + NH ₄] ⁺																
					383	[M + Na] ⁺																
					399	[M + K] ⁺																
					390	[M + NH ₄] ⁺																
					395	[M + Na] ⁺																
					411	[M + K] ⁺																
					593	[M-H] ⁻																
					629	[M + Cl] ⁻																
41	Orange peel	21	5.74	229, 278	390	[M + NH ₄] ⁺	sinensetin/rangeretin	Anagnostopoulou et al. (2005), Li et al. (2006)	X	X	X	X	X	X	X	X	X	X	X	X	X	
					395	[M + Na] ⁺																
					411	[M + K] ⁺																
					593	[M-H] ⁻																
					629	[M + Cl] ⁻																
					595	[M + H] ⁺																
					617	[M + Na] ⁺																
					633	[M + K] ⁺																
					577	[M-H] ⁻																
					613	[M + Cl] ⁻																
41	Orange peel	21	5.74	229, 278	579	[M + H] ⁺	didymin	Anagnostopoulou et al. (2005)	X	X	X	X	X	X	X	X	X	X	X	X	X	
					601	[M + Na] ⁺																
					617	[M + K] ⁺																
					607	[M-H] ⁻																
					643	[M + Cl] ⁻																
					609	[M + H] ⁺																
					631	[M + Na] ⁺																
					647	[M + K] ⁺																
					595	[M-H] ⁻																
					631	[M + Cl] ⁻																
41	Orange peel	21	5.74	229, 278	597	[M + H] ⁺	apigenin-7-O-rutinoside (sorhofolin)	Anagnostopoulou et al. (2005)	X	X	X	X	X	X	X	X	X	X	X	X	X	X
					619	[M + Na] ⁺																
					635	[M + K] ⁺																
					579	[M-H] ⁻																
					615	[M + Cl] ⁻																
					642	[M + NO ₃] ⁻																
					581	[M + H] ⁺																
					603	[M + Na] ⁺																
					619	[M + K] ⁺																
					609	[M-H] ⁻																
41	Orange peel	21	5.74	229, 278	609	[M + Cl] ⁻	diosmin	Anagnostopoulou et al. (2005)	X	X	X	X	X	X	X	X	X	X	X	X	X	X
					645	[M + NO ₃] ⁻																
					672	[M + H] ⁺																
					611	[M + Na] ⁺																
					633	[M + K] ⁺																
					649	[M + Cl] ⁻																
					601	[M + Na] ⁺																
					617	[M + K] ⁺																
					607	[M-H] ⁻																
					643	[M + Cl] ⁻																
41	Orange peel	21	5.74	229, 278	601	[M + Na] ⁺	erfocitrin	Manthey and Grohmann (1996), Anagnostopoulou et al. (2005)	X	X	X	X	X	X	X	X	X	X	X	X	X	X
					617	[M + K] ⁺																
					607	[M-H] ⁻																
					643	[M + Cl] ⁻																
					609	[M + H] ⁺																
					631	[M + Na] ⁺																
					647	[M + K] ⁺																
					595	[M-H] ⁻																
					631	[M + Cl] ⁻																
					597	[M + H] ⁺																
41	Orange peel	21	5.74	229, 278	619	[M + Na] ⁺	naringin	Anagnostopoulou et al. (2005); Sawalha et al. (2009), Puranik et al. (2019)	X	X	X	X	X	X	X	X	X	X	X	X	X	X
					635	[M + K] ⁺																
					579	[M-H] ⁻																
					615	[M + Cl] ⁻																
					642	[M + NO ₃] ⁻																
					581	[M + H] ⁺																
					603	[M + Na] ⁺																
					619	[M + K] ⁺																
					609	[M-H] ⁻																
					645	[M + NO ₃] ⁻																
41	Orange peel	21	5.74	229, 278	672	[M + H] ⁺	hesperidin	Anagnostopoulou et al. (2005), Sawalha et al. (2009), Puranik et al. (2019)	X	X	X	X	X	X	X	X	X	X	X	X	X	X
					611	[M + Na] ⁺																
					633	[M + K] ⁺																
					649	[M + Cl] ⁻																

(Continued on following page)

TABLE 2 | (Continued) NP-HPTLC-EDA-RP-HPLC-DAD-HESI-MS signals of bioactive zones and respective activity (X) in *B. subtilis* (A), *A. fischeri* (B), AChE/BChE (C), α -/ β -glucosidase (D), β -glucuronidase (E), tyrosinase (F), pYAS (G), pYES (H), pYAES (I), pYAES (J) and α -amylase (K). In blue: analytes and respective bioactivity, which were confirmed by a standard; in rose: rebutted ones.

No	Botanical	hR _F (±1)	RT [min]	UV λ_{max} [nm]	m/z	Mass signal	Tentative assignment	Literature	A	B	C	D	E	F	G	H	I	J	K					
42	Oregano	32 ^a	2.88	219, 270	261	[M + H] ⁺	meranzin	Dugo et al. (2000)			X			X					X	X				
					278	[M + NH ₄] ⁺	hexamethoxyflavone (nobiletin)	Anagnostopoulou et al. (2005), Li et al. (2006)		X		X		X		X						X		
					403	[M + H] ⁺																		
					425	[M + Na] ⁺																		
					441	[M + K] ⁺																		
					827	[2M + Na] ⁺																		
					373	[M + H] ⁺	8.44	—																
					395	[M + Na] ⁺																		
					411	[M + K] ⁺																		
					304	[M + NH ₄] ⁺																		
					309	[M + Na] ⁺																		
					325	[M + K] ⁺																		
					331	[M + H] ⁺																		
					367	[M + Cl] ⁻	62	7.36	241															
377	[M + HCOO] ⁻																							
391	[M + H ₂ C-COO] ⁻																							
333	[M + H] ⁺																							
350	[M + NH ₄] ⁺																							
355	[M + Na] ⁺																							
371	[M + K] ⁺																							
379	[M + Cl] ⁻	81	5.81/ 6.20	—																				
367	[M + Na] ⁺																							
383	[M + K] ⁺																							
331	[M + H] ⁺	93	5.99	238																				
353	[M + Na] ⁺																							
369	[M + K] ⁺																							
331	[M + H] ⁺																							
367	[M + Cl] ⁻																							
333	[M + H] ⁺																							
371	[M + K] ⁺																							
271	[M + H] ⁺	99	7.51	238, 279																				
269	[M + H] ⁺																							
271	[M + H] ⁺																							
315	[M + H] ⁺																							
317	[M + H] ⁺																							
339	[M + Na] ⁺																							
355	[M + K] ⁺																							
313	[M + H] ⁺																							
315	[M + H] ⁺																							
337	[M + Na] ⁺																							
353	[M + K] ⁺																							
607	[M + H] ⁺	20	7.05	249, 344																				
609	[M + H] ⁺																							
631	[M + Na] ⁺																							
647	[M + K] ⁺																							
577	[M + H] ⁺	26	7.00	267, 267, 339																				
613	[M + Cl] ⁻																							
579	[M + H] ⁺																							

(Continued on following page)

TABLE 2 | (Continued) NP-HPTLC-EDA-RP-HPLC-DAD-HESI-MS signals of bioactive zones and respective activity (X) in *B. subtilis* (A), *A. fischeri* (B), AChE/BChE (C), α - β -glucosidase (D), β -glucuronidase (E), tyrosinase (F), pYAS (G), pYES (H), pYAES (I), pYAES (J) and α -amylase (K). In blue: analytes and respective bioactivity, which were confirmed by a standard; in rose: rebutted ones.

No	Botanical	hRF _F (± 1)	RT [min]	UV λ_{max} [nm]	m/z	Mass signal	Tentative assignment	Literature	A	B	C	D	E	F	G	H	I	J	K							
46	Rosemary	93	6.23	235, 286	601	[M + Na] ⁺	rosmarinic acid	Fecka et al. (2004)	X	X	X	X	X	X												
					617	[M + K] ⁺																				
					359	[M-H] ⁻																				
					395	[M + Cl] ⁻																				
					383	[M + Na] ⁺																				
					399	[M + K] ⁺																				
					577	[M-H] ⁻			6.99	236	577	[M-H] ⁻	apigenin-7-O-rutinoside (isorhoifolin)	Hossain et al. (2010)	X	X	X	X	X	X						
					613	[M + Cl] ⁻					613	[M + Cl] ⁻														
					640	[M + NO ₃] ⁻					640	[M + NO ₃] ⁻														
					579	[M + H] ⁺					579	[M + H] ⁺														
					601	[M + Na] ⁺					601	[M + Na] ⁺														
					617	[M + K] ⁺					617	[M + K] ⁺														
					46	Rosemary			25	4.89	232, 269	337	[M + Na] ⁺	circimaritin	Ezzat et al. (2016), Krüger et al. (2017), Pérez-Mendoza et al. (2020)	X	X	X	X	X	X					
353	[M + K] ⁺																									
362	[M + NH ₄] ⁺	5.44	226, 285	362			[M + NH ₄] ⁺	rosmadial				Mena et al. (2016), Pérez-Mendoza et al. (2020)	X			X	X	X	X							
367	[M + Na] ⁺			367			[M + Na] ⁺																			
383	[M + K] ⁺			383			[M + K] ⁺	medioresinol				Mena et al. (2016)	X			X	X	X	X	X						
387	[M-H] ⁻	5.78	224, 263	387			[M-H] ⁻																			
406	[M + NH ₄] ⁺			406			[M + NH ₄] ⁺																			
411	[M + Na] ⁺			411			[M + Na] ⁺																			
427	[M + K] ⁺			427			[M + K] ⁺																			
315	[M-H] ⁻	6.06	233	315			[M-H] ⁻	3-O-methylquercetin (isorhamnetin)				Mena et al. (2016)	X			X	X	X	X	X						
351	[M + Cl] ⁻			351			[M + HCOO] ⁻																			
361	[M + HCOO] ⁻			361			[M + HCOO] ⁻																			
46	Rosemary	41	4.05/5.05	220, 263			375	[M + H ₃ C-COO] ⁻				quercetin-3-O-hexoside (isoquercitrin)	Hossain et al. (2010)			X	X	X	X	X	X					
					317	[M + H] ⁺																				
					339	[M + Na] ⁺			339	[M + Na] ⁺																
					355	[M + K] ⁺			355	[M + K] ⁺																
					499	[M + Cl] ⁻	6.13	235	499	[M + Cl] ⁻																
					503	[M + K] ⁺	6.99	236	503	[M + K] ⁺	apigenin-7-O-rutinoside (isorhoifolin)			Mena et al. (2016)	X	X	X	X	X	X						
					577	[M-H] ⁻			577	[M-H] ⁻																
					613	[M + Cl] ⁻			613	[M + Cl] ⁻																
					579	[M + H] ⁺			579	[M + H] ⁺																
					601	[M + Na] ⁺			601	[M + Na] ⁺																
					617	[M + K] ⁺			617	[M + K] ⁺																
					46	Rosemary	62 ^a	6.48	236	299	[M-H] ⁻			diosmetin/6-O-methylapigenin (hispidulin)	Pérez-Mendoza et al. (2020)	X	X	X	X	X	X					
										335	[M + Cl] ⁻															
301	[M + H] ⁺			301						[M + H] ⁺																
318	[M + NH ₄] ⁺			318						[M + NH ₄] ⁺																
323	[M + Na] ⁺			323						[M + Na] ⁺																
339	[M + K] ⁺			339						[M + K] ⁺																
302	[M + Cl] ⁻			302						[M + Cl] ⁻	7-O-methylapigenin (genkwanin)/ acacetin	Ezzat et al. (2016), Mena et al. (2016), Krüger et al. (2017), Pérez-Mendoza et al. (2020)	X			X	X	X	X	X						
307	[M + Na] ⁺			307						[M + Na] ⁺																
323	[M + K] ⁺			323						[M + K] ⁺																
461	[M-H] ⁻	6.89	236	461						[M-H] ⁻	luteolin-7-O-glucuronide	Mena et al. (2016), Pérez-Mendoza et al. (2020)	X			X	X	X	X	X						
463	[M + H] ⁺			463						[M + H] ⁺																
485	[M + Na] ⁺			485						[M + Na] ⁺																

(Continued on following page)

TABLE 2 | (Continued) NP-HPTLC-EDA-RP-HPLC-DAD-HESI-MS signals of bioactive zones and respective activity (X) in *B. subtilis* (A), *A. fischeri* (B), AChE/BChE (C), α -/ β -glucosidase (D), β -glucuronidase (E), tyrosinase (F), pYAS (G), pYES (H), pYAES (I), pYAES (J) and α -amylase (K). In blue: analytes and respective bioactivity, which were confirmed by a standard; in rose: rebutted ones.

No	Botanical	R/Rf (\pm 1)	RT [min]	UV λ_{max} [nm]	m/z	Mass signal	Tentative assignment	Literature	A	B	C	D	E	F	G	H	I	J	K																															
48	Sea buckthorn	21	6.74/ 7.02	254, 354	501	[M + K] ⁺	caffeic acid hexoside	Hossain et al. (2010)	X	X	X	X	X	X	X	X	X	X	X																															
					377	[M + O] ⁻																																												
					401	[M + H ₃ C-COO] ⁻																																												
					365	[M + Na] ⁺																																												
					381	[M + K] ⁺																																												
					359	[M-H] ⁻														rosmarinic acid	Hossain et al. (2010), Mena et al. (2016), Pérez-Mendoza et al. (2020)	X	X	X	X	X	X	X	X	X	X	X	X	X	X															
					395	[M + O] ⁻																																												
					719	[2M-H] ⁻																																												
					378	[M + NH ₄] ⁺																																												
					383	[M + Na] ⁺																																												
					399	[M + K] ⁺																																												
					743	[2M + Na] ⁺																																												
331	[M-H] ⁻	camosic acid	Ezzat et al. (2016), Mena et al. (2016), Pérez-Mendoza et al. (2020)	X	X	X	X	X	X	X	X	X	X	X	X	X	X																																	
333	[M + H] ⁺																																																	
355	[M + Na] ⁺																																																	
371	[M + K] ⁺																																																	
287	[M + H] ⁺																																																	
309	[M + Na] ⁺																																																	
325	[M + K] ⁺																																																	
623	[M-H] ⁻																	luteolin	Mena et al. (2016)	X	X	X	X	X	X	X	X	X	X	X	X	X	X																	
659	[M + O] ⁻																																																	
669	[M + HCOO] ⁻																																																	
625	[M + H] ⁺																																																	
647	[M + Na] ⁺																																																	
663	[M + K] ⁺																																																	
353	[M-H] ⁻	isorhamnetin-3-O-rutinoside (neorissin)/ isorhamnetin-3-glucoside-7- rhamnoside (brassicidin)	Zheng et al. (2016)	X	X	X	X	X	X	X	X	X	X	X	X	X	X																																	
377	[M + H] ⁺																																																	
393	[M + K] ⁺																																																	
377	[M + Na] ⁺																																																	
355	[M + H] ⁺																																																	
377	[M + Na] ⁺																																																	
393	[M + K] ⁺																																																	
377	[M + Na] ⁺																																																	
377	[M + Na] ⁺																																																	
377	[M + Na] ⁺																																																	
377	[M + Na] ⁺																																																	
377	[M + Na] ⁺																																																	
50	Yarrow	40	3.80	221, 325	663	[M + K] ⁺	chlorogenic acid ^b	Giorgi et al. (2009)	X	X	X	X	X	X	X	X	X	X																																
55	Licorice	31	6.52/ 6.63 6.52/ 6.63	217, 228, 271 218, 276	549	[M-H] ⁻	liquiritin apioside	Wong et al. (2018)	X	X	X	X	X	X	X	X	X	X	X																															
					585	[M + O] ⁻																																												
					257	[M + H] ⁺																																												
					561	[M-H] ⁻														2',4',4'-trihydroxychalcone	Li et al. (2016)	X	X	X	X	X	X	X	X	X	X	X	X	X																
					597	[M + O] ⁻																																												
					621	[M + H ₃ C-COO] ⁻																																												
					563	[M + H] ⁺																																												
					585	[M + Na] ⁺																																												
					601	[M + K] ⁺																																												
					821	[M-H] ⁻																													glycyrrhizic acid	Kong et al. (2014); Li et al. (2016), Krüger et al. (2017)	X	X	X	X	X	X	X	X	X	X	X	X	X	X
					843	[M-2H + Na] ⁻																																												
					859	[M-2H + K] ⁻																																												
549	[M-H] ⁻	liquiritin apioside	Krüger et al. (2017), Wong et al. (2018)	X	X	X	X	X	X	X	X	X	X	X	X	X	X																																	
257	[M-C ₂ H ₅ O ₄ +H] ⁺																																																	
419	[M-C ₂ H ₅ O ₉ +H] ⁺																																																	
573	[M + Na] ⁺																																																	
589	[M + K] ⁺																																																	

(Continued on following page)

TABLE 2 | (Continued) NP-HPTLC-EDA-RP-HPLC-DAD-HESI-MS signals of bioactive zones and respective activity (X) in *B. subtilis* (A), *A. fischeri* (B), AChE/BChE (C), α - β -glucosidase (D), β -glucuronidase (E), tyrosinase (F), pYAS (G), pYES (H), pYAES (I), pYAES (J) and α -amylase (K). In blue: analytes and respective bioactivity, which were confirmed by a standard; in rose: rebutted ones.

No	Botanical	<i>h</i> R _F (\pm 1)	RT [min]	UV λ_{max} [nm]	<i>m/z</i>	Mass signal	Tentative assignment	Literature	A	B	C	D	E	F	G	H	I	J	K			
56	Siberian ginseng	62	7.15	249	695	[M-H] ⁻	licorice glycoside B/D1/D2	Wong et al. (2018)					X							X		
					719	[M + Na] ⁺																
					735	[M + K] ⁺																
		77	6.49/7.15/7.24	234, 288, 372	417	[M-H] ⁻	(iso)liquiritin	Krüger et al. (2017), Wong et al. (2018)		X	X				X	X					X	
					453	[M + Cl] ⁻																
					419	[M + H] ⁺																
					441	[M + Na] ⁺																
					457	[M + K] ⁺																
		93	7.17	218, 276	255	[M-H] ⁻	(iso)liquiritigenin	Kong et al. (2014), Boonnuen et al. (2016), Li et al. (2016), Montero et al. (2016)		X	X	X	X	X	X						X	
					257	[M + H] ⁺																
					279	[M + Na] ⁺																
					253	[M-H] ⁻	daidzein	Liu et al. (2001), Nomura et al. (2002), Cornwell et al. (2004)		X	X	X	X	X	X							X
					255	[M + H] ⁺																
					277	[M + Na] ⁺																
					293	[M + K] ⁺																
					283	[M-H] ⁻	biochanin A	Liu et al. (2001)		X	X	X	X	X	X							X
					285	[M + H] ⁺																
			307	[M + Na] ⁺																		
			323	[M + K] ⁺																		
			267	[M-H] ⁻	coumestrol	Cornwell et al. (2004)		X	X	X	X	X	X							X		
			269	[M + H] ⁺																		
			291	[M + Na] ⁺																		
14		6.48			307	[M + Cl] ⁻	quercetin-3-O-galactoside (hyperoside)/quercetin-3-O-glucopyranoside (isoquercitrin)	Wang et al. (2019)	X	X		X	X	X						X		
					423	[M + H ₃ C-COO] ⁻																
					487	[M + Na] ⁺																
					503	[M + K] ⁺	chlorogenic acid ^b	Wang et al. (2019)	X	X	X	X	X	X								
36		2.81/3.68/4.45/4.66	217, 324		353	[M-H] ⁻																
					355	[M + H] ⁺																
					372	[M + NH ₄] ⁺																
					377	[M + Na] ⁺																
					393	[M + K] ⁺																
					439	[M-H] ⁻	akebonoic acid	Ge et al. (2017)	X	X	X	X	X	X								
					475	[M + Cl] ⁻																
					499	[M + H ₃ C-COO] ⁻																
					463	[M + Na] ⁺																
					479	[M + K] ⁺																
					469	[M + Cl] ⁻	naringenin-7-O-glucoside (prunin)	Kuzniowski et al. (2018)	X	X	X	X	X	X								
					479	[M + HCOO] ⁻																
					493	[M + H ₃ C-COO] ⁻																
					452	[M + NH ₄] ⁺																
					457	[M + Na] ⁺																
					473	[M + K] ⁺																
					483	[M + Cl] ⁻	kaempferol-3-O-glucoside (astragaln)/quercetin-3-O-rhamnoside (quercitrin)	Kuzniowski et al. (2018), Wang et al. (2019)	X	X	X	X	X	X							X	
					493	[M + HCOO] ⁻																
					507	[M + H ₃ C-COO] ⁻																
					466	[M + NH ₄] ⁺																
					471	[M + Na] ⁺																
					487	[M + K] ⁺																

(Continued on following page)

TABLE 2 | (Continued) NP-HPTLC-EDA-RP-HPLC-DAD-HESI-MS signals of bioactive zones and respective activity (X) in *B. subtilis* (A), *A. fischeri* (B), AChE/BChE (C), α -/ β -glucosidase (D), β -glucuronidase (E), tyrosinase (F), pYAS (G), pYES (H), pYAES (I), pYAES (J), pYAES (K), in blue: analytes and respective bioactivity, which were confirmed by a standard; in rose: rebutted ones.

No	Botanical	hR _F (±1)	RT [min]	UV λ_{max} [nm]	m/z	Mass signal	Tentative assignment	Literature	A	B	C	D	E	F	G	H	I	J	K									
57	Thyme	22	6.62	235	557	[M + Cl] ⁻	rosmarinyl glucoside (rosmarinic acid-O-hexoside)	Vallverdú-Queralt et al. (2014)	X	X	X	X	X	X	X													
58	Grape seed	92	5.13	204, 279	289	[M-H] ⁻	rosmarinic acid	Krüger et al. (2017)	X	X	X	X	X	X	X													
62-64	Hawthorn	41	6.14	234, 280	325	[M + Cl] ⁻	(ep)catechin	Yilmaz and Toledo (2004)	X	X	X	X	X	X	X													
62-64	Hawthorn	41	6.54	—	421	[M + Cl] ⁻	laricresinol/solaricresinol/cyclolaricresinol dimethylinaitaresinol	Huang et al. (2018), Rocchetti et al. (2020) Rocchetti et al. (2020)	X	X	X	X	X	X	X													
62-64	Hawthorn	58	4.70/5.32	234, 310	337	[M-H] ⁻	4 ^{'''} -acetylvitexin 2 ^{'''} -O-rhamnoside	Krüger et al. (2017)	X	X	X	X	X	X	X													
62-64	Hawthorn	58	6.82	255, 355	339	[M + H] ⁺	3- <i>p</i> -coumaroylquinic acid/4- <i>p</i> -coumaroylquinic acid/5- <i>p</i> -coumaroylquinic acid/	Rocchetti et al. (2020)	X	X	X	X	X	X	X													
62-64	Hawthorn	58	7.64	—	417	[M-H] ⁻	syringaresinol/oleoside dimethylester	Rocchetti et al. (2020)	X	X	X	X	X	X	X													

(Continued on following page)

TABLE 2 | (Continued) NP-HPTLC-EDA-RP-HPLC-DAD-HESI-MS signals of bioactive zones and respective activity (X) in *B. subtilis* (A), *A. fischeri* (B), AChE/BChE (C), α - β -glucosidase (D), β -glucuronidase (E), tyrosinase (F), pYAS (G), pYES (H), pYAES (I), pYAES (J) and α -amylase (K). In blue: analytes and respective bioactivity, which were confirmed by a standard; in rose: rebutted ones.

No	Botanical	IR _F (±1)	RT [min]	UV λ_{max} [nm]	m/z	Mass signal	Tentative assignment	Literature	A	B	C	D	E	F	G	H	I	J	K	
					463	[M + HCOO] ⁻														
					477	[M + H ₃ C-COO] ⁻														
					441	[M + Na] ⁺														
					457	[M + K] ⁺														
		98	7.24	—	286	[M-H] ⁻	cyanidin	Rocchetti et al. (2020)	X	X	X									X
					288	[M + H] ⁺														
					326	[M + K] ⁺														
			7.60	—	197	[M-H] ⁻	syringic acid	Rocchetti et al. (2020)	X	X	X									X
					199	[M + H] ⁺														
					221	[M + Na] ⁺														
					237	[M + K] ⁺														
			8.09	—	305	[M-H] ⁻	(+)-galliccatechin/(-)-epigallocatechin	Rocchetti et al. (2020)	X	X	X									X
					341	[M + Cl] ⁻														
					307	[M + H] ⁺														
					329	[M + Na] ⁺														
					345	[M + K] ⁺														
			8.65		517	[M-H] ⁻	6"-O-malonylgenistin	Rocchetti et al. (2020)	X	X	X									X
					541	[M + Na] ⁺														
					557	[M + K] ⁺														
			8.65	—	487	[M-H] ⁻	luteolin-6-C-glucoside/6"-O-acetylglyctin	Rocchetti et al. (2020)	X	X	X									X
					489	[M + H] ⁺														
					506	[M + NH ₄] ⁺														
					511	[M + Na] ⁺														
					527	[M + K] ⁺														
			9.27	-	471	[M-H] ⁻	crataegolic acid (maslinic acid)	Vierling et al. (2003)	X	X	X									X
					495	[M + Na] ⁺														
					511	[M + K] ⁺														
67	Lemon peel	95	7.46	—	469	[M-H] ⁻	limonin	Baldi et al. (1995)		X										X
					505	[M + Cl] ⁻														
					515	[M + HCOO] ⁻														
					529	[M + H ₃ C-COO] ⁻														
					471	[M + H] ⁺														
					488	[M + NH ₄] ⁺														
					493	[M + Na] ⁺														
					509	[M + K] ⁺														
68	Lemon verbena	42	6.51	—	639	[M-H] ⁻	β -OH-(iso)verbascoside	Bilia et al. (2008)	X	X	X	X	X	X						X
					663	[M + Na] ⁺														
					679	[M + K] ⁺														
			6.66/	222, 330	623	[M-H] ⁻	(iso)verbascoside	Bilia et al. (2008), Quirantes-Piné et al. (2010), Krüger et al. (2017)	X	X	X	X	X	X						X
			6.82/		642	[M + NH ₄] ⁺														
			6.93		647	[M + Na] ⁺														
					663	[M + K] ⁺														

^aStandard eluted at another IR_F value.
^bOr neochlorogenic or cryptochlorogenic acid.

synergistic effect detection strategy was reported here for the first time.

3.2.7 Compounds With Genotoxic Effects

In recent decades, there has been a steady trend away from industrial medical care towards phytotherapy based on medicinal herbs, which have been used in traditional medicine for years. The common belief that phytochemicals are gentler than synthetic medicines may prove to be a fallacy, as most toxic compounds originate in nature (Efferth and Kaina, 2011). The SOS-Umu-C assay is a reporter gene assay indicating genotoxicity based on a genetically modified test organism *Salmonella typhimurium* TA1535 [pSK1002]. Under genotoxic stress, the SOS-DNA repair mechanism is induced. The SOS-Umu response activates the *lacZ* gene, encoding for β -galactosidase, which enables substrate cleavage into detectable products (Meyer et al., 2020). As the analyzed botanicals are commonly used as spices, in herbal medicine, or as tea, no genotoxic substances were expected. Nevertheless, pyrrolizidine alkaloids are known for genotoxic properties and their occurrence in herbal formulations (Habs et al., 2017), e.g., only a few micrograms per liter of tea (6 $\mu\text{g/L}$) (Mulder et al., 2015). The European Food and Safety Authority calculated a margin of exposure to 237 g/kg body weight per day for pyrrolizidine alkaloids and their *N*-oxides (Knutsen et al., 2017; Kaltner et al., 2020). No genotoxicity was detected as pink fluorescent zone for the 68 botanical extracts applied at 400 $\mu\text{g/}$ band (Figures 2–40). This bioassay was repeated to prove for the absence of genotoxic effects at a 2.5-fold (Supplementary Figure S6) and 12.5-fold higher amount applied, which latter at 5 mg/band was closest to overloading the chromatographic system (Supplementary Figure S7).

3.2.8 Compounds Inhibiting α -Amylase

In the context of hypoglycemic drugs from nature, not only the mentioned α - and β -glucosidase inhibitors, but also α -amylase inhibitors play a role in ethnopharmacological remedies with less toxic side effects. Hyperglycemic blood levels could be reduced by inhibiting α -amylases of the saliva and pancreas. The inhibition reduces the cleavage of starch into oligo- and disaccharides, and so the release of glucose molecules absorbed postprandially into the blood. Plant-derived flavones as luteolin present in celery, parsley, broccoli, carrot, peppers, cabbage, and apple peel can inhibit α -amylase (Bai et al., 2019). HPTLC coupled to α -amylase assay (Figures 2–4P) showed only a few inhibiting signals in white horehound (no. 2, hR_F 43, 83, 91, and 93), artichoke (no. 4, hR_F 94), fenugreek (no. 6, hR_F 81), ginkgo (no. 14, hR_F 46), licorice (no. 55, hR_F 59 and 68), and lemon peel (no. 67, hR_F 93 and 95). An α -amylase inhibitory activity has already been described for artichoke extracts from bracts (Turkiewicz et al., 2019), but it was not assigned to any single compound. In *Ginkgo biloba* extracts the compound sciadopitysin ($\text{C}_{33}\text{H}_{24}\text{O}_{10}$) was found to potentially inhibit α -amylase (Petersen et al., 2019).

3.3 Assigning Bioactivity to Single Compounds

In previous work, the samples were applied twice (as two sets). After plate cut, the assay was performed on one plate part, and the

positions of bioactive zones were analogously marked on the other plate part for zone elution and transfer into the MS (Krüger et al., 2017). The challenge of this parallel handling was the accurate positioning of the elution head on the zone. Instead, the elution directly from the bioassay plate would avoid any possible mismatch. In addition, the orthogonal HPLC separation would solve coelution. Hence, zones of interest were heart-cut eluted directly out of the bioassay plate and transferred through an online desalting device to RP-HPLC–DAD–HESI-MS. This reduced the interfering salts and nutrients from the bioassay, separated possibly coeluting substances via the orthogonal chromatographic system, and added value via spectral and mass spectrometric data (Schreiner and Morlock, 2021). Through this straightforward comprehensive workflow, the 60 most bioactive compounds in the botanicals were assigned (Table 2). Several plant extracts out of the 68 botanicals contained multipotent compounds which were active in different assays. Among striking botanicals, such as galangal (no. 13), ginkgo (no. 14), yerba mate green (no. 37), orange peel (no. 41), licorice (no. 55), or Siberian ginseng (no. 56), four botanicals were exemplarily highlighted to demonstrate the targeted assignment of bioactive compounds (orange peel, Figure 7; licorice, Figure 8; galangal, Figure 9; yerba mate green, Figure 10). By transferring residual bioassay salts, different ion species were formed for a molecule, which was found to be helpful as it confirmed the assignment made several times. The adduct $[\text{M}+62]^-$ has not been described in HPTLC-MS literature so far, but appeared frequently during this study (Figures 7C,D, Figures 8C,D, Figures 11A,C). It was proposed to be the nitrate adduct. Nitrate is taken up by the root and transported via the xylem to leaves, shoots, and grains. If too much nitrate is available in the short term, which is the case as it is discussed as a global environmental challenge (Zhang et al., 2021), it passes through the cytoplasm into the vacuoles to be stored and thus can be found in botanicals (Dechognat et al., 2011). Consequently, it may also appear as a pronounced adduct in the mass spectrum.

3.3.1 Hormonal Antagonists in Orange Peel (No. 41)

For orange peel, manifold positive responses across the different assays were observed at hR_F 34 (Figure 7A, marked*). Using the pYEAS bioautogram, this zone was heart-cut eluted directly to RP-HPLC–DAD–HESI-MS. In the DAD chromatogram, three compound peaks were evident in the range of RT 6.87–7.07 min, apart from the 4-methylumbelliferone background signal at RT 5.71 min (Figure 7B). The corresponding mass spectral data led to the tentative identification of naringin (Figure 7C), hesperidin (Figure 7D), and meranzin (Figure 7E, coeluting with an unknown marked blue) and is discussed as follows. The total ion current (TIC) peak at RT 6.87 min revealed mass signals in the positive ionization mode at m/z 581 $[\text{M} + \text{H}]^+$, 603 $[\text{M} + \text{Na}]^+$, and 619 $[\text{M} + \text{K}]^+$. Corresponding mass signals in the negative ion mode were detected at m/z 579 $[\text{M}-\text{H}]^-$, 615 $[\text{M} + \text{Cl}]^-$, and 642 $[\text{M} + \text{NO}_3]^-$ (Figure 7C). The resulting neutral mass of 580 Da together with the absorption spectrum and maximal wavelengths ($\lambda_{\text{max}} = 220$ and 284 nm) suggested naringin, which was confirmed via co-chromatography against a bought standard (Supplementary Figure S8E). The extracted mass spectra of the TIC peak at RT

6.99 min showed positive ions at m/z 611 $[M + H]^+$, 633 $[M + Na]^+$, and 649 $[M + K]^+$ and negative ions at m/z 609 $[M - H]^-$, 645 $[M + Cl]^-$, and 672 $[M + NO_3]^-$ (Figure 7D). The absorption spectrum revealed a maximum wavelength at 284 nm. Based on this data, hesperidin was assumed. The third peak at RT 7.06 min had a major response in TIC-HESI⁺ and a minor response in TIC-HESI⁻ and DAD chromatograms. The UV absorbance spectrum and respective mass spectra suggested two different constituents. The HESI⁺ mass signals at m/z 261 $[M1 + H]^+$ and 278 $[M1 + NH_4]^+$ potentially belong to the coumarin derivate meranzin (Figure 7E). The HESI⁺ mass signals at m/z 441 $[M2 + H]^+$, 458 $[M2 + NH_4]^+$, 463 $[M2 + Na]^+$, and 479 $[M2 + K]^+$ and corresponding HESI⁻ mass signals at m/z 475 $[M2 + Cl]^-$, 485 $[M2 + HCOO]^-$, and 499 $[M2 + H_3C-COO]^-$ were assigned to a component with the neutral mass of 440 Da, which is not yet known in orange peel. The UV maxima at 258 and 325 nm provided additional evidence for meranzin (Fan et al., 2012). Other UV maxima at 223 and 288 nm were possibly induced by the unknown.

Citrus sinensis is rich in beneficial secondary metabolites and therefore traditionally used in the treatment of gastrointestinal malfunction, diseases of the upper respiratory tracts, or menstrual disorders (Favela-Hernández et al., 2016). Both naringin and hesperidin have been shown to bind to the antagonist pocket (3ERT) of hER α , and thereby cause an antiestrogenic effect (Puranik et al., 2019). This effect was verified for both via co-chromatography of standards and samples (Supplementary Figure S8E, Supplementary Table S1), whereby an estrogenic activity was not observed for the applied amount (4 μ g/band). Furthermore, naringin was reported to slightly bind to the androgen receptor (Fang et al., 2003). The pronounced antiandrogenic effects observed in the pYAAS bioautogram confirmed this (Figure 3M, no. 41). Tyrosinase activity attributed to naringin (Itoh et al., 2009) and hesperidin (Zhang et al., 2007) has already been demonstrated. The only bioactivity reported for meranzin was no effect (Smyth et al., 2009) or a minor (Rosselli et al., 2007) antibacterial effect against *B. subtilis*. After NP-HPTLC-FLD comparison to a standard, meranzin was located at hR_F 99 (Supplementary Figure S8G), where antibacterial activity against *B. subtilis* and *A. fischeri* was detected in orange peel (no. 41). Hence, the assumption that meranzin was co-eluting with hesperidin and naringin at hR_F 34 was discarded.

3.3.2 Enzyme Inhibition and Endocrine Activity in Licorice (No. 55) and Galangal (No. 13)

In licorice (no. 55) a few bioactive analytes were found in the zone at hR_F 31 with antibacterial, tyrosinase, and β -glucuronidase inhibitory, antidiabetic, and endocrine-antagonistic properties (Figure 8A, marked*). These results illustrate the diverse pharmacological activities of this root, which has long been used in traditional medicine as remedy to treat gastrointestinal problems (β -glucuronidase inhibition) and respiratory infections (antibacterial activity). Moreover, *Glycyrrhiza glabra* extracts were subject of many pharmacological studies showing neuroprotective, antimicrobial, estrogenic and skin-whitening activity (Pastorino et al., 2018). The second chromatography produced five individual signals with pure mass spectra (Figures 8B–E). The mass spectral data extracted from the

peaks at RT 6.52/6.63 min (colored blue) were identical, indicating a single analyte in different configurations (Figure 8C). The ESI⁻ signals at m/z 549 $[M - H]^-$, 585 $[M + Cl]^-$, and 612 $[M + NO_3]^-$ were correlated to the highly plant-specific liquiritin apioside with a neutral mass of 550 Da. In positive ion mode, the signals at m/z 573 and 589 were identified as sodium and potassium adducts, respectively. The ESI⁺ mass signals at m/z 257 $[M - C_{11}H_{18}O_9 + H]^+$ and 419 $[M - C_5H_8O_4 + H]^+$ could be assigned to fragments with a loss of carbohydrates. Additionally, the experimental UV absorbance spectra were consistent with the ones of liquiritin apioside found in literature (Wong et al., 2018). The isomeric isoliquiritin apioside probably caused the second peak at RT 6.63 min. ESI⁺ mass signals at RT 7.10 min were m/z 563 $[M + H]^+$, 585 $[M + Na]^+$ and 601 $[M + K]^+$ (Figure 8D). (Iso)liquiritin apioside was found to inhibit capsaicin-induced cough, confirming its traditional use (Pastorino et al., 2018). In negative ion mode, signals were detected at m/z 561 $[M - H]^-$, 597 $[M + Cl]^-$, 621 $[M + H_3C-COO]^-$, and 624 $[M + NO_3]^-$. The less abundant DAD signal showed a UV absorption maximum at 250 nm. The spectral data could indicate glycyroside found in licorice root extracts (Montero et al., 2016), which is not known for any bioactivity. The third signal at RT 7.86 min (colored orange) was identified as glycyrrhizic acid against a standard (Supplementary Figure S8E). The ESI⁻ and ESI⁺ ions at m/z 821 $[M - H]^-$, 843 $[M - 2H + Na]^-$, 859 $[M - 2H + K]^-$, 845 $[M + H]^+$, and 861 $[M + K]^+$ originated from the neutral molecule of 822 Da. Lacking a π -electron system and conjugated double bonds, the UV absorbance spectrum showed background absorbance maxima at 251 nm. Glycyrrhizic acid was reported to have anti-inflammatory effects (Yu et al., 2015) similar to those of glucocorticoids (Pastorino et al., 2018), antitussive activity through increased tracheal mucus secretion (Sharma et al., 2018), and neuroprotective (Kao et al., 2009) properties.

Galangal extract (no. 13) responded in almost all assays at hR_F 99 (Figure 9A, marked*). After separating this zone with RP-HPLC-DAD-HESI-MS, multiple signals were observed (Figure 9B). The spectral details and tentative identifications are listed in the table below (Figure 9C). Traditionally, *Alpinia officinarum* is used against cold, which antibacterial effects were confirmed by the Gram-negative *A. fischeri* and Gram-positive *B. subtilis* bioassays. Other traditional applications were described for gynecological disorders, diabetes treatments, and skin washing (Abubakar et al., 2018). All these bioactivities were verified by the respective assays. To assign the bioactivity to one single component out of the coeluting substances from HPTLC, fractionation after column separation is necessary. The fractions can be applied again on a new plate followed by EDA and MS characterization. Alternatively, the mobile phase for planar chromatography has to be optimized in order to separate the previously coeluting substances during HPTLC analysis.

3.3.3 Separating Multipotent Isomers in Yerba Mate Green (No. 37) via 8D-Hyphenation

Biologically active isomers were also separated and detected, shown for example in yerba mate green (no. 37). A multipotent bioactive compound zone (hR_F 40) was observed in AChE, tyrosinase, and

α -/ β -glucosidase inhibition autograms (**Figure 10A**, marked*). This zone was separated into three distinct signals via RP-HPLC (**Figure 10B**), all providing the same absorbance and mass spectra (**Figure 10D**) and assigned to chlorogenic acid isomers, which differed only in quinic acid positioning (**Figure 10C**). The most common isomers of mono-caffeoylquinic acid are 3-*O*-caffeoylquinic acid (neochlorogenic acid), 4-*O*-caffeoylquinic acid (cryptochlorogenic acid), and 5-*O*-caffeoylquinic acid (5-QCA, chlorogenic acid). The mass signals at m/z 353 $[M-H]^-$ and 707 $[2M-H]^-$ in the negative ionization mode and at m/z 355 $[M+H]^+$, 377 $[M+Na]^+$, 393 $[M+K]^+$ and 747 $[2M+K]^+$ in the positive ionization mode matched to the neutral mass of mono-caffeoylquinic acids of 354 Da. The UV absorbance spectra with maxima at 218 and 325 nm that we obtained were also consistent with literature (Velkoska-Markovska et al., 2020). While chlorogenic acids are reported to have antioxidant (Huang et al., 2017), anti-inflammatory (Willems et al., 2016; Huang et al., 2017), and anti-HIV (Tamayose et al., 2019) properties, this screening revealed even more bioactive potential for these phenolics. For instance, the assigned bioactive compound zone also showed anti-Alzheimer, antidiabetic, and skin-whitening effects in this study. Co-chromatography against standards (**Supplementary Figure S8A,B** and **D**, **Supplementary Table S1**) confirmed that these beneficial health effects of yerba mate green (no. 37, **Figure 10**) come from the mono-caffeoylquinic acids. The various effects of *Ilex paraguariensis* traditionally consumed as herbal beverage qualify this botanical for its new role as functional food (Cardozo Junior and Morand, 2016).

3.3.4 Universal Potential of 8D-Hyphenation

The characterization of additional multipotent bioactive zones, partially plant-specific, is shown in **Figure 11**. Artichoke (no. 4) showed bioactivity at hR_F 42 in the tyrosinase and α -/ β -glucosidase inhibition assays. Transferring this zone to RP-HPLC-DAD-HESI-MS provided five signals (**Table 2**), one of which is specific for artichoke. At RT 6.30 min, cynarascoside C was assumed (**Figure 11A**). Spectral data showed no UV absorbance, referring to structural properties of cynarascoside C which possess neither a π -electron system nor conjugated double bonds. The mass signals at m/z 444 $[M+NH_4]^+$, 449 $[M+Na]^+$, 465 $[M+K]^+$, 461 $[M+Cl]^-$, 471 $[M+HCOO]^-$, 485 $[M+H_3C-COO]^-$, and 488 $[M+NO_3]^-$ indicated a neutral mass of 426 Da. Cynarascoside C was not suspected to have bioactive effects. The bioactivity was probably attributed to the coeluting derivatives of chlorogenic acid as in yerba mate green (no. 37, **Figure 10**). Nevertheless, *Cynara scolymus* has been used since the 4th century B.C. as medicinal product due to its health benefits and bioactive constituents, responsible for the hypoglycemic, anti-inflammatory, antimicrobial, and antioxidant properties (Turkiewicz et al., 2019).

Eucalyptus (no. 9) is known for its beneficial health properties against infections of the upper respiratory tracts or as antiseptic and is therefore widely used in the pharmaceutical industry (Hasegawa et al., 2008; Ács et al., 2018). The species *Eucalyptus* is closely associated with herbal medicine and traditional health care in various human cultures. Its leaf extracts are administered to fight against cold and cough, bacterial infections, high blood glucose levels, and to boost the immune system and skin health

(Salehi et al., 2019). Planar bioanalytical screening confirmed most of those traditional uses, showing many positive responses through the assays in a wide hR_F range (**Figure 11B**). Focusing on hR_F 57, highly plant-specific eucaglobulin was identified with UV ($\lambda_{max} = 222$ and 261 nm) and mass spectral data (Boulekbache-Makhlouf et al., 2010). Both the positive ion species at m/z 521 $[M+Na]^+$ and 537 $[M+K]^+$, and the deprotonated molecule $[M-H]^-$ confirmed this suspicion. Anti-melanogenesis activity was attributed to eucaglobulin (Hasegawa et al., 2008) and proved with a planar tyrosinase bioassay. Extracts of eucalyptus fruits were demonstrated to have antibacterial effects against *B. subtilis* (Boulekbache-Makhlouf et al., 2013), which so far have not been directly correlated to the monoterpene conjugate eucaglobulin. The anti-cholinesterase activity was only described for the whole methanolic extract of *Eucalyptus globulus* (Amat-ur-Rasool et al., 2020) but not directly correlated to eucaglobulin.

Extracts of *Ginkgo biloba* seeds and leaves were applied as herbal remedies all over the globe. Originating from traditional Chinese medicine, it is used to treat bacterial skin diseases, cognitive decline (Chassagne et al., 2019), and cardiovascular diseases (Shu et al., 2018). Affirming the ethnopharmacological usage, EDA of ginkgo leaf extract (no.14) demonstrated a variety of bioactivity at hR_F 93, i.e., antibacterial and antidiabetic effects, as well as β -glucuronidase and tyrosinase inhibition, and antiandrogenic activity (**Figure 11C**). RP-HPLC-DAD-HESI-MS analysis revealed the three ginkgolides A–C incorporated in this bioactive zone. Ginkgolide C eluted earlier from RP column (RT 6.42 min). Despite the second chromatography, ginkgolides A and B were not separated (both RT 6.86 min) and were thus detected in the same UV and mass spectra. Structurally they only differ in one additional hydroxy group of ginkgolide B. The high abundance of different ion species describing the two compounds is listed in **Table 2** and displayed in **Figure 11C**. The wide bioactive spectrum of these two diterpenes was confirmed against standards (**Supplementary Figure S8B**, **Supplementary Table S1**).

As an alternative to coffee, the leaves of *Ilex paraguariensis* are widely consumed as beverage in Latin America. Due to its chemical composition, mainly alkaloids and polyphenols, yerba mate exhibits many bioactive effects, e.g., antibacterial, cardiovascular-protective, neuroprotective, and antidiabetic activities (Gan et al., 2018). In yerba mate green (no. 37), a multipotent bioactive analyte zone was detected at hR_F 20 (**Figure 11D**). Showing signals at m/z 609 $[M-H]^-$ in ESI⁻ and at m/z 611 $[M+H]^+$, 633 $[M+Na]^+$, and 649 $[M+K]^+$ in ESI⁺ at an RT of 6.84 min, the flavonoid rutin was assumed. Its antibacterial (Orhan et al., 2010) potential against *B. subtilis*, anti-tyrosinase activity (Kishore et al., 2018), and glucosidase inhibition (Li et al., 2009) have already been demonstrated. The assumption was verified against a standard (**Supplementary Figure S8A** and **D**, **Supplementary Table S1**).

Salvia rosmarinus, predominantly growing in Mediterranean regions, is independently used in Mexican and Spanish ethnopharmacology. As medicinal plant, it was used to fight bacterial skin diseases, colds, intestinal parasites, and headaches (Heinrich et al., 2006). A very broad spectrum of bioactivities was confirmed by the presented study. The comprehensive NP-

HPTLC-EDA-heart-cut RP-HPLC-DAD-HESI-MS analysis of rosemary (no. 46) showed antibacterial activity in the *A. fischeri* bioassay and antidiabetic properties in the β -glucosidase assay at hR_F 25. Several ions at m/z 387 $[M-H]^-$, 406 $[M + NH_4]^+$, 411 $[M + Na]^+$, and 427 $[M + K]^+$ in positive and negative ion mode were correlated to the neutral molecular weight of 388 Da (Figure 11E). The mass spectrometric data substantiate the suspicion that this bioactivity is related to medioresinol. In rosemary extracts, various bioactive compounds have been described. Carnosic acid and carnosol are known to inhibit the growth of human cancer cell lines and operate as anti-inflammatory agents (Bai et al., 2010; Wang et al., 2018) or antioxidants (Loussouarn et al., 2017). Rosmarinic acid and rosmanol were found to have antioxidant potential (Vallverdú-Queralt et al., 2014), but to our knowledge, there is no bioactivity reported for medioresinol.

Many more examples could be explained in detail. All have in common that the effect profiles we obtained explain why consuming green tea and using fresh herbs and spices as seasoning can reduce the risk of diabetes by inhibiting α - and β -glucosidases, why healthy nutrition can protect the intestinal flora from severe impairment caused by β -glucuronidases from *Enterobacteriaceae*, why plant-derived cosmetics can reduce skin abnormalities via its tyrosinase-inhibiting potential, and why Alzheimer's disease can be prevented by daily intake of chlorogenic acid or rosmarinic acid from herbs such as artichoke, lemon balm, peppermint, thyme and rosemary, and so on. The wealth of effect information obtained inspires the mind and could fuel further studies. An enormous diversity in bioactivity was revealed in the effect-profiles of the 68 botanicals, contributing to human health by drug-like properties. It clearly shows the potential and spectrum of nature as basis for alternative medicines.

4 CONCLUSION

Since the major part, and especially, the important active part of natural food and traditional medicines is presently not under analytical control, a paradigm shift from quality control based on marker compounds to effect profiles is postulated for plant-based samples. Considering the global production chain, whose influences on the product cannot be controlled, at least entries or changes regarding the effect should be kept under control. The Chemical Abstracts database (www.cas.org) contains over 190 million chemicals, and thousands of compounds are added daily. There is of little help, if we can measure some thousands of them with ever lower limits of determination. By doing so, this does not come close to doing justice to the complexity of plant extracts, nor to the metabolic networking of natural processes, nor to the contamination-prone global production chain. The implementation of effect-directed profiles would substantially improve quality control, ensure the expected activities and detect unexpected activities. Even small amounts of compounds can be highly active. Disruptive thinking is essential to better control our natural food and traditional medicines. Sophisticated instrumentation does not solve

pressing challenges, but combining orthogonal areas does. The complexity of plant extracts requires modern non-target methods that combine chromatography with effect-directed assays to prioritize active compounds that show an effect and thus require utmost attention. This combination is indispensable for routine quality control to prioritize substances among the thousands of individual compounds in a plant extract. The modular NP-HPTLC-UV/Vis/FLD-EDA-heart-cut RP-HPLC-DAD-HESI-MS coupling can be used in routine and makes it easy to recognize the essence. It is said that a picture is worth a thousand words, but the effect image is worth even more. It visualizes the impressive power of nature to supply the body with important building blocks (multipotent chemicals). Several innovations were demonstrated. The pYES equipped with the hER β or in combination with the simulated S9 metabolism were applied for the first time. In the antagonistic hormonal assays, the proof for false-positive results was newly included. Synergistic effects were revealed in the hormonal effect-profiles for the first time. The developed workflows can be transferred to any other assays or samples. The array of effect-directed profiles clearly showed that natural food has the power to contribute to our homeostasis in various effective ways. The 1,292 profiles (68 samples x 19 detections) obtained within a few weeks showed the versatility of the activity potential of natural food. Artificial intelligence could help evaluate the wealth of information obtained. Exemplarily, the 60 most bioactive components were identified as proof of principle. The developed non-targeted effect-directed hyphenation highlights the advantages of analytical speed, efficiency, and economy. First, the samples were freed from the interfering matrix via planar chromatographic separation. Secondly, the focus was exclusively laid on bioactive compounds, providing targeted characterization. Calculated per sample, the robust profiling takes 3–15 min and costs 0.5–1 Euro, depending on incubation time and material consumption, respectively. One current limitation is the low resolution of the single quadrupole MS instrument. Potential drug candidates were only tentatively assigned and confirmed in an additional run against standards. At the same time, this limitation can be an opportunity for further research. Upgrading the MS instrument to a high-resolution MS with fractionation possibility enables unambiguous assignment of molecular formulas and structure elucidation through fragmentation. This makes effect profiling even more attractive for routine analysis.

DATA AVAILABILITY STATEMENT

The original contributions presented in the study are included in the article/**Supplementary Material**, further inquiries can be directed to the corresponding author.

AUTHOR CONTRIBUTIONS

TS carried out all bioassays and mass spectrometry experiments, analyzed the data, and wrote the manuscript draft. DS and MF

prepared the *B. subtilis*, α - β -glucosidase, β -glucuronidase, pYAS, pYES, pYAAS, pYAES (bio)autograms. JH prepared the samples and *A. fischeri*, tyrosinase, and α -amylase (bio) autograms. GM initiated the project, concept and methodology, obtained research funding, supervised the study, and revised the manuscript.

FUNDING

This work was supported by the Instrumentation was partially funded by the Deutsche Forschungsgemeinschaft (DFG; INST 162/536-1 FUGG).

REFERENCES

- Abubakar, I. B., Malami, I., Yahaya, Y., and Sule, S. M. (2018). A Review on the Ethnomedicinal Uses, Phytochemistry and Pharmacology of *Alpinia officinarum* Hance. *J. Ethnopharmacol* 224, 45–62. doi:10.1016/j.jep.2018.05.027
- Ács, K., Balázs, V. L., Kocsis, B., Bencsik, T., Böszörményi, A., and Horváth, G. (2018). Antibacterial Activity Evaluation of Selected Essential Oils in Liquid and Vapor Phase on Respiratory Tract Pathogens. *BMC Complement. Altern. Med.* 18, 227. doi:10.1186/s12906-018-2291-9
- Agatonovic-Kustrin, S., Kustrin, E., Gegechkori, V., and Morton, D. W. (2019). High-Performance Thin-Layer Chromatography Hyphenated with Microchemical and Biochemical Derivatizations in Bioactivity Profiling of Marine Species. *Mar. Drugs* 17. doi:10.3390/md17030148
- Agatonovic-Kustrin, S., and Morton, D. W. (2017). High-performance Thin-Layer Chromatography HPTLC-Direct Bioautography as a Method of Choice for Alpha-Amylase and Antioxidant Activity Evaluation in marine Algae. *J. Chromatogr. A* 1530, 197–203. doi:10.1016/j.chroma.2017.11.024
- Amat-ur-Rasool, H., Symes, F., Tooth, D., Schaffert, L. N., Elmorsy, E., Ahmed, M., et al. (2020). Potential Nutraceutical Properties of Leaves from Several Commonly Cultivated Plants. *Biomolecules* 10, 1556. doi:10.3390/biom10111556
- Amessis-Ouchemoukh, N., Abu-Reidah, I. M., Quirantes-Piné, R., Madani, K., and Segura-Carretero, A. (2014). Phytochemical Profiling, *In Vitro* Evaluation of Total Phenolic Contents and Antioxidant Properties of *Marrubium Vulgare* (Horehound) Leaves of Plants Growing in Algeria. *Ind. Crops Prod.* 61, 120–129. doi:10.1016/j.indcrop.2014.06.049
- Anagnostopoulou, M. A., Kefalas, P., Kokkalou, E., Assimopoulou, A. N., and Papegeorgiou, V. P. (2005). Analysis of Antioxidant Compounds in Sweet orange Peel by HPLC-Diode Array Detection-Electrospray Ionization Mass Spectrometry. *Biomed. Chromatogr.* 19, 138–148. doi:10.1002/bmc.430
- Azadnia, E., Thomä, I., Baake, J., and Morlock, G. E. (2021). High-throughput Enzyme Inhibition Screening of 44 Iranian Medicinal Plants via Piezoelectric Spraying of Planar Cholinesterase Assays. *J. Chromatogr. B* 1184, 122956. doi:10.1016/j.jchromb.2021.122956
- Bai, L., Li, X., He, L., Zheng, Y., Lu, H., Li, J., et al. (2019). Antidiabetic Potential of Flavonoids from Traditional Chinese Medicine: A Review. *Am. J. Chin. Med.* 47, 933–957. doi:10.1142/S0192415X19500496
- Bai, N., He, K., Roller, M., Lai, C. S., Shao, X., Pan, M. H., et al. (2010). Flavonoids and Phenolic Compounds from *Rosmarinus Officinalis*. *J. Agric. Food Chem.* 58, 5363–5367. doi:10.1021/jf100332w
- Baldi, A., Rosen, R. T., Fukuda, E. K., and Ho, C.-T. (1995). Identification of Nonvolatile Components in Lemon Peel by High-Performance Liquid Chromatography with Confirmation by Mass Spectrometry and Diode-Array Detection. *J. Chromatogr. A* 718, 89–97. doi:10.1016/0021-9673(95)00676-1
- Belwal, T., Devkota, H. P., Hassan, H. A., Ahluwalia, S., Ramadan, M. F., Mocan, A., et al. (2018a). Phytopharmacology of *Acerola* (*Malpighia* Spp.) and its Potential as Functional Food. *Trends Food Sci. Technology* 74, 99–106. doi:10.1016/j.tifs.2018.01.014

ACKNOWLEDGMENTS

We would like to thank Merck, Darmstadt, Germany, for providing the plates, Waters, Eschborn, Germany, for technical support, and Prof. Dr. Erwin Herberle-Bors, University of Vienna, Austria, for donation of *Saccharomyces cerevisiae* cells equipped with the hER β .

SUPPLEMENTARY MATERIAL

The Supplementary Material for this article can be found online at: <https://www.frontiersin.org/articles/10.3389/fphar.2021.755941/full#supplementary-material>

- Belwal, T., Ezzat, S. M., Rastrelli, L., Bhatt, I. D., Daglia, M., Baldi, A., et al. (2018b). A Critical Analysis of Extraction Techniques Used for Botanicals: Trends, Priorities, Industrial Uses and Optimization Strategies. *Trac Trends Anal. Chem.* 100, 82–102. doi:10.1016/j.trac.2017.12.018
- Bilia, A. R., Giomi, M., Innocenti, M., Gallori, S., and Vincieri, F. F. (2008). HPLC-DAD-ESI-MS Analysis of the Constituents of Aqueous Preparations of Verbena and Lemon Verbena and Evaluation of the Antioxidant Activity. *J. Pharm. Biomed. Anal.* 46, 463–470. doi:10.1016/j.jpba.2007.11.007
- Boonmueng, N., Gong, P., Ali, Z., Chittiboyina, A. G., Khan, I., Doerge, D. R., et al. (2016). Licorice Root Components in Dietary Supplements Are Selective Estrogen Receptor Modulators with a Spectrum of Estrogenic and Anti-estrogenic Activities. *Steroids* 105, 42–49. doi:10.1016/j.steroids.2015.11.006
- Boulekbache-Makhlouf, L., Meudec, E., Chibane, M., Mazauric, J. P., Slimani, S., Henry, M., et al. (2010). Analysis by High-Performance Liquid Chromatography Diode Array Detection Mass Spectrometry of Phenolic Compounds in Fruit of *Eucalyptus Globulus* Cultivated in Algeria. *J. Agric. Food Chem.* 58, 12615–12624. doi:10.1021/jf1029509
- Boulekbache-Makhlouf, L., Slimani, S., and Madani, K. (2013). Total Phenolic Content, Antioxidant and Antibacterial Activities of Fruits of *Eucalyptus Globulus* Cultivated in Algeria. *Ind. Crops Prod.* 41, 85–89. doi:10.1016/j.indcrop.2012.04.019
- Brantner, A., and Grein, E. (1994). Antibacterial Activity of Plant Extracts Used Externally in Traditional Medicine. *J. Ethnopharmacol* 44, 35–40. doi:10.1016/0378-8741(94)90096-5
- Bravo, L., Goya, L., and Lecumberri, E. (2007). LC/MS Characterization of Phenolic Constituents of *Mate* (*Ilex Paraguariensis*, St. Hil.) and its Antioxidant Activity Compared to Commonly Consumed Beverages. *Food Res. Int.* 40, 393–405. doi:10.1016/j.foodres.2006.10.016
- Caesar, L. K., Kellogg, J. J., Kvalheim, O. M., and Cech, N. B. (2019). Opportunities and Limitations for Untargeted Mass Spectrometry Metabolomics to Identify Biologically Active Constituents in Complex Natural Product Mixtures. *J. Nat. Prod.* 82, 469–484. doi:10.1021/acs.jnatprod.9b00176
- Cardozo Junior, E. L., and Morand, C. (2016). Interest of *Mate* (*Ilex Paraguariensis* A. St.-Hil.) as a New Natural Functional Food to Preserve Human Cardiovascular Health - A Review. *J. Funct. Foods* 21, 440–454. doi:10.1016/j.jff.2015.12.010
- Celik, S. E., Tufan, A. N., Bekdeser, B., Özyürek, M., Güçlü, K., and Apak, R. (2017). Identification and Determination of Phenolics in *Lamiaceae* Species by UPLC-DAD-ESI-MS. *J. Chromatogr. Sci.* 55, 291–300. doi:10.1093/chromsci/bmw184
- Chassagne, F., Huang, X., Lyles, J. T., and Quave, C. L. (2019). Validation of a 16th Century Traditional Chinese Medicine Use of *Ginkgo Biloba* as a Topical Antimicrobial. *Front. Microbiol.* 10, 775. doi:10.3389/fmicb.2019.00775
- Chen, E., Ding, C., and Lindsay, R. C. (2005). Qualitative and Quantitative Analyses of *Ginkgo* Terpene Trilactones by Liquid Chromatography/sonic spray Ionization Ion Trap Mass Spectrometry. *Anal. Chem.* 77, 2966–2970. doi:10.1021/ac048510p
- Cock, I. E., Ndlovu, N., and van Vuuren, S. F. (2021). The Use of South African Botanical Species for the Control of Blood Sugar. *J. Ethnopharmacol* 264, 113234. doi:10.1016/j.jep.2020.113234
- Cornwell, T., Cohick, W., and Raskin, I. (2004). Dietary Phytoestrogens and Health. *Phytochemistry* 65, 995–1016. doi:10.1016/j.phytochem.2004.03.005

- da Silva, G. S., Canuto, K. M., Ribeiro, P. R. V., de Brito, E. S., Nascimento, M. M., Zocolo, G. J., et al. (2017). Chemical Profiling of Guarana Seeds (*Paullinia Cupana*) from Different Geographical Origins Using UPLC-QTOF-MS Combined with Chemometrics. *Food Res. Int.* 102, 700–709. doi:10.1016/j.foodres.2017.09.055
- de Souza, L. M., Dartora, N., Scoparo, C. T., Cipriani, T. R., Gorin, P. A., Iacomini, M., et al. (2011). Comprehensive Analysis of Maté (*Ilex Paraguariensis*) Compounds: Development of Chemical Strategies for Matesaponin Analysis by Mass Spectrometry. *J. Chromatogr. A* 1218, 7307–7315. doi:10.1016/j.chroma.2011.08.047
- Dechornat, J., Nguyen, C. T., Armengaud, P., Jossier, M., Diatloff, E., Filleur, S., et al. (2011). From the Soil to the Seeds: the Long Journey of Nitrate in Plants. *J. Exp. Bot.* 62, 1349–1359. doi:10.1093/jxb/erq409
- Díaz, R., Ibáñez, M., Sancho, J. V., and Hernández, F. (2012). Target and Non-target Screening Strategies for Organic Contaminants, Residues and Illicit Substances in Food, Environmental and Human Biological Samples by UHPLC-QTOF-MS. *Anal. Methods* 4, 196–209. doi:10.1039/C1AY05385J
- Ding, S., Dudley, E., Plummer, S., Tang, J., Newton, R. P., and Brenton, A. G. (2006). Quantitative Determination of Major Active Components in Ginkgo Biloba Dietary Supplements by Liquid Chromatography/mass Spectrometry. *Rapid Commun. Mass. Spectrom.* 20, 2753–2760. doi:10.1002/rcm.2646
- Du, Z., Li, J., Zhang, X., Pei, J., and Huang, L. (2018). An Integrated LC-MS-Based Strategy for the Quality Assessment and Discrimination of Three Panax Species. *Molecules* 23, 2988. doi:10.3390/molecules23112988
- Dugo, P., Mondello, L., Dugo, L., Stancanelli, R., and Dugo, G. (2000). LC-MS for the Identification of Oxygen Heterocyclic Compounds in Citrus Essential Oils. *J. Pharm. Biomed. Anal.* 24, 147–154. doi:10.1016/S0731-7085(00)00400-3
- Efferth, T., and Kaina, B. (2011). Toxicities by Herbal Medicines with Emphasis to Traditional Chinese Medicine. *Curr. Drug Metab.* 12, 989–996. doi:10.2174/138920011798062328
- El Senousy, A. S., Farag, M. A., Al-Mahdy, D. A., and Wessjohann, L. A. (2014). Developmental Changes in Leaf Phenolics Composition from Three Artichoke Cvs. (*Cynara Scolymus*) as Determined via UHPLC-MS and Chemometrics. *Phytochemistry* 108, 67–76. doi:10.1016/j.phytochem.2014.09.004
- Erenler, R., Sen, O., Aksit, H., Demirtas, I., Yagliglu, A. S., Elmastas, M., et al. (2016). Isolation and Identification of Chemical Constituents from *Origanum Majorana* and Investigation of Antiproliferative and Antioxidant Activities. *J. Sci. Food Agric.* 96, 822–836. doi:10.1002/jsfa.7155
- European Committee for Standardization (2009). *Water Quality - Determination of the Inhibitory Effect of Water Samples on the Light Emission of Vibrio Fischeri (Luminescent Bacteria Test): Part 1: Method Using Freshly Prepared Bacteria*.
- Ezzat, S. M., Salama, M. M., ElMeshad, A. N., Teaima, M. H., and Rashad, L. A. (2016). HPLC-DAD-MS/MS Profiling of Standardized Rosemary Extract and Enhancement of its Anti-wrinkle Activity by Encapsulation in Elastic Nanovesicles. *Arch. Pharm. Res.* 39, 912–925. doi:10.1007/s12272-016-0744-6
- Fan, R., Huang, X., Wang, Y., Chen, X., Ren, P., Ji, H., et al. (2012). Ethnopharmacokinetic- and Activity-Guided Isolation of a New Antidepressive Compound from Fructus Aurantii Found in the Traditional Chinese Medicine Chaihu-Shugan-San: a New Approach and its Application. *Evid. Based Complement. Alternat Med.* 2012, 607584. doi:10.1155/2012/607584
- Fang, H., Tong, W., Branham, W. S., Moland, C. L., Dial, S. L., Hong, H., et al. (2003). Study of 202 Natural, Synthetic, and Environmental Chemicals for Binding to the Androgen Receptor. *Chem. Res. Toxicol.* 16, 1338–1358. doi:10.1021/tx030011g
- Farag, M. A., El-Ahmady, S. H., Elian, F. S., and Wessjohann, L. A. (2013). Metabolomics Driven Analysis of Artichoke Leaf and its Commercial Products via UHPLC-Q-TOF-MS and Chemometrics. *Phytochemistry* 95, 177–187. doi:10.1016/j.phytochem.2013.07.003
- Favela-Hernández, J. M., González-Santiago, O., Ramírez-Cabrera, M. A., Esquivel-Ferriño, P. C., and Camacho-Corona, Mdel. R. (2016). Chemistry and Pharmacology of Citrus Sinensis. *Molecules* 21, 247. doi:10.3390/molecules21020247
- Fecka, I., Kowalczyk, A., and Cisowski, W. (2004). Optimization of the Separation of Flavonoid Glycosides and Rosmarinic Acid from *Mentha Piperita* on HPTLC Plates. *J. Planar Chromatogr. - Mod. TLC* 17, 22–25. doi:10.1556/JPC.17.2004.1.5
- Fu, Y., Zhao, C., Lu, X., and Xu, G. (2017). Nontargeted Screening of Chemical Contaminants and Illegal Additives in Food Based on Liquid Chromatography-High Resolution Mass Spectrometry. *Trac Trends Anal. Chem.* 96, 89–98. doi:10.1016/j.trac.2017.07.014
- Gan, R. Y., Zhang, D., Wang, M., and Corke, H. (2018). Health Benefits of Bioactive Compounds from the Genus *Ilex*, a Source of Traditional Caffeinated Beverages. *Nutrients* 10, 1682. doi:10.3390/nu10111682
- Ge, Y. W., Zhu, S., Yoshimatsu, K., and Komatsu, K. (2017). MS/MS Similarity Networking Accelerated Target Profiling of Triterpene Saponins in *Eleutherococcus Senticosus* Leaves. *Food Chem.* 227, 444–452. doi:10.1016/j.foodchem.2017.01.119
- Giorgi, A., Mingozzi, M., Madeo, M., Speranza, G., and Cocucci, M. (2009). Effect of Nitrogen Starvation on the Phenolic Metabolism and Antioxidant Properties of Yarrow (*Achillea Collina* Becker Ex Rchb.). *Food Chem.* 114, 204–211. doi:10.1016/j.foodchem.2008.09.039
- Guldiken, B., Ozkan, G., Catalkaya, G., Ceylan, F. D., Ekin Yalcinkaya, I., and Capanoglu, E. (2018). Phytochemicals of Herbs and Spices: Health versus Toxicological Effects. *Food Chem. Toxicol.* 119, 37–49. doi:10.1016/j.fct.2018.05.050
- Habs, M., Binder, K., Krauss, S., Müller, K., Ernst, B., Valentini, L., et al. (2017). A Balanced Risk-Benefit Analysis to Determine Human Risks Associated with Pyrrolizidine Alkaloids (PA)-The Case of Tea and Herbal Infusions. *Nutrients* 9, 717. doi:10.3390/nu9070717
- Hage, S., and Morlock, G. E. (2017). Bioprofiling of Salicaceae Bud Extracts through High-Performance Thin-Layer Chromatography Hyphenated to Biochemical, Microbiological and Chemical Detections. *J. Chromatogr. A* 1490, 201–211. doi:10.1016/j.chroma.2017.02.019
- Halvorsen, B. L., Holte, K., Myhrstad, M. C., Barikmo, I., Hvattum, E., Remberg, S. F., et al. (2002). A Systematic Screening of Total Antioxidants in Dietary Plants. *J. Nutr.* 132, 461–471. doi:10.1093/jn/132.3.461
- Hasegawa, T., Takano, F., Takata, T., Niyama, M., and Ohta, T. (2008). Bioactive Monoterpene Glycosides Conjugated with Gallic Acid from the Leaves of *Eucalyptus Globulus*. *Phytochemistry* 69, 747–753. doi:10.1016/j.phytochem.2007.08.030
- Hawryl, M. A. (2014). HPLC-diode Array Detector Fingerprints of Various *Mentha* Species. *J. AOAC Int.* 97, 1268–1273. doi:10.5740/jaoacint.SGEHawryl
- Heinrich, M., Kufer, J., Leonti, M., and Pardo-de-Santayana, M. (2006). Ethnobotany and Ethnopharmacology-Interdisciplinary Links with the Historical Sciences. *J. Ethnopharmacol.* 107, 157–160. doi:10.1016/j.jep.2006.05.035
- Hossain, M. B., Camphuis, G., Aguiló-Aguayo, I., Gangopadhyay, N., and Rai, D. K. (2014). Antioxidant Activity Guided Separation of Major Polyphenols of Marjoram (*Origanum Majorana* L.) Using Flash Chromatography and Their Identification by Liquid Chromatography Coupled with Electrospray Ionization Tandem Mass Spectrometry. *J. Sep. Sci.* 37, 3205–3213. doi:10.1002/jssc.201400597
- Hossain, M. B., Rai, D. K., Brunton, N. P., Martin-Diana, A. B., and Barry-Ryan, C. (2010). Characterization of Phenolic Composition in Lamiaceae Spices by LC-ESI-MS/MS. *J. Agric. Food Chem.* 58, 10576–10581. doi:10.1021/jf102042g
- Hu, Y., Zeng, H., Huang, J., Jiang, L., Chen, J., and Zeng, Q. (2020). Traditional Asian Herbs in Skin Whitening: The Current Development and Limitations. *Front. Pharmacol.* 11, 982. doi:10.3389/fphar.2020.00982
- Huang, W. Y., Fu, L., Li, C. Y., Xu, L. P., Zhang, L. X., and Zhang, W. M. (2017). Quercetin, Hyperin, and Chlorogenic Acid Improve Endothelial Function by Antioxidant, Antiinflammatory, and ACE Inhibitory Effects. *J. Food Sci.* 82, 1239–1246. doi:10.1111/1750-3841.13706
- Huang, X. X., Xu, Y., Bai, M., Zhou, L., Song, S. J., and Wang, X. B. (2018). Lignans from the Seeds of Chinese Hawthorn (*Crataegus Pinnatifida* Var. Major N.E.Br.) against β -amyloid Aggregation. *Nat. Prod. Res.* 32, 1706–1713. doi:10.1080/14786419.2017.1399378
- Itoh, K., Hirata, N., Masuda, M., Naruto, S., Murata, K., Wakabayashi, K., et al. (2009). Inhibitory Effects of Citrus Hassaku Extract and its Flavanone Glycosides on Melanogenesis. *Biol. Pharm. Bull.* 32, 410–415. doi:10.1248/bpb.32.410
- Jabir, N. R., Khan, F. R., and Tabrez, S. (2018). Cholinesterase Targeting by Polyphenols: A Therapeutic Approach for the Treatment of Alzheimer's Disease. *CNS Neurosci. Ther.* 24, 753–762. doi:10.1111/cns.12971

- Kaltner, F., Rychlik, M., Gareis, M., and Gottschalk, C. (2020). Occurrence and Risk Assessment of Pyrrolizidine Alkaloids in Spices and Culinary Herbs from Various Geographical Origins. *Toxins (Basel)* 12, 155. doi:10.3390/toxins12030155
- Kao, T. C., Shyu, M. H., and Yen, G. C. (2009). Neuroprotective Effects of Glycyrrhizic Acid and 18beta-Glycyrrhetic Acid in PC12 Cells via Modulation of the PI3K/Akt Pathway. *J. Agric. Food Chem.* 57, 754–761. doi:10.1021/jf802864k
- Kirchmayer, T. (2009). *Reconstitution of ERβ Transactivation in Yeast. Diploma Thesis*. Vienna: University of Vienna, Faculty of Life Science. Available at: <https://othes.univie.ac.at/8017> (Accessed October 06, 2021).
- Kishore, N., Twilley, D., Blom van Staden, A., Verma, P., Singh, B., Cardinali, G., et al. (2018). Isolation of Flavonoids and Flavonoid Glycosides from *Myrsine Africana* and Their Inhibitory Activities against Mushroom Tyrosinase. *J. Nat. Prod.* 81, 49–56. doi:10.1021/acs.jnatprod.7b00564
- Klingelhöfer, I., Hockamp, N., and Morlock, G. E. (2020). Non-targeted Detection and Differentiation of Agonists versus Antagonists, Directly in Bioprofiles of Everyday Products. *Anal. Chim. Acta* 1125, 288–298. doi:10.1016/j.aca.2020.05.057
- Klingelhöfer, I., and Morlock, G. E. (2015). Bioprofiling of Surface/Wastewater and Bioquantitation of Discovered Endocrine-Active Compounds by Streamlined Direct Bioautography. *Anal. Chem.* 87, 11098–11104. doi:10.1021/acs.analchem.5b03233
- Knutsen, H. K., Knutsen, H. K., Alexander, J., Barregård, L., Bignami, M., Brüschweiler, B., et al. (2017). Risks for Human Health Related to the Presence of Pyrrolizidine Alkaloids in Honey, tea, Herbal Infusions and Food Supplements. *EFSA J.* 15, e04908. doi:10.2903/j.efsa.2017.4908
- Kong, W., Wen, J., Yang, Y., Qiu, F., Sheng, P., and Yang, M. (2014). Simultaneous Targeted Analysis of Five Active Compounds in Licorice by Ultra-fast Liquid Chromatography Coupled to Hybrid Linear-Ion Trap Tandem Mass Spectrometry. *Analyst* 139, 1883–1894. doi:10.1039/c3an02209a
- Kongstad, K. T., Özdemir, C., Barzak, A., Wubshet, S. G., and Staerk, D. (2015). Combined Use of High-Resolution α-glucosidase Inhibition Profiling and High-Performance Liquid Chromatography-High-Resolution Mass Spectrometry-solid-phase Extraction-Nuclear Magnetic Resonance Spectroscopy for Investigation of Antidiabetic Principles in Crude Plant Extracts. *J. Agric. Food Chem.* 63, 2257–2263. doi:10.1021/jf506297k
- Krüger, S., Bergin, A., and Morlock, G. E. (2018). Effect-directed Analysis of Ginger (*Zingiber Officinale*) and its Food Products, and Quantification of Bioactive Compounds via High-Performance Thin-Layer Chromatography and Mass Spectrometry. *Food Chem.* 243, 258–268. doi:10.1016/j.foodchem.2017.09.095
- Krüger, S., Hüskens, L., Fornasari, R., Scainelli, L., and Morlock, G. E. (2017). Effect-directed Fingerprints of 77 Botanical Extracts via a Generic High-Performance Thin-Layer Chromatography Method Combined with Assays and Mass Spectrometry. *J. Chromatogr. A* 1529, 93–106. doi:10.1016/j.chroma.2017.10.068
- Kuźniński, R., Załuski, D., Olech, M., Banaszczyk, P., and Nowak, R. (2018). LC-ESI-MS/MS Profiling of Phenolics in the Leaves of *Eleutherococcus Senticosus* Cultivated in the West Europe and Anti-hyaluronidase and Anti-acetylcholinesterase Activities. *Nat. Prod. Res.* 32, 448–452. doi:10.1080/14786419.2017.1308369
- Lall, N., and Kishore, N. (2014). Are Plants Used for Skin Care in South Africa Fully Explored? *J. Ethnopharmacol.* 153, 61–84. doi:10.1016/j.jep.2014.02.021
- Li, G., Nikolic, D., and van Breemen, R. B. (2016). Identification and Chemical Standardization of Licorice Raw Materials and Dietary Supplements Using UHPLC-MS/MS. *J. Agric. Food Chem.* 64, 8062–8070. doi:10.1021/acs.jafc.6b02954
- Li, K., Ji, S., Song, W., Kuang, Y., Lin, Y., Tang, S., et al. (2017). Glycybridins A-K, Bioactive Phenolic Compounds from *Glycyrrhiza Glabra*. *J. Nat. Prod.* 80, 334–346. doi:10.1021/acs.jnatprod.6b00783
- Li, S., Yu, H., and Ho, C. T. (2006). Nobiletin: Efficient and Large Quantity Isolation from orange Peel Extract. *Biomed. Chromatogr.* 20, 133–138. doi:10.1002/bmc.540
- Li, Y. Q., Zhou, F. C., Gao, F., Bian, J. S., and Shan, F. (2009). Comparative Evaluation of Quercetin, Isoquercetin and Rutin as Inhibitors of Alpha-Glucosidase. *J. Agric. Food Chem.* 57, 11463–11468. doi:10.1021/jf903083h
- Lin, L. Z., and Harnly, J. M. (2012). LC-PDA-ESI/MS Identification of the Phenolic Components of Three Compositae Spices: Chamomile, Tarragon, and Mexican Arnica. *Nat. Prod. Commun.* 7, 749–752. doi:10.1177/1934578X1200700615
- Liu, J., Burdette, J. E., Xu, H., Gu, C., van Breemen, R. B., Bhat, K. P., et al. (2001). Evaluation of Estrogenic Activity of Plant Extracts for the Potential Treatment of Menopausal Symptoms. *J. Agric. Food Chem.* 49, 2472–2479. doi:10.1021/jf0014157
- Liu, J. Q., Peng, X. R., Li, X. Y., Li, T. Z., Zhang, W. M., Shi, L., et al. (2013). Norfriedelins A-C with Acetylcholinesterase Inhibitory Activity from *Acerola* Tree (*Malpighia Emarginata*). *Org. Lett.* 15, 1580–1583. doi:10.1021/ol4003702
- Loussouarn, M., Krieger-Liszky, A., Svalar, L., Bily, A., Birtic, S., and Havaux, M. (2017). Carnosic Acid and Carnosol, Two Major Antioxidants of Rosemary, Act through Different Mechanisms. *Plant Physiol.* 175, 1381–1394. doi:10.1104/pp.17.01183
- Mahran, E., Keusgen, M., and Morlock, G. E. (2020). New Planar Assay for Streamlined Detection and Quantification of β-glucuronidase Inhibitors Applied to Botanical Extracts. *Anal. Chim. Acta X* 4, 100039. doi:10.1016/j.acax.2020.100039
- Manthey, J. A., and Grohmann, K. (1996). Concentrations of Hesperidin and Other Orange Peel Flavonoids in Citrus Processing Byproducts. *J. Agric. Food Chem.* 44, 811–814. doi:10.1021/jf950572g
- Marston, A., Kissling, J., and Hostettmann, K. (2002). A Rapid TLC Bioautographic Method for the Detection of Acetylcholinesterase and Butyrylcholinesterase Inhibitors in Plants. *Phytochem. Anal.* 13, 51–54. doi:10.1002/pca.623
- Marston, A. (2011). Thin-layer Chromatography with Biological Detection in Phytochemistry. *J. Chromatogr. A* 1218, 2676–2683. doi:10.1016/j.chroma.2010.12.068
- Mateos, R., Baeza, G., Sarriá, B., and Bravo, L. (2018). Improved LC-MSn Characterization of Hydroxycinnamic Acid Derivatives and Flavonols in Different Commercial Mate (*Ilex Paraguariensis*) Brands. Quantification of Polyphenols, Methylxanthines, and Antioxidant Activity. *Food Chem.* 241, 232–241. doi:10.1016/j.foodchem.2017.08.085
- Mauri, P., Migliazza, B., and Pietta, P. (1999). Liquid Chromatography/electrospray Mass Spectrometry of Bioactive Terpenoids in *Ginkgo Biloba* L. *J. Mass Spectrom.* 34, 13612–13676. doi:10.1002/(SICI)1096-9888(199912)34:12<1361::AID-JMS895>3.0.CO;2-6
- Mbachu, O. C., Howell, C., Simmler, C., Malca Garcia, G. R., Skowron, K. J., Dong, H., et al. (2020). SAR Study on Estrogen Receptor α/β Activity of (Iso) flavonoids: Importance of Prenylation, C-Ring (Un)Saturation, and Hydroxyl Substituents. *J. Agric. Food Chem.* 68, 10651–10663. doi:10.1021/acs.jafc.0c03526
- Mena, P., Cirilini, M., Tassotti, M., Herrlinger, K. A., dall'Asta, C., and Del Rio, D. (2016). Phytochemical Profiling of Flavonoids, Phenolic Acids, Terpenoids, and Volatile Fraction of a Rosemary (*Rosmarinus Officinalis* L.) Extract. *Molecules* 21, 1576. doi:10.3390/molecules21111576
- Meyer, D., Marin-Kuan, M., Debon, E., Serrant, P., Cottet-Fontannaz, C., Schilter, B., et al. (2020). Detection of Low Levels of Genotoxic Compounds in Food Contact Materials Using an Alternative HPTLC-SOS-Umu-C Assay. *Altex* 38, 387–397. doi:10.14573/altex.2006201
- Montero, L., Ibáñez, E., Russo, M., Di Sanzo, R., Rastrelli, L., Piccinelli, A. L., et al. (2016). Metabolite Profiling of Licorice (*Glycyrrhiza Glabra*) from Different Locations Using Comprehensive Two-Dimensional Liquid Chromatography Coupled to Diode Array and Tandem Mass Spectrometry Detection. *Anal. Chim. Acta* 913, 145–159. doi:10.1016/j.aca.2016.01.040
- Morlock, G. E., and Heil, J. (2020). H1-HPTLC-UV/Vis/FLD-HESI-HRMS and Bioprofiling of Steviol Glycosides, Steviol, and Isosteviol in Stevia Leaves and Foods. *Anal. Bioanal. Chem.* 412, 6431–6448. doi:10.1007/s00216-020-02618-4
- Morlock, G. E., Heil, J., Bardot, V., Lenoir, L., Cotte, C., and Dubourdeaux, M. (2021a). Effect-Directed Profiling of 17 Different Fortified Plant Extracts by High-Performance Thin-Layer Chromatography Combined with Six Planar Assays and High-Resolution Mass Spectrometry. *Molecules* 26, 1468. doi:10.3390/molecules26051468
- Morlock, G. E., Heil, J., Inarejos-Garcia, A. M., and Maeder, J. (2021b). Effect-Directed Profiling of Powdered Tea Extracts for Catechins, Theaflavins, Flavonols and Caffeine. *Antioxidants (Basel)* 10, 117. doi:10.3390/antiox10010117
- Morlock, G. E. (2021). High-performance Thin-Layer Chromatography Combined with Effect-Directed Assays and High-Resolution Mass Spectrometry as an Emerging Hyphenated Technology: A Tutorial Review. *Anal. Chim. Acta* 1180, 338644. doi:10.1016/j.aca.2021.338644

- Morlock, G. E., and Klingelhöfer, I. (2014). Liquid Chromatography-Bioassay-Mass Spectrometry for Profiling of Physiologically Active Food. *Anal. Chem.* 86, 8289–8295. doi:10.1021/ac501723j
- Morlock, G. E. (2014). Background Mass Signals in Tlc/hptlc-Esi-Ms and Practical Advices for Use of the Tlc-Ms Interface. *J. Liquid Chromatogr. Relat. Tech.* 37, 2892–2914. doi:10.1080/10739149.2014.907000
- Motohashi, N., Wakabayashi, H., Kurihara, T., Fukushima, H., Yamada, T., Kawase, M., et al. (2004). Biological Activity of barbados Cherry (Acerola Fruits, Fruit of *Malpighia Emarginata* DC) Extracts and Fractions. *Phytother Res.* 18, 212–223. doi:10.1002/ptr.1426
- Mulder, P. P. J., Sánchez, P. L., These, A., Preiss-Weigert, A., and Castellari, M. (2015). Occurrence of Pyrrolizidine Alkaloids in Food. *EFSA Supporting Publications* 12. doi:10.2903/sp.efsa.2015.EN-859
- Niu, X., Luo, J., Xu, D., Zou, H., and Kong, L. (2017). Hydrogen/deuterium Exchange, a Unique and Effective Method for MS Fragmentation Behavior Elucidation of Ginkgolides and its Application to Systematic Research in Ginkgo Biloba. *J. Pharm. Biomed. Anal.* 134, 181–186. doi:10.1016/j.jpba.2016.11.043
- Nomura, T., Fukai, T., and Akiyama, T. (2002). Chemistry of Phenolic Compounds of Licorice (*Glycyrrhiza* Species) and Their Estrogenic and Cytotoxic Activities. *Pure Appl. Chem.* 74, 1199–1206. doi:10.1351/pac200274071199
- Önder, F. C., Ay, M., and Sarker, S. D. (2013). Comparative Study of Antioxidant Properties and Total Phenolic Content of the Extracts of *Humulus Lupulus* L. And Quantification of Bioactive Components by LC-MS/MS and GC-MS. *J. Agric. Food Chem.* 61, 10498–10506. doi:10.1021/jf4031508
- Orhan, D. D., Özçelik, B., Özgen, S., and Ergun, F. (2010). Antibacterial, Antifungal, and Antiviral Activities of Some Flavonoids. *Microbiol. Res.* 165, 496–504. doi:10.1016/j.micres.2009.09.002
- Palombo, E. A., and Semple, S. J. (2001). Antibacterial Activity of Traditional Australian Medicinal Plants. *J. Ethnopharmacol.* 77, 151–157. doi:10.1016/S0378-8741(01)00290-2
- Pastorino, G., Cornara, L., Soares, S., Rodrigues, F., and Oliveira, M. B. P. P. (2018). Liquorice (*Glycyrrhiza Glabra*): A Phytochemical and Pharmacological Review. *Phytother Res.* 32, 2323–2339. doi:10.1002/ptr.6178
- Pérez-Mendoza, M. B., Llorens-Escobar, L., Vanegas-Espinoza, P. E., Cifuentes, A., Ibáñez, E., and Villar-Martínez, A. A. D. (2020). Chemical Characterization of Leaves and Calli Extracts of *Rosmarinus Officinalis* by UHPLC-MS. *Electrophoresis* 41, 1776–1783. doi:10.1002/elps.201900152
- Petersen, M. J., de Cássia Lemos Lima, R., Kjaerulff, L., and Staerk, D. (2019). Immobilized α -amylase Magnetic Beads for Ligand Fishing: Proof of Concept and Identification of α -amylase Inhibitors in Ginkgo Biloba. *Phytochemistry* 164, 94–101. doi:10.1016/j.phytochem.2019.04.016
- Prencipe, F. P., Brighenti, V., Rodolfi, M., Mongelli, A., dall'Asta, C., Ganino, T., et al. (2014). Development of a New High-Performance Liquid Chromatography Method with Diode Array and Electrospray Ionization-Mass Spectrometry Detection for the Metabolite Fingerprinting of Bioactive Compounds in *Humulus Lupulus* L. *J. Chromatogr. A.* 1349, 50–59. doi:10.1016/j.chroma.2014.04.097
- Puranik, N. V., Srivastava, P., Bhatt, G., John Mary, D. J. S., Limaye, A. M., and Sivaraman, J. (2019). Determination and Analysis of Agonist and Antagonist Potential of Naturally Occurring Flavonoids for Estrogen Receptor (ER α) by Various Parameters and Molecular Modelling Approach. *Sci. Rep.* 9, 7450. doi:10.1038/s41598-019-43768-5
- Quirantes-Piné, R., Arráez-Román, D., Segura-Carretero, A., and Fernández-Gutiérrez, A. (2010). Characterization of Phenolic and Other Polar Compounds in a Lemon Verbena Extract by Capillary Electrophoresis-Electrospray Ionization-Mass Spectrometry. *J. Sep. Sci.* 33, 2818–2827. doi:10.1002/jssc.201000228
- Rejeb, I. B., Dhen, N., Gargouri, M., and Boulila, A. (2020). Chemical Composition, Antioxidant Potential and Enzymes Inhibitory Properties of Globe Artichoke By-Products. *Chem. Biodivers.* 17, e2000073. doi:10.1002/cbdv.202000073
- Rocchetti, G., Senizza, B., Zengin, G., Mahomodally, M. F., Senkardes, I., Lobine, D., et al. (2020). Untargeted Metabolomic Profiling of Three *Crataegus* Species (Hawthorn) and Their *In Vitro* Biological Activities. *J. Sci. Food Agric.* 100, 1998–2006. doi:10.1002/jsfa.10216
- Rosselli, S., Maggio, A., Bellon, G., Formisano, C., Basile, A., Cicala, C., et al. (2007). Antibacterial and Anticoagulant Activities of Coumarins Isolated from the Flowers of *Magyaris Tomentosa*. *Planta Med.* 73, 116–120. doi:10.1055/s-2006-951772
- Rusko, J., Perkons, I., Rasinger, J. D., and Bartkevics, V. (2020). Non-target and Suspected-Target Screening for Potentially Hazardous Chemicals in Food Contact Materials: Investigation of Paper Straws. *Food Addit. Contam. Part. A. Chem. Anal. Control. Expo. Risk Assess.* 37, 649–664. doi:10.1080/19440049.2020.1711969
- Salehi, B., Sharifi-Rad, J., Quispe, C., Llaique, H., Villalobos, M., Smeriglio, A., et al. (2019). Insights into Eucalyptus Genus Chemical Constituents, Biological Activities and Health-Promoting Effects. *Trends Food Sci. Technology* 91, 609–624. doi:10.1016/j.tifs.2019.08.003
- Santos, S. A., Freire, C. S., Domingues, M. R., Silvestre, A. J., and Pascoal Neto, C. (2011). Characterization of Phenolic Components in Polar Extracts of *Eucalyptus Globulus* Labill. Bark by High-Performance Liquid Chromatography-Mass Spectrometry. *J. Agric. Food Chem.* 59, 9386–9393. doi:10.1021/jf201801q
- Sawalha, S. M. S., Arráez-Román, D., Segura-Carretero, A., and Fernández-Gutiérrez, A. (2009). Quantification of Main Phenolic Compounds in Sweet and Bitter orange Peel Using CE-MS/MS. *Food Chem.* 116, 567–574. doi:10.1016/j.foodchem.2009.03.003
- Schreiner, T., and Morlock, G. E. (2021). Non-target Bioanalytical Eight-Dimensional Hyphenation Including Bioassay, Heart-Cut Trapping, Online Desalting, Orthogonal Separations and Mass Spectrometry. *J. Chromatogr. A.* 1647, 462154. doi:10.1016/j.chroma.2021.462154
- Schulte-Oehlmann, U., Oehlmann, J., and Keil, F. (2011). Before the Curtan Falls: Endocrine-Active Pesticides-Aa German Contamination Legacy. *Rev. Environ. Contam. Toxicol.* 213, 137–159. doi:10.1007/978-1-4419-9860-6_5
- Schütz, K., Kammerer, D., Carle, R., and Schieber, A. (2004). Identification and Quantification of Caffeoylquinic Acids and Flavonoids from Artichoke (*Cynara Scolymus* L.) Heads, Juice, and Pomace by HPLC-DAD-ESI/MS(n). *J. Agric. Food Chem.* 52, 4090–4096. doi:10.1021/jf049625x
- Sharma, R., Kuca, K., Nepovimova, E., Kabra, A., Rao, M. M., and Prajapati, P. K. (2019). Traditional Ayurvedic and Herbal Remedies for Alzheimer's Disease: from Bench to Bedside. *Expert Rev. Neurother.* 19, 359–374. doi:10.1080/14737175.2019.1596803
- Sharma, V., Katiyar, A., and Agrawal, R. C. (2018). "Glycyrrhiza Glabra: Chemistry and Pharmacological Activity," in *Sweeteners*. Editors J.-M. Mérillon and K. G. Ramawat (Cham: Springer International Publishing), 87–100. doi:10.1007/978-3-319-27027-2_21
- Shu, P., Fei, Y., Li, J., Liu, A., Zhang, L., Niu, H., et al. (2020). Two New Phenylethanoid Glycosides from Ginkgo Biloba Leaves and Their Tyrosinase Inhibitory Activities. *Carbohydr. Res.* 494, 108059. doi:10.1016/j.carres.2020.108059
- Shu, Z., Hussain Sh. A., Shahen, M., Wang, H., Alagawany, M., Abd El-Hac, M. E., et al. (2018). Pharmacological Uses of Ginkgo Biloba Extracts for Cardiovascular Disease and Coronary Heart Diseases. *Int. J. Pharmacol.* 15, 1–9. doi:10.3923/ijp.2019.1.9
- Simões-Pires, C. A., Hmicha, B., Marston, A., and Hostettmann, K. (2009). A TLC Bioautographic Method for the Detection of Alpha- and Beta-Glucosidase Inhibitors in Plant Extracts. *Phytochem. Anal.* 20, 511–515. doi:10.1002/pca.1154
- Smyth, T., Ramachandran, V. N., and Smyth, W. F. (2009). A Study of the Antimicrobial Activity of Selected Naturally Occurring and Synthetic Coumarins. *Int. J. Antimicrob. Agents* 33, 421–426. doi:10.1016/j.ijantimicag.2008.10.022
- Soković, M., Glamočlija, J., Marin, P. D., Brkić, D., and van Griensven, L. J. (2010). Antibacterial Effects of the Essential Oils of Commonly Consumed Medicinal Herbs Using an *In Vitro* Model. *Molecules* 15, 7532–7546. doi:10.3390/molecules15117532
- Sommella, E., Pagano, F., Salviati, E., Chieppa, M., Bertamino, A., Manfra, M., et al. (2018). Chemical Profiling of Bioactive Constituents in Hop Cones and Pellets Extracts by Online Comprehensive Two-Dimensional Liquid Chromatography with Tandem Mass Spectrometry and Direct Infusion Fourier Transform Ion Cyclotron Resonance Mass Spectrometry. *J. Sep. Sci.* 41, 1548–1557. doi:10.1002/jssc.201701242
- Su, Q. Z., Vera, P., and Nerín, C. (2020). Direct Immersion-solid-phase Microextraction Coupled to Gas Chromatography-Mass Spectrometry and Response Surface Methodology for Nontarget Screening of (Semi-) Volatile Migrants from Food Contact Materials. *Anal. Chem.* 92, 5577–5584. doi:10.1021/acs.analchem.0c00532

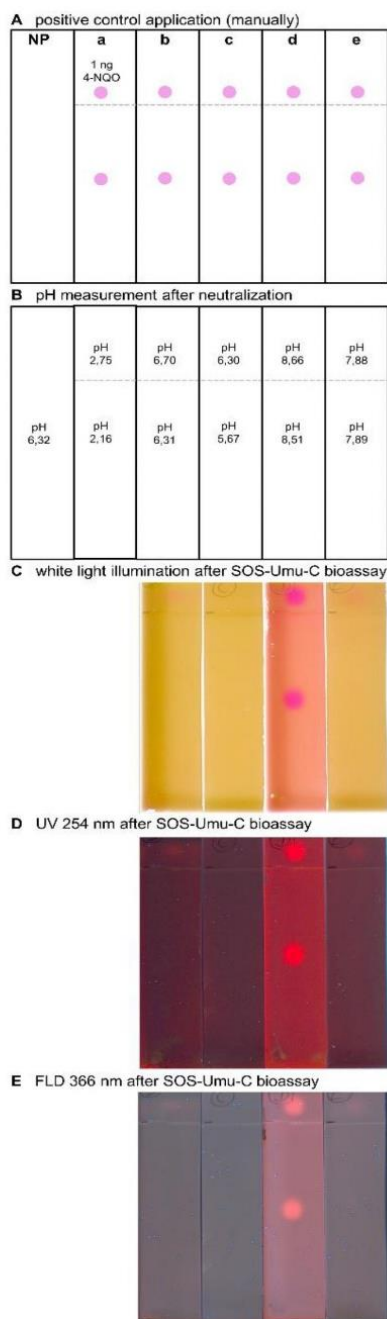
- Sun, C. P., Yan, J. K., Yi, J., Zhang, X. Y., Yu, Z. L., Huo, X. K., et al. (2020). The Study of Inhibitory Effect of Natural Flavonoids toward β -glucuronidase and Interaction of Flavonoids with β -glucuronidase. *Int. J. Biol. Macromol.* 143, 349–358. doi:10.1016/j.ijbiomac.2019.12.057
- Taibon, J., Ankli, A., Schwaiger, S., Magnenat, C., Boka, V. I., Simões-Pires, C., et al. (2015). Prevention of False-Positive Results: Development of an HPTLC Autographic Assay for the Detection of Natural Tyrosinase Inhibitors. *Planta Med.* 81, 1198–1204. doi:10.1055/s-0035-1546250
- Tamayose, C. I., Torres, P. B., Roque, N., and Ferreira, M. J. P. (2019). HIV-1 Reverse Transcriptase Inhibitory Activity of Flavones and Chlorogenic Acid Derivatives from *Moquiastrium Floribundum* (Asteraceae). *South Afr. J. Bot.* 123, 142–146. doi:10.1016/j.sajb.2019.02.005
- Tresserra-Rimbau, A., Lamuela-Raventos, R. M., and Moreno, J. J. (2018). Polyphenols, Food and Pharma. Current Knowledge and Directions for Future Research. *Biochem. Pharmacol.* 156, 186–195. doi:10.1016/j.bcp.2018.07.050
- Tundis, R., Bonesi, M., Menichini, F., and Loizzo, M. R. (2016). Recent Knowledge on Medicinal Plants as Source of Cholinesterase Inhibitors for the Treatment of Dementia. *Mini Rev. Med. Chem.* 16, 605–618. doi:10.2174/1389557515666150709104731
- Turkiewicz, I. P., Wojdylo, A., Tkacz, K., Nowicka, P., and Hernández, F. (2019). Antidiabetic, Anticholinesterase and Antioxidant Activity vs. Terpenoids and Phenolic Compounds in Selected New Cultivars and Hybrids of Artichoke *Cynara Scolymus* L. *Molecules* 24. doi:10.3390/molecules24071222
- Umeno, A., Horie, M., Murotomi, K., Nakajima, Y., and Yoshida, Y. (2016). Antioxidative and Antidiabetic Effects of Natural Polyphenols and Isoflavones. *Molecules* 21. doi:10.3390/molecules21060708
- Vallverdú-Queralt, A., Regueiro, J., Martínez-Huélamo, M., Rinaldi Alvarenga, J. F., Leal, L. N., and Lamuela-Raventos, R. M. (2014). A Comprehensive Study on the Phenolic Profile of Widely Used Culinary Herbs and Spices: Rosemary, Thyme, Oregano, Cinnamon, Cumin and bay. *Food Chem.* 154, 299–307. doi:10.1016/j.foodchem.2013.12.106
- Velkoska-Markovska, L., Jankulovska, M. S., Petanovska-Ilievska, B., and Hristovski, K. (2020). Development and Validation of RRLC-UV Method for Determination of Chlorogenic Acid in green Coffee. *Acta Chromatographica* 32, 34–38. doi:10.1556/1326.2019.00547
- Vierling, W., Brand, N., Gaedcke, F., Sensch, K. H., Schneider, E., and Scholz, M. (2003). Investigation of the Pharmaceutical and Pharmacological Equivalence of Different Hawthorn Extracts. *Phytomedicine* 10, 8–16. doi:10.1078/094471103321648601
- Wang, L. C., Wei, W. H., Zhang, X. W., Liu, D., Zeng, K. W., and Tu, P. F. (2018). An Integrated Proteomics and Bioinformatics Approach Reveals the Anti-inflammatory Mechanism of Carnosic Acid. *Front. Pharmacol.* 9, 370. doi:10.3389/fphar.2018.00370
- Wang, S., Ouyang, B., Aa, J., Geng, J., Fei, F., Wang, P., et al. (2016). Pharmacokinetics and Tissue Distribution of Ginkgolide A, Ginkgolide B, and Ginkgolide K after Intravenous Infusion of Ginkgo Diterpene Lactones in a Rat Model. *J. Pharm. Biomed. Anal.* 126, 109–116. doi:10.1016/j.jpba.2016.04.035
- Wang, Y. H., Meng, Y., Zhai, C., Wang, M., Avula, B., Yuk, J., et al. (2019). The Chemical Characterization of *Eleutherococcus Senticosus* and *Ci-Wu-jia* Tea Using UHPLC-UV-QTOF/MS. *Int. J. Mol. Sci.* 20. doi:10.3390/ijms20030475
- Willems, J. L., Khamis, M. M., Mohammed Saaid, W., Purves, R. W., Katselis, G., Low, N. H., et al. (2016). Analysis of a Series of Chlorogenic Acid Isomers Using Differential Ion Mobility and Tandem Mass Spectrometry. *Anal. Chim. Acta* 933, 164–174. doi:10.1016/j.aca.2016.05.041
- Wilson, W. B., and Sander, L. C. (2018). Method Development for the Certification of a Ginsenoside Calibration Solution via Liquid Chromatography with Absorbance and Mass Spectrometric Detection. *J. Chromatogr. A.* 1574, 114–121. doi:10.1016/j.chroma.2018.09.011
- Wojdylo, A., Oszmianski, J., and Czemerly, R. (2007). Antioxidant Activity and Phenolic Compounds in 32 Selected Herbs. *Food Chem.* 105, 940–949. doi:10.1016/j.foodchem.2007.04.038
- Wong, Y. F., Cacciola, F., Feras, S., Riga, S., James, D., Manzin, V., et al. (2018). Untargeted Profiling of Glycyrrhiza Glabra Extract with Comprehensive Two-Dimensional Liquid Chromatography-Mass Spectrometry Using Multi-Segmented Shift Gradients in the Second Dimension: Expanding the Metabolic Coverage. *Electrophoresis* 39, 1993–2000. doi:10.1002/elps.201700469
- Wu, B., Song, H. P., Zhou, X., Liu, X. G., Gao, W., Dong, X., et al. (2016). Screening of Minor Bioactive Compounds from Herbal Medicines by In Silico Docking and the Trace Peak Exposure Methods. *J. Chromatogr. A.* 1436, 91–99. doi:10.1016/j.chroma.2016.01.062
- Ye, Y., Chou, G. X., Mu, D. D., Wang, H., Chu, J. H., Leung, A. K., et al. (2010). Screening of Chinese Herbal Medicines for Antityrosinase Activity in a Cell Free System and B16 Cells. *J. Ethnopharmacol.* 129, 387–390. doi:10.1016/j.jep.2010.04.009
- Yilmaz, M. A. (2020). Simultaneous Quantitative Screening of 53 Phytochemicals in 33 Species of Medicinal and Aromatic Plants: A Detailed, Robust and Comprehensive LC-MS/MS Method Validation. *Ind. Crops Prod.* 149, 112347. doi:10.1016/j.indcrop.2020.112347
- Yilmaz, Y., and Toledo, R. T. (2004). Major Flavonoids in Grape Seeds and Skins: Antioxidant Capacity of Catechin, Epicatechin, and Gallic Acid. *J. Agric. Food Chem.* 52, 255–260. doi:10.1021/jf030117h
- Yu, J. Y., Ha, J. Y., Kim, K. M., Jung, Y. S., Jung, J. C., and Oh, S. (2015). Anti-Inflammatory Activities of Licorice Extract and its Active Compounds, Glycyrrhizic Acid, Liquiritin and Liquiritigenin, in BV2 Cells and Mice Liver. *Molecules* 20, 13041–13054. doi:10.3390/molecules200713041
- Yuan, H., Ma, Q., Ye, L., and Piao, G. (2016). The Traditional Medicine and Modern Medicine from Natural Products. *Molecules* 21, 559. doi:10.3390/molecules21050559
- Zhang, C., Lu, Y., Tao, L., Tao, X., Su, X., and Wei, D. (2007). Tyrosinase Inhibitory Effects and Inhibition Mechanisms of Nobiletin and Hesperidin from Citrus Peel Crude Extracts. *J. Enzyme Inhib. Med. Chem.* 22, 91–98. doi:10.1080/14756360600953876
- Zhang, X., Zhang, Y., Shi, P., Bi, Z., Shan, Z., and Ren, L. (2021). The Deep challenge of Nitrate Pollution in River Water of China. *Sci. Total Environ.* 770, 144674. doi:10.1016/j.scitotenv.2020.144674
- Zheng, J., Kallio, H., and Yang, B. (2016). Sea Buckthorn (*Hippophaë Rhamnoides* Ssp. *Rhamnoides*) Berries in Nordic Environment: Compositional Response to Latitude and Weather Conditions. *J. Agric. Food Chem.* 64, 5031–5044. doi:10.1021/acs.jafc.6b00682
- Zhou, Y.-Q., Liu, H., He, M.-X., Wang, R., Zeng, Q.-Q., Wang, Y., et al. (2018). “A Review of the Botany, Phytochemical, and Pharmacological Properties of Galangal,” in *Natural And Artificial Flavoring Agents and Food Dyes*. Editors A. M. Grumezescu and A. M. Holban (London: Academic Press, an imprint of Elsevier), 351–396. doi:10.1016/b978-0-12-811518-3.00011-9

Conflict of Interest: The authors declare that the research was conducted in the absence of any commercial or financial relationships that could be construed as a potential conflict of interest.

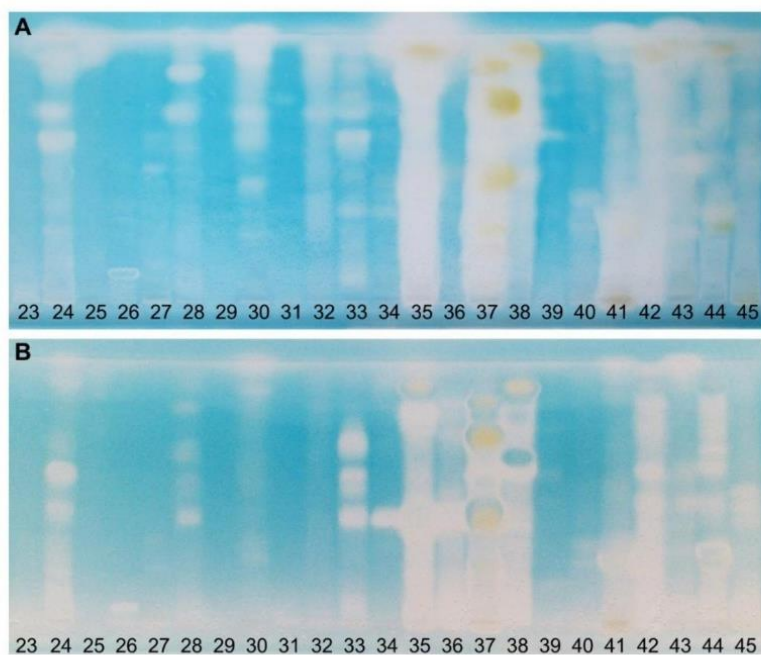
Publisher’s Note: All claims expressed in this article are solely those of the authors and do not necessarily represent those of their affiliated organizations, or those of the publisher, the editors, and the reviewers. Any product that may be evaluated in this article, or claim that may be made by its manufacturer, is not guaranteed or endorsed by the publisher.

Copyright © 2021 Schreiner, Sauter, Friz, Heil and Morlock. This is an open-access article distributed under the terms of the Creative Commons Attribution License (CC BY). The use, distribution or reproduction in other forums is permitted, provided the original author(s) and the copyright owner(s) are credited and that the original publication in this journal is cited, in accordance with accepted academic practice. No use, distribution or reproduction is permitted which does not comply with these terms.

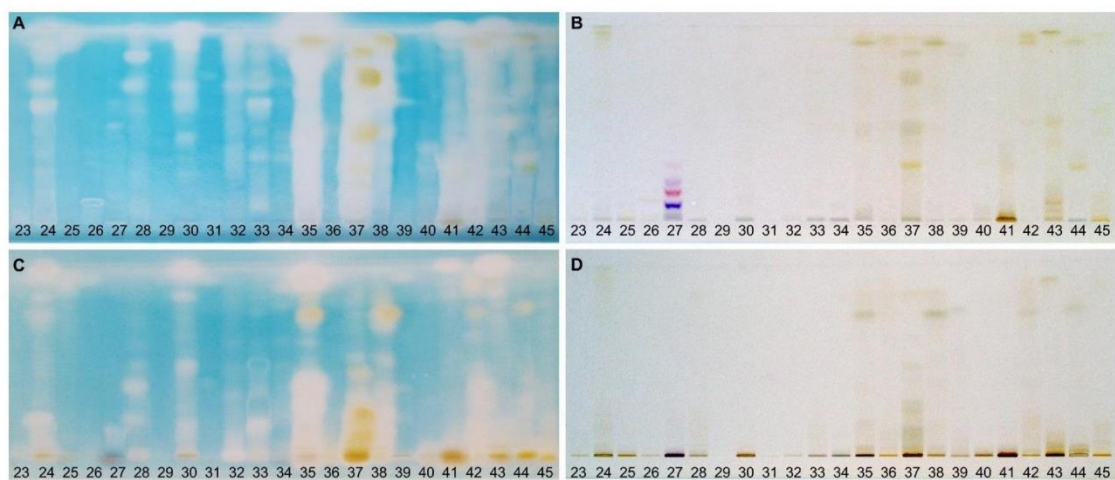
Supplementary Material



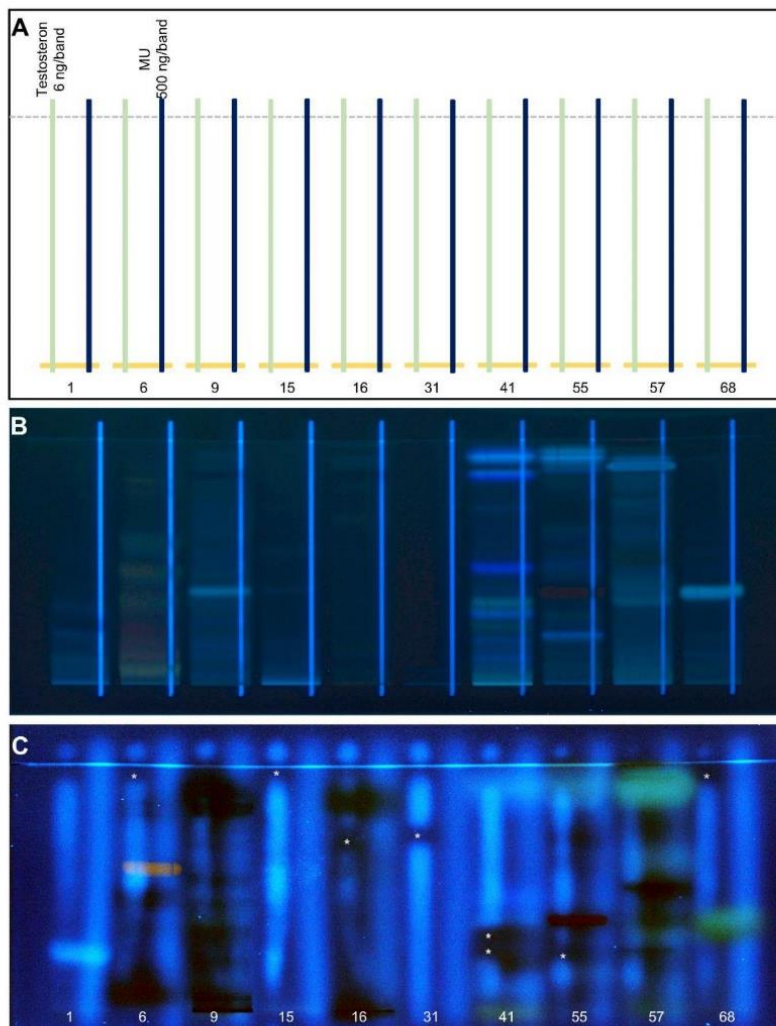
Supplementary Figure 1. NP-HPTLC–SOS-Umu-C neutralization study. An empty HPTLC plate silica gel 60 was developed with ethyl acetate – toluene – formic acid – water (16:4:3:2, *V/V/V/V*), up to 70 mm and cut into 5 pieces (A). 4-nitroquinoline 1-oxide (1 μ L, 1 ng/ μ L) was applied within and above the solvent front. The pH of differently treated plate pieces was measured with a contact electrode (B): untreated plate (NP), not neutralized (a), immersion (3.5 cm/s, 2 s) in citrate buffer pH 12 (b), spraying (yellow nozzle, level 2) 2.8 mL citrate buffer pH 12 (c), immersion (3.5 cm/s, 2 s) in 2.5% sodium bicarbonate buffer pH 8 (d), 20 min ammonia vapor (e). After the SOS-Umu-C bioassay, plates were detected at white light illumination (C), UV 254 nm (D) and FLD 366 nm (E).



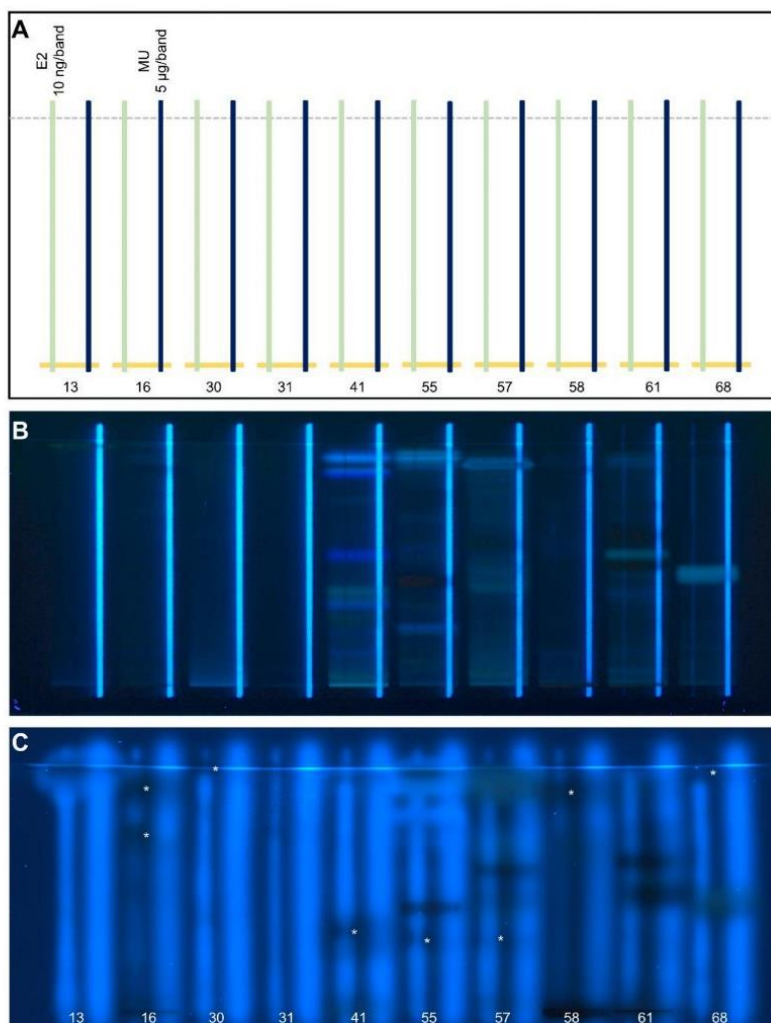
Supplementary Figure 2. NP-HPTLC- β -glucosidase inhibition profiles of the plant extracts nos. 23–45 (assignments in Table 1) applied as 4 μ L/band (**A**) and 1 μ L/band (**B**) on HPTLC plate silica gel 60 F₂₅₄ MS-grade, developed with ethyl acetate – toluene – formic acid – water (16:4:3:2, *V/V/V/V*), up to 70 mm, detected at white light illumination after the β -glucuronidase inhibition assay.



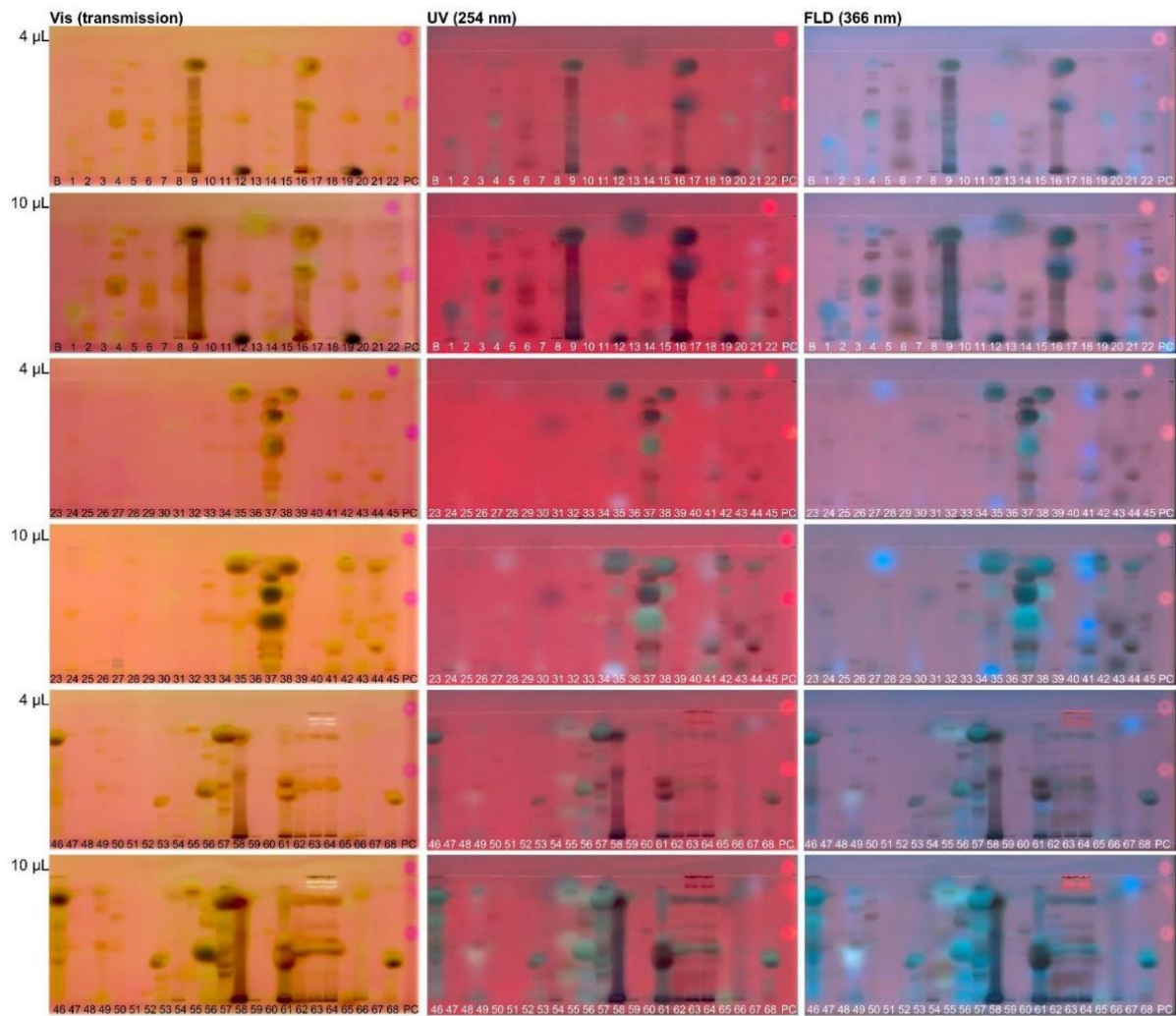
Supplementary Figure 3. NP-HPTLC- β -glucosidase inhibition profiles of the plant extracts nos. 23–45 (4 μ L/band, assignments in Table 1) applied on HPTLC plate silica gel 60 F₂₅₄ MS-grade, developed with ethyl acetate – toluene – formic acid – water (16:4:3:2, *V/V/V/V*) (**A, B**) or ethyl acetate – toluene – formic acid (10:4:1, *V/V/V*) (**C, D**) up to 70 mm, detected at white light illumination before (**B, D**) and after (**A, C**) the β -glucuronidase inhibition assay.



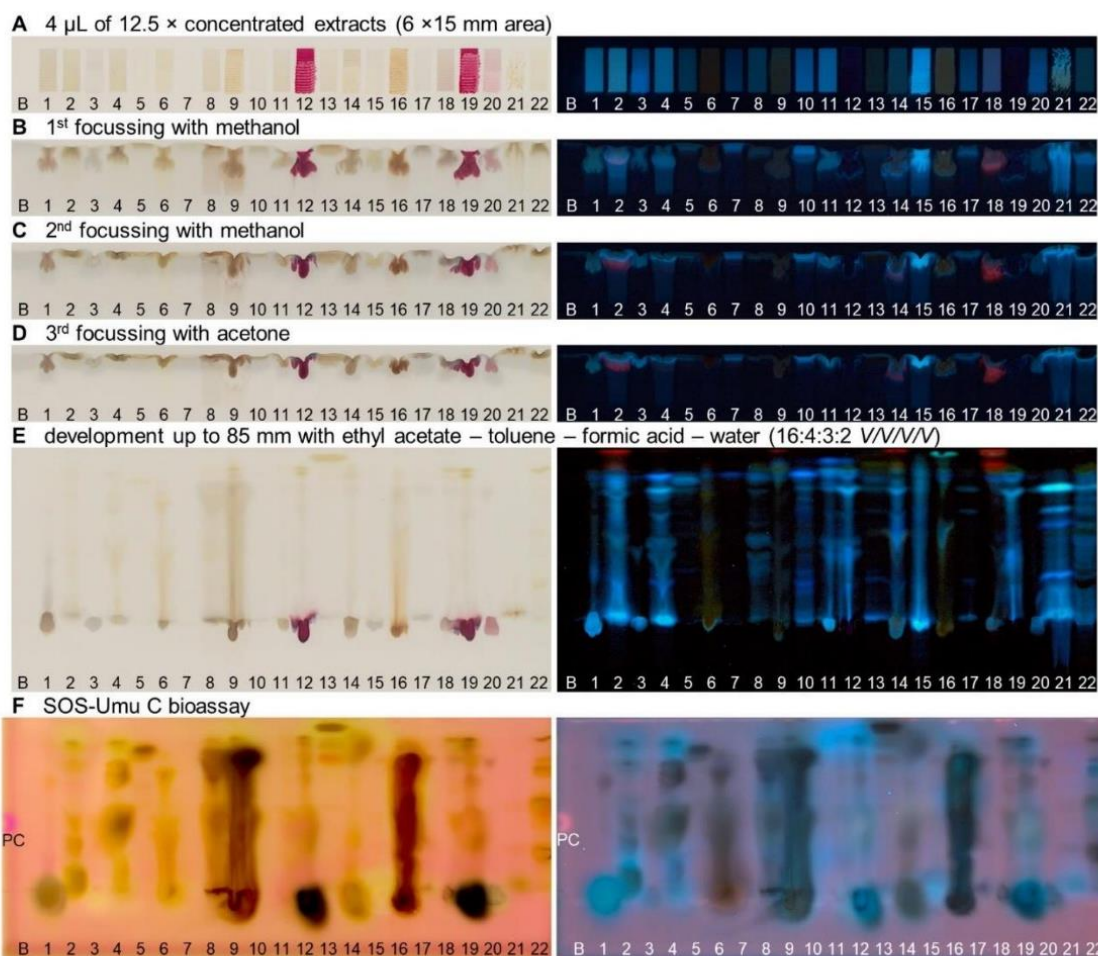
Supplementary Figure 4. Exclusion of false-positive results in NP-HPTLC-pYAAS bioassay. The samples (assignments in Table 1) assumed to have antiandrogen-like effects were investigated for false positive results by application as 15 mm bands (5 μ L) and development up to 70 mm with ethyl acetate – toluene – formic acid – water (16:4:3:2, *V/V/V/V*). 4-Methylumbelliferone (500 ng/band) and testosterone (6 ng/band) were applied as an overlapping 1 mm \times 70 mm area on each track according to plate design (A). Application was monitored at FLD 366 nm (B). Comparison of testosterone and 4-methylumbelliferone fluorescence deletion after performing the pYAAS bioassay documented at FLD 366 nm (C). Antiandrogen-like zones only delete fluorescence in overlapping testosterone area (marked*).



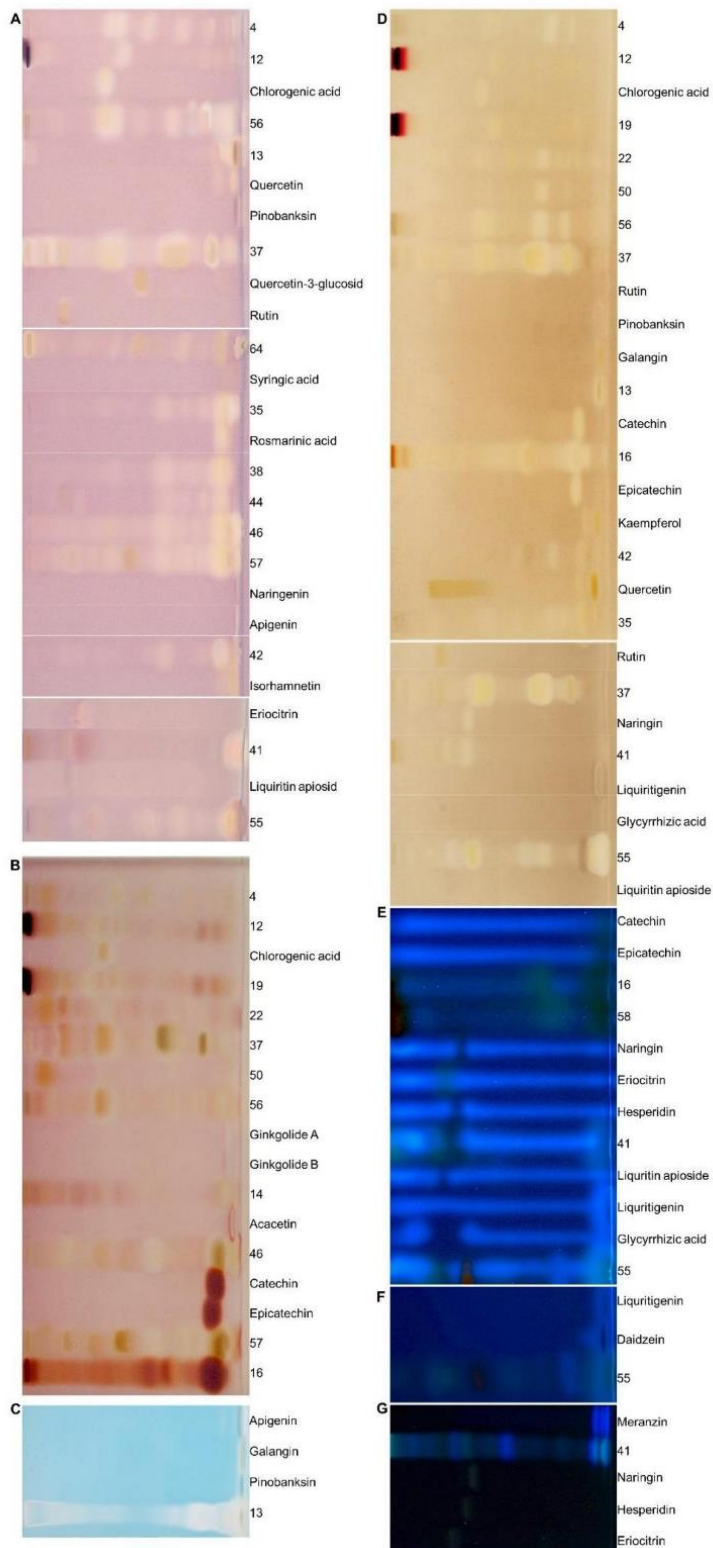
Supplementary Figure 5. First report of the NP-HPTLC-pYAES bioassay with the integrated exclusion of false-positive results. Selected botanicals (nos. 13–68 assigned in Table 1) assumed to have antiestrogen-like effects were proven for truly anti-estrogenic or false positive results according to the plate design (A): application each as 15-mm band (5 μ L), development up to 70 mm with ethyl acetate – toluene – formic acid – water (16:4:3:2, *V/V/V/V*) and detection at FLD 366 nm (B); 4-methylumbelliferone (5 μ g/band) and 17- β -estradiol (10 ng/band) were oversprayed as 1 mm \times 70 mm area on each separated track, followed by the bioassay application and documentation at FLD 366 nm (C). Comparing the 17- β -estradiol and 4-methylumbelliferone fluorescence reduction reveals truly antiestrogen-like zones which only reduce the fluorescence in the 17- β -estradiol area (marked*).



Supplementary Figure 6. NP-HPTLC–SOS-Umu-C profiles of the plant extract nos. 1–68 (4 or 10 µL/band respectively; assignments in Table 1; solvent blank B for comparison) and positive control (4-nitroquinoline 1-oxide 1 µL, 1 ng/µL) on HPTLC plate silica gel 60 with ethyl acetate – toluene – formic acid – water (16:4:3:2, *V/V/V/V*), up to 70 mm, detected at white light illumination (Vis), UV 254 nm and FLD 366 nm after the SOS-Umu-C bioassay.



Supplementary Figure 7. NP-HPTLC–SOS-Umu-C profiles of the plant extracts nos. 1–22. Area application (6 mm \times 15 mm) of the 12.5-fold concentrated botanicals (4 $\mu\text{L}/\text{area}$ respectively, assignments in Table 1; solvent blank B for comparison) and positive control (1 μL , 1 ng/ μL 4-nitroquinoline 1-oxide) on HPTLC plate silica gel 60 (**A**). Focusing of the areas with methanol (**B**, **C**) and acetone (**D**) to 25 mm and development with ethyl acetate – toluene – formic acid – water (16:4:3:2, V/V/V/V) up to 85 mm (**E**), detected at white light illumination (Vis) and FLD 366 nm after the SOS-Umu-C bioassay (**F**).



Supplementary Figure 8. NP-HPTLC-UV/Vis/FLD-EDA profiles of the plant extracts (4 μ L/band, assignments in Table 1) co-chromatographed with standards (5 μ L/band, 1 μ g/ μ L) on HPTLC plate silica gel 60 F₂₅₄ MS-grade with ethyl acetate – toluene – formic acid – water (16:4:3:2, V/V/V/V), up to 70 mm, detected at white light illumination (A–D) and FLD 366 nm (E–F) and after the BChE (A), β -glucosidase (B), β -glucuronidase (C) and tyrosinase (D) inhibition assays as well as pYAES (E) and pYES (F) bioassays.



Supplementary Table 1. NP-HPTLC-EDA-RP-HPLC-DAD-HESI-MS confirmation with standards and respective activity (X) in the AChE/BChE (C), α -/ β -glucosidase (D), β -glucuronidase (E), and tyrosinase (F) inhibition assays as well as pYES (H) and pYAES (J) bioassays.

Substance	<i>t</i> R _F (\pm 1)	RT [min]	UV λ _{max} [nm]	<i>m/z</i>	Mass signal	Found in	C	D	E	F	H	J
Acacetin	98	8.31	268, 330	283 285	[M-H] ⁻ [M+H] ⁺	Rosemary (no. 46)		X				
Apigenin	98	7.79	239, 267, 339	269 271	[M-H] ⁻ [M+H] ⁺	Oregano (no. 42)	X		X			
Catechin	94	5.16	279	289 325 403 291 329	[M-H] ⁻ [M+Cl] ⁻ [M+TFA-H] ⁻ [M+H] ⁺ [M+K] ⁺	Guarana (no. 16)		X		X		X
Chlorogenic acid	37	3.59	217, 324	353 355 372 377 393	[M-H] ⁻ [M+H] ⁺ [M+NH ₄] ⁺ [M+Na] ⁺ [M+K] ⁺	Artichoke (no. 4) Fruit tea, red (no. 12) Hibiscus (no. 19) Elder blossom (no. 22) Siberian ginseng (no. 56)	X	X		X		
Daidzein	98	7.32	248	253 255 277 293	[M-H] ⁻ [M+H] ⁺ [M+Na] ⁺ [M+K] ⁺	Licorice (no. 55)					X	
Epicatechin	93	6.02	203, 279	289 325 403 291 313 329	[M-H] ⁻ [M+Cl] ⁻ [M+TFA-H] ⁻ [M+H] ⁺ [M+Na] ⁺ [M+K] ⁺	Guarana (no. 16)		X		X		X
Eriocitrin	26	6.59	284	595 631 658 709 597 614 619 635	[M-H] ⁻ [M+Cl] ⁻ [M+NO ₃] ⁻ [M+TFA-H] ⁻ [M+H] ⁺ [M+NH ₄] ⁺ [M+Na] ⁺ [M+K] ⁺	Orange peel (no. 41)	X					
Galangin	99	8.35	209, 266	269 271	[M-H] ⁻ [M+H] ⁺	Galangal (no. 13)			X	X		
Ginkgolide A	95	6.95	224	407	[M-H] ⁻	Ginkgo (no. 14)		X				

Substance	<i>hRf</i> (± 1)	RT [min]	UV λ_{max} [nm]	<i>m/z</i>	Mass signal	Found in	C	D	E	F	H	J
			272	443 467 815 426 431 447	[M+Cl] ⁻ [M+H ₃ C-COO] ⁻ [2M-H] ⁻ [M+NH ₄] ⁺ [M+Na] ⁺ [M+K] ⁺							
Ginkgolide B	95	6.95	224, 272	423 459 537 442 447 463	[M-H] ⁻ [M+Cl] ⁻ [M+TFA-H] ⁻ [M+NH ₄] ⁺ [M+Na] ⁺ [M+K] ⁺	Ginkgo (no. 14)	X					
Glycyrrhizic acid	25	7.84	-	410 821 861	[M-2H] ⁻ [M-H] ⁻ [M+K] ⁺	Licorice (no. 55)			X			X
Hesperidin	31	6.92	285	609 645 611 623 649	[M-H] ⁻ [M+Cl] ⁻ [M+H] ⁺ [M+Na] ⁺ [M+K] ⁺	Orange peel (no. 41)						X
Isorhamnetin	97	7.79	-	315 317	[M-H] ⁻ [M+H] ⁺	Oregano (no. 42)	X					
Kaempferol	95	n.d.	n.d.	n.d.	n.d.	Supposed in Oregano (no. 42)				X		
Liquiritigenin	98	7.21	219, 231, 276	255 257 279	[M-H] ⁻ [M+H] ⁺ [M+Na] ⁺	Licorice (no. 55)			X	X		
Liquiritin apiosid	23	6.65	217, 276	549 585 612 663 551 568 573 589	[M-H] ⁻ [M+Cl] ⁻ [M+NO ₃] ⁻ [M+TFA-H] ⁻ [M+H] ⁺ [M+NH ₄] ⁺ [M+Na] ⁺ [M+K] ⁺	Licorice (no. 55)	X		X		X	
Naringenin	97	7.51	226, 290	271 273	[M-H] ⁻ [M+H] ⁺	Oregano (no. 42)	X					
Naringin	33	6.87	284	579 615 639 642 581 603	[M-H] ⁻ [M+Cl] ⁻ [M+H ₃ C-COO] ⁻ [M+NO ₃] ⁻ [M+H] ⁺ [M+Na] ⁺	Orange peel (no. 41)			X			X

Substance	<i>t</i> _R (±1)	RT [min]	UV λ_{max} [nm]	<i>m/z</i>	Mass signal	Found in	C	D	E	F	H	J
Pinobanksin	99	7.53	214, 291	619 271	[M+K] ⁺ [M-H] ⁻	Galangal (no. 13)	X		X	X		
Quercetin	97	7.40	255, 371	301 603 303	[M-H] ⁻ [2M-H] ⁻ [M+H] ⁺	Supposed in Galangal (no. 13) → rebutted	X			X		
Quercetin-3-glucosid	54	6.86	256, 356	463 465 487 503	[M-H] ⁻ [M+H] ⁺ [M+Na] ⁺ [M+K] ⁺	Supposed in Yerba mate, green (no. 37) → rebutted	X					
Rosmarinic acid	90	6.18	218, 326	359 395 719 361 378 383 399	[M-H] ⁻ [M+Cl] ⁻ [2M-H] ⁻ [M+H] ⁺ [M+NH ₄] ⁺ [M+Na] ⁺ [M+K] ⁺	Marjoram (no. 35) Lemon balm (no. 38) Peppermint (no. 44) Rosemary (no. 46) Thyme (no. 57)	X					
Rutin	19	6.84	256, 356	609 611 633 649	[M-H] ⁻ [M+H] ⁺ [M+Na] ⁺ [M+K] ⁺	Yerba mate, green (no. 37)	X			X		
Syringic acid	94	4.80	213, 264	197	[M-H] ⁻	Supposed in Hawthorn (nos. 62-64) → rebutted	X					

4. Publication 3

**Effects of Gastrointestinal Digestion on Bioactivity of Convenience
Tomato Products Studied by Ten-Dimensional Hyphenation**

Tamara Schreiner, Naila M. Eggerstorfer, Gertrud E. Morlock*

Justus Liebig University Giessen, Institute of Nutritional Science, Chair of Food Science,
Heinrich-Buff-Ring 26-32, 35392 Giessen, Germany

Submitted to

Journal of Agricultural and Food Chemistry

Received August 2022

1

2

3 **Effects of Gastrointestinal Digestion on Bioactivity of**
4 **Convenience Tomato Products Studied by**
5 **Ten-Dimensional Hyphenation**

6

7

8 *Tamara Schreiner, Naila M. Eggerstorfer, Gertrud E. Morlock**

9

10

11 Justus Liebig University Giessen, Institute of Nutritional Science, Chair of Food Science,

12

Heinrich-Buff-Ring 26-32, 35392 Giessen, Germany

13

14

15

16

17

18

19 *Corresponding author. Tel.: +49 641 9939141, fax: +49 641 9939149, E-mail address:

20 Gertrud.Morlock@uni-giessen.de (G.E. Morlock)

1

21 **Abstract**

22 Current non-target screening strategies for food focus mainly on adulterants, contaminants, or
23 migrates from packaging instead of beneficial, naturally derived, bioactive constituents. It is
24 long overdue to develop a multi-hyphenated effect-directed non-target screening strategy to
25 study bioavailability, including bioactivity and bioaccessibility in terms of digestion and
26 metabolization processes to mimic true-to-life conditions. A streamlined ten-dimensional
27 hyphenation was established employing on-surface digestion (1D), planar chromatographic
28 separation (2D), visualization using white light (3D), UV light (4D), and fluorescence light (5D),
29 effect-directed assay analysis (6D), heart-cut zone elution to an orthogonal reversed phase
30 column chromatography including online desalting (7D) with subsequent diode array detection
31 (8D), high-resolution mass-spectrometry (9D), and fragmentation (10D). As proof-of-principle,
32 nine convenience tomato products *versus* a freshly prepared one were digested by porcine
33 pancreatin and their metabolic profiles were analyzed via the ten-dimensional hyphenation.
34 The workflow showed robust and reliable results for the screening of bioactive compounds in
35 tomato products.

36 **Keywords**

37 ten-dimensional hyphenation, high-performance thin-layer chromatography, high-performance
38 liquid chromatography, high-resolution mass spectrometry, on-surface digestion, metabolic
39 activation

40 Introduction

41 Non-target screening strategies of food mostly prioritize emerging hazardous chemicals from
42 packaging materials,¹ antibiotic residues in animal products,²⁻⁴ or pesticide residues in fruits
43 and vegetables.^{5,6} The proactive screening for hazardous substances in our daily diet is
44 important to ensure food safety and consumer protection. Screening for health-promoting
45 compounds and their bioavailability is as important, since beneficial compounds also present
46 in a complex sample could mitigate hazardous effects. However, setting priority criteria, which
47 unknowns from complex matrices (as given for food or environmental samples, *etc.*) are worth
48 elucidating, remains challenging.⁷ Advantages of using multi-hyphenated strategies for non-
49 target bioactive compound screening in foods were recently described.⁸⁻¹¹ However, these
50 strategies were not hyphenated with bioavailability tools, neglecting changes in bioactivity and
51 bioaccessibility through digestion.¹²⁻¹⁴ Bioaccessibility is defined by the release of dietary
52 nutrients from the food matrix, solubilization, digestive stability, and the efficiency of absorption
53 through the gut walls.¹⁴⁻¹⁶ Bioactivity could also be influenced through metabolization, *e.g.*
54 proteolysis, split-off of sugar moiety, or hydrolysis of acylglycerols to free fatty acids (FFAs).
55 The prioritization of substances should also take into account substance activation or
56 deactivation through digestive or metabolic processes. Both hazardous and beneficially
57 bioactive compounds as well as their metabolic fate (activation/deactivation) need to be known
58 to ensure proactive consumer protection and wellness. In particular, the focus of new non-
59 target screening strategies should clearly be on digestibly stable bioactive substances from
60 the daily diet, and those getting activated by digestion/metabolization. Such prioritized
61 bioactive compounds are worth elucidating.

62 Static on-surface¹⁷ and *in vitro*^{12,15,18,19} digestion models are subdivided into oral, gastric, and
63 intestinal phase,^{17,18} trying to mimic *in vivo* digestion conditions dependent on microflora, pH,
64 and temperature¹⁶. The enzymatic composition of the intestinal fluids differs between the three
65 phases. While α -amylase is the predominant enzyme in the oral phase, it is the protease pepsin
66 for the acidic gastric phase, and proteolytic, lipolytic, and amylolytic enzymes in the intestinal

67 phase¹⁶. Since the main enzymatic activities from all three phases are united in the latter, this
68 is the most common to work with.^{13,15,18}

69 Most protocols are employing chromatographic separation,^{12,13,17,19} biochemical,^{12,13,15,17,19} or
70 biological assays¹³ after *in vitro* or on-surface metabolization to evaluate changes through
71 digestion. The separation of a complex mixture by column chromatography into many
72 substance peaks/fractions on the one hand and the determination of each bioactivity as a sum
73 parameter in 96-well plates on the other hand prohibit the direct assignment of bioactivity and
74 metabolic changes to individual substances. Moreover, the analysis time is doubled since all
75 experiments are performed twice, for non-digested samples as well as digested ones. To
76 overcome these problems, the simulated static digestion was developed on the adsorbent
77 surface and integrated into the planar chromatography workflow¹⁷, allowing side-by-side
78 comparison of non-digested and digested samples, and on-surface bioassays with direct link
79 to bioactive compounds. Expanding this workflow by a structure identification method, such as
80 tandem high-resolution mass spectrometry (HRMS/MS), a highly streamlined workflow for
81 non-target screening of bioactive compounds in complex samples was aimed.

82 In this study, a ten-dimensional (10D) hyphenation strategy for non-target screening of
83 bioactive compounds in food was developed which included the identification of changes in
84 bioactive compounds through simulated metabolic processes. Therefore, a miniaturized on-
85 surface gastrointestinal tract digestion at the nanomolar compound scale (nanoGIT) was
86 integrated into the workflow. Different normal phase high-performance thin-layer
87 chromatography (NP-HPTLC) solvent systems, reversed phase high-performance liquid
88 chromatography (RP-HPLC) gradients, and HRMS/MS acquisition methods were studied,
89 resulting in an NP-HPTLC–nanoGIT^{+active}–UV/Vis/FLD–EDA–heart cut–RP-HPLC–DAD–
90 HESI–HRMS/MS workflow. As a proof-of-concept, bioactivity profiles of nine convenience
91 tomato products *versus* a freshly prepared one were compared as raw extracts directly and
92 after pancreatic digestion. It was hypothesized that this disruptive strategy will provide a non-
93 target food screening which is more efficient, and in particular, more proactive regarding food
94 safety and consumer protection compared to the status quo.

95 **Materials and Methods**

96 **Chemicals and Materials.** Double distilled water was prepared by a Heraeus Destamat Bi-
97 18E from Thermo Fisher Scientific, Dreieich, Germany. All solvents were chromatography
98 grade, and all salts of p.a. quality unless stated otherwise. Rivastigmine ($\geq 98\%$), sodium
99 acetate ($>99\%$), peptone from casein (for microbiology), caffeine (reagent plus), imidazole
100 ($\geq 99.5\%$), acarbose ($\geq 95\%$), quercetin ($\geq 95\%$), l-ascorbic acid (reagent grade), naringenin
101 ($\geq 95\%$), myristic acid ($\geq 99\%$), palmitic acid ($>99\%$), linoleic acid (60–74%), bile extract
102 (porcine), pancreatin from porcine pancreas (8 × USP specifications), acetylcholinesterase
103 (AChE) from *Electrophorus electricus* (≥ 245 U/mg, 10 kU/vial), and α -glucosidase from
104 *Saccharomyces cerevisiae* (1,000 U/vial) were purchased from Sigma-Aldrich, Steinheim
105 Germany. Ammonium carbonate (extra pure) was delivered by Bernd Kraft, Duisburg, Germany.
106 β -Glucosidase from almonds (3040 U/mg) and 2-naphtyl- β -D-glucopyranoside (95%) were
107 provided by ABCR, Karlsruhe, Germany. Acetonitrile (ACN, $\geq 99.8\%$, Honeywell, Riedel-de
108 Haën), ammonium acetate ($\geq 99\%$), ammonium formate (LC-MS grade, $\geq 99\%$), and sodium
109 bicarbonate ($\geq 99.7\%$) were obtained from Fluka, Sigma-Aldrich, Steinheim, Germany.
110 Chlorogenic acid ($\geq 95\%$) was from Cayman Chemical, Ann Arbor, MI, USA. Bovine serum
111 albumin (BSA, fraction V, $\geq 98\%$), tris(hydroxymethyl)aminomethane (TRIS, $\geq 99.9\%$),
112 hydrochloric acid (HCl, purest, 37%), ethanol, glacial acetic acid (100%), sodium dihydrogen
113 phosphate monohydrate ($\text{NaH}_2\text{PO}_4 \cdot \text{H}_2\text{O}$, 99%), dipotassium hydrogen phosphate trihydrate
114 ($\text{K}_2\text{HPO}_4 \cdot 3 \text{H}_2\text{O}$, $\geq 99\%$), glycerol (Rotipuran, 86%), stearic acid ($>98\%$), oleic acid ($>99\%$),
115 *n*-hexane ($\geq 98\%$), calcium chloride (CaCl_2 , $\geq 98\%$), potassium dihydrogen phosphate (KH_2PO_4 ,
116 $\geq 99\%$), magnesium chloride hexahydrate ($\text{MgCl}_2 \cdot 6 \text{H}_2\text{O}$, $\geq 98\%$), and disodium hydrogen
117 phosphate (Na_2HPO_4 , $\geq 99\%$) were delivered by Carl Roth, Karlsruhe, Germany.
118 2-Naphtyl- α -D-glucopyranoside (99%) was from Fluorochem, Hadfield Derbyshire, UK. HPTLC
119 silica gel 60 F₂₅₄ MS-grade plates, magnesium sulfate heptahydrate ($\text{MgSO}_4 \cdot 7 \text{H}_2\text{O}$, 99.5%),
120 and potassium chloride (KCl, $\geq 99.5\%$) were provided by Merck, Darmstadt, Germany. Water
121 (MS grade), methanol, formic acid (99%), and sodium chloride (NaCl, $\geq 99\%$) were obtained
122 from VWR, Darmstadt, Germany. Fast Blue B salt (95%) was purchased from MP Biomedicals,

123 Eschwege, Germany. Diammonium hydrogen phosphate ($[\text{NH}_4]_2\text{HPO}_4$, $\geq 99\%$), linolenic acid
124 (99%), *n*-butanol, and diisopropyl ether ($\geq 99\%$) were delivered by Acros Organics, Morris
125 Plains, NJ, USA. Dichloromethane, ethyl acetate, and yeast extract powder (for microbiology)
126 were obtained from Th. Geyer, Renningen, Germany. The culture medium preparation for the
127 bioluminescent *Aliivibrio fischeri* bacteria (DSM-7151, German Collection of Microorganisms
128 and Cell Cultures, Berlin, Germany), is listed elsewhere.²⁰ The solvent toluene ($\geq 99.8\%$) was
129 provided by Fisher Scientific, Schwerte, Germany. Butyrylcholinesterase (BChE, ≥ 245 U/mg)
130 from equine serum was purchased from SERVA, Heidelberg, Germany, and its substrate
131 1-naphthyl acetate ($\geq 98\%$) from AppliChem, Darmstadt, Germany.

132 **Preparation of Standard Mixture, Positive Control and Simulated Intestinal Fluid.** Stock
133 solutions (10 mg/mL) of the FFAs myristic (C14:0), palmitic (C16:0), stearic (C18:0), oleic
134 (C18:1), linoleic (C18:2), and linolenic (C18:3) acid were prepared in *n*-hexane. The secondary
135 plant metabolites quercetin, naringenin, ascorbic acid, and chlorogenic acid were prepared
136 each as 1-mg/mL stock solution in methanol. A standard mixture was obtained by diluting
137 100 μL of each FFA, and 1 mL of each secondary plant metabolite stock solution in a 10-mL
138 volumetric flask which was filled with methanol to the mark. The final concentration was
139 100 $\mu\text{g/mL}$ for each substance. As positive control (PC) solution for intestinal digestion,
140 rapeseed oil was diluted in *n*-hexane (1 mg/mL). The preparation of the simulated intestinal
141 fluid (SIF),¹⁶ pancreatin solution (panc, 20 mU/ μL in SIF)¹⁶ containing bile extract,¹⁷ and CaCl_2
142 (6 pmol/ μL) solution¹⁷ were described elsewhere.

143 **Preparation of Tomato Samples.** Nine different convenience tomato products were prepared
144 according to each manufacturer's instruction, and a further tenth sample (fresh tomato soup)
145 was self-prepared (Table S1). Each sample (5 g) was mixed with 5 mL *n*-butanol, vortexed for
146 10 min, and ultrasonicated (Sonores Digiplus, Bandelin, Berlin, Germany) for 15 min. After
147 centrifugation at $3,000 \times g$ for 5 min (Labofuge 400, Heraeus, Hanau, Germany), supernatants
148 were filtered through a 0.45 μm cellulose acetate filter (VWR, Darmstadt, Germany), and
149 transferred into autosampler vials.

150 **NP-HPTLC–nanoGIT^{active}–UV/Vis/FLD–EDA Workflow.** For studying HPLC gradients and
151 MS acquisition methods, the standard mixture was applied 40-fold, each as
152 4 mm × 2 mm-area (500 ng/area) on one HPTLC plate silica gel 60 F₂₅₄ MS-grade (Automatic
153 TLC Sampler 4 controlled by Freemod Option of winCATS software version 1.4.7.2018,
154 CAMAG, Muttenz, Switzerland). For the final method, *n*-butanol extracts were applied twice as
155 6-mm bands (5 µL/band) on pre-washed⁸ HPTLC plates silica gel 60 F₂₅₄ MS-grade. The PC
156 solution (5 µL/band) was co-applied. Then, one sample track each and the PC were
157 oversprayed according to the on-surface protocol¹⁷ with the bile-extract-containing panc
158 solution (5 µL) and with CaCl₂ solution (1 µL). Additionally, one track containing only panc and
159 CaCl₂ was applied as negative control (NC). The top 8 cm of the plate were covered with a
160 second plate (layer faced upwards), so that exclusively the application zone was wetted by
161 piezoelectrical spraying of a 0.1 M sodium chloride solution (Derivatizer; 1.25 mL, yellow
162 nozzle, level 6). Both plates²¹ were transferred in a moistened polypropylene box
163 (26.5 cm × 16 cm × 10 cm, KIS, ABM, Wolframs-Eschenbach, Germany) with filter-paper
164 lining and incubated for 1 h at 37 °C in an oven (Memmert, Schwabach, Germany). The cover
165 plate remains on the sample plate during incubation to prevent the first two centimeters from
166 running dry through the hygroscopic activity of the dry covered silica gel. After incubation, the
167 plate was dried for 4 min in a stream of cold air. Plates were developed with *n*-hexane –
168 dichloromethane – methanol – water (40:50:10:1, V/V/V/V) up to 70 mm (further studied mobile
169 phases as in Table S2 and Figure S1) in a twin trough chamber (20 cm × 10 cm, CAMAG) and
170 documented under white light illumination (Vis), UV 254 nm, and FLD 366 nm (TLC Visualizer
171 3, CAMAG). HPTLC instruments were controlled by visionCATS software
172 (version 3.1.21109.3, CAMAG). Subsequently, effect-directed analysis (EDA) with *A. fischeri*
173 bioassay as well as α-/β-glucosidase and AChE/BChE enzyme inhibition assays was
174 performed as described.⁸

175 **Heart cut–RP-HPLC–DAD–HESI-HRMS/MS.** Bioactive zones were heart-cut eluted from the
176 HPTLC plate using a fully automated autoTLC-MS interface^{22,23} with an oval elution head

177 (4 mm × 2 mm). An HPLC standalone pump (MX010PFT, Teledyne SSI, State College, PA,
178 USA) provided the eluent water – methanol (9:1, V/V) at a flow rate of 0.1 mL/min. Elution time
179 was set to 60 s, including 20 s safety time. The elution head was rinsed for 1 min at
180 half-gradient time, when the autoTLC-MS interface was isolated from the working system.
181 Analytes were transferred through a biocompatible inline filter (IDEX Health & Science,
182 Rohnert Park, CA, USA) to a two-position six-port switching valve (MXT series, PD715-000,
183 Rheodyne, IDEX) with an installed 50- μ L sample loop and desalting cartridge (Accucore RP-
184 MS, 10 mm × 2.1 mm, 2.6 μ m, Thermo Fisher Scientific).⁹ Analytes were trapped on the
185 cartridge within the first 40 s elution time, until the valve was switched, and the 12-min HPLC
186 gradient transferred the analytes with a flow rate of 0.4 mL/min to the main column (Accucore
187 RP-MS 100 mm × 2.1 mm, 2.6 μ m, thermostated at 40 °C, Thermo Fisher Scientific). The
188 gradient consisted of eluent A (water with 2.5 mM ammonium acetate, pH adjusted to 4.5 with
189 acetic acid), and eluent B (methanol). Starting conditions were 2% B for 2 min (elution), which
190 were increased to 100% B (2–7 min), and held for 3 min (7–10 min), followed by 2 min
191 equilibration time (gradient optimizations in Figure S2). The Dionex Ultimate HPLC system
192 (Dionex Softron, Germering, Germany) used was equipped with a binary pump (HPG-
193 3200SD), an autosampler (WPS-3000TXRS), a column oven (TCC-3000RS), and a diode
194 array detector (DAD-3000RS), connected to a Q Exactive Plus Hybrid Quadrupole-Orbitrap
195 mass spectrometer, with an Ion-Max HESI-II probe (both Thermo Fisher Scientific). Detection
196 was performed with DAD (wavelength scan 200–400 nm and at specific wavelengths of
197 240 nm, 280 nm, and 320 nm) and HRMS/MS in polarity switching full-scan data-dependent
198 MS2 (ddMS2) mode. Ionization settings were equal for all MS acquisition methods: sheath gas
199 20 AU, aux gas 10 AU, spray voltage 3.5 kV, capillary temperature 320 °C, probe heater
200 temperature 350 °C, S-lens RF level 50 AU. The settings for full scan were a mass range of
201 m/z 100–1100, resolving power of 70,000 (at m/z 200, full width at half-maximum, FWHM),
202 and automatic gain control (AGC) target 3e6. Fragmentation scans followed in Top5 ddMS2
203 acquisition mode at a mass range of m/z 80–1000, resolution of 17,500 FWHM, AGC target
204 1e6, and stepped normalized collision energy of 20, 40, and 60 eV (further MS acquisition

205 methods in Figure S3). The mass spectrometer was calibrated daily with Pierce TM LTQ Velos
206 ESI positive/negative ion calibration solution (Thermo Fisher Scientific). The instrument was
207 controlled and spectra were recorded with Xcalibur 4.2.47 with Foundation 3.1.261.0 and SII
208 for Xcalibur 1.5.0.10747 (Thermo Fisher Scientific).

209 **Results and Discussion**

210 The recently developed nano-molar NP-HPTLC–nanoGIT^{+active} system¹⁷ and the latest eight-
211 dimensional (8D) hyphenation⁹ were combined to an overall 10D hyphenation and adapted to
212 a high-resolution tandem mass spectrometer (Figure 1), *i.e.* NP-HPTLC–nanoGIT^{+active}–
213 UV/Vis/FLD–EDA–heart cut–RP-HPLC–DAD–HESI–HRMS/MS. As first dimension (1D), the
214 on-surface digestion of tomato samples with pancreatic enzymes simulated the human
215 gastrointestinal tract metabolism (nanoGIT). Separating side-by-side digested *versus* non-
216 digested raw extract samples via NP-HPTLC represented the second dimension (2D).
217 Detection at white light illumination (3D), UV 254 nm (4D), and fluorescence detection FLD
218 366 nm (5D) gave information about chromophores, UV-absorbing, and natively fluorescing
219 molecules, respectively. To prioritize compounds among the hundreds or thousands of
220 unknown compounds in a complex food sample, an effect-directed assay (EDA, ^{+active}) was
221 included as sixth dimension (6D). Zones showing bioactivity were heart-cut eluted to an
222 orthogonal RP-HPLC column (7D) and further characterized with DAD (8D) and HRMS/MS
223 (9D/10D). The resulting 10D hyphenation focused on unknown bioactive compounds which
224 were influenced by simulated human gastrointestinal digestion. The performance, versatility,
225 and robustness of the workflow were examined by nine convenience tomato products in
226 comparison to a freshly prepared one and by using one antibacterial bioassay and four enzyme
227 inhibiting assays.

228 **Mobile Phase Development for NP-HPTLC–nanoGIT^{+active}–UV/Vis/FLD–EDA.** As a broad
229 compound spectrum in a wide polarity range was expected in the *n*-butanol extracts of the
230 tomato products, different mobile phases (Table S2 and Figure S1) were tested to detect a

231 difference between digested *versus* non-digested raw extract samples. The pancreatic enzyme
232 mixture contained three classes of enzymes, *i.e.* lipases, amylases, and peptidases.
233 Therefore, mobile phase development focused on cleavage products of those enzymes.
234 Although apolar solvents, such as *n*-hexane, ethyl acetate, and toluene, were considered basic
235 solvents, others were added for selectivity and band sharpness improvement, *e.g.*
236 dichloromethane, methanol, water, and organic acids (Table S2). The resulting bioautograms
237 were exemplarily compiled for tomato product sample 8 detected via the *A. fischeri* bioassay
238 (Figure S1). The mobile phase *n*-hexane – dichloromethane – methanol – water (40:50:10:1
239 V/V/V/V; Table S2, no. 16) was the best choice to separate both the polar and mid polar
240 components at lower hR_F values as well as the apolar substances in the upper part of the
241 chromatogram. As almost 90% of the selected mobile phase consisted of highly volatile
242 organic solvent, it was inevitable to run the chromatography in a tightly closed twin trough
243 chamber.

244 **Method Development for Automated Non-Target RP-HPLC–HESI-HRMS/MS.** By
245 extending the latest 8D hyphenation to a 10D hyphenation, instrumentation had to be changed
246 from an ultra-performance HPLC⁹ to a standard-pressure HPLC. Adapting the column gradient
247 to an instrument that can sustain less pressure, was challenging. The used Dionex system has
248 an upper pressure limit of only 62 MPa (620 bar), and in addition, the backpressure from the
249 HESI probe was higher than for the previously employed Waters probe.⁹ To prevent the
250 instrumentation from working on its limit, the gradient was adjusted to the given circumstances
251 (Figure S2). The applied standard mixture was heart-cut eluted with water – methanol (9:1 V/V)
252 to RP-HPLC–DAD–HESI-HRMS/MS. The eluents (A: 2.5 mM ammonium acetate adjusted to
253 pH 4.5 with acetic acid; B: methanol) remained the same. The gradient program of the
254 8D-hyphenation⁹ was first tested at half of the flow rate. As a result, the peak shapes were not
255 satisfactory, adjacent peaks were not baseline-separated, and FFAs did not elute at all from
256 the RP column (Figure S2A). Thus, the organic gradient portion was raised to 100%, and the
257 duration was shortened to 10 min, however, baseline separation and the elution of the most

258 apolar stearic acid (C18:0) were not satisfactory (Figure S2B). A less steep increase in organic
259 solvent (Figure S2C), a longer time holding at 100% B, and a higher flow rate of 0.4 mL/min
260 (Figure S2D) completed the gradient optimization.

261 To evaluate the best non-target acquisition settings for hybrid Q-Orbitrap, all ion fragmentation
262 (AIF) and ddMS2 fragmentation were employed in polarity switching mode and compared with
263 multiplexed and variable data-independent acquisitions (m/vDIA) in single polarity mode. A
264 detailed description of the parameters set in the different acquisition modes is summarized
265 (Figure S3). Full scan extracted ion chromatograms (XIC) and corresponding MS2 scan events
266 at higher-energy collisional dissociation, HCD 40.00) are exemplarily shown for the flavonoid
267 naringenin (m/z 271.0614, $[M-H]^-$) in Figure 2. A drawback of AIF acquisition (Figure 2A) is
268 that no precursor molecule is selected for fragmentation and all ions were transferred to the
269 collision cell at the same time resulting in high background ion interference.³ Furthermore, the
270 assignment of fragments to a precursor cannot be made unambiguously for several analytes
271 eluting at the same time. The shown XIC MS2 chromatogram at m/z 119.0503 ($C_6H_7O^-$) is
272 based on a known fragment of naringenin, which also illustrates the lack of potential as a non-
273 target screening acquisition method. In contrast, data-dependent analysis (Figure 2B)
274 obliterated all disadvantages mentioned for AIF. For non-target data acquisition, no inclusion
275 list is available to determine the precursors for fragmentation.³ Hence, the used Top5 ddMS2
276 method, isolated the five most abundant precursors in each full scan event and transferred
277 them to the collision cell. These settings entailed advantages and disadvantages at the same
278 time. Fragments could be assigned to a precursor and fragmentation spectra are almost
279 interference-free. Still, the method is limited to only five precursors which could be fragmented
280 at the same time, neglecting low abundant ones. Further, the low MS2 scan rate (only four
281 fragmentation scans, Figure 2B) was additionally minimized by polarity switching, which is,
282 however, indispensable for non-target analysis. In contrast, DIA methods are suitable for
283 non-target data acquisition, but cycle time is the limiting factor disabling polarity switching.^{5,24}
284 The missing opportunity for polarity switching in both DIA acquisition methods Figure 2C and
285 D) is therefore their main drawback. Compared to AIF, smaller m/z ranges (isolation window,

286 Figure S3) were isolated by the quadrupole and guided to the fragmentation cell. A complete
287 scan cycle consisted therefore of a full scan followed by the DIA m/z windows which were
288 worked off in sequence.^{3,4,24} The smaller the isolation windows, the longer the cycle time. In
289 mDIA methods, the isolation window is fixed for a certain mass range, but several m/z ranges
290 could be simultaneously fragmented and analyzed by multiplexing (Figure S3, MSX ID 9, m/z
291 500.00000–550.00000, and 550.00000–600.00000). Since the bioactive compounds in the
292 tomato products were expected to be small molecules of low molecular weight, the higher m/z
293 ranges were multiplexed, and the lower m/z ranges were left singly to provide interference-free
294 MS2 spectra. In contrast, multiple isolation windows were selected in vDIA acquisition mode,
295 in which the isolation windows for higher m/z values were set wider than for lower m/z for the
296 same reasons mentioned above. Since DIA lacks polarity switching and acquisition is always
297 a decision between resolution and scan speed as well as width of isolation windows and
298 number of MS2 scan events,²⁴ it was discarded as a non-target screening acquisition method.
299 Since AIF acquisition is too impurity-prone and non-selective, it was also discarded as an
300 option. Hence, a ddMS2 acquisition method was selected for automated non-target RP HPLC–
301 HESI HRMS/MS analysis of the eluted zones.

302 **NP-HPTLC–nanoGIT^{+active}–UV/Vis/FLD–EDA–heart cut–RP-HPLC–DAD–HESI-HRMS/MS**

303 **Non-Target Screening Results.** One set of the tomato product extracts was used directly,
304 whereas the other set was metabolized by simulated static pancreatic digestion (1D). After
305 their separation (2D), their UV/Vis/FLD chromatograms (3D–5D) showed only a few zones
306 (Figure S4). For the bioactivity detection (6D), the *A. fischeri* bioassay (Figure 3A) was selected
307 due to its simplicity and more universal detectability. Glucosidase (Figure 3B/C) and
308 cholinesterase (Figure 3D/E) inhibition assays were employed to focus on the relationship
309 between the diet and mainstream civilization diseases, e.g., diabetes type II and Alzheimer's.⁸
310 After bioactivity screening, the most prominent zones I–IX (Figure 3) were heart-cut eluted and
311 analyzed via RP-HPLC–DAD–HESI-HRMS/MS (7D–10D).

312 Comparing the bioactive profiles of non-digested (-) and digested (+) raw extracts of
313 convenience tomato product samples 1–9 (Figure 3) only slight differences were detectable
314 due to the same main ingredient (tomatoes). Zone I (hR_F 99±1) exhibited bioactivity through
315 all assays but did not show any significant HRMS signals. Presumably, lipids, e.g.
316 triacylglycerols (TAGs), from vegetable oils were chromatographed to the solvent front.
317 Missing lipid signals in HRMS/MS were explained by their high apolar properties, which
318 prohibited them to elute from the plate with 90% water. It was assumed, that zone I is partially
319 metabolized by the pancreatic enzymes. Sample 5 (Figure 3B) illustrated this hypothesis.
320 While in the non-digested raw extract 5 (-), zone I (hR_F 99±1) is very intensive, the
321 α -glucosidase inhibition capacity was weakened in the digested sample 5 (+). In contrast,
322 zone IV (Figure 3, hR_F 55–80, depending on plate activity) significantly increased through
323 digestion. This intensification was detected through all assays, suggesting products of
324 metabolization. The recording of HRMS signals revealed a whole pattern of FFAs with chain
325 lengths from C12–C18 (Table 1) as possible degradation products of the TAGs cleavage via
326 the pancreatic lipases. Myristic, palmitic, stearic, oleic, linoleic, and linolenic acid were not
327 separated by NP-HPTLC, but by the orthogonal RP-HPLC. A remarkable difference comparing
328 convenience products with the self-made tomato soup is the comparatively very low content
329 of FFA in the non-digested raw extract of the self-made tomato soup. The freshly prepared
330 food contained fewer FFA degradation products which indicated a good quality and edibility of
331 oils.²⁵

332 The importance of the second orthogonal chromatography was once more highlighted by the
333 following example. At hR_F 81±1 in samples 1–4, 7, 9, and 10, in both digested and non-
334 digested samples, the two antibacterial zones II and III were observed in the *A. fischeri*
335 bioautogram (Figure 3A). In the self-made tomato soup (sample 10) the antibacterial response
336 of zone II is unequivocally affiliated with piperine (Table 1), the main alkaloid in black pepper.²⁶
337 In conclusion, being at a similar migration distance, zone III in sample 7 could also contain
338 piperine (regardless of a slightly different zone shape). But the ingredients list (Table S1)
339 neither showed pepper, spices, nor any declaration indicating the alkaloid. Instead, the two

340 herbicides dinoseb and dinoterb were found in zone **II** (Table 1, Figure 4). According to
341 European Commission Regulation EU 2015/868²⁷ maximum residue levels (MRL) for the
342 herbicides are 0.02 mg/kg each in fruiting vegetables (tomatoes), berries and small fruits (wine
343 grapes), and bulb vegetables (onion and garlic). All these ingredients were present in sample
344 7. Since the *A. fischeri* bioassay and the HRMS/MS analysis are very sensitive, even traces of
345 dinoseb and dinoterb can be found in the sample because authorized herbicides are normally
346 highly active and potent. The bioactive zone at hR_F 81±1 of samples 1–4, all containing pepper
347 or seasoning, was caused by piperine and assigned as zone **II**. Neither the alkaloid nor the
348 herbicides are influenced by the on-surface intestinal digestion.

349 In the *A. fischeri* bioautogram (Figure 3A), an extra zone **V** (hR_F 49±1) was visible after
350 digestion, exclusively for samples 8 and 9. Short-chain FFAs, such as capric (C10:0) and lauric
351 (C12:0) acid were found in this zone (Figure 3A, Table 1) formed by enzymatic digestion of
352 TAGs of animal origin.²⁸ Comparing the ingredients lists (Table S1), samples 5, 8, and 9
353 contained cream and skim milk powder as sources of animal fat, which explained the findings.
354 In sample 5, the skim milk powder was added in a lower quantity explained by the higher
355 tomato content (89% tomatoes *versus* only 48% and 56% in samples 8 and 9, respectively).

356 Zones **VI** and **VII** (both hR_F 28±1, Figure 3A/C/D) revealed several signals, but could not be
357 assigned to any ingredient listed. Calculated molecular formulas $C_{15}H_{26}O_5$, $C_{12}H_{22}O_5$,
358 $C_{14}H_{25}O_5$, and $C_{13}H_{26}O_6$ (Table 1) indicated partially oxidized mono- or diacylglycerols. This
359 was plausible as mono- and diacylglycerols are used as emulsifying agents in convenience
360 tomato products. This assumption was also supported by the presence of these zones in the
361 digested rapeseed oil (PC, hR_F 28) as well as their increase in the digested samples and their
362 absence in the self-made freshly prepared tomato product. Recently, especially the
363 monoacylglycerols were proven to act antibacterial against *A. fischeri*.²⁹

364 The flavonoid naringenin caused the antibacterial effect of zone **VIII** (hR_F 18±1) in the *A.*
365 *fischeri* bioautogram (Figure 3A, Table 1). The bacterial inhibition response was pronounced
366 for samples 1, 3, 4, 6–9, weak for samples 2 and 5, and absent for sample 10. The flavonoid
367 content in tomatoes is dependent on the stage of maturation. Ripe tomato fruits have a high

368 amount of flavonoids accumulated in the peel.^{30,31} Since the tomatoes were peeled for the
369 self-made soup, it was expected that no naringenin was found in sample 10.

370 The β -glucosidase inhibiting zone **IX** (hR_F 0, Figure 3C, Table 1) was assigned to tuberonic
371 acid glucoside,³² and rutin.³¹ Due to the amylolytic activity of pancreatin, these two analytes
372 are expected to be metabolized to their aglycons tuberonic acid and quercetin.

373 **Elucidated structures in health-promoting context.** The new hyphenated strategy
374 successfully provided an efficient and straightforward non-target food screening, exemplarily
375 shown for tomato products. Due to the detection of biological effects and prioritization of
376 important bioactive compounds, it was more proactive regarding food safety and consumer
377 protection compared to the analytical status quo. As the sample amount applied was the same
378 for all assays, the bioactive responses can directly be compared. All studied tomato samples
379 showed a similar bioprofile due to the same main ingredient (tomatoes) and possessed
380 health-promoting constituents with the potential to prevent or at least curtail civilization
381 diseases such as Alzheimer's or diabetes type II. Most striking were the antibacterial, then
382 α -glucosidase, and then BChE inhibition activities among the five different activity mechanisms
383 studied. The effects were observed for an extracted 5-g sample portion taken out of a 250-g
384 meal and considered to be meaningful since the 50-fold effect response has to be imagined to
385 be taken up with a meal. In terms of bioactivity and health benefits, the quality of the
386 convenience tomato products 1–9 can compete, especially after intestinal digestion, with the
387 self-made tomato soup sample 10, which is commonly supposed to be the healthier alternative.
388 The most pronounced and most versatile effects were observed for the FFAs (zone **IV**). This
389 effect substantially increased after the simulated intestinal digestion. The self-made tomato
390 soup sample 10 showed *ab initio* the lowest content of FFAs since it was freshly prepared, but
391 after the simulated intestinal digestion, it was similar in the effect responses to the convenience
392 products. FFAs are known to influence health and disease status of humans. Particularly the
393 antibacterial effect against both Gram-negative and Gram-positive bacteria was
394 emphasized.^{33–35} Despite various ways of acting against pathogens,^{33,35} FFAs support to

395 balance the gut microbiota.³⁶ The cholinesterase inhibition capacities of myristic, oleic,
396 palmitic, and stearic acid were already proved against standards.³⁷ In context with Alzheimer's
397 disease, the inhibition of acetylcholine breakdown via AChE and BChE is one therapeutic
398 option to slow down symptoms.³⁸

399 Piperine (zone II) and the two co-eluting dinitrophenol herbicides dinoseb and dinoterb
400 (zone III) were also prominent in their antibacterial activity against the *A. fischeri* bacteria. Only
401 piperine has been reported so far to act against human pathogens³⁹. The piperine, almost
402 100% absorbed, does not undergo metabolic alterations⁴⁰, which is consistent with our results.
403 Also the herbicides were not influenced by the on-surface intestinal digestion and thus can
404 stay active inside our body. The cellular uptake of herbicides is dependent on the gut
405 microbiota composition, whereby the intestinal absorption of pesticides decreased in presence
406 of microbiota.⁴¹

407 Further, the health-promoting effects of naringenin (zone VIII) are well reported including
408 antidiabetic effects.⁴² The antimicrobial properties of the flavonoid were studied against several
409 model organisms⁴³, but not explicitly *A. fischeri*. The partially oxidized mono- or diacylglycerols
410 (zones VI/VII), but also the FFAs (zone IV), should be tested for the presence of epoxidized
411 forms in future since healthy oils rich in unsaturated fatty acids were recently found to be
412 genotoxic.⁴⁴

413

414 **Abbreviations used**

415 AChE – acetylcholinesterase, AGC – automatic gain control, AIF – all ion fragmentation, BChE –
416 butyrylcholinesterase, DAD – diode array detector, ddMS2 – data-dependent MS2, EDA –
417 effect-directed analysis, FFA – free fatty acids, FLD – fluorescence light detection, FWHM – full
418 width at half maximum, GIT – gastrointestinal tract, HCD – high-energy collisional dissociation,
419 HESI – heated electrospray ionization, HPLC – high-performance liquid chromatography, HPTLC
420 – high-performance thin-layer chromatography, HRMS/MS – high-resolution tandem mass
421 spectrometry, mDIA – multiplexed data-independent acquisition, MSX – multiplexing mode, NC –
422 negative control, NCE – normalized collision energy, NP – normal phase, PC – positive control,

16

423 RP – reversed phase, SIF – simulated intestinal fluid, SIM – single ion monitoring, TAG –
424 triacylglyceride, TIC – total ion count, vDIA – variable data-independent acquisition

425 **Supporting information**

426 The Supporting Information is available free of charge at ...

427 Sample list, investigation of HPTLC mobile phases, investigation of HPLC gradient, detailed
428 overview of MS2 acquisition methods, NP-HPTLC–nanoGIT^{active}–UV/Vis/FLD profiles

429 **Author contributions**

430 **Tamara Schreiner:** Conceptualization, Methodology, Investigation, Data Analysis, Writing –
431 Original Draft. **Naila M. Eggerstorfer:** Investigation. **Gertrud E. Morlock:** Conceptualization,
432 Methodology, Supervision, Writing – Review and Editing.

433 **Notes**

434 The authors declare no competing financial interest.

435 **Acknowledgments**

436 Thank is owed to Merck, Darmstadt for supply of plates. Instrumentation was partially funded
437 by the *Deutsche Forschungsgemeinschaft* (DFG, German Research Foundation) – INST
438 162/536-1 FUGG and INST 162/471-1 FUGG.

439 **References**

- 440 (1) Rusko, J.; Perkons, I.; Rasinger, J. D.; Bartkevics, V. Non-target and suspected-target
441 screening for potentially hazardous chemicals in food contact materials: investigation of paper
442 straws, *Food Addit. Contam.* **2020**, *37*, pp. 649–664.
- 443 (2) Mehl, A.; Schmidt, L. J.; Schmidt, L.; Morlock, G. E. High-throughput planar solid-phase
444 extraction coupled to orbitrap high-resolution mass spectrometry via the autoTLC-MS interface
445 for screening of 66 multi-class antibiotic residues in food of animal origin, *Food Chem.* **2021**,
446 *351*, p. 129211.
- 447 (3) Jia, W.; Shi, L.; Chu, X. Untargeted screening of sulfonamides and their metabolites in
448 salmon using liquid chromatography coupled to quadrupole Orbitrap mass spectrometry, *Food*
449 *Chem.* **2018**, *239*, pp. 427–433.
- 450 (4) Jia, W.; Shi, L.; Chu, X.; Chang, J.; Chen, Y.; Zhang, F. A strategy for untargeted screening
451 of macrolides and metabolites in bass by liquid chromatography coupled to quadrupole orbitrap
452 mass spectrometry, *Food Chem.* **2018**, *262*, pp. 110–117.
- 453 (5) Wang, J.; Chow, W.; Wong, J. W.; Leung, D.; Chang, J.; Li, M. Non-target data acquisition
454 for target analysis (nDATA) of 845 pesticide residues in fruits and vegetables using
455 UHPLC/ESI Q-Orbitrap, *Anal Bioanal Chem.* **2019**, *411*, pp. 1421–1431.
- 456 (6) García-Reyes, J. F.; Hernando, M. D.; Molina-Díaz, A.; Fernández-Alba, A. R.
457 Comprehensive screening of target, non-target and unknown pesticides in food by LC-TOF-
458 MS, *TrAC, Trends Anal. Chem.* **2007**, *26*, pp. 828–841.
- 459 (7) González-Gaya, B.; Lopez-Herguedas, N.; Bilbao, D.; Mijangos, L.; Iker, A. M.; Etxebarria,
460 N.; Irazola, M.; Prieto, A.; Olivares, M.; Zuloaga, O. Suspect and non-target screening: the last
461 frontier in environmental analysis, *Anal. Methods.* **2021**, *13*, pp. 1876–1904.
- 462 (8) Schreiner, T.; Sauter, D.; Friz, M.; Heil, J.; Morlock, G. E. Is Our Natural Food Our
463 Homeostasis? Array of a Thousand Effect-Directed Profiles of 68 Herbs and Spices, *Front.*
464 *Pharmacol.* **2021**, *12*, p. 3310.

- 465 (9) Schreiner, T.; Morlock, G. E. Non-target bioanalytical eight-dimensional hyphenation
466 including bioassay, heart-cut trapping, online desalting, orthogonal separations and mass
467 spectrometry, *J Chromatogr A*. **2021**, *1647*, p. 462154.
- 468 (10) Caesar, L. K.; Kellogg, J. J.; Kvalheim, O. M.; Cech, N. B. Opportunities and Limitations
469 for Untargeted Mass Spectrometry Metabolomics to Identify Biologically Active Constituents in
470 Complex Natural Product Mixtures, *J. Nat. Prod.* **2019**, *82*, pp. 469–484.
- 471 (11) Kongstad, K. T.; Özdemir, C.; Barzak, A.; Wubshet, S. G.; Staerk, D. Combined use of
472 high-resolution α -glucosidase inhibition profiling and high-performance liquid chromatography-
473 high-resolution mass spectrometry-solid-phase extraction-nuclear magnetic resonance
474 spectroscopy for investigation of antidiabetic principles in crude plant extracts, *J Agric Food*
475 *Chem.* **2015**, *63*, pp. 2257–2263.
- 476 (12) Liu, X.; Shi, J.; Yi, J.; Zhang, X.; Ma, Q.; Cai, S. The effect of in vitro simulated
477 gastrointestinal digestion on phenolic bioaccessibility and bioactivities of *Prinsepia utilis* Royle
478 fruits, *LWT - Food Sci. Technol.* **2021**, *138*, p. 110782.
- 479 (13) Correa-Betanzo, J.; Allen-Vercoe, E.; McDonald, J.; Schroeter, K.; Corredig, M.; Paliyath,
480 G. Stability and biological activity of wild blueberry (*Vaccinium angustifolium*) polyphenols
481 during simulated in vitro gastrointestinal digestion, *Food Chem.* **2014**, *165*, pp. 522–531.
- 482 (14) Dima, C.; Assadpour, E.; Dima, S.; Jafari, S. M. Bioavailability and bioaccessibility of food
483 bioactive compounds; overview and assessment by in vitro methods, *Compr. Rev. Food Sci.*
484 *Food Saf.* **2020**, *19*, pp. 2862–2884.
- 485 (15) Ketnawa, S.; Suwannachot, J.; Ogawa, Y. In vitro gastrointestinal digestion of crisphead
486 lettuce: Changes in bioactive compounds and antioxidant potential, *Food Chem.* **2020**, *311*,
487 p. 125885.
- 488 (16) Minekus, M.; Alming, M.; Alvito, P.; Ballance, S.; Bohn, T.; Bourlieu, C.; Carrière, F.;
489 Boutrou, R.; Corredig, M.; Dupont, D.; Dufour, C.; Egger, L.; Golding, M.; Karakaya, S.;
490 Kirkhus, B.; Le Feunteun, S.; Lesmes, U.; Macierzanka, A.; Mackie, A.; Marze, S.;
491 McClements, D. J.; Ménard, O.; Recio, I.; Santos, C. N.; Singh, R. P.; Vegarud, G. E.;

- 492 Wickham, M. S. J.; Weitschies, W.; Brodkorb, A. A standardised static in vitro digestion method
493 suitable for food - an international consensus, *Food Funct.* **2014**, *5*, pp. 1113–1124.
- 494 (17) Morlock, G. E.; Drotleff, L.; Brinkmann, S. Miniaturized all-in-one nanoGIT+active system
495 for on-surface metabolization, separation and effect imaging, *Anal. Chim. Acta.* **2021**, *1154*,
496 p. 338307.
- 497 (18) Sollano-Mendieta, X. C.; Meza-Márquez, O. G.; Osorio-Revilla, G.; Téllez-Medina, D. I.
498 Effect of In Vitro Digestion on the Antioxidant Compounds and Antioxidant Capacity of 12 Plum
499 (*Spondias purpurea* L.) Ecotypes, *Foods.* **2021**, *10*.
- 500 (19) Rodríguez-Roque, M. J.; Rojas-Graü, M. A.; Elez-Martínez, P.; Martín-Belloso, O. Soymilk
501 phenolic compounds, isoflavones and antioxidant activity as affected by in vitro gastrointestinal
502 digestion, *Food Chem.* **2013**, *136*, pp. 206–212.
- 503 (20) European Committee for Standardization (2009) Water Quality - Determination of the
504 Inhibitory Effect of Water Samples on the Light Emission of *Vibrio Fischeri* (Luminescent
505 Bacteria Test). Part 1: Method Using Freshly Prepared Bacteria.
- 506 (21) Müller, I.; Morlock, G. E. Validation and quantification of the saccharide release of
507 hydrothermally treated flours after salivary and pancreatic amylolysis by the HPTLC
508 nanoGIT^{+active} method, *in submission*.
- 509 (22) Häbe, T. T.; Morlock, G. E. Open-source add-on kit for automation of zone elution in planar
510 chromatography, *Rapid Commun. Mass Spectrom.* **2020**, *34*, e8631.
- 511 (23) Mehl, A.; Schwack, W.; Morlock, G. E. On-surface autosampling for liquid
512 chromatography-mass spectrometry, *J. Chromatogr. A.* **2021**, *1651*, p. 462334.
- 513 (24) Wu, I.-L.; Turnipseed, S. B.; Storey, J. M.; Andersen, W. C.; Madson, M. R. Comparison
514 of data acquisition modes with Orbitrap high-resolution mass spectrometry for targeted and
515 non-targeted residue screening in aquacultured eel, *Rapid Commun. Mass Spectrom.* **2020**,
516 *34*, e8642.

- 517 (25) Chew, S. C.; Nyam, K. L. Refining of edible oils. In *Lipids and edible oils. Properties,*
518 *processing and applications*; Galanakis, C. M., Ed.; Academic Press, an imprint of Elsevier:
519 London, 2020, pp. 213–241.
- 520 (26) Liu, J.; Bi, Y.; Luo, R.; Wu, X. Simultaneous UFLC-ESI-MS/MS determination of piperine
521 and piperlonguminine in rat plasma after oral administration of alkaloids from *Piper longum* L.:
522 application to pharmacokinetic studies in rats, *Journal of chromatography. B, Analytical*
523 *technologies in the biomedical and life sciences*. **2011**, *879*, pp. 2885–2890.
- 524 (27) European Commission (2015) Commission Regulation (EU) 2015/868 of 26 May 2015
525 amending Annexes II, III and V to Regulation (EC) No 396/2005 of the European Parliament
526 and of the Council as regards maximum residue levels for 2,4,5-T, barban, binapacryl,
527 bromophos-ethyl, camphechlor (toxaphene), chlorbufam, chloroxuron, chlozolate, DNOC, di-
528 allate, dinoseb, dinoterb, dioxathion, ethylene oxide, fentin acetate, fentin hydroxide,
529 flucycloxuron, flucythrinate, formothion, mecarbam, methacrifos, monolinuron, phenothrin,
530 propham, pyrazophos, quinalphos, resmethrin, tecnazene and vinclozolin in or on certain
531 products.
- 532 (28) Gallier, S.; Cui, J.; Olson, T. D.; Rutherford, S. M.; Ye, A.; Moughan, P. J.; Singh, H. In
533 vivo digestion of bovine milk fat globules: effect of processing and interfacial structural
534 changes. I. Gastric digestion, *Food Chem*. **2013**, *141*, pp. 3273–3281.
- 535 (29) Schreiner, T.; Eggerstorfer, N. M.; Morlock, G. E. Effects of gastrointestinal digestion on
536 bioactivity of meal replacement products studied by ten-dimensional hyphenation, *in revision*.
537 **2022**.
- 538 (30) Chaudhary, P.; Sharma, A.; Singh, B.; Nagpal, A. K. Bioactivities of phytochemicals
539 present in tomato, *J. Food Sci. Technol*. **2018**, *55*, pp. 2833–2849.
- 540 (31) Martí, R.; Roselló, S.; Cebolla-Cornejo, J. Tomato as a Source of Carotenoids and
541 Polyphenols Targeted to Cancer Prevention, *Cancers*. **2016**, *8*.
- 542 (32) van Meulebroek, L.; Bussche, J. V.; Steppe, K.; Vanhaecke, L. Ultra-high performance
543 liquid chromatography coupled to high resolution Orbitrap mass spectrometry for metabolomic

- 544 profiling of the endogenous phytohormonal status of the tomato plant, *J. Chromatogr. A*. **2012**,
 545 1260, pp. 67–80.
- 546 (33) Casillas-Vargas, G.; Ocasio-Malavé, C.; Medina, S.; Morales-Guzmán, C.; Del Valle, R.
 547 G.; Carballeira, N. M.; Sanabria-Ríos, D. J. Antibacterial fatty acids: An update of possible
 548 mechanisms of action and implications in the development of the next-generation of
 549 antibacterial agents, *Prog. Lipid Res.* **2021**, 82, p. 101093.
- 550 (34) Georgel, P.; Crozat, K.; Lauth, X.; Makrantonaki, E.; Seltmann, H.; Sovath, S.; Hoebe, K.;
 551 Du, X.; Rutschmann, S.; Jiang, Z.; Bigby, T.; Nizet, V.; Zouboulis, C. C.; Beutler, B. A toll-like
 552 receptor 2-responsive lipid effector pathway protects mammals against skin infections with
 553 gram-positive bacteria, *Infect Immun.* **2005**, 73, pp. 4512–4521.
- 554 (35) Desbois, A. P.; Smith, V. J. Antibacterial free fatty acids: activities, mechanisms of action
 555 and biotechnological potential, *Appl. Microbiol. Biotechnol.* **2010**, 85, pp. 1629–1642.
- 556 (36) Costantini, L.; Molinari, R.; Farinon, B.; Merendino, N. Impact of Omega-3 Fatty Acids on
 557 the Gut Microbiota, *Int. J. Mol. Sci.* **2017**, 18.
- 558 (37) Chandana, N. G. A. S. S.; Morlock, G. E. Eight different bioactivity profiles of 40
 559 cinnamons by multi-imaging planar chromatography hyphenated with effect-directed assays
 560 and high-resolution mass spectrometry, *Food Chem.* **2021**, 357, p. 129135.
- 561 (38) Howes, M.-J. R.; Houghton, P. J. Plants used in Chinese and Indian traditional medicine
 562 for improvement of memory and cognitive function, *Pharmacol. Biochem. Behav.* **2003**, 75,
 563 pp. 513–527.
- 564 (39) Umadevi, P.; Deepti, K.; Venugopal, D. V. R. Synthesis, anticancer and antibacterial
 565 activities of piperine analogs, *Med. Chem. Res.* **2013**, 22, pp. 5466–5471.
- 566 (40) Haq, I.-U.; Imran, M.; Nadeem, M.; Tufail, T.; Gondal, T. A.; Mubarak, M. S. Piperine: A
 567 review of its biological effects, *Phytotherapy research : PTR.* **2021**, 35, pp. 680–700.
- 568 (41) Shi, Y.-H.; Xiao, J.-J.; Liu, Y.-Y.; Deng, Y.-J.; Feng, W.-Z.; Wei, D.; Liao, M.; Cao, H.-Q.
 569 Gut microbiota influence on oral bioaccessibility and intestinal transport of pesticides in
 570 *Chaenomeles speciosa*, *Food Chem.* **2021**, 339, p. 127985.

- 571 (42) Salehi, B.; Fokou, P. V. T.; Sharifi-Rad, M.; Zucca, P.; Pezzani, R.; Martins, N.; Sharifi-
572 Rad, J. The Therapeutic Potential of Naringenin: A Review of Clinical Trials, *Pharmaceuticals*
573 *(Basel, Switzerland)*. **2019**, *12*.
- 574 (43) Kozłowska, J.; Potaniec, B.; Żarowska, B.; Anioł, M. Synthesis and Biological Activity of
575 Novel O-Alkyl Derivatives of Naringenin and Their Oximes, *Molecules (Basel, Switzerland)*.
576 **2017**, *22*.
- 577 (44) Meyer, D.; Morlock, G. E. Healthy oils are not necessarily healthy, *in revision*. **2022**.
- 578 (45) Orsavova, J.; Misurcova, L.; Ambrozova, J. V.; Vicha, R.; Mlcek, J. Fatty Acids
579 Composition of Vegetable Oils and Its Contribution to Dietary Energy Intake and Dependence
580 of Cardiovascular Mortality on Dietary Intake of Fatty Acids, *Int. J. Mol. Sci.* **2015**, *16*,
581 pp. 12871–12890.
- 582

583 **Figure legends**

584 **Figure 1.** Schematic workflow of the straightforward 10D hyphenated NP-
585 HPTLC–nanoGIT^{+active}–UV/Vis/FLD–EDA–heart cut–RP–HPLC–DAD–HESI–HRMS/MS taking
586 2.5–4.0 h per sample with consumption costs of 2.90 € per sample plus 0.15 € per substance
587 elution.

588 **Figure 2.** Study of HRMS acquisition modes: Extracted ion chromatograms (XIC) from full scan
589 and respective MS2 chromatograms from different acquisition modes analysed by a Q Exactive
590 Plus Hybrid Quadrupole–Orbitrap. Naringin (500 ng/area each) applied on an HPTLC silica gel
591 60 F₂₅₄ MS-grade plate was eluted with water – methanol (9:1, V/V) to RP–HPLC–HESI–
592 HRMS/MS. The full scans (displayed as stick) of the deprotonated naringin (*m/z* 271.0614,
593 [M–H][–]) were combined with (A) All Ion Fragmentation (AIF, product ion spectra of *m/z*
594 199.0503 C₈H₇O[–]), (B) data-dependent MS2 (ddMS2, directly from the isolated precursor), (C)
595 multiplexed data independent acquisition (mDIA), and (D) variable DIA (vDIA) both latter from
596 the MS2 scan event *m/z* 250–300.

597 **Figure 3.** Food screening for bioactive compounds: NP–HPTLC–nanoGIT^{+active}–UV/Vis/FLD–
598 EDA profiles of non-digested (–) versus panc-digested (+) raw extracts of tomato products
599 (5 µL/band each, assignments in Table S1) along with positive control (PC, digested rapeseed
600 oil) and negative control (NC, pancreatic enzyme mix and bile salts) on HPTLC plate silica gel
601 60 F₂₅₄ MS-grade, developed with *n*-hexane – dichloromethane – methanol – water
602 (40:50:10:1, V/V/V/V) up to 70 mm and detected via the bioluminescence (depicted as a
603 greyscale image) after the *A. fischeri* bioassay (A), and at white light illumination after the
604 α-glucosidase (B), β-glucosidase (C), acetylcholinesterase (D), and butyrylcholinesterase (E)
605 inhibition assays. Bioactive zones I–IX were heart-cut eluted for further characterization by RP–
606 HPLC–DAD–HRMS/MS. *hR_F* values were dependent on plate activity, as evident for zone IV
607 (D).

608 **Figure 4.** NP-HPTLC-nanoGIT^{+active}-UV/Vis/FLD-EDA-heart cut-RP-HPLC-DAD-HESI-
609 HRMS/MS spectra of zones **II** and **III**, both at hR_F 81 ± 1 .

610 **Table 1.** Tentative signal assignments of bioactive zones I–IX in tomato products without (–) and with (+) simulated intestinal on-surface digestion
 611 obtained by NP-HPTLC–nanoGIT⁺–active–UV/Vis/FLD–EDA–heart cut–RP–HPLC–DAD–HESI–HRMS/MS (n.d. not detected)

Zone	Sample	Observed effect	<i>hRf</i> (±1)	Retention time [min]	Molecular formula	Ion species	Precursor [<i>m/z</i>]	$\Delta m/z$ [ppm]	MS2 fragments [<i>m/z</i>]	λ_{max} [nm]	Tentative assignment	Lit.	
I	1–5(–/+)	A. <i>fischeri</i> enhancing, inhibition of AChE/BChE, α - β -glucosidase	99	n.d.			286.1438	0.00	201.0540 ⁺	245.	piperine	26	
	308.1254						0.92	143.0488 ⁺	330				
II	1(–/+)	A. <i>fischeri</i>	82	7.77	C ₁₇ H ₁₉ O ₃ N	[M+H] ⁺	571.2805	–0.38	135.0437 ⁺				
						[M+Na] ⁺	593.2622	0.08	115.0541 ⁺				
						[2M+Na] ⁺	609.2362	–0.07					
						[2M+K] ⁺	239.0675	–0.64	207.0409 [–]			dinoseb (pesticide)	27
		A. <i>fischeri</i>	80	7.21	C ₁₀ H ₁₂ O ₅ N ₂	[M–H] [–]	239.0675	–0.64	192.0668 [–]				
				7.43	C ₁₀ H ₁₂ O ₅ N ₂	[M–H] [–]	239.0675	–0.64	136.0402 [–]		dinoterb (pesticide)	27	
IV	all(–/+)	inhibition of A. <i>fischeri</i> , AChE/BChE, α - β -glucosidase	55–80	9.00	C ₁₄ H ₂₈ O ₂	[M–H] [–]	227.2018	–0.55	no fragments			myristic acid	45
						[M–H] [–]	277.2174	–0.38	no fragments			linolenic acid	45
						[M–H] [–]	279.2332	–0.99	no fragments			linoleic acid	45
						[M–H] [–]	255.2331	–0.53	no fragments			palmitic acid	45
						[M–H] [–]	281.2488	–0.73	no fragments			oleic acid	45
						[M–H] [–]	283.2646	–1.04	no fragments			stearic acid	45
						[M–H] [–]	171.1391	–0.27	no fragments			capric acid	28
V	8(+)	A. <i>fischeri</i>	49	8.31	C ₁₀ H ₂₀ O ₂	[M–H] [–]	199.1704	–0.43	no fragments			lauric acid	28
						[M–H] [–]	285.1710	–0.74	211.1338 [–]			unknown	
						[M+Cl] [–]	321.1476	–0.48	183.1388 [–]			(diglycerides/oxidated monoglycerides)	
						[M+HCOO] [–]	331.1765	–0.85	269.1744 ⁺				
VI	all(–/+)	A. <i>fischeri</i> , AChE/BChE, α - β -glucosidase	28	7.38	C ₁₃ H ₂₆ O ₅	[M+H ₃ C–COO] [–]	195.1920	–0.32	195.1379 ⁺				
						[M–H ₂ O+H] ⁺	269.1746	0.47	149.1325 ⁺				
						[M+H] ⁺	287.1852	0.53					
						[M+NH ₄] ⁺	304.2118	0.13					

Zone	Sample	Observed effect	<i>h</i> / <i>R</i> (±1)	Retention time [min]	Molecular formula	Ion species	Precursor [<i>m/z</i>]	$\Delta m/z$ [ppm]	MS2 fragments [<i>m/z</i>]	λ_{max} [nm]	Tentative assignment	Lit.
VII	7(-)	weak inhibition of AChE	28	6.11	C ₁₈ H ₃₁ O ₇ N	[M+Na] ⁺	309.1669	1.05		-	unknown	
						[M+K] ⁺	325.1409	0.74				
						[M+H] ⁺	348.2032	-1.07	274.1663 ⁻			
						[M+Cl] ⁻	384.1801	-1.70	226.1451 ⁻			
						[M+HCOO] ⁻	394.2087	-1.10	208.1344 ⁻			
						[M+H ₃ C-COO] ⁻	408.2243	-1.03	91.0401 ⁻			
						[M+H] ⁺	350.2174	-0.31	104.0711 ⁺			
						[M+Na] ⁺	372.1994	-0.44				
						[M+K] ⁺	388.1733	-0.33				
						[M+H] ⁺	245.1395	-0.09	171.1026 ⁻			
						[M+Cl] ⁻	281.1163	-0.65	173.1164 ⁺			
						[M+HCOO] ⁻	291.1453	-1.14	155.1059 ⁺			
[M+H ₃ C-COO] ⁻	305.1608	-0.76	109.1009 ⁺									
[M+H ₂ O+H] ⁺	229.1431	1.55	67.0547 ⁺									
[M+NH ₄] ⁺	264.1801	1.74										
[M+Na] ⁺	269.1353	2.44										
[M+K] ⁺	285.1093	1.90										
[M+Cl] ⁻	313.1426	-0.73	269.1362 ⁺									
[M+HCOO] ⁻	323.1713	-0.33	(sodium fragment)									
[M+H ₃ C-COO] ⁻	337.1870	-0.64										
[M+NH ₄] ⁺	296.2062	1.84										
[M+Na] ⁺	301.1617	1.66										
[M+K] ⁺	317.1355	1.88										
[M+H] ⁺	271.1554	-1.18	233.8611 ⁻									
[M+Cl] ⁻	307.1321	-0.99	197.1183 ⁻									
[M+HCOO] ⁻	317.1607	-0.44	169.1232 ⁻									
[M+H ₃ C-COO] ⁻	331.1766	-1.24	181.1223 ⁺									
[M+H ₂ O+H] ⁺	255.1590	0.30	135.1170 ⁺									
[M+H] ⁺	273.1695	0.48	107.0859 ⁺									
[M+NH ₄] ⁺	290.1962	0.03	93.0704 ⁺									
[M+Na] ⁺	295.1515	0.26										
[M+K] ⁺	311.1254	0.39										
[M+H] ⁺	271.0614	-0.89	177.0192 ⁻									
[M+Cl] ⁻	307.0381	-0.79	151.0036 ⁻									
			119.0501 ⁻									
			107.0138 ⁻									
			159.1026 ⁺									
			140.0829 ⁻									
			123.0564 ⁻									
			105.0457 ⁻									
VIII	1-9(-/+)	inhibition of <i>A. fischeri</i>	18	6.99	C ₁₅ H ₂₄ O ₅					215, 290	naringenin	30
IX	7(-)	inhibition of β -glucosidase	0	5.13	C ₁₄ H ₂₅ O ₃ N ₃	[M+H] ⁻	282.1825	-0.62		-	unknown	
						[M+Cl] ⁻	318.1591	-0.33	140.0829 ⁻			
						[M+H] ⁺	284.1972	-1.06	123.0564 ⁻			
							306.1791	-0.81	105.0457 ⁻			

Zone	Sample	Observed effect	hR_f (± 1)	Retention time [min]	Molecular formula	Ion species	Precursor [m/z]	$\Delta m/z$ [ppm]	MS2 fragments [m/z]	λ_{max} [nm]	Tentative assignment	Lit.
						[M+K] ⁺	322.1530	-0.69	266.1867 ⁺ 124.0873 ⁺ 107.0608 ⁺ 81.0455 ⁺	-		
				5.13	C ₂₇ H ₃₂ O ₁₀	[M-H] ⁻ [M+Cl] ⁻ [M+H] ⁺ [M+NH ₄] ⁺ [M+Na] ⁺ [M+K] ⁺	443.1926 479.1693 445.2076 462.2341 467.1898 483.1634	-0.83 -0.75 -1.76 -1.61 -2.14 -1.33	265.1435 ⁺ 247.1324 ⁺ (ammonia fragments)	-	unknown	
				5.30	C ₁₈ H ₂₈ O ₉	[M-H] ⁻ [M+Cl] ⁻ [M+NH ₄] ⁺ [M+Na] ⁺ [M+K] ⁺	387.1666 423.1428 406.2073 411.1626 427.1368	-1.42 -0.13 -0.34 -0.03 -0.74	163.1128 ⁻ 59.0133 ⁻ 209.1175⁺ 191.1068 ⁺ 149.0963 ⁺ 131.0858 ⁺	220, 280	tuberonic acid glucoside	32
				5.87	C ₁₈ H ₃₀ O ₈	[M+Cl] ⁻ [M+HCOO] ⁻ [M+H ₃ C-COO] ⁻ [M+H] ⁺ [M+NH ₄] ⁺ [M+Na] ⁺ [M+K] ⁺	421.1640 431.1925 445.2082 387.2015 404.2282 409.1836 425.1576	-1.16 -0.51 -0.69 -0.37 -0.85 -0.68 -0.88	no fragments	-	unknown	
				6.24	C ₂₇ H ₃₀ O ₁₆	[M-H] ⁻ [M+Cl] ⁻ [M+H] ⁺ [M+Na] ⁺ [M+K] ⁺	609.1469 645.1235 611.1613 633.1433 649.1173	-1.21 -1.04 -1.05 -1.12 -1.21	301.0713⁻ 303.0501⁺	260, 355	rutin	31

612

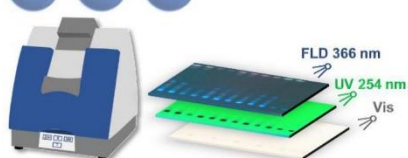
1D On-surface metabolization (nanoGIT)



2D NP-HPTLC separation



3D 4D 5D Detection



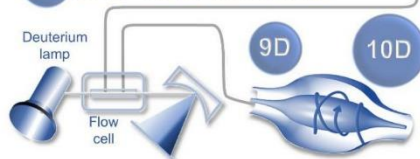
6D Effect-directed analysis (+active)



7D RP-HPLC separation



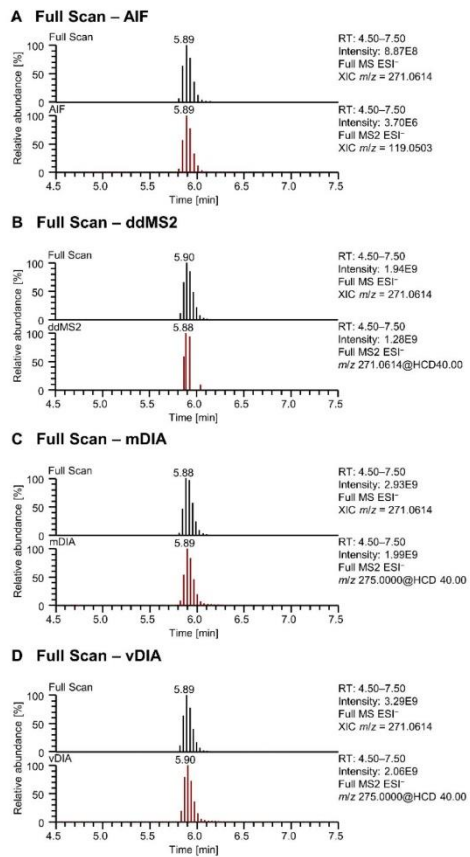
8D DAD-HESI-HRMS/MS



613

614 **Figure 1**

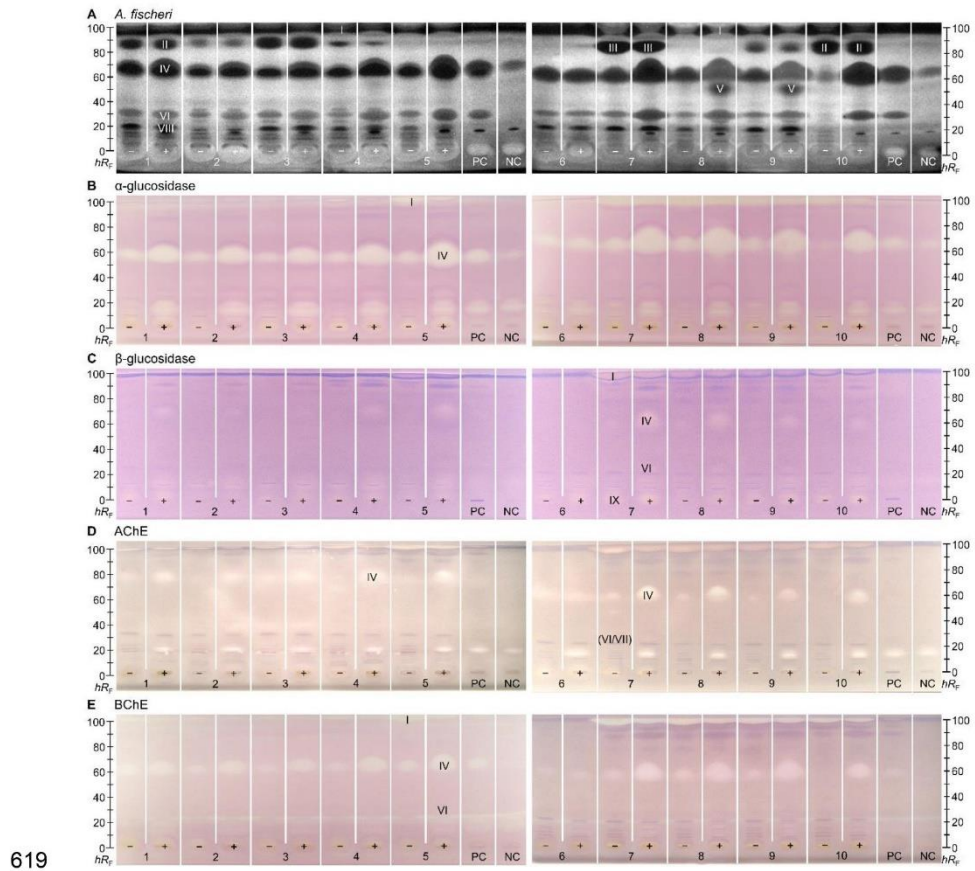
615



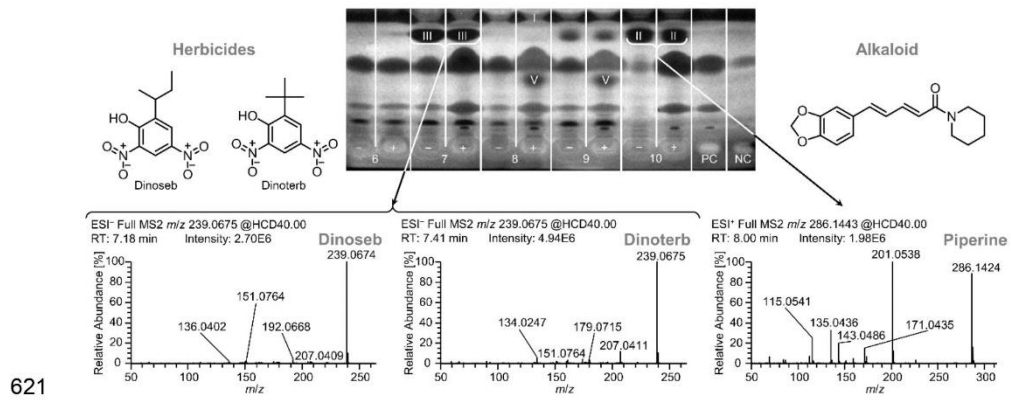
616

617 **Figure 2**

618

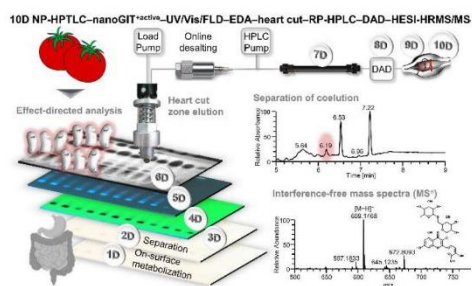


620 **Figure 3**



622 **Figure 4**

623 For TOC only



Supplementary Information

Effects of Gastrointestinal Digestion on Bioactivity of Convenience Tomato Products Studied by Ten-Dimensional Hyphenation

*Tamara Schreiner, Naila M. Eggerstorfer, Gertrud E. Morlock**

Justus Liebig University Giessen, Institute of Nutritional Science, Chair of Food Science,
Heinrich-Buff-Ring 26-32, 35392 Giessen, Germany

*Corresponding author. Tel.: +49 641 9939141, fax: +49 641 9939149, E-mail address:
Gertrud.Morlock@uni-giessen.de (G.E. Morlock)

S-1

Table of contents

Page S–4	Table S1. List of the ten investigated tomato products extracted with 5 mL <i>n</i> -butanol and filtered through 0.45 µm cellulose acetate filter.
Page S–6	Table S2. Investigation of mobile phase systems for tomato extract separation on HPTLC silica gel 60 F ₂₅₄ MS-grade plates up to a migration distance of 75 mm (*70 mm).
Page S–7	Fig. S1. Investigation of mobile phase systems (no. 1–24, Table S2) on HPTLC plates silica gel 60 F ₂₅₄ MS-grade for the NP-HPTLC–nanoGIT ^{+active} – <i>Aliivibrio fischeri</i> separation of the raw (–) versus panc-digested (+) extract of tomato product no. 8 (Table S1) along with positive control (PC, rapeseed oil) and negative control (NC, enzyme mix and bile salts) applied (all 5 µL/band each), developed and detected via the bioluminescence (depicted as greyscale image) after the <i>A. fischeri</i> bioassay.
Page S–8	Fig. S2. Development of the RP-HPLC gradient consisting of eluent A (2.5 mM ammonium acetate pH adjusted with acetic acid to 4.5) and eluent B (methanol) using standard mixture (500 ng/area, 4 mm × 2 mm) applied on HPTLC silica gel 60 F ₂₅₄ MS-grade plate and heart-cut eluted with water – methanol (9:1 V/V) to the column and HRMS showing the total ion current (TIC) chromatogram in the negative ionization mode.
Page S–9	Fig. S3. RP-HPLC–HESI–HRMS/MS settings for the evaluation of a non-target acquisition strategy. Full scan settings were maintained while MS2 settings were varied as all ion fragmentation (AIF), data-dependent MS2 (ddMS2), multiplexed data-independent acquisition (mDIA), and variable data-independent acquisition (vDIA).

Page S-10	Fig. S4. NP-HPTLC-nanoGIT ^{+active} -UV/Vis/FLD profiles of 10 raw (-) <i>versus</i> panc-digested (+) tomato products (5 µL/band, Table S1) along with positive control (PC, rapeseed oil), and negative control (NC, pancreatic enzyme mix and bile salts) on HPTLC silica gel 60 F ₂₅₄ MS-grade plate, developed with <i>n</i> -hexane – dichloromethane – methanol – water (40:50:10:1, V/V/V/V) up to 70 mm and detected at white light illumination (A), UV 254 nm (B), and FLD 366 nm (C).
-----------	--

Table S1. List of the ten investigated tomato products extracted with 5 mL *n*-butanol and filtered through 0.45 µm cellulose acetate filter.

No.	Product name	German Manufacturer	LOT no.	W [g]	Ingredients
1	Knorr Tomato al Gusto Basilikum	Unilever, Heilbronn	L113102852	5.00	88% tomatoes ^a (65% diced, 23% strained), 4.2% tomato paste ^a , 3.5% onion ^a , herbs (basil ^a , parsley ^a , basil powder), sugar iodized table salt, starch, native olive oil, spices (garlic, pepper), acidity regulator: citric acid. ^a from sustainable production.
2	Maggi rustikale Tomatencremesuppe	Nestlé, Lüdinghausen	12070703U	5.03	30% tomatoes, wheat flour, corn starch, sugar, iodized salt, spices (onion, bell pepper, garlic, pepper), herbs (laurel, majoram), smoked bacon (bacon, smoke), sunflower oil, yeast extract, flavours, thickening agents: guar gum. May contain traces of milk, egg, mustard, soy, and celery.
3	Maggi Spaghetti Napoli	Nestlé, Lüdinghausen	121607Q3R	5.02	39.4% tomatoes ^b , pea starch ^b , potato starch ^b , sugar ^b , iodized salt (salt, potassium iodate), spices ^b (onion, garlic, pepper), herbs ^b (parsley, oregano, basil, majoram, thyme), sunflower oil ^b , salt ^b , seasoning ^b (from wheat), flavours, acidity regulator: citric acid ^b . ^b natural ingredients. May contain traces of milk, egg, celery, mustard, and soy.
4	Kania Tomatensuppe toskanische Art	Radolf Nahrungsmittel, Radolfzell	L1175520658/A	5.01	36% tomatoes, starch, wheat semolina, palm fat, sweet whey powder, sugar, table salt; wheat flour, 2.9% roasted onion (onion, sunflower oil), spices, herbs, yeast extract, acidity regulator: citric acid, beet powder, garlic, dye: beta-carotene, seasoning extract, thickening agents: guar gum. Celery. (May contain traces of egg and soy.)

No.	Product name	German Manufacturer	LOT no.	W [g]	Ingredients
5	Heinz Cream of Tomato Soup	KraftHeinz Company, Düsseldorf	Not available	5.26	89% tomatoes, water, modified starch, sugar, rapeseed oil, skim milk powder, table salt, cream (milk), whey products (milk), acidity regulator: citric acid, seasoning extracts, herbal extracts.
6	Campo Verde Tomaten Sauce Classico	Campo Verde, Uhdingen-Mühlhofen	1163 ST K8	5.09	94.2% tomatoes, 2% native olive oil, 2% basil, 1.2% onion, grape juice, sea salt
7	Bertolli Siciliana	Unilever, Heilbronn	L11820086	5.11	76% tomatoes, 11% tomato paste, sunflower oil, white wine, onion, carrot, white wine vinegar, garlic, 0,9% dried tomatoes, table salt, sugar, native olive oil, oregano, thyme, basil, rosemary, laurel leaves, acidity regulator: citric acid, chili.
8	Ja! Tomaten-Creme-Suppe	Buss Fertiggerichte, Ottersberg	TCSV 3	5.06	48% tomato paste, water, 14% tomatoes, 5% cream, sugar, table salt, rapeseed oil, modified starch, thickening agents: guar gum, xanthan gum, wheat flour, coloring food bell pepper extract, chicken egg white, skim milk powder, spices (containing celery, mustard).
9	REWE Tomatencremsupe	Buss Fertiggerichte, Ottersberg	TCR 3	5.10	56% tomato, water, 5% cream, sugar, table salt, rapeseed oil, modified starch, herbs, thickening agents: guar gum, spices (containing mustard, celery), antioxidants: ascorbic acid, wheat flour, skim milk powder, chicken egg white
10	Self-made tomato soup	Tamara Schreiner, Giessen		5.04	8 tomatoes (skinned, sliced), 1 onion (sautéed), 1 garlic clove (sautéed), 1 soup spoon olive oil, thyme, dried, 6 leaves of basil, 1 teaspoon walnut oil, salt, pepper

Table S2. Investigation of mobile phase systems for tomato extract separation on HPTLC silica gel 60 F₂₅₄ MS-grade plates up to a migration distance of 75 mm (*70 mm).

No.	Mobile Phase (V/V/V/V)
1	<i>n</i> -hexane – ethyl acetate – methanol (6:3:2)
2	<i>n</i> -hexane – ethyl acetate – methanol (6:3:1)
3	<i>n</i> -hexane – toluene – ethyl acetate – methanol – formic acid (20:20:15:5:3)
5	<i>n</i> -hexane – toluene – ethyl acetate – methanol – formic acid (20:20:15:5:1)
5*	ethyl acetate – methanol – water (80:13:7)
6*	ethyl acetate – methanol – water (75:17:8)
7*	toluene – ethyl acetate – formic acid (45:30:2)
8*	toluene – acetonitrile – formic acid (45:30:2)
9	toluene – ethyl acetate – formic acid (45:40:2)
10*	<i>n</i> -hexane – toluene – ethyl acetate – methanol (4:4:3:2)
11*	ethyl acetate – methanol – water (16:2:1)
12	ethyl acetate – toluene – methanol – water (16:4:2:1)
13*	diisopropyl ether – <i>n</i> -butanol – methanol (1:1:1)
14*	ethyl acetate – toluene – methanol – water (16:2:2:1)
15	<i>n</i> -hexane – dichloromethane – methanol – water (40:50:12:1)
16	<i>n</i> -hexane – dichloromethane – methanol – water (40:50:10:1)
17	<i>n</i> -hexane – dichloromethane – methanol – water (40:55:12:1)
18	<i>n</i> -hexane – dichloromethane – methanol – water (40:60:15:1)
19	<i>n</i> -hexane – dichloromethane – methanol – water (50:55:15:1)
20	<i>n</i> -hexane – dichloromethane – methanol – water (50:60:15:1)
21	<i>n</i> -hexane – dichloromethane – methanol – acetic acid (40:50:10:1)
22	<i>n</i> -hexane – dichloromethane – methanol – acetic acid (80:100:20:1)
23	<i>n</i> -hexane – dichloromethane – methanol – water (90:100:24:1)
24	<i>n</i> -hexane – dichloromethane – methanol – water (30:50:7:1)

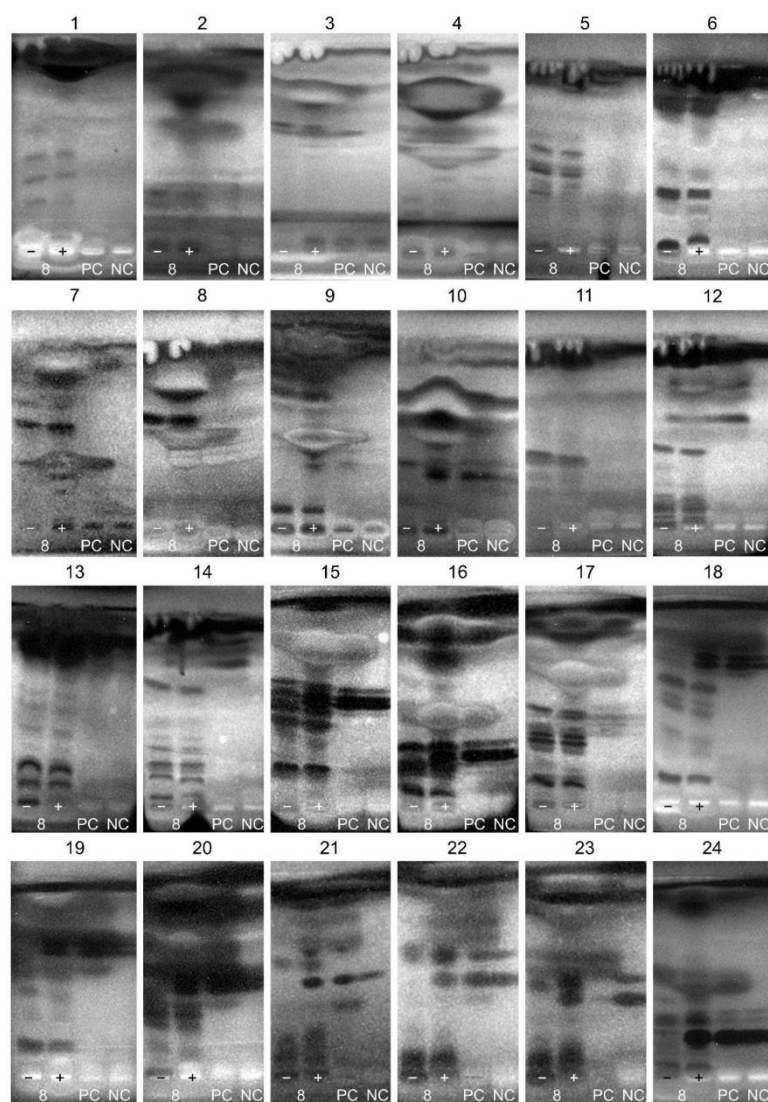


Fig. S1. Investigation of mobile phase systems (no. 1–24, Table S2) on HPTLC plates silica gel 60 F₂₅₄ MS-grade for the NP-HPTLC–nanoGIT^{active}–*Aliivibrio fischeri* separation of the raw (-) versus panc-digested (+) extract of tomato product no. 8 (Table S1) along with positive control (PC, rapeseed oil) and negative control (NC, enzyme mix and bile salts) applied (all 5 µL/band each), developed and detected via the bioluminescence (depicted as greyscale image) after the *A. fischeri* bioassay.

S-7

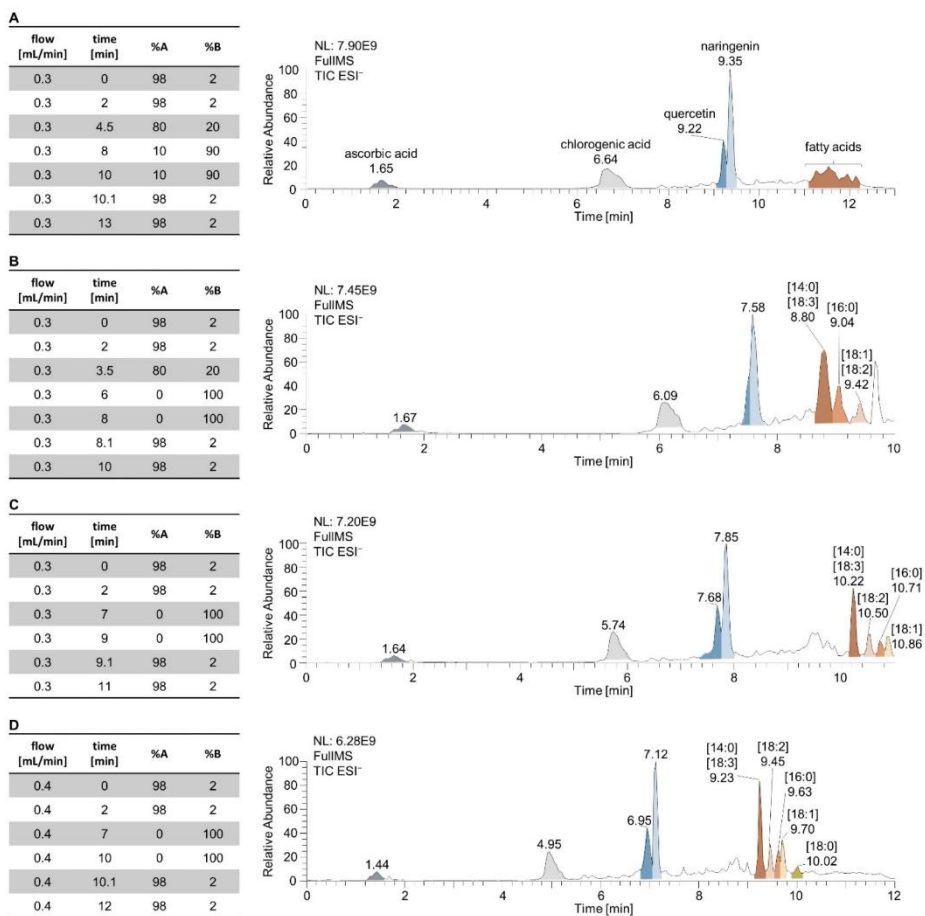


Fig. S2. Development of the RP-HPLC gradient consisting of eluent A (2.5 mM ammonium acetate pH adjusted with acetic acid to 4.5) and eluent B (methanol) using standard mixture (500 ng/area, 4 mm × 2 mm) applied on HPTLC silica gel 60 F₂₅₄ MS-grade plate and heart-cut eluted with water – methanol (9:1 V/V) to the column and HRMS showing the total ion current (TIC) chromatogram in the negative ionization mode.

HPLC Gradient		Full Scan – AIF		Full Scan – ddMS2		Full Scan – mDIA		Full Scan – vDIA	
Properties Gradient		Properties Full Scan		Properties Full Scan		Properties Full Scan		Properties Full Scan	
General	Runtime 0 to 10 min Flow 0.3 mL/min	General	Runtime 0 to 10 min Polarity switching (+/-)	General	Runtime 0 to 10 min Polarity switching (+/-)	General	Runtime 0 to 10 min Polarity negative	General	Runtime 0 to 10 min Polarity negative
Eluents	A 4 mM ammonium formate + 0.1% FA in water B 4 mM ammonium formate + 0.1% FA in methanol	Full MS	Resolution 70,000 AGC target 3e6 Scan range 100 to 1000 m/z	Full MS	Resolution 70,000 AGC target 3e6 Scan range 100 to 1000 m/z	Full MS – SIM	Resolution 70,000 AGC target 3e6 Scan range 100 to 1000 m/z	Full MS – SIM	Resolution 70,000 AGC target 3e6 Scan range 100 to 1000 m/z
Gradient composition	Time [min] %A %B	Properties AIF	Runtime 0 to 10 min Polarity switching (+/-) AIF 70,000 AGC target 3e6 (NICE/stepped) (NICE) 20, 40, 60 Scan range 100 to 1000 m/z Lock masses TopN 5 Isolation window 4.0 m/z (NICE/stepped) (NICE) 20, 40, 60 Scan range 100 to 1000 m/z	Properties ddMS2	Runtime 0 to 10 min Polarity switching (+/-) AIF 17,500 AGC target 3e6 Loop count 5 MSX count 1 TopN 5 Isolation window 4.0 m/z (NICE/stepped) (NICE) 20, 40, 60 Scan range 100 to 1000 m/z Lock masses 301, 14103 positive 413, 26623 positive 112, 98563 negative	Properties mDIA	Runtime 0 to 10 min Polarity negative mDIA 35,000 AGC target 3e6 Loop count 18 MSX count 6 Isolation window 50.0 m/z (NICE/stepped) (NICE) 20, 40, 60 Scan range 100 to 1000 m/z Lock masses 112, 98563 negative	Properties vDIA	Runtime 0 to 10 min Polarity negative vDIA (1) 35,000 AGC target 3e6 Loop count 8 MSX count 1 Isolation window 50.0 m/z (NICE/stepped) (NICE) 20, 40, 60 Scan range 100 to 1000 m/z vDIA (2) 35,000 AGC target 3e6 Loop count 2 MSX count 1 Isolation window 100.0 m/z (NICE/stepped) (NICE) 20, 40, 60 Scan range 100 to 1000 m/z vDIA (3) 35,000 AGC target 3e6 Loop count 1 MSX count 1 Isolation window 300.0 m/z (NICE/stepped) (NICE) 20, 40, 60 Scan range 100 to 1000 m/z Lock masses 112, 98563 negative Inclusion list polarity MSX ID Mass [m/z] 125,00000 negative 1 225,00000 negative 2 275,00000 negative 3 325,00000 negative 4 375,00000 negative 5 425,00000 negative 6 475,00000 negative 7 525,00000 negative 8 575,00000 negative 9 625,00000 negative 10 675,00000 negative 11 725,00000 negative 11 775,00000 negative 11 825,00000 negative 11 875,00000 negative 11 925,00000 negative 11 975,00000 negative 11

Fig. S3. RP-HPLC–HESI-HRMS/MS settings for the evaluation of a non-target acquisition strategy. Full scan settings were maintained while MS2 settings were varied as all ion fragmentation (AIF), data-dependent MS2 (ddMS2), multiplexed data-independent acquisition (mDIA), and variable data-independent acquisition (vDIA).

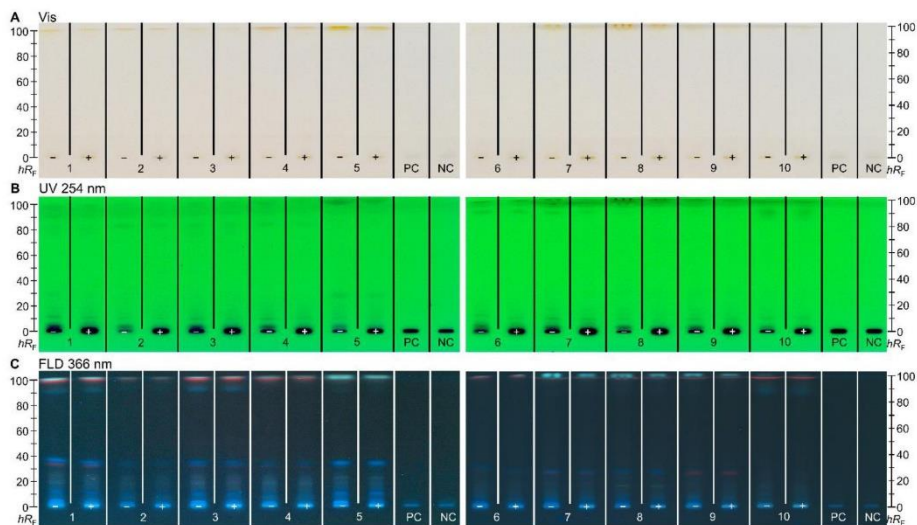


Fig. S4. NP-HPTLC-nanoGIT^{active}-UV/Vis/FLD profiles of 10 raw (-) versus panc-digested (+) tomato products (5 µL/band, Table S1) along with positive control (PC, rapeseed oil), and negative control (NC, pancreatic enzyme mix and bile salts) on HPTLC silica gel 60 F₂₅₄ MS-grade plate, developed with *n*-hexane – dichloromethane – methanol – water (40:50:10:1, V/V/V/V) up to 70 mm and detected at white light illumination (A), UV 254 nm (B), and FLD 366 nm (C).

5. Publication 4

**Effects of gastrointestinal digestion on bioactivity of meal
replacement products studied by ten-dimensional hyphenation**

Tamara Schreiner, Naila M. Eggerstorfer, Gertrud E. Morlock*

Justus Liebig University Giessen, Institute of Nutritional Science, Chair of Food Science,
Heinrich-Buff-Ring 26-32, 35392 Giessen, Germany

Submitted to

Food and Function

Received August 2022

ARTICLE

Effects of gastrointestinal digestion on bioactivity of meal replacement products studied by ten-dimensional hyphenation†

Tamara Schreiner, Naila Margot Eggerstorfer and Gertrud Elisabeth Morlock *

Received 00th January 20xx,
Accepted 00th January 20xx

DOI: 10.1039/x0xx00000x

Meal replacement products are normally consumed in weight-loss interventions and the treatment of obesity and diabetes. Changing lifestyles and eating habits rendered meal replacement products in the forms of shakes and bars a good alternative as “to-go-meals” promoted as healthier compared to other ready-to-eat meals. This study aimed to evaluate the bioactivity of six differently flavoured powdered meal replacement products analyzed by the recently developed ten-dimensional hyphenation. The latter incorporated miniaturized on-surface digestion, normal-phase high-performance thin-layer chromatography, multi-imaging, bioassay detection, reversed-phase high-performance liquid chromatography with diode array detection, and high-resolution tandem mass spectrometry. The breakdown of saccharides, fats, and proteins through intestinal enzymatic activity revealed new metabolites. These exhibited bioactivity in their different effect-profiles obtained by the Gram-negative *Allivibrio fischeri* bioassay as well as α -/ β -glucosidase, and acetyl-/butyrylcholinesterase inhibition assays. The main bioactive compounds arising through pancreatic digestion were saturated and unsaturated free fatty acids. The synthetic sweetener sucralose was not influenced by intestinal digestion, but showed antimicrobial activity. Also, the acetylcholinesterase-inhibiting methylxanthines caffeine and theobromine were identified in the prepared drinking meals with coffee and choco flavour. Despite the proven bioactivity, some other ingredients could not be assigned to specific molecules and require further analyses. In addition to the advertised balanced composition of the tested meal replacement products, they showed further health-beneficial properties through antimicrobial properties or inhibition of enzymes involved in the expression of the civilisation diseases, such as diabetes and Alzheimer’s, but plant foods, herbs and spices were shown to be even more rich and versatile in bioactive compounds.

1. Introduction

The nutritional status plays an important role in health and disease.^{1,2} Overweight, obesity, and health complaints are often consequences of malnutrition and a lack of micronutrients.² A poor diet is influenced by many factors, e.g., higher consumption of processed foods^{3,4} such as sugar-sweetened beverages^{5–7} or fast food,⁶ portion sizes,^{6,7} or snacking habits.⁴ Researchers hypothesized that long-term consumption of highly processed food plays a key role in the development of overweight, obesity,⁴ diabetes type 2,^{2,5} aggravation of Alzheimer’s,^{8,9} and other civilization diseases.³ Food processing includes all processes that alter food from its natural state by drying, freezing, grinding, heating, mixing, pasteurizing, fermenting, packaging, adding salts or sugars, etc.^{1,3} Through various processing steps, food safety and security are thought to be maintained,¹ but can be impaired as for the nutritional value.¹⁰ Nevertheless, highly processed meal replacement products (MRPs) are applied in the treatment of obesity or

diabetes.^{11,12} This seems contradictory at first sight, but usually, MRPs have been formulated by nutrition professionals and represent the ideal composition for a balanced diet, which consists of the optimal ratio of proteins, fat, fibre, vitamins, and minerals.¹ Due to better nutritional values, MRPs are generally promoted as healthy^{4,13} and often preferred over whole food in weight-loss interventions.^{4,14} It is clear that such surrogates can not substitute the versatility of bioactive compounds present in natural plant foods, herbs and spices.¹⁵ Thus, the impact of excessive longer use is unclear. Moreover, MRPs also aim for a time-saving opportunity to maintain a balanced diet. Meal replacement bars or shakes (e.g., <https://uk.yfood.eu>) could be a good alternative for busy lifestyles not allowing constant eating habits.¹⁶ Regardless of the purpose for which the MRPs are consumed, health-promoting properties are advertised to users.¹³

Besides a balanced diet through MRPs, it is assumed, that individual biologically active ingredients can contribute the health positively as well. As the human metabolism alters the bioactivity,^{17–20} it is significant if active compounds survive the gastrointestinal passage to exhibit their effects. Versatile metabolic transformation pathways of the gastrointestinal tract (GIT), e.g., microbial or enzymatic reactions, metabolise food components to get absorbed or influence the microbiome.¹⁸ Most prominent enzyme classes of the intestine are lipases, amylases, and proteases, responsible for the breakdown of fats,

Justus Liebig University Giessen, Institute of Nutritional Science. Chair of Food Science, Heinrich-Buff-Ring 26–32, 35392 Giessen, Germany. E-mail:

Gertrud.Morlock@uni-giessen.de; Tel.: +49 641 9939141; fax: +49 641 9939149,

† Electronic Supplementary Information (ESI) available: Details of samples (Table S1), nutritional values of samples (Table S2) Migration behaviour of lipidic standards (Fig. S1). See DOI: 10.1039/x0xx00000x

saccharides, and proteins, respectively. Through digestive processes, previously active ingredients could either lose their properties, are not influenced, or new biologically active metabolites or degradation products are produced. Therefore, screening for health-beneficial substances from processed foods should always consider further processing by the human metabolism.

In this study, the recently developed ten-dimensional bioanalytical hyphenation²¹ was employed to screen for stable, degraded or metabolised bioactive compounds in six differently flavoured MRPs. The bioanalytical workflow incorporated a miniaturized on-surface digestion (1D, nanoGIT), followed by normal-phase high-performance thin-layer chromatography (2D, NP-HPTLC) with multi-imaging at UV light (3D), white light illumination (4D, Vis), and fluorescence light detection (5D, FLD) plus effect-directed assay analysis (6D, EDA, ^{active}). Dimensions 1D–6D were performed on the same planar surface. Active zones were further evaluated by heart-cut elution, online desalting, reversed-phase high-performance liquid chromatography (7D, RP-HPLC) with diode array detection (8D, DAD), and high-resolution tandem mass spectrometry (9D/10D, HRMS/MS). This streamlined NP-HPTLC–nanoGIT^{active}–UV/Vis/FLD–EDA–heart cut–RP-HPLC–DAD–HRMS/MS workflow was used for non-target screening of bioactive substances from highly processed foods, such as MRPs.

2. Materials and methods

2.1. Chemicals and materials

All solvents were chromatography grade, and all salts of p.a. quality unless stated otherwise. HPTLC silica gel 60 F₂₅₄ MS-grade plates, potassium chloride (KCl, ≥99.5%), and magnesium sulfate heptahydrate (MgSO₄ · 7 H₂O, 99.5%) were obtained from Merck, Darmstadt, Germany. Dipotassium hydrogen phosphate trihydrate (K₂HPO₄ · 3 H₂O, ≥99%), magnesium chloride hexahydrate (MgCl₂ · 6 H₂O, ≥98%), sodium dihydrogen phosphate monohydrate (NaH₂PO₄ · H₂O, 99%), calcium chloride (CaCl₂, ≥98%), potassium dihydrogen phosphate (KH₂PO₄, ≥99%), disodium hydrogen phosphate (Na₂HPO₄, ≥99%), bovine serum albumin (BSA, fraction V, ≥98%), tris(hydroxymethyl)aminomethane (TRIS, ≥99.9%), hydrochloric acid (HCl, purest, 37%), glycerol (Rotipuran, 86%), glacial acetic acid (100%), *n*-hexane (≥98%), capric acid (>98%), stearic acid (>98%), and oleic acid (>99%) were purchased from Carl Roth, Karlsruhe, Germany. Bile extract (porcine), pancreatin from porcine pancreas (8 × USP specifications), acarbose (≥95%), rivastigmine (≥98%), caffeine (reagent plus), sodium acetate (>99%), peptone from casein (for microbiology), imidazole (≥99.5%), acetylcholinesterase (AChE) from *Electrophorus electricus* (≥245 U/mg, 10 kU/vial), α-glucosidase from *Saccharomyces cerevisiae* (1,000 U/vial), ethanol (≥99.8%), lauric acid (98%), myristic acid (≥99%), palmitic acid (>99%), linoleic acid (60–74%), 1-oleoyl-*rac*-glycerol (≥99%, monoacylglycerols, MAGs), dioleoylglycerol (≥99%, diacylglycerols, DAGs), and glyceryl trioleate (≥99%, triacylglycerols, TAGs) were delivered by Sigma-Aldrich,

Steinheim Germany. Butyrylcholinesterase (BChE, ≥245 U/mg) from equine serum was obtained from SERVA, Heidelberg, Germany, and its substrate 1-naphthyl acetate (≥98%) from AppliChem, Darmstadt, Germany. 2-Naphtyl-β-D-glucopyranoside (95%) and β-glucosidase from almonds (3040 U/mg) were provided by ABCR, Karlsruhe, Germany. Sodium bicarbonate (≥99.7%) and ammonium acetate (≥99%) were purchased from Fluka, Sigma-Aldrich, Steinheim, Germany. Yeast extract powder (for microbiology) and dichloromethane were delivered by Th. Geyer, Renningen, Germany. 2-Naphtyl-α-D-glucopyranoside (99%) was from Fluorochem, Hadfield Derbyshire, United Kingdom. Methanol, water (MS-grade), formic acid (99%), and sodium chloride (NaCl, ≥99%) were from VWR, Darmstadt, Germany. Ammonium carbonate (extra pure) was purchased from Bernd Kraft, Duisburg, Germany. *n*-Butanol, diammonium hydrogen phosphate ([NH₄]₂HPO₄, ≥99%), diethyl ether (99%), and linolenic acid (99%) were obtained from Acros Organics, Morris Plains, NJ, United States of America. Fast Blue B salt (95%) was delivered by MP Biomedicals, Eschwege, Germany. The culture medium preparation for the bioluminescent *Allivibrio fischeri* bacteria (DSM-7151, German Collection of Microorganisms and Cell Cultures, Berlin, Germany), is listed elsewhere.²² Rhodamine 6G (100 ± 3%) was delivered by Alfa Aesar, Kandel, Germany. Double distilled water was prepared by a Heraeus Destamat Bi 18E from Thermo Fisher Scientific, Dreieich, Germany.

2.2. Standard and sample preparation

Capric, lauric, myristic, palmitic, stearic, oleic, linoleic, and linolenic acid, 1-oleoyl-*rac*-glycerol (MAGs), dioleoylglycerol (DAGs), and glyceryl trioleate (TAGs) were prepared as 10-mg/mL stock solutions in *n*-hexane and diluted to 1-mg/mL working standards each.

Powdered MRPs in different flavours were purchased from yfood Labs, Munich, Germany and prepared according to the manufacturer's instructions. Briefly, 29 g of each powder were solved in 100 mL double distilled water and homogenised by manual shaking. Then, 5 g of each liquid nutrient (Table S1) were mixed with 5 mL *n*-butanol, vortexed for 10 min, and ultrasonicated (Sonoress Digiplus, Bandelin, Berlin, Germany) for 15 min. After centrifugation at 3,000 × *g* for 5 min (Labofuge 400, Heraeus, Hanau, Germany), supernatants were filtered through a 0.45 μm cellulose acetate filter (VWR, Darmstadt, Germany), and transferred into autosampler vials.

2.3. NP-HPTLC–nanoGIT^{active}–UV/Vis/FLD–EDA workflow

The simulated intestinal fluid (SIF) was prepared^{23,24} and the NP-HPTLC–nanoGIT^{active}–UV/Vis/FLD–EDA workflow was performed²¹ as described. All HPTLC instruments were from CAMAG, Muttenz, Switzerland, and controlled by visionCATS software (version 3.1.21109.3) if not stated otherwise. In brief, HPTLC silica gel 60 F₂₅₄ MS-grade plates were prewashed twice with methanol – water (4:1, V/V) in a Simultaneous TLC Developing Chamber (Macherey-Nagel, Düren, Germany) and dried at 110 °C in a clean oven (Mettler, Schwabach, Germany) for 20 min.²⁵ Plates were stored wrapped in

Please do not adjust margins

Journal Name

ARTICLE

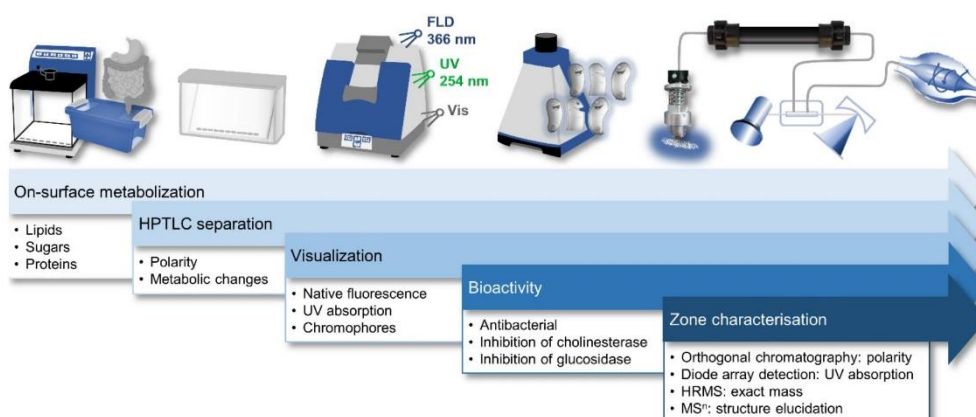


Fig. 1. Schematic ten-dimensional workflow and information obtained by streamlined hyphenation.

aluminium foil in a desiccator until use. *n*-Butanol extracts were applied twice as 6-mm bands (5 μ L/band) on pre-washed plates with a track distance of 13.5 mm (Automated TLC Sampler 4). The positive control (PC) rapeseed oil (1 mg/mL in *n*-hexane, 5 μ L) and the negative control (NC) pancreatin solution (panc, 20 mU/ μ L in SIF with bile extract, 5 μ L) with respective co-factors (CaCl₂, 6 pmol/ μ L, 1 μ L) were co-applied. The PC and one sample track each were oversprayed with panc and CaCl₂. To simulate the digestion, the lower 2 cm of the plate were moistened with 0.1 M sodium chloride solution (1.25 mL, yellow nozzle, level 6). Thereby, the top 8 cm of the plate were covered with a second plate, so that exclusively the 2-cm lower application area was wetted.²⁶ The stacked plates were placed horizontally in a moistened polypropylene box (KIS, 26.5 cm \times 16 cm \times 10 cm, ABM, Wolframs-Eschenbach, Germany) and incubated for 1 h at 37 $^{\circ}$ C in an oven (Memmert, Schwabach, Germany). The sample-loaded plate was dried for 4 min in a stream of cold air and chromatographed with *n*-hexane – dichloromethane – methanol – water (40:50:10:1, V/V/V/V) up to 70 mm in a twin trough chamber. Note that the mobile phase consisted of almost 90% highly volatile organic solvents, *i.e.* *n*-hexane and dichloromethane, necessitating an absolutely tight development chamber. Documentation followed at Vis, UV 254 nm, and FLD 366 nm (TLC Visualizer 3). The selected enzyme-inhibition assays α -/ β -glucosidase and AChE/BChE as well as the *A. fischeri* bioassay were performed as previously described.¹⁵ Functionality of the assays was proven by the application of PCs on the upper plate edge. PCs used were caffeine (1 mg/mL in methanol, 0.5, 1.5, and 3 μ L/band) for *A. fischeri* bioassay, rivastigmine (0.1 mg/mL in methanol, 2, 4, and 8 μ L/band) for AChE and BChE inhibition assays, acarbose (3 mg/mL in ethanol, 1, 3, and 6 μ L/band) for α -glucosidase, and imidazole (1 mg/mL, 3, 5, and 7 μ L/band) for β -glucosidase inhibition assay.

2.4. Heart cut–RP–HPLC–DAD–HESI–HRMS/MS

In a previous study, a 10D-workflow was established.²¹

All instrumental settings concerning standalone pump, autoTLC–MS interface, switching valve, desalting unit, LC, and HRMS/MS parameters were adopted. Shortly, bioactive zones were selected using the respective (bio)autogram, then automatically eluted from the plate by an oval elution head (2 mm \times 4 mm), desalted by trapping on a pre-column and valve switching, and further characterized by RP–HPLC–DAD–HESI–HRMS/MS.

3. Results and discussion

The 10D-hyphenation is a powerful tool to maximize the information gained from a single run (Fig. 1).²¹ In a minimalistic approach, pancreatic digestion was simulated through lipolytic, amyolytic, and proteolytic activity in the GIT, and revealed information about possibly present digestible lipids, saccharides, or proteins present in the sample. NP–HPTLC separation showed metabolic changes through digestion and side-by-side comparison of non-digested and digested samples. Further, HPTLC gave evidence about substance polarity via the hR_F value. Due to the different detection modes at Vis, UV 254 nm, and FLD 366 nm, chemical properties of sample components, such as chromophores, UV absorption, and natively fluorescent structure moieties, respectively, were evaluated. Subsequent effect-directed analysis (EDA) revealed antibacterial compounds against *A. fischeri* as well as inhibitors of α -glucosidase, β -glucosidase, AChE and BChE. Tracking of metabolic activation or deactivation was also embedded in the workflow. Final heart cut–RP–HPLC–DAD–HRMS/MS analysis of the bioactive zone allowed a variety of information about polarity (retention time in RP column), UV absorption (DAD), exact mass (HRMS), and fragmentation (MS/MS), ultimately leading to structure elucidation.

3.1. NP–HPTLC–nanoGIT⁺active–UV/Vis/FLD–EDA screening results

Effect-directed profiling showed bioactive zones in all five assays (Fig. 2). Since the basic formulation of the six differently

Please do not adjust margins

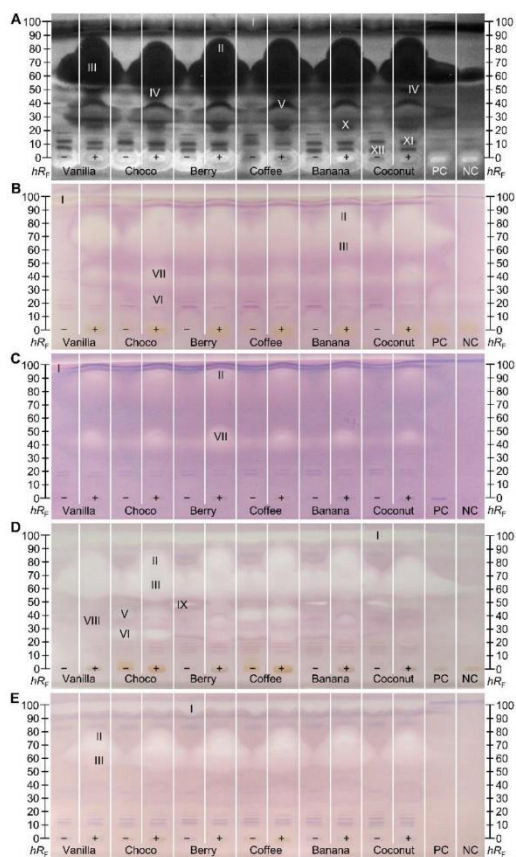


Fig. 2. NP-HPTLC–nanoGIT^{active}–UV/Vis/FLD–EDA profiles of five flavoured food substitutes. Side-by-side comparison of non-digested (–) and enzymatically digested (+) yfood products (5 μ l/band, assignments in Table S1) with positive control (PC, rapeseed oil), and negative control (NC, pancreatic enzyme mix, and bile salts) applied on HPTLC plate silica gel 60 F₂₅₄ MS-grade, developed with *n*-hexane–dichloromethane–methanol–water (40:50:10:1, v/v/v/v) up to 70 mm and detected after *A. fischeri* bioassay with bioluminescence depicted as a greyscale image (A), and under white light illumination after α -glucosidase (B), β -glucosidase (C), acetylcholinesterase (D), and butyrylcholinesterase (E) inhibition assays. Heart-cut eluted zones which were further characterized with RP-HPLC–DAD–HRMS/MS were marked with Roman numbers.

flavoured MRPs is very similar or even the same (Tables S1 and 2), an observed similar effect-profile across the different MRPs pointed to active compounds which are ingredients of the basic formulation. Non-digested (–) and digested (+) samples were screened in parallel to visualize differences through pancreatic digestion. Active zones of interest (marked I–XII) were further analysed via heart cut–RP–HPLC–DAD–HRMS/MS.

Antibacterial effects against the Gram-negative *A. fischeri* bacteria were evident as dark zones on the bioluminescent background (depicted as greyscale image, Fig. 2A). Compounds with positive impact on the energetic cell metabolism are brighter than the background. Zone I almost migrated to the solvent front (hR_F 99) and its bioactive response was hard to distinguish from the solvent front. The amount of antimicrobial substances increased through on-surface digestion (Fig. 2A),

especially in the upper hR_F region (hR_F 60–90, zones II and III). This effect was so strong that the substances even diffused to the neighbouring tracks under aqueous bioassay conditions. Since this effect was also observed in the PC (digested rapeseed oil) and NC, albeit in an attenuated form, it was expected that the substances must be lipids. The same holds for the antibacterial zones at hR_F 23 (zone X). Zones IV (hR_F 50) and V (hR_F 35) also exhibited antibacterial properties against *A. fischeri*. Both originated from metabolic digestion processes, missing in the non-digested samples. Only in this bioassay, the zone IV could be clearly differentiated from the blurred zones II and III. Some compounds enhancing the energetic cell metabolism of the *A. fischeri* bacteria remained in the application zone. At least in the digested samples (+), this effect originated from the pancreatic enzyme, as it was also recognized in the NC. Nevertheless, the non-digested (–) MRPs also showed bright zones, which could not be explained by pancreatic enzyme activity, since no panc was applied on the left track of each sample. Minor antibacterial effects were observed between hR_F values ≤ 10 (zones XI and XII) in all samples, which were not affected by digestion.

Inhibitors of α - and β -glucosidase were evident as colourless zones on a purple background (Fig. 2B/C). They only differed in the inhibition intensity, which was apparently stronger towards α -glucosidase. The ingredients of yfood are thus more potent in inhibiting the cleavage of α -1,4- or α -1,6-linked polysaccharides such as starch. In non-digested samples, a colourless inhibiting zone was detected within the solvent front (hR_F 99, zone I), especially in the MRP vanilla and choco. The chromatographic behaviour of this substance suggested that it has apolar properties since it did not interact with the polar silica gel plate. This substance was suspected to be digested, missing in these samples. Further inhibitory zones were detected at hR_F 60–90 (zones II and III) as in the *A. fischeri* bioassay. Exclusively for the choco-flavoured MRP, another weak α -glucosidase inhibitory zone (VI, hR_F 27) was determined which was also apparent in the AChE assay (Fig. 2D). The latter proved no metabolic changes through digestion that were not obvious for the α -glucosidase assay. At hR_F 40–50, zone VII was solely observed in the glucosidase inhibition assay (Fig. 2B/C). The intensity of the inhibitory zone increased through digestion in all samples.

The cholinesterase inhibition profiles (Fig. 2D/E) were similar regarding the lipid part (zones I–III) in the response and intensity to the glucosidase inhibition (Fig. 2B/C). This highlighted the influence of lipids on different metabolic processes. Screening for AChE inhibitors (Fig. 2D) revealed four further zones (V, VI, VIII, and IX), one predominantly active in varieties of choco (hR_F 27, zone VI) and the other in coffee (hR_F 38, zone V) which were not influenced by pancreatic digestion. These substances are assumed to originate from the yfood sort-specific ingredients (Table S1), i.e., fat-reduced cacao and coffee extract in choco- and coffee-flavoured MRPs, respectively. Zone VIII (hR_F 37) was only apparent in the AChE inhibition assay for the digested samples except for coconut. Since there is no response at the same hR_F value in non-digested analogues, it was suggested, that the pancreatic digestion provided new AChE inhibition properties to metabolites. At hR_F

Please do not adjust margins

Journal Name

ARTICLE

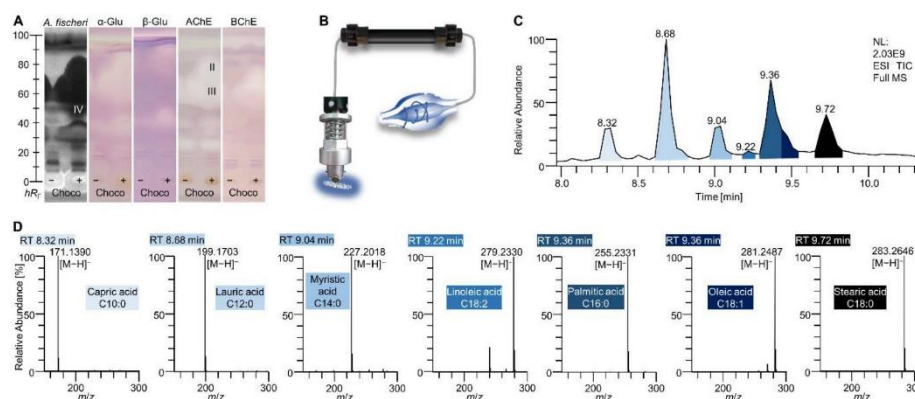


Fig. 3. NP-HPTLC–nanoGIT^{active}–UV/Vis/FLD–EDA–heart cut–RP-HPLC–DAD–HRMS/MS results of zone III (zones II and IV with a similar profile but differing emphasis). NP-HPTLC–nanoGIT^{active} profiles of the choco-flavoured MRP as in Fehler! Verweisquelle konnte nicht gefunden werden. (A). Zones II–IV were heart cut eluted, separated on an RP-HPLC column, and detected via orbitrap HRMS/MS as schematically shown (B), resulting in a chromatographic fatty acid profile (C), and respective mass spectra (D). Related peaks and mass spectra were highlighted in the same colour.

48, a colourless zone (IX) was detectable in the non-digested fruit-based MRPs berry, coffee, banana, and coconut, while this response was missing in the flavours vanilla and choco. After digestion, this effect was no longer detected. Modified chemical properties of the digestion product compared to its educt, resulted in either a change in the retention behavior on the NP plate or the loss of interaction with the binding site of AChE. The BChE inhibition profiles (Fig. 2E) showed the lipidic zones I–III very similar in intensity to the α -glucosidase.

3.2. Heart cut–RP-HPLC–DAD–HRMS/MS non-target screening results

Interesting active zones for elution were selected as coordinates on the respective (bio)autogram. The fully automated TLC–MS interface moves to the position selected, puts down the elution head, and elutes directly from the (bio)autogram one zone after the other.²⁷ Most bioactive ingredients identified were not explicitly listed in the ingredients list, but hidden behind super categories such as vegetable oils, coffee extract, or cacao, which hindered a direct assignment. The very apolar zone I (close to the solvent front, not so prominent) did not provide a mass signal in the heart cut–RP-HPLC–DAD–HESI–HRMS/MS analysis. It was assumed that triacylglycerols (TAGs) from animal fats and vegetable oils (Table S1) migrated to the solvent front (hR_F 99) on the NP-HPTLC plate. This assumption was intensified as the migration behaviour of lipidic standards was already comprehensible in a comparable chromatographic system (Fig. S1). The missing signals for TAGs originated from the setup of the 10D hyphenation. The zone elution solvent consists of 90% water and only 10% organic solvent. The aqueous solvent has good elution strength on NP-HPTLC plates, but solubility for TAGs is poor. The highly apolar TAGs could not be transferred from the plate to be detected with HRMS/MS. In addition, the installed HESI ionization source is not suited for ionisation of apolar compounds. The most striking zones II–IV were detected

in all assays. After heart cut–RP-HPLC–DAD–HESI–HRMS/MS, the benefit of the orthogonal separation (Fig. 3) was evident. Seven fatty acids (Table 1, Fig. 3D) were detected at an hR_F of approx. 60–95. To cover the broad retardation range, three independent elutions were performed (zones II–IV). All revealed comparable chromatograms with differing emphases of the fatty acid profile. It was expected that all fatty acids migrate to a similar hR_F value in this chromatographic system. This hypothesis was confirmed with the respective standards and the *A. fischeri* bioassay (Fig. 4). Supposedly pure standards of unsaturated fatty acids, *i.e.* C18:1, C18:2, and C18:3, were prone to impurities and oxidized degradation products. Lipolytic activity of pancreatic enzymes hydrolysed TAGs from milk protein and vegetable oils to their respective free fatty acids. Capric (C10:0) and lauric acid (C12:0) were cleavage products from animal fats,²⁸ while myristic (C14:0), palmitic (C16:0), stearic (C18:0), oleic (C18:1), linoleic (C18:2), and linolenic acid (C18:3) resulted rather from sunflower and rapeseed oil²⁹. According to the nutritional values list of the tested MRPs (Table S2), the overall amount of fat is indicated as 18.17 ± 0.37 g per 300 mL shake, of which only 2.42 ± 0.09 g are saturated. C12:0 is reported to interrupt the membrane integrity of Gram-positive and Gram-negative bacteria, inducing its antibacterial effect.³⁰ Weaker antimicrobial properties are described for the saturated C10:0, C16:0, and C18:0.³⁰ Despite the antimicrobial activity, the fatty acids, particularly *n*-3 (omega-3) polyunsaturated fatty acids, do not destroy the natural intestinal microbiome but help to establish a balance between the main bacterial genera *Firmicutes* and *Bacteroidetes*.^{31,32} Omega-3 fatty acids are reported to exhibit AChE inhibitory activities.³³ Of the detected fatty acids (Table 1), only C18:3 belongs to the omega-3 family. Since the AChE inhibition signal is very broad, it was assumed that other fatty acids also contribute to the overall inhibitory capacity. In a previous study, standards of C14:0, C16:0, C18:0, and C18:1 were also found to inhibit AChE as well as BChE, although the

Please do not adjust margins

Table 1. Tentative HRMS signal assignments for six flavoured food substitutes. NP-HPTLC–nanoGIT[®]–UV/Vis/FLD–EDA–heart cut–RP-HPLC–DAD–HESI-HRMS/MS signals of bioactive zones as in Fig. 2.

Zone	<i>hR_z</i> (±1)	<i>t_R</i> [min]	Molecular formula	Ion species	Precursor [<i>m/z</i>]	$\Delta m/z$ [ppm]	MS ² [<i>m/z</i>]	λ_{max} [nm]	Tentative assignment	Lit.
I	99					n.d.				
II	60–	8.32	C ₁₀ H ₂₀ O ₂	[M–H] [–]	171.1390	0.49	no fragments	–	capric acid	28
III	95									
IV		8.68	C ₁₂ H ₂₄ O ₂	[M–H] [–]	199.1703	0.42	no fragments	–	lauric acid	28
		8.78	C ₁₈ H ₃₄ O ₃	[M–H] [–] [M+Cl] [–] [M+HCOO] [–]	297.2436 333.2204 343.2492	–0.24 –0.64 –0.47	no fragments	–	unknown	
		9.00	C ₁₄ H ₂₈ O ₂	[M–H] [–] [2M–H] [–]	227.2019 455.4112	–0.95 –1.37	no fragments	–	myristic acid	29
		9.00	C ₁₈ H ₃₀ O ₂	[M–H] [–]	277.2174	–0.49	no fragments	–	linolenic acid	29
		9.21	C ₁₈ H ₃₂ O ₂	[M–H] [–] [2M–H] [–]	279.2330 559.4735	–0.13 –0.65	no fragments	–	linoleic acid	29
		9.43sh	C ₁₆ H ₃₂ O ₂	[M–H] [–] [2M–H] [–]	255.2331 511.4734	–0.65 –0.46	no fragments	–	palmitic acid	29
		9.43	C ₁₈ H ₃₄ O ₂	[M–H] [–] [2M–H] [–]	281.2486 563.5048	–0.09 –0.49	no fragments	–	oleic acid	29
		9.68	C ₁₈ H ₃₆ O ₂	[M–H] [–] [2M–H] [–]	283.2644 567.5364	–0.34 –1.03	no fragments	–	stearic acid	29
V	38	5.50	C ₈ H ₁₀ O ₂ N ₄	[M+H] ⁺	195.0879	–1.48	138.0664 ⁺ 110.0718 ⁺	205, 275	caffeine	36
VI	27	4.45	C ₇ H ₈ O ₂ N ₄	[M+H] ⁺ [M+NH ₄] ⁺ [M+Na] ⁺ [M+K] ⁺	181.0720 198.0989 203.0539 219.0278	0.23 –1.81 0.08 0.29	163.0615 ⁺ 138.0663 ⁺ 110.0717 ⁺	205, 275	theobromine	35
VII	48	6.63	C ₁₂ H ₂₂ O ₅	[M–H] [–] [M+Cl] [–] [M+HCOO] [–] [M+H ₃ C–COO] [–] [M–H ₂ O+H] ⁺ [M+NH ₄] ⁺ [M+Na] ⁺ [M+K] ⁺	245.1395 281.1164 291.1453 305.1609 229.1427 264.1797 269.1349 285.1089	–0.37 –0.86 –1.31 –0.92 3.12 3.10 4.04 3.62	171.1028 [–] 173.1168 ⁺ 155.1063 ⁺ 109.1012 ⁺ 67.0549 ⁺	–	unknown	
		7.37	C ₁₅ H ₂₆ O ₅	[M–H] [–] [M+Cl] [–] [M+HCOO] [–] [M+H ₃ C–COO] [–] [M–H ₂ O+H] ⁺ [M+H] ⁺ [M+NH ₄] ⁺ [M+Na] ⁺ [M+K] ⁺	285.1710 321.1476 331.1765 345.1921 269.1746 287.1852 304.2117 309.1670 325.1410	–0.88 –0.54 –0.82 –0.64 0.51 0.53 0.49 0.73 0.56	211.1337 [–] 187.1337 [–] 247.0965 ⁺ 215.0703 ⁺ 187.0754 ⁺	–	unknown	
VIII	37	6.12	C ₁₈ H ₃₁ O ₇ N	[M–H] [–] [M+Cl] [–] [M+HCOO] [–] [M+H ₃ C–COO] [–] [M+H] ⁺ [M+Na] ⁺ [M+K] ⁺	348.2031 384.1800 394.2086 408.2243 350.2174 372.1994 388.1733	–0.95 –1.36 –0.97 –1.03 –0.11 –0.23 –0.18	274.1662 [–] 226.1450 [–] 208.1344 [–] 104.0711 ⁺	–	unknown	
IX	48	6.95	C ₁₀ H ₁₁ O ₄ N	[M–H] [–]	208.0616	–0.18	151.0275 [–] 121.0295 [–]	215, 275, 360	unknown (fruit based powders)	

Please do not adjust margins

Journal Name

ARTICLE

Table 1 (continued)

Zone	hR_f (± 1)	t_R [min]	Molecular formula	Ion species	Precursor [m/z]	$\Delta m/z$ [ppm]	MS^2 [m/z]	λ_{max} [nm]	Tentative assignment	Lit.
X	23	8.07	$C_{24}H_{38}O_4$	[M-H] ⁻	389.2702	-1.25	373.2741 ⁺	-	Bile acid (7-Ketolithocholic acid)	
				[M+Cl] ⁻	425.2468	-1.01	355.2634 ⁺			
				[M+HCOO] ⁻	435.2756	-0.88	337.2517 ⁺			
				[M+H ₃ C-COO] ⁻	449.2914	-1.10	319.2416 ⁺			
				[2M-H] ⁻	779.5474	-0.79	159.1170 ⁺			
				[2M+Na-2H] ⁻	801.5300	-1.66				
				[2M+Cl] ⁻	815.5245	-1.32				
				[2M+HCOO] ⁻	825.5545	-2.70				
				[2M+H ₃ C-COO] ⁻	839.5697	-2.20				
				[M-2H ₂ O+H] ⁺	355.2634	-0.63				
				[M-H ₂ O+H] ⁺	373.2741	-0.99				
				[M+H] ⁺	391.2847	-0.98				
				[M+NH ₄] ⁺	408.3111	-0.75				
				[M+K] ⁺	429.2405	-0.80				
				[2M+H] ⁺	781.5623	-1.27				
				[2M+NH ₄] ⁺	798.5888	-1.23				
				[2M+Na] ⁺	803.5444	-1.48				
[2M+K] ⁺	819.5184	-1.44								
XI	15	8.10, 8.46	$C_{24}H_{40}O_4$	[M-H] ⁻	391.2859	-1.27	no fragments	-	Bile acids (hydoxycholic acid, ursodeoxycholic acid, chenodeoxycholic acid, deoxycholic acid)	37
				[M+Cl] ⁻	427.2623	-0.56				
				[M+HCOO] ⁻	437.2913	-1.02				
				[M+H ₃ C-COO] ⁻	451.3070	-1.03				
				[2M-H] ⁻	783.5789	-1.14				
				[2M+Na-2H] ⁻	805.5609	-1.09				
				[2M+Cl] ⁻	819.5561	-1.63				
				[M-2H ₂ O+H] ⁺	357.2789	-0.35				
				[M-H ₂ O+H] ⁺	375.2894	0.06				
				[M+NH ₄] ⁺	410.3266	-0.33				
				[M+Na] ⁺	415.2817	0.41				
				[M+K] ⁺	431.2558	0.06				
				[2M+H] ⁺	785.5927	-0.13				
				[2M+NH ₄] ⁺	802.6190	0.13				
				[2M+Na] ⁺	807.5749	-0.40				
				[2M+K] ⁺	823.5485	0.03				
				XII	7	5.73				
[M+Cl] ⁻	430.9840	-0.19	323.0538 ⁻							
[M+HCOO] ⁻	441.0126	0.36								
[M+H ₃ C-COO] ⁻	455.0285	-0.20								
[M+NH ₄] ⁺	414.0488	-1.02								
[M+K] ⁺	434.9779	-0.46								

hR_f : 100-fold retardation factor on NP-HPTLC, t_R : retention time on RP-HPLC column, n.d.: not detected, sh: shoulder

inhibition of the latter was weaker.³⁴ Further, α - and β -glucosidase inhibition properties for those four fatty acids were determined.³⁴ The intense response of zones II–IV through all (bio)assays resulted from additive effects of the single fatty acids, impossible to separate on NP-HPTLC plates (Fig. 4), but on the RP-HPLC column (Fig. 3). Furthermore, MRP product-specific bioactive compounds were identified as caffeine (zone V, Table 1 and Fig. 2A/D) in coffee and choco-flavoured MRP, and theobromine (zone VI, Table 1 and Fig. 2B/D) only in the choco-flavoured shake. Both substances were not influenced by pancreatic digestion. Theobromine is known to have a stronger AChE (about 39%) inhibition capacity compared to BChE (about 4%),³⁵ confirming the presented assay results (Fig. 2D versus E). Inhibitory activity of caffeine against

AChE *in vivo* was already proved by Souza *et al.*³⁶ This confirms that the on-surface methodology is suited to study highly efficiently complex samples and preselect active compounds with potential impact *in vivo*.

The bioactive zones VII–IX (Fig. 2A–D) revealed HRMS mass signals that were used to calculate possible molecular formulae (Table 1), but were not assigned to individual substances. In zone VII, two polyphenols were assumed, while alkaloids were suspected in zones VIII and IX.

Zones X and XI in the *A. fischeri* bioautogram (Fig. 2A) were assigned to 7-ketolithocholic acid and hydoxycholic, ursodeoxycholic, chenodeoxycholic, or deoxycholic acid³⁷ (Table 1) as constituents of the porcine bile salts added to the panc enzyme mixture. Since those antibacterial effects were not

Please do not adjust margins

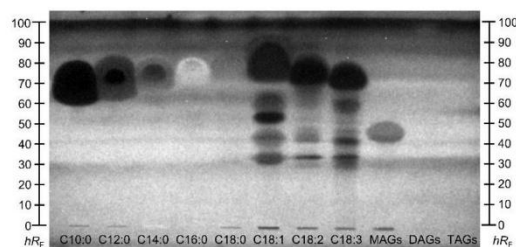


Fig. 4. NP-HPTLC-*Allivibrio fischeri* bioautogram of eight fatty acids (C10:0–C18:3), monoacylglycerols (MAGs), diacylglycerols (DAGs), and triacylglycerols (TAGs) (5 µg/band) applied on HPTLC plate silica gel 60 F₂₅₄ MS-grade, developed with *n*-hexane–dichloromethane–methanol–water (40:50:10:1, v/v/v/v) up to 70 mm and detected after *A. fischeri* bioassay with bioluminescence depicted as a greyscale image.

observed in the NC (only porcine bile salt, panc, and CaCl₂), it was initially suspected that these antimicrobial effects originated from yfoods, however, the identified compounds are not explainable by the list of ingredients. Based on the absence of any signal in the 7D–10D of the hyphenation, the substance exhibiting the bioactivity against *A. fischeri* bacteria does not have UV-absorption properties and is not ionizable, and was therefore not detected.

The isotope pattern of the unknown substance found in zone XII, indicated a trichlorinated compound. The precursor ion was obtained as 27:27:9:1 quadruplet at *m/z* 395.0071, 397.0041, 399.0010, and 400.9976. HRMS signals revealed a molecular formula of C₁₂H₁₉O₈³⁵Cl₃ for *m/z* 395.0071. Further evidence of a trichlorinated compound is provided by the fragmentation spectrum, where two times chlorine split-off was observed (Table 1). According to spectral data and in accordance with the ingredients list, the sweetener sucralose was identified. Besides the antibacterial effect against *A. fischeri* (Fig. 2A), the synthetic sweetener has also been shown to have antimicrobial properties against other Gram-negative bacteria such as different *Escherichia coli* strains (HB101 and K-12).³⁸ Further, sucralose altered the gut microbiome concerning the phyla *Firmicutes* and *Bacteroidetes*.³⁸

4. Conclusions

The applied 10D-hyphenation provided information about bioactive ingredients and activities of food constituents that are not directly listed as such on the packaging, as not regulated. The highly streamlined workflow was able to analyse six samples in parallel at a minimum of time (2.5–4.0 h depending on the assay) and material costs of 2.90 € per sample plus 0.15 € per substance elution to RP-HPLC–DAD–HESI-HRMS/MS. The health benefits of MRPs claimed by manufacturers were rapidly verified. Additionally, information about bioavailability and bioactivity after digestion of highly processed food was gained. Besides the advertised balanced diet, the analysed MRPs demonstrated further health-beneficial properties in form of bioactivity. The bioprofiling was exemplarily focused on detecting antibacterial compounds and inhibitors of glucosidases and cholinesterases, but other mechanisms can be studied in future. Depending on the processing, potential bioactive compounds from MRPs were stable against

mechanical, physical, or chemical influences and had bioactive properties even after intestinal digestion, also demonstrating biological stability. The obtained results showed that food and its digestion products inhibited the main enzymes involved in the development of hyperglycaemia and cognitive decline, *i.e.* glucosidases and cholinesterases, respectively. Remedies packaged in food for the treatment of diabetes and Alzheimer's disease could ease the daily lives of some patients. The famous quote by Hippocrates "Let food be thy medicine, and let medicine be thy food", summarises the results of the present work.

Author Contributions

Tamara Schreiner: Conceptualization, Methodology, Investigation, Data curation, Writing – Original Draft. **Naila M. Eggerstorfer:** Investigation. **Gertrud E. Morlock:** Conceptualization, Methodology, Supervision, Funding Acquisition, Writing – Review and Editing.

Conflicts of interest

There are no conflicts to declare.

Acknowledgements

Thank is owed to Merck, Darmstadt, for supply of plates. Instrumentation was partially funded by the *Deutsche Forschungsgemeinschaft* (INST 162/536-1 FUGG and INST 162/471-1 FUGG).

Abbreviations

AChE – acetylcholinesterase, BChE – butyrylcholinesterase, C10:0 – capric acid, C12:0 – lauric acid, C14:0 – myristic acid, C16:0 – palmitic acid, C18:0 – stearic acid, C18:1 – oleic acid, C18:2 – linoleic acid, C18:3 – linolenic acid, DAD – diode array detection, DAG – diacylglycerols, EDA – effect-directed analysis, FLD – fluorescence light detection, GIT – gastrointestinal tract, HPLC – high-performance liquid chromatography, HPTLC – high-performance thin-layer chromatography, HRMS – high-resolution mass spectrometry, MAGs – monoacylglycerols, MRP – meal replacement products, NC – negative control, NP – normal phase, panc – porcine pancreatin, PC – positive control, RP – reversed-phase, sh – shoulder, SIF – simulated intestinal fluid, TAGs – triacylglycerols, UV – ultraviolet, Vis – visible light (white light detection)

References

1. L. Sammugam and V. R. Pasupuleti, Balanced diets in food systems: Emerging trends and challenges for human health, *Crit. Rev. Food Sci. Nutr.*, 2019, **59**, 2746–2759.
2. M. I. Gómez, C. B. Barrett, T. Raney, P. Pinstrup-Andersen, J. Meerman, A. Croppenstedt, B. Carisma and B. Thompson, Post-green revolution food systems and the triple burden of malnutrition, *Food Policy*, 2013, **42**, 129–138.

- 3 J. M. Poti, M. A. Mendez, S. W. Ng and B. M. Popkin, Is the degree of food processing and convenience linked with the nutritional quality of foods purchased by US households?, *Am. J. Clin. Nutr.*, 2015, **101**, 1251–1262.
- 4 A. E. Mohr, C. Ramos, K. Tavarez and P. J. Arciero, Lower Postprandial Thermogenic Response to an Unprocessed Whole Food Meal Compared to an Iso-Energetic/Macronutrient Meal Replacement in Young Women: A Single-Blind Randomized Cross-Over Trial, *Nutrients*, 2020, **12**.
- 5 Y. Li, D. D. Wang, S. H. Ley, M. Vasanti, A. G. Howard, Y. He and F. B. Hu, Time Trends of Dietary and Lifestyle Factors and Their Potential Impact on Diabetes Burden in China, *Diabetes care*, 2017, **40**, 1685–1694.
- 6 L. A. Moreno, G. Rodríguez, J. Fleta, M. Bueno-Lozano, A. Lazaro and G. Bueno, Trends of dietary habits in adolescents, *Crit. Rev. Food Sci. Nutr.*, 2010, **50**, 106–112.
- 7 R. R. Briefel and C. L. Johnson, Secular trends in dietary intake in the United States, *Annu. Rev. Nutr.*, 2004, **24**, 401–431.
- 8 B. Vellas, S. Lauque, S. Gillette-Guyonnet, S. Andrieu, F. Cortes, F. Nourhashemi, C. Cantet, P. J. Ousset and H. Grandjean, Impact of nutritional status on the evolution of Alzheimer's disease and on response to acetylcholinesterase inhibitor treatment, *J. Nutr. Health Aging*, 2005, **9**, 75–80.
- 9 S. M. de La Monte and M. Tong, Mechanisms of nitrosamine-mediated neurodegeneration: potential relevance to sporadic Alzheimer's disease, *J. Alzheimers Dis.*, 2009, **17**, 817–825.
- 10 S. Sommano, in *Advances in food science and nutrition*, ed. P. M. Visakh, et al., John Wiley & Sons, Hoboken, NJ, 2014, pp. 361–390.
- 11 J. Peng, J. Lu, X. Ma, L. Ying, W. Lu, W. Zhu, Y. Bao and J. Zhou, Breakfast replacement with a liquid formula improves glycaemic variability in patients with type 2 diabetes: a randomised clinical trial, *Br. J. Nutr.*, 2019, **121**, 560–566.
- 12 I. Yip, V. L. Go, S. DeShields, P. Saltsman, M. Bellman, G. Thames, S. Murray, H. J. Wang, R. Elashoff and D. Heber, Liquid meal replacements and glycemic control in obese type 2 diabetes patients, *Obes. Res.*, 2001, **9 Suppl 4**, 341–347.
- 13 C. Hartmann, C. Keller and M. Siegrist, Compensatory beliefs, nutrition knowledge and eating styles of users and non-users of meal replacement products, *Appetite*, 2016, **105**, 775–781.
- 14 D. Q. Rothacker, B. A. Staniszewski and P. K. Ellis, Liquid Meal Replacement vs Traditional Food: A Potential Model for Women Who Cannot Maintain Eating Habit Change, *J. Am. Diet. Assoc.*, 2001, **101**, 345–347.
- 15 T. Schreiner, D. Sauter, M. Friz, J. Heil and G. E. Morlock, Is Our Natural Food Our Homeostasis? Array of a Thousand Effect-Directed Profiles of 68 Herbs and Spices, *Front. Pharmacol.*, 2021, **12**, 3310.
- 16 Noël Bollmann and Benjamin Kremer, The story behind yfood, <https://uk.yfood.eu/pages/story>, Accessed July 4, 2022.
- 17 J. Correa-Betanzo, E. Allen-Vercoe, J. McDonald, K. Schroeter, M. Corredig and G. Paliyath, Stability and biological activity of wild blueberry (*Vaccinium angustifolium*) polyphenols during simulated in vitro gastrointestinal digestion, *Food Chem.*, 2014, **165**, 522–531.
- 18 S. Ketnawa, J. Suwannachot and Y. Ogawa, In vitro gastrointestinal digestion of crisphead lettuce: Changes in bioactive compounds and antioxidant potential, *Food Chem.*, 2020, **311**, 125885.
- 19 X. Liu, J. Shi, J. Yi, X. Zhang, Q. Ma and S. Cai, The effect of in vitro simulated gastrointestinal digestion on phenolic bioaccessibility and bioactivities of *Prinsepia utilis* Royle fruits, *LWT - Food Sci. Technol.*, 2021, **138**, 110782.
- 20 X. C. Sollano-Mendieta, O. G. Meza-Márquez, G. Osorio-Revilla and D. I. Téllez-Medina, Effect of In Vitro Digestion on the Antioxidant Compounds and Antioxidant Capacity of 12 Plum (*Spondias purpurea* L.) Ecotypes, *Foods*, 2021, **10**.
- 21 T. Schreiner, N. M. Eggerstorfer and G. E. Morlock, Effects of gastrointestinal digestion on the bioactivity of convenience tomato products examined by ten-dimensional hyphenation, *in submission*.
- 22 European Committee for Standardization, *Water Quality - Determination of the Inhibitory Effect of Water Samples on the Light Emission of Vibrio Fischeri (Luminescent Bacteria Test)*, 2009.
- 23 M. Minekus, M. Alving, P. Alvito, S. Ballance, T. Bohn, C. Bourlieu, F. Carrière, R. Boutrou, M. Corredig, D. Dupont, C. Dufour, L. Egger, M. Golding, S. Karakaya, B. Kirkhus, S. Le Feunteun, U. Lesmes, A. Macierzanka, A. Mackie, S. Marze, D. J. McClements, O. Ménard, I. Recio, C. N. Santos, R. P. Singh, G. E. Vegarud, M. S. J. Wickham, W. Weitschies and A. Brodkorb, A standardised static in vitro digestion method suitable for food - an international consensus, *Food Funct.*, 2014, **5**, 1113–1124.
- 24 G. E. Morlock, L. Drotleff and S. Brinkmann, Miniaturized all-in-one nanoGIT+active system for on-surface metabolism, separation and effect imaging, *Anal. Chim. Acta*, 2021, **1154**, 338307.
- 25 G. E. Morlock, Background Mass Signals in TLC/HPTLC–ESI-MS and Practical Advices for Use of the TLC-MS Interface, *J. Liq. Chromatogr. Related Technol.*, 2014, **37**, 2892–2914.
- 26 I. Müller and G. E. Morlock, Validation and quantification of the saccharide release of hydrothermally treated flours after salivary and pancreatic amylolysis by the HPTLC nanoGIT+active method, *in submission*.
- 27 A. Mehl, W. Schwack and G. E. Morlock, On-surface autosampling for liquid chromatography-mass spectrometry, *J. Chromatogr. A*, 2021, **1651**, 462334.
- 28 S. Gallier, J. Cui, T. D. Olson, S. M. Rutherford, A. Ye, P. J. Moughan and H. Singh, In vivo digestion of bovine milk fat globules: effect of processing and interfacial structural changes. I. Gastric digestion, *Food Chem.*, 2013, **141**, 3273–3281.
- 29 J. Orsavova, L. Misurcova, J. V. Ambrozova, R. Vicha and J. Mlcek, Fatty Acids Composition of Vegetable Oils and Its Contribution to Dietary Energy Intake and Dependence of Cardiovascular Mortality on Dietary Intake of Fatty Acids, *Int. J. Mol. Sci.*, 2015, **16**, 12871–12890.
- 30 G. Casillas-Vargas, C. Ocasio-Malavé, S. Medina, C. Morales-Guzmán, R. G. Del Valle, N. M. Carballeira and D. J. Sanabria-Ríos, Antibacterial fatty acids: An update of possible mechanisms of action and implications in the development of the next-generation of antibacterial agents, *Prog. Lipid Res.*, 2021, **82**, 101093.
- 31 L. Costantini, R. Molinari, B. Farinon and N. Merendino, Impact of Omega-3 Fatty Acids on the Gut Microbiota, *Int. J. Mol. Sci.*, 2017, **18**.
- 32 M. Balfegó, S. Canivell, F. A. Hanzu, A. Sala-Vila, M. Martínez-Medina, S. Murillo, T. Mur, E. G. Ruano, F. Linares, N. Porras, S. Valladares, M. Fontalba, E. Roura, A. Novials, C. Hernández, G. Aranda, A. Sisó-Almirall, G. Rojo-Martínez, R. Simó and R. Gomis, Effects of sardine-enriched diet on metabolic control, inflammation and gut microbiota in drug-naïve patients with type 2 diabetes: a pilot randomized trial, *Lipids Health Dis.*, 2016, **15**, 78.
- 33 A. I. Zugno, H. Chipindo, L. Canever, J. Budni, A. Alves de Castro, M. Bittencourt de Oliveira, A. S. Heylmann, P. Gomes Wessler, F. Da Rosa Silveira, L. S. Damázio, G. A. Mastella, L. W. Kist, M. R. Bogo, J. Quevedo and C. S. Gama, Omega-3 fatty acids prevent the ketamine-induced increase in acetylcholinesterase activity in an animal model of schizophrenia, *Life Sci.*, 2015, **121**, 65–69.
- 34 N. G. A. S. S. Chandana and G. E. Morlock, Eight different bioactivity profiles of 40 cinnamons by multi-imaging planar chromatography hyphenated with effect-directed assays and

- high-resolution mass spectrometry, *Food Chem.*, 2021, **357**, 129135.
- 35 G. Brunhofer, A. Fallarero, D. Karlsson, A. Batista-Gonzalez, P. Shinde, C. Gopi Mohan and P. Vuorela, Exploration of natural compounds as sources of new bifunctional scaffolds targeting cholinesterases and beta amyloid aggregation: the case of chelerythrine, *Bioorg. Med. Chem.*, 2012, **20**, 6669–6679.
- 36 A. C. Souza, A. Souza, L. F. Medeiros, C. de Oliveira, V. L. Scarabelot, R. S. Da Silva, M. R. Bogo, K. M. Capiotti, L. W. Kist, C. D. Bonan, W. Caumo and I. L. S. Torres, Maternal caffeine exposure alters neuromotor development and hippocampus acetylcholinesterase activity in rat offspring, *Brain Res.*, 2015, **1595**, 10–18.
- 37 X. Qiao, M. Ye, D. Pan, W. Miao, C. Xiang, J. Han and D. Guo, Differentiation of various traditional Chinese medicines derived from animal bile and gallstone: simultaneous determination of bile acids by liquid chromatography coupled with triple quadrupole mass spectrometry, *J. Chromatogr. A*, 2011, **1218**, 107–117.
- 38 Q.-P. Wang, D. Browman, H. Herzog and G. G. Neely, Non-nutritive sweeteners possess a bacteriostatic effect and alter gut microbiota in mice, *PLoS one*, 2018, **13**, e0199080.

Electronic Supplementary Information

Effects of gastrointestinal digestion on bioactivity of meal replacement products studied by ten-dimensional hyphenation

*Tamara Schreiner, Naila Margot Eggerstorfer, Gertrud Elisabeth Morlock**

Justus Liebig University Giessen, Institute of Nutritional Science, Chair of Food Science,
Heinrich-Buff-Ring 26-32, 35392 Giessen, Germany

*Corresponding author. Tel.: +49 641 9939141, fax: +49 641 9939149, E-mail address:
Gertrud.Morlock@uni-giessen.de (G.E. Morlock)

S-1

Table of contents

Page S-3	Table S1. Flavour, expiration date, ingredients, and sample weights (<i>W</i>), extracted with 5 mL <i>n</i> -butanol and filtered through a 0.45 µm cellulose acetate filter.
Page S-4	Table S2. Nutritional values of the six investigated MRPs.
Page S-5	Fig. S1. NP-HPTLC-Rhodamine 6G-FLD of eight fatty acids (C10:0–C18:3), monoacylglycerols (MAGs), diacylglycerols (DAGs), and triacylglycerols (TAGs) (10 µg/band) applied on HPTLC plate silica gel 60 F ₂₅₄ MS-grade, developed with <i>n</i> -hexane – diethyl ether – formic acid (70:30:2, V/V/V) up to 60 mm and detected after chemical derivatisation with rhodamine 6G (0.1% in ethanol).

Table S1. Flavour, expiration date, ingredients, and sample weights (*W*), extracted with 5 mL*n*-butanol and filtered through a 0.45 µm cellulose acetate filter.

Sample flavor	Best before	Ingredients	W [g]
Vanilla	03/19/2022	milk protein, vegetable oils (sunflower, rapeseed), chicory root fibre, coconut milk, gluten-free oat fibre, vitamins (A, C, D, E, K, B1, B3, B5, B6, folic acid, biotin), minerals (potassium, magnesium, iron, zinc, copper, manganese, selenium, chromium, molybdenum, chloride, iodine), modified starch, maltodextrin, sweetener sucralose; natural flavourings.	5.00
Choco	03/19/2022	milk protein, vegetable oils (sunflower, rapeseed), fat-reduced cocoa 7.3%, chicory root fibre, coconut milk, gluten-free oat fibre, vitamins (A, C, D, E, K, B1, B3, B5, B6, folic acid, biotin), minerals (potassium, magnesium, iron, zinc, copper, manganese, selenium, chromium, molybdenum, chloride, iodine), modified starch, maltodextrin, sweetener sucralose; natural flavourings.	5.00
Berry	03/19/2022	milk protein, vegetable oils (sunflower, rapeseed), chicory root fibre, coconut milk, gluten-free oat fibre, raspberry puree 0.2%, dried strawberries 0.2%, vitamins (A, C, D, E, K, B1, B3, B5, B6, folic acid, biotin), minerals (potassium, magnesium, iron, zinc, copper, manganese, selenium, chromium, molybdenum, chloride, iodine), modified starch, maltodextrin, sweetener sucralose; colouring beetroot concentrate; acidity regulator citric acid; natural flavourings.	5.09
Coffee	03/11/2022	milk protein, vegetable oils (sunflower, rapeseed), chicory root fibre, coffee extract 3.2%, coconut milk, gluten-free oat fibre, vitamins (A, C, D, E, K, B1, B3, B5, B6, folic acid, biotin), minerals (potassium, magnesium, iron, zinc, copper, manganese, selenium, chromium, molybdenum, chloride, iodine), modified starch, maltodextrin, sweetener sucralose; natural flavourings.	5.02
Banana	03/11/2022	milk protein, vegetable oils (sunflower, rapeseed), chicory root fibre, coconut milk, gluten-free oat fibre, banana powder 0.2%, vitamins (A, C, D, E, K, B1, B3, B5, B6, folic acid, biotin), minerals (potassium, magnesium, iron, zinc, copper, manganese, selenium, chromium, molybdenum, chloride, iodine), modified starch, maltodextrin, sweetener sucralose; natural flavourings.	5.04
Coconut	03/19/2022	milk protein, vegetable oils (sunflower, rapeseed), chicory root fibre, gluten-free oat fibre, coconut milk 0.4%, vitamins (A, C, D, E, K, B1, B3, B5, B6, folic acid, biotin), minerals (potassium, magnesium, iron, zinc, copper, manganese, selenium, chromium, molybdenum, chloride, iodine), modified starch, maltodextrin, sweetener sucralose; natural flavourings.	5.10

Table S2. Nutritional values of the six investigated MRPs.

Nutritional values	*
Calories [kcal]	400.00 ± 0
Carbohydrates [g]	30.33 ± 0.47
of which sugars [g]	15.17 ± 0.69
Protein [g]	25.00 ± 0
Fat [g]	18.17 ± 0.37
of which saturated fats [g]	2.42 ± 0.09
fiber [g]	6.62 ± 0.47
salt [g]	0.53 ± 0
Vitamins	
Vitamin A [µg]	241.00 ± 0
Vitamin D [µg]	1.50 ± 0
Vitamin E [mg]	3.60 ± 0
Vitamin K [µg]	23.00 ± 0
Vitamin C [mg]	24.00 ± 0
Thiamin [mg]	0.33 ± 0
Riboflavin [mg]	0.70 ± 0
Niacin [mg]	4.80 ± 0
Vitamin B6 [mg]	0.42 ± 0
Folic acid [µg]	60.40 ± 0
Vitamin B12 [µg]	1.20 ± 0
Biotin [µg]	20.00 ± 0
Pantothenic acid [mg]	1.80 ± 0
Minerals	
Potassium [mg]	633.33 ± 74.54
Chloride [mg]	240.00 ± 0
Calcium [mg]	722.67 ± 2.98
Phosphorus [mg]	498.83 ± 13.04
Magnesium [mg]	119.17 ± 13.79
Iron [mg]	4.55 ± 0.78
Zinc [mg]	3.00 ± 0
Copper [mg]	0.34 ± 0.09
Manganese [mg]	0.60 ± 0
Selenium [µg]	17.00 ± 0
Chromium [µg]	12.00 ± 0
Molybdenum [µg]	15.00 ± 0
Iodine [µg]	45.22 ± 0.04

*data were calculated as mean ± standard deviation per portion (300 mL)

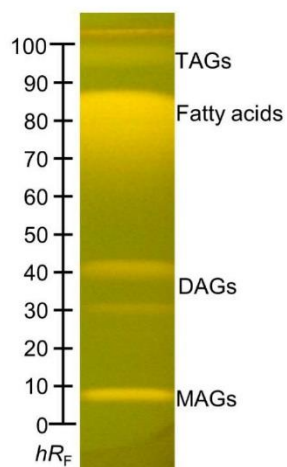


Fig. S1. NP-HPTLC-Rhodamine 6G-FLD of eight fatty acids (C10:0–C18:3), monoacylglycerols (MAGs), diacylglycerols (DAGs), and triacylglycerols (TAGs) (10 $\mu\text{g}/\text{band}$) applied on HPTLC plate silica gel 60 F₂₅₄ MS-grade, developed with *n*-hexane – diethyl ether – formic acid (70:30:2, V/V/V) up to 60 mm and detected after chemical derivatisation with rhodamine 6G (0.1% in ethanol).

6. **Publication 5**

**Multiplex planar bioassay with reduced diffusion on normal phase,
identifying androgens, verified antiandrogens and synergists in
botanicals via 12D hyphenation**

Tamara Schreiner, Alisa Ronzheimer, Maren Friz, Gertrud E. Morlock*

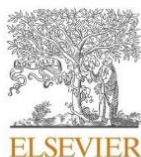
Justus Liebig University Giessen, Institute of Nutritional Science, Chair of Food Science,
Heinrich-Buff-Ring 26-32, 35392 Giessen, Germany

Dedicated to the 70th birthday of Prof. Dr. Wolfgang Schwack, University of Hohenheim,
Germany

Published in

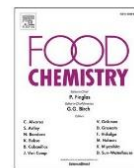
Food Chemistry, 395 (2022) 133610

Received 29 January 2022; Received in revised form 29 May 2022; Accepted 28 June 2022



Contents lists available at ScienceDirect

Food Chemistry

journal homepage: www.elsevier.com/locate/foodchem

Analytical Methods

Multiplex planar bioassay with reduced diffusion on normal phase, identifying androgens, verified antiandrogens and synergists in botanicals via 12D hyphenation

T. Schreiner, A. Ronzheimer, M. Friz, G.E. Morlock*

Justus Liebig University Giessen, Institute of Nutritional Science, Chair of Food Science, Heinrich-Buff Ring 26-32, 35392 Giessen, Germany



ARTICLE INFO

Dedicated to the 70th birthday of Prof. Dr. Wolfgang Schwack, University of Hohenheim, Stuttgart, Germany.

Keywords:

Agonist
Antagonist
Synergist
False-positive
Planar yeast antagonist androgen screen (pYAAS) bioassay
Zone diffusion reduction
High-performance thin-layer chromatography coupled with high-resolution mass spectrometry (HPTLC-HRMS)

ABSTRACT

Hormonal active compounds affecting health by altering the hormonal system are present in food. The planar yeast antagonist androgen screen (pYAAS) bioassay is a powerful tool to detect individual hormonal active compounds in complex samples separated by high-performance thin-layer chromatography (HPTLC). Previous methods lacked either detection sensitivity or zone sharpness. To overcome diffusion caused by long bioassay incubation on the normal-phase (NP) plate, zone fixation (^{fix}) was achieved with a new polyisobutyl methacrylate coating, leading to enhanced zone sharpness. The exclusion of false-positive antagonists was integrated in the workflow, which allowed the verification (V) of true antagonists, apart from the detection of synergists. With the new multiplex bioassay providing information on 4 activities, 68 different botanicals were screened and hormonal active zones were identified by elution from the bioautogram to orthogonal reversed-phase high performance liquid chromatography with diode array detection and high-resolution mass spectrometry including fragmentation, resulting in the 12D hyphenation NP-HPTLC^{fix}-UV/Vis/FLD-pYAVAS-FLD-heart cut-RP-HPLC-DAD-HRMS/MS.

1. Introduction

The consumption of plant-based food is known to be good for human health, as botanicals contain various bioactive compounds that have for example antidiabetic or antibacterial properties (Schreiner, Sauter, Friz, Heil, & Morlock, 2021), but there are also adverse effects. Substances that interfere with the human endocrine system are attracting increased attention (Riegraf et al., 2019; Klingelhöfer, Hockamp, & Morlock, 2020; Mertl et al., 2014). Such endocrine-disrupting chemicals mimic or alter the activity of steroid hormones (Mertl et al., 2014; Lee, Lee, Kwon, & Lee, 2003). Testosterone-like substances bind the human androgen receptor (hAR) and can act as androgens by receptor activation or act in an antiandrogenic way by blocking the binding site of the receptor (Azhagiya Singam, Tachachartvanich, La Merrill, Smith, & Durkin, 2019). Especially antiandrogens can cause male developmental disorders. One of the first studied antiandrogens is the dicarboximide fungicide vinclozolin, which has long been shown to affect mammalian

reproduction (Gray, Ostby, & Kelce, 1994). Effects on the reproductive system have also been demonstrated for esters of 4-hydroxybenzoic acid (parabens), which are known for their antiandrogenic properties (Oishi, 2001; Chen et al., 2007). There are also many phytochemicals that act as antiandrogens by binding the hAR (Singh, Baruah, & Sharma, 2017). Antiandrogenic activity has been proven especially for phytoestrogens (Singh et al., 2017) such as apigenin (Mbachu et al., 2020). As natural plant-based compounds can have antiandrogenic effects, it is likely that edible plants also contain such substances (Kuroyanagi et al., 1996; Zierau et al., 2003; Schleich, Papaioannou, Baniahmad, & Matusch, 2006).

Several bioassays were developed to detect endocrine-disrupting chemicals in food (Bovee et al., 1998; Bownes et al., 2009; Bovee et al., 2009). The yeast androgen screen (YAS) uses genetically modified *Saccharomyces cerevisiae* containing the hAR and is usually performed in microtiter plates, whereby only a sum parameter (sum effect) can be obtained for a complex sample or multi-component mixture (Sohoni &

* Corresponding author.

E-mail address: Gertrud.Morlock@uni-giessen.de (G.E. Morlock).<https://doi.org/10.1016/j.foodchem.2022.133610>

Received 29 January 2022; Received in revised form 29 May 2022; Accepted 28 June 2022

Available online 3 July 2022

0308-8146/© 2022 Elsevier Ltd. All rights reserved.

Sumpter, 1998). A combination with a chromatographic separation is, therefore, eligible (Mertl et al., 2014; Schönborn et al., 2017; Klingelhöfer et al., 2020). High-performance thin-layer chromatography (HPTLC) is well suited for complex samples due to its matrix robustness (Morlock, Morlock, & Lemo, 2014; Morlock & Prabha, 2007). Matrix-rich samples can be used almost in their native form and separated with virtually no loss of substance, in contrast to high-performance liquid chromatography (HPLC), which requires more complex sample preparation (Morlock, 2021; Schick & Schwack, 2017). The hyphenation of planar chromatography with biological detection led to the planar YAS (pYAS) bioassay, which allowed detecting straightforwardly individual substances in a complex mixture (Klingelhöfer et al., 2020). Separated androgens activated the hAR, leading to the production of β -galactosidase in the zone (Schick & Schwack, 2017). By the application of the substrate 4-methyl umbelliferyl- β -D-galactopyranoside (MUG), its galactose moiety was enzymatically cleaved by the YAS-reporter β -D-galactosidase, releasing the blue fluorescent 4-methyl umbelliferone (MU) recorded at 366 nm by fluorescence light detection (FLD). Hence, an androgen present in the sample was detected as a blue fluorescent zone. In contrast, an antiandrogen, blocking the binding site of the hAR, was indirectly detected as a fluorescence-reducing zone, when an agonist-stripe was overlaid orthogonally along each sample track after chromatography (Klingelhöfer et al., 2020). Thus, on the planar format, the additional detection of the opposite antagonistic effect was easily performed via an overlaid stripe of testosterone (T), which is the most common androgen or agonist. As water has almost no elution power on wettable reversed-phase HPTLC plates (RP-18 W), almost no desorption and diffusion of compounds occurred during the applied bioassay (despite long incubation times and a polar bioassay medium), preserving the sharpness of the zones which is especially important for complex mixtures (Klingelhöfer & Morlock, 2014). This multiplex planar yeast antagonist androgen screen (pYAS) bioassay was recently demonstrated (Klingelhöfer et al., 2020).

The application of this bioassay on normal-phase (NP)-HPTLC plates would improve detectability as well as multiplex functionality and reduce plate costs, but a major disadvantage is the strong diffusion (Schönborn et al., 2017) caused by the combination of a polar layer and an aqueous bioassay during long incubation times. Hence, for the first time, the reduction of diffusion on the NP-HPTLC plate was investigated by coating the layer with different fixation agents. A substance fixation (^{fix}) and resulting zone sharpness would especially improve the evaluation of hormonal compounds in complex samples. First, this sharpness would also allow extending the workflow pattern by another stripe to include the detection and exclusion of false-positive antagonistic responses. The overlay of the end product MU as additional stripe could prove true antagonists leading to their verification (V). The assay conditions on NP, such as incubation time, agonist-stripe amount, and end-product-stripe amount, had to be studied. The resulting NP-HPTLC^{fix}-UV/Vis/FLD-pYAS-FLD bioassay tailored for the detection of androgens, antiandrogens, false-positive antiandrogens, and synergists in complex mixtures was intended to provide more efficiency and profound information compared to status quo methods. Bioactive zones are to be eluted straightforwardly from the bioassay plate to orthogonal reversed-phase high-performance liquid chromatography with diode array detection and high-resolution mass spectrometry including fragmentation (heart cut-RP-HPLC-DAD-HRMS/MS).

2. Materials and methods

2.1. Chemicals and materials

Double-distilled water was prepared using a Destamat Bi 18E, Heraeus, Hanau, Germany. *Saccharomyces cerevisiae* BJ1991, genetically modified to contain the hAR, was purchased from Xenometrix, Allschwil, Switzerland. Ethyl acetate (HPLC grade) was from Th. Geyer, Renningen, Germany. *n*-Hexane (HPLC grade) was purchased from

Honeywell, Seelze, Germany and ethanol (HPLC grade), methanol (LC-MS grade), and water (LC-MS grade) from Fisher Scientific, Schwerte, Germany. Wettable reversed-phase HPTLC plates silica gel 60 RP-18 W and silica gel 60 F₂₅₄ MS-grade (NP), as well as *L*-tyrosine (for biochemistry), sodium chloride (NaCl, $\geq 99\%$), citric acid monohydrate ($\geq 99.5\%$), and *L*-arginine ($>99\%$) were obtained from Merck, Darmstadt, Germany. Testosterone (T, $\geq 99\%$), D-(+)-glucose (99.5%), *L*-glutamic acid (99%), *L*-serine (99%), *L*-valine (99%), *L*-leucine (99%), *L*-methionine (98%), *L*-aspartic acid (99.5%), *L*-threonine (for laboratory use), *L*-isoleucine (99%), *L*-glycine (99%), copper (II) sulfate pentahydrate, yeast nitrogen base without amino acids (p. a.), 4-methyl umbelliferone (MU, $>98\%$), ethyl 4-hydroxybenzoate (ethyl paraben, ethyl ester, EE, 99%), and ammonium formate (LC-MS grade, $\geq 99\%$) were delivered by Sigma-Aldrich Fluka, Steinheim, Germany. *L*-Lysine and *L*-histidine (both p. a.) were provided by Serva, Heidelberg, Germany. *L*-Phenylalanine (99%) was delivered from Bachem, Bubendorf, Switzerland. *L*-Adenine ($>99\%$) was purchased from TCI Deutschland, Eschborn, Germany. Formic acid ($\geq 98\%$), 4-methyl umbelliferyl- β -D-galactopyranoside (MUG, for biochemistry), dimethyl sulfoxide ($\geq 99.8\%$), sodium hydroxide ($\geq 99\%$), disodium hydrogen phosphate ($\geq 99\%$), and toluene (HPLC grade) were obtained from Carl Roth, Karlsruhe, Germany. Methanol (HPLC grade) was from VWR, Darmstadt, Germany. Degalan® P 28 N (Degalan), former Plexigum P 28, was obtained from Röhm, Darmstadt, Germany. Purity grades were listed when available. Dried botanical powders (Table S1) were obtained from Martin Bauer Group, Vestenbergsgreuth, Germany.

2.2. HPTLC plate pre-treatment

To improve layer stability, RP-18 W plates were heated at 120 °C in a clean oven (Memmert, Schwabach, Germany) for 1 h, then prewashed up to approx. 90 mm, first with methanol and second with ethyl acetate in a Simultaneous TLC Developing Chamber (Macherey-Nagel, Düren, Germany). NP plates were prewashed twice with methanol – water (4:1, V/V) and dried at 110 °C in the oven for 20 min (Morlock, 2014). All plates were stored wrapped in aluminum foil in a desiccator.

2.3. Preparation of yeast cell medium and culture

A minimal medium was prepared in double-distilled sterilized water. Through sterile filtration (mixed cellulose ester syringe filter, $<0.22 \mu\text{m}$, Merck, Darmstadt, Germany) 6.8 g/L yeast nitrogen base without amino acids, 5 g/L D-(+)-glucose, and 14 amino acids (20 mg/L *L*-adenine, 20 mg/L *L*-arginine, 100 mg/L *L*-aspartic acid, 100 mg/L *L*-glutamic acid, 20 mg/L *L*-histidine, 30 mg/L *L*-isoleucine, 100 mg/L *L*-leucine, 30 mg/L *L*-lysine, 20 mg/L *L*-methionine, 50 mg/L *L*-phenylalanine, 400 mg/L *L*-serine, 200 mg/L *L*-threonine, 30 mg/L *L*-tyrosine, and 150 mg/L *L*-valine) were added. A 1 mL cryostock *Saccharomyces cerevisiae* BJ1991 (modified to contain the hAR, Purvis et al., 1991) was diluted in 39 mL minimal medium in a 100 mL plastic baffled flask. The inoculated medium was incubated (Cultura M Incubator 70700, Almedica, Giffers, Switzerland) overnight (18–19 h) at 30 °C and 75 rpm on an orbital shaker (Edmund Bühler, Hechingen, Germany). The cell number was determined with a hemocytometer (Brand, Wertheim, Germany) out of a 1:20 dilution (50 μL cell suspension and 950 μL 0.9% (W/V) NaCl in double-distilled water). To adjust the cell number to 0.8×10^8 cells/mL, the respective volume of cell suspension was centrifuged (centrifuge 5702, Eppendorf, Hamburg, Germany) at $2,500 \times g$ for 5 min. The supernatant was discarded, while the sedimented cells were resuspended in 2 mL or 4 mL fresh medium with 150 μM copper sulfate (Klingelhöfer et al., 2020).

2.4. Standard solutions

A standard solution of the agonist T was prepared as dilution from a 1 mg/mL methanolic stock solution to a concentration of 1.5 $\mu\text{g/mL}$. The

antagonist EE solution was prepared as a 1 mg/mL solution in methanol. For detection of false-positive antagonistic responses, 1 mg of the fluorescent end product MU was dissolved in 1 mL methanol and diluted to 100 µg/mL with methanol.

2.5. Sample preparation

Each botanical sample (500 mg, Table S1) was dissolved in 5 mL methanol to prepare 10% (W/V) extract solutions. Extraction was performed by ultrasonication (Sonorex Digiplus, Bandelin, Berlin, Germany) for 30 min and centrifugation (Labofuge 400, Heraeus, Hanau, Germany) at $3,000 \times g$ for 15 min. Turbid extracts were additionally filtered through polytetrafluoroethylene syringe filters (0.45 µm, Macherey-Nagel, Düren, Germany, marked* in Table S1) before being transferred into autosampler vials. Extracts were stored at $-20\text{ }^{\circ}\text{C}$.

2.6. Investigation of assay parameters and layer coating

If not stated otherwise, HPTLC instrumentation was from CAMAG, controlled by Freemode option of winCATS software (version 1.4.7.2018) and visionCATS software (version 3.1.21109.3). Band patterns and orthogonal stripes were sprayed (Freemode, Automated TLC Sampler 4) on NP MS-grade plates and dried for 4 min (stream of cold air, hair dryer). Optimization of the assay parameters and first attempts on diffusion reduction are provided in the [supplementary information](#) (Text S1). To investigate the reduction in zone diffusion via Degalan on an NP plate, EE was applied two times as four stacked 6-mm bands of 1 µg/band and four times as four stacked 10-mm bands of 1.5 µg/band, and still on the same plate, the sample kola (no. 31) was applied as two 6-mm bands (4 µL each). The plate piece with the kola sample was cut (5 cm \times 10 cm) and developed in a 10 cm \times 10-cm twin trough chamber (as in 2.7). All tracks or patterns were oversprayed orthogonally with T either as 1 mm \times 70-mm stripe (6 µg/area) or 2 mm \times 70-mm stripe (12 µg/area). The larger 10-mm EE-bands were additionally oversprayed orthogonally with MU (1 mm \times 70 mm, 500 ng/area). The plate was cut to obtain 2.5 cm \times 10-cm pieces. From each plate piece with two identical applications, one was used as control reference and the other for Degalan coating before the bioassay application.

2.7. NP-HPTLC^{fix}-UV/Vis/FLD-pYAVAS-FLD workflow

Less sample volume had to be sprayed on the thinner-coated NP MS-grade plates (80–120 µm layer thickness), if compared to the RP-18 W plates (150–200 µm layer thickness). The extracts (as 6-mm bands, 4 µL on NP or 8 µL on RP-18 W, and as 12-mm bands, 8 µL on NP) were applied bandwise (Automated TLC Sampler 4). As mobile phase ethyl acetate – toluene – formic acid – water (16:4:3:2, V/V/V/V) was used up to a migration distance of 70 mm (Krüger, Hüskens, Fornasari, Scainelli, & Morlock, 2017; Schreiner et al., 2021) in a twin trough chamber (20 cm \times 10 cm). After plate drying, T was applied as a partially overlaid area along each track (1 mm \times 70 mm; 6 ng/area on NP; 2 mm \times 70 mm; 12 ng/area on NP^{fix}; 3 mm \times 66 mm; 230 ng/area on RP-18 W). Additionally, a MU area (1 mm \times 70 mm; 500 ng/area) was applied on each right track side. The HPTLC chromatograms were recorded (TLC Visualizer 2) at 254 nm (UV), white light illumination (Vis), and 366 nm (FLD). For neutralization of the acidic layer, citrate phosphate buffer (6 g/L citric acid monohydrate and 10 g/L disodium hydrogen phosphate in double-distilled water, adjusted to pH 12 by solid sodium hydroxide) was piezoelectrically sprayed onto the plate (1.4 mL on NP or 2.8 mL on RP-18 W, yellow ultra nozzle, level 2, Derivatizer), followed by plate drying. For fixation, NP plates were coated with Degalan solution (0.25% (W/V) in *n*-hexane; 250 mL in a crystallizing dish) for 10 min and then dried. The prepared yeast cell culture was piezoelectrically sprayed onto the plates (1.4 mL on NP or 2.8 mL on RP-18 W, red nozzle, level 6, Derivatizer). The planar chromatogram was placed in a polypropylene box (KIS 26.5 cm \times 16 cm \times 10 cm, ABM, Wolframs-

Eschenbach, Germany; pre-moistened with water for 30 min) and incubated at $30\text{ }^{\circ}\text{C}$ for 4 h, followed by drying. The substrate solution (2 mg MUG in 100 µL dimethyl sulfoxide and 3 mL citrate buffer) was piezoelectrically sprayed (1.5 mL on NP or 2.3 mL on RP-18 W, yellow ultra nozzle, level 2, Derivatizer). The plate was incubated at $37\text{ }^{\circ}\text{C}$ for 1 h, dried, and documented at FLD 366 nm. Digital evaluation was carried out by generating a videodensitogram out of the image at FLD 366 nm using quantTLC (Fichou & Morlock, 2018).

2.8. Heart cut-RP-HPLC-DAD-HRMS/MS workflow

Dionex Ultimate HPLC system was equipped with a binary pump (HPG-3200SD), an autosampler (WPS-3000TXRS), a column oven (TCC-3000RS), and a diode array detector (DAD-3000RS, all Dionex Softron, Germering, Germany) and connected to a Q Exactive Plus Hybrid Quadrupole-Orbitrap (Thermo Scientific, Bellefonte, PA, United States). Ion-Max HESI-II probe operated according to the following conditions: sheath gas 20 AU, aux gas 10 AU, spray voltage 3.5 kV, capillary temperature $320\text{ }^{\circ}\text{C}$, probe heater temperature $350\text{ }^{\circ}\text{C}$, S-lens RF level 50 AU).

Verified antiandrogens and compounds with synergistic effects were heart-cut eluted from the HPTLC plate with the fully automated autoTLC-MS interface (Mehl, Schwack, & Morlock, 2021; Häbe & Morlock, 2020) equipped with an oval elution head (2 mm \times 4 mm). Elution solvent (water – methanol, 9:1 V/V, with 4 mM ammonium formate and 0.1% formic acid) was provided by an HPLC standalone pump (MX010PFT, Teledyne SSI, State College, PA, United States) at a flow rate of 0.1 mL/min. Analytes were guided to a two-position six-port switching valve (MXT series, PD715-000, Rheodyne, IDEX Health & Science, Rohnert Park, CA, United States) on which a 50-µL sample loop and a desalting cartridge (Accucore RP-MS, 10 mm \times 2.1 mm, 2.6 µm, Thermo Scientific) were installed. By switching after 40 s elution time, HPLC gradient flushed the cartridge and transferred analytes to the main column (Accucore RP-MS 100 mm \times 2.1 mm, 2.6 µm, thermostated at $40\text{ }^{\circ}\text{C}$, Thermo Scientific) (Schreiner & Morlock, 2021). Mobile phase A was water, while mobile phase B was methanol, both with 4 mM ammonium formate and 0.1% formic acid. Gradient started at 5% B at a flow rate of 0.3 mL/min for 1 min (elution), then increased to 50% B (1–2 min) and to 95% B (2–6 min). Gradient composition was held for 2 min (6–8 min) followed by 2 min equilibration time resulting in a 10-min gradient. After orthogonal column separation, analytes were detected with DAD (wavelength scan 200–400 nm, and at specific wavelengths, i.e. 240 nm, 280 nm, and 320 nm) and HRMS/MS in polarity switching full-scan data-dependent MS² (ddMS²) mode. MS instrument performed a full scan event at a mass range of *m/z* 100–1100, with a resolving power of 70,000 full width at half-maximum (FWHM) and automated gain control (AGC) target 3e6, followed by a Top5 ddMS² fragmentation without inclusion list at a mass range of *m/z* 80–1000, resolution of 17,500 FWHM, AGC target 1e6, and normalized stepped collision energy of 20, 40, and 60 eV. External mass calibration was performed weekly with Pierce TM LTQ Velos ESI positive/negative ion calibration solution. The instrument was controlled by Xcalibur 3.0.63.3 with Foundation 3.0.152 under DCMS link 2.14 (all Thermo Scientific).

3. Results and discussion

For thorough evaluation of a sample, four microtiter plate assays are currently needed for differentiation of agonistic, antagonistic, false-positive, and synergistic effects, whereby the latter are difficult to detect. For the analysis of sample mixtures (non-separated extracts), only the sum of the activity of all contained substances (sum parameter) can be determined via *in vitro* microtiter plate assays. In a mixture, individual opposing effects and thus opposing signals can cancel each other out and give a false sum result. Therefore, a planar multiplex bioassay was sought because it would provide due to the separation and effect differentiation more in-depth information about complex

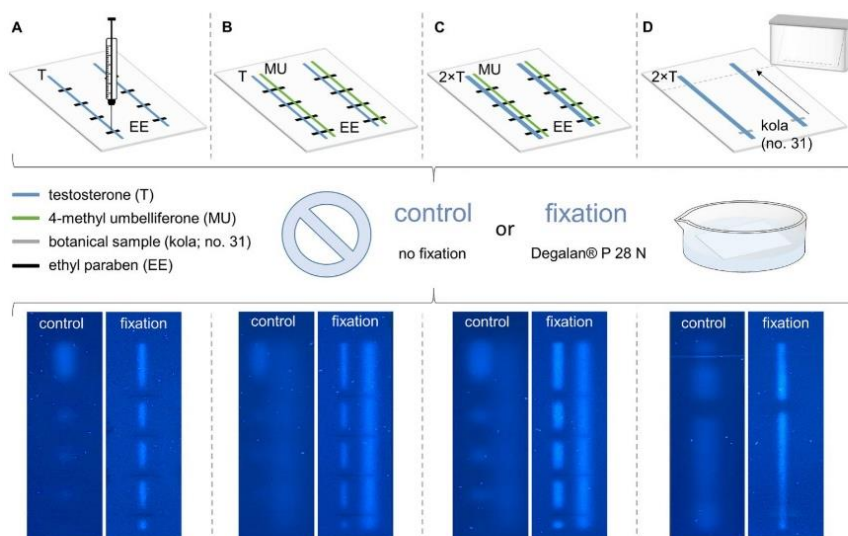


Fig. 1. Diffusion reduction via Degalan coating for NP-HPTLC^{fix}-pYAVAS. Application scheme and pYA(V)AS bioassay of ethyl paraben (A; 6-mm band, 1 µg/band; B and C; 10-mm band, 1.5 µg/band) and the sample kola (D; 6-mm band, 4 µL, separated with ethyl acetate – toluene – formic acid – water 16:4:3:2, V/V/V/V, up to 70 mm) on silica gel 60 F₂₅₄ MS-grade plates. Testosterone (T) was overlaid as 1 mm × 70-mm (A and B; 6 ng) or 2 mm × 70-mm (C and D; 12 ng) area and 4-methyl umbelliferone (MU, 500 ng) as 1 mm × 70-mm area (B and C). For each approach, one plate piece was coated with Degalan (0.25% W/V in *n*-hexane; 10 min) and the other one was carried as a control reference to check diffusion reduction at FLD 366 nm.

mixtures than the status quo. However, the reduction of zone diffusion was a prerequisite and critical to the success of this planar multiplex bioassay.

3.1. Tailoring the assay parameters, integrating the fixation (^{fix}) and verification (V)

Status quo pYAAS assays on RP-18 W- and NP-HPTLC plates (the latter without diffusion reduction) either have insufficient sensitivity or are prone to diffusion. RP and NP plates differ in their ability to adsorb and desorb substances in the aqueous bioassay buffer. A reduced sensitivity on RP-18 W plates is caused and explained as follows. After application and development, the molecules are mainly inside the porous layer. Since the microorganism are only applied to the upper surface layer (cells are too big to penetrate through the 6-nm particle pores), there is limited interaction between molecules and microorganism, since aqueous buffers have almost no elution strength and can hardly desorb the molecules from the RP-18 W-layer. In contrast, due to the opposite high elution strength of aqueous buffers on NP layers, molecules tend to diffuse here, enhancing interaction between substances and microorganism, resulting in higher sensitivity but diffuse zones.

Most comparable results to RP-18 W regarding T-stripe broadening and signal intensity were given on NP for 6 ng T (Fig. S1). The applied 1-mm T-stripe on the NP plate broadened to 3 mm during the long incubation with the aqueous bioassay, whereas the 3-mm stripe on the RP-18 W plate kept the same size. However, the diffusion complicated the evaluation of the bioautograms, especially for the intended multiplex bioassay and multicomponent sample mixtures arranged close together for side-by-side screening on the same plate. Parameters to overcome diffusion were studied based on an applied band pattern. Thus, results were obtained faster, as for integrating a development step. The applied band pattern of the antagonist EE was oversprayed by an agonist stripe to assess the influence on the antiandrogenic effect in the bioautogram. First attempts to reduce diffusion were carried out by varying the second incubation time for the substrate MUG. A 15-min incubation was too short, whereas a 30-min incubation was already found to be sufficient in the response (Fig. S2B). Hence, a 30-min incubation was selected for further experiments.

A zone fixation agent could reduce diffusion and improve the bioautogram evaluation. To the best of our knowledge, studies on the

reduction of zone diffusion on NP-HPTLC bioautograms have not been published to date, which is however, precondition for the analysis of multi-component mixtures. To fixate substances on the NP-HPTLC plate, the application of a polymer solution could be useful. Poly-D-lysine and polyethylene glycol seemed to be a good choice, as they are biocompatible and have already been used for experiments with cells (Kim, Baek, Han, Chung, & Jung, 2011; Alcantar, Aydil, & Israelachvili, 2000). Another method that can be taken into account is immersing the plate into Degalan, a polymerizing agent made of polyisobutyl methacrylate. It was reported to fixate the silica gel layer and thus overcome layer detachment during immunoassay applications (Brockhaus et al., 1981). The fixation of the silica gel layer could also lead to a fixation of the substances in the layer and thus a reduction in the observed zone diffusion.

The investigation and comparison of the different diffusion reduction agents mentioned showed that only Degalan had a positive influence on the sharpness of the bands (Fig. S3). A 10-min immersion in a 0.25% (W/V) Degalan solution in *n*-hexane was suited best. However, the automated immersion caused streaks upon plate withdrawal, especially for high T amounts. Hence, the plates were placed horizontally in a glass dish filled with Degalan. The robustness of the method was confirmed based on the usage of different glass dishes and inter-day and intra-day precisions (Fig. S4). Additionally, a one-month-old Degalan solution was used. All led to comparable results.

Optimal parameters regarding T amount and incubation time for the diffusion-reduced bioassay workflow on the NP plate were studied using EE-band patterns overlaid with a 2-mm T-stripe. The applied amounts were 0.2-fold, 2-fold, and 20-fold compared to the usually applied 6 ng onto a 1-mm broad area on the unfixated NP plate (Fig. S5A). The best results were achieved with 12 ng T per area and a cell incubation time of 4 h at 30 °C (Fig. S5B). A 37-°C incubation temperature was tested to simplify the workflow as the substrate incubation temperature was also 37 °C, which is the optimal temperature for substrate conversion by β-galactosidase (Purvis et al., 1991) but led to slightly poorer sensitivity with higher diffusion (Fig. S5C). So the 30-°C incubation for the cells was kept, as specified by the manufacturer.

Fluorescence reduction, obtained in the T-stripe of a sample track, may also be caused by physico-chemical quenching properties of a substance, which would lead to a false-positive antagonistic response. The identification and thereby exclusion of false-positive antagonists was newly integrated in the same workflow via overlay of a stripe of the



Fig. 2. Scheme of the new NP-HPTLC^{fix}-UV/Vis/FLD-pYAVAS-FLD workflow. The individual steps are listed for profiling of twelve samples on a 20-cm x 10-cm plate.

end product MU. If a dark zone was caused by fluorescence quenching and not by an antiandrogenic response, the fluorescence would similarly be reduced in this MU-stripe. In other words, an uninterrupted, homogeneous MU-stripe would verify a true antiandrogenic response. The conditions for the MU-stripe amount and area had to be studied to integrate the exclusion of false-positive antiandrogens and thus the verification (V) of true antiandrogens in complex mixtures. In reference to the example of kola (no. 31), which showed an antiandrogenic zone, the new pYAVAS-FLD bioassay protocol was developed. Different amounts from 10 ng to 5 µg of the 1 mm x 70-mm MU-stripe (Fig. S6A) were investigated to determine the equivalent fluorescent response as the 12-ng T-stripe, applied as reference on each plate. With decreasing amount of MU, the natural fluorescence decreased, already evident after application (Fig. S6B). After bioassay application, for MU-stripe amounts of 1–5 µg (500-ng interval), the fluorescence intensity was too bright and no stripe matched to the T-stripe intensity (Fig. S6C).

With regard to MU-stripe amounts of 100–500 ng (50-ng interval), a comparable fluorescence intensity to the T-stripe was achieved for the highest amount of MU (500 ng). For MU-stripe amounts of 10–50 ng (5-ng interval), fluorescence intensities were too low in comparison to the T-stripe in the bioautogram. After this fine-tuning of the relevant stripe amounts, the overlay of the two stripes made it a multiplex bioassay that provided biological signals of agonists and antagonists as well as physico-chemical signals of false-positives from the same sample in the same planar assay.

With the Degalan coating, the bioautogram revealed sharper T-stripes and EE-bands compared to the control reference plate without fixation. This proved a successful zone fixation (Fig. 1A). Using the same geometry of 1 mm x 70 mm for both stripes, the 6-ng T-stripe remained thinner than the MU-stripe (Fig. 1B). This was explained by the lower substance amounts of T (6 ng) versus MU (500 ng) and that the fluorescence of T was biologically produced on the plate (first upon reaction with the receptor) later than MU (present from the very beginning of the incubation and thus having more time for diffusion). Doubling the T width and volume resulted in comparable stripe intensities and geometries, which were equivalent in the fluorescence response (Fig. 1C).

In conclusion, the optimal assay parameters were found to be a T-stripe (2 mm x 70 mm, 12 ng) for antiandrogen detection, a MU-stripe (1 mm x 70 mm, 500 ng) for its verification, an integrated Degalan coating (0.25% W/V in *n*-hexane, 10 min) for diffusion reduction, as well as 4-h cell and 30-min substrate incubations. As proof, the developed zone fixation protocol (^{fix}) was applied to the sample kola (no. 31), which showed successfully a reduced diffusion on the NP plate (Fig. 1D).

3.2. Screening of 68 different botanicals for hormonal active substances and comparison to the status quo

The newly developed NP-HPTLC^{fix}-UV/Vis/FLD-pYAVAS-FLD protocol (Fig. 2) was applied to the effect-directed analysis of 68 different botanical samples and a solvent blank. The chromatograms at UV 254 nm, Vis, and FLD 366 nm provided additional information on how to interpret the bioassay (Fig. S7, Schreiner et al., 2021). Pigments have been reported to cause false-negative antiandrogenic responses (Klingelhöfer et al., 2020). UV-active substances could also reduce the fluorescence at FLD 366 nm. The very good reproducibility of the analysis is exemplarily given for the FLD 366 nm chromatogram (Fig. S7C versus Fig. 3A repeated after 6 months). A comparison of the images at FLD 366 nm before and after the bioassay is always recommended (Fig. 3A versus B). Natively blue fluorescent zones at FLD 366 nm may interfere with the biologically produced MU-blue fluorescence response. The native fluorescence could shine through after the bioassay and lead to false-positive androgenic responses, whereas a fluorescence quenching property could lead to false-positive results for antiandrogenic responses.

The bioautograms (Fig. 3B) showed MU-blue fluorescent bands in elder berry (no. 21), orange peel (no. 41), and lemon peel (no. 67) indicating androgens. One or more fluorescence-reducing zones indicating possible antiandrogens were detected for eucalyptus (no. 9), guarana (no. 16), kola (no. 31), orange peel (no. 41), licorice (no. 55), grape seeds and leaves (nos. 58 and 61), and hawthorn samples (nos. 62–64). Droplet formation caused by Degalan fixation was observed on some application zones (nos. 1, 4, 12, 15, 21, 41, 56, and 65) and whole tracks (nos. 16 and 37). However, such substance-dependent influences on the Degalan coating did not interfere with the result interpretation. The analysis of the 68 botanicals was compared with two status-quo methods to highlight the achieved progress. Firstly, the performance of the same workflow but without zone fixation showed highly diffused zones, which complicated the evaluation of the bioautogram (Fig. 3C, NP) and underlined the importance of fixation on the NP plate. In the samples nos. 6 and 15, and less in sample no. 37, some substances at a lower *hR_F* diffused more strongly and thereby bent the neighbouring T-stripes. This spreading effect was explained by substance structures

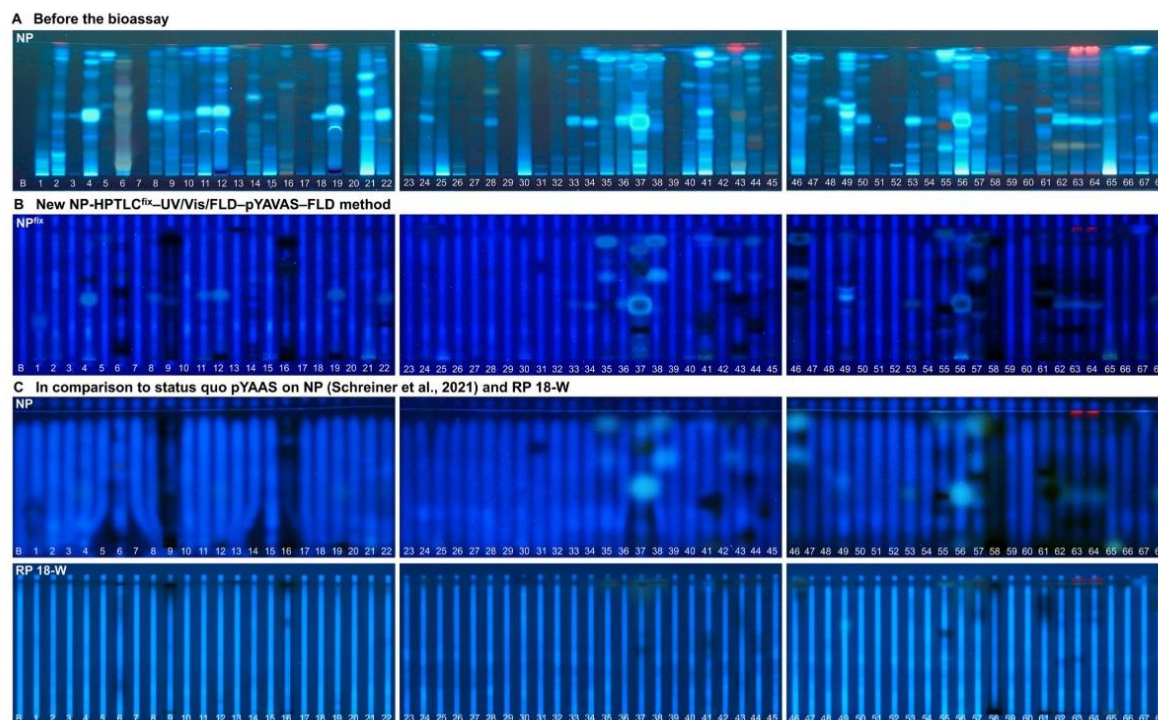


Fig. 3. NP-HPTLC^{fix}-UV/Vis/FLD-pYAVAS analysis of 68 botanicals compared to status quo on NP and RP-18 W. Botanical samples (4 μ L, 6-mm bands, nos. 1–68 assigned in Table S1 and solvent blank B for comparison) separated with ethyl acetate – toluene – formic acid – water (16:4:3:2; V/V/V/V) up to 70 mm on silica gel 60 F₂₅₄ MS-grade plates and RP-18 W. Chromatograms (A) and pYAVAS bioautograms of NP-HPTLC^{fix} (B; 12 ng testosterone (T) per 2 mm \times 70-mm area and coating with Degalan 0.25% W/V in *n*-hexane; 10 min). The bioautograms were compared with the status-quo bioautograms (C) on NP (6 ng T per 1 mm \times 70-mm area, as studied (Schreiner et al., 2021) and RP-18 W plates (230 ng T per 3 mm \times 66-mm area). All detected at FLD 366 nm.

highly prone to diffusion when getting in contact with the bioassay salts. In contrast, this spreading effect was effectively hindered via the Degalan coating (Fig. 3B), resulting in bioautograms with accurate T-stripes and sharp-bounded zones. Secondly, the performance of the reported workflow on RP-18 W plates (Klingelhöfer & Morlock, 2014) led to hardly detectable antagonistic zones (Fig. 3C, RP-18 W). Consequently, higher sample amounts need to be applied. Note that the hR_F values are only partially comparable between the NP and RP-18 W separations. The comparison to both status-quo methods clearly confirmed that the developed NP-HPTLC^{fix}-UV/Vis/FLD-pYAVAS-FLD protocol was more sensitive and led to sharper bands. The new bioassay was repeated several times and the good reproducibility and outcome were confirmed. This achievement was very helpful for the evaluation of complex mixtures. Especially presumed antagonistic zones near the solvent front were clearly detectable, as for ginger (no. 25), garlic (no. 30), star anise (no. 54), and chicory (no. 65). The best of two worlds, *i. e.* the sensitivity in detection on the NP and the zone sharpness on the RP-18 W, were combined in the new approach.

Twelve out of the 68 botanical samples showed a fluorescence reduction (Fig. 3B, nos. 4, 6, 9, 16, 25, 30, 31, 41, 54, 55, 65, and 66). These were applied again with increased band length to verify the antiandrogenic effect via the added MU-stripe (Fig. 4A). After separation, the samples revealed blue fluorescence in the chromatogram at FLD 366 nm (Fig. 4B). The T-stripe was not fluorescent after application, while the MU-stripe was already natively fluorescent. First in the bioautogram, both stripes exhibited fluorescence (Fig. 4C). True antagonistic activity was observed as fluorescence reduction of the T-stripe, whereas the MU-stripe had to be fluorescent at this position. This was given for several zones (Fig. 4C, marked*), *i. e.* in globe artichoke (no.

4), eucalyptus (no. 9), ginger (no. 25), garlic (no. 30), kola (no. 31), star anise (no. 54), chicory (no. 65), and cinnamon bark (no. 66). Digital evaluation of the antiandrogenic activity in the bioautogram at FLD 366 nm was exemplarily shown for garlic (no. 30) and kola (no. 31) using the open-source software quanTLC (Fichou & Morlock, 2018). Note that the inversion of negative peaks in case of a fluorescence reduction was not possible by the visionCATS software. Fenugreek (no. 6), guarana (no. 16), orange peel (no. 41), and licorice (no. 55) revealed a fluorescence reduction in both stripes. These were false-positive antiandrogenic zones and excluded as hits. Additionally, some substance zones (Fig. 4C, marked^o) enhanced the fluorescence of the T-stripe, which was interpreted as synergistic effect. This slight synergistic effects from the intensified signal response (>1) by combining a non-observed-effect compound (0) and an effect compound (1), *i. e.* $0 + 1 > 1$, were observed in various botanicals (Fig. 3B and 4C). After the bioassay, some samples revealed MU-blue fluorescent zones, which seemed to be androgenic (Fig. 4C). As they already fluoresced after chromatography (Fig. 4B), it had to be determined whether this fluorescence is generated by the biological response in the pYAVAS bioassay or shines through despite the bioassay treatment. The same workflow was repeated without cells in the medium. Since one zone showed a fluorescence on the plate without cells, this zone was proven not to be androgenic (Fig. 4D, marked[#]). For samples rich in such natively blue fluorescent substance zones, the exchange of the substrate is recommended. Fluorescein-di- β -D-galactopyranoside is suited, which generates the green fluorescent end product fluorescein. Then, the workflow needs not to be repeated without cells, as the natively blue fluorescent compounds can directly be differentiated from the green fluorescent androgens.

In conclusion, several antiandrogenic zones have been unequivocally

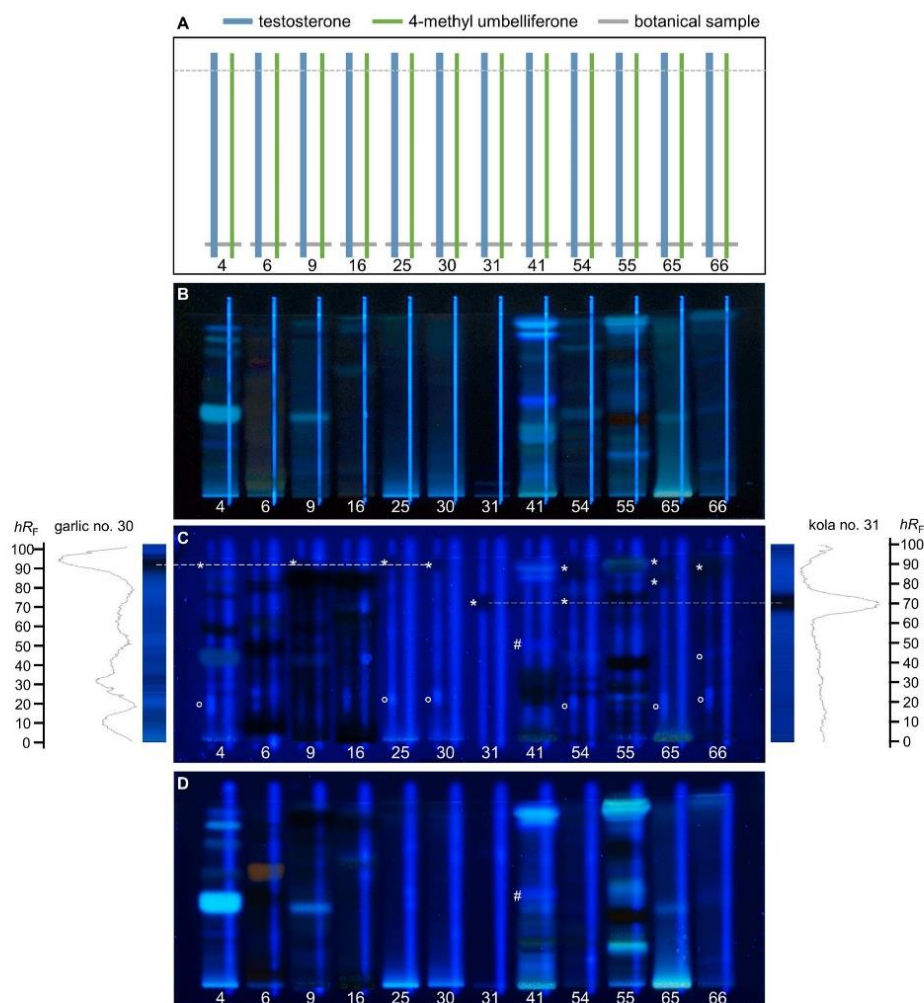


Fig. 4. NP-HPTLC^{fix}-UV/Vis/FLD-pYAVAS-FLD as multiplex planar assay. Botanical samples assumed to have antiandrogenic effects (8 μ L, 12-mm bands, separated with ethyl acetate – toluene – formic acid – water (16:4:3:2; V/V/V/V) up to 70 mm on silica gel 60 F₂₅₄ MS-grade) were overlaid with testosterone (T, 12 ng, 2 mm \times 70 mm) and 4-methyl umbelliferone (MU, 500 ng, 1 mm \times 70 mm) according to the plate design (A). The native fluorescence pattern (B; UV and Vis images not shown) and the HPTLC^{fix}-pYAVAS bioautogram (C; fixation with Degalan coating, 0.25% W/V in n-hexane; 10 min) were recorded at FLD 366 nm. Antiandrogenic zones reduced the fluorescence signal in the overlaid T-stripe (marked*), whereas synergistic zones enhanced it (marked#). One fluorescent zone (marked^o) was excluded to be an androgen, as its native fluorescence (B) was proven to be present after bioassay treatment without cells (D). Videodensitometric evaluation was exemplarily shown for garlic (no. 30) and kola (no. 31).

verified by this powerful multiplex bioassay that have not been previously reported in the literature. It is of general interest to elucidate the structures of these naturally occurring antiandrogens, which were observed for the first time in this study.

3.3. Identification of hormonal active substances via HRMS/MS

The combination with nuclear magnetic resonance spectroscopy could be an option for structure elucidation of the detected hormonal active substances (Azadniya, Goldoni, Bandiera, & Morlock, 2020). However, the recently reported 8D hyphenation for effect-directed non-target screening with automated zone elution and on-line HPLC-DAD-HRMS/MS (Schreiner & Morlock, 2021; Schreiner et al., 2021; Mehl et al., 2021) was found to be more straightforward. The selected botanicals were separated and evaluated with regard to UV-absorbing (Fig. 5A), native fluorescent (Fig. 5B), and bioactive

compounds (Fig. 5C). The correct position of each zone elution was successfully proven via the bioassay performance after heart cut elution (Fig. 5D). Since most of the antiandrogenic zones were near the solvent front and therefore many analytes were assumed at the same hR_F values, the eluted zone was orthogonally separated via an RP-HPLC column and detected by DAD-HRMS/MS to obtain pure mass and fragmentation spectra for structure elucidation (Fig. 5E). The information gained by heart cut-RP-HPLC-DAD-HRMS/MS measurement led to the tentative assignment of analytes, possibly responsible for the observed hormonal activity (Table S2). Proposed fragmentation pathways of most of these analytes are provided in Supplementary Schemes S1–S19. Spectral information for selected antiandrogenic compounds is exemplarily shown (Fig. 5F). Together with the exact monoisotopic masses, fragment profiles, and UV absorbance spectra the following compounds were identified to possess antiandrogenic potential. Apigenin (m/z 269.0457 [M – H][–]) was found in artichoke (no. 4, zone b). In a previous study

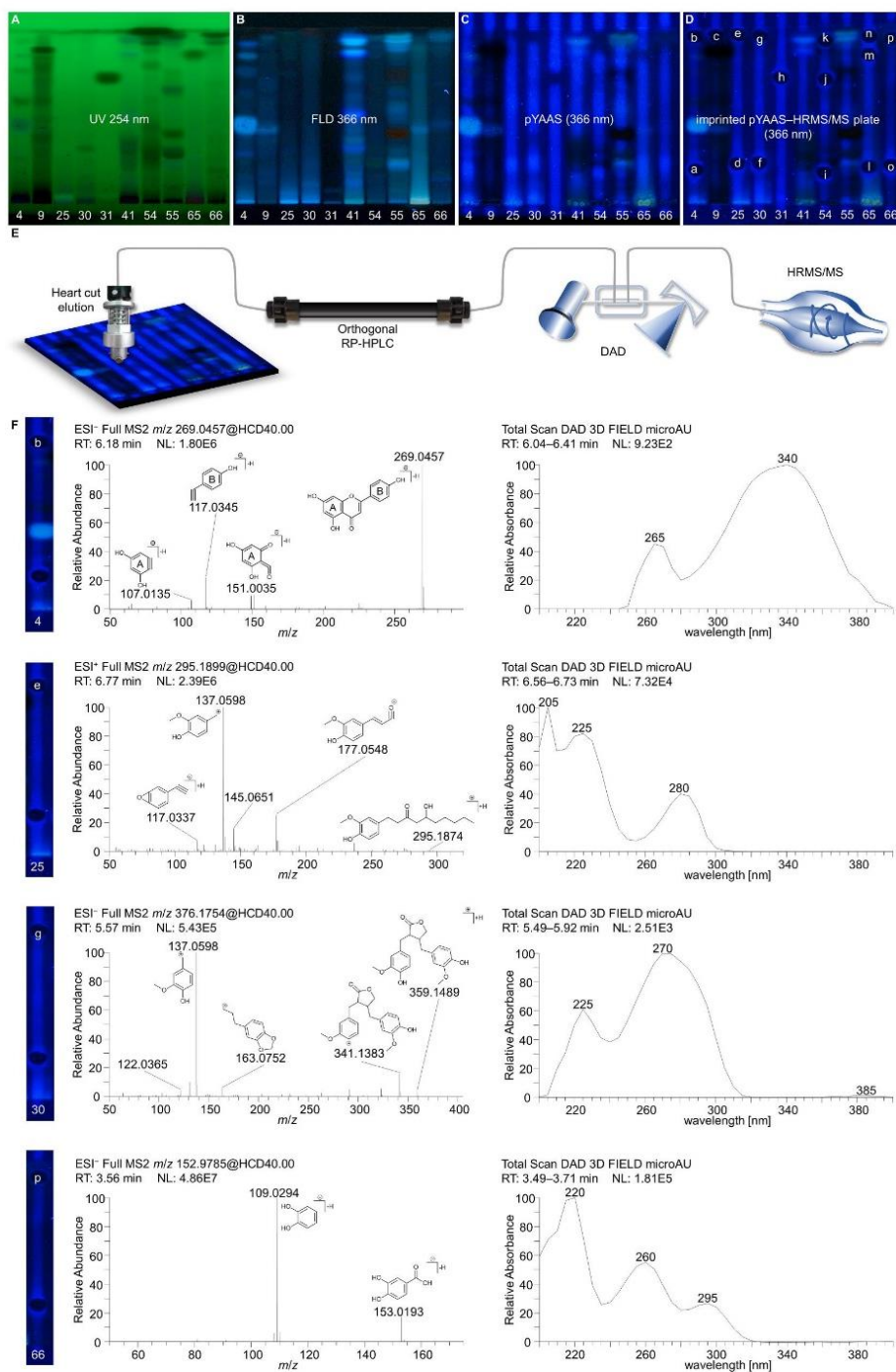


Fig. 5. NP-HPTLC^{fix}-UV/Vis/FLD-pYAAS-FLD heart cut-RP-HPLC-DAD-HRMS/MS of synergistic and antiandrogenic zones. Chromatograms of botanical samples with antiandrogenic effects (4 μ L, 6-mm bands, separated with ethyl acetate – toluene – formic acid – water (16:4:3:2; V/V/V/V) up to 70 mm on silica gel 60 F₂₅₄ MS-grade) at UV 254 nm (A), FLD 366 nm (B), and pYAAS bioautogram at FLD 366 nm (C). After heart cut elution of certain zones (D), RP-HPLC-DAD-HRMS/MS measurement was performed (E). Structure elucidation is exemplarily shown for apigenin in artichoke (no. 4, zone b), [6]-gingerol in ginger (no. 25, zone e), matairesinol in garlic (no. 30, zone g), and protocatechuic acid in cinnamon (no. 66, zone p) based on HRMS/MS and UV spectra (F).

(Schreiner et al., 2021), an apigenin standard was co-chromatographed under the same conditions, confirming its migration to the solvent front. Further studies proved, that this well-known phytoestrogen (Mbachu et al., 2020) also binds to the hAR (Singh et al., 2017). MS² fragments (Scheme S2) at m/z 117.0345 [M – H][–] and 151.0035 [M – H][–] originated according to Retro-Diels-Alder fragmentation mechanisms. The signal at m/z 107.0135 [M – H][–] was formed by a neutral CO₂-loss, matching with literature (Fabre, Rustan, de Hoffmann, & Quetin-Leclercq, 2001; Troalen, Phillips, Pegg, Barran, & Hulme, 2014). Another identified compound was [6]-gingerol (m/z 295.1899 [M + H]⁺) in ginger (no. 25, zone e). The obtained fragment ion at m/z 177.0909 [C₁₀H₁₁O₂]⁺ resulted from dehydration (–H₂O) and partial elimination of the oxidized alkyl chain (Scheme S4). Other fragments and the UV spectrum were consistent with literature (Asamenew et al., 2019). Except antiandrogenic properties, versatile bioactivities were described for [6]-gingerol, e. g., antioxidant (Dugasani et al., 2010), anti-inflammatory (Dugasani et al., 2010; Young et al., 2005), and analgesic (Young et al., 2005) activities. Besides [6]-gingerol, gingerenone A, [4]-gingerol, and [6]-shogaol (Table S2) were also found in this antiandrogenic zone, so it is not certain from which of these compounds the observed bioactivity actually originates. Zone g from garlic (no. 30) revealed two distinct signals: a highly abundant signal with a sulfuric isotope pattern and exact mass of allicin and a second one with spectral properties of matairesinol (m/z 359.1489 [M + H]⁺). Allicin was not assumed to bind to the hAR due to structural properties, whereas matairesinol was proven to interact with the hAR (Selvaraj et al., 2021). Positive fragment ions of m/z 137.0598, 163.0752, and 341.1383 (Mornar et al., 2020) confirmed matairesinol (Scheme S7). The latter fragment originated from dehydration, while others were adapted from common proposed lignan fragmentation pathways (Eklund, Backman, Kronberg, Smeds, & Sjöholm, 2008). In cinnamon bark (no. 66, zone p), the hydroxylated benzoic acid derivate protocatechuic acid was found as the most abundant signal. Experimental spectral data with a precursor ion at m/z 153.0193 [M – H][–], a product ion at m/z 109.0294 [M – H][–] (Ali et al., 2021), and the UV-absorbance maxima (Robbins, 2003) are consistent with theoretical data. The small benzoic acid derivate revealed only one fragment through the neutral loss of carboxylic acid (CO₂, Scheme S12). Androgen antagonistic effects for protocatechuic acid are not described. Only its interaction with the estrogenic steroid-hormone receptor was reported (Hu et al., 2014), which makes its binding also to the hAR plausible (Sohoni & Sumpter, 1998). Zone p incorporated hydroxybenzoic acid, cinnzeylanine, and anhydrocinnzeylanine (Table S2). Each of the analytes could be responsible for the observed antiandrogenic effect, what still needs to be confirmed with standards.

Complex mixtures were thoroughly analyzed by this 12D hyphenation from crude extract to the identification of individual hormonally active compounds. Each spectral/chromatographic information obtained from the same chromatographic run on the same surface about the sample is considered as one dimension (D) of hyphenation (Morlock & Schwack, 2010; Schreiner et al., 2021). The here developed 12D hyphenation provided information on substance polarity and hR_F value via chromatographic separation (1), on UV/Vis/FLD responses (2–4), on agonistic, antagonistic, false-positive, and synergistic effects (5–8), on coeluting compounds via orthogonal separation (9), on its individual signal responses via DAD (10) and HRMS (11) with fragmentation (12). For identification of a responsible compound with regard to the hormonal effect, all this information is important to find a reasonable data-supported match. The more information obtained from the sample zone, the easier it is to assign and prove identity.

4. Conclusions

For the first time, the developed workflow for a planar bioassay was shown to provide sharp zones on a normal phase plate. The achieved multiplex bioassay provided information on agonists, antagonists, false-

positives, and synergists from the same sample in the same planar bioassay. The powerful NP-HPTLC^{fix}-UV/Vis/FLD-pYAVAS-FLD method allowed, for the first time, unambiguous and accurate screening for androgens, verified antiandrogens, and synergists in the 68 botanicals. The innovative workflow is considered a milestone and transferable to other planar bioassays with long incubation times. Substantial improvements were achieved compared to state of the art bioassays. The hormonal activity of separated substances was detected with improved sensitivity compared to RP-18 W and with enhanced zone sharpness compared to NP due to the new Degalan coating technique HPTLC^{fix}. Integrating the identification of false-positive antagonistic responses verified the detection of antiandrogens. For the first time, true antiandrogenic substances were found in globe artichoke, eucalyptus, ginger, garlic, kola, star anise, chicory, and cinnamon. Synergistic effects that have not yet been described before were also discovered with this method in several samples. The presented generic screening is suitable for complex mixtures, although it is not possible to separate all analytes. An orthogonal column separation confirmed the co-elution of several substances in bioactive zones, and if so, an additional experiment has to be made to determine which analyte is responsible for the observed effect. Via HRMS/MS known phytochemicals such as apigenin and matairesinol were found in synergistic or antiandrogenic zones and for some of these substances hormonal activity has been described (considered as method proof). So these can be responsible for the effect, but for some identified compounds no interaction with the hAR has been described so far, which needs further in-depth studies for confirmation. To investigate bioactive analytes in individual samples in more detail, a 2D development on HPTLC could be used. The here demonstrated generic workflow of the developed 12D hyphenation NP-HPTLC^{fix}-UV/Vis/FLD-pYAVAS-FLD-heart cut-RP-HPLC-DAD-HRMS/MS can be transferred to other planar assays to gain in-depth knowledge and understanding of the actual effects in complex samples.

CRedit authorship contribution statement

T. Schreiner: Methodology, Investigation, Formal analysis, Writing – original draft. **A. Ronzheimer:** Methodology, Investigation, Formal analysis, Writing – original draft. **M. Friz:** Investigation. **G.E. Morlock:** Conceptualization, Methodology, Supervision, Funding acquisition, Project administration, Writing – review & editing.

Declaration of Competing Interest

The authors declare that they have no known competing financial interests or personal relationships that could have appeared to influence the work reported in this paper.

Acknowledgments

Thank is owed to Dorena Sauter for preparing plates, to Julia Heil for sample preparation, both in the Food Science working group, to Merck, Darmstadt, Germany for providing plates as well as to Röhm, Darmstadt, Germany for providing Degalan® P 28N. Instrumentation was partially funded by the Deutsche Forschungsgemeinschaft (DFG, German Research Foundation) - INST 162/536-1 FUGG and INST 162/471-1 FUGG.

Appendix A. Supplementary data

Supplementary data to this article can be found online at <https://doi.org/10.1016/j.foodchem.2022.133610>.

References

- Alcantar, N. A., Aydil, E. S., & Israelachvili, J. N. (2000). Polyethylene glycol-coated biocompatible surfaces. *Journal of Biomedical Materials Research*, *51*, 343–351.

- Ali, A., Wu, H., Ponnampalam, E. N., Cottrell, J. J., Dunshea, F. R., & Suleria, H. A. R. (2021). Comprehensive Profiling of Most Widely Used Spices for Their Phenolic Compounds through LC-ESI-QTOF-MS2 and Their Antioxidant Potential. *Antioxidants (Basel, Switzerland)*, 10.
- Asamenew, G., Kim, H. W., Lee, M. K., Lee, S. H., Kim, Y. J., Cha, Y. S., Yoo, S. M., & Kim, J.-B. (2019). Characterization of phenolic compounds from normal ginger (*Zingiber officinale* Rosc.) and black ginger (*Kaempferia parviflora* Wall.) using UPLC-DAD-QToF-MS. *European Food Research and Technology*, 245, 653–665.
- Azadnia, E., Goldoni, L., Bandiera, T., & Morlock, G. E. (2020). Same analytical method for both (bio)assay and zone isolation to identify/quantify bioactive compounds by quantitative nuclear magnetic resonance spectroscopy. *Journal of Chromatography A*, 1628, 461434.
- Azhagiya Singam, E. R., Tachachartvanich, P., La Merrill, M. A., Smith, M. T., & Durkin, K. A. (2019). Structural Dynamics of Agonist and Antagonist Binding to the Androgen Receptor. *Journal of Physical Chemistry B*, 123, 7657–7666.
- Bovee, T. F., Hoogenboom, L. A., Hamers, A. R., Traag, W. A., Zuidema, T., Aarts, J. M., ... Kuiper, H. A. (1998). Validation and use of the CALUX-bioassay for the determination of dioxins and PCBs in bovine milk. *Food additives and contaminants*, 15, 863–875.
- Bovee, T. F. H., Bor, G., Heskamp, H. H., Lasaroms, J. J. P., Sanders, M. B., & Nielen, M. W. F. (2009). Validation and application of a yeast bioassay for screening androgenic activity in calf urine and feed. *Analytica Chimica Acta*, 637, 225–234.
- Bowens, P., Lancova, K., Dip, R., Povilaityte, V., Stroka, J., & Naegeli, H. (2009). A new PCR-based bioassay strategy for the detection of type A trichothecenes in food. *The Analyst*, 134, 939–944.
- Brockhaus, M., Magnani, J. L., Blaszczyk, M., Steplewski, Z., Koprowski, H., Karlsson, K. A., ... Ginsburg, V. (1981). Monoclonal antibodies directed against the human Leu b blood group antigen. *Journal of Biological Chemistry*, 256, 13223–13225.
- Chen, J., Ahn, K. C., Gee, N. A., Gee, S. J., Hammock, B. D., & Lasley, B. L. (2007). Antiandrogenic properties of parabens and other phenolic containing small molecules in personal care products. *Toxicology and Applied Pharmacology*, 221, 278–284.
- Dugasani, S., Pichika, M. R., Nadarajah, V. D., Balijepalli, M. K., Tandra, S., & Korlakunta, J. N. (2010). Comparative antioxidant and anti-inflammatory effects of 6-gingerol, 8-gingerol, 10-gingerol and 6-shogaol. *Journal of Ethnopharmacology*, 127, 515–520.
- Eklund, P. C., Backman, M. J., Kronberg, L. A., Smeds, A. I., & Sjöholm, R. E. (2008). Identification of lignans by liquid chromatography-electrospray ionization ion-trap mass spectrometry. *Journal of Mass Spectrometry*, 43, 97–107.
- Fabre, N., Rustan, I., de Hoffmann, E., & Quetin-Leclercq, J. (2001). Determination of flavone, flavonol, and flavanone aglycones by negative ion liquid chromatography electrospray ion trap mass spectrometry. *Journal of the American Society for Mass Spectrometry*, 12, 707–715.
- Fichou, D., & Morlock, G. E. (2018). quanTLC, an online open-source solution for videodensitometric quantification. *Journal of chromatography. A*, 1560, 78–81.
- Gray, L. E., Ostby, J. S., & Kelce, W. R. (1994). Developmental effects of an environmental antiandrogen: The fungicide vinclozolin alters sex differentiation of the male rat. *Toxicology and Applied Pharmacology*, 129, 46–52.
- Häbe, T. T., & Morlock, G. E. (2020). Open source add on kit for automation of zone elution in planar chromatography. *Rapid Communications in Mass Spectrometry*, 34, e8631.
- Hu, F., Wang, J., Luo, H., Zhang, L., Luo, Y., Sun, W., ... Zou, K. (2014). Estrogenic and Antiestrogenic Activities of Protocatechic Acid. In S. Li, Q. Jin, X. Jiang, & J. J. Park (Eds.), *Frontier and Future Development of Information Technology in Medicine and Education* (pp. 3319–3327). Dordrecht: Springer Netherlands.
- Kim, Y. H., Back, N. S., Han, Y. H., Chung, M. A., & Jung, S. D. (2011). Enhancement of neuronal cell adhesion by covalent binding of poly-D-lysine. *Journal of Neuroscience Methods*, 202, 38–44.
- Klingelhofer, I., Hockamp, N., & Morlock, G. E. (2020). Non-targeted detection and differentiation of agonists versus antagonists, directly in bioprofiles of everyday products. *Analytica Chimica Acta*, 1125, 288–298.
- Klingelhofer, I., & Morlock, G. E. (2014). Sharp bounded zones link to the effect in planar chromatography-bioassay-mass spectrometry. *Journal of Chromatography A*, 1360, 288–295.
- Kröger, S., Hüskens, L., Fornasari, R., Scainelli, I., & Morlock, G. E. (2017). Effect directed fingerprints of 77 botanical extracts via a generic high-performance thin-layer chromatography method combined with assays and mass spectrometry. *Journal of Chromatography A*, 1529, 93–106.
- Kuroyanagi, M., Ueno, A., Hirayama, Y., Hakamata, Y., Gokita, T., Ishimaru, T., ... Sekita, S. (1996). Anti-Androgen Active Constituents from *Dalbergia cochinchinensis* Pierre. *Natural Medicines*, 50, 408–412.
- Lee, H. J., Lee, Y. S., Kwon, H. B., & Lee, K. (2003). Novel yeast bioassay system for detection of androgenic and antiandrogenic compounds. *Toxicology in Vitro*, 17, 237–244.
- Mbachtu, O. C., Howell, C., Simmler, C., Malca Garcia, G. R., Skowron, K. J., Dong, H., ... Dietz, B. M. (2020). SAR Study on Estrogen Receptor α/β Activity of (Iso)flavonoids: Importance of Prenylation, C-Ring (Un)Saturation, and Hydroxyl Substituents. *Journal of Agricultural and Food Chemistry*, 68, 10651–10663.
- Mehl, A., Schwack, W., & Morlock, G. E. (2021). On surface autosampling for liquid chromatography-mass spectrometry. *Journal of Chromatography A*, 1651, Article 462334.
- Mertl, J., Kirchnawy, C., Osorio, V., Grininger, A., Richter, A., Bergmair, J., ... Tacker, M. (2014). Characterization of estrogen and androgen activity of food contact materials by different in vitro bioassays (YES, YAS, ER α and AR CALUX) and chromatographic analysis (GC-MS, HPLC-MS). *PLoS One*, 9, e100952.
- Morlock, G. E. (2021). High-performance thin-layer chromatography combined with effect directed assays and high resolution mass spectrometry as an emerging hyphenated technology: A tutorial review. *Analytica Chimica Acta*, 1180, Article 338644.
- Morlock, G. E., Morlock, L. P., & Lemo, C. (2014). Streamlined analysis of lactose-free dairy products. *Journal of Chromatography A*, 1324, 215–223.
- Morlock, G. E., & Prabha, S. (2007). Analysis and stability of sucralose in a milk-based confection by a simple planar chromatographic method. *Journal of Agricultural and Food Chemistry*, 55, 7217–7223.
- Mornar, A., Buhac, T., Klarić, D. A., Klarić, I., Sertić, M., & Nigović, B. (2020). Multi-targeted Screening of Phytoestrogens in Food, Raw Material, and Dietary Supplements by Liquid Chromatography with Tandem Mass Spectrometry. *Food Analytical Methods*, 13, 482–495.
- Oisli, S. (2001). Effects of butylparaben on the male reproductive system in rats. *Toxicology and Industrial Health*, 17, 31–39.
- Purvis, I. J., Chotai, D., Dykes, C. W., Lubahn, D. B., French, F. S., Wilson, E. M., & Hobden, A. N. (1991). An androgen-inducible expression system for *Saccharomyces cerevisiae*. *Gene*, 106, 35–42.
- Riegraf, C., Reifferscheid, G., Belkin, S., Moscovici, L., Shakibai, D., Hollert, H., & Buchinger, S. (2019). Combination of yeast based in vitro screens with high performance thin-layer chromatography as a novel tool for the detection of hormonal and dioxin-like compounds. *Analytica Chimica Acta*, 1081, 218–230.
- Robbins, R. J. (2003). Phenolic acids in foods: An overview of analytical methodology. *Journal of Agricultural and Food Chemistry*, 51, 2866–2887.
- Schick, D., & Schwack, W. (2017). Planar yeast estrogen screen with resorufin- β -D-galactopyranoside as substrate. *Journal of Chromatography A*, 1497, 155–163.
- Schleich, S., Papaioannou, M., Baniahmad, A., & Matusch, R. (2006). Extracts from *Pygeum africanum* and other ethnobotanical species with antiandrogenic activity. *Planta Medica*, 72, 807–813.
- Schönborn, A., Schmid, P., Bräm, S., Reifferscheid, G., Ohlig, M., & Buchinger, S. (2017). Unprecedented sensitivity of the planar yeast estrogen screen by using a spray-on technology. *Journal of Chromatography A*, 1530, 185–191.
- Schreiner, T., & Morlock, G. E. (2021). Non target bioanalytical eight dimensional hyphenation including bioassay, heart-cut trapping, online desalting, orthogonal separations and mass spectrometry. *Journal of Chromatography A*, 1647, Article 462154.
- Schreiner, T., Sauter, D., Friz, M., Heil, J., & Morlock, G. E. (2021). Is Our Natural Food Our Homeostasis? Array of A Thousand Effect-Directed Profiles of 68 Herbs and Spices. *Frontiers in Pharmacology*, 12.
- Selvaraj, D., Muthu, S., Kotha, S., Siddamsetty, R. S., Andavar, S., & Jayaraman, S. (2021). Syringaresinol as a novel androgen receptor antagonist against wild and mutant androgen receptors for the treatment of castration resistant prostate cancer: Molecular docking, in-vitro and molecular dynamics study. *Journal of biomolecular structure & dynamics*, 39, 621–634.
- Singh, A. N., Baruah, M. M., & Sharma, N. (2017). Structure Based docking studies towards exploring potential anti-androgen activity of selected phytochemicals against Prostate Cancer. *Scientific Reports*, 7, 1955.
- Sohni, P., & Sumpter, J. P. (1998). Several environmental oestrogens are also anti-androgens. *Journal of Endocrinology*, 158, 327–339.
- Troalen, L. G., Phillips, A. S., Peggie, D. A., Barran, P. E., & Hulme, A. N. (2014). Historical textile dyeing with *Genista tinctoria* L.: A comprehensive study by UPLC MS/MS analysis. *Analytical Methods*, 6, 8915–8923.
- Young, H.-Y., Luo, Y.-L., Cheng, H.-Y., Hsieh, W.-C., Liao, J.-C., & Peng, W.-H. (2005). Analgesic and anti-inflammatory activities of 6-gingerol. *Journal of Ethnopharmacology*, 96, 207–210.
- Zierau, O., Morrissey, C., Watson, R. W. G., Schwab, P., Kolba, S., Metz, P., & Vollmer, G. (2003). Antiandrogenic activity of the phytoestrogens naringenin, 6-(1,1-dimethylallyl)naringenin and 8-prenylnaringenin. *Planta Medica*, 69, 856–858.

Supplementary Information

Multiplex planar bioassay with reduced diffusion on normal phase, identifying androgens, verified antiandrogens and synergists in botanicals via 12D hyphenation

*T. Schreiner, A. Ronzheimer, M. Friz, G.E. Morlock**

Justus Liebig University Giessen, Institute of Nutritional Science, Chair of Food Science,
Heinrich-Buff-Ring 26-32, 35392 Giessen, Germany

Dedicated to the 70th birthday of
Prof. Dr. Wolfgang Schwack, University of Hohenheim, Stuttgart, Germany

*Corresponding author. Tel.: +49 641 9939141, fax: +49 641 9939149, E-mail address:
Gertrud.Morlock@uni-giessen.de (G.E. Morlock)

Table of contents

Page S–5	Text S1. Materials and methods
Page S–7	Table S1. List of the 68 investigated botanicals. Botanical name, plant part, and sample weights (<i>W</i>), extracted with 5 mL methanol (*marked: filtered through 0.45 µm syringe PTFE filter).
Page S–8	Table S2. Tentative HRMS signal assignments. NP-HPTLC–pYAAS–RP–HPLC–DAD–HRMS/MS signals of bioactive zones.
Page S–12	Fig. S1. Agonist stripes of the status quo for comparison. pYAAS bioautograms at FLD 366 nm of parabens overlaid with testosterone on NP silica gel 60 F ₂₅₄ MS-grade (6 ng, 1 mm × 70 mm) compared to less sensitive but more sharp RP-18 W (230 ng, 3 mm × 70 mm).
Page S–14	Fig. S2. Determination of substrate incubation time. Application scheme (A) and pYAAS bioassay recorded at FLD 366 nm (B) of ethyl paraben (1 µg/band) overlaid with testosterone (6 ng, 1 mm × 70 mm) on silica gel 60 F ₂₅₄ MS-grade plate cut into four 2 cm × 10-cm pieces. 4-Methyl umbelliferyl-β-D-galactopyranoside (MUG) incubation time varied from 15–60 min.
Page S–15	Fig. S3. Diffusion reduction potential of different reagents. pYAAS bioautograms at FLD 366 nm of 5–50 ng per 6-mm band testosterone (T) on silica gel 60 F ₂₅₄ MS-grade. A plate without fixation was used as control (A). Diffusion reduction was investigated with sprayed on 0.01% (<i>W/V</i>) solution of poly-D-lysine (B), by immersion in 0.25% (C–E), or 0.5% (F–H) Degalan (<i>W/V</i>) for 5 min (C and F), 10 min (D and G), or 15 min (E and H), as well as with sprayed on 5% (I and K), or 10% (J and L) polyethylene glycol (PEG) 2000 (<i>W/V</i>), and 5% (M and O), 8% (P), or 10% (N) PEG 8000 (<i>W/V</i>), added either to the yeast cell suspension (I–J , M–N) or to the 4-methyl umbelliferyl-β-D-galactopyranoside substrate solution (K–L , O–P).
Page S–16	Fig. S4. Robustness of fixation with Degalan. pYAAS bioautograms at FLD 366 nm of 0.5–5 ng per 6-mm band testosterone (T) on silica gel 60 F ₂₅₄ MS-grade. A plate without fixation was used as control and the others were coated with freshly prepared Degalan (0.25% <i>W/V</i> in <i>n</i> -hexane; 10 min) in a crystallizing

	dish or a rectangular deco glass bowl. For one plate, a one-month-old Degalan solution was used.
Page S–17	Fig. S5. Experimental determination of testosterone amount and incubation time for NP-HPTLC^{fix}-pYAAS. Ethyl paraben (EE; 1 µg/band, 6-mm bands) was overlaid with different amounts of testosterone (T, 1.2–120 ng/area, 2 mm × 70 mm) on silica gel 60 F ₂₅₄ MS-grade according to plate design (A). Comparison of fluorescence intensity after Degalan coating (0.25% W/V in <i>n</i> -hexane; 10 min) and performing the pYAAS bioassay at 30 °C (B) versus 37 °C (C), studying a 2–5 h of incubation period; resulting bioautogram detected at FLD 366 nm.
Page S–18	Fig. S6. Experimental determination of MU reference area for NP-HPTLC^{fix}-pYAVAS. Kola (no. 31, 4 µL, 6-mm bands, separated with ethyl acetate – toluene – formic acid – water (16:4:3:2; V/V/V/V) up to 70 mm on silica gel 60 F ₂₅₄ MS-grade) was overlaid with 4-methyl umbelliferone (MU, 10–5000 ng/area, 1 mm × 70 mm) and testosterone (T, 12 ng/area, 2 mm × 70 mm) according to plate design (A). Application (B) and the HPTLC ^{fix} -pYAVAS bioautogram (C; fixation with Degalan coating, 0.25% W/V in <i>n</i> -hexane; 10 min) were recorded at FLD 366 nm. The fluorescence intensity of the MU-stripes was compared to the T-stripe containing an antiandrogenic zone (marked*).
Page S–19	Fig. S7. NP-HPTLC–UV/Vis/FLD of 68 botanicals (Schreiner et al., 2021). Chromatograms of botanical samples (4 µL, 6-mm bands, nos. 1–68 assigned in Table S1 and solvent blank B for comparison) separated with ethyl acetate – toluene – formic acid – water (16:4:3:2; V/V/V/V) up to 70 mm on silica gel 60 F ₂₅₄ MS-grade plates recorded at UV 254 nm (A), white light illumination (B), and FLD 366 nm (C).
Page S–20	Scheme S1. Proposed fragmentation pathway of luteolin according to Retro-Diels-Alder fragmentation mechanisms.
Page S–21	Scheme S2. Proposed fragmentation pathway of apigenin.
Page S–22	Scheme S3. Proposed fragmentation pathway of eucalyptone.

Page S–23	Scheme S4. Proposed fragmentation pathways of [4]- and [6]-gingerol.
Page S–24	Scheme S5. Proposed fragmentation pathways of gingerenone A.
Page S–25	Scheme S6. Proposed fragmentation pathway of [6]-shogaol.
Page S–26	Scheme S7. Proposed fragmentation pathway of matairesinol.
Page S–27	Scheme S8. Proposed fragmentation pathway of caffeine.
Page S–28	Scheme S9. Proposed fragmentation pathway of quercetin.
Page S–29	Scheme S10. Proposed fragmentation pathway of naringenin.
Page S–30	Scheme S11. Proposed fragmentation pathway of eugenol (glucoside).
Page S–31	Scheme S12. Proposed fragmentation pathway of protocatechuic acid.
Page S–32	Scheme S13. Proposed fragmentation pathway of veranisatin B.
Page S–33	Scheme S14. Proposed fragmentation pathway of 5-hydroxymethylfurfural.
Page S–34	Scheme S15. Proposed fragmentation pathway of ferulic acid.
Page S–35	Scheme S16. Proposed fragmentation pathway of hydroxytyrosol O-glucoside.
Page S–36	Scheme S17. Proposed fragmentation pathway of apipaeonoside.
Page S–37	Scheme S18. Proposed fragmentation pathway of cinnzeylanine.
Page S–38	Scheme S19. Proposed fragmentation pathway of anhydrocinnzeylanine.
Page S–39	References for Table S2

Text S1. Materials and methods

Chemicals and materials

Methyl 4-hydroxybenzoate (methyl paraben, $\geq 99\%$), polyethylene glycol (PEG) 2000 (molecular weight 1,800–2,200 Da), and PEG 8000 (molecular weight 7,300–9,000 Da) were obtained from Carl Roth, Karlsruhe, Germany. Propyl 4-hydroxybenzoate (propyl paraben, $>99\%$) and poly-D-lysine hydrobromide (lyophilized, molecular weight 70,000–150,000 Da) were delivered by Sigma-Aldrich Fluka, Steinheim, Germany. Butyl 4-hydroxybenzoate (butyl paraben, $>99.0\%$) were purchased from TCI Deutschland, Eschborn, Germany.

Standard solutions

Additional standard solutions of T were prepared as dilution series to concentrations of 50 $\mu\text{g/mL}$, 10 $\mu\text{g/mL}$, and 150 ng/mL . The EE solution was further diluted to 100 $\mu\text{g/mL}$ and MU was further diluted to 50 $\mu\text{g/mL}$, 10 $\mu\text{g/mL}$, and 5 $\mu\text{g/mL}$.

Investigation of assay parameters and layer coating

EE (1 $\mu\text{g/band}$) was applied four times as four stacked 6-mm bands on a 2 cm \times 10-cm plate and oversprayed orthogonally with a 1 mm \times 70-mm area of T (6 $\mu\text{g/area}$). The dried plate was cut into four 2 cm \times 10-cm pieces and the bioassay was performed as in 2.7 without fixation and verification and with MUG incubation times of 15–60 min.

Band patterns of T were applied as four stacked 6-mm bands in ascending amounts of 5, 10, 20, and 50 ng/band on 2 cm \times 10-cm plate pieces. The pYAAS bioassay was performed (as in 2.7) on one plate piece without fixation agent as control. On another plate piece, the poly-D-lysine hydrobromide solution (0.01% in ethanol, *W/V*) was piezoelectrically sprayed (1 mL, yellow nozzle, level 6, Derivatizer), followed by plate drying for 1 min. For Degalan coating, plates were immersed in 0.25% or 0.5% Degalan solution (each *W/V* in *n*-hexane; each 40 mL in a 10 cm \times 10-cm glass chamber of TLC Chromatogram Immersion Device) for 5–15 min, followed by plate drying for 1 min. After poly-D-lysine or Degalan application, the bioassay was performed, whereas PEG 2000 and 8000 (each 40% aqueous, *W/V*) were

applied during the bioassay either in the cell suspension or in the substrate. For preparation of the PEG-containing cell suspensions, the cells were prepared each in medium containing 5% (1.75 mL medium and 250 μ L PEG) and 10% PEG (1.5 mL medium and 500 μ L PEG), instead of 2 mL pure medium. The bioassay was performed as described in 2.7. For preparation of the PEG-containing substrate solutions, the substrate was dissolved in 3 mL citrate buffer containing 5% (2.613 mL buffer and 387 μ L PEG) and 10% PEG (2.225 mL buffer and 775 μ L PEG), instead of pure citrate buffer. These substrate solutions were sprayed (red nozzle, level 6) on the incubated plates. The PEG 8000 had to be further diluted by another 750 μ L of citrate buffer because of its viscosity, resulting in a PEG 8000 concentration of only 8% and a lower amount of MUG.

Degalan fixation was further analyzed by applying band patterns of T as four stacked 6-mm bands in descending amounts of 0.5, 1, 2, and 5 ng/band on 2 cm \times 10-cm plate pieces. On one plate piece, the pYAAS bioassay was performed without fixation as control. The other plates were coated with Degalan by placing them horizontally in the 0.25% Degalan solution (W/V in *n*-hexane) for 10 min in a crystallizing dish (23 cm \times 10 cm; Schott, Mayence, Germany) covered with aluminium foil or in a rectangular deco glass tank (21 cm \times 11 cm \times 4 cm) covered with a rectangular glass plate (27 cm \times 13 cm). Experiments were repeated on another day.

To optimize the parameters for a bioassay with Degalan fixation, a band pattern of EE was applied as four stacked 6-mm bands in ascending amounts of 0.1, 0.2, 0.5, and 1 μ g/band on two 20 cm \times 10-cm plate. EE was oversprayed with 2 mm \times 70-mm T-stripes of 1.2, 12, and 120 ng/area. The plate was coated with Degalan (0.25% W/V in *n*-hexane, 10 min, 250 mL filled in a crystallizing dish, 23 cm \times 10 cm Schott, Mayence, Germany) and cut into 7 pieces to investigate different bioassay incubation times of 2–5 h at temperatures of 30 °C and 37 °C. The sample kola (no. 31) was applied 30-times on three 10 cm \times 10-cm plates, developed in a 10 cm \times 10-cm twin trough chamber (as in 2.7) and oversprayed orthogonally with descending amounts of MU (5–10 ng/area) on nine tracks each and one T-stripe of 12 ng/area. Plates were coated with Degalan and bioassay was performed as described.

Table S1. List of the 68 investigated botanicals: Botanical name, plant part, and sample weights (*W*), extracted with 5 mL methanol (*marked: filtered through 0.45 µm syringe PTFE filter).

No.	Common name	Botanical name	Plant part	<i>W</i> [mg]
1	Acerola	<i>Malpighia glabra</i> L. [Malpighiaceae].	fruits	501.5
2	Horehound, white	<i>Marrubium vulgare</i> L. [Lamiaceae]	herb	500.1
3	Apple*	<i>Malus sylvestris</i> (L.) Mill. [Rosaceae]	peel	500.7
4	Artichoke, globe	<i>Cynara cardunculus</i> subsp. <i>scolymus</i> (L.) [Asteraceae]	leaves	501.3
5	Basil	<i>Ocimum basilicum</i> L. [Lamiaceae]	herb	500.6
6	Fenugreek	<i>Trigonella foenum-graecum</i> L. [Fabaceae]	seeds	499.9
7	Stinging nettle*	<i>Urtica dioica</i> L. [Urticaceae]	leaves	501.5
8	Blackberry	<i>Rubus fruticosus</i> L. [Rosaceae]	leaves	500.6
9	Eucalyptus	<i>Eucalyptus globulus</i> Labill. [Myrtaceae]	leaves	499.7
10	Fennel	<i>Foeniculum vulgare</i> Mill. [Apiaceae]	fruits	499.9
11	Fruit tea, yellow	not available	unknown	501.3
12	Fruit tea, red	not available	unknown	502.6
13	Galangal	<i>Alpinia officinarum</i> Hance. [Zingiberaceae]	roots	501.8
14	Ginkgo	<i>Ginkgo biloba</i> L. [Ginkgoaceae]	leaves	502.7
15	Ginseng	<i>Panax ginseng</i> C.A.Mey. [Araliaceae]	roots	502.3
16	Guarana	<i>Paullinia cupana</i> Kunth [Sapindaceae]	seeds	498.8
17	Dog rose	<i>Rosa canina</i> L. [Rosaceae]	fruits	501.0
18	Blueberry, European	<i>Vaccinium myrtillus</i> L. [Ericaceae]	fruits	501.2
19	Hibiscus	<i>Hibiscus rosa-sinensis</i> L. [Malvaceae]	blossoms	499.6
20	Raspberry	<i>Rubus idaeus</i> L. [Rosaceae]	juice concentrate from fruits	503.0
21	Elder berry	<i>Sambucus nigra</i> L. [Adoxaceae]	fruits	501.4
22	Elder flower	<i>Sambucus nigra</i> L. [Adoxaceae]	blossoms	502.5
23	Honeybush*	<i>Cyclopia genistoides</i> (L.) R.Br. [Fabaceae]	leaves, branches, blossoms	499.3
24	Hop	<i>Humulus lupulus</i> L. [Cannabaceae]	blossoms	502.1
25	Ginger	<i>Zingiber officinale</i> Roscoe [Zingiberaceae]	roots	499.0
26	Jasmine*	<i>Jasminum officinale</i> L. [Oleaceae]	blossoms	499.2
27	Cassis	<i>Ribes nigrum</i> L. [Grossulariaceae]	juice concentrate from fruits	500.7
28	Chamomile	<i>Matricaria chamomilla</i> L. [Asteraceae]	blossoms	499.3
29	Cardamom*	<i>Elettaria cardamomum</i> (L.) Maton [Zingiberaceae]	fruits	499.6
30	Garlic	<i>Allium sativum</i> L. [Amaryllidaceae]	bulbs	499.9
31	Kola*	<i>Cola nitida</i> (Vent.) Schott & Endl. [Malvaceae]	seeds	500.8
32	Coriander	<i>Coriandrum sativum</i> L. [Apiaceae]	fruits	501.3
33	Caraway	<i>Carum carvi</i> L. [Apiaceae]	fruits	500.0

No.	Common name	Botanical name	Plant part	W [mg]
34	Lovage	<i>Levisticum officinale</i> W.D.J.Koch [Apiaceae]	roots	499.6
35	Marjoram	<i>Origanum majorana</i> L. [Lamiaceae]	herb	502.4
36	Yerba mate*	<i>Ilex paraguariensis</i> A.St.-Hil. [Aquifoliaceae]	leaves, roasted	499.6
37	Yerba mate	<i>Ilex paraguariensis</i> A.St.-Hil. [Aquifoliaceae]	leaves	500.2
38	Lemon balm	<i>Melissa officinalis</i> L. [Lamiaceae]	leaves	500.6
39	Clove*	<i>Syzygium aromaticum</i> (L.) Merr. & L.M. Perry [Myrtaceae]	flower buds	501.9
40	Orange	<i>Citrus × aurantium</i> L. [Rutaceae]	blossoms	499.7
41	Orange	<i>Citrus × aurantium</i> L. [Rutaceae]	peel	501.1
42	Oregano	<i>Origanum vulgare</i> L. [Lamiaceae]	herb	501.5
43	Passionflower	<i>Passiflora incarnata</i> L. [Passifloraceae]	blossoms	501.1
44	Peppermint	<i>Mentha × piperita</i> L. [Lamiaceae]	leaves	500.3
45	Rooibos*	<i>Aspalathus linearis</i> (Burm.f.) R. Dahlgren [Fabaceae]	leaves	500.7
46	Rosemary*	<i>Salvia Rosmarinus</i> Spenn. [Lamiaceae]	leaves	500.9
47	Sage	<i>Salvia officinalis</i> L. [Lamiaceae]	leaves	499.9
48	Sea buckthorn	<i>Hippophae rhamnoides</i> L. [Elaeagnaceae]	fruits	501.9
49	Horsetail	<i>Equisetum arvense</i> L. [Equisetaceae]	herb	499.3
50	Yarrow*	<i>Achillea millefolium</i> L. [Asteraceae]	herb	501.6
51	Celeriac	<i>Apium graveolens</i> L. [Apiaceae]	bulb	501.3
52	Coneflower	<i>Echinacea angustifolia</i> DC. [Asteraceae]	herb and roots	499.1
53	Plantain	<i>Plantago lanceolata</i> L. [Plantaginaceae]	leaves	500.5
54	Star anise	<i>Illicium verum</i> Hook.f. [Schisandraceae]	fruits	500.3
55	Licorice	<i>Glycyrrhiza glabra</i> L. [Fabaceae]	roots	500.3
56	Siberian ginseng	<i>Eleutherococcus senticosus</i> (Rupr. & Maxim.) Maxim. [Araliaceae]	roots	503.4
57	Thyme	<i>Thymus vulgaris</i> L. [Lamiaceae]	herb	499.6
58	Grape*	<i>Vitis vinifera</i> L. [Vitaceae]	seed	499.9
59	Grape	<i>Vitis vinifera</i> L. [Vitaceae]	peel	499.7
60	Juniper	<i>Juniperus communis</i> L. [Cupressaceae]	fruits	501.5
61	Grape	<i>Vitis vinifera</i> L. [Vitaceae]	leaves	501.2
62	Hawthorn	<i>Crataegus</i> sp. [Rosaceae]	leaves and blossoms	499.7
63	Hawthorn leaves (Batch 1)	<i>Crataegus</i> sp. [Rosaceae]	leaves	501.8
64	Hawthorn leaves (Batch 2)	<i>Crataegus</i> sp. [Rosaceae]	leaves	499.9
65	Chicory	<i>Cichorium intybus</i> L. [Asteraceae]	roots	501.1
66	Cinnamon	<i>Cinnamomum verum</i> J.Presl [Lauraceae]	bark	501.5
67	Lemon	<i>Citrus × limon</i> (L.) Osbeck [Rutaceae]	peel	500.7
68	Lemon verbena	<i>Aloysia citridora</i> Paláu [Verbenaceae]	leaves	500.4

Table S2. Tentative HRMS signal assignments: NP-HPTLC-pYAAS-RP-HPLC-DAD-HRMS/MS signals of bioactive zones.

Zone	Botanical (no.4)	Observed effect	hR_f	Retention time [min]	Molecular formula	Adduct	Precursor [m/z]	$\Delta m/z$ [ppm]	MS^2 fragments [m/z]	Proposed fragment formula	$\Delta m/z$ [ppm]	λ_{max} [nm]	Tentative assignment	Literature
a	artichoke (no.4)	synergy	19	4.04	$C_9H_{10}O_3$	[M+H] ⁺	167.0703	-0.11	123.0443 106.0417	$[C_7H_6O_2+H]^+$ $[C_7H_5O+H]^+$	-1.74 -3.53		p -dihydrocoumaric acid unknown	(Rouphael et al., 2016)
							424.2566	0.49	389.1734*	[M+NH ₄] ⁺				
							429.2121	0.27	341.1518*	[M+Na] ⁺				
							445.1859	0.50	209.1550*	[M+K] ⁺				
b	artichoke (no.4)	antiandrogen	96	5.83	$C_{15}H_{10}O_6$	[M+H] ⁺	287.0550	0.16	199.0400	$[C_{12}H_{10}O_3-H]^-$	0.30		luteolin	(Abu-Reidah et al., 2013; Sánchez-Rabateda et al., 2003; Singh et al., 2017)
							285.0405	-0.09	175.0400	[M-H] ⁻	0.45			(Singh et al., 2017; Abu-Reidah et al., 2013; Sánchez-Rabateda et al., 2003; Kolle et al., 2010)
							269.0457	-0.41	151.0035	[M-H] ⁻	-0.20	265, 340	apigenin	
									117.0345	$[C_8H_6O-H]^-$	0.95			
c	eucalyptus (no. 9)	antiandrogen	97	5.95	$C_{10}H_{14}O_3$	[M+H] ⁺	183.1014	1.10	137.0972	$[C_8H_{10}O-H]^-$	-0.08		4-ethylsyringol	(del Rio et al., 2005)
							181.0871	-0.50		[M-H] ⁻				
							485.2550	-0.99	207.0300	[M-H] ⁻	-0.68		eucalyptone	(Osawa et al., 1995; Dos Santos et al., 2019)
									153.1278*	[M+H] ⁺			unknown	
d	ginger (no. 25)	synergy	23	4.58	$C_{18}H_{30}O_8$	[M+H] ⁺	351.2022	-2.32	153.1278*	$[C_{11}H_{15}O_2]^-$	1.33		[4]-gingerol	(Jiang et al., 2005)
							368.2290	-3.11	135.1172*	[M+NH ₄] ⁺	1.86			
							373.1842	-2.38	107.0860*	[M+Na] ⁺	2.35		gingerone A	(Han et al., 2015)
							389.1579	-1.78	81.0708*	[M+K] ⁺	2.18			
e	ginger (no. 25)	antiandrogen	97	5.90	$C_{21}H_{32}O_4$	[M+H] ⁺	349.1869	-0.42	177.0913	$[C_{10}H_{11}O_2]^-$	2.52		[6]-gingerol	(Park & Jung, 2012)
							385.1640	-1.37		[M+Cl] ⁻	2.29			
							395.1924	-0.34		[M+HCOO] ⁻	3.70	220, 280		
							249.1487	-0.56	145.0651	[M-H ₂ O+H] ⁺	4.09			
		267.1592	-0.54	*145.0651	[M+H] ⁺									
		289.1411	-0.13	137.0600	[M+Na] ⁺									
		305.11494	0.09	*117.0703	[M+K] ⁺									
		357.1710	-3.86	179.0704	[M+H] ⁺									
		374.1965	-0.88	163.0756	[M+NH ₄] ⁺									
		379.1516	-0.06	137.0599	[M+Na] ⁺									
		395.1256	-0.25	131.0494	[M+Na] ⁺									
		277.1795	1.30	177.0909	[M+K] ⁺									
		295.1899	1.78	*145.0651	[M+H] ⁺									
		312.2165	1.55	137.0597	[M+NH ₄] ⁺									
		317.1719	1.39	117.0337	[M+Na] ⁺									
		333.1457	1.67		[M+K] ⁺									

Zone	Botanical	Observed effect	hR_F	Retention time [min]	Molecular formula	Adduct	Precursor [m/z]	$\Delta m/z$ [ppm]	MS ² fragments [m/z]	Proposed fragment formula	$\Delta m/z$ [ppm]	λ_{max} [nm]	Tentative assignment	Literature		
f	garlic (no. 30)	synergy	23	4.04	$C_{19}H_{14}O_3$	[M-H] ⁻	293.1760	1.67								
							[M+H] ⁺	277.1796	0.94	177.0909	[C ₁₁ H ₁₃ O ₃] ⁺	3.70		[6]-shogaol	(Deng et al., 2015; Park & Jung, 2012; Jiang et al., 2005)	
							[M+NH ₄] ⁺	294.2060	1.26	137.0597	[C ₈ H ₉ O ₂] ⁺	4.34				
							[M+Na] ⁺	299.1614	1.19							
							[M+K] ⁺	315.1352	1.56	no						
							[M+H] ⁺	291.1030	-4.94	no						
							[M-H] ⁻	289.0865	1.66	fragments						
							[M+H] ⁺	163.1329	-0.42	no						
							[M+NH ₄] ⁺	180.1595	-0.50	fragments						
							[M+Na] ⁺	185.1146	1.06							
g	garlic (no. 30)	antiandrogen	96	5.56	$C_{20}H_{22}O_6$	[M-H ₂ O+H] ⁺	341.1385	-0.44	341.1383	[C ₂₀ H ₂₁ O ₆] ⁺	1.82				(Horn-Ross et al., 2000; Selvaraj et al., 2021)	
							[M+H] ⁺	359.1489	0.16	163.0752	[C ₁₀ H ₁₁ O ₃] ⁺	4.45				
							[M+NH ₄] ⁺	376.1757	-0.49	137.0598	[C ₈ H ₉ O ₂] ⁺	3.03				
							[M+Na] ⁺	381.1310	-0.23							
							[M+K] ⁺	397.1049	-0.28	no						
							[M-H ₂ O+H] ⁺	145.0140	-0.08							
							[M+H] ⁺	163.0245	0.33	fragments						
							[M+H] ⁺	195.0877	-0.04	138.0660	[C ₆ H ₇ N ₃ O+H] ⁺	1.07	230,	caffeine	(Nyamien et al., 2014)	
							[M+Na] ⁺	217.0690	2.61	110.0715	[C ₅ H ₈ N ₃] ⁺	2.74	270			
							[M-H] ⁻	301.0353	0.23	178.9986	[C ₈ H ₄ O ₅ -H] ⁻	-0.01		quercetin	(Singh et al., 2017)	
h	kola (no. 31)	antiandrogen	75	5.65	$C_{15}H_{10}O_7$	[M-H] ⁻	151.0036	0.42								
							[M+H] ⁺	107.0138	0.61	121.0294	[C ₇ H ₆ O ₂ -H] ⁻	0.42				
							[M+H] ⁺	107.0138	0.88							
							[M+H] ⁺	177.0195	-0.77	177.0195	[C ₆ H ₄ O ₂ -H] ⁻	0.88		naringenin	(Singh et al., 2017)	
							[M+H] ⁺	151.0036	0.42	151.0036	[C ₆ H ₆ O ₄ -H] ⁻	0.42				
							[M+H] ⁺	119.0502	-0.01	119.0502	[C ₇ H ₄ O ₅ -H] ⁻	-0.01				
							[M+H] ⁺	107.0137	1.07	107.0137	[C ₈ H ₄ O ₂ -H] ⁻	1.07				
							[M+H] ⁺	289.0918	0.09	127.0392						
							[M+Na] ⁺	311.0737	0.54	85.0290*						
							[M+K] ⁺	327.0475	0.39							
i	star anise (no.54)	synergy	19	3.60	$C_{12}H_{16}O_8$	[M+H] ⁺	360.1289	0.11	no							
							[M+NH ₄] ⁺	365.0841	0.56	fragments						
							[M+Na] ⁺	341.0879	-0.15							
							[M-H] ⁻	165.0910	-0.08	147.0805	[C ₁₀ H ₁₁ O] ⁺	3.26	215,	eugenol	(Salem et al., 2021)	
							[M+H] ⁺			*132.0571			255,			
										*123.0807			310			
										91.0548						
										165.0902						
										344.1703	0.38	147.0797	[C ₁₀ H ₁₂ O ₂ +H] ⁺	0.05		
										349.1255	0.85	91.0543	[C ₁₀ H ₁₁ O] ⁺	4.88	225,	eugenol
j	star anise (no.54)	antiandrogen	75	5.12	$C_{10}H_{12}O_2$	[M+H] ⁺	365.0996	0.31	147.0797	[C ₁₀ H ₁₁ O] ⁺	8.91	270	eugenol	(Salem et al., 2021)		
							[M+K] ⁺	675.2622	0.19	91.0543	[C ₇ H ₇] ⁺	5.66		glucoside (Citrusin C)		
							[2M+Na] ⁺									

Zone	Botanical (no.54)	Observed effect	<i>hR_f</i>	Retention time [min]	Molecular formula	Adduct	Precursor [m/z]	$\Delta m/z$ [ppm]	MS ² fragments [m/z]	Proposed fragment formula	$\Delta m/z$ [ppm]	λ_{max} [nm]	Tentative assignment	Literature					
k	star anise (no.54)	antiandrogen	94	3.62	C ₇ H ₆ O ₄	[M+HCOO] ⁻	371.1348	-0.22		[C ₆ H ₆ O ₂ -H] ⁻	0.68	215, 260, 295	protocatechuic acid	(Lu et al., 2011; Shan et al., 2005; Salem et al., 2021)					
						[M-H] ⁻	153.0192	0.68	109.0294										
						[M-H] ⁻	137.0244	0.28	no fragments								3-hydroxybenzoic acid (Ali et al., 2021)		
						[M+NH ₄] ⁺	374.1448	-0.59	281.1022										
						[M+Na] ⁺	379.1000	-0.04	249.0759										
l	chicory (no. 65)	synergy	19	4.91	C ₉ H ₁₇ O ₃ N	[M+H] ⁺	170.1179	-2.20	no fragments					unknown					
						[M+Na] ⁺	210.1105	-2.07											
						[M-H ₂ O+H] ⁺	109.0288	-3.80	109.0288										
						[M+H] ⁺	127.0392	-2.04	81.0338										
						[M+H] ⁺	455.2277	-0.39	233.1539*										
						[M+NH ₄] ⁺	472.2545	-0.76	187.0602*										
						[M+Na] ⁺	477.2096	-0.28	159.1169*										
						[M+K] ⁺	493.1835	-0.18	109.0288*										
						[M-H] ⁻	453.2138	-1.70											
						[M+Cl] ⁻	489.1902	-1.05											
m	chicory (no. 65)	antiandrogen	88	3.20	C ₆ H ₆ O ₃	[M+HCOO] ⁻	499.2191	-1.22											
						[M+NO ₃] ⁻	516.2089	-1.50											
						[M-H] ⁻	137.0244	0.50	no fragments										
						[M-H] ⁻	193.0506	0.38	149.0608										
						[M+H] ⁺	284.1853	1.07	249.1489*										
						[M+Na] ⁺	289.1407	1.28	231.1383*										
						[M+K] ⁺	305.1146	1.20	203.1434*										
						[M+H] ⁺	249.1477	3.13	231.1371*										
						[M+Na] ⁺	271.1295	3.49	203.1424*										
						[M-H] ⁻	247.1339	0.12	176.1189*										
n	chicory (no. 65)	antiandrogen	97	4.23	C ₇ H ₆ O ₃	[M+HCOO] ⁻	499.2191	-1.22											
						[M+NO ₃] ⁻	516.2089	-1.50											
						[M-H] ⁻	137.0244	0.50	no fragments										
						[M-H] ⁻	193.0506	0.38	149.0608										
						[M+H] ⁺	284.1853	1.07	249.1489*										
						[M+Na] ⁺	289.1407	1.28	231.1383*										
						[M+K] ⁺	305.1146	1.20	203.1434*										
						[M+H] ⁺	249.1477	3.13	231.1371*										
						[M+Na] ⁺	271.1295	3.49	203.1424*										
						[M-H] ⁻	247.1339	0.12	176.1189*										
o	cinnamon (no. 66)	synergy	23	3.68	C ₁₁ H ₂₀ O ₈	[M+NH ₄] ⁺	334.1494	0.61	137.0598										
						[M+Na] ⁺	339.1048	0.71	73.0292*										
						[M+HCOO] ⁻	499.2191	-1.22											
						[M+NO ₃] ⁻	516.2089	-1.50											
						[M-H] ⁻	137.0244	0.50	no fragments										
						[M-H] ⁻	193.0506	0.38	149.0608										
						[M+H] ⁺	284.1853	1.07	249.1489*										
						[M+Na] ⁺	289.1407	1.28	231.1383*										
						[M+K] ⁺	305.1146	1.20	203.1434*										
						[M+H] ⁺	249.1477	3.13	231.1371*										
p	cinnamon (no. 66)	synergy	23	3.68	C ₁₁ H ₂₀ O ₈	[M+NH ₄] ⁺	334.1494	0.61	137.0598										
						[M+Na] ⁺	339.1048	0.71	73.0292*										
						[M+HCOO] ⁻	499.2191	-1.22											
						[M+NO ₃] ⁻	516.2089	-1.50											
						[M-H] ⁻	137.0244	0.50	no fragments										
						[M-H] ⁻	193.0506	0.38	149.0608										
						[M+H] ⁺	284.1853	1.07	249.1489*										
						[M+Na] ⁺	289.1407	1.28	231.1383*										
						[M+K] ⁺	305.1146	1.20	203.1434*										
						[M+H] ⁺	249.1477	3.13	231.1371*										
q	cinnamon (no. 66)	synergy	23	3.68	C ₁₁ H ₂₀ O ₈	[M+NH ₄] ⁺	334.1494	0.61	137.0598										
						[M+Na] ⁺	339.1048	0.71	73.0292*										
						[M+HCOO] ⁻	499.2191	-1.22											
						[M+NO ₃] ⁻	516.2089	-1.50											
						[M-H] ⁻	137.0244	0.50	no fragments										
						[M-H] ⁻	193.0506	0.38	149.0608										
						[M+H] ⁺	284.1853	1.07	249.1489*										
						[M+Na] ⁺	289.1407	1.28	231.1383*										
						[M+K] ⁺	305.1146	1.20	203.1434*										
						[M+H] ⁺	249.1477	3.13	231.1371*										

Zone	Botanical	Observed effect	hR_F	Retention time [min]	Molecular formula	Adduct	Precursor [m/z]	$\Delta m/z$ [ppm]	MS ² fragments [m/z]	Proposed fragment formula	$\Delta m/z$ [ppm]	λ_{max} [nm]	Tentative assignment	Literature						
p	cinnamon (no. 66)	antianthrogen	94	4.65	C ₂₀ H ₂₈ O ₁₂	[M+K] ⁺	355.0787	0.70												
						[M+NH ₄] ⁺	478.1932	-2.71	165.0557	[C ₆ H ₆ O ₃] ⁻	-3.27									
						[M+Na] ⁺	483.1482	-1.92	147.0452	[C ₆ H ₆ O ₃ -H ₂ O] ⁻	-3.98					apiopaenonoside	(Wang et al., 2020)			
						[M+K] ⁺	499.1227	-2.95	*121.0659											
						[M-H] ⁻	459.1511	-0.56	*106.0423											
						[M-H] ⁻	153.0193	0.42	109.0294	[C ₆ H ₆ O ₂ -H] ⁻	0.95	215, 260, 295, 280, 310	protocatechuic acid	(Jayaprakasha et al., 2006; Ali et al., 2021)						
						[M-H] ⁻	137.0244	-0.01	108.0218											
						[M-H] ⁻	425.2185	-0.93	365.1971											
						[M+Cl] ⁻	461.1953	-1.17	*279.1238											
						[M+HCOO] ⁻	471.2238	-0.37	* 261.1132											
[M+NO ₃] ⁻	488.2141	-1.85	*137.0608																	
[M-H] ⁻	407.2079	-0.94	347.1863																	
[M+Cl] ⁻	443.1845	-0.68	*285.1860																	
[M+HCOO] ⁻	453.2133	-0.64	*149.0970																	
[M+NO ₃] ⁻	470.2035	-1.80	59.0133																	

*not matching the proposed fragmentation pathway

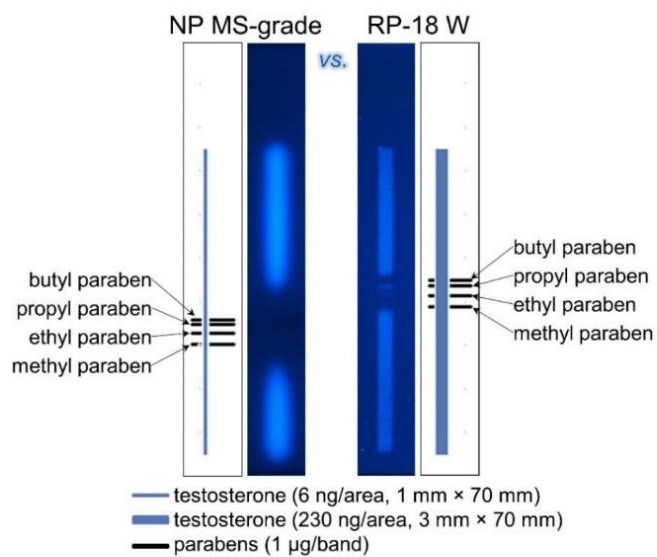


Fig. S1. Comparison of two stripes of the agonist testosterone applied on different phases. pYAAS bioautograms at FLD 366 nm of parabens overlaid with testosterone on the NP silica gel 60 F₂₅₄ MS-grade plate (6 ng, 1 mm × 70 mm) compared to the less sensitive but more sharp response on the RP-18 W plate (230 ng, 3 mm × 70 mm).

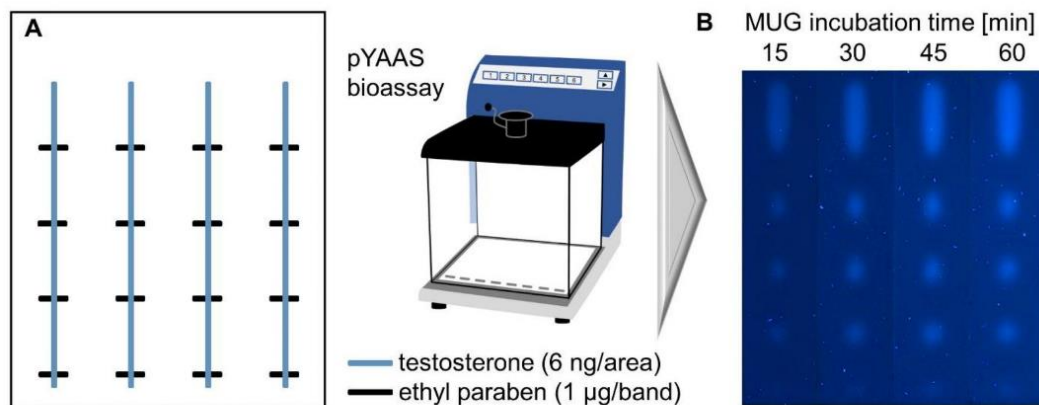


Fig. S2. Determination of substrate incubation time. Application scheme (A) and pYAAS bioassay recorded at FLD 366 nm (B) of ethyl paraben (1 µg/band) overlaid with testosterone (6 ng, 1 mm × 70 mm) on silica gel 60 F₂₅₄ MS-grade plate cut into four 2 cm × 10-cm pieces. 4-Methyl umbelliferyl-β-D-galactopyranoside (MUG) incubation time varied from 15–60 min.

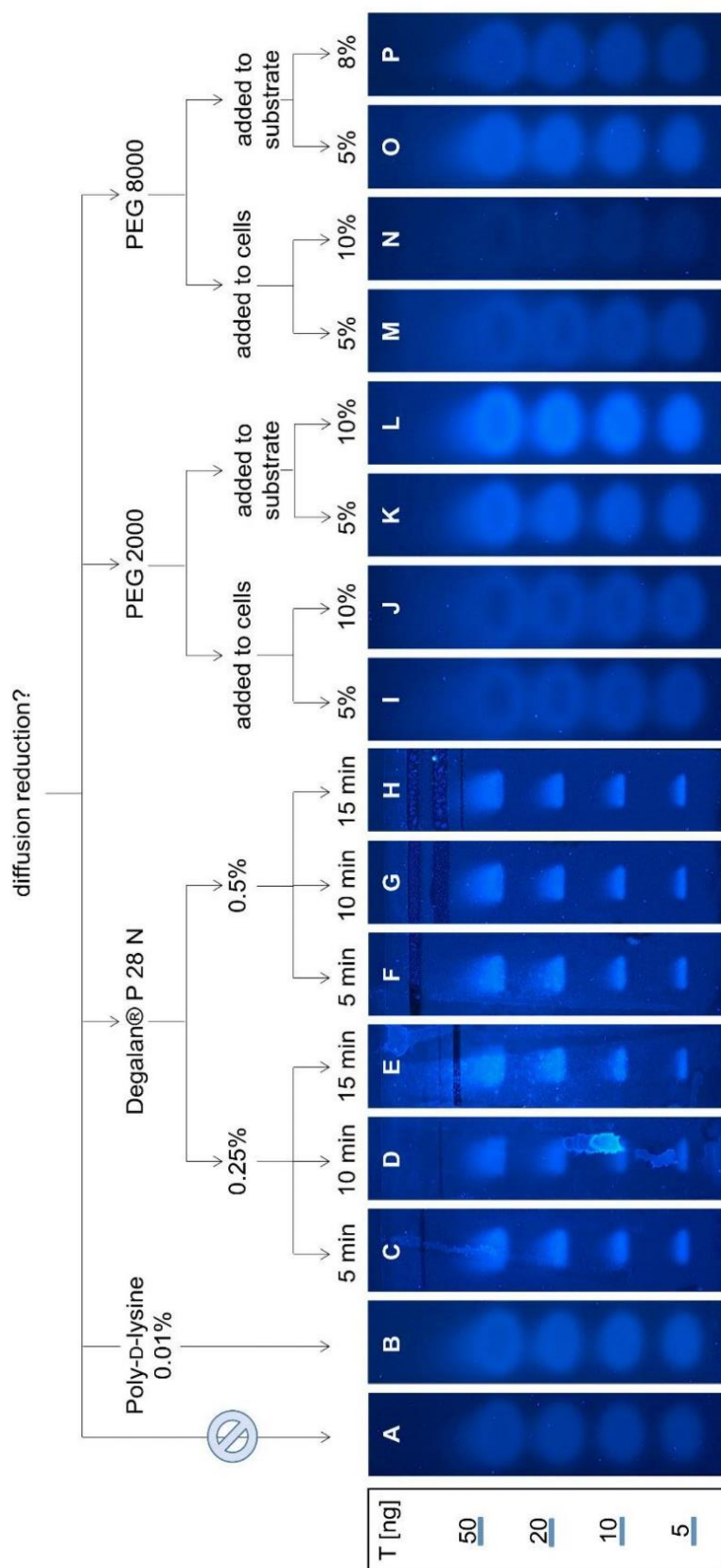


Fig. S3. Diffusion reduction potential of different reagents. pYAS bioautograms at FLD 366 nm of 5–50 ng per 6-mm band testosterone (T) on silica gel 60 F₂₅₄ MS-grade. A plate without fixation was used as control (A). Diffusion reduction was investigated with sprayed on 0.01% (W/V) solution of poly-D-lysine (B), by immersion in 0.25% (C–E), or 0.5% (F–H) Degalan (W/V) for 5 min (C and F), 10 min (D and G), or 15 min (E and H), as well as with sprayed on 5% (I and K), or 10% (J and L) polyethylene glycol (PEG) 2000 (W/V), and 5% (M and O), 8% (P), or 10% (N) PEG 8000 (W/V), added either to the yeast cell suspension (I–J, M–N) or to the 4-methyl umbelliferyl- β -D-galactopyranoside substrate solution (K–L, O–P).

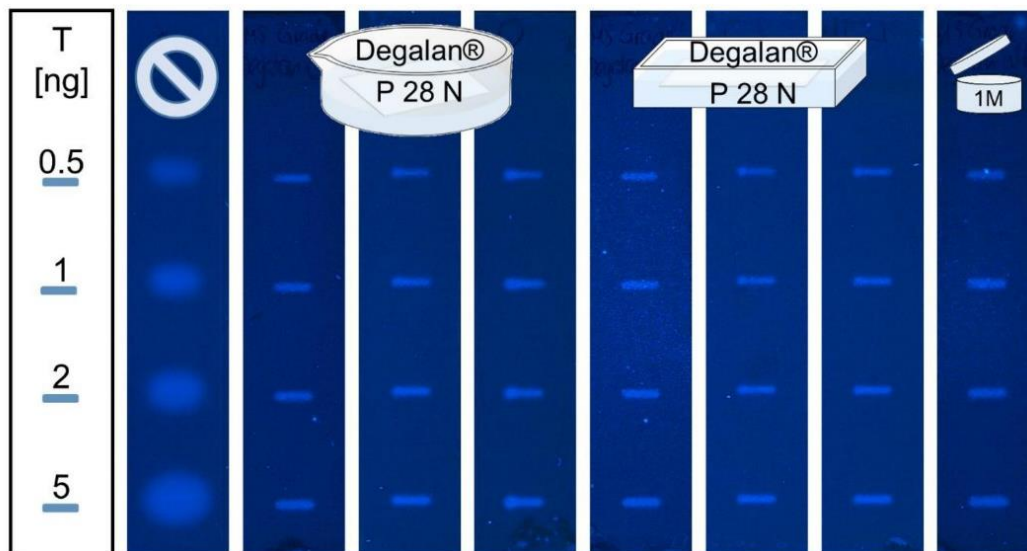


Fig. S4. Robustness of fixation with Degalan. pYAAS bioautograms at FLD 366 nm of 0.5–5 ng per 6-mm band testosterone (T) on silica gel 60 F₂₅₄ MS-grade. A plate without fixation was used as control and the others were coated with freshly prepared Degalan P 28 N (0.25% W/V in *n*-hexane; 10 min) in a crystallizing dish or a rectangular deco glass bowl. For one plate, a one-month-old (1M) Degalan solution was used.

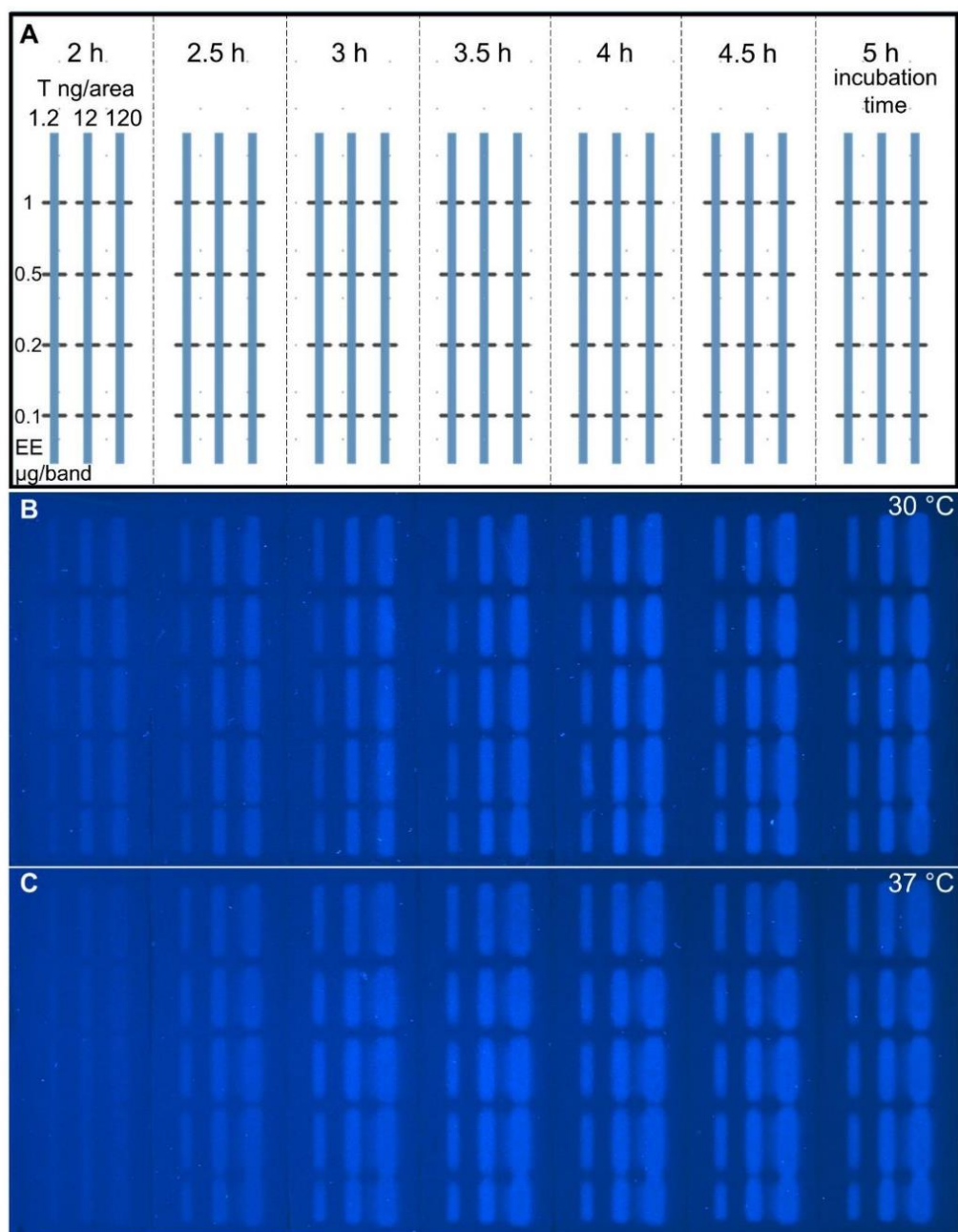


Fig. S5. Experimental determination of testosterone amount and incubation time for NP-HPTLC^{fix}-pYAAS. Ethyl paraben (EE; 1 µg/band, 6-mm bands) was overlaid with different amounts of testosterone (T, 1.2–120 ng/area, 2 mm × 70 mm) on silica gel 60 F₂₅₄ MS-grade according to plate design (A). Comparison of fluorescence intensity after Degalan coating (0.25% W/V in *n*-hexane; 10 min) and performing the pYAAS bioassay at 30 °C (B) versus 37 °C (C), studying a 2–5 h of incubation period; resulting bioautogram detected at FLD 366 nm.

S-17

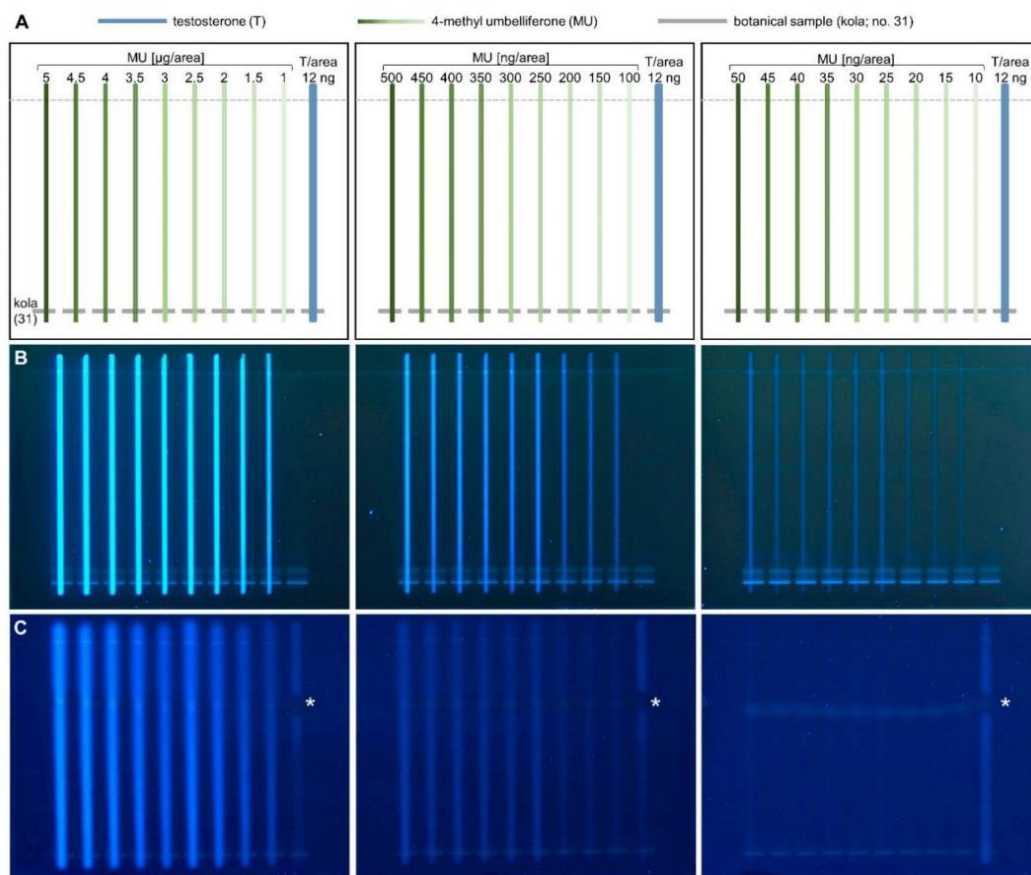


Fig. S6. Experimental determination of MU reference area for NP-HPTLC^{fix}-pYAVAS. Kola (no. 31, 4 μL , 6-mm bands, separated with ethyl acetate – toluene – formic acid – water (16:4:3:2; *V/V/V/V*) up to 70 mm on silica gel 60 F₂₅₄ MS-grade) was overlaid with 4-methyl umbelliferone (MU, 10–5000 ng/area, 1 mm \times 70 mm) and testosterone (T, 12 ng/area, 2 mm \times 70 mm) according to plate design (A). Application (B) and the HPTLC^{fix}-pYAVAS bioautogram (C; fixation with Degalan coating, 0.25% *W/V* in *n*-hexane; 10 min) were recorded at FLD 366 nm. The fluorescence intensity of the MU-stripes was compared to the T-stripe containing an antiandrogenic zone (marked*).

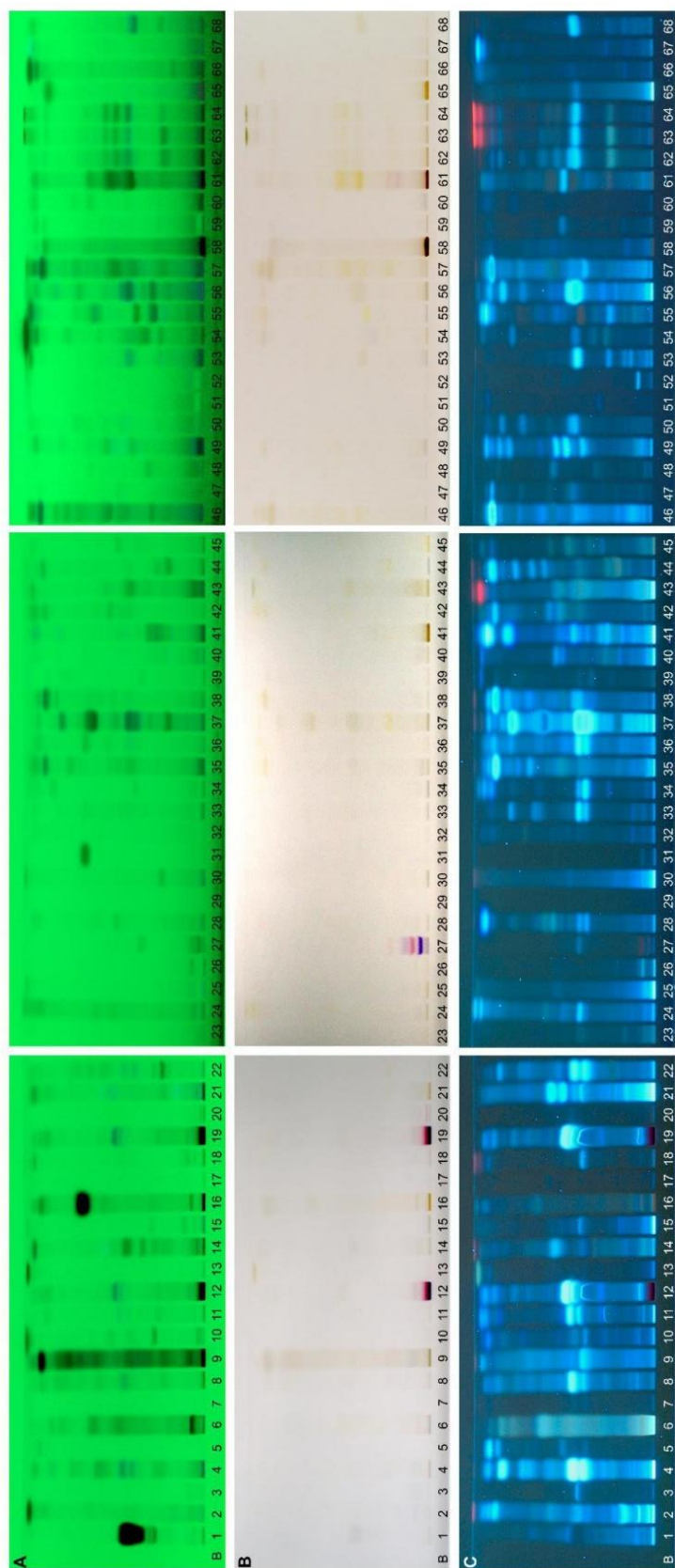
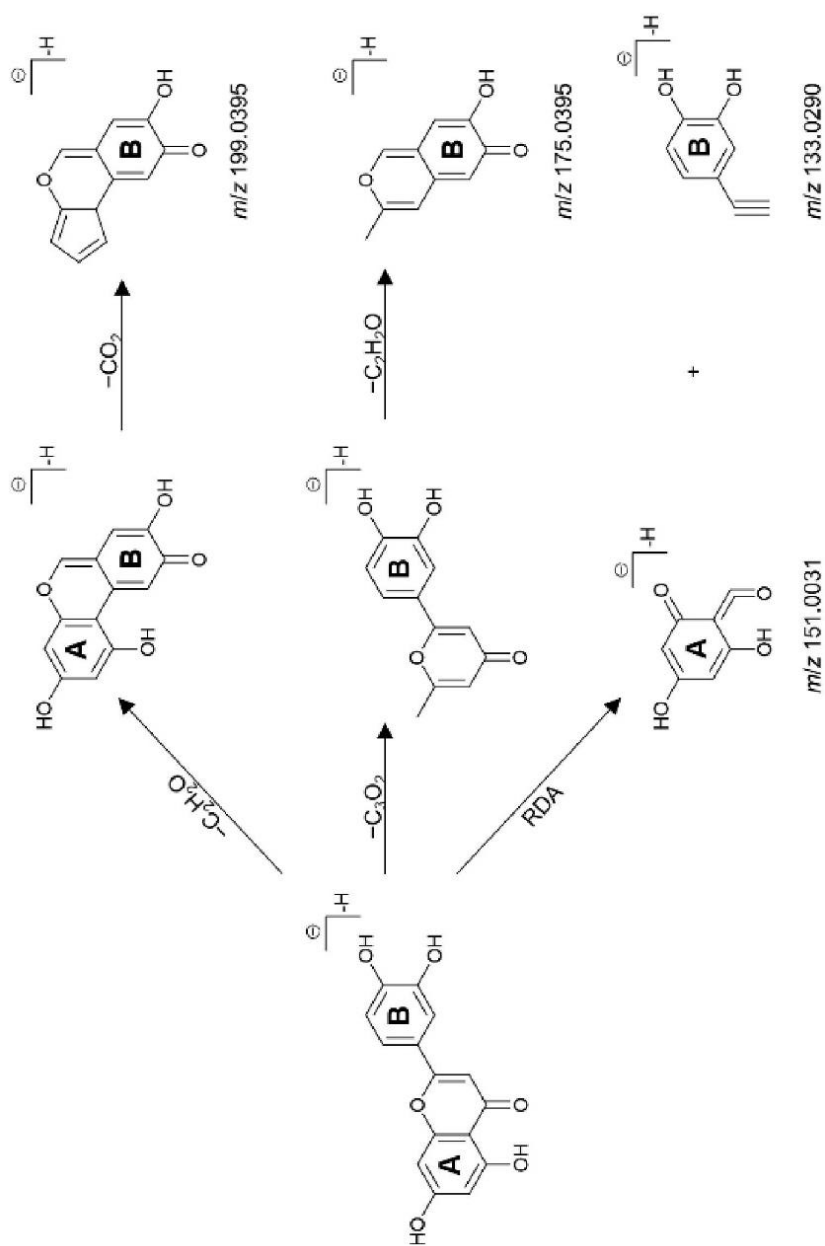
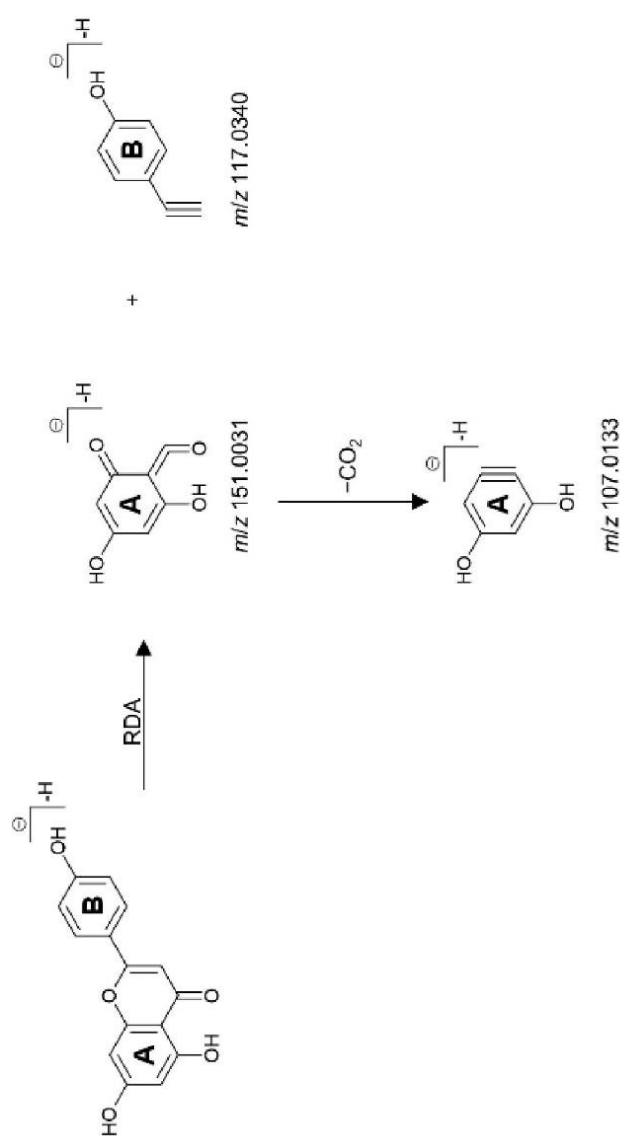


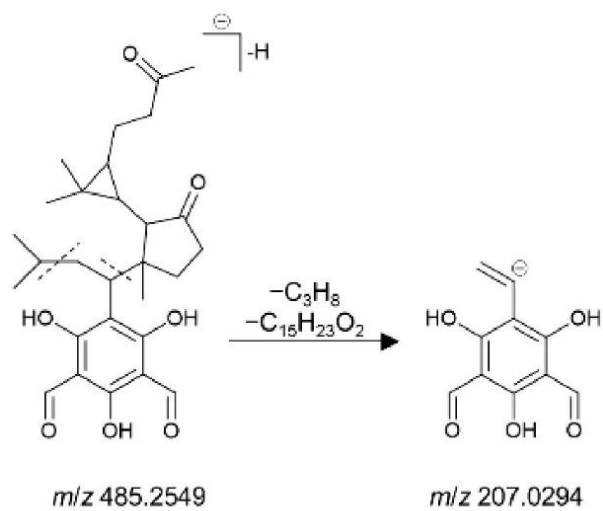
Fig. S7. NP-HPTLC-UV/Vis/FLD of 68 botanicals (Schreiner et al., 2021). Chromatograms of botanical samples (4 μ L, 6-mm bands, nos. 1–68 assigned in Table S1 and solvent blank B for comparison) separated with ethyl acetate – toluene – formic acid – water (16:4:3:2; V/V/V/V) up to 70 mm on silica gel 60 F₂₅₄ MS-grade plates recorded at UV 254 nm (A), white light illumination (B), and FLD 366 nm (C).



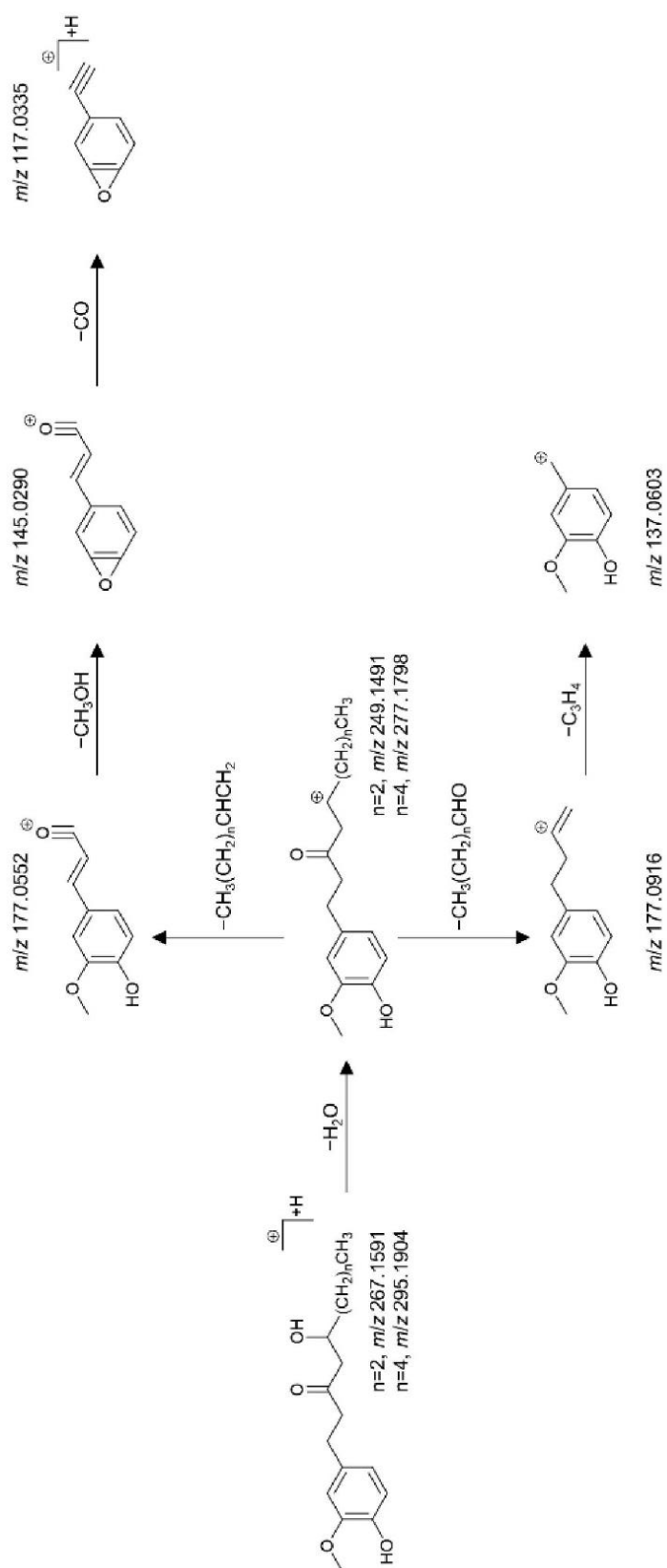
Scheme S1. Proposed fragmentation pathway of luteolin including Retro-Diels-Alder mechanism.



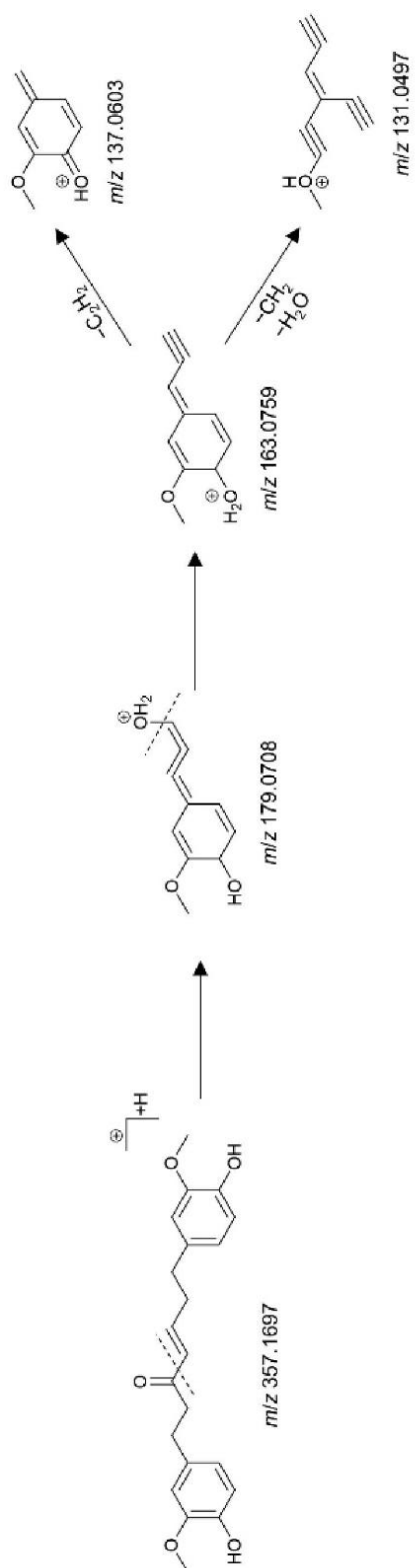
Scheme S2. Proposed fragmentation pathway of apigenin including Retro-Diels-Alder mechanism.



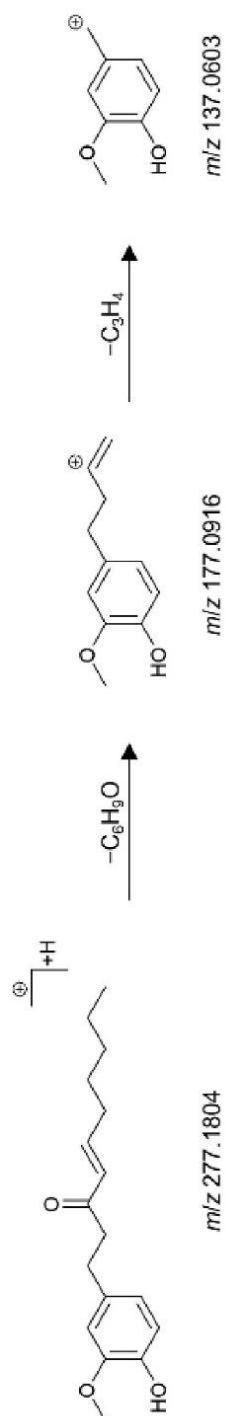
Scheme S3. Proposed fragmentation pathway of eucalyptone.



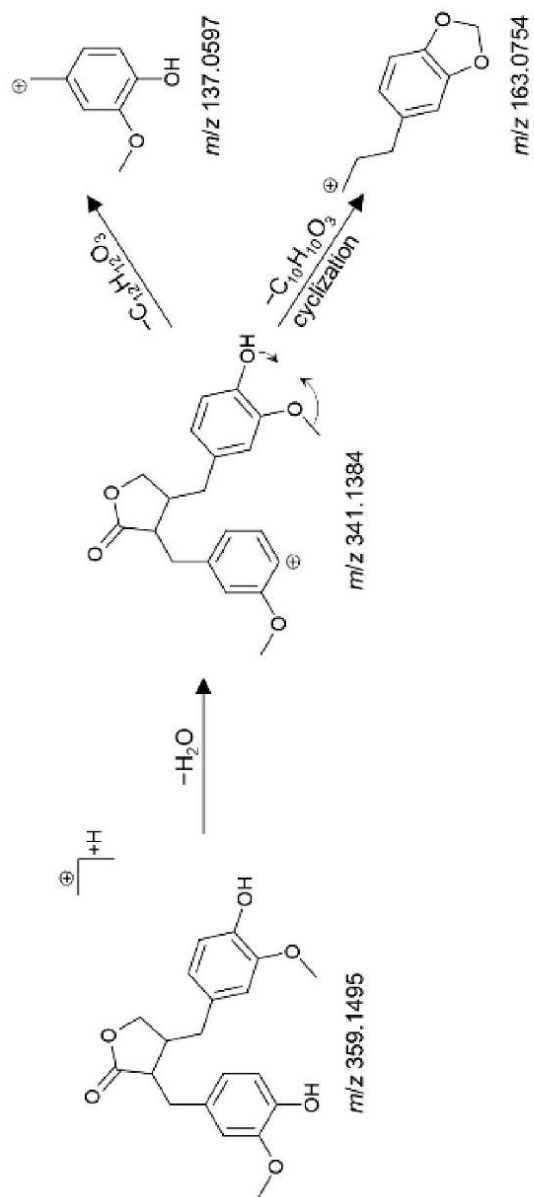
Scheme S4. Proposed fragmentation pathways of [4]- and [6]-gingerol.



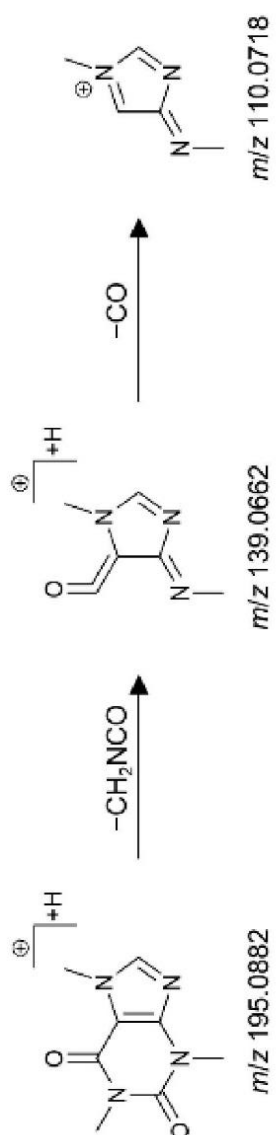
Scheme S5. Proposed fragmentation pathways of gingerenone A.



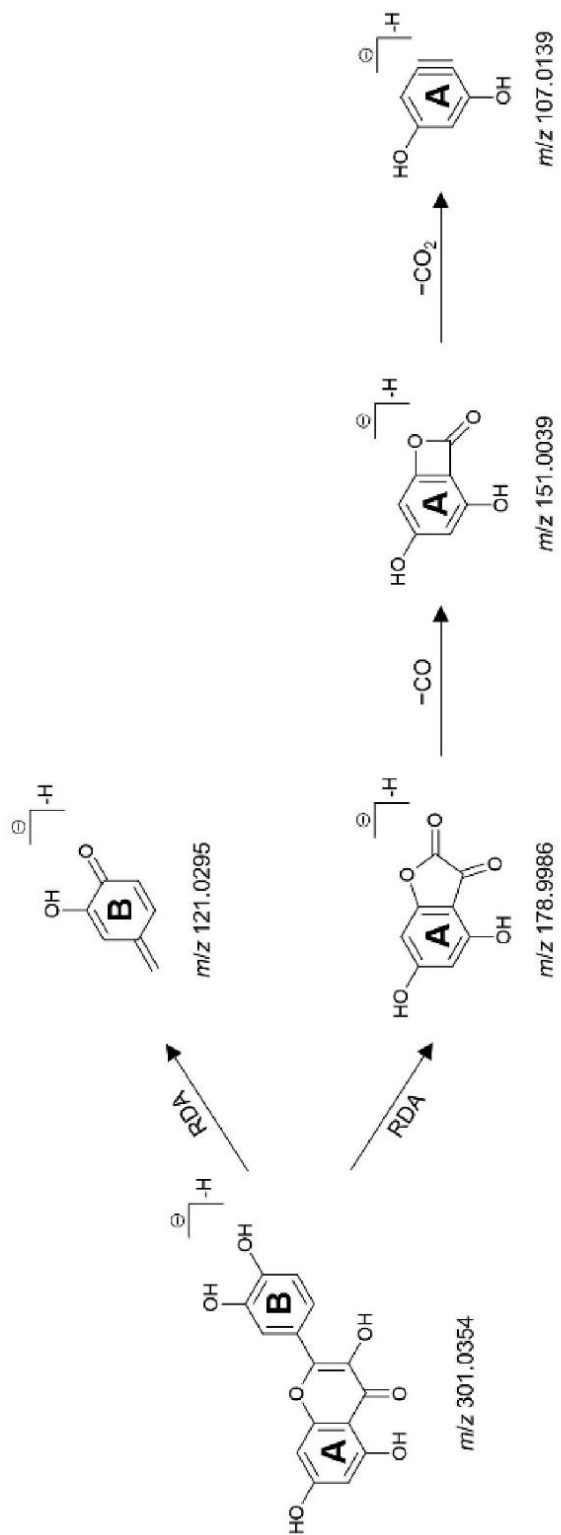
Scheme S6. Proposed fragmentation pathway of [6]-shogaol.



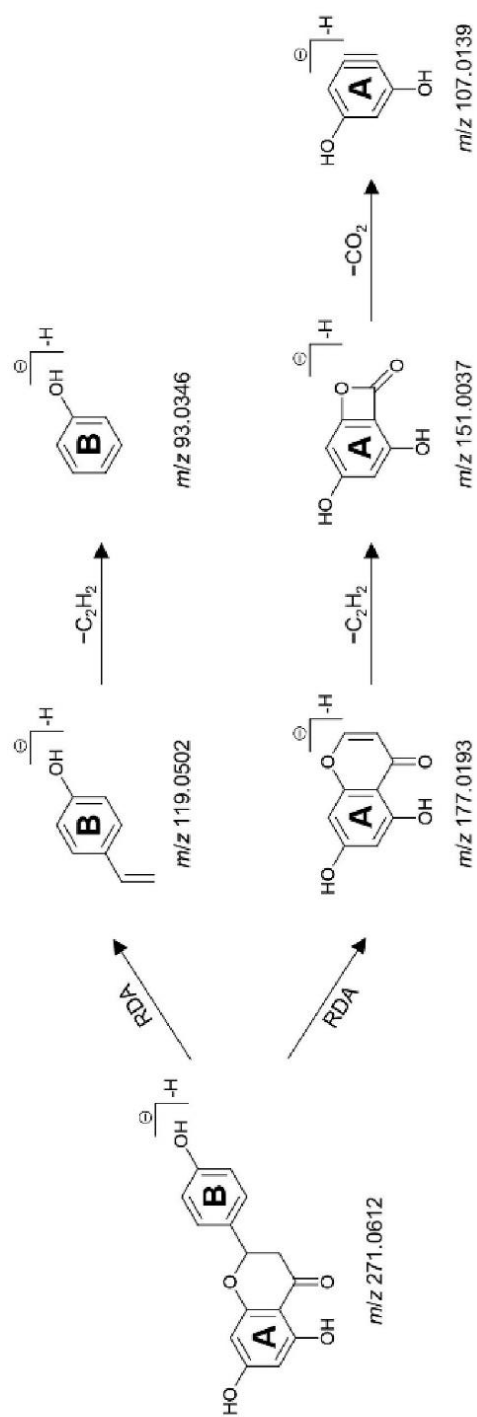
Scheme S7. Proposed fragmentation pathway of matairesinol.



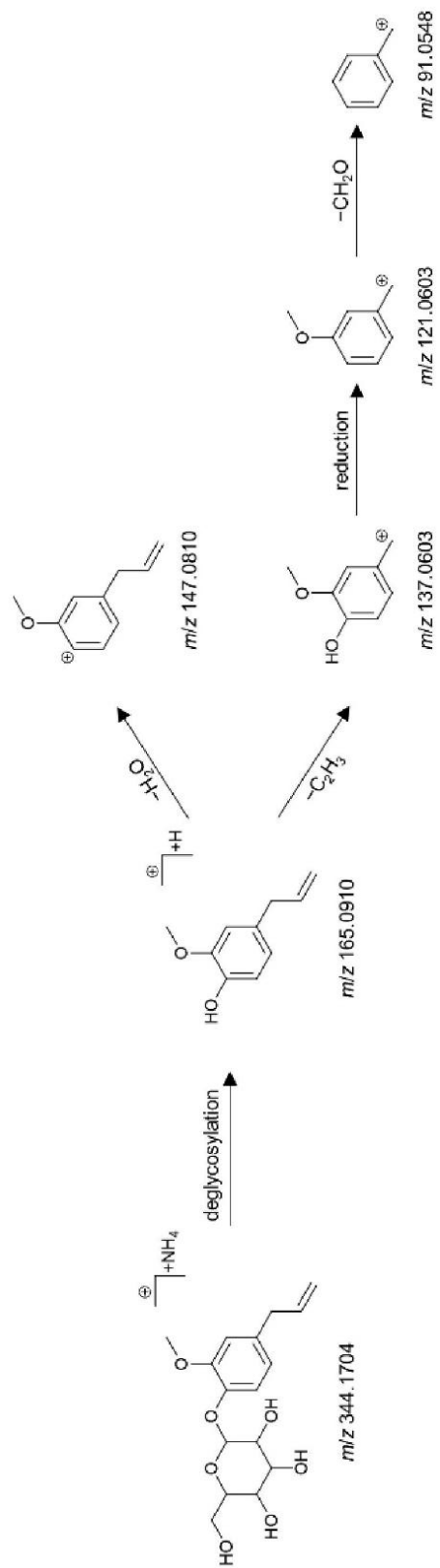
Scheme S8. Proposed fragmentation pathway of caffeine.



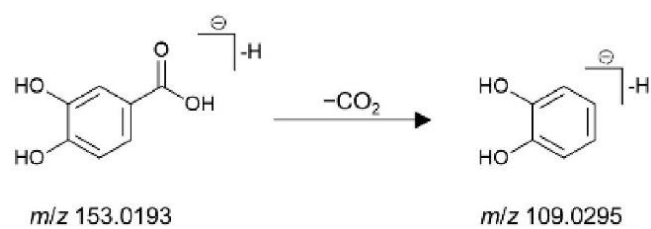
Scheme S9. Proposed fragmentation pathway of quercetin including Retro-Diels-Alder mechanism.



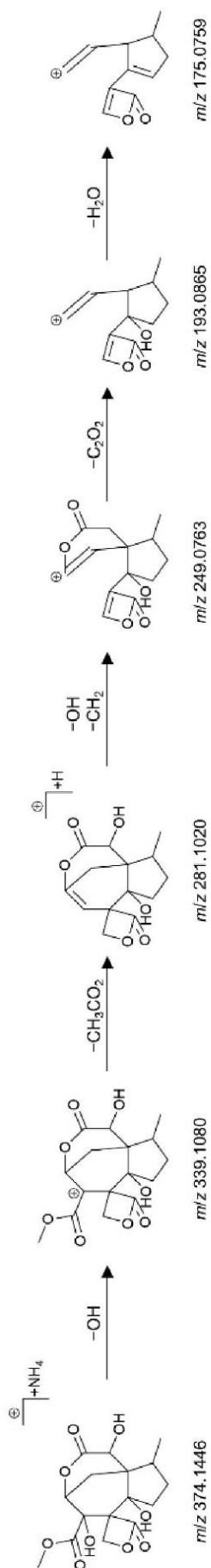
Scheme S10. Proposed fragmentation pathway of naringenin including Retro-Diels-Alder mechanism.



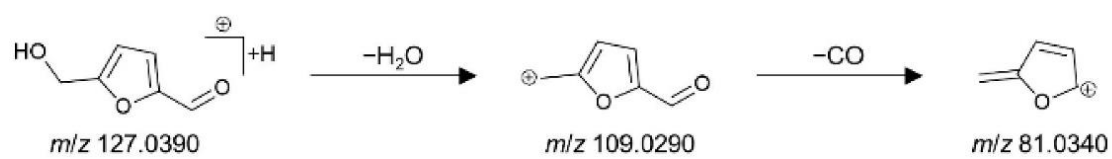
Scheme S11. Proposed fragmentation pathway of eugenol (glucoside).



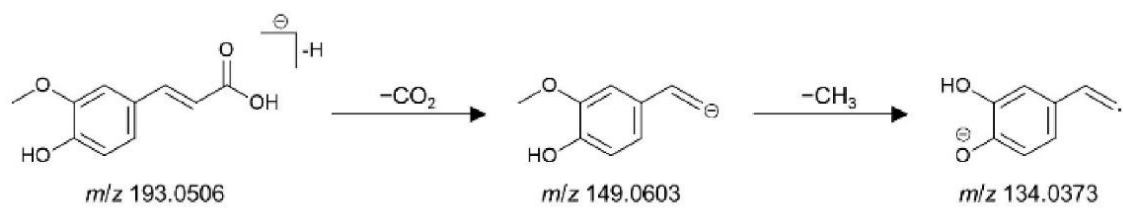
Scheme S12. Proposed fragmentation pathway of protocatechuic acid.



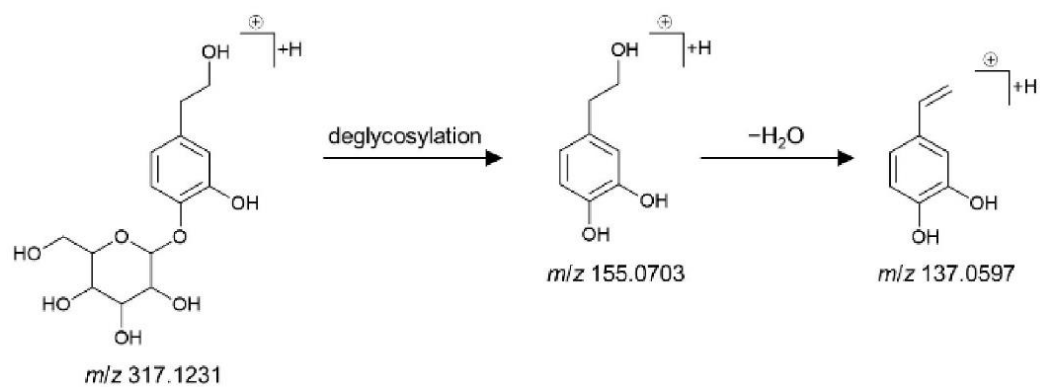
Scheme S13. Proposed fragmentation pathway of veranisatin B.



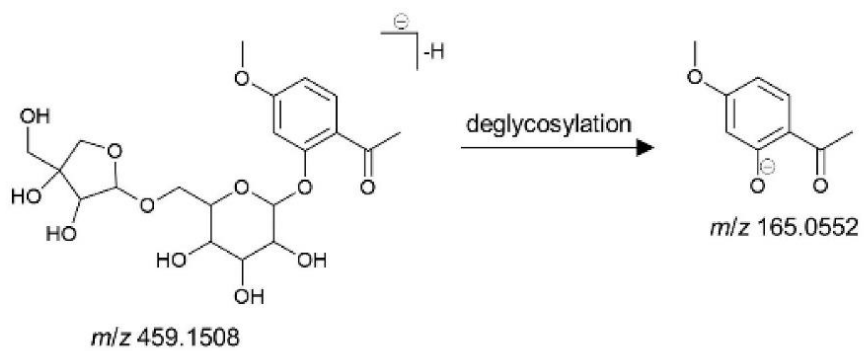
Scheme S14. Proposed fragmentation pathway of 5-hydroxymethylfurfural.



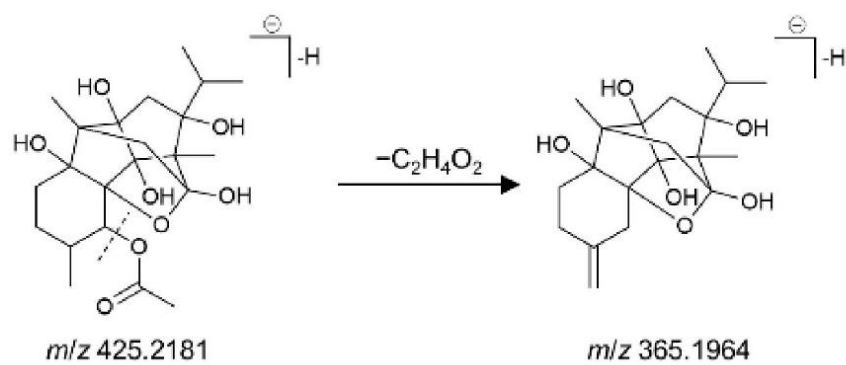
Scheme S15. Proposed fragmentation pathway of ferulic acid.



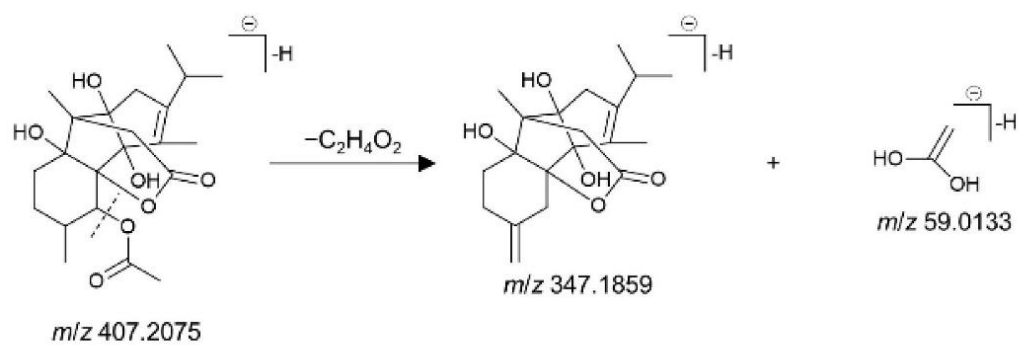
Scheme S16. Proposed fragmentation pathway of hydroxytyrosol O-glucoside.



Scheme S17. Proposed fragmentation pathway of apipaeonoside.



Scheme S18. Proposed fragmentation pathway of cinnzeylanine.



Scheme S19. Proposed fragmentation pathway of anhydrocinnzeylanine.

References

- Abu-Reidah, I. M., Arráez-Román, D., Segura-Carretero, A., & Fernández-Gutiérrez, A. (2013). Extensive characterisation of bioactive phenolic constituents from globe artichoke (*Cynara scolymus* L.) by HPLC-DAD-ESI-QTOF-MS. *Food Chemistry*, *141*, 2269–2277.
- Ali, A., Wu, H., Ponnampalam, E. N., Cottrell, J. J., Dunshea, F. R., & Suleria, H. A. R. (2021). Comprehensive Profiling of Most Widely Used Spices for Their Phenolic Compounds through LC-ESI-QTOF-MS2 and Their Antioxidant Potential. *Antioxidants (Basel, Switzerland)*, *10*.
- Block, E., Dane, A. J., Thomas, S., & Cody, R. B. (2010). Applications of direct analysis in real time mass spectrometry (DART-MS) in *Allium* chemistry. 2-propenesulfenic and 2-propenesulfinic acids, diallyl trisulfane S-oxide, and other reactive sulfur compounds from crushed garlic and other *Alliums*. *Journal of agricultural and food chemistry*, *58*, 4617–4625.
- Cova, C. M., Boffa, L., Pistocchi, M., Giorgini, S., Luque, R., & Cravotto, G. (2019). Technology and Process Design for Phenols Recovery from Industrial Chicory (*Chicorium intybus*) Leftovers. *Molecules (Basel, Switzerland)*, *24*.
- del Río, J. C., Gutiérrez, A., Hernando, M., Landín, P., Romero, J., & Martínez, Á. T. (2005). Determining the influence of eucalypt lignin composition in paper pulp yield using Py-GC/MS. *Journal of Analytical and Applied Pyrolysis*, *74*, 110–115.
- Deng, X., Yu, J., Zhao, M., Zhao, B., Xue, X., Che, C., Meng, J., & Wang, S. (2015). Quality assessment of crude and processed ginger by high-performance liquid chromatography with diode array detection and mass spectrometry combined with chemometrics. *Journal of Separation Science*, *38*, 2945–2952.
- Dos Santos, B. M., Zibrandtsen, J. F. S., Gunbilig, D., Sørensen, M., Cozzi, F., Boughton, B. A., Heskes, A. M., & Neilson, E. H. J. (2019). Quantification and Localization of Formylated Phloroglucinol Compounds (FPCs) in *Eucalyptus* Species. *Frontiers in Plant Science*, *10*, 186.

- Han, J. S., Lee, S., Kim, H. Y., & Lee, C. H. (2015). MS-Based Metabolite Profiling of Aboveground and Root Components of *Zingiber mioga* and *Officinale*. *Molecules (Basel, Switzerland)*, *20*, 16170–16185.
- Horn-Ross, P. L., Barnes, S., Lee, M., Coward, L., Mandel, J. E., Koo, J., John, E. M., & Smith, M. (2000). Assessing phytoestrogen exposure in epidemiologic studies: development of a database (United States). *Cancer causes & control CCC*, *11*, 289–298.
- Jayaprakasha, G. K., Ohnishi-Kameyama, M., Ono, H., Yoshida, M., & Jaganmohan Rao, L. (2006). Phenolic constituents in the fruits of *Cinnamomum zeylanicum* and their antioxidant activity. *Journal of Agricultural and Food Chemistry*, *54*, 1672–1679.
- Jiang, H., Sólyom, A. M., Timmermann, B. N., & Gang, D. R. (2005). Characterization of gingerol-related compounds in ginger rhizome (*Zingiber officinale* Rosc.) by high-performance liquid chromatography/electrospray ionization mass spectrometry. *Rapid Communications in Mass Spectrometry*, *19*, 2957–2964.
- Kisiel, W., & Zielińska, K. (2001). Guaianolides from *Cichorium intybus* and structure revision of *Cichorium* sesquiterpene lactones. *Phytochemistry*, *57*, 523–527.
- Kolle, S. N., Kamp, H. G., Huener, H.-A., Knickel, J., Verlohner, A., Woitkowiak, C., Landsiedel, R., & van Ravenzwaay, B. (2010). In house validation of recombinant yeast estrogen and androgen receptor agonist and antagonist screening assays. *Toxicology in Vitro*, *24*, 2030–2040.
- Lu, M., Yuan, B., Zeng, M., & Chen, J. (2011). Antioxidant capacity and major phenolic compounds of spices commonly consumed in China. *Food Research International*, *44*, 530–536.
- Malik, B., Pirzadah, T. B., Tahir, I., Abdin, M. Z., & Ul Rehman, R. (2016). Phytochemical studies on *Cichorium intybus* L. (chicory) from Kashmir Himalaya using GC-MS. *Journal of Pharmacy Research*, *10*.
- Nakamura, T., Okuyama, E., & Yamazaki, M. (1996). Neurotropic components from star anise (*Illicium verum* Hook. fil.). *Chemical and Pharmaceutical Bulletin*, *44*, 1908–1914.

- Nyamien, Y., Adje, F., Niamké, F., Chatigre, O., Adima, A., & Biego, G. (2014). Caffeine and Phenolic Compounds in *Cola nitida* (Vent.) Schott and Endl and *Garcinia kola* Heckel Grown in Côte d'Ivoire. *British Journal of Applied Science & Technology*, *4*, 4846–4859.
- Osawa, K., Yasuda, H., Morita, H., Takeya, K., & Itokawa, H. (1995). Eucalyptone from *Eucalyptus globulus*. *Phytochemistry*, *40*, 183–184.
- Park, J. S., & Jung, M. Y. (2012). Development of high-performance liquid chromatography-time-of-flight mass spectrometry for the simultaneous characterization and quantitative analysis of gingerol-related compounds in ginger products. *Journal of agricultural and food chemistry*, *60*, 10015–10026.
- Renaud, J. B., & Sumarah, M. W. (2016). Data independent acquisition-digital archiving mass spectrometry: application to single kernel mycotoxin analysis of *Fusarium graminearum* infected maize. *Analytical and Bioanalytical Chemistry*, *408*, 3083–3091.
- Rouphael, Y., Bernardi, J., Cardarelli, M., Bernardo, L., Kane, D., Colla, G., & Lucini, L. (2016). Phenolic Compounds and Sesquiterpene Lactones Profile in Leaves of Nineteen Artichoke Cultivars. *Journal of agricultural and food chemistry*, *64*, 8540–8548.
- Salem, M. A., El-Shiekh, R. A., Hashem, R. A., & Hassan, M. (2021). In vivo Antibacterial Activity of Star Anise (*Illicium verum* Hook.) Extract Using Murine MRSA Skin Infection Model in Relation to Its Metabolite Profile. *Infection and drug resistance*, *14*, 33–48.
- Sánchez-Rabaneda, F., Jáuregui, O., Lamuela-Raventós, R. M., Bastida, J., Viladomat, F., & Codina, C. (2003). Identification of phenolic compounds in artichoke waste by high-performance liquid chromatography–tandem mass spectrometry. *Journal of Chromatography A*, *1008*, 57–72.
- Selvaraj, D., Muthu, S., Kotha, S., Siddamsetty, R. S., Andavar, S., & Jayaraman, S. (2021). Syringaresinol as a novel androgen receptor antagonist against wild and mutant androgen receptors for the treatment of castration-resistant prostate cancer: molecular docking, in-vitro and molecular dynamics study. *Journal of biomolecular structure & dynamics*, *39*, 621–634.

- Shan, B., Cai, Y. Z., Sun, M., & Corke, H. (2005). Antioxidant capacity of 26 spice extracts and characterization of their phenolic constituents. *Journal of Agricultural and Food Chemistry*, *53*, 7749–7759.
- Singh, A. N., Baruah, M. M., & Sharma, N. (2017). Structure Based docking studies towards exploring potential anti-androgen activity of selected phytochemicals against Prostate Cancer. *Scientific Reports*, *7*, 1955.
- Singh, R., & Chahal, K. K. (2019). Cichorium intybus from India: GC-MS Profiling, Phenolic Content and in vitro Antioxidant Capacity of Sequential Soxhlet Extracted Roasted Roots. *Brazilian Archives of Biology and Technology*, *62*.
- Wang, Y., Harrington, P. d. B., & Chen, P. (2020). Metabolomic profiling and comparison of major cinnamon species using UHPLC-HRMS. *Analytical and Bioanalytical Chemistry*, *412*, 7669–7681.
- Wu, M., Ni, L., Lu, H., Xu, H., Zou, S., & Zou, X. (2020). Terpenoids and Their Biological Activities from Cinnamomum A Review. *Journal of Chemistry*, *2020*, 1–14.

7. Publication 6

**Multiplex planar bioassay detecting estrogens, antiestrogens,
false-positives and synergists as sharp zones on normal phase**

Tamara Schreiner, Alisa Ronzheimer, Gertrud E. Morlock*

Justus Liebig University Giessen, Institute of Nutritional Science, Chair of Food Science,
Heinrich-Buff-Ring 26-32, 35392 Giessen, Germany

Dedicated to the 75th birthdays of Elke Hahn-Deinstrop and Dr. Heinz Hauck, Germany

Published in

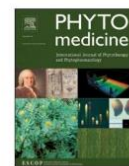
Phytomedicine, 103 (2022) 154230

Received 08 March 2022; Received in revised form 28 May 2022; Accepted 31 May 2022



Contents lists available at ScienceDirect

Phytomedicine

journal homepage: www.elsevier.com/locate/phymed

Original Article

Multiplex planar bioassay detecting estrogens, antiestrogens, false-positives and synergists as sharp zones on normal phase

A. Ronzheimer, T. Schreiner, G.E. Morlock*

Justus Liebig University Giessen, Institute of Nutritional Science, Chair of Food Science, Heinrich-Buff-Ring 26-32, 35392, Giessen, Germany



ARTICLE INFO

Dedicated to the 75th birthdays of Elke Hahn-Deinstrop and Dr. Heinz Hauck, Germany.

Keywords:

Botanicals
Zone diffusion
Planar yeast antagonist estrogen screen
Synergistic effects
12D Hyphenation
High-resolution mass spectrometry

ABSTRACT

Background: Phytoestrogens are found in many plants used in traditional medicines. Increasingly, plant extracts (botanicals) are also being added to foods or marketed as dietary supplements. Especially such powder formulations are susceptible to adulteration and falsification, given the global processing chain. To detect estrogen-like compounds in such multicomponent mixtures, non-target screening for hormonally active or endocrine disrupting compounds in plant products is becoming more important. Unfortunately, the current planar yeast estrogen screen (pYES) is prone to zone diffusion on the normal-phase high-performance thin-layer chromatography (NP-HPTLC) plate due to long incubation times in the aqueous bioassay.

Purpose: The present study aimed to reduce zone diffusion on NP plates, which provides the basis for extending pYES to a multiplex bioassay, offering 4 different biological activity principles, followed by targeted identification of active zones.

Study design and methods: The reduction of substance diffusion via a polyisobutyl methacrylate polymer coating was studied. After successful zone fixation (^{fix}), a multiplex bioassay was developed, in which a 17 β -estradiol-strip was applied along each sample track to detect synergists and antagonists (A), and for verification (V), a 4-methyl umbelliferone-strip to exclude false-positives. After multiplex bioassay screening of 68 botanicals, the zones with hormonal activities were heart-cut eluted to reversed-phase high-performance liquid chromatography–diode array detection–high-resolution tandem mass spectrometry (RP-HPLC–DAD–HESI-HRMS/MS).

Results: The separated substances were successfully fixed by the chromatogram coating. The zone sharpness (achieved after the bioassay) made it possible to add two strips, the 17 β -estradiol-strip for antagonistic and synergistic, and the 4-methyl umbelliferone-strip for false-positive effect detection, resulting in a multiplex bioassay. Using the 12D hyphenation NP-HPTLC^{fix}–UV/Vis/FLD–pYAVES–FLD heart-cut RP-HPLC–DAD–HESI-HRMS/MS, it was possible to obtain information on estrogens, antiestrogens, false-positives, and synergists, and (tentatively) assign 17 hormonally active compounds, of which only 7 have been known to affect the human estrogen receptor, while another 4 had structural similarity to common phytoestrogens and antiestrogens.

Conclusions: The streamlined 12D hyphenation including a multiplex bioassay has been shown to differentiate hormonal effects, leading to new insights and better understanding. It can generally be used to identify unknown hormonally active compounds in complex samples.

List of Abbreviations: A, antagonist; AGC, automated gain control; DAD, diode array detection; ddMS², data-dependent tandem mass spectrometry; E2, 17 β -estradiol; F, fluorescein; FDG, fluorescein-di-(β -D-galactopyranoside); ^{fix}, fixated; FLD, fluorescence detection; FWHM, full width at half-maximum; (h)ER, (human) estrogen receptor; (H)ESI, (heated) electrospray ionization; *hR_f*, retardation factor multiplied by 100; HRMS/MS, high-resolution tandem mass spectrometry; MU, 4-methyl umbelliferone; MUG, 4-methyl umbelliferyl- β -D-galactopyranoside; NP-HPTLC, normal-phase high-performance thin-layer chromatography; pYES, planar yeast estrogen screen; RP-HPLC, reversed-phase high-performance liquid chromatography; RP-18 W, wetttable reversed-phase; UV, ultra violet; V, verification; Vis, visible.

* Corresponding author.

E-mail address: Gertrud.Morlock@uni-giessen.de (G.E. Morlock).

<https://doi.org/10.1016/j.phymed.2022.154230>

Received 8 March 2022; Received in revised form 28 May 2022; Accepted 31 May 2022

Available online 2 June 2022

0944-7113/© 2022 Elsevier GmbH. All rights reserved.

Introduction

There are a wealth of traditional medicines and many of them are based on plants such as ginkgo, ginseng, or Siberian ginseng (Kaufmann et al., 2016). In addition, plant-based extracts (botanicals) are increasingly used as food supplements due to their characteristic bioactive ingredients. Health effects are often claimed for both dietary supplements and plant-based medicines, despite different quality control standards for food and medicine. Due to country-specific term definitions, regulatory frameworks, and legal systems, a consensus on standardized quality control for the different types of health-promoting food products is not available (Dwyer et al., 2018). As health claims require scientific evidence, there is a need for better analytical techniques to ensure the product quality of plant-derived food supplements (Working group Fragen der Ernährung, Society of Food Chemistry, Germany 2022; Jobst et al., 2021). The combination of physico-chemical separation of plant extracts by planar chromatography and biological effect detection using an on-surface bioassay is capable to prioritize important active compounds in multicomponent mixtures (Morlock, 2021). Non-target planar (bio)assay imaging has recently been used to compare 68 different botanicals with regard to their potential effects on human metabolism, microbiome, enzymatic processes, and endocrine system (Schreiner et al., 2021).

In particular, the hormonally active ingredients of plants and environmental samples have gained much interest in recent decades. Many bioassays which are commonly used for the detection of estrogens or antiestrogens are employing estrogen reporter organisms, such as chemically activated luciferase expression (CALUX) (Sonneveld et al., 2005; van der Linden et al., 2008), MELN (Balaguer et al., 1999), or yeast estrogen screen (YES) (Routledge and Sumpter, 1996; Murk et al., 2002) cell lines. These sum parameter assay methods, typically performed in the microtiter-plate or centrifuge-tube format, either address target estrogens only (Balaguer et al., 1999; Sonneveld et al., 2005) or cannot differentiate individual effects in complex mixtures, as the estrogenic potency is often determined as 17 β -estradiol equivalents (Murk et al., 2002; van der Linden et al., 2008). Contributions of unknown compounds, opposing effects, or effects deriving from mixtures are neglected by these methods (Houtman et al., 2007), which could lead to false results.

The planar yeast estrogen screen (pYES) is an easy and fast alternative to screen for estrogenic substances in complex mixtures (Morlock, 2021). It combines the separation of complex samples via high-performance thin-layer chromatography (HPTLC) with the biological detection of estrogen-like substances via the human estrogen receptor (hER) containing yeast (Müller et al., 2004). Right from the beginning, there was a problem with zone diffusion on normal-phase (NP) HPTLC plates for long incubation times due to the polar layer and aqueous bioassay medium. Diffuse bioautogram zones made it difficult to interpret correctly complex sample mixtures (Buchinger et al., 2013; Schönborn and Grimmer, 2013). In contrast, zone sharpening was achieved on wettable reversed-phase HPTLC plates (RP-18 W), but depending on the analytes led to a more or less lower detectability (Klingelhöfer and Morlock, 2014). The use of automated spray-on technology instead of automated immersion resulted in sharper zones on NP with improved sensitivity (Schönborn et al., 2017; Azadnija and Morlock, 2019). However, although diffusion was reduced, the zones did not achieve the same sharpness as with RP-18 W. Especially for complex mixtures like botanicals, many substance zones often only present in small quantities are close to each other, and thereby sharp zones are indispensable.

Consequently, the planar pYES bioassay was sought to be improved in terms of sensitivity and sharpness. Polymerizing agents such as polyisobutyl methacrylate had already been used to fixate silica gel layers for immunoassay detection (Brockhaus et al., 1981). Studying such polymerizing agents for planar bioassays could lead to a substance fixation and thereby sharper zones with reduced diffusion. A fixation

step (^{fix}) can easily be integrated into the workflow. The achieved zone sharpness would in turn allow the extension of the pYES workflow by applying along each sample track a 17 β -estradiol-strip for antagonistic effects (A) and a control-strip for verification (V). The resulting multiplex bioassay method NP-HPTLC^{fix}-UV/Vis/FLD-pYAVES-FLD would provide information on estrogens, antiestrogens, and false-positive antiestrogens. In addition, an enhanced fluorescence of the agonist strip would imply a fortified activation of the hER and thereby indicate synergistic effects. For traditional medicines in particular, synergistic effects have been widely explored but are difficult to identify (Zhou et al., 2016). Synergistic activation of the hER has been suspected for phytochemicals, but could not be proven so far (Arnold et al., 1996; Graumann et al., 1999). To further investigate zones of interest in the bioautogram, orthogonal separation is useful, especially in case of possible co-elution, followed by spectroscopic and mass spectrometric detections. In particular, high-resolution mass spectrometry (HRMS) and fragmentation (HRMS/MS) are useful for structural assignment to molecules described in the literature (Schreiner et al., 2021).

Materials and methods

Chemicals and materials

Double-distilled water was prepared with a Destamat Bi 18E, Heraeus, Hanau, Germany. *Saccharomyces cerevisiae* BJ3505 was genetically modified to contain the hER α (McDonnell et al., 1991). Silica gel 60 HPTLC plates, silica gel 60 F₂₅₄ MS-grade plates, L-tyrosine (for biochemistry), sodium chloride ($\geq 99\%$), citric acid monohydrate ($\geq 99.5\%$), magnesium sulfate heptahydrate (MgSO₄ • 7 H₂O, 99.5%), and L-arginine ($> 99\%$) were obtained from Merck, Darmstadt, Germany. L-Phenylalanine (99%) was delivered by Bachem, Bubendorf, Switzerland, and L-histidine monohydrochloride monohydrate (for cell culture) was provided by Alfa Aesar, Karlsruhe, Germany. L-Lysine and L-histidine (both p. a.) were obtained from Serva, Heidelberg, Germany. L-Adenine ($> 99\%$) was purchased from TCI Deutschland, Eschborn, Germany. L-Aspartic acid (99.5%), L-glutamine (99%), L-glycine (99%), L-isoleucine (99%), L-leucine (99%), L-methionine (98%), L-serine (99%), L-threonine (for laboratory use), L-valine (99%), D-(+)-glucose (99.5%), yeast nitrogen base without amino acids (p. a.), 4-methyl umbelliferone (MU, $> 98\%$), resazurin sodium salt, fluorescein sodium salt (F), fluorescein-di-(β -D-galactopyranoside) (FDG, $\geq 98\%$), menadione (analytical standard), sodium bicarbonat ($\geq 99.7\%$), and ammonium acetate (LC-MS grade, $\geq 99\%$) were from Sigma-Aldrich Fluka, Steinheim, Germany. Sodium hydroxide ($\geq 99\%$), disodium hydrogen phosphate (Na₂HPO₄, $\geq 99\%$), 4-methyl umbelliferyl- β -D-galactopyranoside (MUG, for biochemistry), potassium dihydrogen phosphate (KH₂PO₄, $\geq 99\%$), potassium chloride (KCl, 98.5%), dimethyl sulfoxide (DMSO, $\geq 99.8\%$), formic acid ($\geq 98\%$), acetic acid (Rotipuran Supra, 100%), and toluene (HPLC grade) were obtained from Carl Roth, Karlsruhe, Germany. Ethyl acetate (HPLC grade) was delivered by Th. Geyer, Renningen, Germany and n-hexane (HPLC grade), methanol (LC-MS grade), and copper (II) sulfate pentahydrate ($\geq 99\%$) by Honeywell, Seelze, Germany. Ethanol (HPLC grade) and water (LC-MS grade) were purchased from Fisher Scientific, Schwerte, Germany. Methanol (HPLC grade) was from VWR, Darmstadt, Germany. 17 β -Estradiol (E2, 98.5%) was delivered by Dr. Ehrenstorfer, Augsburg, Germany. Degalan® P 28 N (Degalan) was provided by Röhm, Darmstadt, Germany. Daidzein was delivered by Cayman Chemicals, Ann Arbor, MI, United States. Dried botanical powders (Table S1) were obtained from Martin Bauer Group, Vestenbergsgreuth, Germany. Purity grades were listed when available.

Preparation of standard solutions, buffers, and samples

A methanolic E2 standard solution (2 ng/ml) was prepared as 1:500,000 dilution from a methanolic stock solution (1 mg/ml). For

dose-response-curves, further E2 standard solutions (200 ng/ml, 100 ng/ml, 20 ng/ml) were required. Daidzein standard solutions were prepared as 1 mg/ml stock solutions in methanol and diluted in a linear descending series to concentrations of 100 µg/ml, 10 µg/ml, 1 µg/ml, and 100 ng/ml. The fluorescent end product MU (1 mg) was dissolved in 1 ml methanol. The alternative end product F was prepared as a 1-mg/ml stock solution in methanol and diluted 1:100 and 1:1000. Citrate buffer consisted of 6 g/l citric acid monohydrate and 10 g/l Na₂HPO₄ in double-distilled water, adjusted to pH 12 by solid sodium hydroxide (Klingelhöfer and Morlock, 2014). Phosphate buffer was prepared by dissolving 40.8 g/l KH₂PO₄, 42.6 g/l Na₂HPO₄, 1.2 g/l MgSO₄ • 7 H₂O, and 3.7 g/l KCl in double-distilled water, adjusted to pH 7 with solid sodium hydroxide (Schick and Schwack, 2017). Sodium bicarbonate solution (2.5%, W/V) was prepared in double-distilled water. Botanical samples (Table S1) were prepared as 100 mg/ml methanolic extracts according to (Schreiner et al., 2021).

Preparation of yeast cell medium and culture

Minimal medium and yeast cell culture were prepared via a modified version of Klingelhöfer and Morlock, 2014. For the medium, double-distilled water was sterilized. Through sterile filtration (mixed cellulose ester syringe filter, <0.22 µm, Merck, Darmstadt, Germany) 10 g/l D-(+)-glucose, 6.8 g/l yeast nitrogen base without amino acids, and 14 amino acids (200 mg/l L-adenine, 200 mg/l L-arginine, 1,000 mg/l L-aspartic acid, 1,000 mg/l L-glutamic acid, 200 mg/l L-histidine, 300 mg/l L-isoleucine, 1,000 mg/l L-leucine, 300 mg/l L-lysine, 200 mg/l L-methionine, 500 mg/l L-phenylalanine, 4,000 mg/l L-serine, 2,000 mg/l L-threonine, 300 mg/l L-tyrosine, and 1,500 mg/l L-valine) were added. A 1-ml cryostock (−80 °C) yeast suspension was diluted in 29 ml minimal medium in a 100 ml glass baffled flask. The inoculated medium was incubated (Cultura M Incubator 70700, Almedica, Giffers, Switzerland) overnight (18–19 h) at 30 °C and 75 rpm on an orbital shaker (Edmund Bühler, Hechingen, Germany). The cell number was determined with a fluidlab R-300 (anvajo, Dresden, Germany) out of a 1:20 dilution (50 µl cell suspension and 950 µl 0.9% sodium chloride in double-distilled water, W/V). To adjust the cell number to 0.8×10^8 cells/µl, the respective volume of cell suspension was centrifuged (centrifuge 5702, Eppendorf, Hamburg, Germany) at $2,500 \times g$ for 5 min. The supernatant was discarded, while the sedimented cells were resuspended in 2 µl fresh medium with 150 µM copper (II) sulfate. For cytotoxicity testing, 1 mg resazurin sodium salt was added to the 2 µl resuspended cells as 50 µl of a 20 mg/µl resazurin solution in double-distilled water.

NP-HPTLC^{fix}-UV/Vis/FLD-pYAVES-UV/Vis/FLD workflow

Experiments were carried out on silica gel 60 F₂₅₄ MS-grade plates, except for those with FDG substrate. Since the FDG response is evaluated at UV 254 nm, silica gel 60 plates without fluorescence indicator were used. Both plate types were prewashed twice with methanol – water (4:1, V/V) in a Simultaneous TLC Developing Chamber (Macherey-Nagel, Düren, Germany) and dried at 110 °C in a clean oven (Memmert, Schwabach, Germany) for 20 min (Morlock, 2014). The plates were stored wrapped in aluminum foil in a desiccator. HPTLC instrumentation was from CAMAG, Muttenz, Switzerland, controlled by visionCATS software (version 3.1.21109.3). Applications were performed using an Automated TLC Sampler 4. Sample extracts were applied as 6-mm bands (4 µl, pYES) or 10-mm bands (6.7 µl, pYAVES) and separated with ethyl acetate – toluene – formic acid – water (16:4:3:2, V/V/V/V) up to a migration distance of 70 mm (Krüger et al., 2017; Schreiner et al., 2021) in a twin trough chamber (20 cm × 10 cm). Plates were dried for 4 min (stream of cold air, hairdryer, if not stated otherwise). Strips were partially overlaid along each track using Freemode option of winCATS software (version 1.4.7.2018). The E2-strip was applied on NP (1 mm × 70 mm; 10 pg/area) or on NP^{fix} (2 mm × 70 mm; 20 pg/area), and

the MU strip (1 mm × 70 mm; 5 µg/area) was applied to the right of each. Alternatively to MU-strips, F-strips (1 mm × 70 mm; 10 ng/area) were applied. The planar chromatograms were recorded (TLC Visualizer 2) at 254 nm (UV), white light illumination (Vis), and 366 nm (FLD).

To neutralize the acidic layer, buffering (all sprayed with yellow nozzle, level 2, Derivatizer) was substrate-specific. For MUG substrate, citrate buffer was piezoelectrically sprayed onto the plate (1.4 ml). For FDG substrate, 2.8 ml sodium bicarbonate buffer was used. For resazurin substrate, the plate was buffered twice with 1.4 ml sodium bicarbonate buffer. All buffering steps were followed by plate drying. For fixation, plates were coated according to Schreiner et al. (2022) with Degalan by placing them horizontally in 400 ml of a 0.25% Degalan solution in *n*-hexane (rectangular deco glass tank of 21 cm × 11 cm × 4 cm covered with a rectangular glass plate of 27 cm × 13 cm) for 10 min and then dried.

The prepared yeast cell culture was piezoelectrically sprayed onto the plates (1.4 ml, red nozzle, level 6), placed in a polypropylene box (KIS 26.5 cm × 16 cm × 10 cm, ABM, Wolframs-Eschenbach, Germany; pre-moistened with water for 30 min), and incubated at 30 °C for 3 h, followed by drying. Two different substrate-solutions were tested, which were piezoelectrically sprayed (yellow nozzle, level 4): MUG substrate (1.5 ml citrate buffer and 50 µl of 20 mg/µl MUG in DMSO) or FDG substrate (1.4 ml phosphate buffer and 25 µl of 5 mg/µl FDG in DMSO). The plate was incubated at 37 °C for either 15 min (FDG) or 30 min (MUG), dried, and documented at UV 254 nm (FDG), FLD 366 nm (MUG), or white light illumination (resazurin). To ensure functionality of the assays, 10 pg E2 were applied onto each upper plate part above the solvent front as positive control, whereas menadione (1, 1.5, and 2 µg) was used to prove the cytotoxicity assay. For pYAVES experiments the E2-strip acts as a positive control. For the evaluation of dose-response curves, plates were additionally scanned (TLC Scanner 3) at 366 nm to generate peak profiles for integration (visionCATS). Dose-response curves were generated using the online tool IC₅₀ calculator from AAT Bioquest, Sunnyvale, CA, United States.

Heart cut-RP-HPLC-DAD-HESI-HRMS/MS

The Dionex Ultimate HPLC system (Dionex Softron, Germering, Germany) consisted of a binary pump (HPG-3200SD), an autosampler (WPS-3000TXRS), a column oven (TCC-3000RS), and a diode array detector (DAD-3000RS). It was connected to a Q Exactive Plus Hybrid Quadrupole-Orbitrap, equipped with an Ion-Max HESI-II probe (both Thermo Scientific, Bellefonte, PA, United States). Ionization settings were: sheath gas 20 AU, aux gas 10 AU, spray voltage 3.5 kV, capillary temperature 270 °C, probe heater temperature 200 °C, S-lens RF level 50 AU.

Verified antiestrogens were heart-cut eluted from the HPTLC plate with water – methanol (9:1, V/V), using a fully automated autoTLC-MS interface (Häbe and Morlock, 2020; Mehl et al., 2021) with oval elution head (4 mm × 2 mm). An eluent flow of 0.1 ml/min was provided by an HPLC standalone pump (MX010PFT, Teledyne SSI, State College, PA, United States). On a two-position six-port switching valve (MXT series, PD715-000, Rheodyne, IDEX Health & Science, Rohnert Park, CA, United States), a 50-µl sample loop and a desalting cartridge (Accucore RP-MS, 10 mm × 2.1 mm, 2.6 µm, Thermo Scientific) were installed (Schreiner and Morlock, 2021). After 40 s elution time, the valve was switched and HPLC gradient flushed the cartridge, transferring the analytes to the main column (Accucore RP-MS 100 mm × 2.1 mm, 2.6 µm, thermostated at 40 °C, Thermo Scientific). Eluent A was water with 2.5 mM ammonium acetate (pH adjusted to 4.5 with acetic acid), eluent B was methanol and the flow rate was set to 0.4 ml/min. The 12-min gradient started at 2% B for 2 min (elution), then increased to 100% B (2 min–7 min), was held for 3 min (7 min–10 min), followed by 2 min equilibration time. Analytes were detected with DAD (wavelength scan 200–400 nm and at specific wavelengths $\lambda_1=240$ nm, $\lambda_2=280$ nm, and $\lambda_3=320$ nm) and HRMS/MS in polarity switching full-scan

data-dependent MS² (ddMS²) mode. Full scan at a mass range of m/z 100–1100 had a resolving power of 70,000 full width at half-maximum (FWHM) and automated gain control (AGC) target 3e6, which was followed by a Top5 ddMS² fragmentation at a mass range of m/z 80–1000, resolution of 17,500 FWHM, AGC target 1e6, and collision energy of 40 eV. External mass calibration was performed weekly with Pierce TM LTQ Velos ESI positive/negative ion calibration solution. The instrument was controlled by Xcalibur 3.0.63.3 with Foundation 3.0.152 under DCMS link 2.14 (all Thermo Scientific).

Results and discussion

A multiplex bioassay format was developed offering 4 different biological activity principles to evaluate estrogenic agonists, antagonists, synergists, and false-positives in complex botanical samples. The reduction of diffusion through Degalan fixation on NP planar chromatograms was a critical step to provide multiplex conditions. The Degalan-fixed bioautograms were compared to the status quo without fixation for estrogenic responses (pYES) and by overlaying an E2-strip for antiestrogenic responses (pYAES). The overlaid E2-strip also revealed synergists. Adding a strip of the substrate cleavage product led to the detection of false-positive antiestrogens and thereby the verification of true antiestrogenic responses (pYAVES). Several bioactive zones were further analyzed using HPLC–DAD–HESI–HRMS/MS.

Screening of 68 botanicals via HPTLC^{fix}–UV/Vis/FLD–pYES and comparison to status quo

The HPTLC–UV/Vis/FLD–pYES bioautograms revealed many more blue-fluorescent zones on the plate with fixation agent (Fig. S1B) than the status quo without fixation (Fig. S1C, Schreiner et al., 2021). Since zone response can be caused by excessive native fluorescence, the bioautogram at FLD 366 nm always has to be compared to the chromatogram at FLD 366 nm (Fig. S1A). With the status-quo method, estrogenic substances were found in botanical sample nos. 1, 13, 24, 28, 35, 41, 42, 55, 59, 60, 62–64, and 67 (Schreiner et al., 2021). Fixating the substances led to a bioassay with sharper zones, and additional estrogenic substances were found in botanical sample nos. 8, 14, 16, 22, 38, 45, and 54. The fluorescent zone at hR_F 40 appeared in many samples (nos. 4, 8, 11, 12, 19, 22, 33, 34, 36, 37, 50, 53, 56, 62–64, and 68) but derived from the native fluorescence of chlorogenic acid, as described for nos. 4, 12, 19, 22, 37, 50, and 56 in Schreiner et al., 2021. Estrogenic zones in sample nos. 24, 28, 55, and 59 disappeared with the Degalan fixation and were investigated again (Fig. S2). The estrogens in 24 and 59 were not detectable in the repetition even on the unfixated plate despite the botanicals were freshly extracted. The age of the plant powders could have an influence, as the first unfixated bioautograms were from a previous study. Estrogens in the middle hR_F area of 28 and 55 were missing after fixation, whereby the estrogenic responses in the solvent front were detected. This was explained by the fact that Degalan fixation could compromise the sensitivity of the assay. The dose-response-curves of E2 of a fixed and an unfixated bioautogram led to comparable results, whereby the dose-response curves of the phytoestrogen daidzein differed (Fig. S3). Hence, the fixation may have an influence on the estrogenic response but is substance-specific.

Screening of 68 botanicals via HPTLC^{fix}–UV/Vis/FLD–pYAVES and comparison to status quo

The improved sharpness via the Degalan coating was particularly noticeable in the HPTLC^{fix}–UV/Vis/FLD–pYAVES bioautograms, as the E2-strips were less diffuse and the interruptions were more distinct (Fig. 1A) compared to plates with unfixated substances (Fig. 1B, Schreiner et al., 2021). Additionally, a bending of the neighboring E2-strips was observed in the status quo for the samples nos. 6, 15, and 37 at lower hR_F values, presumably caused by strongly diffusing

substances. This problem was prevented by the respective HPTLC^{fix} workflow. The status-quo bioassay revealed many enhancements of the E2-strip fluorescence (compared to the blank B), implying synergistic effects, and some fluorescence reductions indicating antiestrogens (Schreiner et al., 2021). With fixation, the fluorescence of the E2-strip was less detectable indicating a loss of sensitivity exemplarily observed for sample nos. 7 and 29, but the profiles and meaning of the described effects could be reproduced and sharpened, assigning the effects even more precisely to certain zones. For example, botanical sample no. 47 revealed many small interruptions of the fluorescence, not seen in the status-quo bioassay (unfixated). The detection of non-fluorescent zones and thus possible antiestrogens was also improved, as shown by the example of botanical sample no. 53.

Screening of 13 selected botanicals via HPTLC^{fix}–UV/Vis/FLD–pYAVES–UV/Vis/FLD

Selected botanical samples with presumed antiestrogenic compounds (nos. 16, 22, 24, 34, 37, 41, 43, 53, 55, 58, 61, 67, and 68) were subjected to the newly developed HPTLC^{fix}–UV/Vis/FLD–pYAVES method. To also investigate the multiplex bioassay with another substrate than MUG, FDG was used and the amount of end product F was adjusted to the fluorescence of the E2-strip, whereby 10 ng seemed to be the most suitable (Fig. S4). Native fluorescence of the botanical samples at 254 nm (Fig. 2A) or 366 nm (Fig. 2C) complicated the bioassay evaluation. Using MUG as substrate, the bioautogram (Fig. 2D) showed less native fluorescence than the one with the FDG-substrate (Fig. 2B). The response of the Vis-evaluable substrate resorufin- β -D-galactopyranoside was pH sensitive and not usable with the acidic mobile phase despite testing of various buffers. The multiplex pYAVES bioautograms confirmed and verified many antiestrogenic effects by the reduced fluorescent E2-strip and at the same time remaining fluorescent F- or MU-strip in this antiestrogenic zone (Fig. 2B/D). Except for botanical sample nos. 58 and 61, all investigated samples contain true antiestrogens. To ensure, that the antiestrogenic effect was not a cytotoxic effect, cell viability staining with resazurin was performed (Fig. 2E). As positive control menadione was used detected as colorless zone (concentration-dependent halos) on a purple background. No cytotoxic effects were observed in any of the zones, further verifying the antiestrogens. The estrogenic effects in botanical sample nos. 41, 55, and 67 were also detected. Contrarily, the estrogen-like substances detected in sample nos. 16 and 22, still seen in pYAVES were not detectable in the pYAVES bioautogram (Fig. S5A). The reason for this could be that the chromatography is slightly shifted upwards, as can be seen in the chromatograms at UV 254 nm (Fig. S5B) and FLD 366 nm (Fig. S5C), whereby fluorescence-quenching substances were moved over the estrogenic zone.

With the new NP-HPTLC^{fix}–UV/Vis/FLD–pYAVES workflow, 13 samples were simultaneously analyzed for four different effects (Fig. 3). Estrogens were detected as MU-blue fluorescent zones, whereas antiestrogens caused a fluorescence reduction of the overlaid E2-strip. False-positive antiestrogens were identified by fluorescence reduction of the MU-strip at the same horizontal zone position where the E2-strip was interrupted. An enhanced E2-strip indicated synergistic effects. Often it cannot be distinguished between synergistic and additive effects (Zhou et al., 2016), but with the presented multiplex approach, both phenomena could be detected simultaneously. According to the terminology (Roell et al., 2017; Rajapakse et al., 2002) slightly modified as $0 + 1 > 1$, synergy is raised from the intensified signal response (>1) by combining a non-observed-effect compound (0) and an effect-compound (1) (Fig. 3). Contrarily, additive effects are described as the sum of two individually active compounds (1), when applied in combination, amplifying to more intense signals ($1 + 1 = 2$, Seeger et al., 2016). Studying all these effects for 13 samples on one plate was only possible with the sharpening due to the fixation with Degalan. The four bioassay responses were merged on the same plate and obtained in parallel,

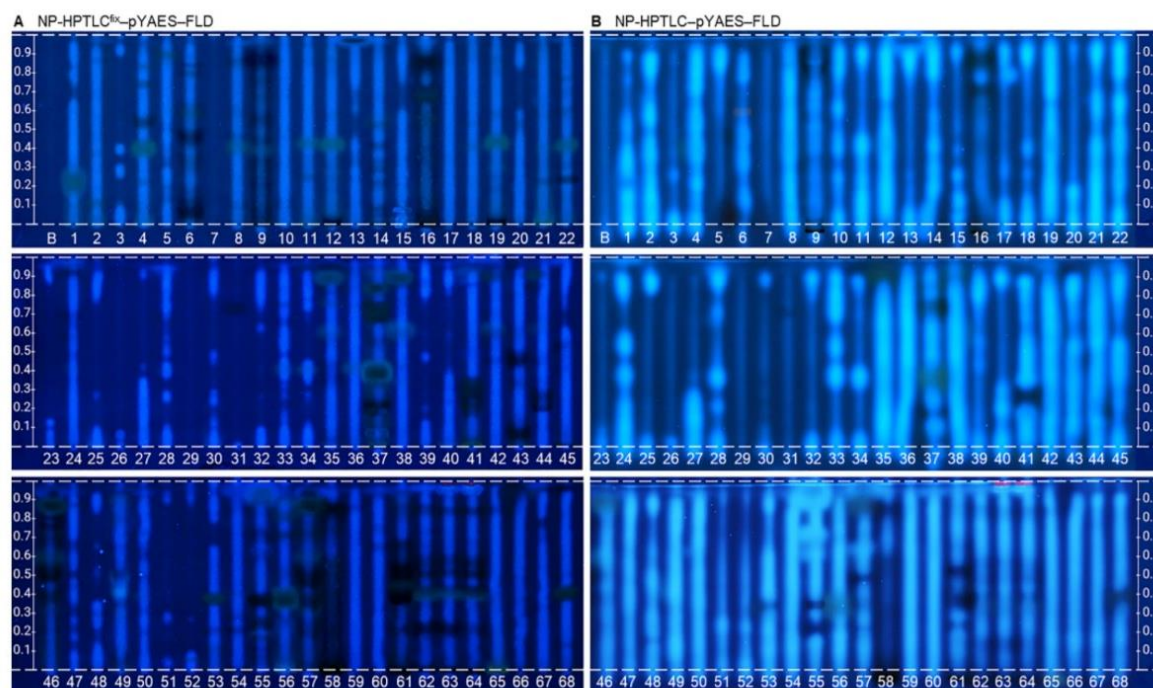


Fig. 1. NP-HPTLC^{fix}-pYAES-FLD analysis of 68 botanicals compared to status quo without fixation. Botanical samples (4 μ l, 6-mm bands, nos. 1–68 assigned in Table S1 and solvent blank B for comparison) separated on HPTLC plates silica gel 60 F₂₅₄ MS-grade with ethyl acetate – toluene – formic acid – water (16:4:3:2; V/V/V/V) up to 70 mm. NP-HPTLC^{fix}-pYAES bioautograms at FLD 366 nm (A, with 20 μ g E2-strip of 2 mm \times 70 mm and Degalan coating) compared with respective status-quo bioautograms (B, 10 μ g E2-strip of 1 mm \times 70 mm, Schreiner et al., 2021).

which saves time and costs, and makes the multiplex bioassay highly reliable and less error-prone.

NP-HPTLC^{fix}-UV/Vis/FLD-pYAVES-heart cut-RP-HPLC-DAD-HESI HRMS/MS

Selected bioactive zones (marked as lowercase letters in Fig. 2D) were eluted directly from the fixated pYAVES bioautogram and subjected to RP-HPLC-DAD-HESI-HRMS/MS (Fig. 4A). Mass spectrometric results of the recorded zones a–n were summarized in Table 1. Out of 28 mass signals detected, 17 were identified, six of which are known to possess estrogenic (antagonistic) activity, and four which could affect an estrogen-like response due to structural similarity. Zone a in guarana (no. 16, hR_F 75) was divided into three signals by orthogonal separation. First, theophylline (Fig. 4B), which was distinguished from the related theobromine based on its fragment spectrum (Bartella et al., 2019), highlighted the benefit of MS/MS measurement. The two other signals were assigned to procyanidin B2 and caffeine since their UV spectra, mass spectra, and fragmentation pattern were consistent with literature (Bartella et al., 2019). All of them are known to be contained in guarana (Cynara de Oliveira Salles et al., 2022) but none of them is known for antiestrogenic activity. Since procyanidin B2 structurally originates of two catechin subunits, and catechin is known to have effects on ER-regulated estrogenic activity (Kuruto-Niwa et al., 2000), the dimer could be responsible for the detected antiestrogenic effect. This assumption has to be verified with a standard. Zone b of elder flower (no. 22, hR_F 21) indicated the presence of icaraside F2, which fragments in ESI-negative mode are consistent with literature (Amessis-Ouchemoukh et al., 2014, Fig. 4C). Its estrogenic activity was already presumed in parsley by Yoshikawa et al. (2000) but was never proved. Besides, in the presented case an estrogen antagonistic effect is

postulated. Hop (no. 24) revealed two different antiestrogenic zones at hR_F 47 (zone c) and 76 (zone d), both with two distinct mass signals. At lower hR_F value, m/z 379.1763 [M–H][–] was assigned to 4'-hydroxyallo-(*cis*-)cohumulinone, and m/z 393.1925 [M–H][–] to 4'-hydroxyallo-humulonone, either in *cis*-conformation or as *ad*- or *n*-isomers, respectively (Taniguchi et al., 2015). Since they were only described as hop constituents, they were only assumed to cause antiestrogenic activity. In the upper zone, none of the mass signals were found as compounds comprised in hop, nor as estrogenically active. Zone e in lovage (no. 34, hR_F 86) did not show any mass signals differing from the plate and assay background. The phytohormone abscisic acid, found in yerba mate (no. 37, hR_F 98, zone f), is known to play an important role in signaling pathways when the plant is exposed to drought (Acevedo et al., 2019). Its effects on the human endocrine system and affinity to hERs have not been discovered so far. Its identification is certain, since UV spectrum (Gao et al., 2016) and fragmentation spectrum (Durgbanshi et al., 2005) are consistent with literature (Fig. 4D). In orange peel (no. 41, hR_F 40, both zone g), the well-documented phytoestrogens naringin (Fig. 4E) and hesperidin were found (Favela-Hernández et al., 2016; Puranik et al., 2019). Zone h in passionflower (no. 43, hR_F 72, Fig. 4F) contained (iso)vitexin, also called (6-) β -glycosyl-apigenin. The aglycon apigenin is known to bind the hER (Mbachu et al., 2020) and affects an estrogenic response. Often glycosylated molecules and their aglycones exhibit contrary effects, e.g. naringin and naringenin, hesperidin and hesperetin, or genistin and genistein. Plantain (no. 53) contained two antiestrogenic zones i (hR_F 45) and j (hR_F 85) both comprising a single mass signal, which could not be assigned to known substances found in plantain, nor to antagonistic phytoestrogens. At least the molecular formulae of C₁₉H₃₄O₁₀ (i) and C₁₂H₁₈O₆ (j) were determined. In licorice (no. 55) an antiestrogenic zone (hR_F 36, zone k) and an estrogenic zone (hR_F 96, zone l) were found. The estrogenic zone revealed four distinct

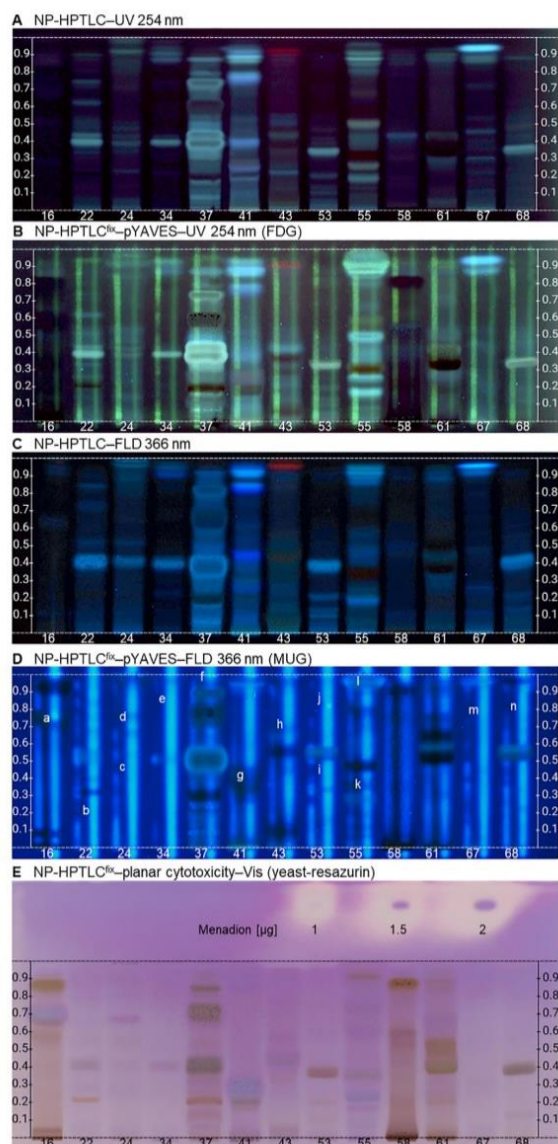


Fig. 2. NP-HPTLC^{fix}-UV/FLD-pYAVES of 13 selected botanicals. Chromatogram at UV 254 nm (A) and FLD 366 nm (C) of botanical samples (nos. assigned in Table S1, 6.7 µl, 10-mm bands) with tentative antiestrogenic effects separated on HPTLC plate silica gel 60 F₂₅₄ MS-grade with ethyl acetate – toluene – formic acid – water (16:4:3:2; V/V/V/V) up to 70 mm, overlaid with E2-strip (20 pg, 2 mm × 70 mm) and fluorescein (10 ng) or 4-methyl umbelliferone (5 µg) strips (1 mm × 70 mm). NP-HPTLC^{fix}-pYAVES bioautograms with FDG-substrate at UV 254 nm (B) or MUG-substrate at FLD 366 nm (D). Marked zones a–n were analyzed via heart cut–RP-HPLC–DAD–HESI-HRMS/MS (Figs. 4 and 5). Planar cytotoxicity assay with YES cells and resazurin staining at white light illumination with menadion as positive control (E).

signals assigned to formononetin (Fig. 4G), liquiritigenin, daidzein (both Fig. 5), and calycosin (not displayed) identified according to published UV and fragmentation spectra (Xu et al., 2013; Zhang et al., 2013; Vlasisavljević et al., 2018). The estrogenic activity for daidzein (Nishihara et al., 2000) and liquiritigenin (Boonmuen et al., 2016) is already

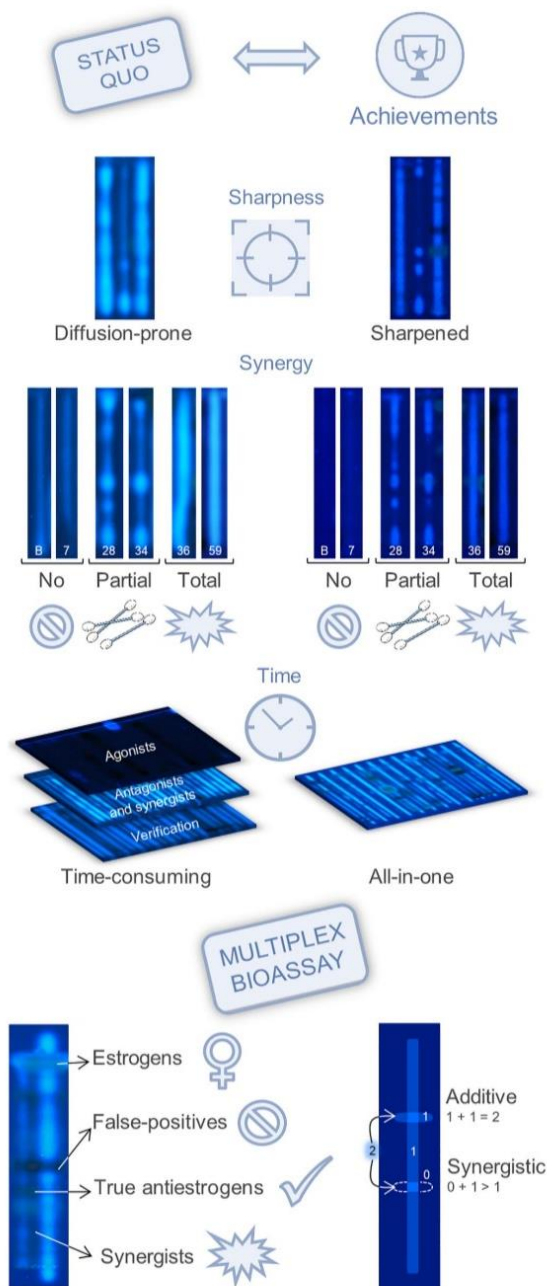


Fig. 3. Achievements in estrogen screening by the new multiplex bioassay. Improved zone sharpness and a time-saving combination of different bioassays led to the multiplex bioassay giving information on estrogens, antiestrogens, false-positives and synergists. The difference between additive effects and synergistic is explained.

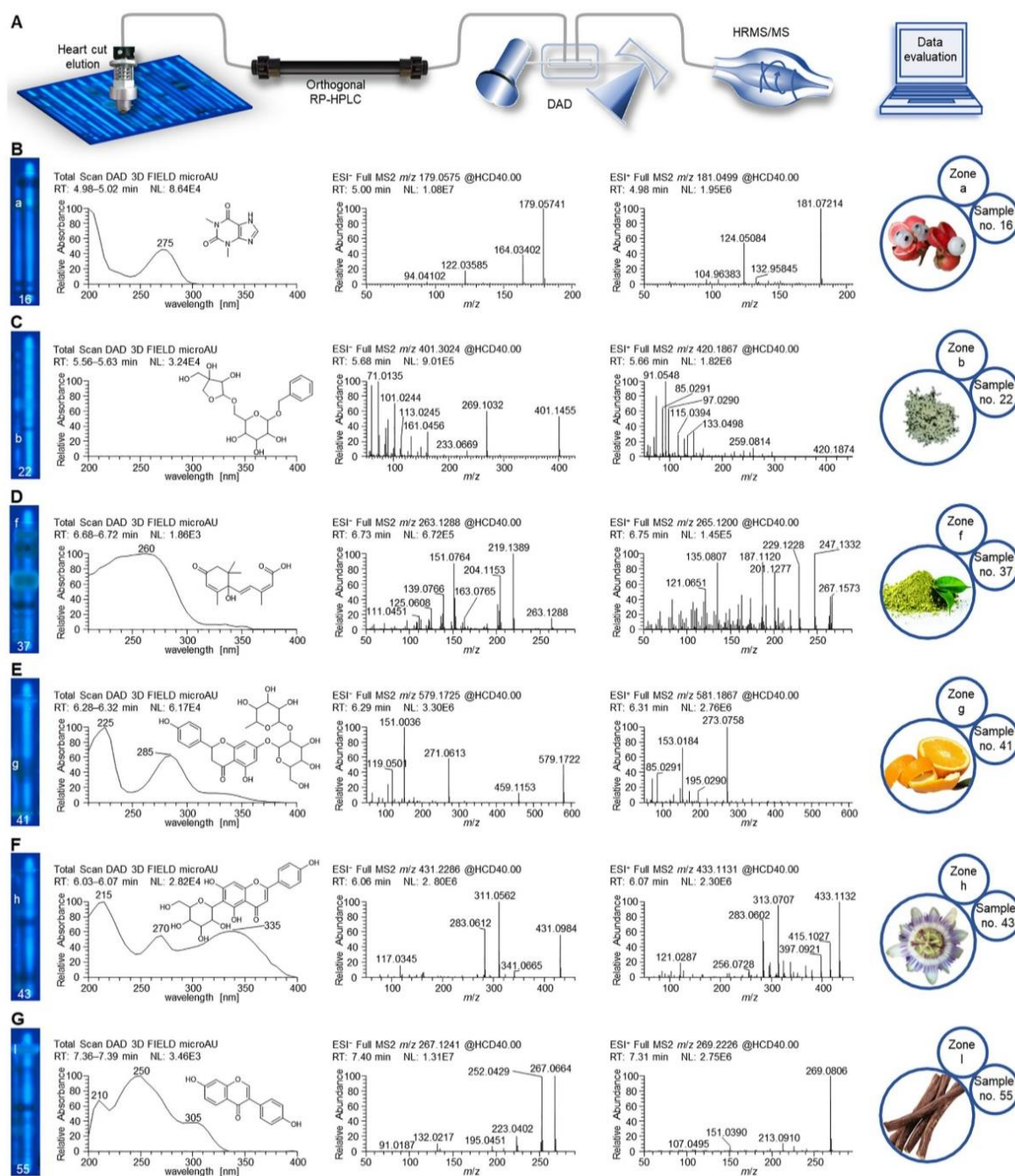


Fig. 4. NP-HPTLC^{fix}-pYAVES-FLD-heart cut-RP-HPLC-DAD-HESI-HRMS/MS. Schematic overview of the fully automated heart cut elution, orthogonal separation, diode array detection and high-resolution tandem mass spectrometry (A). UV and fragmentation spectra shown for theophylline in guarana (no. 16, B), icaraside F2 in elder flower (no. 22, C), abscisic acid in yerba mate (no. 37, D), naringin in orange peel (no. 41, E), isovitexin in passionflower (no. 43, F), and formononetin in licorice (no. 55, G).

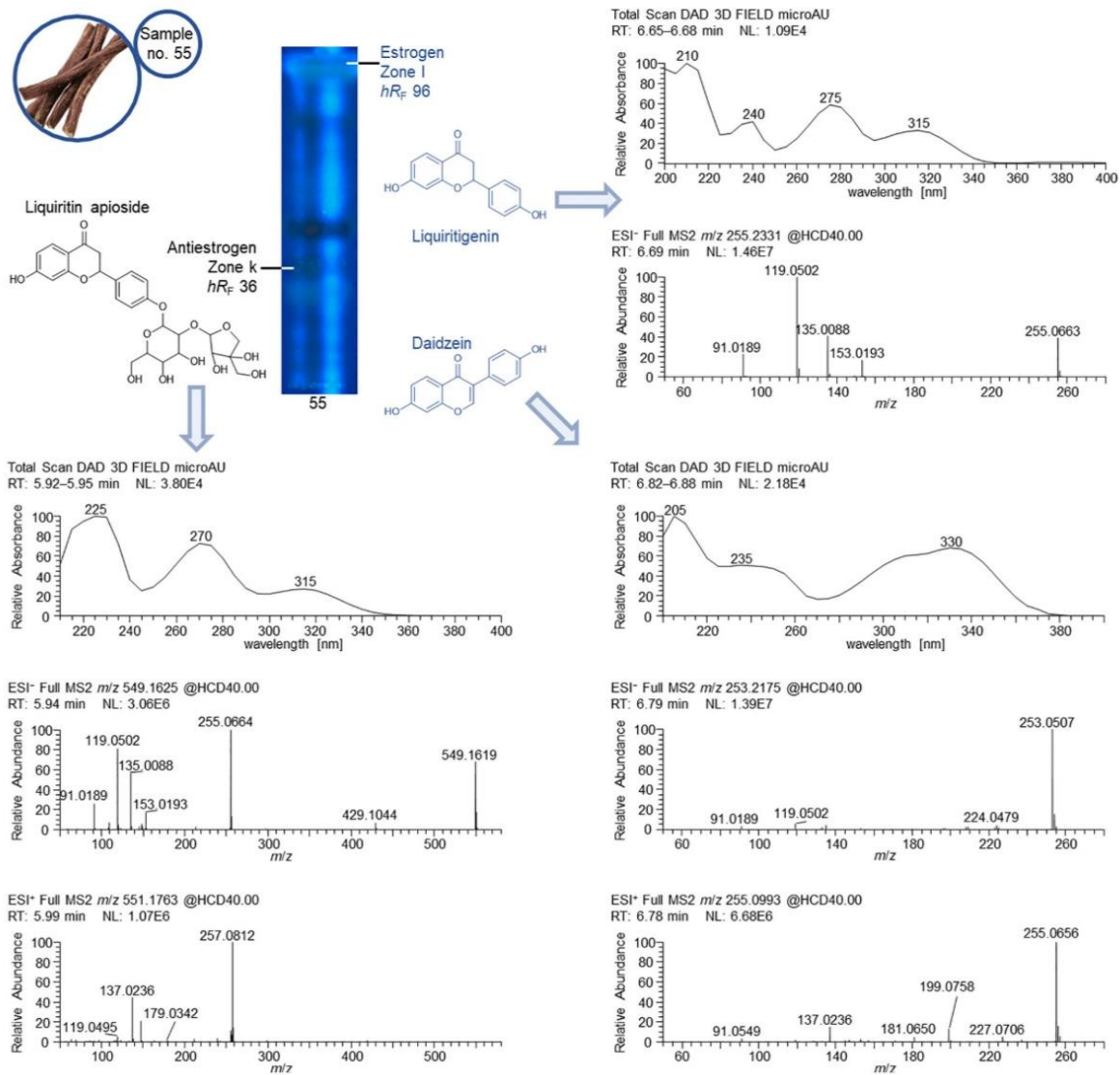


Fig. 5. NP-HPTLC^{fix}-pYAVES-FLD-heart cut-RP-HPLC-DAD-HESI-HRMS/MS of licorice zones k and l. Antiestrogenic zone k was caused by liquiritin apioside verified by UV absorption and HRMS fragmentation spectra in both ionization modes. Formononetin (Fig. 4G), liquiritigenin, and daidzein identified by respective spectra in the estrogenic zone I.

Table 1
Tentative HRMS signal assignments. NP-IPITLC^{6x}-pYAVES-RP-HPLC-DAD-HESI-IRMS/MS signals of bioactive zones.

Zone	Botanical	Observed effect	hR _f	Retention time [min]	Molecular formula	Ion species	Precursor [m/z]	Δm/z [ppm]	MS ² fragments [m/z]	Proposed fragment formula	Δm/z [ppm]	λ _{max} [nm]	Tentative assignment	Literature
a	Guarana (no. 16)	antiestrogen	75	5.05	C ₇ H ₆ O ₂ N ₄	[M-H] ⁻	179.0576	-0.56	164.0340	[C ₆ H ₄ O ₂ N ₄ -H] ⁻	-0.03	275	theophylline	(Bartella et al., 2019)
						[M+HCOO] ⁻	225.0631	-0.89	122.0360	[C ₆ H ₄ ON ₃ -H] ⁻	0.29			
						[M+H] ⁺	181.0719	0.40	94.0410	[C ₆ H ₅ N ₃ -H] ⁻	0.97			
						[M+N ₃] ⁺	203.0539	0.18	124.0308	[C ₆ H ₅ ON ₃ +H] ⁺	2.43			
						[M+K] ⁺	219.0278	0.42						
						[M-H] ⁻	577.1359	-1.34	407.0774	[C ₂₂ H ₁₆ O ₈ -H] ⁻	-0.36	280	procyanidin B2	(Cymara de Oliveira Sallies et al., 2022)
						[M+Cl] ⁻	613.1125	-1.07	289.0720	[C ₁₆ H ₁₀ -H] ⁻	-0.78			
						[M+NO ₂] ⁻	640.1317	-2.28	125.0244	[C ₁₀ H ₆ O ₃ -H] ⁻	-0.17			
						[M+H] ⁺	579.1505	-1.34	409.0931	[C ₂₂ H ₁₇ O ₈] ⁺	-1.94			
						[M+NH ₄] ⁺	596.1766	-0.60	291.0865	[C ₁₃ H ₄ O ₆ +H] ⁺	-0.53			
						[M+N ₃] ⁺	601.1323	-1.00	139.0390	[C ₇ H ₆ O ₃ +H] ⁺	-0.71			
						[M+K] ⁺	617.1060	-0.78	127.0392	[C ₈ H ₆ O ₃ +H] ⁺	-1.49			
b	Elder flower (no. 22)	antiestrogen	21	5.68	C ₁₈ H ₂₆ O ₁₀	[M+H] ⁺	195.0877	-0.04	138.0662	[C ₈ H ₇ ON ₃ +H] ⁺	0.06	275	caffeine	(Bartella et al., 2019)
						[M+N ₃] ⁺	217.0694	0.86	110.0716	[C ₃ H ₆ N ₃] ⁺	2.29			
						[M+K] ⁺	233.0436	-0.24	83.0609	[C ₃ H ₇ N ₂] ⁺	-0.20			
						[M+K] ⁺	401.1459	-1.54	269.1032	[C ₃ H ₆ N ₂] ⁺	-2.71			
						[M-H] ⁻	437.1221	-0.27	161.0456	[C ₃ H ₆ O ₃ -H] ⁻	-0.54			
						[M+Cl] ⁻	447.1510	-0.46	113.0245	[C ₆ H ₁₀ O ₃ -H] ⁻	-0.25			
						[M+HCOO] ⁻	461.1666	-0.40	101.0244	[C ₃ H ₆ O ₃ -H] ⁻	-0.58			
						[M+H ₂ C-COO] ⁻	420.1866	-0.49	259.0814	[C ₁₀ H ₄ O ₇ +H] ⁺	-0.73			
						[M+NH ₄] ⁺	425.1417	0.26	145.0497	[C ₃ H ₆ O ₃ +H] ⁺	-1.34			
						[M+N ₃] ⁺	441.1157	0.11	115.0394	[C ₃ H ₇ O ₃] ⁺	-1.39			
						[M+K] ⁺	379.1763	-0.24	163.0763	[C ₇ H ₇] ⁺	-0.49			
						c	Hop (no. 24)	antiestrogen	47	6.36	C ₂₀ H ₂₆ O ₇	[M-H] ⁻	381.1912	-1.15
[M+H] ⁺	398.2178	-1.28	111.0461	[C ₈ H ₁₂ O-H] ⁻	0.66									
[M+NH ₄] ⁺	403.1736	-1.07		[C ₈ H ₈ O ₂ -H] ⁻	0.85									
[M+K] ⁺	419.1471	-1.07												
[M+H] ⁺	393.1925	-1.48	335.1499	[C ₁₈ H ₂₀ O ₆ -H] ⁻	0.43									
[M+H] ⁺	395.2067	-0.71	183.0664	[C ₈ H ₁₂ O ₂ -H] ⁻	-0.36									
[M+N ₃] ⁺	417.1891	-1.83	125.0608	[C ₃ H ₁₀ O ₂ -H] ⁻	0.19									
[M+K] ⁺	433.1632	-2.00												
[M+H] ⁺	174.1128	-1.84	113.0602											
[M+N ₃] ⁺	196.0948	-1.86												
[M+K] ⁺	212.0686	-1.08												
d	Hop (no. 24)	antiestrogen	76	4.61	C ₈ H ₁₃ O ₃ N							[M-H] ⁻	351.0877	-0.79
						[M+H] ⁺	353.1018	0.47	292.0738			325	unknown	
						[M+K] ⁺	419.1471	-1.07	311.0914					
						[M+K] ⁺	433.1632	-2.00	243.0653					
						[M+H] ⁺	174.1128	-1.84	201.0548					
						[M+N ₃] ⁺	196.0948	-1.86						
						[M+K] ⁺	212.0686	-1.08						
						[M+H] ⁺	351.0877	-0.79						
						[M+H] ⁺	353.1018	0.47						
						[M+K] ⁺	419.1471	-1.07						
						[M+K] ⁺	433.1632	-2.00						
						e	Lovage (no. 34)	antiestrogen	86	u. d.	C ₁₅ H ₂₀ O ₄	[M-H] ⁻	263.1289	-0.17
[M+Cl] ⁻	299.1054	0.44	204.1153	[C ₁₃ H ₁₇ O ₂ -H] ⁻	1.46									
[M+H ₂ O+H] ⁺	247.1331	-0.81	151.0764	[C ₈ H ₁₂ O ₂ -H] ⁻	0.23									
[M+H] ⁺	265.1436	-0.51	139.0766	[C ₈ H ₁₂ O ₂ -H] ⁻	-0.83									
[M+NH ₄] ⁺	282.1701	-0.51												
[M+N ₃] ⁺	287.1254	-0.21												
[M+K] ⁺	303.0995	-0.57												
[M+H] ⁺	331.2491	-0.40	157.1233											
[M+Cl] ⁻	367.2256	0.32	127.1128											
[M+NO ₂] ⁻	394.2446	-1.38	297.2425											
[M+K] ⁺	419.1471	-1.07												
[M+K] ⁺	433.1632	-2.00												
f	Yerba mate (no. 37)	antiestrogen	98	6.73	C ₁₈ H ₂₆ O ₅	[M-H] ⁻	381.1912	-1.15	135.0815	[C ₁₀ H ₁₂ O ₂ -H] ⁻	0.70	-	4'-hydroxyallo-	(Taniguchi et al., 2015)
						[M+H] ⁺	398.2178	-1.28	111.0461	[C ₈ H ₁₂ O-H] ⁻	0.66			
						[M+NH ₄] ⁺	403.1736	-1.07		[C ₈ H ₈ O ₂ -H] ⁻	0.85			
						[M+K] ⁺	419.1471	-1.07						
						[M+H] ⁺	393.1925	-1.48	335.1499	[C ₁₈ H ₂₀ O ₆ -H] ⁻	0.43			
						[M+H] ⁺	395.2067	-0.71	183.0664	[C ₈ H ₁₂ O ₂ -H] ⁻	-0.36			
						[M+N ₃] ⁺	417.1891	-1.83	125.0608	[C ₃ H ₁₀ O ₂ -H] ⁻	0.19			
						[M+K] ⁺	433.1632	-2.00						
						[M+H] ⁺	174.1128	-1.84	113.0602					
						[M+N ₃] ⁺	196.0948	-1.86						
						[M+K] ⁺	212.0686	-1.08						
						[M+H] ⁺	351.0877	-0.79						
[M+H] ⁺	353.1018	0.47												

(Continued on next page)

Table 1 (continued)

Zone	Botanical	Observed effect	hR_f	Retention time [min]	Molecular formula	Ion species	Precursor [m/z]	$\Delta m/z$ [ppm]	MS ² fragments [m/z]	Proposed fragment formula	$\Delta m/z$ [ppm]	λ_{max} [nm]	Tentative assignment	Literature						
g	Orange peel (no. 41)	antiestrogen	40	6.10	$C_{21}H_{32}O_{11}$	$[M-H_2O+H]^+$	315.2531	-0.33	279.2322 ⁺											
						$[M+H]^+$	333.2636	-0.12	261.2215 ⁺											
						$[M+NH_4]^+$	350.2902	-0.29	243.2113 ⁺											
						$[M+Na]^+$	355.2955	0.07												
						$[M+K]^+$	371.2194	0.01												
						$[M-H]^+$	459.1879	-1.57	297.1343											
						$[M+Cl]^-$	495.1647	-1.66	253.1446 ⁻											
						$[M+NH_4]^+$	478.2289	-1.30	165.0920 ⁻											
						$[M+Na]^+$	483.1843	-1.21	150.0686											
						$[M+K]^+$	499.1582	-1.10	203.1069 ⁻											
									161.0600 ⁺											
									595.1676	-1.31	459.1148									
									631.1443	-1.18	287.0563									
									658.1637	-2.70	151.0036									
									597.1819	-0.94	135.0452									
			614.2082	-0.41	289.0710															
			619.1638	-0.67	195.0291															
			635.1375	-0.41	153.0185															
			579.1728	-1.46	459.1153															
			595.1677	-1.35	271.0613															
			615.1496	-1.52	151.0036															
			642.1685	-2.23	119.0501															
			581.1867	-0.37	173.0758															
			598.2132	-0.33	171.0290															
			603.1684	0.08	153.0184															
			619.1424	-0.02	85.0291															
			439.1612	-0.45	no															
			475.1380	-0.73	fragments															
			485.1669	-0.84																
			499.1826	-0.91																
			441.1756	-0.19																
			458.2022	-0.25																
			463.1573	0.39																
			479.1314	0.10																
			609.1831	-0.99	301.0722															
			645.1597	-0.83	286.0484															
			672.1790	-2.11	164.0117															
			611.1971	-0.01	134.0375															
			628.2236	-0.03	303.0862															
			633.1790	-0.05	177.0546															
			649.1531	-0.32	153.0183															
			431.0988	-0.96	311.0562															
			467.0754	-0.70	283.0612															
			494.0945	-2.05	117.0345															
			433.1136	-1.46	415.1027															
			455.0954	-1.12	397.0921															
			471.0694	-1.17	313.0707															
			283.1189	-0.55	no															
			319.0955	-0.21	fragments															
h	Passionflower (no. 43)	antiestrogen	72	6.08	$C_{21}H_{32}O_{10}$	$[M-H]^+$	609.1831	-0.99	301.0722	$[C_{16}H_{11}O_6-H]^-$	-1.45	255,	hesperidin*	(Augoustopoulos et al., 2005;						
						$[M+Cl]^-$	645.1597	-0.83	286.0484	$[C_{13}H_{11}O_6-H]^-$	-0.49	325								
						$[M+NO_3]^-$	672.1790	-2.11	164.0117	$[C_8H_5O_4-H]^-$	-1.10									
						$[M+H]^+$	611.1971	-0.01	134.0375	$[C_8H_7O_2-H]^-$	-0.98									
						$[M+NH_4]^+$	628.2236	-0.03	303.0862	$[C_8H_7O_2+H]^+$	0.45									
						$[M+Na]^+$	633.1790	-0.05	177.0546	$[C_{10}H_9O_3+H]^+$	-0.11									
						$[M+K]^+$	649.1531	-0.32	153.0183	$[C_7H_4O_4+H]^+$	-0.09									
									85.0290	$[C_4H_5O_2]^+$	-0.41									
									431.0988	$[C_{17}H_{12}O_6-H]^-$	-0.21	215,	(iso)vitecin	(Quercia et al., 1978)						
									467.0754	$[C_{16}H_{10}O_6-H]^-$	-0.14	270,								
									494.0945	$[C_8H_6O-H]^-$	-0.59	335								
									433.1136	$[C_{21}H_{18}O_9+H]^+$	-0.79									
									455.0954	$[C_{21}H_{16}O_8+H]^+$	-0.84									
									471.0694	$[C_{21}H_{17}O_8+H]^+$	-0.24									
									283.1189	$[C_{16}H_{10}O_5+H]^+$	-0.39	235,								
			319.0955	no	315															

(continued on next page)

Table 1 (continued)

Zone	Botanical	Observed effect	hR_f	Retention time [min]	Molecular formula	Ion species	Precursor [m/z]	$\Delta m/z$ [ppm]	MS ² fragments [m/z]	Proposed fragment formula	$\Delta m/z$ [ppm]	λ_{max} [nm]	Tentative assignment	Literature					
i	Plantain (no. 53)	antiestrogen	45	7.13	$C_{19}H_{30}O_{10}$	[M+HCOO] ⁻	329.1244	-0.50											
						[M+H ₃ C-COO] ⁻	343.1399	-0.22											
						[M+H] ⁺	285.1330	0.93											
						[M+NH ₄] ⁺	302.1595	0.98											
						[M+Na] ⁺	307.1146	2.02											
						[M+K] ⁺	323.0888	1.14											
						[M-H] ⁻	421.2087	-1.79	289.1659 ⁻									unknown	
						[M+Cl] ⁻	457.1853	-1.59	161.0455 ⁻										
						[M+HCOO] ⁻	467.2139	-1.00	101.0243 ⁻										
						[M+H ₃ C-COO] ⁻	481.2296	-1.16	71.0135 ⁻										
						[M+H] ⁺	440.2491	-0.17	111.1172 ⁺										
						[M+NH ₄] ⁺	445.2044	0.07	97.0289 ⁺										
[M+Na] ⁺	461.1782	0.38	85.0290 ⁺																
[M+K] ⁺	469.0707 ⁺		69.0707 ⁺																
j	Plantain (no. 53)	antiestrogen	85	6.82	$C_{12}H_{18}O_6$	[M+H] ⁺	259.1176	-0.09	155.0704 ⁺										
						[M+NH ₄] ⁺	276.1442	-0.05	87.0447 ⁺										
						[M+Na] ⁺	281.0994	0.50	69.0343 ⁺										
						[M+K] ⁺	297.0734	0.36											
						[M-H] ⁻	549.1623	-1.68	255.0664 ⁻										
						[M+Cl] ⁻	585.1390	-1.70	135.0088 ⁻										
						[M+HCOO] ⁻	595.1676	-1.26	119.0502 ⁻										
						[M+NO ₂] ⁺	612.1578	-2.25	91.0189 ⁺										
						[M+H] ⁺	551.1767	-1.47	257.0812 ⁺										
						[M+NH ₄] ⁺	568.2035	-1.72	147.0943 ⁺										
						[M+Na] ⁺	573.1587	-1.47	137.0236 ⁺										
						[M+K] ⁺	589.1327	-1.49											
[M-H] ⁻	821.3981	-1.92	351.0566 ⁻																
[M+K-2H] ⁻	843.3788	-0.36	289.0548 ⁻																
[M+R-2H] ⁻	859.3519	0.56	647.3783 ⁻																
[M+H] ⁺	823.4109	0.21																	
[M+NH ₄] ⁺	840.4374	0.28																	
[M+Na] ⁺	845.3923	0.88																	
[M+K] ⁺	861.3662	0.86																	
[M-H] ⁻	255.0666	-1.16	153.0193 ⁻																
[M+Cl] ⁻	291.0433	-1.02	137.0236 ⁻																
l	Licorice (no. 55)	estrogen	96	6.71	$C_{15}H_{12}O_4$	[M-H] ⁻	253.0507	-0.38	199.0758 ⁻										
						[M+Cl] ⁻	289.0273	0.21	137.0236 ⁻										
						[M+HCOO] ⁻	299.0561	0.05											
						[2M-H] ⁻	507.1086	-0.03											
						[2M+Cl] ⁻	543.0854	-0.25											
						[2M+HCOO] ⁻	553.1141	-0.08											
						[M+H] ⁺	255.0646	2.22											
						[M+Na] ⁺	277.0466	1.88											
						[M+K] ⁺	293.0203	2.52											
						[2M+H] ⁺	509.1221	1.88											
						[2M+Na] ⁺	531.1047	0.68											
						[2M+K] ⁺	547.0782	1.40											
[M-H] ⁻	283.0613	-0.22	270.0505 ⁻																
[M+Cl] ⁻	319.0380	-0.26	253.0480 ⁻																
[2M+Cl] ⁻	603.1064	-0.06	225.0532 ⁻																
[M+H] ⁺	285.0752	2.11																	

(continued on next page)

Table 1 (continued)

Zone	Botanical	Observed effect	hR_F	Retention time [min]	Molecular formula	Ion species	Precursor [m/z]	$\Delta m/z$ [ppm]	MS ² fragments [m/z]	Proposed fragment formula	$\Delta m/z$ [ppm]	λ_{max} [nm]	Tentative assignment	Literature					
m	Lemon peel (no. 67)	antiestrogen	81	5.90	$C_{13}H_{18}O_4$	[M+Na] ⁺	307.0570	2.33	137.0225	[C ₇ H ₄ O ₃ +H] ⁺									
						[M+K] ⁺	323.0309	2.42											
						[2M+Na] ⁺	591.1252	1.57											
						[2M+K] ⁺	607.0992	1.58											
						[M-H] ⁻	267.0664	-0.58	7.43	$C_{16}H_{12}O_4$	[M+H] ⁺	269.0807	0.47	252.0429	[C ₁₄ H ₅ O ₃ -H] ⁻	-0.44	210,	formononectin	(Xu et al., 2013)
						[M+H] ⁺	269.0807	0.47			[M+H] ⁺	269.0807	0.47	223.0402	[C ₁₄ H ₅ O ₃ -H] ⁻	-0.50	250,		
						[M+Na] ⁺	291.0626	0.47			[M+Na] ⁺	291.0626	0.47	195.0451	[C ₁₂ H ₄ O ₂ -H] ⁻	0.33	305		
						[M+K] ⁺	307.0366	0.57			[M+K] ⁺	307.0366	0.57	132.0217	[C ₈ H ₆ O ₂ -H] ⁻	-0.01			
														213.0910	[C ₁₄ H ₂ O ₂ +H] ⁺	0.22			
														151.0390	[C ₈ H ₄ O ₃ +H] ⁺	0.07			
n	Lemon verbena (no. 68)	antiestrogen	83	5.90	$C_{13}H_{18}O_4$	[M+H] ⁺	239.1278	0.15	135.1170										
						[M+NH ₄] ⁺	256.1543	0.06	105.0187										
						[M+Na] ⁺	261.1097	0.16	93.0704										
						[M+K] ⁺	277.0837	0.03											
						[2M+NH ₄] ⁺	494.2751	-0.56											
						[2M+Na] ⁺	499.2304	-0.26											
						[2M+K] ⁺	515.2045	-0.65											
						[M+H] ⁺	239.1278	0.03						135.1170					
						[M+NH ₄] ⁺	256.1544	-0.06						105.0187					
						[M+Na] ⁺	261.1097	0.08						93.0704					
[M+K] ⁺	277.0837	-0.01																	
[2M+NH ₄] ⁺	494.2750	-0.29																	
[2M+Na] ⁺	499.2304	-0.30																	
[2M+K] ⁺	515.2045	-0.61																	
[M+H] ⁺	255.1227	0.12						209.1175											
[M+NH ₄] ⁺	272.1493	-0.18		6.02	$C_{13}H_{18}O_5$	[M+H] ⁺	272.1493	-0.18	135.1170										
[M+Na] ⁺	277.1046	0.02				[M+Na] ⁺	277.1046	0.02	121.0135										
[M+K] ⁺	293.0786	0.11				[M+K] ⁺	293.0786	0.11	93.0704										

n. d. not detected

*Confirmed *via* reference compounds in Schreiner et al. (2021).

described. The estrogen antagonistic zone was caused by liquiritin apioside (Fig. 5) which was confirmed via a standard in a previous study (Schreiner et al., 2021). The two antiestrogenic zones m and n are unknown, and further structure-elucidating techniques are needed.

Conclusions

The developed multiplex planar bioassay method NP-HPTLC^{FLX}-UV/Vis/FLD-pYAVES enabled the sophisticated non-target screening for hormonal activity. For the first time, sharp zones were obtained after the pYES bioassay on normal-phase HPTLC plates due to substance fixation with Degalan coating. Both estrogen- and antiestrogen-like substances were unambiguously detected, and in addition, false-positives and synergists. Further information was obtained on polarity (R_F on NP-HPTLC), chromophores (Vis), UV absorbance (UV 254 nm), fluorophores (FLD 366 nm), and due to hyphenation with RP-HPLC-DAD-HESI-HRMS/MS, on polarity (retention time on RP-HPLC), UV/Vis absorbance, molecular formulae and structures. Several botanical compounds were identified by their exact masses, fragmentation patterns and UV absorbance. The versatile information obtained by the 12 D hyphenation from a single plate for many samples in parallel provides straightforward evaluation of complex sample mixtures.

CRedit authorship contribution statement

A. Ronzheimer: Conceptualization, Methodology, Investigation, Data curation, Writing – original draft. **T. Schreiner:** Conceptualization, Methodology, Investigation, Data curation, Writing – original draft. **G.E. Morlock:** Conceptualization, Methodology, Supervision, Writing – review & editing.

Declaration of interests

The authors declare that they have no known competing financial interests or personal relationships that could have appeared to influence the work reported in this paper.

Supplementary materials

Supplementary material associated with this article can be found, in the online version, at doi:10.1016/j.phymed.2022.154230.

References

- Acevedo, R.M., Avico, E.H., González, S., Salvador, A.R., Rivarola, M., Paniago, N., Nunes-Nesi, A., Ruiz, O.A., Sansberro, P.A., 2019. Transcript and metabolic adjustments triggered by drought in *Ilex paraguariensis* leaves. *Planta* 250, 445–462.
- Amessis-Ouchemoukh, N., Abu-Reidah, I.M., Quirantes-Piné, R., Rodríguez-Pérez, C., Madani, K., Fernández-Gutiérrez, A., Segura-Carretero, A., 2014. Tentative characterisation of iridoids, phenylethanoid glycosides and flavonoid derivatives from *Globularia alypum* L. (Globulariaceae) leaves by LC-ESI QTOF MS. *Phytochem. Anal.* 25, 389–398.
- Anagnostopoulou, M.A., Kefalas, P., Kokkalou, E., Assimopoulou, A.N., Papageorgiou, V. P., 2005. Analysis of antioxidant compounds in sweet orange peel by HPLC-diode array detection-electrospray ionization mass spectrometry. *Biomed. Chromatogr.* 19, 138–148.
- Arnold, S.F., Klotz, D.M., Collins, B.M., Vonier, P.M., Guillet, L.J., McLachlan, J.A., 1996. Synergistic activation of estrogen receptor with combinations of environmental chemicals. *Science* 272, 1489–1492.
- Azadnia, E., Morlock, G.E., 2019. Automated piezoelectric spraying of biological and enzymatic assays for effect-directed analysis of planar chromatograms. *J. Chromatogr. A* 1602, 458–466.
- Balaguer, P., François, F., Comunale, F., Fenet, H., Boussieux, A.-M., Pons, M., Nicolas, J.-C., Casellas, C., 1999. Reporter cell lines to study the estrogenic effects of xenoestrogens. *Sci. Total Environ.* 233, 47–56.
- Bartella, L., Di Donna, L., Napoli, A., Siciliano, C., Sindona, G., Mazzotti, F., 2019. A rapid method for the assay of methylxanthines alkaloids: Theobromine, theophylline and caffeine, in cocoa products and drugs by paper spray tandem mass spectrometry. *Food Chem.* 278, 261–266.
- Boonmuen, N., Gong, P., Ali, Z., Chitriboiyina, A.G., Khan, I., Doerge, D.R., Helferich, W. G., Carlson, K.E., Martin, T., Piyachaturawat, P., Katzenellenbogen, J.A., Katzenellenbogen, B.S., 2016. Licorice root components in dietary supplements are selective estrogen receptor modulators with a spectrum of estrogenic and anti-estrogenic activities. *Steroids* 105, 42–49.
- Brockhaus, M., Magnani, J.L., Blaszczyk, M., Steplewski, Z., Koprowski, H., Karlsson, K. A., Larson, G., Ginsburg, V., 1981. Monoclonal antibodies directed against the human Leb blood group antigen. *J. Biol. Chem.* 256, 13223–13225.
- Buchinger, S., Spira, D., Bröder, K., Schlißner, M., Ternes, T., Reifferscheid, G., 2013. Direct coupling of thin-layer chromatography with a bioassay for the detection of estrogenic compounds: applications for effect-directed analysis. *Anal. Chem.* 85, 7248–7256.
- Cynara de Oliveira Salles, R., Perça Muniz, M., Cássia Saraiva Nunomura, R., de, Massayoshi, Nunomura, S., 2022. Geographical origin of guarana seeds from untargeted UHPLC-MS and chemometrics analysis. *Food Chem.* 371, 131068.
- D'Abrosca, B., DellaGreca, M., Fiorentino, A., Monaco, P., Previtera, L., Simonet, A.M., Zarrelli, A., 2001. Potential allelochemicals from *Sambucus nigra*. *Phytochemistry* 58, 1073–1081.
- Durgbanshi, A., Arbona, V., Pozo, O., Miersch, O., Sancho, J.V., Gómez-Cadenas, A., 2005. Simultaneous determination of multiple phytohormones in plant extracts by liquid chromatography-electrospray tandem mass spectrometry. *J. Agric. Food. Chem.* 53, 8437–8442.
- Dwyer, J.T., Coates, P.M., Smith, M.J., 2018. Dietary Supplements: Regulatory Challenges and Research Resources. *Nutrients* 10.
- Favela-Hernández, J.M.J., González-Santiago, O., Ramírez-Cabrera, M.A., Esquivel-Ferriño, P.C., Del Canacho-Corona, M.R., 2016. Chemistry and Pharmacology of *Citrus sinensis*. *Molecules* 21, 247.
- Gao, F., Hu, T., Tan, W., Yu, C., Li, Z., Zhang, L., Duan, L., 2016. Photoprotectant improves photostability and bioactivity of abscisic acid under UV radiation. *J. Photochem. Photobiol. B* 158, 99–104.
- Graumann, K., Breithofer, A., Jungbauer, A., 1999. Monitoring of estrogen mimics by a recombinant yeast assay: synergy between natural and synthetic compounds? *Sci. Total Environ.* 225, 69–79.
- Häbe, T.T., Morlock, G.E., 2020. Open-source add-on kit for automation of zone elution in planar chromatography. *Rapid Commun. Mass Spectrom.* 34, e8631.
- Houtman, C.J., Leonards, P.E.G., Kapiteijn, W., Bakker, J.F., Brouwer, A., Lamoree, M.H., Legler, J., Klamer, H.J.C., 2007. Sample preparation method for the ER-CALUX bioassay screening of (xeno-)estrogenic activity in sediment extracts. *Sci. Total Environ.* 386, 134–144.
- Jobst, D., Hensel, A., Kraft, K., 2021. Position Paper of the Society for Phytotherapy on the Differentiation of Herbal Medicinal Products and Food Supplements. GPT - Gesellschaft für Phytotherapie e.V. <https://phytotherapie.de/de/die-gpt/publikationen/publikationen/position-paper-2021/>. Accessed 22 February 2022.
- Kaufmann, D., Kaur Dogra, A., Tahrani, A., Herrmann, F., Wink, M., 2016. Extracts from traditional chinese medicinal plants inhibit acetylcholinesterase, a known Alzheimer's disease target. *Molecules* 21, Basel, Switzerland.
- Klingelhöfer, L., Morlock, G.E., 2014. Sharp-bounded zones link to the effect in planar chromatography-bioassay-mass spectrometry. *J. Chromatogr. A* 1360, 288–295.
- Krüger, S., Hüsen, L., Fornasari, R., Scainelli, I., Morlock, G.E., 2017. Effect-directed fingerprints of 77 botanical extracts via a generic high-performance thin-layer chromatography method combined with assays and mass spectrometry. *J. Chromatogr. A* 1529, 93–106.
- Kunito-Niwa, R., Inoue, S., Ogawa, S., Muramatsu, M., Nozawa, R., 2000. Effects of tea catechins on the ERE-regulated estrogenic activity. *J. Agric. Food. Chem.* 48, 6355–6361.
- Mbachu, O.C., Howell, C., Simmler, C., Malca Garcia, G.R., Skowron, K.J., Dong, H., Ellis, S.G., Hitzman, R.T., Hajirahimkhan, A., Chen, S.-N., Nikolic, D., Moore, T.W., Vollmer, G., Pauli, G.F., Bolton, J.L., Dietz, B.M., 2020. SAR study on estrogen receptor α/β activity of (iso)flavonoids: importance of prenylation, C-Ring (Un) Saturation, and hydroxyl substituents. *J. Agric. Food. Chem.* 68, 10651–10663.
- McDonnell, D.P., Nawaz, Z., Densmore, C., Weigel, N.L., Pham, T.A., Clark, J.H., O'Malley, B.W., 1991. High level expression of biologically active estrogen receptor in *Saccharomyces cerevisiae*. *J. Steroid Biochem. Mol. Biol.* 39, 291–297.
- Mehl, A., Schwack, W., Morlock, G.E., 2021. On-surface autosampling for liquid chromatography-mass spectrometry. *J. Chromatogr. A* 1651, 462334.
- Morlock, G.E., 2021. High-performance thin-layer chromatography combined with effect directed assays and high resolution mass spectrometry as an emerging hyphenated technology: a tutorial review. *Anal. Chim. Acta* 1180, 3386–44.
- Müller, M.B., Dausend, C., Weins, C., Frimmel, F.H., 2004. A new bioautographic screening method for the detection of estrogenic compounds. *Chromatographia* 60, 207–211.
- Murk, A.J., Legler, J., van Lipzig, M.M.H., Meerman, J.H.N., Belfroid, A.C., Spenkelink, A., van der Burg, B., Rijs, G.B.J., Vethaak, D., 2002. Detection of estrogenic potency in wastewater and surface water with three *in vitro* bioassays. *Environ. Toxicol. Chem.* 21, 16–23.
- Nishihara, T., Nishikawa, J., Kanayama, T., Dakeyama, F., Saito, K., Inagawa, M., Takatori, S., Kitagawa, Y., Hori, S., Utsuni, H., 2000. Estrogenic activities of 517 chemicals by yeast two-hybrid assay. *J. Health Sci.* 46, 282–298.
- Puranik, N.V., Srivastava, P., Bhatt, G., John Mary, D.J.S., Limaye, A.M., Sivaraman, J., 2019. Determination and analysis of agonist and antagonist potential of naturally occurring flavonoids for estrogen receptor (ER α) by various parameters and molecular modelling approach. *Sci. Rep.* 9, 7450.
- Quercia, V., Turchetto, L., Pierini, N., Cuzzo, V., Percaccio, G., 1978. Identification and determination of vitexin and isovitexin in *Passiflora incarnata* extracts. *J. Chromatogr. A* 161, 396–402.
- Rajapakse, N., Silva, E., Kortenkamp, Andreas, 2002. Combining xenoestrogens at levels below individual no observed effect concentrations dramatically enhances steroid hormone action. *Environ. Health Perspect.* 110, 917–921.

- Roell, K.R., Reif, D.M., Motsinger-Reif, A.A., 2017. An introduction to terminology and methodology of chemical synergy-perspectives from across disciplines. *Front. Pharmacol.* 8, 158.
- Routledge, E.J., Sumpter, J.P., 1996. Estrogenic activity of surfactants and some of their degradation products assessed using a recombinant yeast screen. *Environ. Toxicol. Chem.* 15, 241–248.
- Schick, D., Schwack, W., 2017. Planar yeast estrogen screen with resorufin- β -D-galactopyranoside as substrate. *J. Chromatogr. A* 1497, 155–163.
- Schönborn, A., Grimmer, A., 2013. Coupling sample preparation with effect-directed analysis of estrogenic activity - Proposal for a new rapid screening concept for water samples. *J. Planar. Chromatogr. - Mod. TLC* 26, 402–408.
- Schönborn, A., Schmid, P., Bräm, S., Reifferscheid, G., Ohlig, M., Buchinger, S., 2017. Unprecedented sensitivity of the planar yeast estrogen screen by using a spray on technology. *J. Chromatogr. A* 1530, 185–191.
- Schreiner, T., Morlock, G.E., 2021. Non-target bioanalytical eight-dimensional hyphenation including bioassay, heart-cut trapping, online desalting, orthogonal separations and mass spectrometry. *J. Chromatogr. A* 1647, 462154.
- Schreiner, T., Ronzheimer, A., Friz, M., Morlock, G.E., 2022. Multiplex planar bioassay with reduced diffusion and improved sensitivity on normal phase: androgens and verified antiandrogens in botanicals. In revision.
- Schreiner, T., Sauter, D., Friz, M., Heil, J., Morlock, G.E., 2021. Is our natural food our homeostasis? Array of A thousand effect-directed profiles of 68 herbs and spices. *Front. Pharmacol.* 12.
- Seeger, B., Klawonn, F., Nguema Bekale, B., Steinberg, P., 2016. Mixture effects of estrogenic pesticides at the human estrogen receptor α and β . *PLoS ONE* 11, e0147490.
- Sonneveld, E., Jansen, H.J., Ritco, J.A.C., Brouwer, A., van der Burg, B., 2005. Development of androgen- and estrogen-responsive bioassays, members of a panel of human cell line-based highly selective steroid-responsive bioassays. *Toxicol. Sci.* 83, 136–148.
- Taniguchi, Y., Matsukura, Y., Taniguchi, H., Koizumi, H., Katayama, M., 2015. Development of preparative and analytical methods of the hop bitter acid oxide fraction and chemical properties of its components. *Biosci. Biotechnol., Biochem.* 79, 1684–1694.
- van der Linden, S.C., Heringa, M.B., Mau, H. Y., Sonneveld, E., Puijker, L.M., Brouwer, A., van der Burg, B., 2008. Detection of multiple hormonal activities in wastewater effluents and surface water, using a panel of steroid receptor CALUX bioassays. *Environ. Sci. Technol.* 42, 5814–5820.
- Vlaisavljević, S., Šibul, F., Sinka, I., Zupko, I., Ocsovszki, I., Jovanović-Šanta, S., 2018. Chemical composition, antioxidant and anticancer activity of licorice from Fruska Gora locality. *Ind. Crops Prod.* 112, 217–224.
- Working group *Fragen der Ernährung*, Society of Food Chemistry, Germany, 2022.
- Grundlagenpapier Beurteilung von Pflanzenextrakten (Basic paper on the evaluation of plant extracts). *Lebensmittelchemie* 1, S1–27. Supplementband.
- Xu, T., Yang, M., Li, Y., Chen, X., Wang, Q., Deng, W., Pang, X., Yu, K., Jiang, B., Guan, S., Guo, D., 2013. An integrated exact mass spectrometric strategy for comprehensive and rapid characterization of phenolic compounds in licorice. *Rapid Commun. Mass Spectrom.* 27, 2297–2309.
- Yoshikawa, M., Uemura, T., Shinoda, H., Kishi, A., Kawahara, Y., Matsuda, H., 2000. Medicinal foodstuffs. XVIII. Phytoestrogens from the aerial part of *Petroselinum crispum* Mill. (Parsley) and structures of 6'-acetylapiin and a new monoterpene glycoside, petroside. *Chem. Pharm. Bull.* 48, 1039–1044.
- Zhang, Y., Cao, J., Wang, Y., Xiao, S., 2013. Simultaneous determination of glycyrrhizin and 15 flavonoids in licorice and blood by high performance liquid chromatography with ultraviolet detector. *ISRN Anal. Chem.* 2013, 1–7.
- Zhou, X., Seto, S.W., Chang, D., Kiat, H., Razmovski-Naumovski, V., Chan, K., Bensoussan, A., 2016. Synergistic effects of Chinese herbal medicine: a comprehensive review of methodology and current research. *Front. Pharmacol.* 7, 201.

Supplementary Information

Multiplex planar bioassay detecting estrogens, antiestrogens, false-positives and synergists as sharp zones on normal phase

*A. Ronzheimer, T. Schreiner, G.E. Morlock**

Justus Liebig University Giessen, Institute of Nutritional Science, Chair of Food Science,
Heinrich-Buff-Ring 26-32, 35392 Giessen, Germany

Dedicated to the 75th birthdays of Elke Hahn-Deinstrop and Dr. Heinz Hauck, Germany

*Corresponding author. Tel.: +49 641 9939141, fax: +49 641 9939149, E-mail address: Gertrud.Morlock@uni-giessen.de (G.E. Morlock)

Table of Contents

Page S-4	Tab. S1. List of the 68 investigated botanicals. Botanical name, plant part, and sample weights (W), extracted with 5 mL methanol (*marked: filtered through 0.45 µm syringe PTFE filter).
Page S-6	Fig. S1. NP-HPTLCfix-UV/Vis/FLD-pYES analysis of 68 botanicals compared to status quo without fixation. Botanical samples (4 µL, 6-mm bands, nos. 1–68 assigned in Table S1 and solvent blank B for comparison) separated on HPTLC plates silica gel 60 F254 MS grade with ethyl acetate – toluene – formic acid – water (16:4:3:2; V/V/V/V) up to 70 mm. Chromatograms (A) and NP-HPTLCfix-pYES bioautograms (B, with Degalan coating) compared with respective status-quo bioautograms (C, Schreiner et al., 2021) at FLD 366 nm.
Page S-7	Fig. S2. Investigation of estrogenic zones missing after Degalan fixation in the bioautogram. Estrogenic profiles of botanical samples nos. 24, 28, 55, and 59 were compared with Degalan fixation (^{fix}) and without fixation after separation with ethyl acetate – toluene – formic acid – water (16:4:3:2, V/V/V/V) up to 70 mm on silica gel 60 F254 MS-grade plates, and documentation at UV 254 nm (A), FLD 366 nm (B) and as pYES bioautogram at FLD 366 nm (C).
Page S-8	Fig. S3. Comparison of dose-response-curves with Degalan fixation (red) and without fixation (blue) of the xenoestrogen 17β-estradiol (E2) and the phytoestrogen daidzein. Standards were applied in different amounts as 6-mm band and chromatographed with ethyl acetate – toluene – formic acid – water (16:4:3:2, V/V/V/V) up to 70 mm. Fluorescence was measured at 366 nm.
Page S-9	Fig. S4. Experimental determination of fluorescein reference area for NP-HPTLCfix-pYAVES. Glycyrrhizic acid (5 µg, 6-mm bands, separated with ethyl acetate – toluene – formic acid – water (16:4:3:2; V/V/V/V) up to 70 mm on silica gel 60) was overlaid with fluorescein (F, 1–75 ng/area,

	<p>1 mm × 70 mm) and 17β-estradiol (É2, 20 pg/area, 2 mm × 70 mm) according to plate design (A). Application (B) and the HPTLCfix-pYAVES bioautogram (C; fixation with Degalan coating, 0.25%; 10 min) were recorded at UV 254 nm. The fluorescence intensity of the F-strips was compared to the E2-strip.</p>
Page S–10	<p>Fig. S5. Comparison of the pYES, pYAES, and pYAVES bioautograms. Botanical samples (4 µL, 6-mm bands for pYES and pYAES and 6.7 µL, 10-mm bands for pYAVES, nos. 16 and 22, assigned in Table S1) separated on silica gel 60 F254 MS-grade plates with ethyl acetate – toluene – formic acid – water (16:4:3:2; V/V/V/V) up to 70 mm and coated with Degalan. HPTLCfix–pYES, pYAES, and pYAVES bioautograms at FLD 366 nm (A) and corresponding chromatograms at UV 254 nm (B) and FLD 366 nm (C).</p>

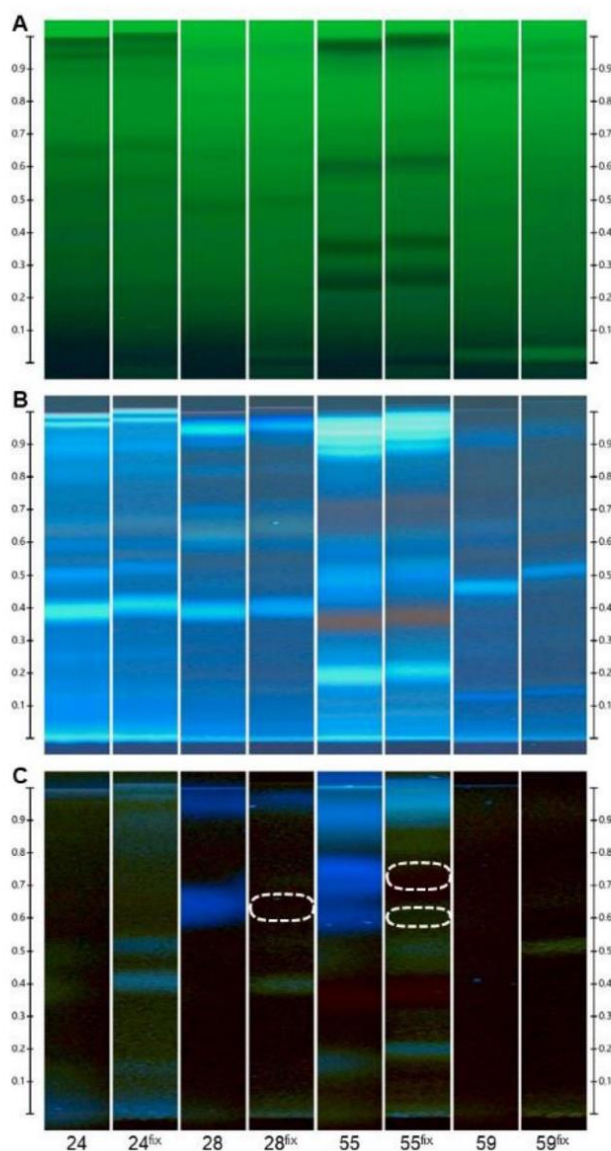
Tab. S1. List of the 68 investigated botanicals. Botanical name, plant part, and sample weights (W), extracted with 5 mL methanol (*marked: filtered through 0.45 µm syringe PTFE filter).

No.	Common name	Botanical name	Plant part	W [mg]
1	Acerola	<i>Malpighia glabra</i> L. [Malpighiaceae].	fruits	501.5
2	Horehound, white	<i>Marrubium vulgare</i> L. [Lamiaceae]	herb	500.1
3	Apple*	<i>Malus sylvestris</i> (L.) Mill. [Rosaceae]	peel	500.7
4	Artichoke, globe	<i>Cynara cardunculus</i> subsp. <i>scolymus</i> (L.) [Asteraceae]	leaves	501.3
5	Basil	<i>Ocimum basilicum</i> L. [Lamiaceae]	herb	500.6
6	Fenugreek	<i>Trigonella foenum-graecum</i> L. [Fabaceae]	seeds	499.9
7	Stinging nettle*	<i>Urtica dioica</i> L. [Urticaceae]	leaves	501.5
8	Blackberry	<i>Rubus fruticosus</i> L. [Rosaceae]	leaves	500.6
9	Eucalyptus	<i>Eucalyptus globulus</i> Labill. [Myrtaceae]	leaves	499.7
10	Fennel	<i>Foeniculum vulgare</i> Mill. [Apiaceae]	fruits	499.9
11	Fruit tea, yellow	not available	unknown	501.3
12	Fruit tea, red	not available	unknown	502.6
13	Galangal	<i>Alpinia officinarum</i> Hance. [Zingiberaceae]	roots	501.8
14	Ginkgo	<i>Ginkgo biloba</i> L. [Ginkgoaceae]	leaves	502.7
15	Ginseng	<i>Panax ginseng</i> C.A.Mey. [Araliaceae]	roots	502.3
16	Guarana	<i>Paullinia cupana</i> Kunth [Sapindaceae]	seeds	498.8
17	Dog rose	<i>Rosa canina</i> L. [Rosaceae]	fruits	501.0
18	Blueberry, European	<i>Vaccinium myrtillus</i> L. [Ericaceae]	fruits	501.2
19	Hibiscus	<i>Hibiscus rosa-sinensis</i> L. [Malvaceae]	blossoms	499.6
20	Raspberry	<i>Rubus idaeus</i> L. [Rosaceae]	juice concentrate from fruits	503.0
21	Elder berry	<i>Sambucus nigra</i> L. [Adoxaceae]	fruits	501.4
22	Elder flower	<i>Sambucus nigra</i> L. [Adoxaceae]	blossoms	502.5
23	Honeybush*	<i>Cyclopia genistoides</i> (L.) R.Br. [Fabaceae]	leaves, branches, blossoms	499.3
24	Hop	<i>Humulus lupulus</i> L. [Cannabaceae]	blossoms	502.1
25	Ginger	<i>Zingiber officinale</i> Roscoe [Zingiberaceae]	roots	499.0
26	Jasmine*	<i>Jasminum officinale</i> L. [Oleaceae]	blossoms	499.2
27	Cassis	<i>Ribes nigrum</i> L. [Grossulariaceae]	juice concentrate from fruits	500.7
28	Chamomile	<i>Matricaria chamomilla</i> L. [Asteraceae]	blossoms	499.3
29	Cardamom*	<i>Elettaria cardamomum</i> (L.) Maton [Zingiberaceae]	fruits	499.6
30	Garlic	<i>Allium sativum</i> L. [Amaryllidaceae]	bulbs	499.9
31	Kola*	<i>Cola nitida</i> (Vent.) Schott & Endl. [Malvaceae]	seeds	500.8
32	Coriander	<i>Coriandrum sativum</i> L. [Apiaceae]	fruits	501.3
33	Caraway	<i>Carum carvi</i> L. [Apiaceae]	fruits	500.0

No.	Common name	Botanical name	Plant part	W [mg]
34	Lovage	<i>Levisticum officinale</i> W.D.J.Koch [Apiaceae]	roots	499.6
35	Marjoram	<i>Origanum majorana</i> L. [Lamiaceae]	herb	502.4
36	Yerba mate*	<i>Ilex paraguariensis</i> A.St.-Hil. [Aquifoliaceae]	leaves, roasted	499.6
37	Yerba mate	<i>Ilex paraguariensis</i> A.St.-Hil. [Aquifoliaceae]	leaves	500.2
38	Lemon balm	<i>Melissa officinalis</i> L. [Lamiaceae]	leaves	500.6
39	Clove*	<i>Syzygium aromaticum</i> (L.) Merr. & L.M. Perry [Myrtaceae]	flower buds	501.9
40	Orange	<i>Citrus × aurantium</i> L. [Rutaceae]	blossoms	499.7
41	Orange	<i>Citrus × aurantium</i> L. [Rutaceae]	peel	501.1
42	Oregano	<i>Origanum vulgare</i> L. [Lamiaceae]	herb	501.5
43	Passionflower	<i>Passiflora incarnata</i> L. [Passifloraceae]	blossoms	501.1
44	Peppermint	<i>Mentha × piperita</i> L. [Lamiaceae]	leaves	500.3
45	Rooibos*	<i>Aspalathus linearis</i> (Burm.f.) R. Dahlgren [Fabaceae]	leaves	500.7
46	Rosemary*	<i>Salvia Rosmarinus</i> Spenn. [Lamiaceae]	leaves	500.9
47	Sage	<i>Salvia officinalis</i> L. [Lamiaceae]	leaves	499.9
48	Sea buckthorn	<i>Hippophae rhamnoides</i> L. [Elaeagnaceae]	fruits	501.9
49	Horsetail	<i>Equisetum arvense</i> L. [Equisetaceae]	herb	499.3
50	Yarrow*	<i>Achillea millefolium</i> L. [Asteraceae]	herb	501.6
51	Celeriac	<i>Apium graveolens</i> L. [Apiaceae]	bulb	501.3
52	Coneflower	<i>Echinacea angustifolia</i> DC. [Asteraceae]	herb and roots	499.1
53	Plantain	<i>Plantago lanceolata</i> L. [Plantaginaceae]	leaves	500.5
54	Star anise	<i>Illicium verum</i> Hook.f. [Schisandraceae]	fruits	500.3
55	Licorice	<i>Glycyrrhiza glabra</i> L. [Fabaceae]	roots	500.3
56	Siberian ginseng	<i>Eleutherococcus senticosus</i> (Rupr. & Maxim.) Maxim. [Araliaceae]	roots	503.4
57	Thyme	<i>Thymus vulgaris</i> L. [Lamiaceae]	herb	499.6
58	Grape*	<i>Vitis vinifera</i> L. [Vitaceae]	seed	499.9
59	Grape	<i>Vitis vinifera</i> L. [Vitaceae]	peel	499.7
60	Juniper	<i>Juniperus communis</i> L. [Cupressaceae]	fruits	501.5
61	Grape	<i>Vitis vinifera</i> L. [Vitaceae]	leaves	501.2
62	Hawthorn	<i>Crataegus</i> sp. [Rosaceae]	leaves and blossoms	499.7
63	Hawthorn leaves (Batch 1)	<i>Crataegus</i> sp. [Rosaceae]	leaves	501.8
64	Hawthorn leaves (Batch 2)	<i>Crataegus</i> sp. [Rosaceae]	leaves	499.9
65	Chicory	<i>Cichorium intybus</i> L. [Asteraceae]	roots	501.1
66	Cinnamon	<i>Cinnamomum verum</i> J.Presl [Lauraceae]	bark	501.5
67	Lemon	<i>Citrus × limon</i> (L.) Osbeck [Rutaceae]	peel	500.7
68	Lemon verbena	<i>Aloysia citridora</i> Paláu [Verbenaceae]	leaves	500.4



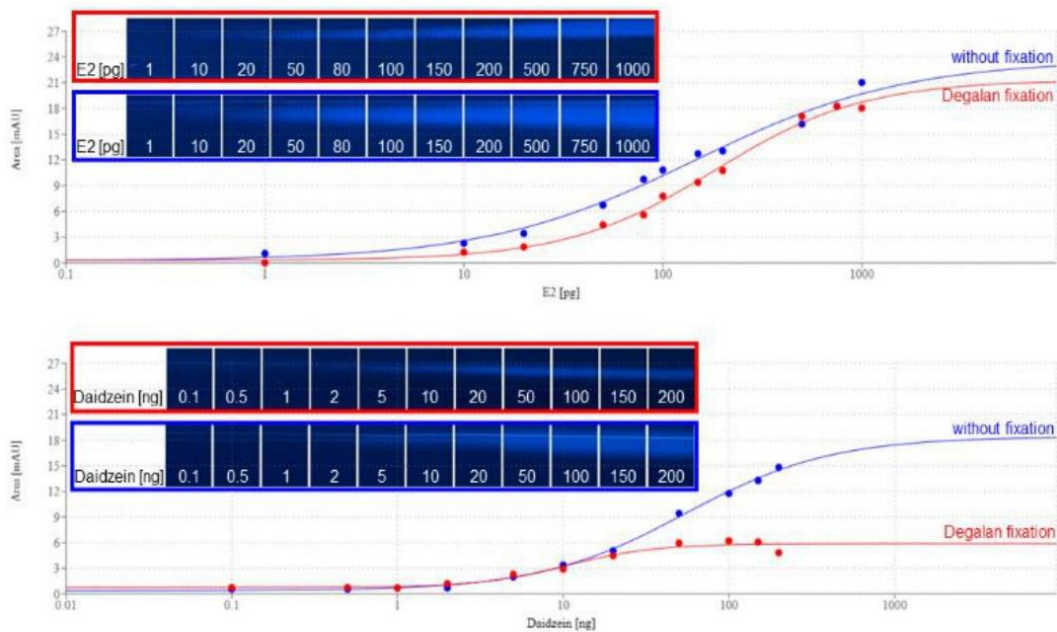
2 **Fig. S1. NP-HPTLC^{fix}-UV/Vis/FLD-pYES analysis of 68 botanicals compared to status quo without fixation.** Botanical samples (4 μ L, 6-mm bands, nos. 1–68 assigned in Table S1 and solvent blank B for comparison) separated on HPTLC plates silica gel 60 F254 MS grade with ethyl acetate – toluene – formic acid – water (16:4:3:2; V/V/V/V) up to 70 mm. Chromatograms (A) and NP-HPTLC^{fix}-pYES bioautograms (B, with Degalan coating) compared with respective status-quo bioautograms (C, Schreiner et al., 2021) at FLD 366 nm.



6

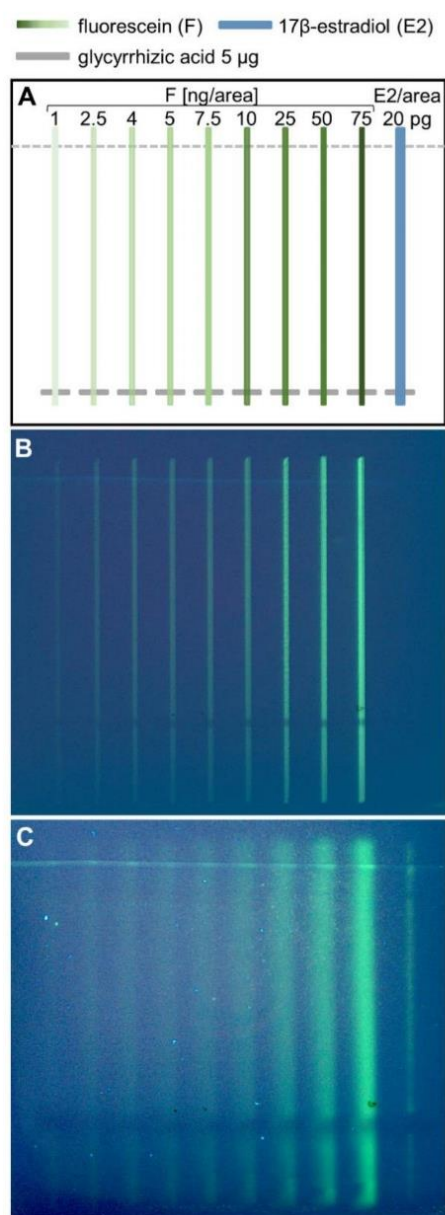
7 **Fig. S2. Investigation of estrogenic zones missing after Degalan fixation in the**
8 **bioautogram.** Estrogenic profiles of botanical samples nos. 24, 28, 55, and 59 were compared
9 with Degalan fixation (^{fix}) and without fixation after separation with ethyl acetate – toluene –
10 formic acid – water (16:4:3:2, V/V/V/V) up to 70 mm on silica gel 60 F₂₅₄ MS-grade plates, and
11 documentation at UV 254 nm (A), FLD 366 nm (B) and as pYES bioautogram at FLD 366 nm
12 (C).

S-7



13

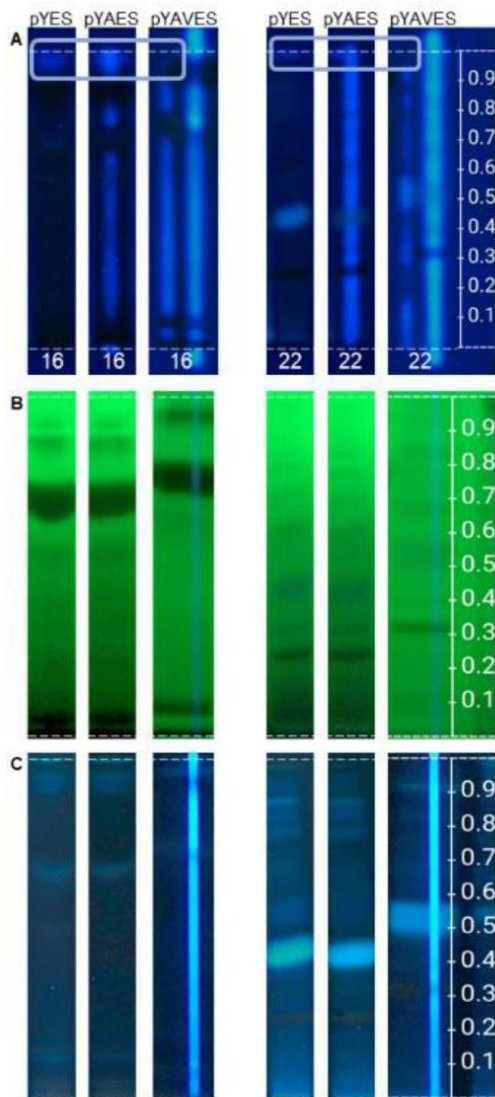
14 **Fig. S3. Comparison of dose-response-curves with Degalan fixation (red) and without**
 15 **fixation (blue) of the xenoestrogen 17 β -estradiol (E2) and the phytoestrogen daidzein.**
 16 Standards were applied in different amounts as 6-mm band and chromatographed with ethyl
 17 acetate – toluene – formic acid – water (16:4:3:2, V/V/V/V) up to 70 mm. Fluorescence was
 18 measured at 366 nm.



19

20 **Fig. S4. Experimental determination of fluorescein reference area for NP-HPTLC^{fix}-**
 21 **pYAVES.** Glycyrrhizic acid (5 μg, 6-mm bands, separated with ethyl acetate – toluene – formic
 22 acid – water (16:4:3:2; V/V/V/V) up to 70 mm on silica gel 60) was overlaid with fluorescein (F,
 23 1–75 ng/area, 1 mm × 70 mm) and 17β-estradiol (É2, 20 pg/area, 2 mm × 70 mm) according
 24 to plate design (A). Application (B) and the HPTLC^{fix}-pYAVES bioautogram (C; fixation with
 25 Degalan coating, 0.25%; 10 min) were recorded at UV 254 nm. The fluorescence intensity of
 26 the F-strips was compared to the E2-strip.

S-9



27

28 **Fig. S5. Comparison of the pYES, pYAES, and pYAVES bioautograms.** Botanical samples
 29 (4 μ L, 6-mm bands for pYES and pYAES and 6.7 μ L, 10-mm bands for pYAVES, nos. 16 and
 30 22, assigned in Table S1) separated on silica gel 60 F₂₅₄ MS-grade plates with ethyl acetate –
 31 toluene – formic acid – water (16:4:3:2; V/V/V/V) up to 70 mm and coated with Degalan. HPT-
 32 LC^{fix}-pYES, pYAES, and pYAVES bioautograms at FLD 366 nm (A) and corresponding chro-
 33 matograms at UV 254 nm (B) and FLD 366 nm (C).

8. Summary

Most NTS strategies for food focus on adulterations to maintain the food quality and safety. Considering thousands of unknown compounds therein, data processing is necessary to properly handle the huge amount of data. If most features of the analysed food are rationalized by processing, how can we evaluate it as safe? Therefore, new NTS strategies should prioritise bioactive compounds which is only possible by interdisciplinary hyphenation of analytical chemistry and biology. As metabolic processes can alter the bioactivity of compounds absorbed into the human body, incorporating metabolomics would provide an utmost holistic approach. The developed multi-hyphenated eight-, ten-, and twelve-dimensional workflows proved to be excellent analysis tools for the identification of new bioactive compounds from complex matrices. The more information one could gain within a comprehensive highly-streamlined workflow, the easier the elucidation of an emerging bioactive unknown is. The basic screening procedure consisted of NP-HPTLC, multi-imaging, (bio)assay, heart cut elution, online-desalting, RP-HPLC, DAD, and mass spectrometric detection (8D). Information provided by this workflow includes polarity, chromophores, UV absorption capability, native fluorescing properties, bioactivity, absorbance, and mass spectra. Extensions were introduced with the nanoGIT^{active} system and HRMS with fragmentation option (10D). Further dimensions were feasible through multiplexed assay formats (12D) after the diffusion susceptibility of substances in the silica gel layer was reduced with a polyisobutyl methacrylate coating. Multiplexed assays for hormonally active compounds were capable to screen for agonists, antagonists, synergists, and false-positives within a single run. Combined with the previous dimensions, comprehensive information about an unknown structure is gained, ultimately leading to structure elucidation. In conclusion, the newly developed multi-dimensional workflows are applicable both, in routine and research. They could fuel drug discovery and pharmaceutical industry, and they can serve as quality control tools to ensure food safety and prevent food fraud.

9. Zusammenfassung

Die meisten NTS-Strategien für Lebensmittel konzentrieren sich auf Kontaminanten, um die Lebensmittelqualität und -sicherheit zu erhalten. Bei Tausenden von unbekanntem Verbindungen in Lebensmitteln ist eine computergestützte Verarbeitung der riesigen Datenmengen erforderlich. Wenn einige dieser Daten durch die Verarbeitung verloren gehen, wie können wir die Lebensmittel dann als sicher bewerten? Neue NTS-Strategien sollten daher den Fokus auf bioaktive Verbindungen legen, was nur durch eine interdisziplinäre Verknüpfung von analytisch-chemischen und biologischen Methoden möglich ist. Da Stoffwechselprozesse im menschlichen Körper die Bioaktivität von Verbindungen verändern können, würde die Einbeziehung der metabolischen Aktivität den Analyse-Ansatz vervollständigen. Die entwickelten acht-, zehn- und zwölfdimensionalen Arbeitsabläufe erwiesen sich als gutes Analysewerkzeug für die Identifizierung neuer bioaktiver Verbindungen aus komplexen Matrices. Je mehr Informationen im Rahmen eines umfassenden Arbeitsablaufs gewonnen werden können, desto einfacher ist es, eine unbekannt bioaktive Substanz zu identifizieren. Das grundlegende Screening-Verfahren bestand aus NP-HPTLC, Mehrfach-Bildgebung, (Bio)Assay, Zonen-Elution, Online-Entsalzung, RP-HPLC, DAD und massenspektrometrischer Detektion (8D). Zu den Informationen, die dieser Arbeitsablauf liefert, gehören Polarität, Chromophore, UV-Absorptionsvermögen, native Fluoreszenzeigenschaften, Bioaktivität, Absorptions- und Massenspektren. Erweiterungen wurden mit dem nanoGIT^{active}-System und HRMS mit Fragmentierungsoption (10D) eingeführt. Weitere Dimensionen wurden durch Multiplex-Assay-Formate möglich (12D), nachdem die Diffusionsanfälligkeit der Kieselgelschicht mit einer Polyisobutylmethacrylatbeschichtung unter Kontrolle gehalten wurde. Multiplex-Assays für hormonell wirksame Verbindungen waren in der Lage, Agonisten, Antagonisten, Synergisten und falsch-positive Ergebnisse in einem einzigen Durchgang zu ermitteln. In Kombination mit den vorhergehenden Dimensionen werden umfassende Details über eine unbekannt Struktur gewonnen, was letztlich zur Strukturaufklärung führt. Zusammenfassend lässt sich sagen, dass die neu entwickelten multidimensionalen Arbeitsabläufe sowohl in der Routine als auch in der Forschung anwendbar sind. Sie könnten die Arzneimittelforschung und die pharmazeutische Industrie voranbringen und als Qualitätssicherungsinstrument zur Kontrolle der Lebensmittelsicherheit und zur Verhinderung von Lebensmittelbetrug dienen.